

AD-A183 783

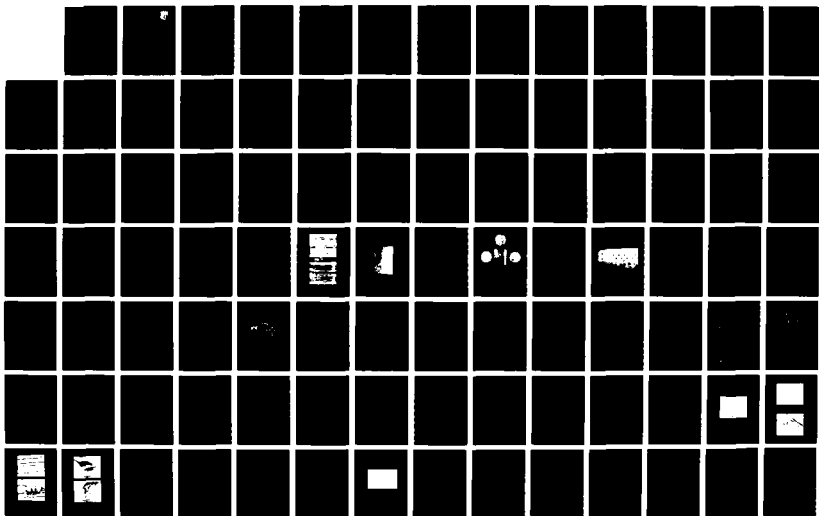
COMPENDIUM OF POST-FAILURE ANALYSIS TECHNIQUES FOR
COMPOSITE MATERIALS(U) BOEING MILITARY AIRPLANE CO
SEATTLE WA R A GROVE ET AL. JAN 87 AFMAL-TR-86-4137
F33615-84-C-5010

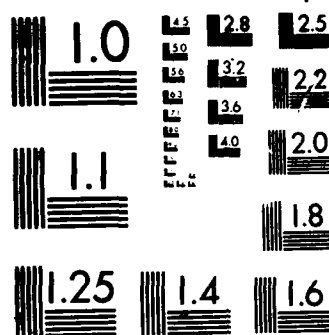
1/5

UNCLASSIFIED

F/G 11/4

NL





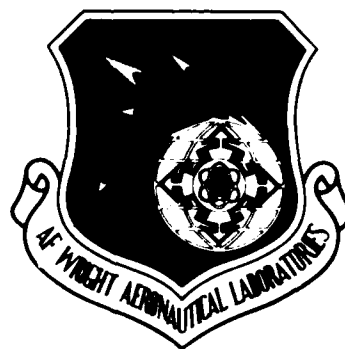
MICROCOPY RESOLUTION TEST CHART

NATIONAL BUREAU OF STANDARDS-1963-A

2

AFWAL-TR-86-4137

DTIC FILE COPY



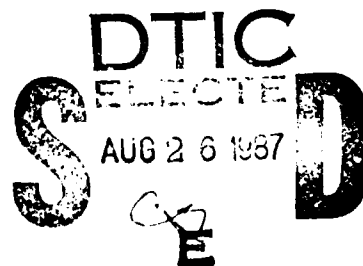
COMPENDIUM OF POST-FAILURE ANALYSIS TECHNIQUES
FOR COMPOSITE MATERIALS

RAY GROVE, BRIAN SMITH
BOEING MILITARY AIRPLANE COMPANY
P. O. BOX 3707
M/S 73-43
SEATTLE, WASHINGTON 98124

JANUARY 1987

INTERIM REPORT FOR PERIOD JULY 1984 - NOVEMBER 1986

APPROVED FOR PUBLIC RELEASE; DISTRIBUTION IS UNLIMITED.



MATERIALS LABORATORY
AIR FORCE WRIGHT AERONAUTICAL LABORATORIES
AIR FORCE SYSTEMS COMMAND
WRIGHT PATTERSON AIR FORCE BASE, OHIO 45433-6533

87 8 25 044

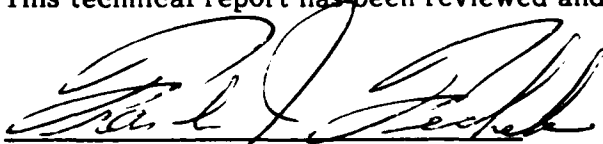
AD-A183 783

NOTICE

When Government drawings, specifications, or other data are used for any purpose other than in connection with a definitely related Government procurement operation, the United States Government thereby incurs no responsibility nor any obligation whatsoever; and the fact that the government may have formulated, furnished, or in any way supplied the said drawings, specifications, or other data, is not to be regarded by implication or otherwise as in any manner licensing the holder or any other person or corporation or conveying any rights or permission to manufacture, use, or sell any patented invention that may in any way be related thereto.

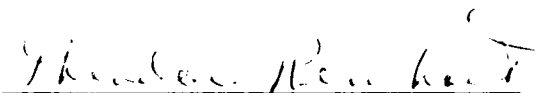
This report has been reviewed by the Office of Public Affairs (ASD/PA) and is releasable to the National Technical Information Service (NTIS). At NTIS, it will be available to the general public, including foreign nations.

This technical report has been reviewed and is approved for publication.



Frank J. Fechek
Air Force Project Engineer

FOR THE COMMANDER



Theodore Reinhart
Chief Materials Engineering Branch
Systems Support Division

If your address has changed, if you wish to be removed from our mailing list, or if the addressee is no longer employed by your organization, please notify AFWAL/MLSE, W-PAFB, OH 45433-6533, to help us maintain a current mailing list.

Copies of this report should not be returned unless return is required by security considerations, contractual obligations, or notice on a specific document.

UNCLASSIFIED

SECURITY CLASSIFICATION OF THIS PAGE

REPORT DOCUMENTATION PAGE

1a REPORT SECURITY CLASSIFICATION Unclassified			1b RESTRICTIVE MARKINGS		
2a SECURITY CLASSIFICATION AUTHORITY			3 DISTRIBUTION / AVAILABILITY OF REPORT Approved for public release; distribution is unlimited.		
2b DECLASSIFICATION / DOWNGRADING SCHEDULE			5 MONITORING ORGANIZATION REPORT NUMBER(S) AFWAL-TR-86-4137		
4. PERFORMING ORGANIZATION REPORT NUMBER(S)			7a NAME OF MONITORING ORGANIZATION Air Force Wright Aeronautical/Laboratories, Materials Laboratory (AFWAL/MLSE)		
6a. NAME OF PERFORMING ORGANIZATION Boeing Military Airplane Co.		6b OFFICE SYMBOL (If applicable)	7b ADDRESS (City, State, and ZIP Code) AFWAL/MLSE Wright Patterson Air Force Base, OH 45433-6533		
6c. ADDRESS (City, State, and ZIP Code) P.O. Box 307, M/S 73-43 Seattle, WA 98124			9 PROCUREMENT INSTRUMENT IDENTIFICATION NUMBER Contract No. F33615-84-C-5010		
8a. NAME OF FUNDING / SPONSORING ORGANIZATION		8b OFFICE SYMBOL (If applicable) AFWAL/MLSE	10 SOURCE OF FUNDING NUMBERS		
8c ADDRESS (City, State, and ZIP Code) Wright Patterson AFB, OH 45433-6533		PROGRAM ELEMENT NO 62102F	PROJECT NO 2418	TASK NO 04	WORK UNIT ACCESSION NO 31
11 TITLE (Include Security Classification) Compendium of Post Failure Analysis Techniques for Composite Materials					
12 PERSONAL AUTHOR(S) Ray Grove and Brian Smith					
13a TYPE OF REPORT Interim		13b TIME COVERED FROM 840718 TO 861118		14 DATE OF REPORT (Year, Month, Day) 1987, January	
15 PAGE COUNT 428					
16 SUPPLEMENTARY NOTATION					
17 COSATI CODES			18 SUBJECT TERMS (Continue on reverse if necessary and identify by block number)		
FIELD 11	GROUP 04	SUB GROUP	Composites; composite structure, failure analysis, fractography, graphite epoxy, stress analysis, non-destructive evaluation, materials characterization.		
19 ABSTRACT (Continue on reverse if necessary and identify by block number) The objective of this document is to describe the analytical and diagnostic techniques that can be used to determine the causes of failure in continuous fiber reinforced composite materials. This is a compendium of procedures which may be used as a reference manual when conducting a post-failure analysis of a composite structure, given the failed part as the starting point of the investigation. Flow charts present a logical sequence of steps for each discipline when conducting a post-failure analysis. The major diagnostic procedures considered are fractography, materials characterization, non-destructive evaluation, and stress analysis. (copy)					
20 DISTRIBUTION AVAILABILITY OF ABSTRACT <input checked="" type="checkbox"/> UNCLASSIFIED/UNLIMITED <input type="checkbox"/> SAME AS RPT <input type="checkbox"/> DTIC USERS			21 ABSTRACT SECURITY CLASSIFICATION Unclassified		
22a NAME OF RESPONSIBLE INDIVIDUAL Frank Fechek			22b TELEPHONE (Include Area Code) (513) 255-7483		22c OFFICE SYMBOL AFWAL/MLSE

DD FORM 1473, 84 MAR

83 APR edition may be used until exhausted

For other editions, see GPO notice

SECURITY CLASSIFICATION OF THIS PAGE

UNCLASSIFIED

SUMMARY

The objective of this document is to describe the analytical and diagnostic techniques that can be used to determine the causes of failure in continuous fiber reinforced composite materials. The material of primary emphasis in this compendium is the continuous carbon fiber-epoxy resin matrix system.

This document is the final product of Task 4 of a five task program:

- Task 1 - An objective review of available literature for various diagnostic techniques and approaches.
- Task 2 - Evaluate the capability of selected test techniques to produce specific types of modes of failure in specimens examined in Task 3.
- Task 3 - Evaluate various diagnostic techniques, particularly fractography, such that crack propagation mechanisms could be related to specific fracture features.
- Task 4 - Compile all the pertinent data and techniques into one source book, or Compendium.
- Task 5 - Verify and demonstrate the applicability of these techniques by conducting failure analyses of three structural components.

This document is a result of the accumulation of knowledge gained through the completion of all of the above tasks (the results of which are also documented in the interim and final reports) as well as experience gained by The Boeing Company and other government, industry and academic investigators over the last ten or so years through R&D programs. The intent is to provide an organized and easily accessible source of information and guidance upon which a composite material structure failure analysis may be performed. The Compendium is organized as follows: (1) a working document of value to the investigator during a failure analysis, (2) a reference document to which one can refer to clarify a point in question or to research a specific new observation, and, (3) a teaching

document from which a new investigator can learn the essentials necessary to do an analysis and from which a "rusty" investigator can brush up on a specific area.

This compendium is a first attempt by the Air Force to provide a reference source on this subject and should be considered as a precursor to a much more comprehensive handbook which will be the final product of two current Air Force programs, F33615-86-C-5071 and F33615-87-C-5212.

This compendium is divided into three major groupings:

- Failure analysis logic networks (FALN), which identify a logical approach toward composite failure analysis investigations are presented in Section 2.0.
- The techniques and analytical procedures to gather information as well as the interpretation of the results obtained, are presented in Sections 3.0 and 4.0.
- Supportive data, such as case histories of actual failure analyses and an extensive atlas of fractographs, to provide a comparative reference source, are presented in Sections 5.0 and 6.0.

FOREWORD

This report documents work performed under Contract F33615-84-C-5010 from July 18, 1984 through November 18, 1986. This contract with the Boeing Military Airplane Company, Seattle, Washington, is monitored by AFWAL/MLSE under the direction of Mr. F. Fecek, Air Force Wright Aeronautical Laboratories, Materials Laboratory, Wright Patterson Air Force Base, Ohio 45433-6533.

The program was conducted by the Materials Technology organization of the Boeing Commercial Airplane Company. Mr. D. F. Sekits is the program manager; Mr. R. A. Grove and Mr. Brian W. Smith are co-principal investigators.

Other contributors to this report are Mr. B. J. McElroy (materials characterization), Mr. T. E. Munns (materials characterization), Mr. R. J. Rothschilds (stress analysis), Mr. M. M. Yamashita (case histories), and Messrs R. E. Smith and E. A. Ledbury (SEM) of the Boeing Materials Technology Group.

The authors wish to thank Mr. F. Fecek (AFWAL/MLSE) and Ms. P. Stumpff (AFWAL/MLSA) for their inputs and guidance. In addition, the authors would like to express their thanks to the numerous publishing houses and authors who granted permission to include their works in this document.

Accession For	
NTIS GRA&I	<input checked="checked" type="checkbox"/>
DTIC TAB	<input type="checkbox"/>
Unannounced	<input type="checkbox"/>
Justification	
By _____	
Distribution/	
Availability Codes	
Dist	Avail and/or Special
A-1	



TABLE OF CONTENTS

	Page
1.0 INTRODUCTION AND PURPOSE	1-1
2.0 FAILURE ANALYSIS LOGIC NETWORKS (FALN)	2-1
2.1 General Concepts	2-1
2.2 Major Failure Analysis Logic Networks (FALN)	2-1
3.0 PROCEDURES FOR USE IN FAILURE ANALYSIS	3-1
3.1 Materials Characterization	3-2
3.1.1 Laminate Layup and Ply Orientation Analyses	3-8
3.1.1.1 Optical Microscopy	3-10
Sectioning	3-10
Metallographic Preparation	3-10
Plies	3-11
3.1.1.2 Image Analysis	3-14
3.1.1.3 Radiography	3-14
3.1.2 Determination of Fiber, Matrix, Void, and Moisture Content	3-16
3.1.2.1 Fiber and Matrix Content	3-16
3.1.2.2 Void Content	3-18
3.1.2.3 Moisture Content	3-18
3.1.3 Material Identification	3-19
3.1.3.1 Uncured Material Identification	3-19
High Pressure Liquid Chromatography (HPLC)	3-20
Infrared Spectroscopy (IR)	3-20
Differential Scanning Calorimetry (DSC)	3-23
Atomic Absorption Spectroscopy (AA)	3-26
X-Ray Fluorescence Spectroscopy (XRF)	3-26

3.1.3.2	Cured Material Identification	3-29
	Pyrolysis Gas Chromatography (PGC)	3-29
	PGC/Mass Spectrometry (PGC/MS)	3-29
	Infrared Spectroscopy (IR)	3-31
	Diffuse Reflectance Infrared Spectroscopy (DRIFTS)	3-31
3.1.4	Degree of Cure Analysis	3-31
3.1.4.1	Glass Transition Temperature (T _g) Analysis	3-35
	Thermomechanical Analysis (TMA)	3-36
	Dynamic Mechanical Analysis (DMA)	3-40
	Differential Scanning Calorimetry (DSC)	3-41
3.1.4.2	Extent of Unreacted Material	3-42
	Differential Scanning Calorimetry (DSC)	3-42
	Dynamic Mechanical Analysis (DMA)	3-42
	Solvent Extraction/Infrared Spectroscopy	3-44
3.1.5	Cured Material Contamination Analysis	3-44
3.1.5.1	Particulate Contamination	3-45
3.1.5.2	Weak Boundary Contamination	3-45
3.1.5.3	Scanning Electron Microscopy (SEM) and Electron Microprobe Analysis (EPMA)	3-51
3.1.5.4	X-Ray Photoelectron Spectroscopy (XPS)	3-56
3.1.5.5	Infrared Spectroscopy (IR) and Fourier Transform Infrared (FTIR)	3-60
3.1.5.6	X-Ray Diffraction (XRD)	3-63
3.1.5.7	Secondary Ion Mass Spectroscopy (SIMS)	3-63
3.1.5.8	Auger Electron Spectroscopy (AES)	3-64
3.1.5.9	Contamination Analysis Example	3-64

3.2	Nondestructive Evaluation (NDE) Techniques	3-67
3.2.1	Ultrasonic Methods	3-76
3.2.1.1	Through-Transmission Ultrasonics (TTU)	3-77
3.2.1.2	Pulse-Echo Ultrasonics	3-80
3.2.1.3	Single-Sided Ultrasonic (Backscatter)	3-83
3.2.2	X-Ray Radiography	3-84
3.2.2.1	Classical Radiography	3-84
3.2.2.2	Penetrant-Enhanced Radiography	3-85
3.2.3	Eddy Current	3-88
3.2.4	Edge Replication	3-88
3.3	Fractography Techniques	3-90
3.3.1	Care, Handling, and Protection of Fracture Surfaces	3-97
3.3.2	Photo Macrography	3-99
3.3.3	Optical Microscopy	3-101
3.3.4	Scanning Electron Microscopy (SEM)	3-104
3.3.4.1	SEM Specimen Preparation	3-105
3.3.4.2	SEM Techniques	3-107
	Interlaminar Fractures	3-112
	Translaminar Fractures	3-115
3.3.5	Transmission Electron Microscopy (TEM)	3-115
3.3.5.1	TEM Specimen Preparation	3-116
3.3.5.2	TEM Techniques	3-118

3.4	Stress Analysis Techniques	3-119
3.4.1	Introduction to Composite Stress Analysis	3-119
3.4.1.1	Relevance to Stress Analysis FALN	3-128
3.4.1.2	Overview of Topics	3-131
3.4.1.3	Analytical Prediction of Strength (Of Unnotched Multidirectional Laminates)	3-132
3.4.1.4	Individual Ply Failure Criteria	3-132
3.4.1.5	Laminate Level Strength Criteria	3-137
	First Ply Failure	3-137
	Ply Discount Methods	3-137
	Finite Element Modeling	3-140
3.4.1.6	Summary - Unnotched Laminate Strength	3-143
3.4.2	Influence of Ply Thickness on Transverse Cracking	3-145
3.4.3	Strength Reductions Incorporated Into Design Notched Laminate Strength	3-147
3.4.4	Introduction to Delamination	3-153
3.4.4.1	Fracture Analysis and Specimens (For Determining Interlaminar Toughness)	3-154
3.4.4.2	Interlaminar Fatigue Crack Growth	3-158
3.4.5	Reductions in Strength Due to Manufacturing Defects	3-159
4.0	FRACTOGRAPHIC APPLICATIONS, EXAMPLES AND INTERPRETIVE METHODS	4-1
4.1	Fracture Types	4-2
4.2	Fracture Modes, Features, and Growth Directions	4-7
4.2.1	Interlaminar and Intralaminar	4-8

4.2.1.1	Mode I Tension Delaminations	4-12
4.2.1.2	Mode II Shear Delaminations	4-22
4.2.1.3	Mixed Mode Delaminations	4-28
4.2.2	Translaminar	4-30
4.2.2.1	Translaminar Tension Fractures	4-30
4.2.2.2	Translaminar Compression Fractures	4-34
4.3	Interlaminar Fracture Mapping	4-39
4.4	Crack Origin Analysis	4-44
4.5	Environment Effects	4-44
4.5.1	Translaminar Fractures	4-46
4.5.2	Delamination Fractures	4-46
4.6	Summary of Composite Materials Fractography	4-50
4.6.1	Brittle Resin Composites Crack Growth	4-50
4.6.2	Ductile Resin Composites Crack Growth	4-51
4.6.3	Fracture Mode Determination (Tension, Shear, and Compression)	4-51
4.6.4	Mixed Mode Loading Effects	4-52
4.6.5	Temperature and Absorbed Moisture Effects	4-52
4.6.6	Processing Defects Effects	4-53
4.6.7	Material Forms Effects	4-53
4.6.8	Post-Failure Environment Effects	4-54
4.6.9	Fatigue Effects	4-54
5.0	CASE HISTORIES OF COMPOSITE FAILURE ANALYSES	5-1
5.1	The 737-300 Elevator Test Box	5-1

5.1.1	Background History	5-1
5.1.2	Nondestructive Examination	5-3
5.1.3	Materials Characterization	5-3
5.1.4	Fractography	5-4
5.1.5	Stress Analyses	5-4
5.2	JVX V-22 Osprey Full Scale Test Box	5-6
5.2.1	Background History	5-6
5.2.2	Nondestructive Evaluation	5-6
5.2.3	Materials Characterization	5-14
5.2.4	Fractography	5-14
5.2.5	Stress Analysis	5-16
5.3	NASA HiMAT Wing	5-17
5.3.1	Background History	5-17
5.3.2	Nondestructive Evaluation	5-17
5.3.3	Materials Characterization	5-20
5.3.4	Fractography	5-24
5.3.5	Stress Analysis	5-24
5.4	Carbon Fiber Reinforced Plastic I-Beam	5-27
5.4.1	Background History	5-27
5.4.2	Nondestructive Evaluation	5-27
5.4.3	Materials Characterization	5-31
5.4.4	Fractography	5-32
5.4.5	Stress Analysis	5-32
6.0	ATLAS OF FRACTOGRAPHS	6-1
6.1	Interlaminar Mode I Tension	6-5
6.2	Interlaminar Mode II Shear	6-31
6.3	Interlaminar Mixed Mode Flexural	6-49

6.4	Translaminar Mode I Tension	6-54
6.5	Translaminar Mode I Compression	6-69
6.6	Translaminar Mode II Shear	6-91
6.7	Translaminar Flexure	6-102
6.8	Interlaminar Fatigue	6-104
6.9	Drill Backside Breakout	6-113
6.10	Compression After Impact (CAI)	6-116
6.11	Contaminants	6-118
6.12	Voids	6-121
6.13	Other Material Systems	6-123
6.13.1	Epoxy Resin Based Systems	6-123
6.13.2	Carbon Fiber Based Systems	6-123
7.0	REFERENCES	7-1
8.0	BIBLIOGRAPHY	8-1

LIST OF FIGURES

	Page
2-1	Simplified Investigative Framework 2-4
2-2	Detailed Investigative Framework 2-5
3-1	Simplified Investigative Framework 3-4
3-2	Material Verification Technique Sub-FALN 3-6
3-3	Failure Analysis Techniques for Materials Characterization 3-7
3-4	Cross-section of a Laminate With Easily Differentiated Ply Separation 3-12
3-5	Identification of Ply Orientation by Fiber End Shape and Ovality 3-13
3-6	Polished Cross-Section at 45 -deg Angle Through the Thickness of the Part 3-15
3-7	A Radiograph in Which the Tracer Yarns are Evident for Determination of the Ply Orientation in a Thin Laminate 3-17
3-8	HPLC Test Setup Schematic and Typical Instrument Parameters 3-21
3-9	LC Chromatogram of Narmco Resin Matrix Showing Major Peak Assignment 3-22
3-10	Standard IR Spectrum of a Commercial Epoxy Resin Formulation 3-24
3-11	Cross-Sectional Diagram of the DSC Cell Used by Du Pont DSC Module 3-25
3-12	DSC Thermogram for 3501-6 Resin 3-27
3-13	Sample Fingerprinting of Various Systems by Way of X-ray Fluorescence 3-28
3-14	Pyrolysis Gas Chromatography (PGC) of Two Difficult Resin Systems 3-30
3-15	Gas Chromatography of DDS, Diaminodiphenyl Sulfone 3-32
3-16	IR Comparison of Resin 3-33
3-17	Drifts of Graphite/Epoxy (AS/3501-5) Composite Before and After Thermal Aging 3-34
3-18	Glass Transition Temperature Determination - TMA Penetration Test Setup 3-37
3-19	Glass Transition Temperature Determination - TMA Penetration Test Measurement 3-37
3-20	Glass Transition Temperature Determination - TMA Flexure Test Setup 3-38

3-21	Glass Transition Temperature Determination - TMA Flexure Test Measurement	3-38
3-22	Determination of Tg by Expansion Method	3-39
3-23	Typical DMA Plot for Cured Epoxy Showing Glass Transition Determination	
3-24	A Typical DMA Plot for Cured Epoxy Illustrating Determination of the Tg and Heat of Additional Reaction	3-40
3-25	DMA Loss Modulus Versus Temperature Showing Effect of Undercure for Epoxy Resin	3-41
3-26	SEM Micrograph of a Teflon Contaminated Tension Specimen	3-43
3-27	SEM Micrograph of a Frekote Release Agent Contaminated Tension Specimen (200X)	3-47
3-28	SEM Micrograph of a Frekote Release Agent Contaminated Tension Specimen (2000X)	3-48
3-29	SEM Micrographs of a Typical Uncontaminated Fracture Specimen	3-49
3-30	SEM Micrographs of Foreign Particle Inclusions Illustrating the Characteristic Fracture Surface Asperity and Radiating Fracture Lines	3-50
3-31	Flow Diagram for the Initial Inspection and Determination of a Foreign Material Contamination	3-52
3-32	Logic Network for Chemical Analysis of Foreign Material Contamination of a Composite Fracture Surface	3-53
3-33	X-ray Emission Lines, Partial Listing	3-55
3-34	Talc Powder Contamination Along a Bond line	3-55
3-35	Approximate XPS Peak Positions and Emission Probabilities for Common Elements	3-57
3-36	A Typical XPS Spectrum of an Epoxy Resin with Elements Identified	3-57
3-37	Carbon Peak Shifts in XPS	3-59
3-38	Rules of Thumb for XPS Identification of Typical Release Agents	3-59
3-39	Partial List of Possible Contamination Sources	3-60
3-40	Infrared Spectrum of an Epoxy Resin	3-61

3-41	AES Spectra of (a) Carbon Fiber and (b) An Exposed Carbon Fiber on a Tensile Fracture	3-65
3-42	Optical Micrograph in Cross Section of a Laminate Skin to Core Buckling Separation	3-66
3-43	SEM Micrographs Showing a Replicated Surface Morphology	3-66
3-44	XPS Spectra of the Disbonded FM-300 Ply Surfaces	3-68
3-45	XPS Spectra of FM-300 Ply Surfaces Separated by Hand in the Laboratory	3-69
3-46	Nondestructive Evaluation Sub-FALN	3-71
3-47a	Failure Analysis Techniques - Nondestructive Evaluation	3-72
3-47b	Method Selection (Listed in Order of Preference)	3-73
3-48	Example of an Ultrasonic Through-Transmission C-Scan	3-78
3-49	Pulse-Echo Ultrasonic C-Scan Using Time Domain Gating Zones to Identify Damage States of Impact	3-81
3-50	Delamination Identified by a Family of Pulse-Echo Ultrasonic A-Scans	3-82
3-51	Pulse-Echo Ultrasonic B-Scan of Delaminated Region	3-83
3-52	Ultrasonic Detection of Simulated Crack in Laminate Plate	3-83
3-53	Penetrant-Enhanced X-Ray Image of Edge Delamination	3-86
3-54	Subsurface Fracture Evaluation	3-89
3-55	Fractography Diagnostic Technique Sub-FALN	3-93
3-56	Failure Analysis Techniques - Fractography	3-94
3-57	Failure Analysis Techniques - Fracture Surface Material and Chemical Characterization	3-95
3-58	Basic Features of the SEM	3-108
3-59	The SEM Beam-Specimen Interaction Details	3-109
3-60	Contrasting Differences in SEM Photomicrographs	3-111
3-61	SEM Photomicrographs of Effect of Tilt on Striation Resolution	3-113
3-62	SEM Fractographs of Mode II Delamination Between Adjacent 0-deg Plies Illustrating the Effect of Tilt Angle	3-114
3-63	The Two-Stage TEM Replication Technique	3-117

3-64	Basic Features of the Transmission Electron Microscope (TEM)	3-118
3-65	High Magnification TEM Photomicrographs Showing Fatigue Striations	3-120
3-66	TEM Photomicrograph of Striation Features from a Crack Lap Shear (CLS) Specimen	3-121
3-67	Stress Analysis Methods	3-124
3-68	Stress Analysis Sub-FALN	3-127
3-69	Computer Analysis Programs	3-129
3-70	Maximum Stress Failure Theory	3-133
3-71	Tsai-Hill Theory	3-134
3-72	Tsai-Wu Tensor Theory	3-136
3-73	Comparison of Calculated Inplane Tensile Strength with Experiment	3-138
3-74	Quadratic Interaction First Ply Failure Envelope for T300/5208	3-139
3-75	Stress Gradients Resulting From Edge Effects	3-141
3-76	Through-Thickness Tensor Polynomial Distributions for Curing Stresses and Stresses at the First Failure (+/-) Laminates	3-142
3-77	Tensor Polynomial Distributions Along the Interface of (+/-) Laminates	3-144
3-78	Comparison of Experimentally Derived <i>In Situ</i> Lamina Elastic Strains at Onset of Matrix Cracking to 2D Shear Lag Model Predictions for (0/90) T300/934 Laminate Family	3-146
3-79	Fracture Toughness of Various Orientations	3-148
3-80	Strength Reduction of Uniaxially Loaded Plate with Circular Hole, According to Average Stress Criterion	3-149
3-81	Strength Reduction of Uniaxial Loaded Hole According to Point Failure Stress Criteria	3-149
3-82	Strength Reductions as a Function of the Hole Radius for (0/+45/-45/90 deg) Graphite-Epoxy Plates with Circular Holes Under Uniaxial Tensile Loading	3-150
3-83	Hole Geometries Analyzed With the Damage Zone Model (DZM)	3-151

3-84	Effect of Impact Damage on the Compressive Strength of a Quasi-Isotropic Laminate	3-152
3-85	Design Details That Cause Interlaminar Stress Concentrations	3-153
3-86	End Notched Flexure (ENF) and Double-Cantilever Beam (DCB) Specimens	3-154
3-87	Modes of Crack Propagation	3-155
3-88	Mixed Modes I and II Delamination Specimens	3-155
3-89	Crack Tip Loading Mechanisms Causing Interlaminar Normal and Shear Stress Concentrations	3-157
3-90	G_{IC} and G_{IIC} Values Obtained from DCB and ENF Testing Reported in Literature	3-157
3-91	Fatigue Crack Growth of AS-1/3501-6	3-158
3-92	Mode II Fatigue	3-159
3-93	Manufacturing Defects Chart	3-161
4-1	Laminate Flexure Specimens	4-3
4-2	Tensile and Compression Translaminar Fractures	4-4
4-3	The Basic Fracture Modes	4-6
4-4	Visual Microscopic Fracture Surface Features	4-7
4-5	V-22 Osprey Wing Box Failure	4-8
4-6	Basic Modes of Loading Involving Different Crack Types and Surface Displacements (Interlaminar and Translaminar)	4-10
4-7	Fracture Surface of 4340M Steel Illustrating Cleavage Fracture Features Indicative of Crack Growth Direction	4-10
4-8	Fracture of Unreinforced Neat Epoxy Resin	4-11
4-9	Mode I Tension Fracture	4-13
4-10	Beach Marks Found in a Delamination Surface Indicative of Crack Front Shape and Growth Direction During Fracture	4-14
4-11	Optical Photomicrographs Intended Fracture Plane Between 0/0 deg Plies, DCB 21°C (70°F) Specimen	4-14
4-12	SEM Fractographs of Mode I Delaminations Between 0/0 -deg Plies	4-16

4-13	Photomicrograph Illustrating Adhesive Fracture Areas of Textured Microflow	4-17
4-14	TEM Image of Resin Microplane with River Marks and Resin Microflow	4-17
4-15	SEM Photomicrographs of Mode I Delamination Between 0/90-deg Plies	4-19
4-16	SEM Photomicrographs of Mode I Delamination Between 0/+45-deg Plies	4-20
4-17	SEM Fractographs of Mode I Delamination Between +45/+45-deg Plies	4-21
4-18	Optical Photomicrographs of Intended Fracture Plane Between 0/0-deg Plies, ENF 21°C (70°F) Specimen	4-22
4-19	SEM Photomicrographs of Mode II Delamination Between 0/0-deg Plies	4-23
4-20	Free Body Diagram of Resolved Tensile Stresses and Inclined Microcracks	4-24
4-21	Microstructure of Cracks Found in Short Beam Shear Specimen Tested at 132°C (270°F)	4-24
4-22	Scalloped Resin Fracture Areas and Their Development	4-25
4-23	Possible Hackle Separation Mechanisms	4-26
4-24	Orthogonally Shaped Symmetrical Hackles	4-27
4-25	Triangular Asymmetric Hackles, with River Marks and Fiber-Matrix Separation	4-27
4-26	Interlaminar Mixed Mode (Tension and Shear) Fracture Morphology	4-29
4-27	Interlaminar Mixed Mode Flexural (MMF) (Tension and Shear) Specimen Fracture Morphology	4-29
4-28	Macroscopic View of a Translaminar Tension Fracture From a Unidirectional Laminate	4-31
4-29	Translaminar Fracture Morphology	4-32
4-30	Typical Tensile Fiber Fracture Characteristics	4-32
4-31	SEM Photomicrograph Showing Direction of Crack Propagation	4-33

4-32	Compression Buckling Failure Damage of Stringer Stiffened Laminate	4-35
4-33	End-View of Translaminar Compression Fracture	4-36
4-34	SEM Micrograph of Compression-Generated Fracture Surface Showing Severe Fracture Surface Damage	4-36
4-35	Cross-Section of Compressively Loaded Laminate with Microbuckling or Kinking of the Fiber Bundles Oriented Parallel to the Axial Compressive Load	4-37
4-36	Typical Flexural Fracture Morphology Found on the Fiber Ends from a Compression Failure	4-38
4-37	Fiber End Fracture Morphology from Compression Buckling Failure	4-40
4-38	Slant or Shear-Type Fracture from Compression-Induced Translaminar Failure	4-40
4-39	SEM Photomicrographic Montage Showing Crack Propagation Direction Mapping	4-43
4-40	Damage Defect Checklist	4-45
4-41	SEM Micrographs of Translaminar Fracture Conditions at Different Temperatures	4-47
4-42	Low Magnification Series of Characteristic 0/0 -deg Interface Mode I Fractures at Each Environmental Condition	4-48
4-43	High Magnification SEM Series of 0/0 -deg Interface Mode II (Shear) Fractures Showing Features of Fiber-Matrix Separation	4-49
5-1	737-300 Elevator Static Test Evaluation	5-2
5-2	737-300 Elevator Static Test Fracture Directions	5-5
5-3	Central Portion of J VX V-22 Central Wing Test Box	5-7
5-4a	J VX Wing Test Box Upper Skin Surface	5-8
5-4b	J VX Wing Test Box Inner Side of Upper Skin	5-10
5-5	J VX Wing Test Box Front and Rear Spars	5-11
5-6	J VX Wing Test Box Lower Skin Surface	5-12
5-7	Ultrasonic C-Scan of Upper Skin Surface	5-13
5-8	J VX Wing Test Box Crack Mapping Results	5-15
5-9	NASA HiMAT Test Wing in the As-Received Condition	5-18

5-10	Upper Skin Inboard Edge Damage	5-19
5-11	NDE Results of the Lower Surface	5-20
5-12	NDE Results of the Upper Surface	5-21
5-13	Fiber Identification by Surface Analysis	5-22
5-14	Photomicrograph of Cross-Section Damage Zone B	5-23
5-15	Cross-Section Illustrating Boron Fiber Misalignment Resulting in Resin-Rich Adjacent Regions	5-23
5-16	Photomicrograph of Beach Marks Indicative of Cyclic Crack Growth and Crack Propagation Direction	5-25
5-17	Fractography Results from NASA HiMAT Wing	5-25
5-18	Crack Mapping Results from Selected Delamination Regions	5-26
5-19	CFRP I-Beam in the As-Received Condition	5-27
5-20	Regions of (a) Compression Buckling and (b) Delamination in the Upper Cap Section of the I-Beam	5-28
5-21	Regions of (a) Compression Buckling and (b) Delamination in the Upper Cap Section of the I-Beam	5-29
5-22	TTU C-Scans of the I-Beam Subcomponents	5-30
5-23	Extensive Porosity and Laminate Deformity in the Web-to-Cap Junction	5-31
5-24	Results of Fractographic Crack Mapping of an Upper Cap Delamination	5-32
6-1	Singular and Multiple-Failure-Condition Test Specimen Matrix (Page 1 of 3)	6-2
6-1	Singular and Multiple-Failure-Condition Test Specimen Matrix (Page 2 of 3)	6-3
6-1	Singular and Multiple-Failure-Condition Test Specimen Matrix (Page 3 of 3)	6-4
6-2	Double Cantilever Beam (DCB) Test Type	6-5
6-3	Overall Crack Growth Direction by Resin Regions Between Fibers	6-6
6-4	Crack Growth Direction by Resin Microflow	6-6
6-5	24-Ply Layup, 0 Plies	6-7

6-6	Fiber Matrix Separation, Fracture, and River Markings	6-8
6-7	-65°F Dry, 70°F Dry, and 270°F Dry Conditions (Optical)	6-9
6-8	70°F Wet Condition (Optical)	6-10
6-9	-65°F Dry and 70°F Dry, and 270°F Dry Conditions (SEM 200X)	6-11
6-10	-65°F Dry and 70°F Dry Conditions (SEM)	6-12
6-11	70°F Wet and 180°F Wet Conditions	6-13
6-12	-65°F Dry, 70°F Dry, and 270°F Dry Conditions (SEM 50X)	6-14
6-13	70°F Wet, 180°F Dry, and 180°F Wet Conditions, With Fiber Separation and River Marks	6-15
6-14	+45/-45 Plies (Optical)	6-16
6-15	+45/-45 Plies with Matrix Fracture, Fiber Separation, River Marks, and Textured Microflow	6-17
6-16	-65°F Dry, 70°F Dry, and 270°F Dry Conditions (Optical 400X)	6-18
6-17	+45/-45 Plies at 70°F Wet Conditions (Optical 400X)	6-19
6-18	+45/-45 Plies at -65°F Dry, 70°F Dry, and 270°F Dry Conditions (Optical 50X)	6-20
6-19	+45/-45 Plies at -65°F Dry, 70°F Dry, and 270°F Dry Conditions (SEM 200X)	6-21
6-20	+45/-45 Plies at 70°F Wet and 180°F Wet Conditions (SEM 400X)	6-22
6-21	0/45 Plies at 21°C Dry (Optical 400X)	6-23
6-22	0/45 Plies with Matrix Fracture, Fiber Separation, River Marks, and Textured Microflow	6-24
6-23	0/+45 Plies at -65°F Dry, 70°F Dry, and 270°F Dry Conditions (Optical 400X)	6-25
6-24	0/90 Plies at 21°C Dry Condition (Optical 100X and 400X)	6-26
6-25	0/90 Plies With Matrix Fracture, Fiber Separation, River Marks, and Textured Microflow	6-27
6-26	0/90 Plies at -65°F Dry and 70°F Dry Conditions (Optical 400X)	6-28
6-27	90/90 Plies at 21°C Dry Condition (Optical 100X and 400X)	6-29
6-28	0/90 Plies at 21°C Dry Condition With Matrix Fracture, Fiber Separation, and River Marks	6-30

6-29	End Notch Flexural (ENF) Test Type	6-31
6-30	0/0 Plies at 21°C Dry Condition (Optical 100X and 400X)	6-32
6-31	0/0 Plies at 21°C Dry Condition with Fiber Separation, River Marks, Hackles, and Textured Microflow	6-33
6-32	0/0 Plies at 70°F Wet, 180°F Dry, and 180°F Wet Conditions (Optical 400X)	6-34
6-33	0/0 Plies at -65°F Dry, 70°F Dry, and 270°F Dry Conditions (Optical 400X)	6-35
6-34	0/0 Plies at -65°F Dry, 70°F Dry, and 270°F Dry Conditions (SEM 400X)	6-36
6-35	0/0 Plies at 70°F Wet and 180°F Wet Conditions With Fiber Separation and Hackles	6-37
6-36	0/0 Plies at -65°F Dry, 70°F Dry, and 270°F Dry Conditions with Fiber Separation and Hackles	6-38
6-37	+45/-45 Plies at 21°C Dry Condition (Optical 100X and 400X)	6-39
6-38	+45/-45 Plies at 21°C Dry Condition with Fiber Separation River Marks and Hackles	6-40
6-39	+45/-45 Plies at -65°F Dry, 70°F Dry, and 270°F Dry Conditions (Optical 400X)	6-41
6-40	+45/-45 Plies at -65°F Dry, 70°F Dry, and 270°F Dry Conditions (SEM 400X)	6-42
6-41	+45/-45 Plies at -65°F Dry, 70°F Dry, and 270°F Dry Conditions (SEM 2000X)	6-43
6-42	0/45 Plies at 21°C Dry Condition (Optical 100X and 400X)	6-44
6-43	0/45 Plies With Fiber Separation, River Marks, Hackles, and Textured Microflow	6-45
6-44	0/90 Plies at 21°C Dry Condition (Optical 100X and 400X)	6-46
6-45	90/90 Plies at 21°C Dry Condition (Optical 100X and 400X)	6-47
6-46	90/90 Plies at 21°C Dry Condition With Fiber Separation, River Marks, and Hackles	6-48
6-47	Mixed Mode Flexural Test Type	6-49
6-48	0/0 Plies at 21°C Dry Condition (SEM 2000X)	6-50

6-49	0/90 Plies at 21°C Dry Condition (SEM 2000X)	6-51
6-50	+45/-45 Plies at 21°C Dry Condition (SEM 2000X)	6-52
6-51	0/45 Plies at 21°C Dry Condition (SEM 1900X and 2000X)	6-53
6-52	Four-Point Bend Test Type (Tension)	6-55
6-53	Fracture of Adjacent Files	6-55
6-54	0/90 Plies at -65°F Dry, 180°F Dry, and 270°F Dry Conditions (SEM Low Magnification)	6-56
6-55	+45/-45 Plies at 70°F Wet, 180°F Wet, and 270°F Wet Conditions (SEM 50X)	6-57
6-56	0/90 Plies at 82°C Dry Condition (Various SEM Magnifications)	6-58
6-57	0/90 Plies at -65°F Dry, 180°F Dry, and 270°F Dry Conditions (SEM)	6-59
6-58	0/90 Plies at 70°F Wet, 180°F Wet, and 270°F Wet Conditions (SEM 50X)	6-60
6-59	0/90 Plies at 70°F Wet, 180°F Wet, and 270°F Wet Conditions (SEM 2000X)	6-61
6-60	0/45/90 Plies at -65°F Dry, 180°F Dry, and 270°F Dry Conditions (SEM 50X)	6-62
6-61	0/45/90 Plies at -65°F Dry, 180°F Dry, and 270°F Dry Conditions (SEM 2000X)	6-63
6-62	0/45/90 Plies at -70°F Wet, 180°F Wet, and 270°F Wet Conditions (SEM 50X)	6-64
6-63	0/45/90 Plies at 70°F Wet, 180°F Wet and 270°F Wet Conditions (SEM 2000X)	6-65
6-64	+45/-45 Plies at -65°F Dry, 180°F Dry, and 270°F Dry Conditions (Fiber Pullout)	6-66
6-65	+45/-45 Plies at -65°F Dry, 180°F Dry, and 270°F Dry Conditions (Fiber Breakage)	6-67
6-66	+45/-45 Plies at 70°F Wet, 180°F Wet, and 270°F Wet Conditions (SEM 2000X)	6-68
6-67	Four-Point Bend Test Type (Compression)	6-69
6-68	Translaminar Compression Fractures	6-70

6-69	0(32) Ply at 21°C Dry Condition (SEM 50X, 400X, and 2000X)	6-71
6-70	0(32) Ply at -65°F Dry, 180°F Dry, 270°F Dry Conditions (SEM Low Magnification)	6-72
6-71	0(32) Ply at -65°F Dry, 180°F Dry, 270°F Dry Conditions (SEM 400X)	6-73
6-72	0(32) Ply at 70°F Wet, 180°F Wet, and 270°F Wet Conditions (SEM 20X)	6-74
6-73	0(32) Ply at 70°F Wet, 180°F Wet, and 270°F Wet Conditions (SEM 400X)	6-75
6-74	0/90 Plies at 21°C Dry Conditions (SEM 50X, 400X, and 2000X)	6-76
6-75	0/90 Plies at -65°F Dry, 180°F Dry, and 270°F Dry Conditions (SEM 20X)	6-77
6-76	0/90 Plies at -65°F Dry, 180°F Dry, and 270°F Dry Conditions (SEM 400X)	6-78
6-77	0/90 Plies at 70°F Wet, 180°F Wet, and 270°F Wet Conditions (SEM 20X)	6-79
6-78	0/90 Plies at 70°F Wet, 180°F Wet, and 270°F Wet Conditions (SEM 400X)	6-80
6-79	0/45/90 Plies at 21°C Condition (SEM 50X, 400X, and 2000X)	6-81
6-80	0/45/90 Plies at -65°F Dry, 180°F Dry, and 270°F Dry Conditions (SEM 20X)	6-82
6-81	0/45/90 Plies at 70°F Wet, 180°F Wet, and 270°F Wet Conditions (SEM 400X)	6-83
6-82	0/45/90 Plies at 70°F Wet, 180°F Wet, and 270°F Wet Conditions (SEM 20X)	6-84
6-83	+45/-45 Plies at 21°C Dry Condition (SEM 50X, 400X, and 2000X)	6-85
6-84	+45/-45 Plies at -65°F dry, 180°F Dry, and 270°F Dry Conditions (SEM 20X)	6-86
6-85	0/45/90 Plies at -65°F Dry, 180°F Dry, and 270°F Dry Conditions (SEM 400X)	6-87
6-86	+45/-45 Plies at -65°F Dry, 80°F Dry, and 270°F Dry Conditions (SEM 400X)	6-88
6-87	+45/-45 Plies at 70°F Wet, 180°F Wet, and 270°F Wet Conditions (SEM 20X)	6-89

6-88	+45/-45 Plies at 70°F Wet, 180°F Wet, and 270°F Wet Conditions (SEM 400X)	6-90
6-89	Side-Notched Rail Shear Test Type	6-91
6-90	0/90 Plies at 21°C Dry (SEM 200X and 2000X)	6-92
6-91	0/90 Plies at -65°F Dry, 180°F Dry, and 270°F Dry Conditions (SEM 400X)	6-93
6-92	0/90 Plies at 65°F Dry, 180°F Dry, and 270°F Dry Conditions (SEM 2000X)	6-94
6-93	0/90 Plies at 70°F Wet, 180°F Wet, and 270°F Wet Conditions (SEM 400X)	6-95
6-94	0/90 Plies at 70°F Wet, 180°F Wet, and 270°F Wet Conditions (SEM 2000X)	6-96
6-95	0/45/90 Plies at 21°C Dry (SEM 200X and 2000X)	6-97
6-96	0/45/90 Plies at -65°F Dry, 180°F Dry, and 270°F Dry Conditions (SEM 400X)	6-98
6-97	0/45/90 Plies at -65°F Dry, 180°F Dry, and 270°F Dry Conditions (SEM 2000X)	6-99
6-98	0/45/90 Plies at 70°F Wet, 180°F Wet, and 270°F Wet Conditions (SEM 400X)	6-100
6-99	0/45/90 Plies at 70°F Wet, 180°F Wet, and 270°F Wet Conditions (SEM 2000X)	6-101
6-100	Laminate Flexure Test Type	6-102
6-101	0(32) Plies at 21°C Dry (SEM 20X, 800X, and 2000X)	6-103
6-102	Double Cantilever Beam (DCB) for Mode I Fractures and Crack Lap Shear (CLS) for Mode II Fractures	6-105
6-103	0/0 Plies at 70°F Dry Condition (Fatigue DCB Mode I, Optical)	6-106
6-104	0/0 Plies at 70°F Dry Condition (Fatigue CLS Mode II, Optical)	6-107
6-105	0/0 Plies at 21°C Dry Condition (Fatigue DCB Mode I, Optical)	6-108
6-106	0/0 Plies at 21°C Dry Condition (Fatigue DCB Mode I, SEM)	6-109
6-107	0/0 Plies at 21°C Dry Condition (Fatigue CLS Mode II, Optical)	6-110

6-108	0/0 Plies at 21°C Dry Condition (Fatigue CLS Mode II, 40-80% Static)	6-111
6-109	0/0 Plies at 21°C Dry Condition (Fatigue CLS Mode II, 20 to 60% Static)	6-112
6-110	Drill Breakout Specimen	6-113
6-111	0/0 Plies at 21°C Dry Condition (Example A)	6-114
6-112	0/0 Plies at 21°C Dry Condition (Example B)	6-115
6-113	0/45/90 Plies, Dry Condition (Compression After Impact)	6-117
6-114	Teflon Contamination	6-119
6-115	Frekote Contamination	6-120
6-116	Voids, DCB and ENF	6-122
6-117	Fiberglass/Epoxy 250°F Cure	6-125
6-118	Fiberglass/Epoxy 350°F Cure	6-126
6-119	Aramid Fibers/Epoxy	6-127
6-120	PEEK/AS4 Fibers	6-128
6-121	PMR-15/Celion-3000	6-129

1.0 INTRODUCTION AND PURPOSE

As a result of their tailorability, high strength, and modulus to density ratios, high performance continuous fiber reinforced composites are being selected in rapidly increasing amounts as structures in the design of each successive military and civilian aircraft. These materials are also seeing increased application in land, sea and space transportation vehicles, as well as less glamorous applications such as mass-produced items for the sport industry. In aerospace applications, where the demands upon materials are the greatest, composites are efficiently meeting the weight, strength, stiffness, fatigue, and corrosion resistance requirements.

This increased usage, combined with design applications progressing toward increased operational strains, will undoubtedly result in more frequent occurrences in part failure. When such a failure occurs, the ability to determine the origin, cause, and sequence of failure constitutes a critical step necessary in providing valuable engineering feedback which will assure the continued integrity of the components during service. These critical steps are necessary so that appropriate corrective actions can be made which are effective as well as rationally based.

In the case of metallic structures, the analytical techniques required to analyze the failed part and determine the cause of failure has been fairly well established since the mid-1950's. Analyses of fractures has been influential in the selection of materials, and the identification of critical design details, processes and operating conditions which must be controlled to prevent failures. This necessary technology, however, should be defined as in its infancy for post-failure analysis of composite structures. Many individuals within the past ten years have applied selected analysis techniques and procedures toward developing portions of the overall capability required for comprehensive failure analysis. The U. S. Air Force, aware of the need for this comprehensive capability which combines the analytical tools with the approach and interpretive skills, awarded The Boeing Company this contract to identify, study, and document these areas for composite failure analysis. This document is a final product of the C-5010 program, #F33615-84-C-5010, "Failure Analysis For Composite Structure Materials" (ref. 1).

The intent of this Compendium is to provide an organized and easily accessible source of information and guidance upon which a composite material structure failure analysis may be performed. The Compendium is organized as follows: (1) a working document of value to the investigator during a failure analysis, (2) a reference document to which one can refer to clarify a point in question or to research a specific new observation, and (3) a teaching document from which a new investigator can learn the essentials necessary to do an analysis and from which a "rusty" investigator can brush up on a specific area.

This document is divided into three major groupings:

- Failure analysis logic networks (FALN), which identify a logical approach toward composite failure analysis investigations are presented in Section 2.0.
- The techniques and analytical procedures used to gather information as well as the interpretation of the results obtained, are presented in Sections 3.0 and 4.0.
- Supportive data such as case histories of actual failure analyses and an extensive atlas of fractographs, to provide a comparative reference source, are presented in Sections 5.0 and 6.0.

2.0 FAILURE ANALYSIS LOGIC NETWORKS (FALN)

2.1 GENERAL CONCEPTS

This section reviews the failure analysis logic network (FALN) flow charts and supporting data tables developed to provide investigators with guidelines delineating a logical sequence of investigative operations. These flow charts are designed to identify the analytical tools necessary for composite failure analysis. The charts, when combined with decision gates, allow an accurate, cost effective, and timely determination of the cause of component failure. Such guidelines have not been available previously due to the relative complexity of composite materials and their fairly recent use in industry, particularly for primary structures. In developing these guidelines, specific objectives were incorporated to provide investigators with a logical sequence that:

- Considers a variety of potential causes including design or fabrication errors, anomalies, and in-service or testing damage.
- Incorporates multiple analytical disciplines, such as nondestructive testing, materials characterization, fractography, and stress analysis.
- Avoids the premature destruction of evidence.
- Builds on gathered information and allows for redirected investigations.

In addition to the general FALN, several specific FALNs are provided for the areas of nondestructive testing, materials characterization, fractography and stress analysis. Both types of FALNs are described in the following paragraphs.

2.2 MAJOR FAILURE ANALYSIS LOGIC NETWORKS (FALN)

Identifying the logical sequence of steps for doing a post-failure analysis is often a complex and difficult process. Sufficient information must be gathered and evaluated so that the cause of fracture may be determined from positive supportive evidence rather than simply by a process of elimination. In many instances, the development of a coherent

set of positive evidence is often complex since: (1) numerous potential cause(s) exist and (2) multiple contributory factors may be involved. In order to accurately identify the cause of fracture, each of these potential contributory factors must be taken into consideration. Identifying the cause of fracture and related contributory factors without examining each and every conceivable cause requires an organized investigation sequence. Developing this plan of attack is further complicated by the fact that many investigative steps may be destructive to remaining evidence, and thus preclude further critical analysis. Consequently, adequate documentation to record existing evidence, as well as the logical flow of information from one analysis to another must be considered.

In order to assist investigators in developing a logical plan of attack, an organizational framework was developed. This framework is based upon well established procedures utilized in the failure analysis of metallic structures, modified to meet the specific analytical requirements for fiber reinforced composite structures. This framework considers each major failure category, potential interrelationships, and the prevention of premature destruction of evidence. Because composite materials differ in many respects from metals, the specific operations involved were modified to address those characteristics specific to composites. This proven framework consists of five basic investigative operations arranged around intermediate decision points. The approach is aimed at simplifying and streamlining the number and complexity of analysis steps involved, usually lowering the overall costs of investigations. The five major investigative operations are:

- Collection and review of background history and information.
- Nondestructive inspection.
- Evaluation of the part conformity to specified requirements.
- Detailed fractographic examinations.
- Stress analysis.

An overall diagram, showing the simplified application sequence of these five operations is illustrated in Figure 2-1. The sequence initially encourages the use of simple, inexpensive examinations, followed by progressively more detailed analyses. Through comprehensive hands-on application and evaluations, a significant amount of detail has been added to the original investigative framework. The expanded version, shown in Figure 2-2, establishes a more detailed and accurate path for investigators. It delineates most of the widely used techniques that may be used and the required decisions involved in carrying out a postmortem analysis.

During the initial stages of investigation, background information on material, fabrication, design, loads, environment, and service or test history is collected and reviewed with the intention of identifying areas of concern. This process helps develop a familiarity with the component, its operation, and its service environment. Nondestructive inspections are then performed to identify and further delineate the extent and nature of nonvisible fracture or damage. The data is documented for later reference. This operation establishes the groundwork to plan more detailed examinations and helps in selection of specimens that may require destructive sectioning. After nondestructive examination, the part is evaluated for conformity with engineering, material, and process specifications. Each initial examination is directed toward identifying items of significance early in the investigation. Through an iterative process, the number of steps can be minimized and future efforts concentrated on items of interest.

Detailed fractographic and stress examinations are the next analytical steps. These operations identify more specific details and assess their significance. Typically, fractographic examinations are used principally to identify the origin and load conditions involved in failure. In many cases, the main benefit of fracture examination is the identification of material defects or anomalies. As such factors are identified, sufficient information may be developed to identify either a specific cause for failure or a point of interest (that is, an origin) for further analyses. After inputs from fractographic analysis have been developed, stress may be performed to evaluate stress states, out-of-compliance conditions, or the critical nature of identified defects. In cases where questions may remain, additional specialized tests or further more detailed stress analyses may be required from the stress specialist to model previously indeterminate conditions.

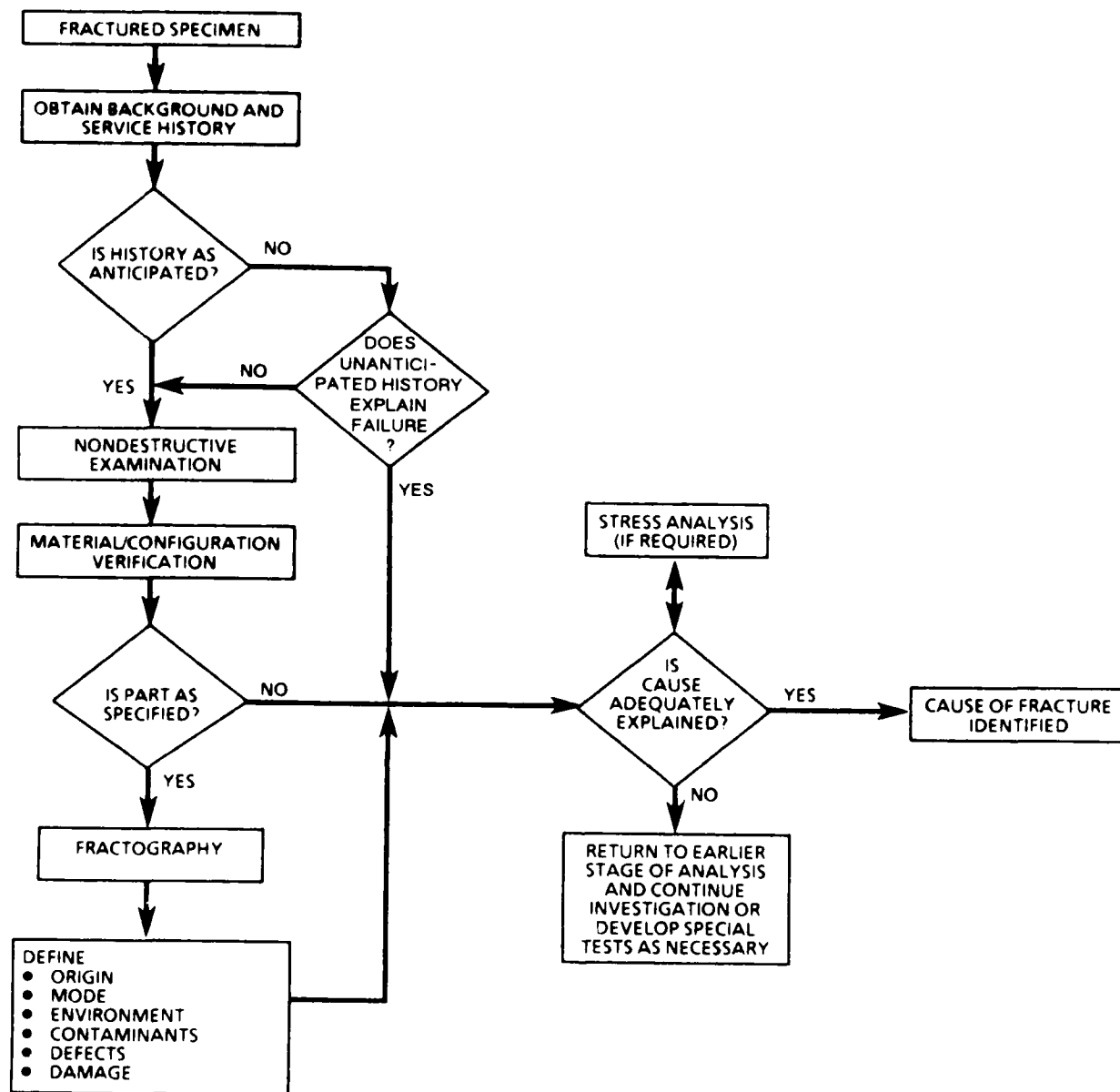


Figure 2-1. Simplified Investigative Framework

5-B70227R1-57

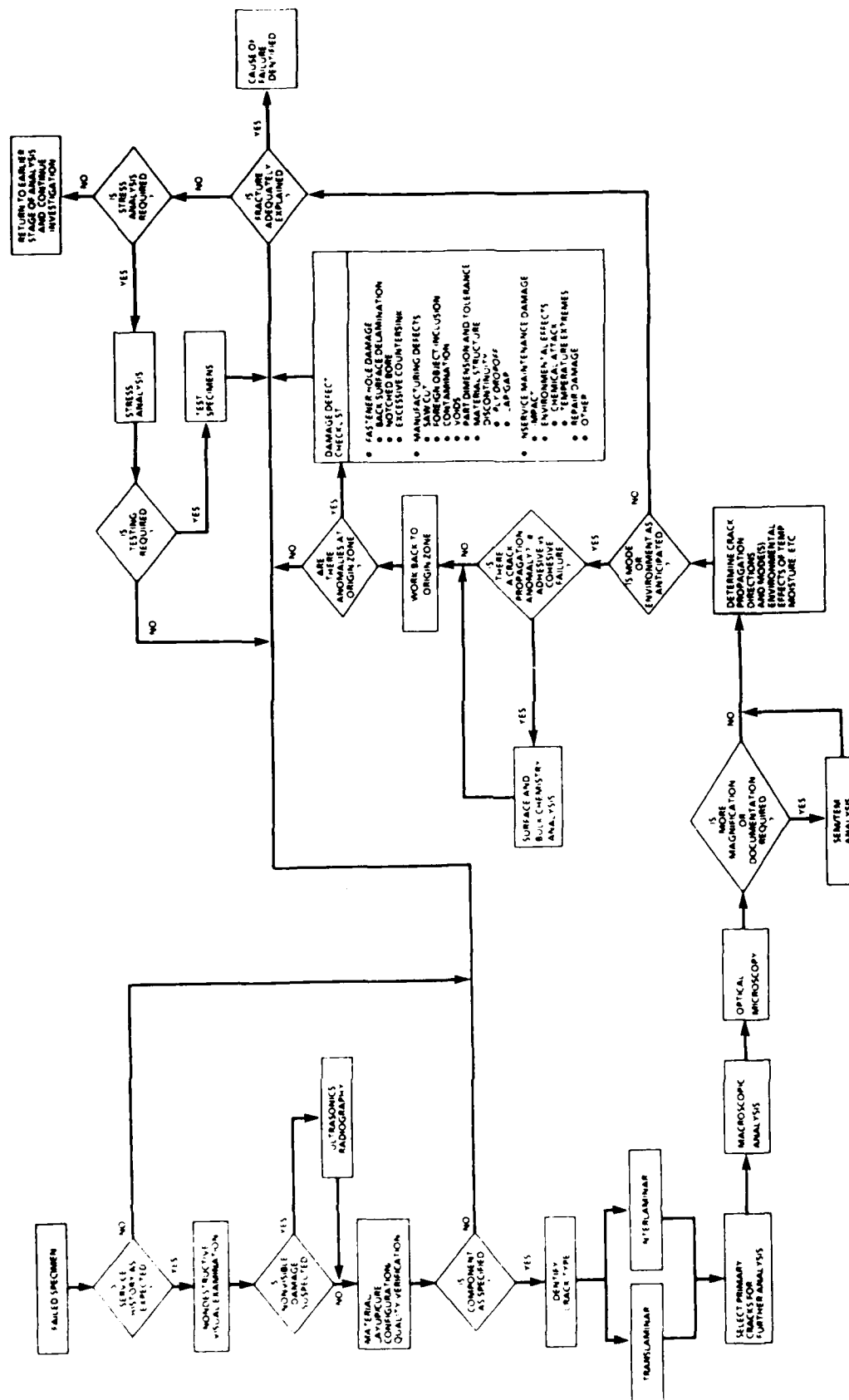


Figure 2-2. Detailed Investigative Framework

3.0 PROCEDURES FOR USE IN FAILURE ANALYSIS

In general, the procedures utilized in the failure analysis of composites are similar to those used for other materials systems. As with any thorough analysis, the investigation should follow a basic sequence which at least includes the following procedures: (1) a review of available inservice or test procedure records, (2) a preliminary nondestructive examination of the extent of damage on the part, (3) verification of use of the correct material in the specified condition, and (4) the fractographic determination of the origin and mode of fracture. In many cases, much more detailed and labor intensive analyses are required, including the evaluation of the stress and fracture mechanics involved in failure so as to adequately determine the sequence and cause of failure.

The specific sequences, or Failure Analysis Logic Networks (FALN), through which these analytical techniques can be applied, were presented in section 2.0.

Many of the analytical procedures presented in this section have been previously developed for metals failure analysis and modified to meet the needs of composite post-mortem analysis. Each technique has been developed, evaluated and verified by the scientific community through strict laboratory analysis and directly applied during composite failure analysis investigations. These state-of-the-art analytical tools and the specific procedures for use in failure analysis are discussed in the following sequence:

- Materials Characterization, paragraph 3.1
- Nondestructive Evaluation, paragraph 3.2
- Fractography, paragraph 3.3
- Stress Analysis, paragraph 3.4

Each of these major topics discuss techniques, procedures, and explain:

- The principles underlying the technique.

- How the technique or procedure is used and applied to analyze a composite material structure.
- How to interpret the data/information obtained.
- How different circumstances affect the data type and its interpretation.
- Alternative approaches or complementary tests to verify accuracy of results.
- Comparisons and effective value between various available techniques.

3.1 MATERIALS CHARACTERIZATION

Errors in material layup, ply orientation, microconstituent chemical formulation, processing and the degree of matrix curing can lead, or contribute, to premature component failures. As a result, the analysis of these basic material and processing errors should be considered a standard operation in most analysis investigations. This paragraph presents the standard techniques currently available for characterizing the material integrity and identifying anomalous conditions, if any, that may have caused or contributed to component failure. These techniques are presented for evaluation and testing of carbon fiber/epoxy resin systems.

In this paragraph, the principal selected topics include the following:

- Material layup analysis - verification of the number, orientation, and sequence of plies in the laminate.
- Determination of fiber, matrix, and void volume fractions.
- Material identification - verify and fingerprint the material chemical composition for both cured laminate and uncured prepreg.
- Degree of cure analysis - determination of glass transition temperature (T_g) and extent of reaction during the cure process.

- Contamination analysis - surface chemical analysis and foreign inclusion identification

In most failure analyses, the examination of part material, configuration, and quality should be considered a routine procedure, necessary for the accurate evaluation of the failure cause. These examinations should identify gross deficiencies, if they exist, that could have significant effect on material properties or the magnitude of local stresses within the part. For composite materials, items of concern include:

- Incorrect materials.
- Resin content and fiber content.
- Undercure.
- Moisture content.
- Ply stacking sequence, placement, and orientation errors.
- Incorrect size, placement, or poor quality of details such as holes, and radii.
- Improper fastener installation, joining, bonding, etc.
- Void content.
- Individual ply thickness.
- Fiber alignment.

Most of these conditions are likely to be rare. However, since they require little effort to examine and have such a critical influence on failure, their inclusion in any complete analysis is a necessity. Configuration and materials characterization examinations are included in the overall FALN illustrated in Figure 3-1. Because of their potential impact on subsequent operations, these examinations have been incorporated in the early stages

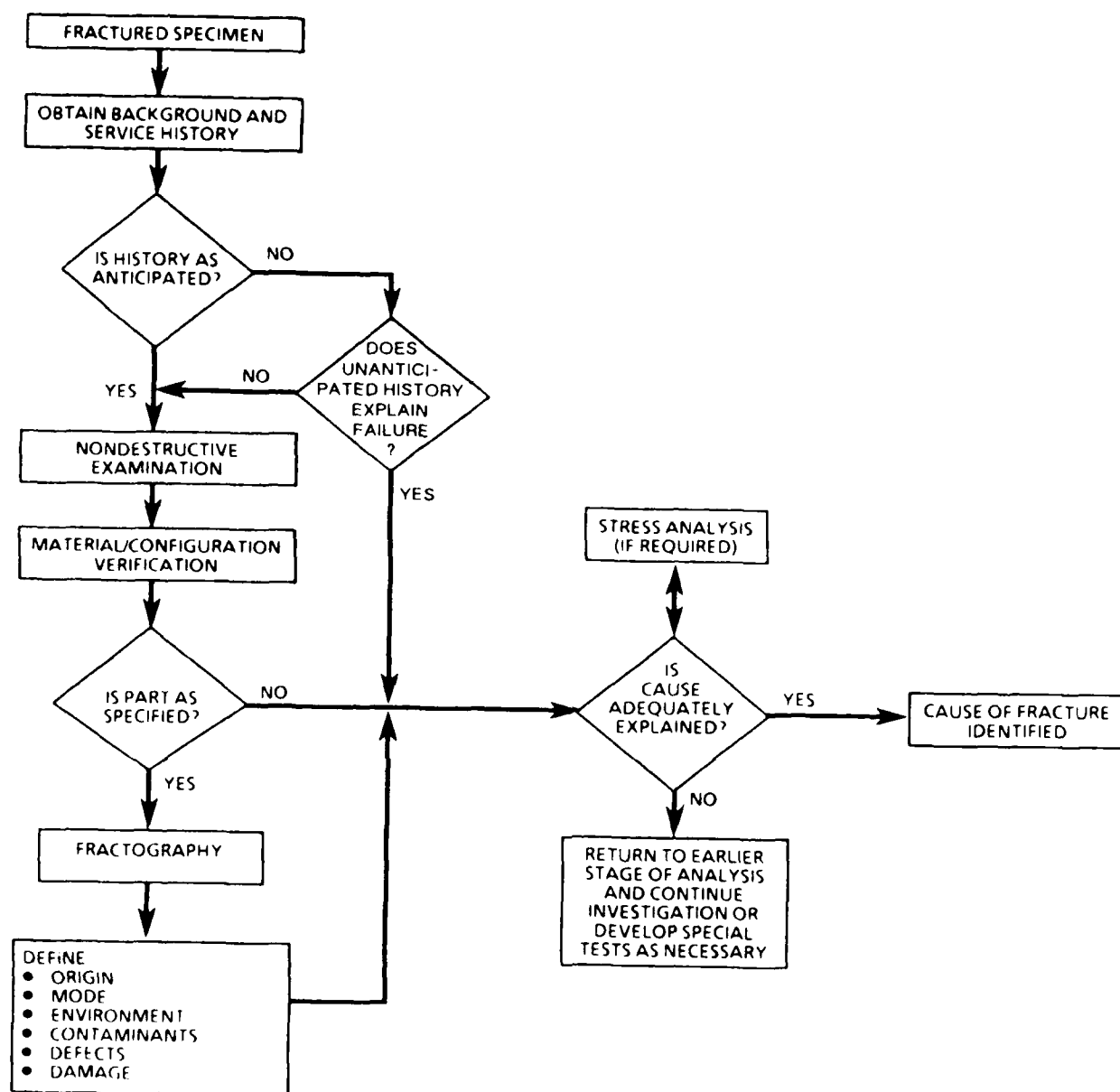


Figure 3-1. Simplified Investigative Framework

5-B70227R1-57

of analysis. In many cases, identification of a major discrepancy (such as using the wrong material), may sufficiently explain the cause of fracture, thus expediting and lowering the cost of the overall investigation, in addition to providing the rationale for appropriate corrective actions.

In support of the overall FALN, a detailed flow chart for configuration and materials characterization was developed. This chart, illustrated in Figure 3-2, provides a detailed guideline for investigators to evaluate critical items such as configuration, ply layup, degree of cure, and the type of resin system used. This FALN employs relatively simple analytical techniques. More complex and difficult analyses occur at later stages of investigation. Figure 3-3 provides a detailed matrix summary of material characterization failure techniques.

In Figure 3-2, one of the more detailed areas of a configuration and materials characterization study is illustrated. Once a thermoset resin material has cured, ascertaining its identity (such as vendor or specific resin formulation family) poses a relatively difficult problem. This is because of the generally similar chemical structure of cross-linked epoxy systems and the tendency of cured resins to resist yielding their identities by typical chemical analyses methods. However, since many of the currently used epoxies exhibit nearly identical properties (within a cure-temperature family), identification of the exact resin system used may not be as crucial as identifying a material with its proper cure-temperature family, for example 121°C (250°F) or 177°C (350°F). Through the combined use of glass transition temperature (T_g) and residual heat of reaction measurements, the particular cure-temperature family of most materials can be established with relative confidence.

For example, when fully cured, most epoxies lack any appreciable residual heat of reaction and the T_g 's are at or slightly above their original cure temperature. When minimum heat of reaction is observed, the measured T_g gives a fairly good indication of the cure temperature family of material used. However, in cases where significant heat of reaction still exists, and the measured T_g is well below the specified cure temperature, the indication is that the proper prepreg material was used but an insufficient degree of cure was generated during processing. In making these analyses, it is important to keep in mind that undercure can arise from several causes: only one of which may be an improper

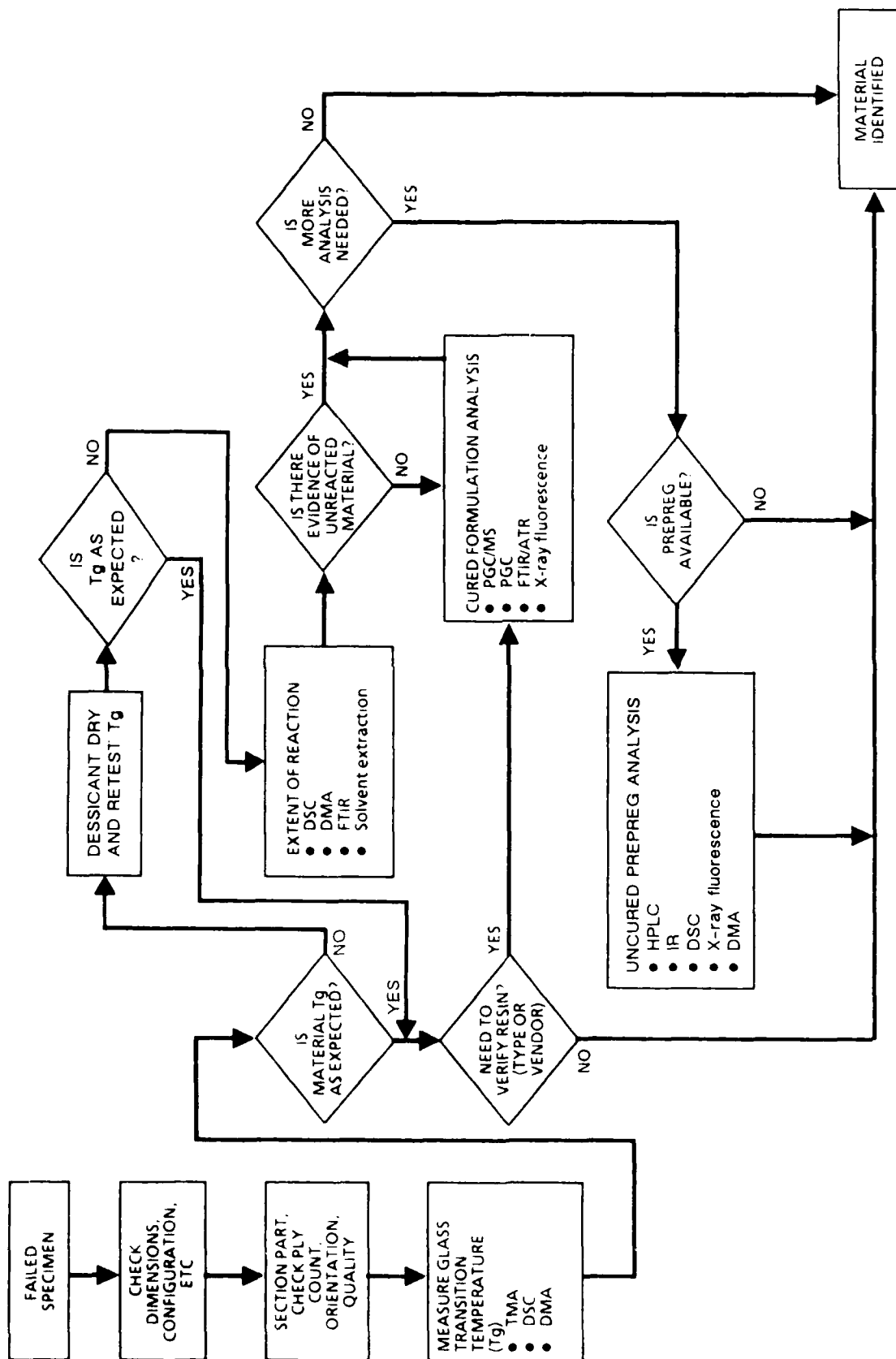


Figure 3-2. Material Verification Technique Sub-FALN

5-B70227-59

	TECHNIQUE	DESCRIPTION	USE	VALUE
Degree-of Cure Analysis	Thermomechanical Analysis (TMA)	Measure probe displacement as a function of sample temperature	Determines glass transition temperature	Indication of degree of cure or environmental effects
	Differential Scanning Calorimetry (DSC)	Performs enthalpy measurements	<ul style="list-style-type: none"> Determines glass transition temperature Determines residual heat of reaction 	Indication of degree of cure or environmental effects
	Dynamic Mechanical Analysis (DMA)	Measures mechanical response to oscillating dynamic loading	<ul style="list-style-type: none"> Determines glass transition temperature Observes mechanical transition due to additional crosslinking 	<ul style="list-style-type: none"> Indication of degree of cure or environmental effects Indication of uncured condition
	Infrared spectroscopy	Measures IR spectrum	Distinguishes between reacted and unreacted functional groups	Indicates amount of unreacted functional groups to determine extent of cure
	Solvent extraction	Exposure to an organic solvent	Removes unreacted material leaving reacted network behind	Indication of the degree of cure
Uncured Material Identification	High-Pressure Liquid Chromatography (HPLC)	Produces liquid chromatograms of any soluble liquid	Identifies individual components of differing solubilities or size	Formulation verification
	Infrared spectroscopy	Measures IR spectra	Identifies functional groups attached to carbon backbone	Formulation verification
	Differential Scanning Calorimetry (DSC)	Performs enthalpy measurements	Determines heat of reaction	Formulation verification
	X-ray fluorescence	Measures X-ray fluorescence spectra	Determines sulfur content	Hardener content
Cured Material Identification	Pyrolysis – Gas Chromatography (PGC)	Determines gas chromatograms formed from nonvolatile organics by thermal decomposition	Qualitative and quantitative analysis of cured epoxy	Formulation/impurity verification
	Pyrolysis – Gas Chromatography / Mass Spectroscopy (PGC/MS)	Allows mass spectrometer to act as a detector for the gas chromatograph	Qualitative and quantitative analysis of cured epoxy	Formulation/impurity verification
	Infrared spectroscopy	Measures IR spectra	Functional group analysis	Formulation verification
	X-ray fluorescence	Measures X-ray fluorescence spectra	Determines sulfur content	Hardener content
	Thermomechanical Analysis (TMA)	Measures material thermal-mechanical response	Determines glass transition	Identify general resin system

Figure 3-3. Failure Analysis Techniques for Materials Characterization

5-B70227-79

cure procedure. Alterations in the prepreg formulation can reduce reaction rates during cure. Therefore, when a sufficient degree of undercure is detected, it is generally recommended that additional tests be carried out on the original prepreg (from that specific lot, if possible) to verify its chemistry.

In some analyses, identifying the specific resin system used may be important; however, the investigator should be aware that analytical capabilities are only partially developed, and are in their infancy for more recent resin formulations and systems. Sufficient differences exist in basic formulations so that relatively simple tests may be used to identify different systems, but for the most part, the ability to identify resin systems within the same temperature-cure family is relatively difficult.

3.1.1 Laminate Lay-Up and Ply Orientation Analyses

Unlike homogeneous materials, most modern composite materials are fabricated by laminating together a large number of relatively thin gage woven or unidirectional plies. For structures made from such materials it is important to recognize that engineering properties, and hence the component's ability to operate without failure, depend upon the correct number, sequence and orientation of plies being used to make up the laminate. In general, the significance of errors depends upon the particular material in question as well as the magnitude of mistake in terms of the overall laminate construction. For example, an overall off-axis rotation of 5 degrees can reduce the ultimate compression strength of a unidirectional graphite epoxy laminate by as much 54 percent. In contrast, a 5 degree rotation of only one ply out of a 30 ply laminate probably would produce less than a 2 percent decrease in ultimate strength. From this standpoint it is critical that the impact of identified discrepancies be accurately identified and taken into consideration prior to their reporting or possible identification as a significant contributor to the cause of failure.

Errors in lay-up can also have significant effects not directly related to those engineering properties considered as part of typical design. The materials' coefficient of thermal expansion represents one such property, where variations in stacking sequence can produce significant amounts of panel warpage or internal residual stresses. These internal stresses have been found to cause damage such as gross delamination and matrix cracking

within the laminate plies. Such damage, while not always directly responsible for failure, may in many cases constitute one of several contributory conditions resulting in premature failure.

For continuous fiber reinforced composite materials, the exact design properties which should be checked as part of a ply lay-up analysis will depend strongly upon the requirements of the specific component examined. However, as a general guideline, critical parameters which should be given consideration in the event discrepancies are detected should include:

- Young's Modulus.
- Basic laminate strength (tension, compression, shear).
- Notch sensitivity (tension and compression).
- Buckling stability.
- Internal thermal stress or residual stress conditions.
- Alterations in environmental susceptibility.

Some of the most common errors in ply layup include:

- Missing or additional plies.
- Improper angular orientation.
- Improper ply type, grade or style.

Several relatively straightforward methods exist for analyzing the orientation, stacking sequence and number of plies making up a composite structure. Optical metallography is the most obvious and direct technique. Adapted from the microstructural analysis of metals, this technique involves the optical examination of finely polished cross sections using a standard reflected-light optical microscope. Other methods, although not as quick or simple, include image analysis and radiography. Specific details of each of these methods are presented in the following paragraphs.

Similar to standard metallurgical failure analysis procedures, selection of areas for examination generally constitutes the critical step involved in understanding internal material characteristics. For most failures, detailed examinations should be carried out

in all areas of the part representative of the typical structure. For example, in a skin panel with attached stringers, a thorough analysis should examine both the skin as well as the stringer constructions regardless of whether the failure occurred in only one of these primary components, for example the skin. Reductions in modulus due to a lay-up error of one component can often produce higher loads in an adjacent part of the panel resulting in premature failure at a location not related to the original error. Generally, as a final step, metallographically prepared cross-sections should also be taken through, or adjacent to, the origin area of failure to examine for local discrepancies and ensure material uniformity.

3.1.1.1 Optical Microscopy (For Determination of Lay-Up and Ply Orientation)

Sectioning—Removal of sections for metallographic preparation can be performed utilizing a wide variety of cutting devices as long as some care and forethought is given to the type and extent of damage likely to be generated. Abrasively coated band saw or circular blades are the most desirable since they generate the least damage (no further than 0.15 inch from the cut) and are widely available. If possible, a coolant such as water should be applied during the cutting operation to prevent heat damage, provided that subsequent contamination of the remaining component structure is not a concern. If abrasive cutting equipment is not available or coolant contamination is a concern, hand operated toothed blades or saws such as hack or coping saws can be used. With these blades every effort should be made to use as fine a toothed blade as possible to limit damage. With these toothed blades, a substantial amount of damage is often created adjacent to the cut edge - such as localized delaminations - which should be removed during subsequent sanding operations.

Metallographic Preparation—The basic preparation procedures for composites are the same as for metals. Depending upon the size of the section, mounting in a supportive resin may be necessary to provide a stable base for sanding and polishing. Resins requiring elevated temperature for cure or forming, such as bakelite, should in general be avoided since many may approach or exceed the materials original cure temperature and thereby introduce additional damage such as embrittlement, creep, or microcracking. For most applications room temperature cure systems such as two part epoxies or methyl methacrylate resins work well.

Sanding should proceed from a relatively coarse paper (120 grit), to the finer grits (600). Typically wet-or-dry sandpapers are used during this procedure with a substantial amount of water being applied at all times to the surface being sanded to remove debris and prevent heat damage. For subsequent operations it is critical that the sanded surface produced is flat to ensure full surface contact during the final polishing operations. For most composite materials, final polishing is best accomplished by utilizing a high speed polishing wheel covered with stretched silk (or other extremely low nap material such as nylon) in combination with either diamond paste or an equivalent alumina polishing compound. Final polishing usually does not require a large number of steps; usually 15 micron followed by 3 micron is adequate. Results are further improved by fairly heavy downward pressure and counter-rotating the specimen to the direction of wheel rotation.

Following polishing, etching is generally not required due to the distinct optical differences which exist between most fibers and the surrounding matrix systems. An exception to this is fiberglass where a dilute hydroformic or hydrofluoric acid etch may be necessary to enhance fiber visibility.

Plies—The orientation, number, and stacking sequence of plies making up the section of interest can be generally identified by optical microscopy at magnifications ranging from 50X to 400X. At the lower magnifications, individual plies can be identified by pronounced alterations in overall reflectivity due to the fiber orientation of each ply, or by the existence of a linear interfacial region of reduced fiber density (matrix-rich layer) between each ply (see Figure 3-4). Determination of the precise angular orientation of each ply requires higher magnification examinations. As illustrated in Figure 3-5, fibers intersecting the polished surface at an angle appear oval in shape. With this method, large differences between ply orientations are easily seen by large variances in the elliptical shape of the cross-sectioned fibers. In determining and reporting ply orientations, it is important to reference the measured angle against the component's defined 0 degree axis to prevent confusion and maintain consistency with other analyses such as stress analysis. Commonly, most sections are taken at 0, 45 or 90 degrees to the defined 0 degree axis, with a vertical section plane. This vertical section does not, however, allow one to distinguish between certain ply orientations such as +45 and -45 degree plies. A recent technique has been developed which provides differentiation of all ply angularities with a single cross-sectional planar view. In this method, the cross-section is prepared



Figure 3-4. Cross Section of a Laminate With Easily Differentiated Ply Separation

5-B70227-1



Figure 3-5. Identification of Ply Orientation by
Fiber End Shape and Ovality

5-B70227-2

such that the polished sectional plane is at a 45 degree angle through the thickness of the part. This technique is presented in Figure 3-6. Small differences in fiber orientation, such as fiber waviness, can be determined by measuring the intersected fiber lengths and utilizing simple trigonometric calculations. For such measurements, the sectional plane should be vertical so that fibers from the primary reference plies are normal to the polished surface. This will result in the reference plies appearing circular and allowing measurement of nominal fiber diameter.

3.1.1.2 Image Analysis (For Determination of Lay-Up and Ply Orientation)

Through the use of fairly low cost image analysis systems, both ply and individual fiber orientations can be determined. Through optical imaging of the polished cross-sections, the intersectional fiber length or the aspect ratio for each fiber is measured. Simple trigonometric calculations with these data is then used to determine overall ply orientation in each region of view or the average and worse case fiber waviness. Fiber waviness can be critical to certain product forms and applications like unidirectional or filament wound structures in which fiber nestling and tow movement occurs. One advantage of image analysis is that an automated or statistical evaluation of material integrity is available. Since fiber resolution and differentiation from the surrounding matrix resin is required, high magnification (400X or more) and various enhancement techniques such as etching (for fiberglass) or staining may be necessary.

Image analyses can also be used to determine the relative percentage of voids in the laminate. Either by cross-sectioning or by evaluation of the fracture surfaces, a quantitative assessment of the planar void content can be performed. By taking several measurements along parallel planes, a fairly accurate determination of the void shape, distribution, and percent can be made.

3.1.1.3 Radiography (For Determination of Lay-Up and Ply Orientation)

A nondestructive technique is available in which a plan view image of ply orientations can be determined. This involves the use of radiographically opaque tracer yarns, such that X-ray imaging can detect these doped fiber bundles. For tape preregs, the tracer yarns are placed in the 0 degree direction parallel to the fiber orientation. For fabric, the yarns

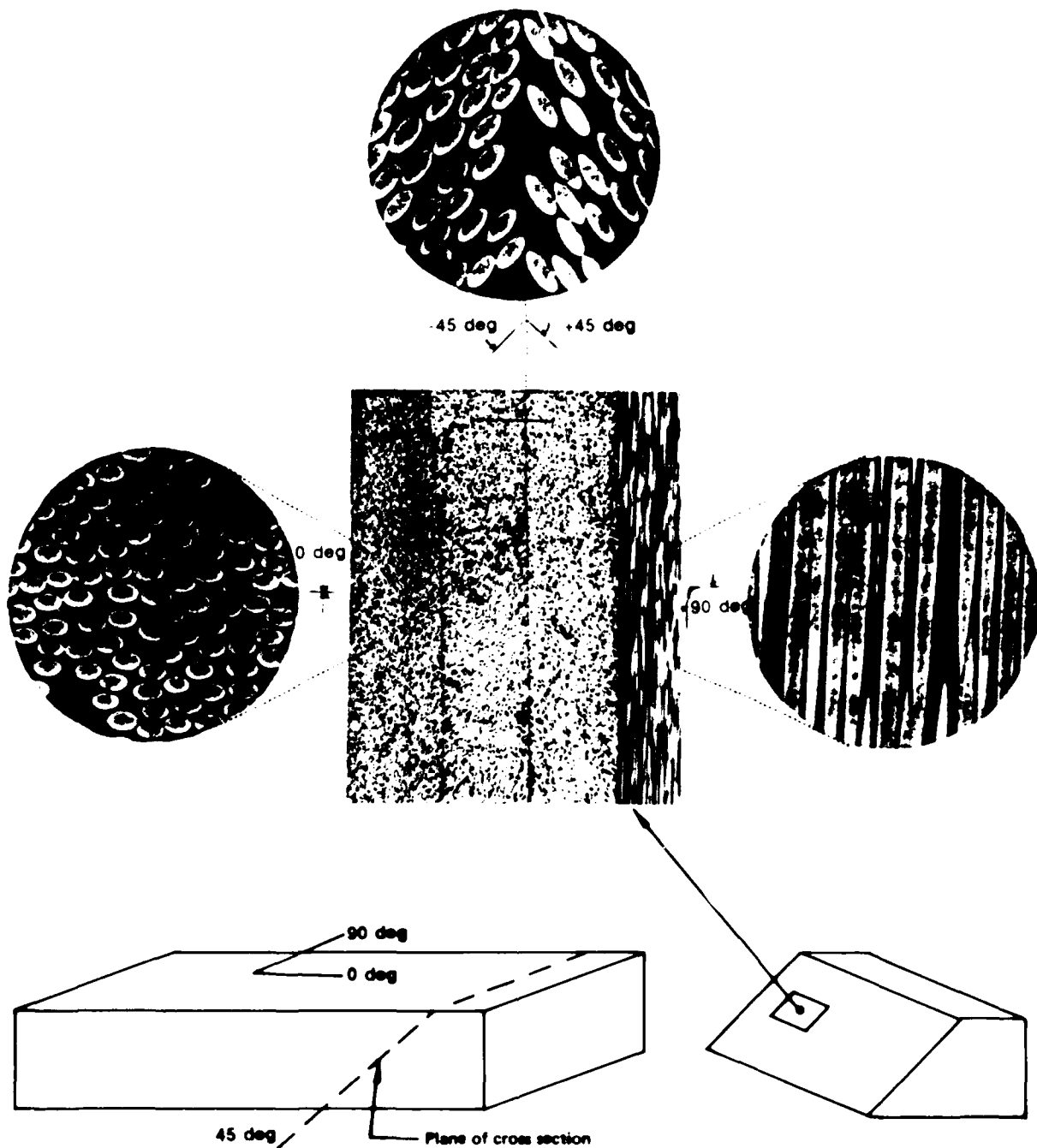


Figure 3-6. Polished Cross Section at 45-deg Angle Through the Thickness of the Part

5-B70227-3

are most often placed in the warp direction. This technique is most useful for thin laminates, where the precise number of plies and orientation can be determined. Thick laminates make it difficult to identify the number of plies, although anomalous conditions such as ply orientation shift and ply dropoffs and pickups are easily detected. Figure 3-7 presents a radiograph in which the tracer yarns are evident.

3.1.2 Determination of Fiber, Matrix, Void, and Moisture Content

The determination of the constituents present in the cured laminate is as important as identifying the layup of the individual plies. These details provide information regarding the microstructure which in turn can be directly related to mechanical properties of the overall laminate. For instance, a 20% shift in the fiber (or matrix) content has been shown to result in a decrease in mechanical properties as large as 50%. Similarly, void contents above 3% (by volume) can significantly reduce interlaminar tension and shear strength, particularly when the voids concentrate between plies.

3.1.2.1 Fiber and Matrix Content

The stiffness and strength of laminates are determined by the internal packing geometry of the fibers and the constitutive behavior of the fiber and matrix. The volume fractions of the fibers or matrices can be determined by three methods: (1) gradient density column, (2) chemical matrix digestion, and (3) photomicrographic.

The gradient density column method is performed by placing the sample in a graduated column containing a solution with a gradient of density from top to bottom. The height at which the sample is suspended in the solution can be used to calculate the overall density of the sample. The specimen density can then be used to calculate fiber volume and resin volume, given the resin density and fiber density as known constants.

The chemical matrix digestion method is performed by dissolving the resin with hot nitric acid and weighing the amount of fibers remaining. The volume fractions of fibers and resin can then be determined from the beginning and final weights and the known identities of the constituent.

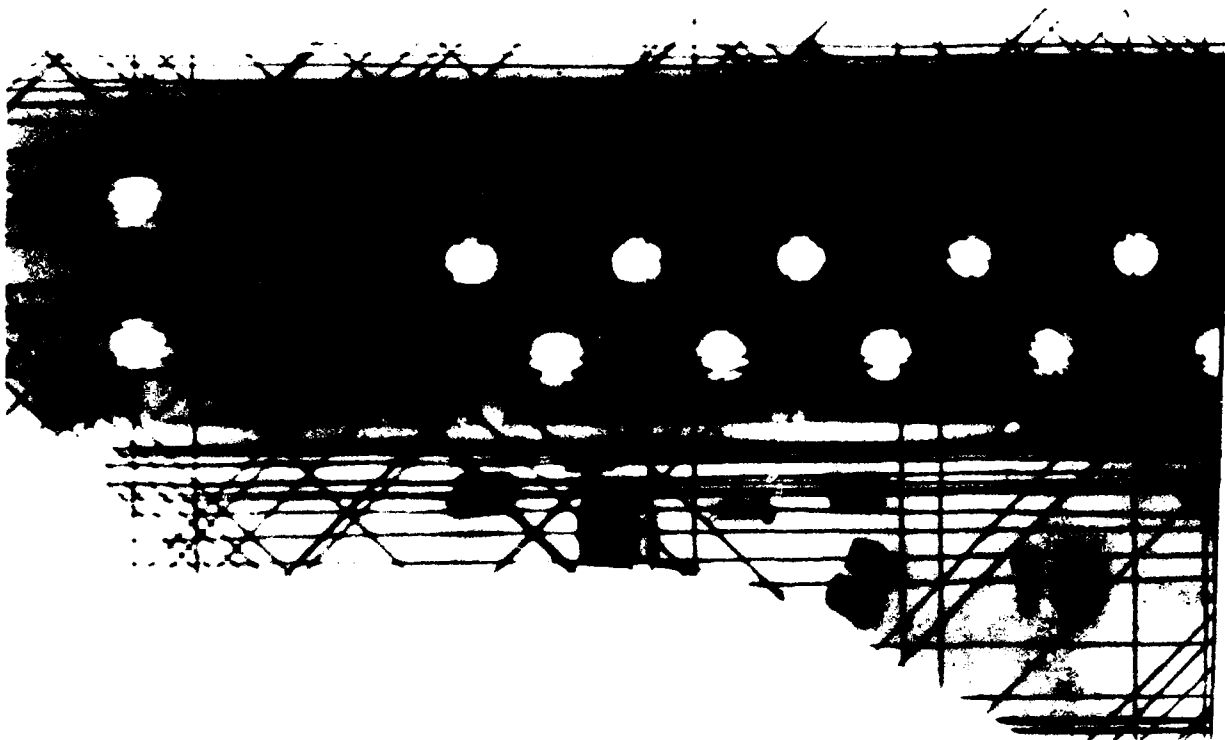


Figure 3-7. A Radiograph in Which the Tracer Yarns Are Evident for Determination of the Ply Orientation in a Thin Laminate

5-B70227-4

In the photomicrographics technique, the number of fibers in a given area of polished cross-section are counted and the volume fractions are determined as the area fractions of each constituent. Both area methods and line intercept methods can be used with an image analyzer to quickly determine fiber volume fractions.

The first two methods require a much larger specimen than the photomicrographic technique. This latter method must use many sampling areas to produce reliable results, since the area viewed is about a hundredth of a square millimeter. It does, however, give an accurate view of the fiber-matrix distribution and void content. The first two methods do not indicate void content, which can result in erroneous data with specimens containing high void content or moisture content.

3.1.2.2 Void Content

The best method for determining void content is the photomicrographic analysis, as discussed in the previous paragraph. When inspecting laminates for void content, the cross-section is usually taken transverse to the laminate plane. In such cases where the voids are concentrated between plies, a polished section in the plane of the laminate can be examined to determine void content specific to the region between plies. As indicated above, a quantitative image analyzer can be used to more quickly and accurately determine void content.

3.1.2.3 Moisture Content

Moisture content of cured laminates can be performed by thermal drying or with a moisture analyzer. The primary difference between the two methods is that the moisture analyzer can differentiate between water vapor and other volatiles which escape from the specimen. Thermal drying only requires an accurate weighing balance and a small drying oven. The specimen is weighed before and after drying to determine moisture content. The temperature selected should be much less than the cure temperature or the glass transition temperature (T_g). For a 177°C (350°F) system, a temperature below 60°C (140°F) is recommended. The moisture analyzer is much quicker (hours versus days) and more accurate, however, the analyzer is relatively an expensive unit that also requires a trained operator.

3.1.3 Material Identification

The identification of the composite material used in a failed part may be necessary to determine the cause of failure. Material identification techniques are available which are suitable for cured or uncured material analysis. Uncured identification techniques are rarely used in failure analysis because the prepreg used in part fabrication is rarely available. Once a material has cured, identification of materials is difficult due to the intractable nature of a thermosetting polymer matrix. Since many of the currently used epoxies exhibit nearly identical properties (within a cure-temperature family), identification of the exact resin system may not be as crucial as identifying a material within a cure-temperature family. Due to the extensive vendor certification, receiving inspection testing, and quality control records maintained throughout the aerospace industry, a large amount of data usually exists on the prepreg used in any specific part. Major formulation or production errors are rare. The following paragraphs describe techniques for identification of cured or uncured composite materials.

3.1.3.1 Uncured Material Identification

Evaluation techniques for uncured epoxy prepreg are fairly well established. Several analytical techniques to characterize the uncured prepreg including High Performance Liquid Chromatography (HPLC), Infrared (IR) Spectroscopy, Differential Scanning Calorimetry (DSC), Automatic Absorption Spectroscopy, and X-ray Fluorescence provide detailed information to the investigator. Each technique is discussed in more detail below.

Generally, uncured material identification techniques are seldom used in failure analysis because the prepreg materials used to fabricate the failed part are not available to analysis. The most commonly used techniques, when the prepreg is available, are HPLC and IR Spectroscopy. HPLC and IR are widely utilized in the aerospace industry to "fingerprint" the prepreg resin formulation. Standard HPLC chromatograms and IR spectra exist for all qualified materials. These standards provide a quick check of resin formulation. DSC is less frequently used for material identification. Although DSC can identify reaction types, specific resin system formulations are difficult. X-ray fluorescence is used to detect sulfonyl groups to verify the amount of DDS hardener present. Atomic

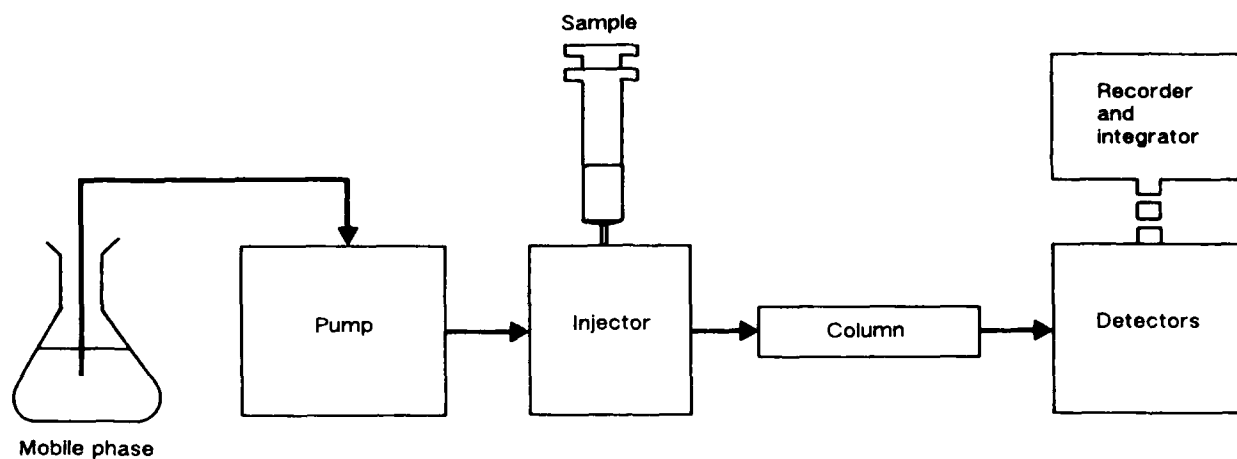
absorption spectroscopy is utilized to detect boron which verifies the level of BF₃ catalyst present. X-ray fluorescence and atomic absorption spectroscopy are usually used only if anomalies are detected in HPLC, IR, or DSC.

High Pressure Liquid Chromatography (HPLC) is a common technique for chemical characterization of composite matrices. HPLC separates individual resin components according to their size or solubility using high efficiency, micro particulate columns.

HPLC test procedures are well established in the aerospace industry because of the widespread usage of HPLC for "fingerprint" inspection of resin formulation. Resin samples are extracted using an HPLC grade solvent such as 63:37 CH₃CN:H₂O. A schematic of a HPLC test setup and instrument parameters are shown in Figure 3-8. The extracted sample is injected into the column and analyzed using an ultraviolet detector. A typical HPLC chromatograph is shown in Figure 3-9. Components can be identified by comparing the peak positions on the chromatograms to a reference standard. Peak areas can be used to determine relative concentrations.

Infrared Spectroscopy (IR) is an organic chemical analysis tool which is extremely sensitive to the overall chemical makeup of a complex chemical formulation. IR measures the absorption of incident infrared radiation, and is used to verify epoxy resin formulation. This technique is well suited for characterizing commercial epoxy resins which often contain several components such as aromatic epoxy main, reactive epoxy diluents for flow control, aliphatic epoxy flexibilizers, elastomers, curing agents, catalysts, or accelerators. IR can accurately fingerprint the total resin formulation by detecting the absorbed frequencies of infrared light associated with the vibrations of specific molecular functional groups. The degree of absorbance is proportional to the amount of functionality in the resin formulation.

Because IR is able to accurately fingerprint a given formulation, it is used as a quality control tool to assure that lot-to-lot variations do not exceed certain limits. IR would also be useful to determine the manufacturer of the material when unidentified material is encountered. The typical application requires that the resin is extracted from the prepreg with reagent grade acetone at room temperature. The extract is then allowed to dry onto a salt pellet for IR analysis. The resultant spectrum is then compared to a standard



Instrument parameters

Column:	microbondapak C18 waters
Mobile phase:	premixed 63% CH ₃ CN/37% H ₂ O
Flow rate:	1.5 mL/min
Injection volume:	10 µL
Detection:	UV 220 nm
Attenuation:	0.2 AUFS
Chart speed:	1 cm/min (0.5 in/min)

Figure 3-8. HPLC Test Setup Schematic and Typical Instrument Parameters

5-B70227-167

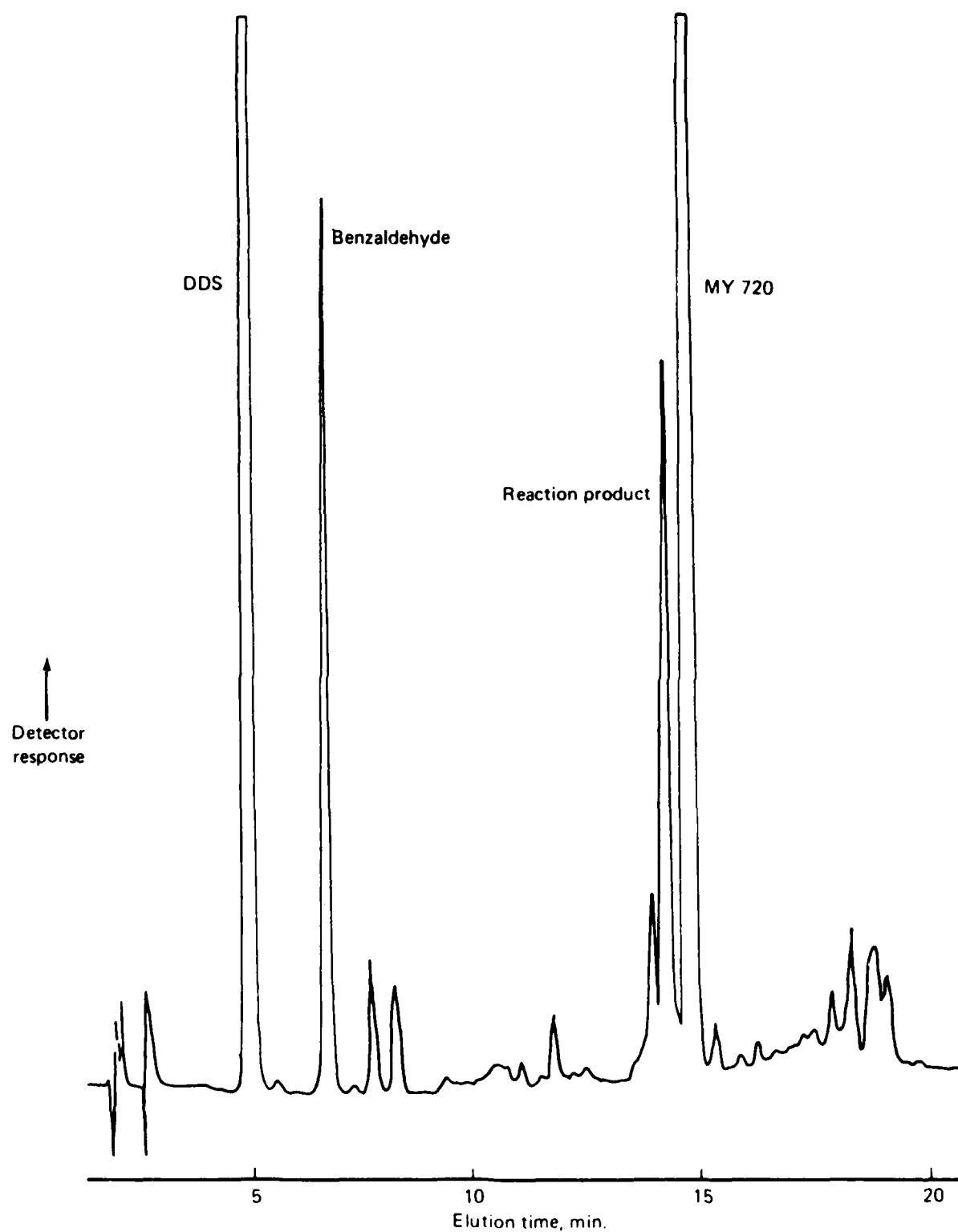


Figure 3-9. LC Chromatogram of Narmco Resin Matrix Showing Major Peak Assignment

5-B70227R1-83

epoxy spectrum acquired from the supplier or on a previous batch of material. The spectrum is examined for contaminants (additional peaks) or gross formulation changes (changes in the relative peak ratios). An example of a standard epoxy resin spectrum is shown in Figure 3-10. If a deviation from the standard spectrum is observed, then each subcomponent should be quantified and compared to standard formulation quantities. Quantitation methods for the curing agent and catalyst are considered below.

A quantitative method for determining the amount of Diaminodiphenyl Sulfone (DDS) curing agent and carbonyl epoxy has been developed for the 3501 resin system (ref. 2). This involves constructing a working calibration curve for DDS concentrations in solution versus IR absorbance for the sulfone peak followed by a measurement of the absorbance of the unknown concentration of DDS in an epoxy prepreg extract. An alternate qualitative approach would rely on comparing the relative change in the ratio between these peaks as the concentration varied.

Differential Scanning Calorimetry (DSC)—DSC is a thermal analysis technique which measures heat flow into or out of a sample by measuring the differential heat (energy) necessary to keep the sample at the same temperature as a reference sample. In the case of a curing epoxy system, DSC measures the heat released during the exothermic cure reactions as the specimen is heated at a constant heating rate.

DSC can be used to identify or characterize uncured prepreg. The cure of typical aerospace epoxy systems consists of several chemical reactions with different reaction rates and activation energies which cause certain cure reactions to be favored over certain temperature ranges. The reaction types occurring in a particular system depends on the formulation of the system. DSC can be used to separate the different cure reactions to help identify a particular resin system.

A typical DSC cell is shown in Figure 3-11. The sample pan and reference pan are placed in the cell. An inert atmosphere of nitrogen is then introduced into the test chamber. Heat is transferred to the pans through the sample platforms and heat flow is monitored by thermocouples. Generally, prepreg sample sizes of approximately 10 mg are used for DSC experiments depending on the size of the sample pan used. Low heating rates of about 2 to 5°C/minute are best to separate the various reaction peaks. Heat flow versus

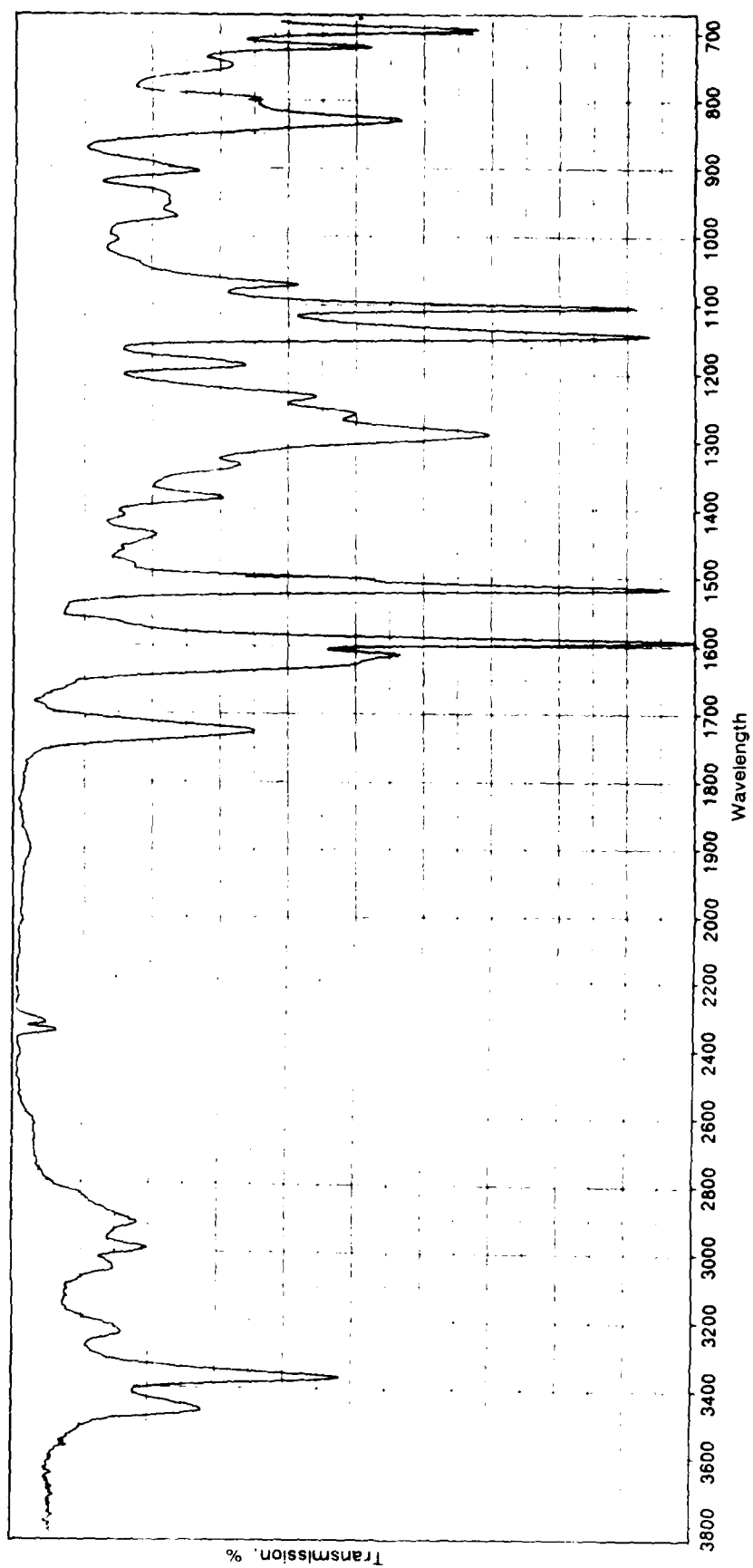


Figure 3-10 Standard IR Spectrum of a Commercial Epoxy Resin Formulation

5-B70227-168

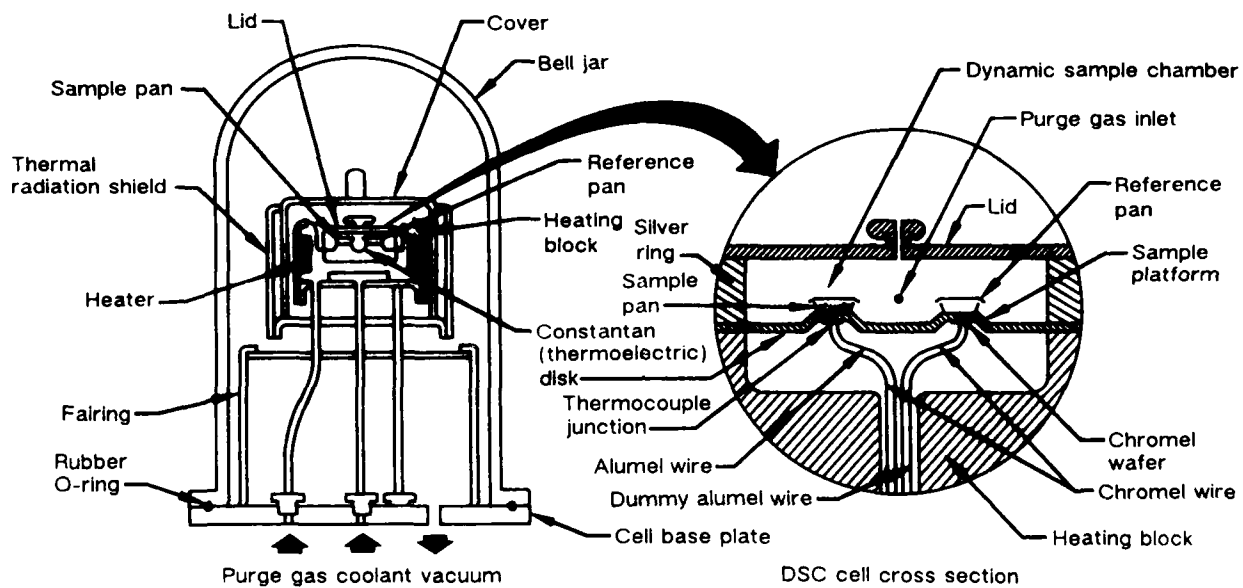


Figure 3-11. Cross-Sectional Diagram of the DSC Cell Used by Du Pont DSC Module

5-B70227-166

temperature or versus time at constant heating rate from ambient to 300°C is measured. An interface with a computer or microprocessor for experiment control, data acquisition, and data analysis provides greater accuracy and more information from each experiment.

A DSC thermogram for the Hercules 3501-6 resin system is shown in Figure 3-12. Exotherm peaks are observed at two temperatures (149°C and 213°C). The lower temperature peak is attributed to the catalyzed cure reactions while the higher temperature peak is attributed to the uncatalyzed cure reactions. The total heat of reaction (the area between the thermogram peaks and baseline T1 to T4), the relative peak size, and reaction temperature can identify resin constituents. Comparison to a standard thermogram can identify a particular resin system.

The advantages of DSC formulation verification are the small sample size and the experimental ease. The disadvantage is the need for standard thermograms and background information for system identification.

Atomic Absorption Spectroscopy (AA)—AA is used to quantify the amount of BF₃ containing catalyst in the epoxy resin. AA determinations for catalyst concentration are initiated when HPLC and IR indicate a significant deviation in resin formulation has occurred. The underlying principle of AA is the absorption of a discrete wavelength of light by a vaporized prepreg resin extract. For boron, 249.7 nm and 208.9 nm wavelength light will be attenuated proportionately to the boron concentration. A boron calibration curve is established using a certified standard. Typical working range of concentrations for boron is 400 to 4000 microliter per milliliter of solution.

X-ray Fluorescence Spectroscopy (XRF)—XRF can be used qualitatively or quantitatively to determine the amount of DDS curing agent in an epoxy prepreg extract by quantifying the amount of sulfur present. XRF measurements are initiated when a formulation change is suspected, based on HPLC or IR evaluation. The XRF determination is based on the emission of X-rays characteristic of sulfur (0.537216 nm) when the sample is irradiated with an X-ray source. The intensity of X-ray emission is proportional to the sulfur concentration. An example of a qualitative comparison of different epoxy resin systems is given in Figure 3-13.

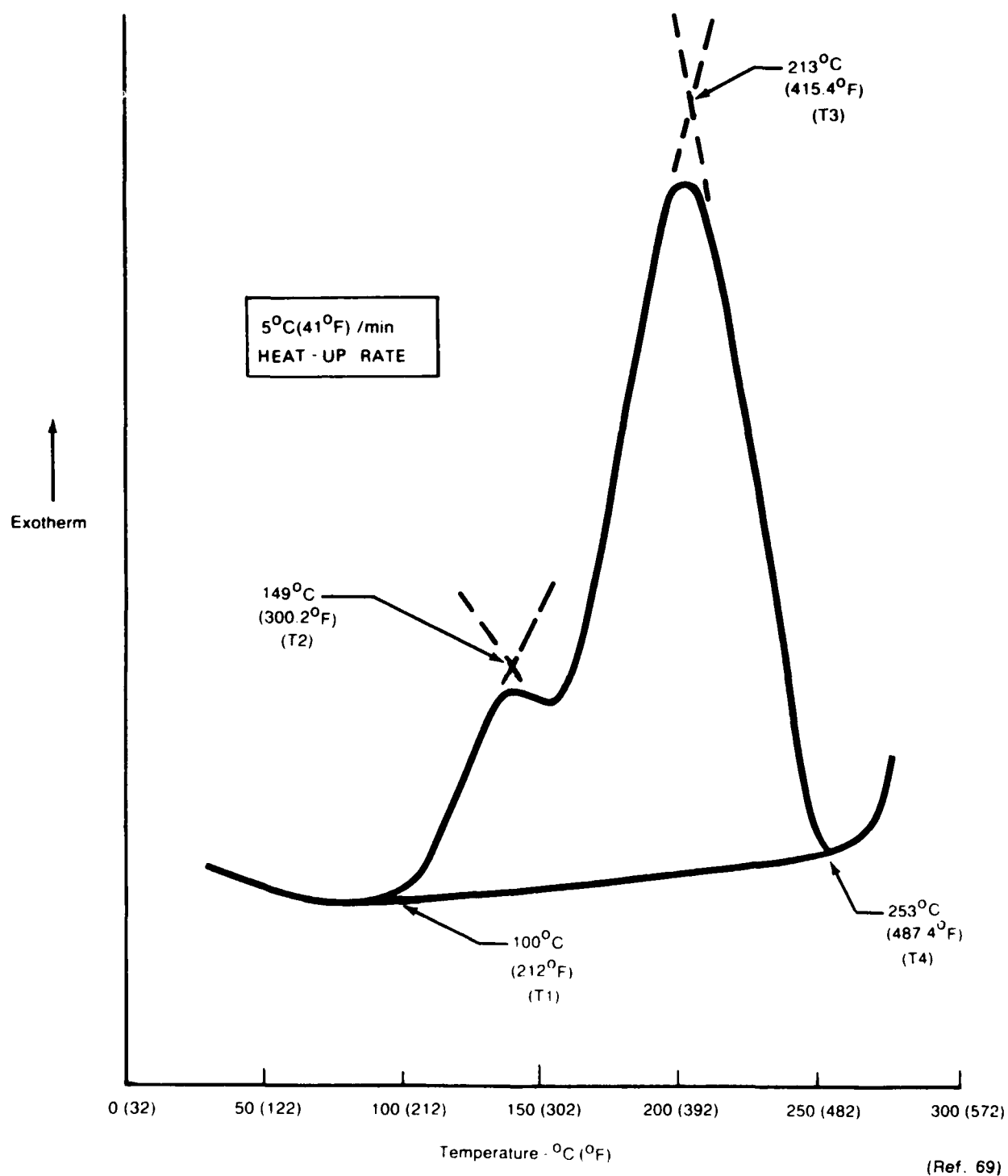


Figure 3-12. DSC Thermogram for 3501-6 Resin

5-B70227R2-84

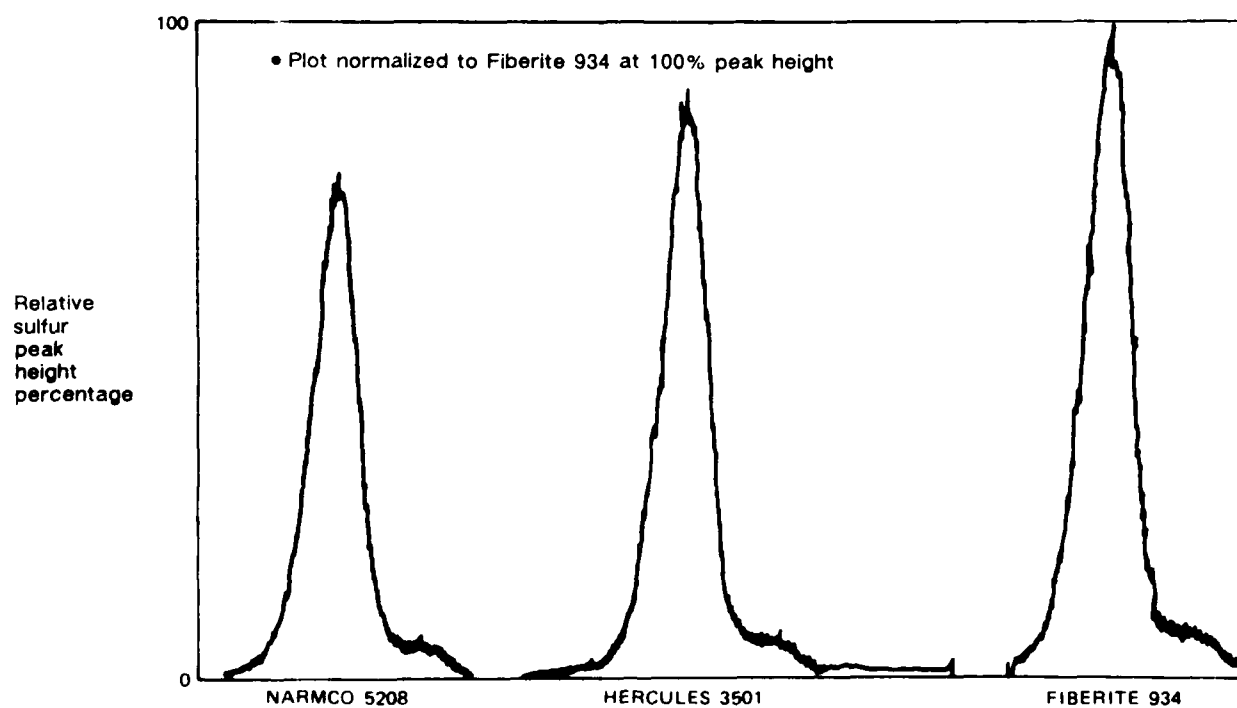


Figure 3-13. Sample Fingerprinting of Various Systems by Way of X-Ray Fluorescence

5-B70227-165

3.1.3.2 Cured Material Identification

Once a material has cured, ascertaining its identity poses a relatively difficult problem arising from the generally similar chemical structure of cross-linked thermosetting systems and the tendency of the cured resins to resist yielding their identities by typical analytical methods. However, since many of the currently used epoxies exhibit nearly identical properties (within a cure-temperature family), identification of the exact resin system used may not be as critical as identifying a material with its proper cure temperature family. Through the combined use of determinations of T_g and residual heat of reaction measurements, the particular cure-temperature family can be determined.

In some isolated cases during post-failure analysis investigations, identifying the specific resin system used to fabricate the failed part may be important; however, the investigator should be aware that extensive capabilities in this area are only partially developed. Sufficient differences exist in basic formulation so that relatively simple tests, such as X-ray fluorescence (XRF) may be used to identify different systems. For the most part, the ability to identify resin systems within the same cure-temperature family is difficult. Two of the most promising techniques are pyrolysis gas chromatography (PGC) and diffuse reflectance (FTIR) spectroscopy. These techniques are discussed in the following paragraphs.

Pyrolysis Gas Chromatography (PGC)—This method is used to determine epoxy matrix chemical formulation. Pyrolysis is the vaporization and degradation of the matrix resin under controlled heating. The resulting decomposed products pass through a gas chromatograph which separates the components by physical or chemical parameters such as molecular size or polarity.

PGC requires samples of approximately 25-50 micrograms. Pyrolysis is accomplished at 1000°C. Typical PGC chromatograms are shown in Figure 3-14 for two commercial epoxy systems. The resulting PGC chromatogram can be used to identify the matrix resin by comparing to a reference fingerprint standard.

PGC/Mass Spectrometry (PGC/MS)—PGC/MS consists of PGC, as described above, coupled with a mass spectrometer (MS). In order to identify separated pyrolysis products and

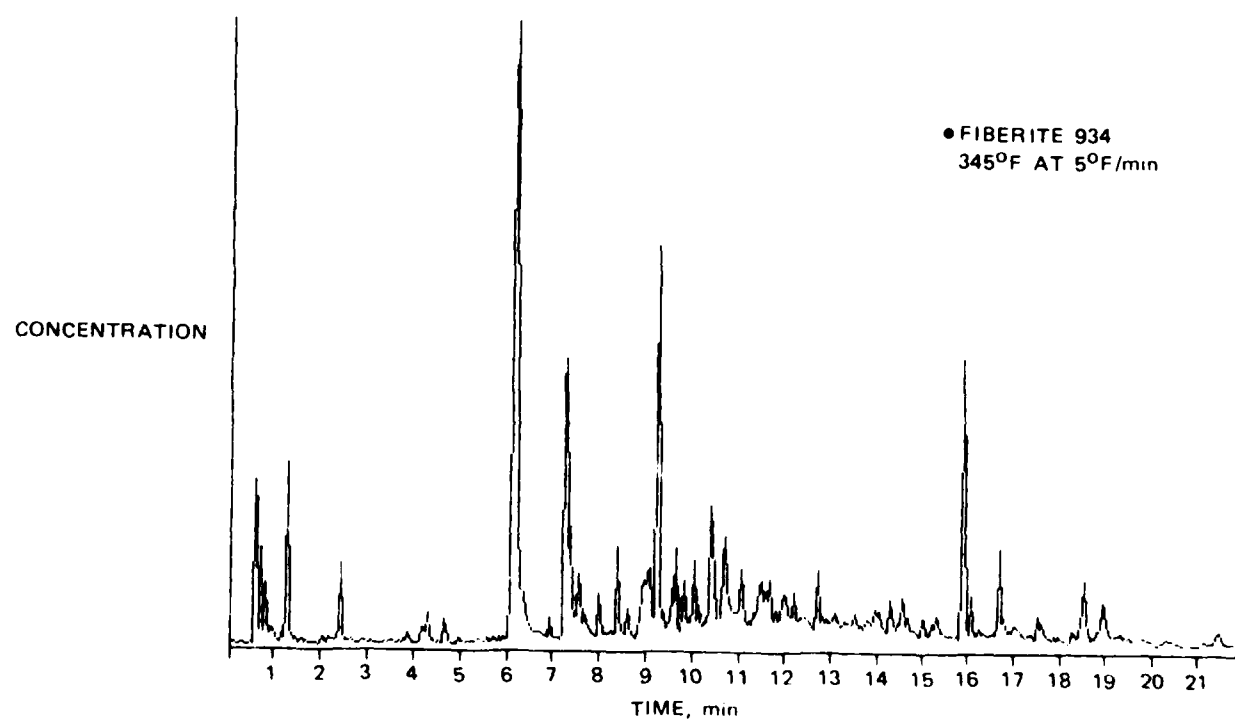
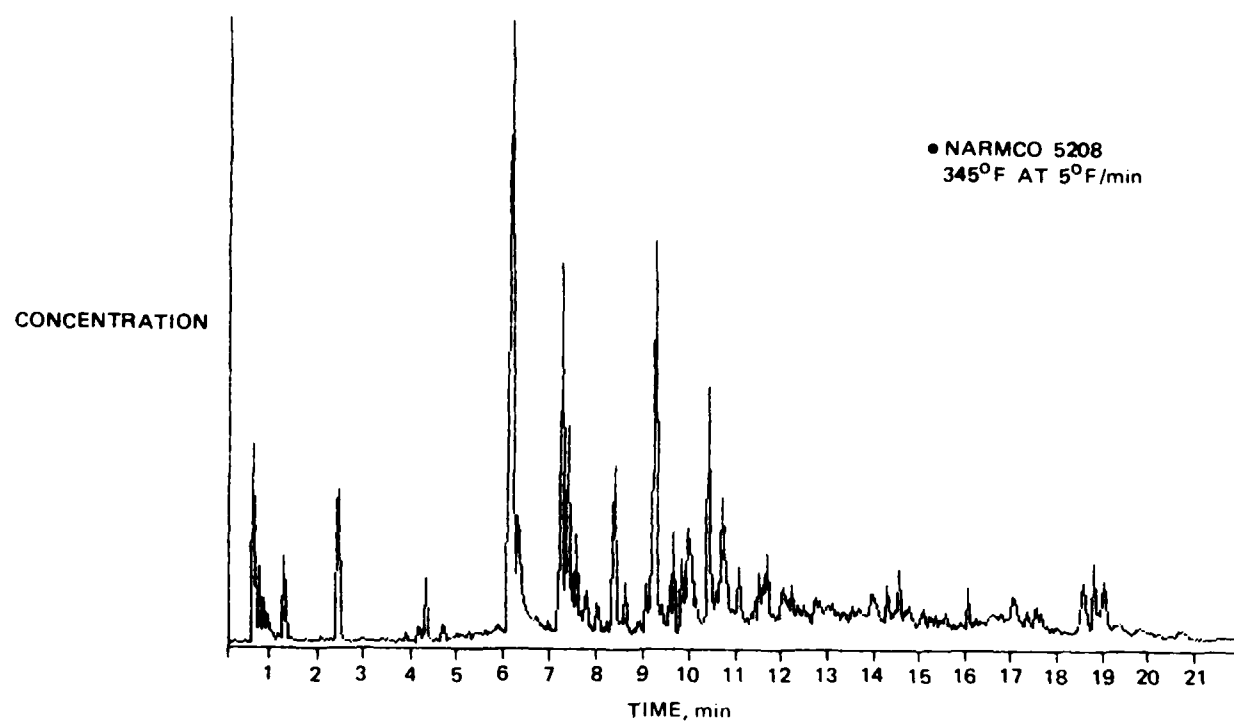


Figure 3-14. Pyrolysis Gas Chromatography (PGC) of Two Difficult Resin Systems

5-B70227-164

assign component structure to chromatographic peaks, the pyrolysis products are passed through a capillary column directly into the mass spectrometer. A typical PGC chromatogram with MS peak assignments is shown in Figure 3-15 for DDS hardener. Identification of resin formulation can be accomplished using PGC/MS.

Infrared Spectroscopy (IR)—Chemical characterization of a cured composite specimen is important in order to establish if the proper resin system was selected and to establish if any environmental degradation has occurred to the chemical structure. Using traditional transmission IR specimen techniques, a cured composite can be analyzed. Small particles are scraped off a resin rich area and ground to a fine particulate using a mortar and pestle. The particulate is then mixed into a potassium-bromide salt pellet for analysis. Figure 3-16 illustrates a comparison between this method for cured resin analysis and the standard spectrum for the uncured resin. Qualitatively these spectra are similar (except for the loss of epoxide groups upon curing) and may prove to be useful in a failure analysis where a database of uncured and cured resin systems has been established.

Diffuse Reflectance Infrared Spectroscopy (DRIFTS)—This method permits direct measurement of the infrared spectrum from a cured composite resin. Infrared radiation is focused on the sample. The resulting diffusely scattered infrared radiation is collected with a large solid angle detector. The spectrum is interpreted as a normal IR spectrum would be; except that a number of potential artifacts due to variations in sample geometry, peak distortions and spectral interferences may occur. Figure 3-17 (ref 3) illustrates DRIFTS spectra of a composite before and after thermal aging where increasing oxidation with aging is observed. Note the increased absorbance levels at 1654 to 1696 nm.

3.1.4 Degree of Cure Analysis

The degree of cure of a thermosetting polymeric composite matrix is a critical variable effecting the performance of the composite, especially in elevated temperature or moist environments. Insufficient cure may occur due to lower than required cure temperatures, shorter than required cure times, or due to errors in resin formulation or chemistry. Errors in resin formulation or chemistry are rare because of the stringent specification requirements, vendor certification, and receiving inspection testing common throughout the aerospace industry. However, because conditions of undercure can significantly

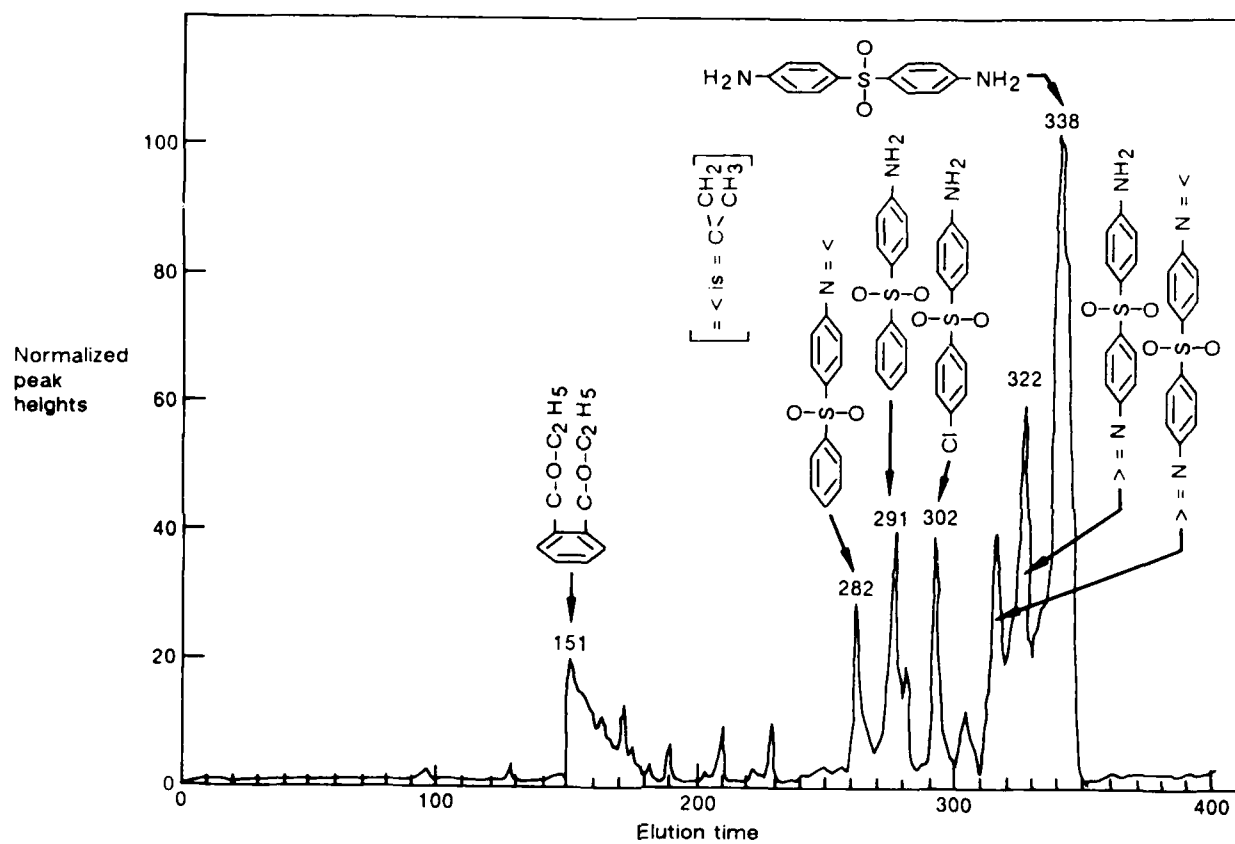


Figure 3-15. Gas Chromatography of DDS, Diaminodiphenyl Sulfone

5-B70227-163

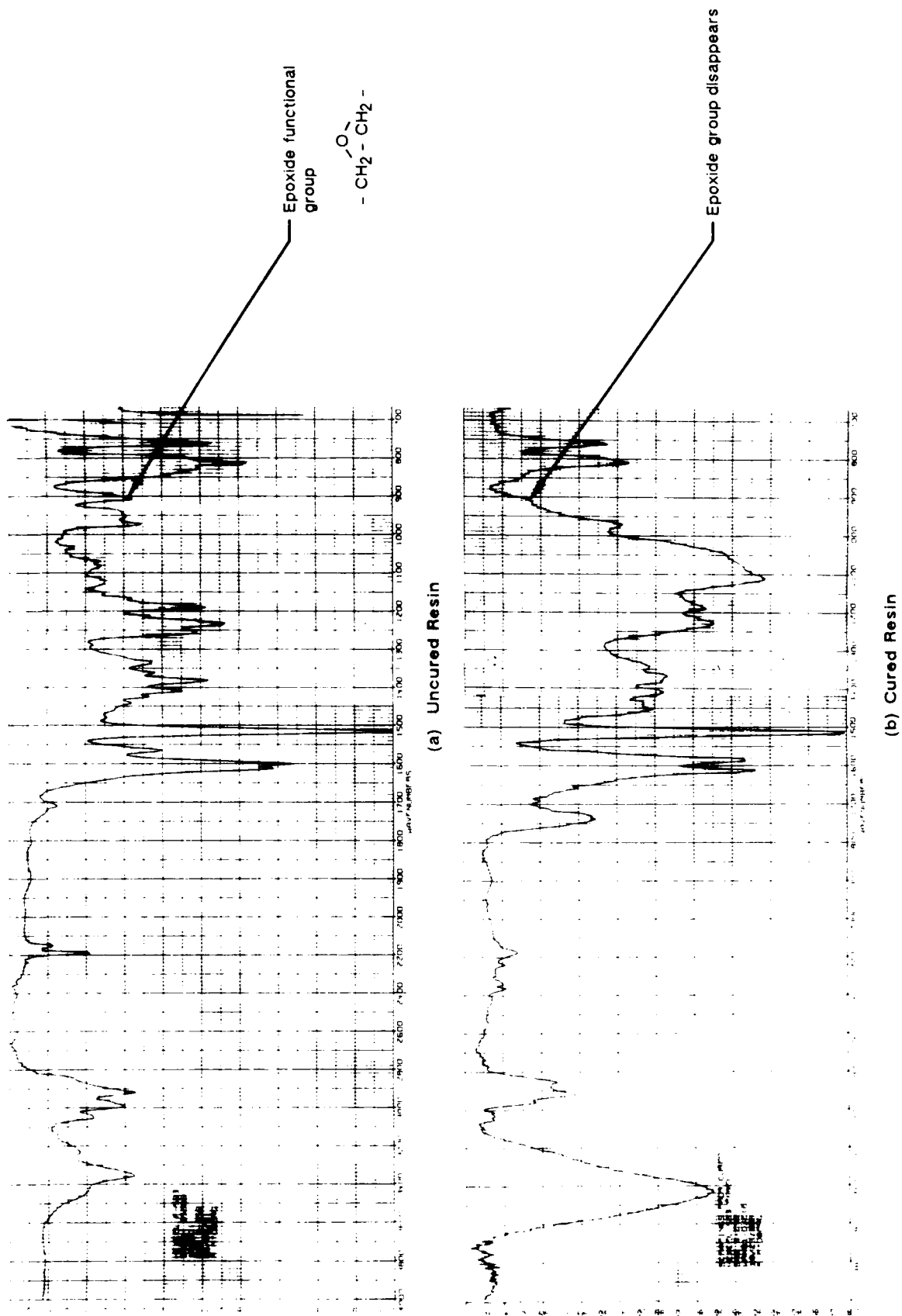
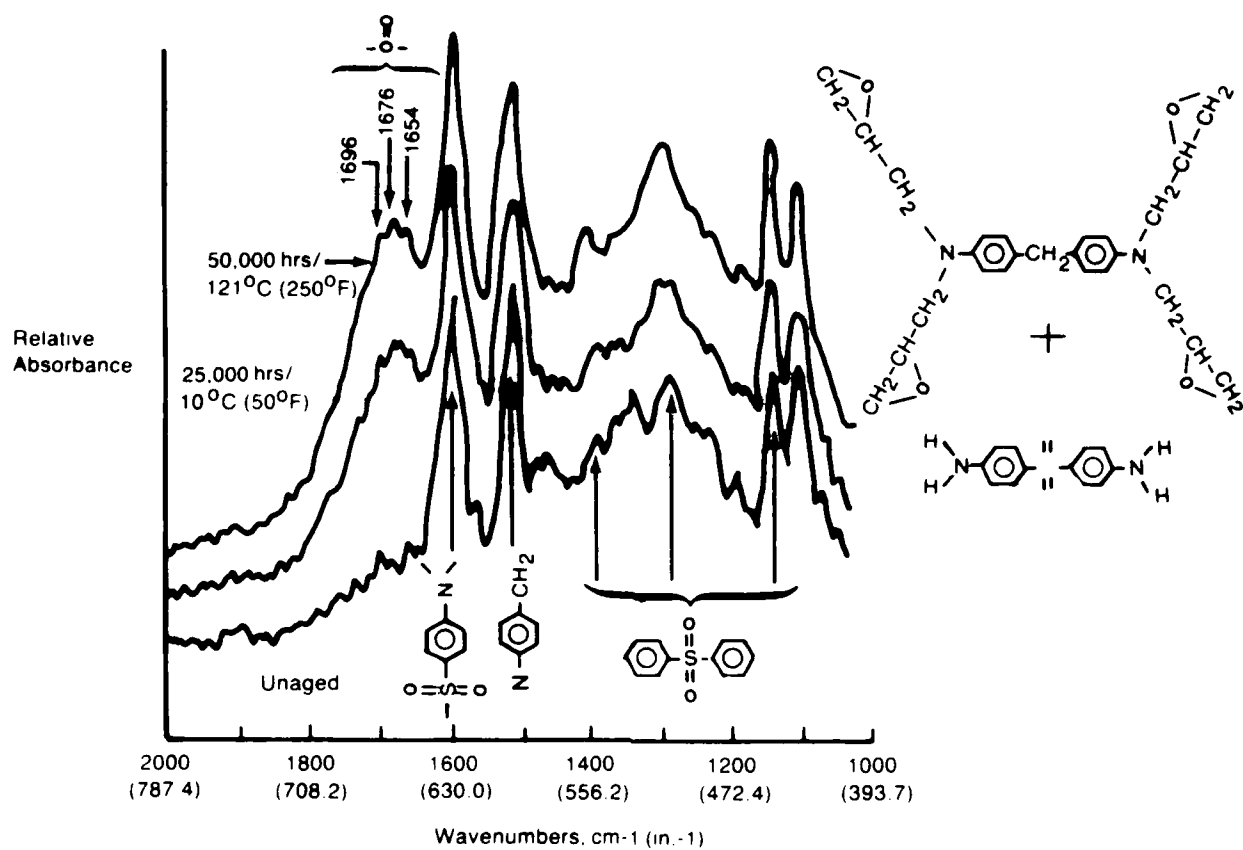


Figure 3-16. IR Comparison of Resin

S-B70227-162



(Ref. 3)

Figure 3-17. Drifts of Graphite-Epoxy (AS/3501-5) Composite Before and After Thermal Aging

5-B70227R1-85

impact structural integrity and can be rapidly and easily checked, their analysis should be included as a routine step in most failure analyses. Verifying the degree of cure is analogous to checking the correct heat treat condition on fractured metal components, a procedure considered routine in metals failure analysis.

As described in the materials characterization FALN contained in paragraph 3.1, verifying the state of cure of a fractured component normally represents the first stage of materials characterization analysis. There are several reasons for performing such analyses during the initial stages of an investigation. Perhaps the most significant reason is that such analyses can be performed quickly and easily and produce results which may have a significant impact on downstream investigative operations.

In most cases, evaluation of the degree of cure of a failed component is best addressed by a two stage process. In the first stage, glass transition temperature (T_g) analysis establishes whether a lower than expected degree of cure may exist. These analyses (paragraph 3.1.3.1) are generally relatively easy to perform and therefore impose a relatively small impact on the amount of effort necessary to carry-out an investigation. As with evaluating the heat treat of metals, most of the time the appropriate thermal processing has been performed, and similarly for composites, the correct degree of cure will be detected and further analyses will not be necessary. However, if the glass transition temperature (T_g) of the laminate and a subsequent retest of a dried (desiccated) laminate does not match that anticipated for the material used, the second stage analyses (paragraph 3.1.3.2) should be performed. This involves determination of the extent of unreacted material - can be performed to evaluate if this anomaly represents a condition of undercure. Here it should be noted that a low T_g may arise both from inadequate processing or resin formulation errors, as well as the accidental use of a wrong material such as a 250°F curing prepreg in place of a 350°F curing prepreg. A detailed description of the logical sequence of steps (FALN) involved in assessing the materials' degree of cure was presented in paragraph 3.1.

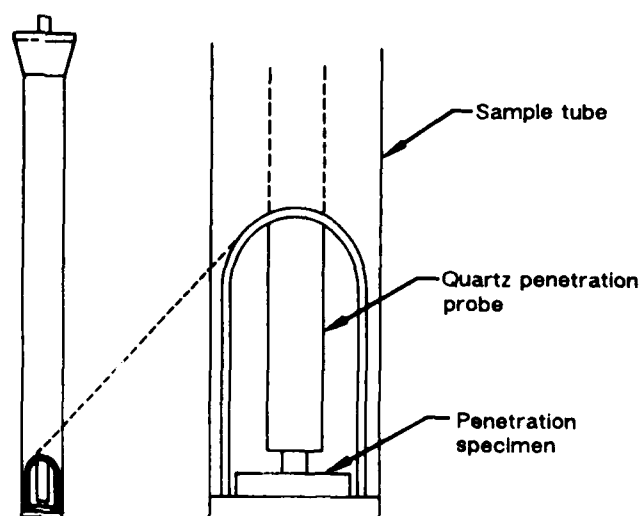
3.1.4.1 Glass Transition Temperature (T_g) Analysis

The temperature at which an amorphous polymer reversibly changes from a brittle, glassy state to a more flexible, rubbery state is the glass transition temperature. In the case of

thermosetting polymers this transition temperature directly reflects the degree of cure achieved by the material. This transition temperature is manifested as a change in slope of the curve obtained by plotting any of the primary thermodynamic properties against temperature. This change in slope falls in the same temperature range as that in which mechanical softening occurs. A variety of techniques exist by which the point of this softening can be determined. The most common are thermal analysis tests such as thermo-mechanical analysis (TMA) and dynamic mechanical analysis (DMA), and differential scanning calorimetry (DSC). TMA is the most common technique for failure analysis because of the small sample requirement and the ease of testing and evaluation. DMA and DSC can be used to determine the T_g , however are less attractive due to specimen preparation, performance, and interpretation difficulties. These methods are more appropriately used in failure analyses for determination of the extent of unreacted material and environmental effects, as discussed in the following paragraph.

Thermomechanical Analysis (TMA)—This method is designed to measure (with extremely high sensitivity) the relative linear displacement of a quartz probe placed in contact with the sample surface. During controlled heating, a record is generated revealing thermally dependent dimensional changes exhibited by the sample and therefore the materials' glass transition temperature. For this method several variations can be used to support the sample and measure dimensional behavior. Specific methods commonly available on most instruments include:

- **Penetration**—In this mode, a probe is placed on the side of a small rectangular specimen cut from the sample. Typically, a cubic shaped specimen with 0.1 to 0.15 inch for each dimension is used for this technique. This small sample size lowers the concern of thermal lag. The generation of any thermal lag between the temperature of the sample (which is uncontrolled) with that of the surrounding chamber (which is controlled) can affect data accuracy. For most samples, the direction of fiber orientation does not represent a critical parameter in this test since only relative dimensional measurements are being made, however placement of the probe directly on the carbon fibers instead of the epoxy resin may interfere with sharp definition of the glass transition. During the test, the specimen is situated as shown in Figure 3-18, heated at a controlled rate, typically 5° to 25°C/minute, and the glass transition temperature



Penetration Method

Figure 3-18. Glass Transition Temperature Determination—TMA Penetration Test Setup

5-B70227R1-161

determined by a pronounced downward movement of the probe indicating matrix softening, Figure 3-19. Typically, several specimens from a part are characterized. The measured T_g can then be averaged to minimize errors due to specimen inhomogeneity on a small scale.

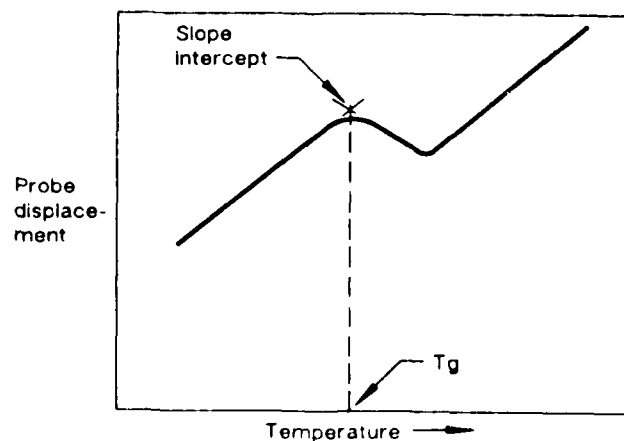


Figure 3-19. Glass Transition Temperature Determination—TMA Penetration Test Measurement

5-B70227R1-160

- Flexure**—In this test mode, a rectangular sample 0.1 inch in width by 0.25 to 0.50 inch in length by 2 to 4 plies in thickness is placed in three point flexural stress within the test chamber as shown in Figure 3-20. With this configuration the probe measures beam deflection as a function of temperature. Again, as the transition temperature is reached the resin softens, the beam (specimen) deflects, and an inflection in the slope of the thermogram being generated occurs. Nominally, the heat-up rate is approximately 20°C/Minute with a probe load of 10 grams. A thermogram of a 177°C (350°F) epoxy system is presented in Figure 3-21, showing the tangents to the slope. The Tg is defined as the temperature at which the tangents intercept. Care should also be taken to not remove specimens from the laminate near a surface which has a different chemistry or cure temperature material attached. This includes adhesively bonded regions, potted areas or surfaces which have had surface prep fabric such as peel-ply.

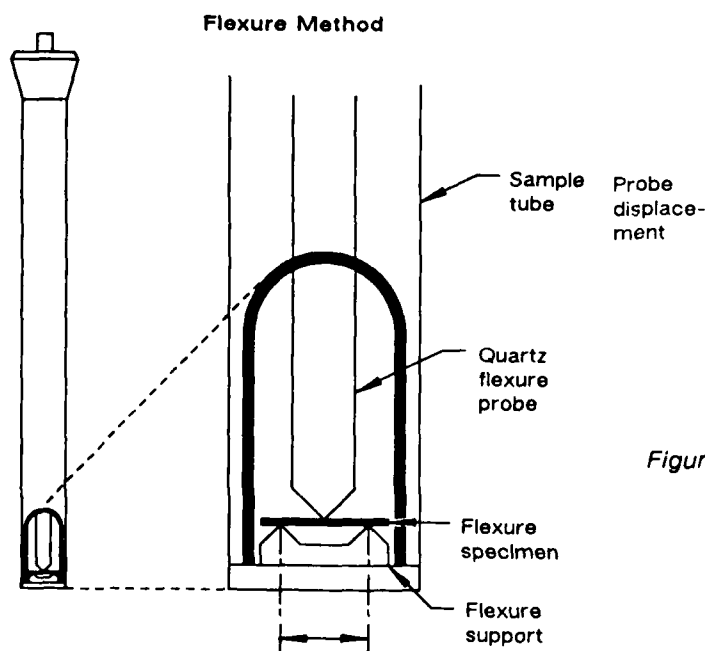


Figure 3-20. Glass Transition Temperature Determination—TMA Flexure Test Setup

5-B70227R1-159

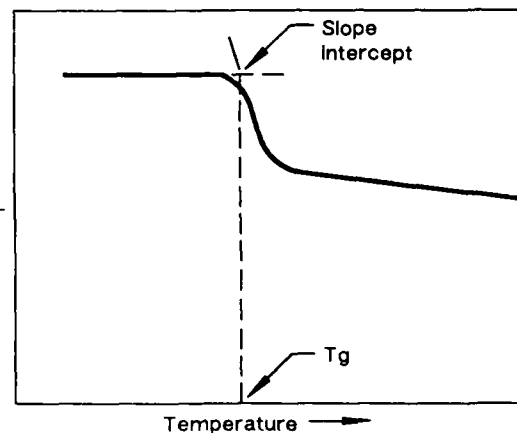


Figure 3-21. Glass Transition Temperature Determination—TMA Flexure Test Measurement

5-B70227R1-158

- **Expansion**—This test is run in much the same manner as penetration, except a larger diameter probe is utilized to prevent penetration into the sample at the point of softening. As the specimen is heated, the resin is free to expand in the transverse or lateral direction. Since a distinct increase in the rate of thermal expansion normally occurs at the glass transition, the thermogram generated by this technique typically provides an additional method by which to determine the materials' glass transition (Figure 3-22). As in the penetration method, placement of the probe directly on carbon fibers may interfere with accurate Tg determination.

Of the three methods discussed above, the preferred method is the flexural technique. Generally, the flexural test method produces sharper, more distinct inflections and only requires a very small sample. The penetration and expansion methods are used less often because of the interference of the carbon fibers with accurate Tg determination.

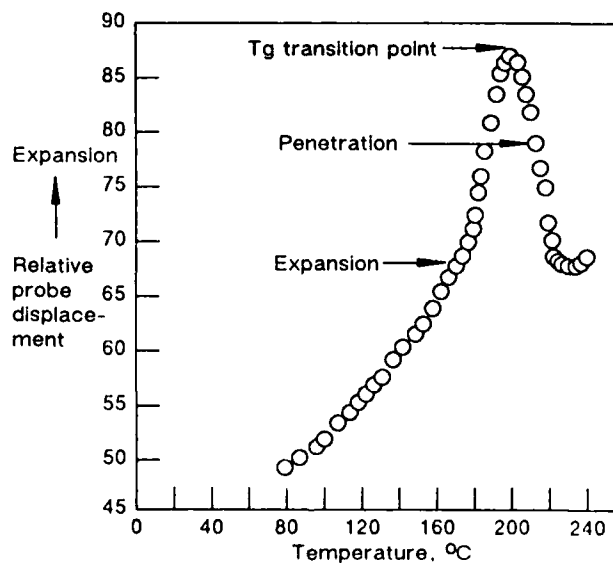


Figure 3-22. Determination of Tg by Expansion Method

5-B70227-157

Dynamic Mechanical Analysis (DMA)—High performance epoxy systems used in composite matrices exhibit a viscoelastic response to applied mechanical strains. Dynamic Mechanical Analysis (DMA) techniques are a useful means of determining the viscoelastic nature of epoxy matrices. The glass transition temperature can be determined from DMA experiments.

DMA involves the application of a sinusoidally oscillating tensile, torsional, or flexural strain to a sample and measuring the response versus increasing temperature from -150°C to 400°C . Heating rates vary from $1^{\circ}\text{C}/\text{minute}$ to $10^{\circ}\text{C}/\text{minute}$ depending on the sample size. Data are presented in terms of storage modulus (elastic component), loss modulus (viscous component) and tangent delta (ratio of loss modulus to storage modulus) versus test temperature.

Typical DMA data are shown in Figure 3-23. The glass transition temperature can be determined as the peak temperature of the high temperature transition in tangent delta or loss modulus or as the knee of the storage modulus curve.

DMA is typically not used where only glass transition temperature measurement is required. Larger sample sizes and more difficult sample preparation and test methods limit the utility of DMA for glass transition measurement. Since carbon fibers tend to diminish the viscoelastic transition magnitudes, samples should be tested in a matrix dominated direction if possible.

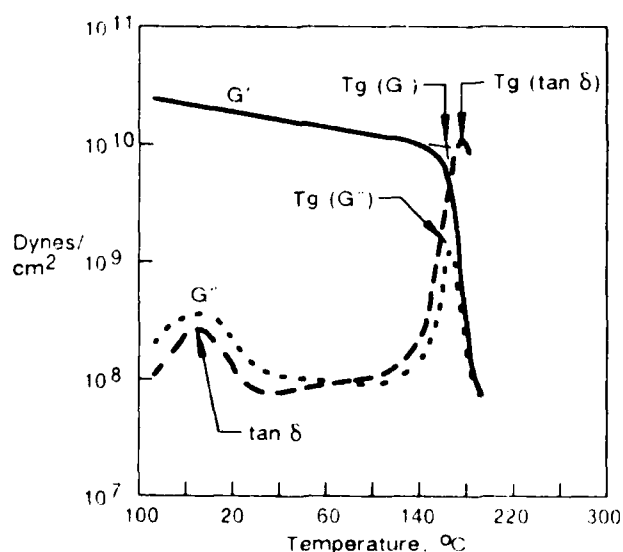


Figure 3-23. Typical DMA Plot for Cured Epoxy Showing Glass Transition Determination

5-B70227-156

Differential Scanning Calorimetry (DSC)—DSC techniques similar to those described in paragraph 3.1.2.1 can be used to determine the glass transition temperature of a cured epoxy composite sample except that sample sizes of approximately 5 mg are tested at approximately 20°C/minute heating rate.

A typical DSC thermogram for a cured epoxy is shown in Figure 3-24. The glass transition will appear as a change in the slope of the DSC thermogram. Determination of glass transition temperature using DSC is sometimes difficult because of the exotherm peaks due to additional reaction during the DSC test.

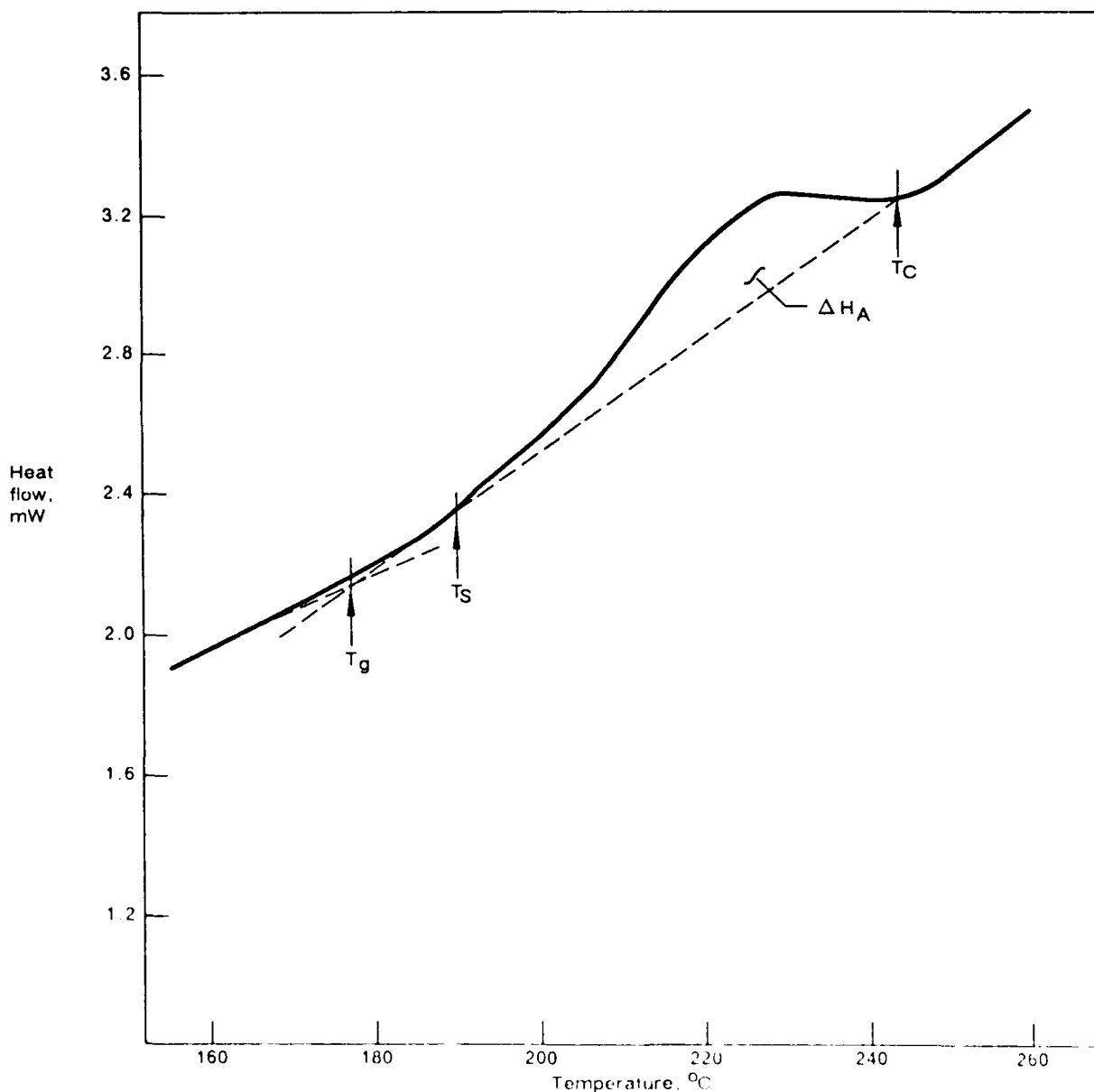


Figure 3-24 A Typical DSC Plot for Cured Epoxy Illustrating Determination of the T_g and Heat of Additional Reaction

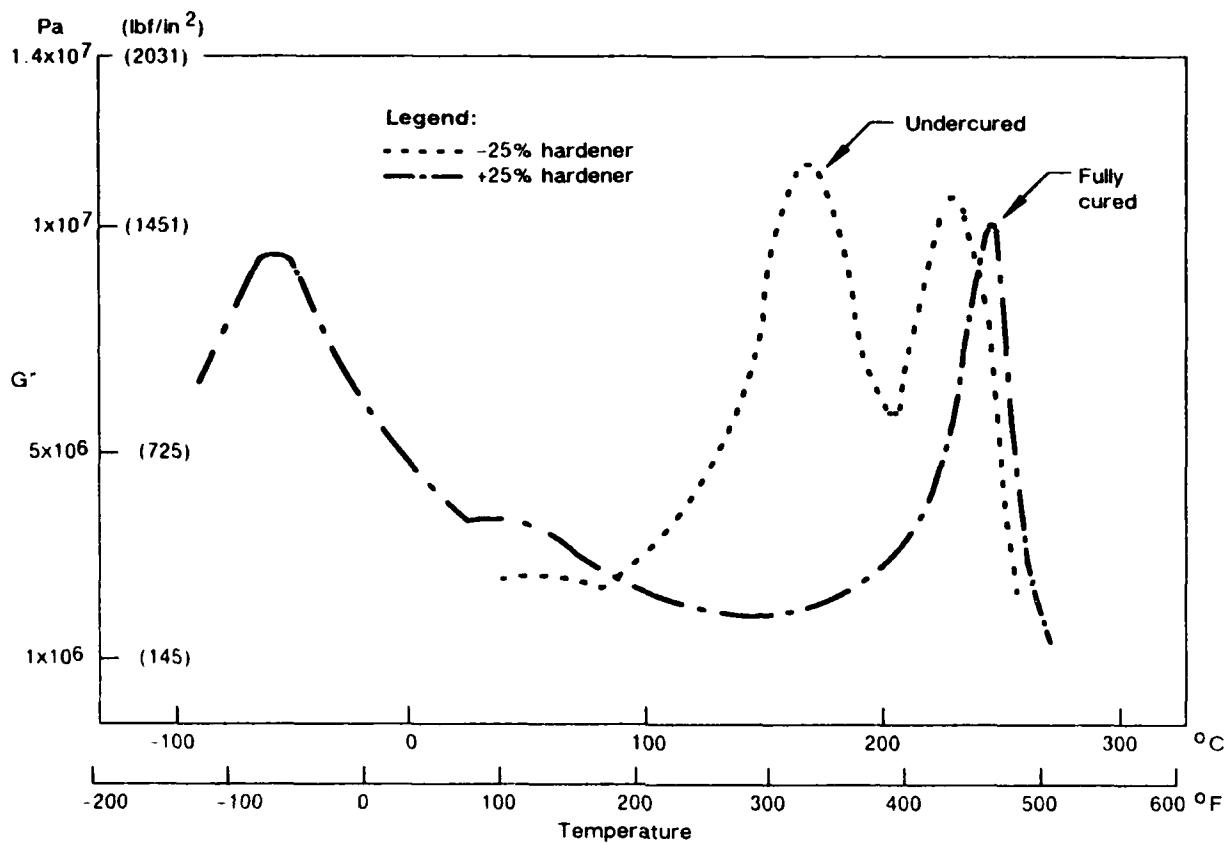
3.1.4.2 Extent of Unreacted Material

An undercured condition may be indicated by a lower than expected glass transition temperature determined as described in paragraph 3.1. However, a low glass transition temperature may also be due to environmental/moisture effects or to formulation errors. To show that the low glass transition temperature is due to undercure it may be necessary to determine the extent of reaction by analysis of the residual unreacted material, as shown in the materials characterization paragraph 3.1. Before testing for extent of reaction, glass transition temperature tests should be rerun on a desiccated laminate to eliminate moisture effects as a cause of low Tg.

The most effective means of determining the extent of unreacted material is by measuring the residual heat of reaction using DSC. This method has the advantage of small sample sizes and fast, simple experimental procedures. DMA can show the effects of both undercure and environmental exposure, although the larger sample size and difficult data analysis discourage widespread usage. Solvent extraction, with or without subsequent analysis using IR spectroscopy, may also be used to indicate extent of unreacted material. Excessive handling and analysis difficulty discourage these techniques.

Differential Scanning Calorimetry (DSC)—DSC can be used to measure the heat of residual reaction in a partially cured epoxy matrix. Experimental procedures as described in paragraph 3.1 are used on cured laminates. The heat of residual reaction is the area between the DSC thermogram and a baseline drawn from the reaction onset temperature, T_s , to the reaction completion temperature, T_c , as shown in Figure 3-24. The presence of measurable heat of residual reaction indicates some undercure. The extent of unreacted material can be calculated by dividing the heat of residual reaction by the total heat of reaction of the prepreg (paragraph 3.1).

Dynamic Mechanical Analysis (DMA)—DMA can be used to detect undercure and moisture degradation of cured laminates. Experimental procedures as described in paragraph 3.1 are used. An undercured laminate will exhibit a double high temperature peak in tangent delta and loss modulus plus an initial loss with subsequent recovery of storage modulus as shown in Figure 3-25. The initial softening (increase in tangent delta, loss modulus; decrease in storage modulus) is attributed to the glass transition of the original under-



Frequency: 1 Hz

Figure 3-25. DMA Loss Modulus Versus Temperature Showing Effect of Undercure for Epoxy Resin

5-B70227-154

cured material. As the test temperature increases, the matrix undergoes further cure allowing a recovery of properties. The final softening is due to the glass transition of the fully cured material. Laminates with absorbed moisture exhibit a peak in tangent delta and loss modulus at approximately 100°C due to the increased activity of moisture at this temperature. The presence of this peak indicates significant absorbed moisture in the laminate.

Solvent Extraction / Infrared Spectroscopy—This method can be used to remove low molecular weight (uncured or partially cured) polymer from the surrounding cured matrix. A solvent such as dimethyl acetamide (DMAc) or reagent grade acetone may be used to extract the uncured segments from a thin sample laminate. By weighing a solvent extracted and desiccated (moisture free) sample the percent of unreacted material can be calculated.

The extracted sample can be analyzed using IR spectroscopy. The test procedure is identical to that described in paragraph 3.1. The unreacted functional groups can be identified by the peaks in the IR spectra. The extent of reaction can be determined from the peak intensities by comparison to standard prepreg spectra.

3.1.5 Cured Material Contamination Analysis

Cured composites may contain defects due to contamination during manufacturing and assembly of composites structures. Foreign material contamination present in the cured composite is readily identified by an array of traditional chemical analysis tools. This paragraph addresses the methods for selecting the technique and interpreting the data. Emphasis is also placed on showing how the contaminant affects the fracture morphology and the ultimate integrity of the failed component.

The essence of a successful material contamination analysis is: (1) Recognition of the anomalous fracture morphology, (2) Exact documentation and interpretation of the anomalous features, (3) Chemical identification of the material contamination, (4) Establishing that the detected contamination is not an artifact of specimen handling or post-failure inservice exposures, (5) Identifying possible sources of contamination, and (6) Evaluating the criticality of the contaminant as related to crack growth and initiation.

Foreign material defects lead to lower crack propagation energies and corresponding a typical fracture morphology. Contamination analysis is initiated when anomalous crack propagation or foreign material inclusions are detected on the fracture surface during the course of the FALN execution. While performing optical microscopy or SEM examination of the fracture surfaces, the specific fracture morphology allows the analyst to classify the contamination as either a particulate or weak boundary layer contamination. This step is crucial to selecting the steps needed to chemically identify the contamination and to relate the analysis to the overall failure analysis and location of the origin. It is also crucial to be able to recognize artifacts created by sample preparation or due to postfailure exposure to contamination sources. The following definitions will serve to classify contamination types.

3.1.5.1 Particulate Contamination

In this case, inhomogeneous resin fracture will be observed with inclusion particles on the fracture plane with the optical or electron microscope. The particulate significantly reduces the net cross-sectional load bearing area leading to lowered properties such as reduced interlaminar shear and tensile strength. Although composites with their fiber reinforced construction are less sensitive to small localized defects, large particulates have been found to initiate failure. An individual particle defect, if located at a critical location, may also act as a crack initiation site with corresponding fracture lines radiating from the defect.

3.1.5.2 Weak Boundary Contamination

The presence of weak boundary surfaces account for the majority of crack initiation and subsequent component failures due to contamination. The weak boundary layer acts as a barrier to adhesive bonding between:

- Adjacent plies.
- Dissimilar materials or microconstituents such as fiber and resin or honeycomb core and laminate.
- Adhesively bonded subcomponents such as stringers and skin.

The weak boundary layer is formed by a chemical compound which interferes with the wetting and adhesion mechanism between the epoxy adhesive layers. Interfering chemicals such as hydrocarbons, fluorocarbons, and silicones are common in composite manufacturing as mold release compounds and parting agents. During the fracture event, the weak boundary layer provides a low energy crack propagation pathway through the structure. The fracture surfaces exhibit localized regions of smooth and featureless mating fracture surfaces, as opposed to normal fractures, where there is significant resin micro-flow deformation, hackle formation and secondary cracking. When stress analysis has indicated that a composite structure failed at a fraction of the design limit strength, and delaminations are present, weak boundary contamination layers should be suspected.

As illustrated in Figures 3-26, 3-27, and 3-28, contamination caused by Teflon paddle and Frekote release agent along the interlaminar ply interface exhibit inhomogeneous resin fracture as compared to a typical uncontaminated baseline fracture specimen illustrated in Figure 3-29. A second example of an isolated foreign particle inclusion, in Figure 3-30 illustrates the distinctive fracture surface asperity and crack initiation lines radiating from the particle. However, isolated particles will not significantly degrade the structural integrity of the composite. This is because the fibers already act as primary sites of crack initiation. As a result, low delamination strengths are expected and incorporated into the designs. Particulate contamination along these directions can be tolerated in moderate amounts without significantly affecting the performance.

Special care must be taken to avoid confusing the post-failure surface debris on the fracture surface with foreign particle inclusions in the resin. By definition the surface debris will not initiate radiating fracture lines. This is especially a problem where the fracture surface has had a long environmental exposure or experienced in-service cyclic loading conditions. Caution should also be exercised when extensive mechanical cutting was required to extract the specimen from the failed component. Often the particle shape can lead to identification of the contamination source where the particulate contains fractured carbon fibers and the source could be traced to machining debris. Another concern in examining a resin system with particles on the fracture surface is that the resin may have intentional particle additions (or phases) which improve properties or manufacturing characteristics. If there is a suspicion that the resin system may have been modified in this way, the analyst must prepare a lab fractured specimen for SEM examination as a reference fracture surface.

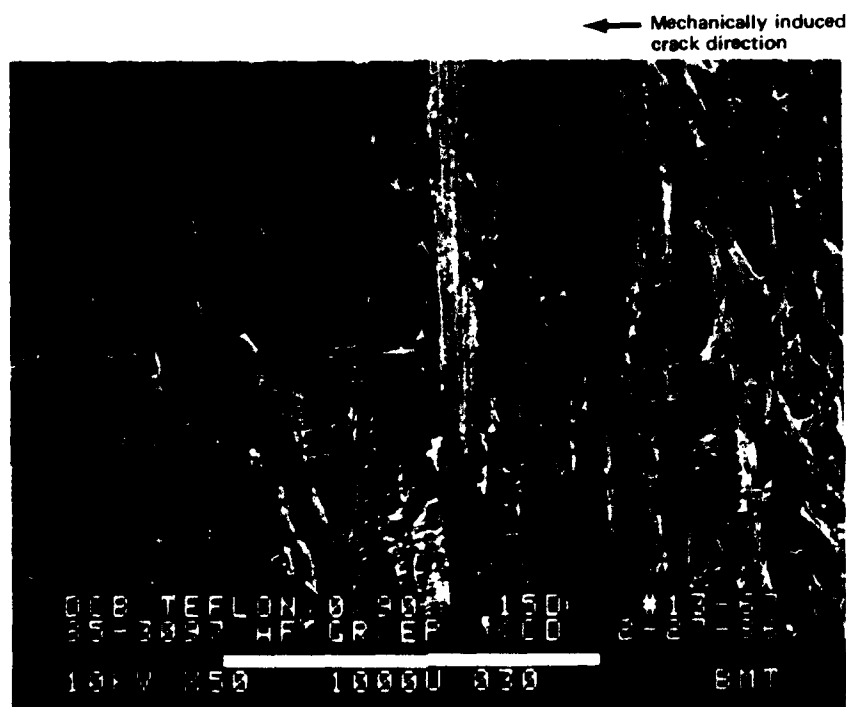


Figure 3-26. SEM Micrograph of a Teflon-Contaminated Tension Specimen

5-B70227-5

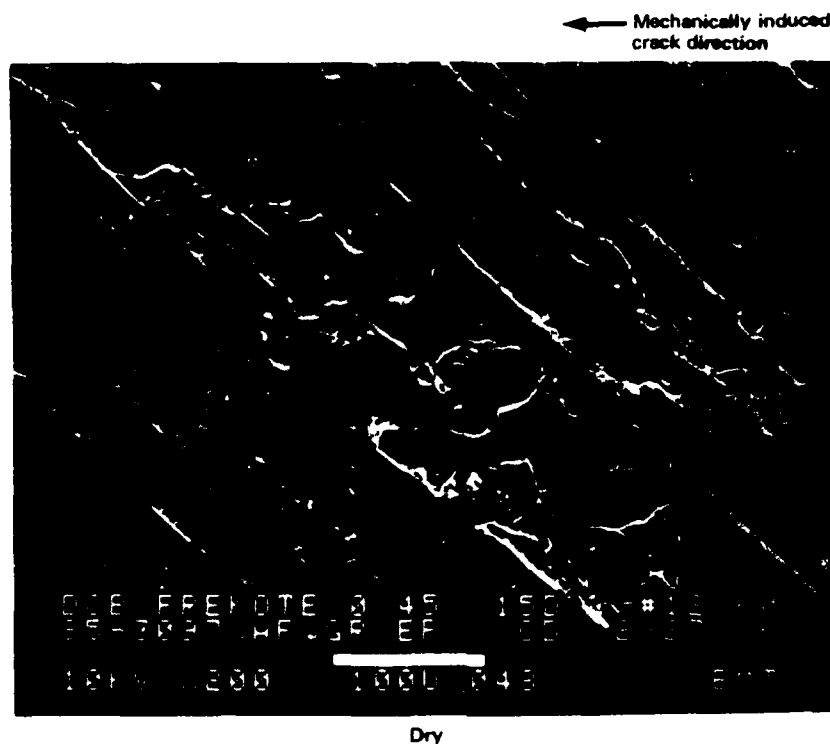


Figure 3-27. SEM Micrograph of a Frekote Release Agent Contaminated Tension Specimen (200X)

5-B70227-6

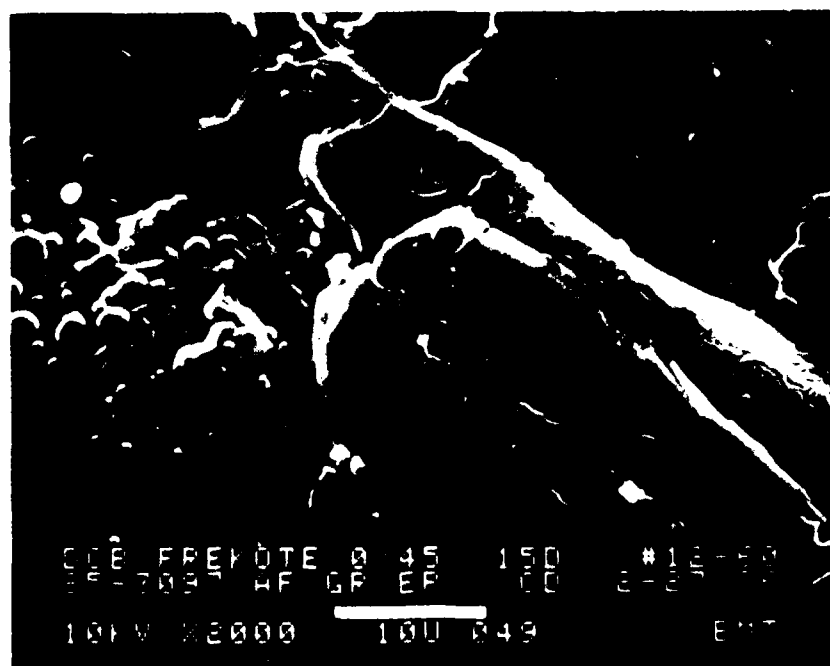


Figure 3-28. SEM Micrograph of a Frekote Release Agent Contaminated Tension Specimen (2000X)

5-B70227-7

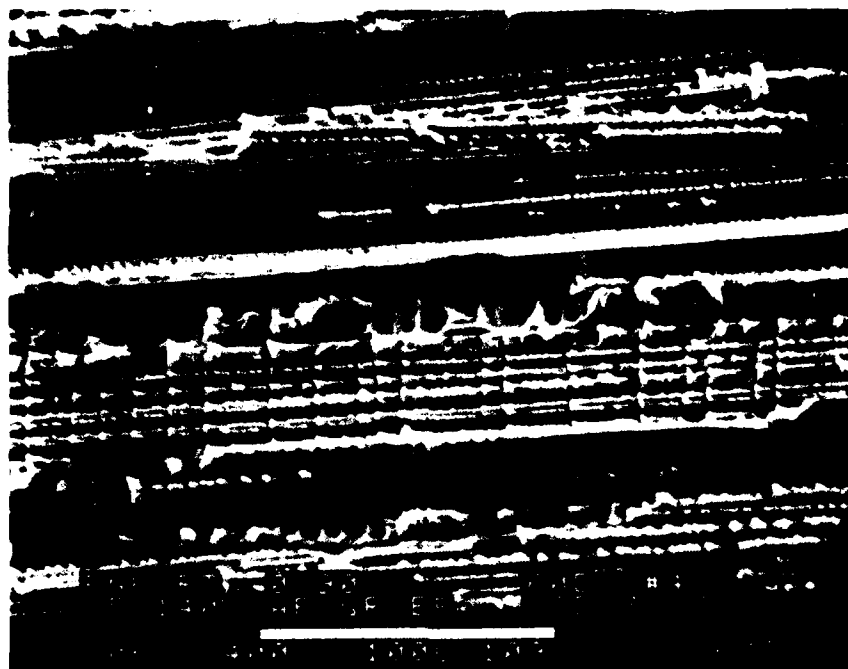
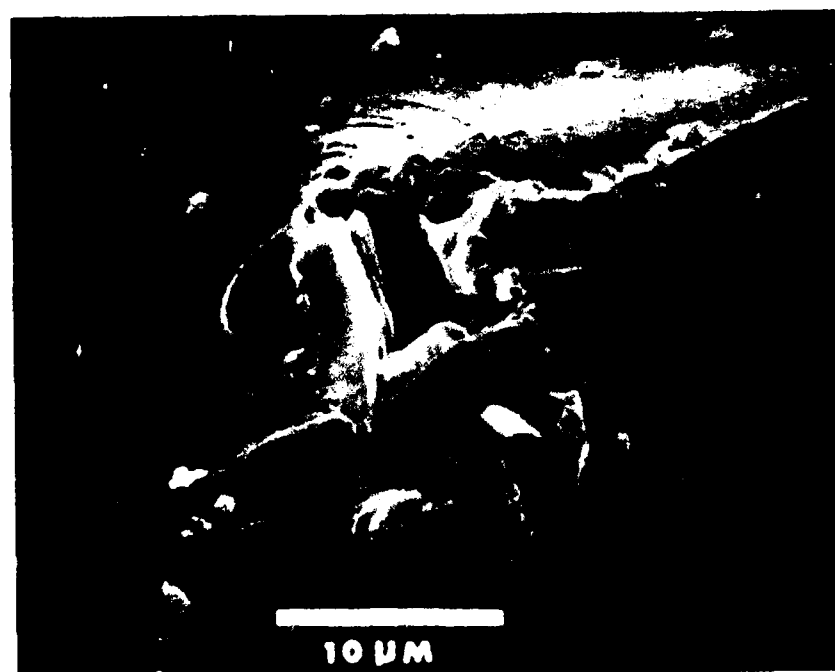


Figure 3-29. SEM Micrographs of a Typical Uncontaminated Fracture Specimen

5-B70227-8



*Figure 3-30. SEM Micrographs of Foreign Particle Inclusions
Illustrating the Characteristic Fracture Surface
Asperity and Radiating Fracture Lines*

5-B70227-9

The flow diagram in Figure 3-31 reviews the sequence of steps taken to perform initial inspections and to classify the contamination type. The next sequence of steps involve selection of the appropriate analytical techniques to make an accurate chemical identification of the contaminant. Direct chemical analysis probes can be very decisive in providing a chemical identification in a cost efficient manner. The flow diagram in Figure 3-32 for analytical work reflects this emphasis. A number of analytical techniques are recommended in order of decreasing information per unit analysis time for each application. There are specialists for each analytical technique whose expertise in instrumentation and spectroscopy will be required. The following paragraphs on analytical techniques are designed to inform the investigator of the special terminology used for these techniques and highlight special concerns which arise during a composite failure analysis. Paragraph 3.1 concludes with an applied example of contamination analysis during a failure analysis.

3.1.5.3 Scanning Electron Microscopy (SEM) and Electron Microprobe Analysis (EPMA)

The scanning electron microscope (SEM) and the electron probe microanalyzer (EPMA), commonly known as the electron microprobe, are powerful tools for identification of contaminant particles on a fracture surface. This paragraph covers the elemental detection capabilities of the SEM and EPMA for foreign particle detection. The microscopic image formation is covered in paragraph 3.3. These instruments are used when a quick qualitative identification is needed and provides information regarding selection of more detailed methods to be performed later.

The SEM and EPMA instruments are equipped with X-ray detectors to monitor the X-ray emission spectrum generated when a finely focused electron beam impinges on a microscopic feature of interest. Electron beam induced X-ray emission produces a spectrum unique to each element present allowing direct determination of particle composition. The analysis volume is determined by the electron beam energy and the density of the specimen surface. Typically the analysis volume is 0.5 to 2 micrometers in diameter. If the X-rays are measured with an energy detector then the analysis is termed Energy Dispersive Spectroscopy (EDS). If the X-rays are measured with a wavelength detector then the process is termed Wavelength Dispersive Spectroscopy (WDS). Each method has its own unique advantages. Conventional EDS can acquire a spectrum for all the elements

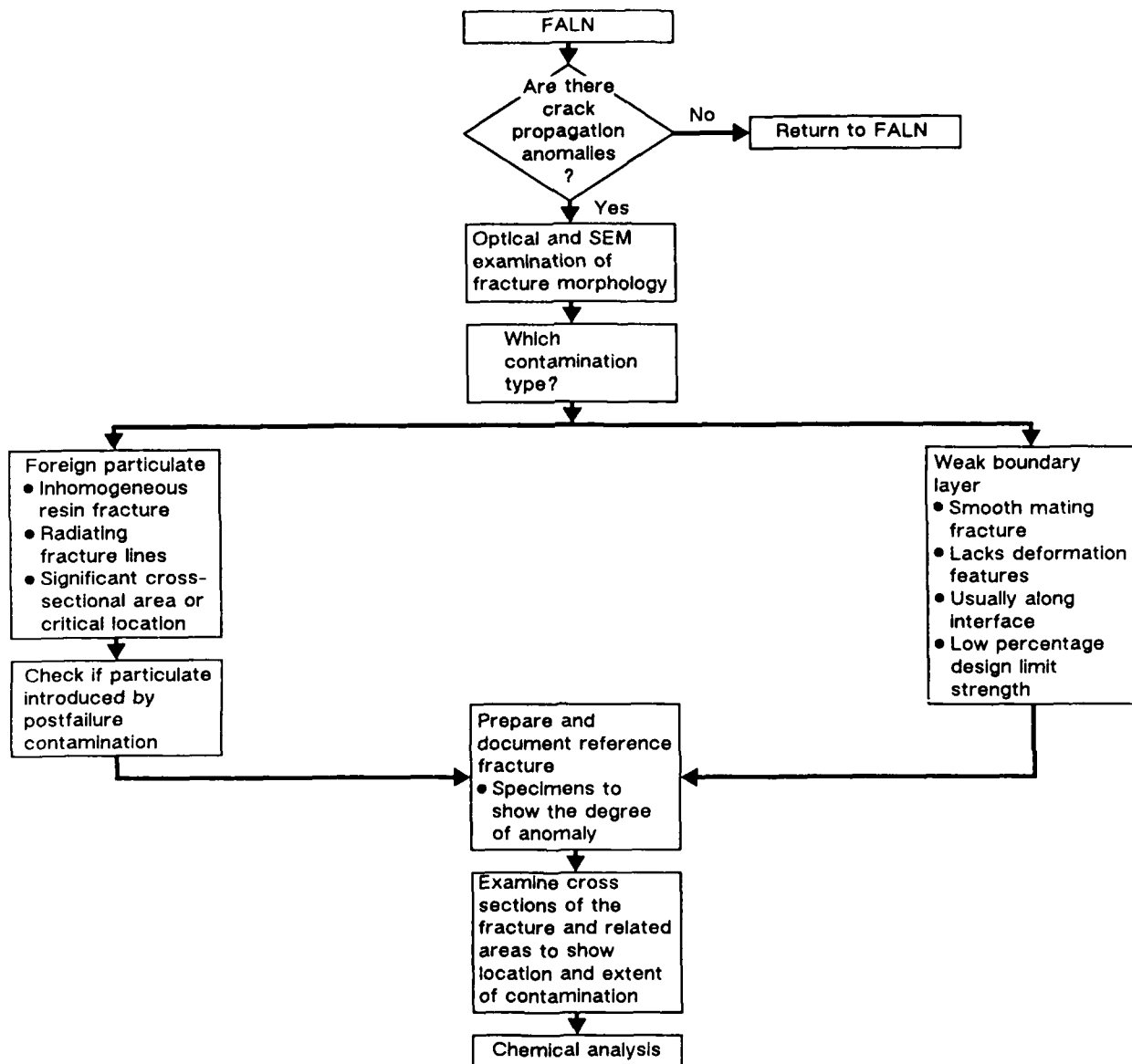


Figure 3-31. Flow Diagram for the Initial Inspection and Determination of a Foreign Material Contamination

5-B70227R1-153

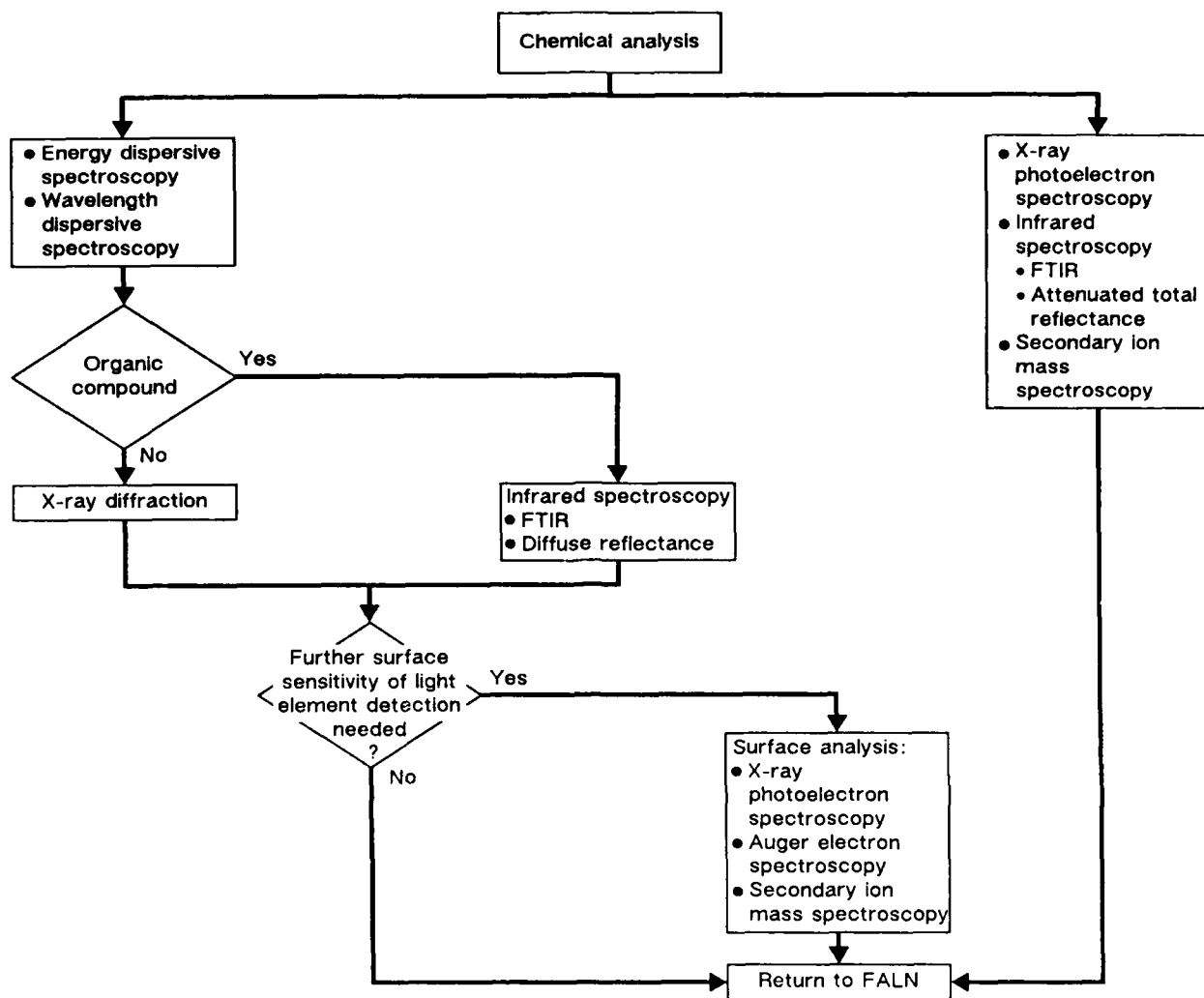


Figure 3-32. Logic Network for Chemical Analysis of Foreign Material Contamination of a Composite Fracture Surface

5-B70227R2-152

from sodium to uranium simultaneously in 30 seconds to a minute. (Ultra thin window EDS detectors can detect elements to the Boron range.) Because of the limited energy resolution of the EDS detector, there are a number of spectral peak overlaps. For example, aluminum and bromine peaks occur at 1.48 KEV. WDS has extremely high signal to noise sensitivity and resolution. WDS can also detect boron, carbon, oxygen and fluorine. The disadvantages are that only a single wavelength at a time can be detected, requiring many minutes to scan even a limited range of elements. Of concern to composites failure analysis is the ability to use WDS for light element detection. A partial list to assist the analyst in identifying elements by EDS and WDS is given in Figure 3-33. A SEM micrograph and EDS spectrum of talc contamination at a bondline is shown in Figure 3-34. The SEM reveals the sheet-like crystalline morphology and the EDS spectrum exhibits the primary elements typical of talc powders, magnesium and silicon, along with other particulate impurities.

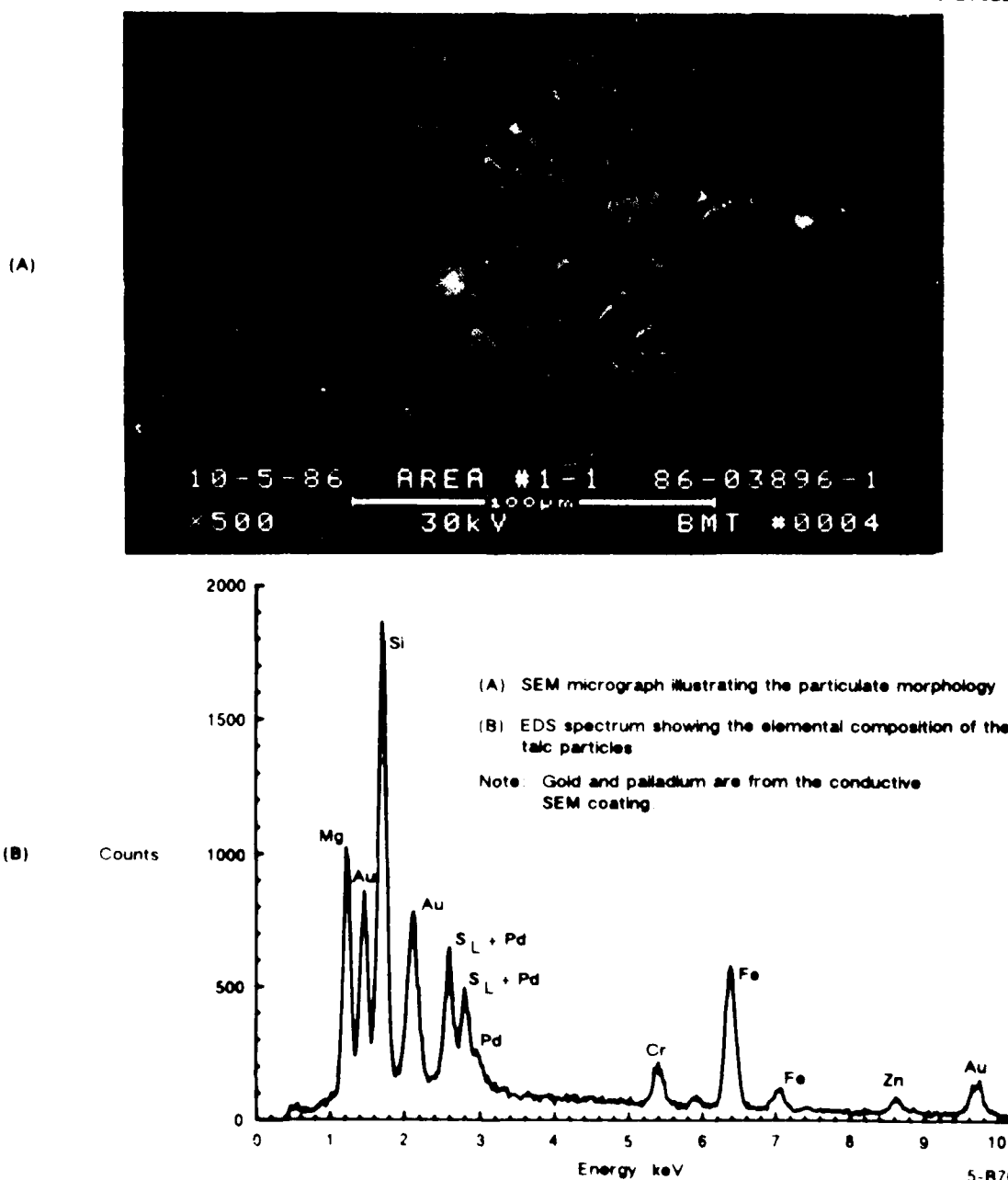
In using EDS or WDS several concerns should be mentioned. First, the composite specimen is introduced into an instrument vacuum chamber at pressure ranging from 1×10^{-8} torr to 1×10^{-4} torr. If the contaminant under investigation is volatile in the instrument's vacuum chamber, there is a possibility that important elemental information will be lost before analysis. Second, these techniques were originally developed as techniques to study conducting metal specimens. Polymers which are nonconductive present a specimen charge build up problem which is reduced by vapor depositing a conductive coating the specimen. Typically a very thin 5 nanometer film of gold or other noble metal alloys are used. These films provide interfering peaks in the X-ray spectrum which may mask elements of interest. When analyzing composite contamination, it is sometimes useful to coat these surfaces with conductive carbon since carbon is to be expected and will not be detected in the EDS spectrum. There is a significant literature base to suggest the electron beam can induce degradation and thermal effects to polymers. The degradation can be minimized by using low electron beam accelerating voltages and low current densities. Since WDS usually requires very high beam currents, this detection method should be used as quickly as possible to reduce the detrimental beam damage effects.

WDS	X-ray wavelengths (K_{α}), nm	EDS	X-ray energies, keV	
			$K_{\alpha 1}$	K_{β}
B	6.76	Na	1.04	1.07
C	4.47	Mg	1.25	1.30
N	3.16	Al	1.49	1.56
O	2.36	Si	1.74	1.84
F	1.83	P	2.01	2.13
		S	2.31	2.46
		Cl	2.62	2.81

(Ref. 4)

Figure 3-33. X-Ray Emission Lines, Partial Listing

5-B70227R1-151



5-B70227-011

Figure 3-34. Talc Powder Contamination Along a Bond Line

3.1.5.4 X-Ray Photoelectron Spectroscopy

X-ray Photoelectron Spectroscopy (XPS) is based on electron emission when a sample is irradiated with low energy X-rays. The process called photoelectron emission causes each element to emit photoelectrons at specific energies. All elements except hydrogen and helium can be detected by this method. Typical instruments analyze a square centimeter of surface area. The latest generation of instruments have a small spot XPS capability to analyze areas 100 micrometers in diameter. This development in XPS will make it increasingly important to the failure analyst. Several unique features arise from the physics of this process. The surface sensitivity of XPS arises from the very short distance that a low energy electron can travel in a solid without losing its initial energy. Since the detected electrons must travel to the detector without losing energy, detected electrons can only originate within this short characteristic distance (called the escape depth) from the surface. Typical escape depths in organic solids are 5 nanometers.

The XPS spectrum is expressed as the detected electron number versus electron energy. The measured kinetic energy (KE) relationship to binding energy (BE) of the electron from the parent atom is expressed as:

$$BE = h\nu - KE - \phi - V \text{ charge} \quad (\text{eq. 1})$$

where:

$h\nu$ = energy of X-ray source

ϕ = spectrometer work function

V charge = correction due to specimen charging.

The binding energies of some typically encountered elements are listed in Figure 3-35. Figure 3-36 is a typical spectrum of an epoxy resin where the elements carbon, nitrogen, oxygen and sulfur are shown. If one is examining a fracture surface for a chemical contaminant, comparison of the surface relative to a fresh cohesive resin fracture surface will provide a very sensitive test for the presence of foreign elements indicative of contamination.

Element	Binding* energy	Relative emission probability (cross section for aluminum X-rays) (Ref. 4)
Boron	195	0.49
Carbon	285	1.00
Nitrogen	399	1.80
Oxygen	531	2.93
Fluorine	689	4.43
Sodium	1072	8.52
Silicon	102	0.82
	151	0.96
Phosphorus	135	1.19
	189	1.18
Sulfur	165	1.68
	229	1.43
Chlorine	199	2.29
	264	1.69
Bromine	69	2.34

*Laminating energies change depending on how the elements are chemically bonded.

Figure 3-35. Approximate XPS Peak Positions and Emission Probabilities for Common Elements

5-B70227R1-150

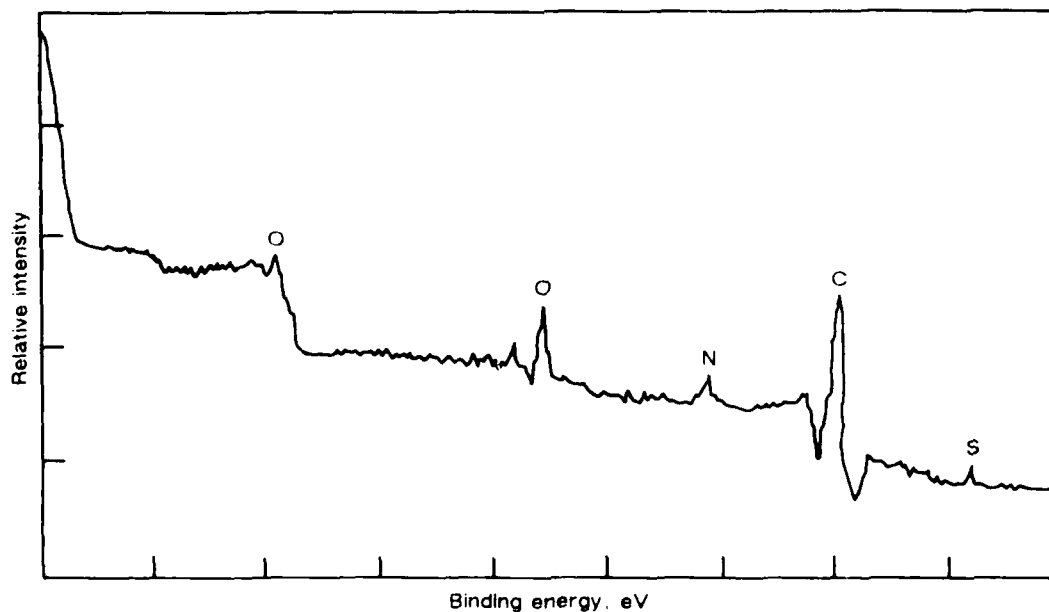


Figure 3-36. A Typical XPS Spectrum of an Epoxy Resin With Elements Identified

5-B70227-149

The details of XPS quantitation are unique to each instrument depending on design and detection efficiency. In Figure 3-35, the relative probabilities for photoelectron emission called cross-sections, are given. These factors would need to be adjusted for detection efficiency to obtain the relative sensitivity factor. Quantitation is accomplished by normalizing the observed intensities for each element and is expressed as:

$$\text{Element } x \text{ atom\%} = \frac{I_x/S_x \times 100}{\sum_i I_i/S_i} \quad (\text{eq. 2})$$

where:

S = relative sensitivity factor

I_x = observed intensities

x = each element

The binding energy concept is important because XPS peaks exhibit small binding energy shifts due to the chemical bonding environment of the parent atom. Chemical functional groups on the surface can be inferred from these binding energy shifts. Inspection of the equation also shows that the binding energy is dependent on the work function constant which is a spectrometer calibration constant and the specimen charge correction factor which is determined for each non-conductive specimen (the usual case for composite specimens). A charge correction can be made by shifting the binding energies so that the carbon 1s peak due to the hydrocarbon like chemical bond present in polymer resins occurs at 285.0 eV. Some investigators use alternate charge correction methods or a slightly different carbon 1s peak correction value (284.6 eV). So when making comparisons to published literature values, the author has to be careful. Figure 3-37 gives a partial list of the carbon 1s peak shifts which might be encountered with composite materials.

When analyzing a composite fracture surface for foreign material contaminants, low surface energy compounds or releasing agents are high on the list of potential contaminants. These compounds are typically hydrocarbon oils, fluorocarbons, or organic silicone oils. Figure 3-38 summarizes a few rules of thumb in interpreting the XPS data for these compounds. Figure 3-39 provides a partial list of materials which could be contamination sources.

Functional group	Binding energy, eV
Hydrocarbon	285.0
Ether or alcohol	286.5
Ketone	288.0
Ester	288.8

(Ref. 5)

Figure 3-37. Carbon Peak Shifts in XPS

5-B70227R1-130

• Hydrocarbon	<ul style="list-style-type: none"> • Excessively high carbon levels on the surface when compared with a cohesive resin fracture • Confirm by FTIR analysis of the residue from a solvent rinse of the fracture surface
• Fluorocarbon	<ul style="list-style-type: none"> • Carbon-shifted peak in the range 288.0 to 292.0 eV; fluorine peak at 689.0 eV • Ascertain whether there is a fluorocarbon additive to the resin • Compare with XPS spectrum of known fluorocarbon release agents or parting films used in manufacturing the part
• Silicone	<ul style="list-style-type: none"> • Silicon peak at 102.0 eV; silicon Auger parameter in the range 1708.5 to 1709.5 eV • Where there are significant silicon levels, the carbon-to-oxygen ratio will exceed the resin value • Because some inorganic minerals exhibit the same XPS shifts, verify that there are no inorganic mineral particulates on the fracture surface with SEM/EDS • Ascertain whether there is a silicon additive to the resin • Confirm by FTIR analysis of the residue from a solvent rinse of the fracture surface • Compare with XPS spectrum of known silicon release agents used in manufacturing the component

Figure 3-38. Rules of Thumb for XPS Identification of Typical Release Agents

5-B70227R1-131

<ul style="list-style-type: none"> • Molding tool release compounds and sprays • Parting films and breather fabrics • Prepreg backing papers and films • Solvent impurity residues • Vacuum pump oils • Machining debris • Plastic resin sweeps • Gloves • Vacuum bags • Molding compounds, vacuum bag sealants

Figure 3-39. Partial List of Possible Contamination Sources

5-B70227-132

3.1.5.5 Infrared Spectroscopy (IR) and Fourier Transform Infrared (FTIR)

Infrared Spectroscopy (IR) is the primary technique for identifying the compound or chemical family in which a foreign organic contaminant belongs. Infrared spectroscopy is much less sensitive than XPS or EDS/WDS but provides more chemical information. Special techniques have been developed to apply IR to the weak boundary layer and the particulate contamination problem. These methods are addressed in the following discussion.

Organic polymer molecules absorb infrared radiation at frequencies which relate to the chemical bonds within the molecule. The physics of this process can be attributed to a mechanism where the infrared light is absorbed at discrete frequencies associated with characteristic molecular vibrations within the molecule. This principle forms the basis of Infrared Spectroscopy as an analytical technique to characterize polymer resins. Each polymer molecule absorbs infrared light in a distinctive pattern which can be used to fingerprint the molecule. Figure 3-40 illustrates a typical IR spectrum of an epoxy spectrum. In a contamination analysis where one is investigating an unknown identification, it is useful to compare the spectrum of the unknown with infrared spectra of model compounds published in an atlas or stored in a data base. Infrared spectra are usually plotted as intensity versus wavenumber (CM-1), wavelength (micrometers or microns), or frequency (s-1).

Intensity can be expressed as percent transmittance or absorbance as shown in the following equations.

Percent Transmittance

$$\%T = \frac{I}{I_0} \quad (\text{eq. 3})$$

where:

%T = percent transmittance

I = selected radiation

I₀ = incident radiation

Absorbance

$$A = \text{Log } (I/I_0) \quad (\text{eq. 4})$$

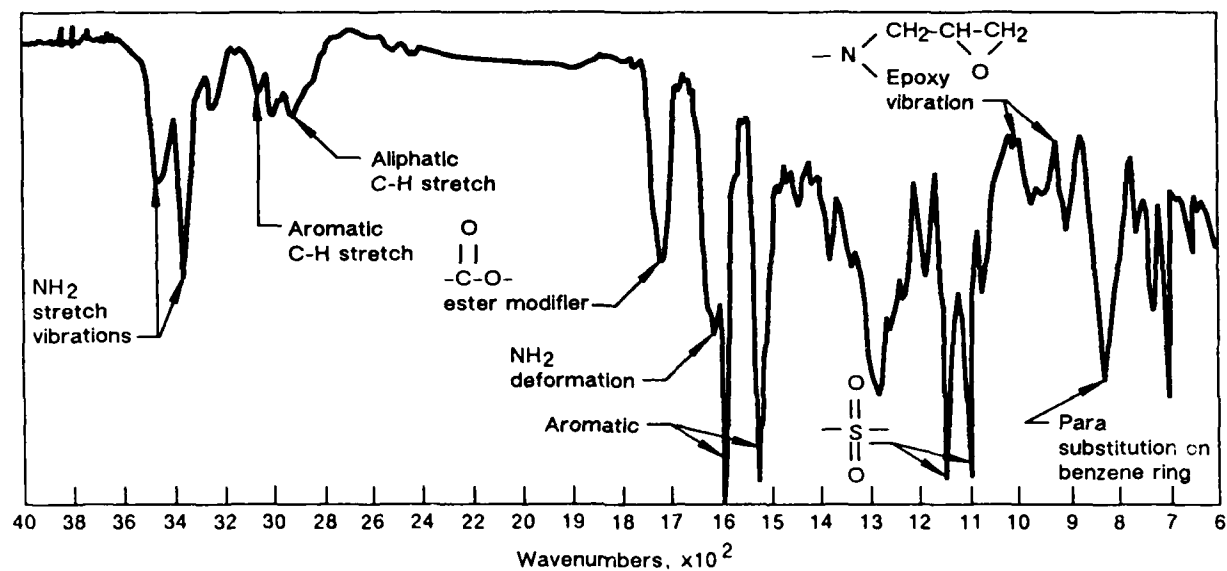


Figure 3-40. Infrared Spectrum of an Epoxy Resin

5-B70227-135

where:

A = absorbance

I = detected radiation

I₀ = incident radiation

Recently several developments in the field of IR analysis have allowed the technique to become more practical for solid materials involved with composite failure analysis and contamination analysis. The first development is the use of Fourier transform infrared (FTIR) instruments. It is orders of magnitude greater in sensitivity than conventional IR instruments. It is almost a necessity to select the FTIR instrument for sensitive contamination detection. The FTIR sensitivity can be used to complement the XPS in weak boundary layer identification. The analysis can be approached from several directions. First, a fracture surface can be rinsed with an ultra-pure solvent, such as methylene chloride, which is allowed to evaporate on a salt pellet (the standard specimen holder). The residue can then be analyzed as in conventional FTIR transmittance analysis. Often there is enough material on a contaminated surface to be detected and the increased chemical information increases the reliability of the contamination source identification. If a large amount of particulate contamination can be isolated then particles can be dispersed into a salt and then consolidated into a pellet. Often a reasonable spectrum can be obtained.

Reflectance methods are desirable in order to avoid the use of removal methods described above. The Attenuated Total Reflectance (ATR) method is implemented on an FTIR instrument which uses an infrared transparent crystal with a high refractive index. The IR radiation is then caused to propagate through the crystal and the near surface region of a specimen. The depth of penetration is typically 0.5 to 2 micrometers. The method has a limited application to fracture surfaces since it requires a fairly smooth and flat surface to obtain a spectrum. Diffuse reflectance, an older reflectance method, is coming back into use on the FTIR instruments. This method relies on the detection of scattered or radiation directly from a solid surface. The technique has seen limited application in analysis of rough surfaces which are usually encountered in composite fracture.

AO-A103 703

COMPENDIUM OF POST-FAILURE ANALYSIS TECHNIQUES FOR
COMPOSITE MATERIALS(U) BOEING MILITARY AIRPLANE CO
SEATTLE WA R A GROVE ET AL. JAN 87 AFMAL-TR-86-4137

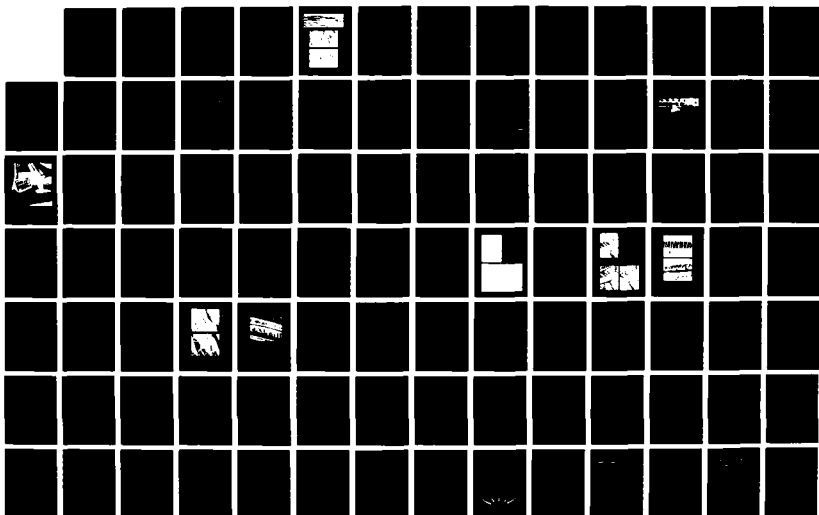
2/5

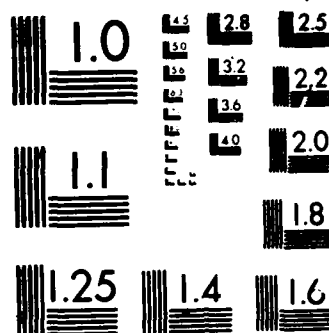
UNCLASSIFIED

F33615-84-C-5010

F/G 11/4

NL





MICROCOPY RESOLUTION TEST CHART
 NATIONAL BUREAU OF STANDARDS 1963 A

3.1.5.6 X-ray Diffraction (XRD)

X-ray diffraction (XRD) techniques are used for a wide variety of crystal structure determinations. In composite failure analysis, XRD is primarily used for crystalline foreign material particulates which can be isolated from a fracture surface. The cylindrical Debye-Scherrer or Gandolfi camera is commonly employed for crystal phases in identification of particles. The basis for X-ray diffraction is given by Bragg's law:

$$\lambda = 2d \sin \theta \quad (\text{eq. 5})$$

where:

λ = wavelength of incident X-ray beam

θ = measured angle of diffracted beam

d = crystal lattice spacing

X-rays diffracted from a particle strike a film from which the diffraction angle θ is measured and consequently the crystal lattice spacing is determined. A tabulated index of lattice planes (ref. 5) can be searched for compound identification.

3.1.5.7 Secondary Ion Mass Spectroscopy (SIMS)

Secondary Ion Mass Spectroscopy (SIMS) can be used to obtain several information levels about the surface and near surface region of a solid material. SIMS is used in composite failure analysis of weak boundary layers when XPS cannot provide sufficient sensitivity or chemical information. SIMS is based on energetic ion beam impact (or sputtering) on a surface with subsequent ionization and removal of the surface atoms. The ejected surface ions are then detected with a mass spectrometer. The plotted spectrum of intensity versus atomic mass units (amu) can be interpreted to identify the elements or molecular fragments of the parent molecule. A number of SIMS instruments exist to perform specific functions. The simplest SIMS instrument (often the most frequently encountered) requires very high sputter removal rates to provide sufficient secondary ions to the detector. These instruments operating in the dynamic SIMS mode can be used for detecting extremely low levels of elements as a function of depth into the surface. Due to the very high current densities involved, this method does not work well on non-conducting composite surfaces due to specimen charging. Static SIMS applications use very low sputter removal rates to characterize the surface molecular layer. Future

improvements in this method to allow routine polymer characterization may find significant uses to complement XPS analysis of composites. The SIMS microprobe, a variation of the static SIMS instrument, has an imaging capability which can be used to characterize particulates and map chemical inhomogeneities across the surface.

3.1.5.8 Auger Electron Spectroscopy (AES)

Auger Electron Spectroscopy (AES) is a surface analysis technique based on electron beam induced Auger electron emission, characteristic energy for each element, and escape from the surface in a manner analogous to XPS. In fact, many surface analysis instruments are designed to perform AES and XPS with the same spectrometer. Since AES requires a conducting specimen its applications are limited in composite analysis. However since the carbon fibers are conductive, AES can be useful in determining whether an exposed carbon fiber failed at the fiber matrix interface or in the resin. The analysis is based on the elemental differences between the fiber and the surrounding resin (which may be a sizing resin different from the nominal epoxy resin composition) as shown in Figure 3-41.

Usually preparation methods are required to provide a conductive path from the fiber to the sample holder.

3.1.5.9 Contamination Analysis Example

A secondarily bonded composite structure was returned from service after visual inspection revealed surface cracks on the outer painted skin surface. The composite construction had a laminated skin bonded to a honeycomb core. The bonding adhesive was a FM-300 adhesive. When the composite part was sectioned, it was noted that the paint cracking resulted from the skin buckling away from the honeycomb. An optical cross section is shown in Figure 3-42. Optical microscopic examination revealed the FM-300 adhesive separated along the centerline of the adhesive layer. SEM micrographs of mating separation surfaces are shown in Figure 3-43. The smooth surfaces lack any significant evidence of fracture features or resin deformation, indicating that a low energy adhesive failure had occurred. The adhesively separated surface followed the contoured boundary between two plies of adhesive. The mating surfaces are perfect replicas of each other. Even the protruding scrim fibers of one ply made an impression on the other ply without showing any evidence of bonding.

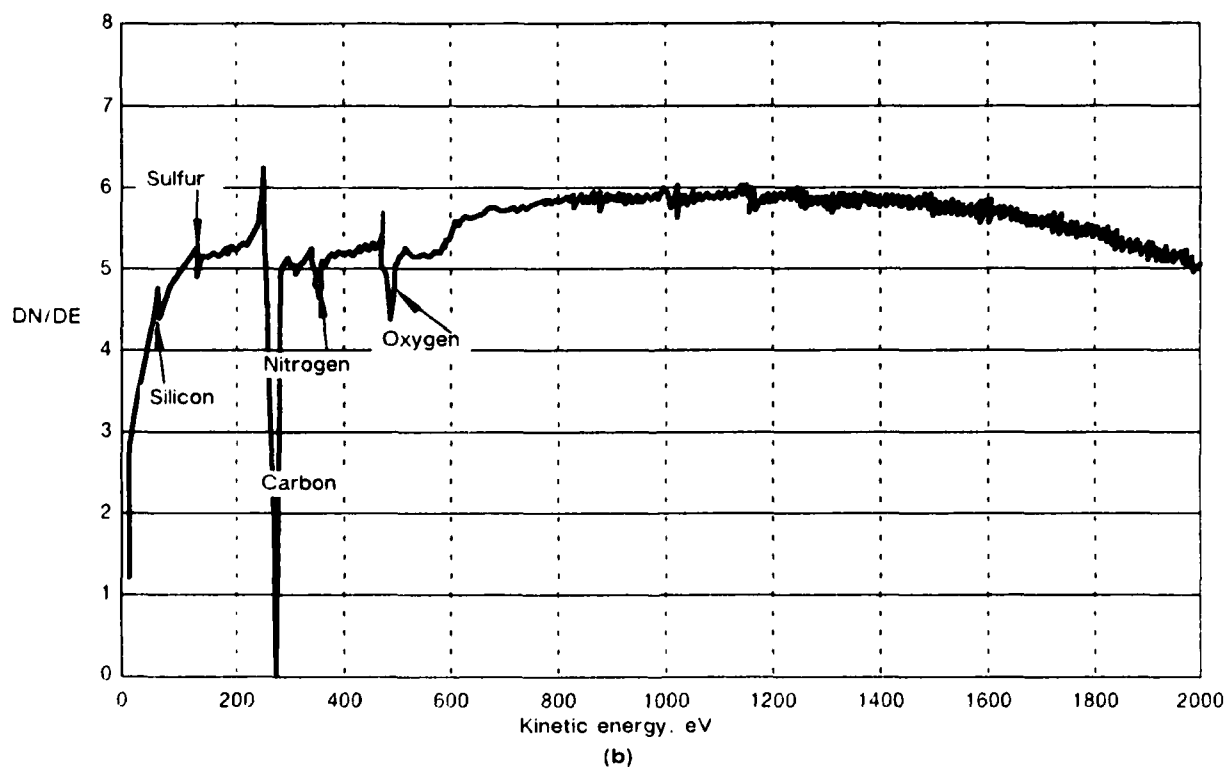
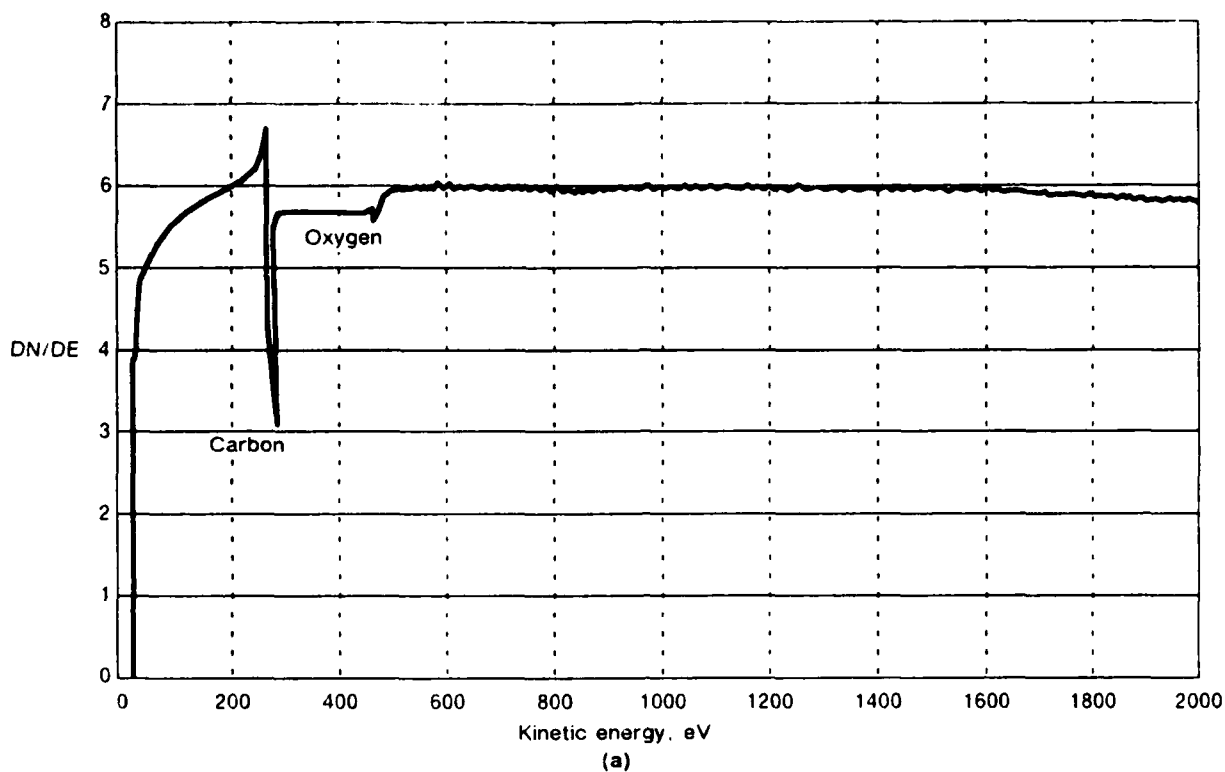


Figure 3-41. AES Spectra of (a) Carbon Fiber and (b) An Exposed Carbon Fiber on a Tensile Fracture

5-B70227-136

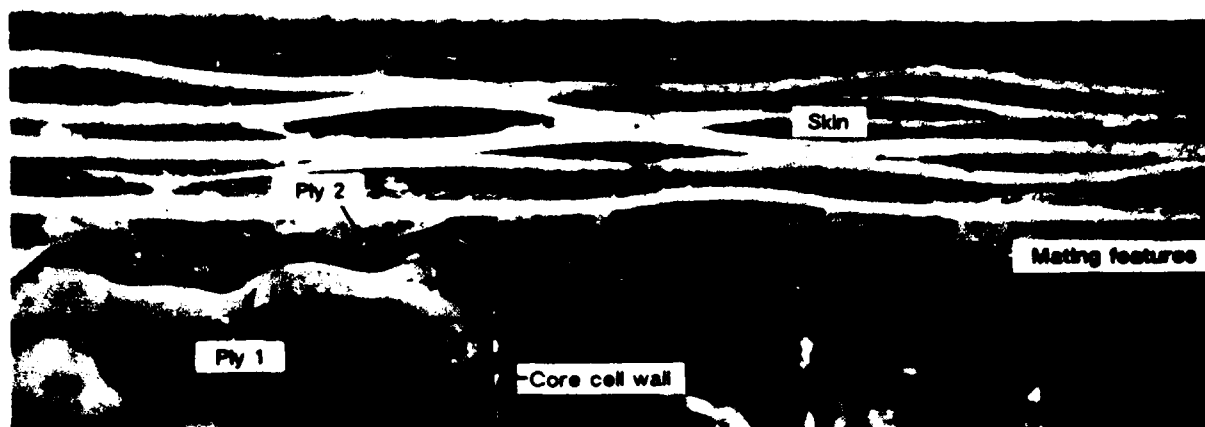
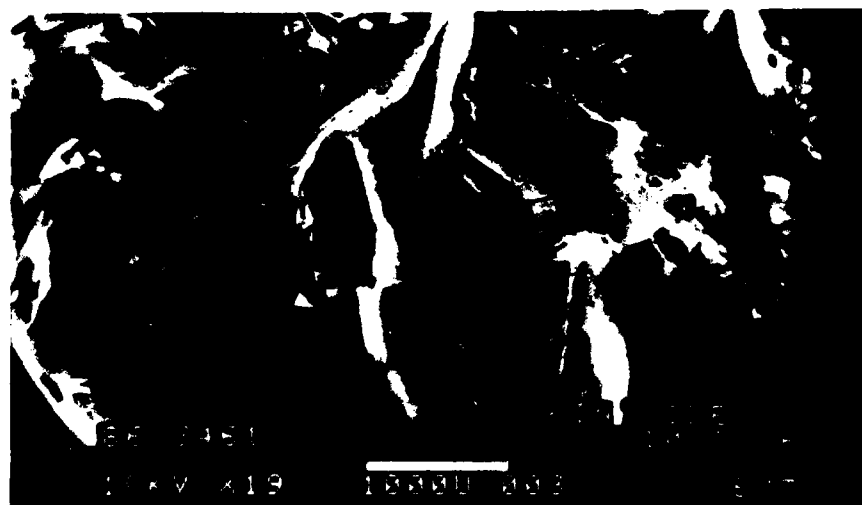


Figure 3-42. Optical Micrograph in Cross Section of a Laminate Skin to Core Buckling Separation

5-B70227-12



Mating features

Scrim impression



5-B70227-13

Figure 3-43. SEM Micrographs Showing a Replicated Surface Morphology

The XPS spectra of the debonded surfaces shown in Figure 3-44 revealed a significant amount of silicon, fluorine and carbon in addition to the expected composition of the adhesive. XPS peak shifts indicate the presence of silicone, fluorocarbon, and hydrocarbon chemical functional groups. The next step was to rinse the fracture surfaces with methylene chloride solvent and allow the soluble residues from the surfaces to precipitate on a salt pellet. The residue was then analyzed with the FTIR where hydrocarbon oils were identified in the spectrum. It was important to remember that these surfaces may have experienced a significant exposure to contaminants from the service environment. Because the SEM micrographs implied the weak boundary layer was present during the curing of the adhesive by the presence of scrim fiber impressions on the mating adhesive plies, the contaminant must have been present during manufacturing and curing of the bondline.

Using this assumption, areas of the composite part with similarities of location and construction (the disbond occurred adjacent to a core dropoff) were examined for bondline integrity. To ensure that no secondary contamination would occur, the part was cut with hand shears (cleaned in a solvent) which produces very little particulate damage. The part was also cut in the analytical lab well away from fabrication and machining areas where contaminants can be easily introduced. The result was that the adhesive bondline was easily separated by hand after being cut out with the shears. Separation occurred in a similar manner at the interface between the two adhesive plies and the mating surfaces were smooth and featureless. The advantage of finding these weak boundaries is that the specimen can be separated and introduced into the XPS spectrometer within minutes thereby ensuring that any contaminant found is directly related to the original debonding. Figure 3-45 shows the XPS spectra in which the primary contaminant is silicon with the appropriate shift expected for a silicone release agent. Subsequent FTIR analysis of the soluble residues rinsed from the surface did not detect any anomalous functional groups, which implies the contamination is very minute.

3.2 NONDESTRUCTIVE EVALUATION (NDE) TECHNIQUES

In the broadest sense, nondestructive evaluation (NDE) includes any examination that assesses material integrity without damaging or destroying a component, and it is used for a variety of tasks such as in-process quality control, in-situ test monitoring, and fleet

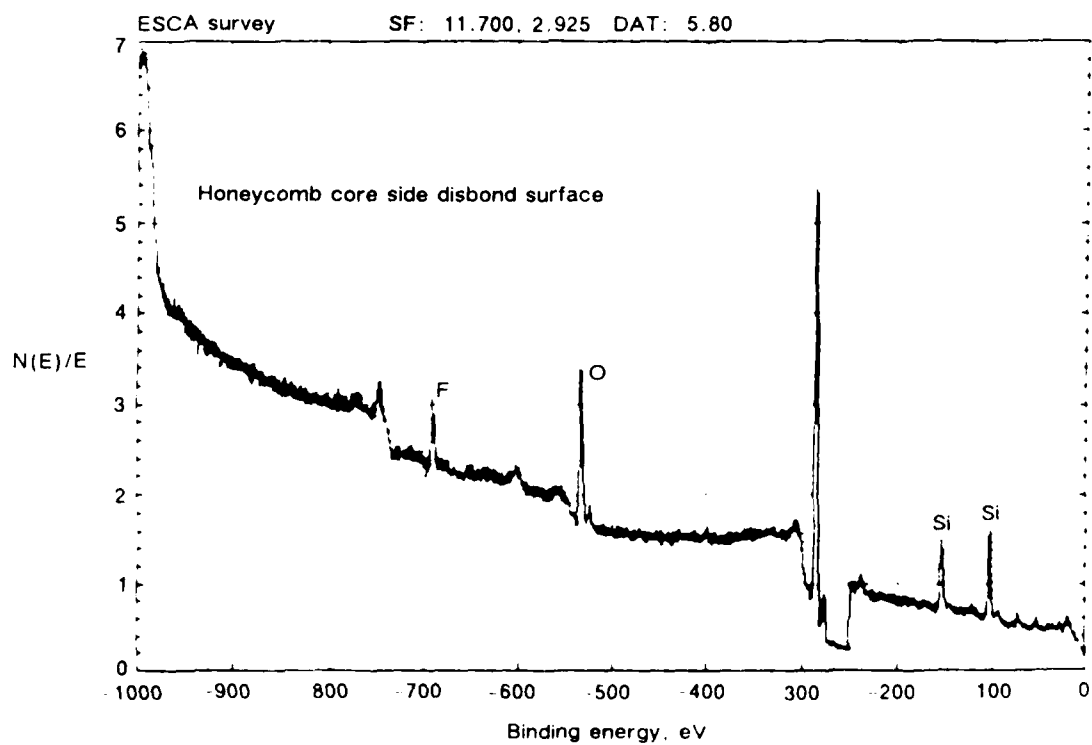
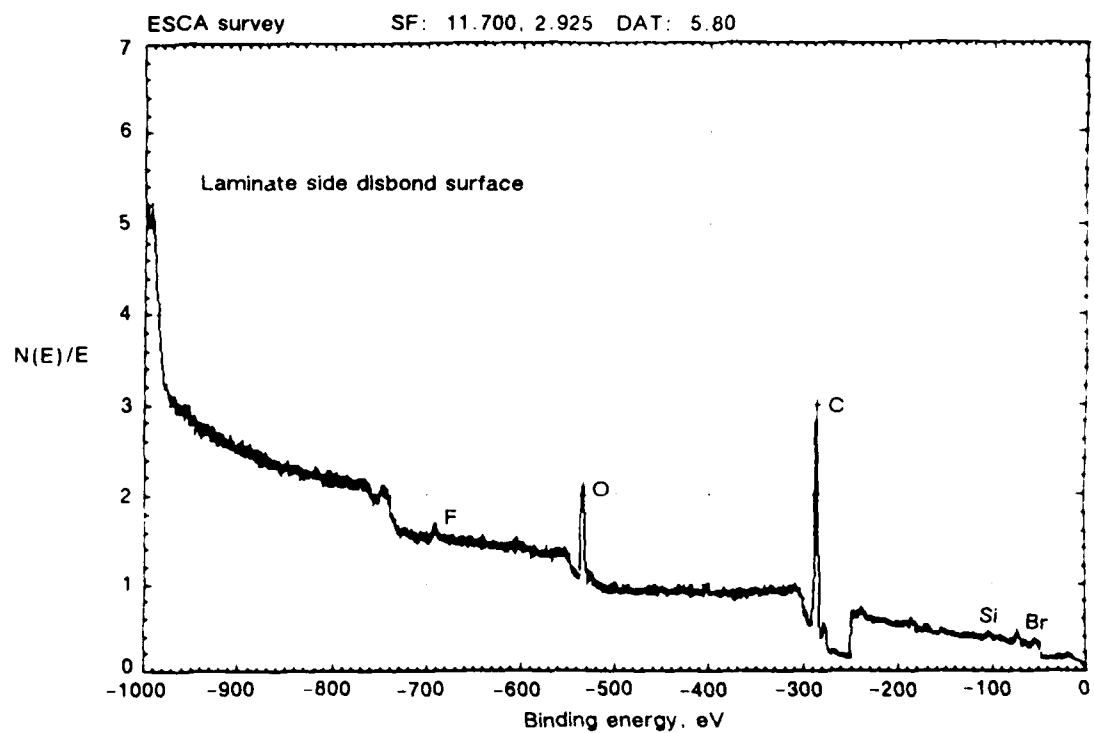


Figure 3-44. XPS Spectra of the Disbonded FM-300 Ply Surfaces

5-B70227-137

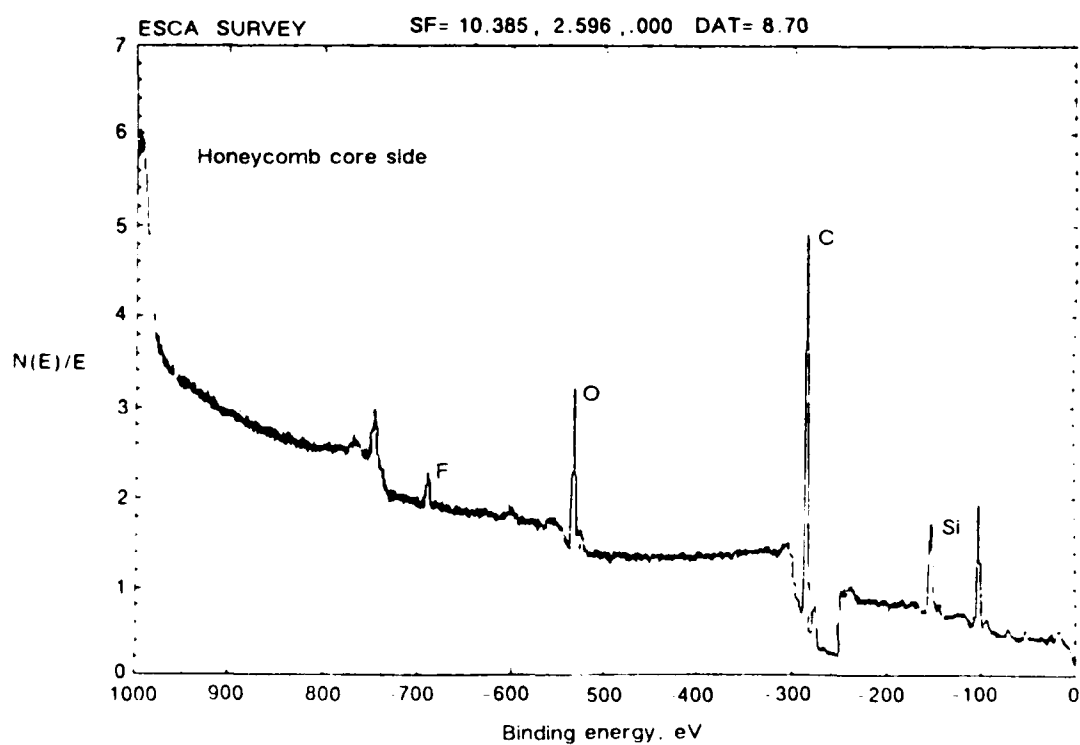
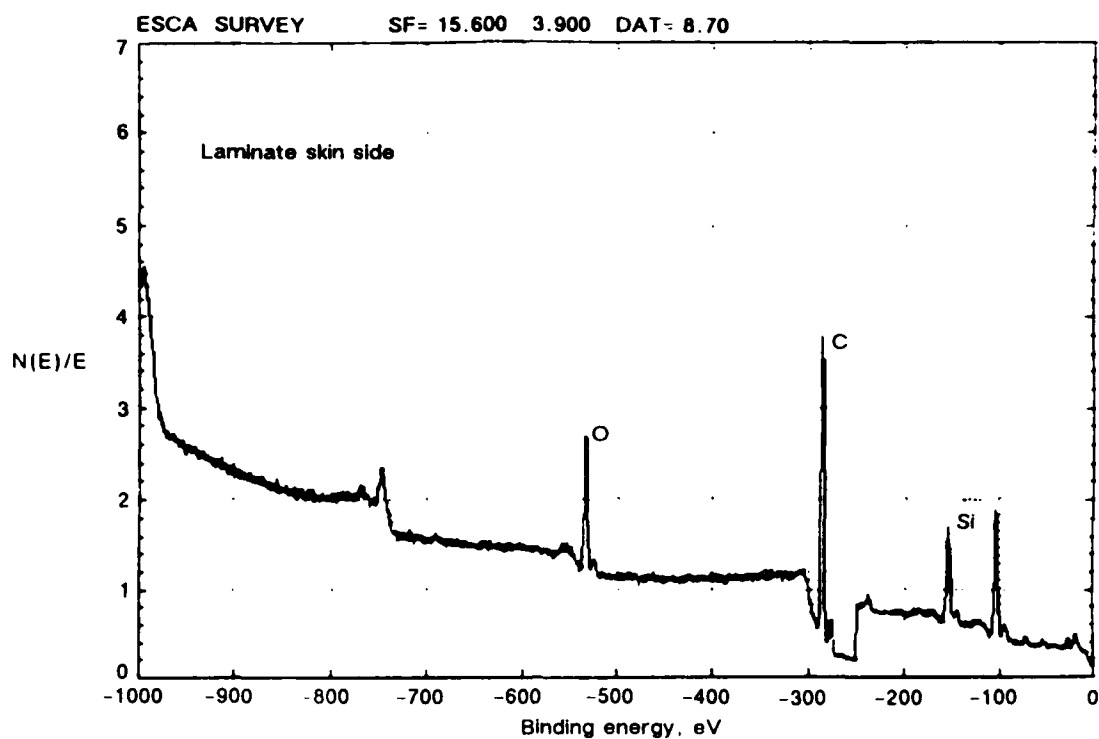


Figure 3-45. XPS Spectra of FM-300 Ply Surfaces Separated by Hand in the Laboratory

5-B70227 138

service inspection. For failure analysis, nondestructive evaluations are useful for identifying the conditions of invisible fracture for documentation, and for planning subsequent destructive evaluations.

Following preliminary visual and macroscopic analysis of the failed component, invisible damage can be identified and evaluated by various techniques outlined below. Figures 3-46 and 3-47 (a and b) present a summary of the various methods commonly used for failure analyses, as related to typical defect or damage conditions. Note that the methods are listed in the order of preference for evaluating and defining each defect condition. The NDE FALN is structured such that inspections involve progressively more detail of the damage condition, including:

- Initial plan view inspections.
- Detailed plan view inspections.
- Through-thickness inspections.

It should be noted that a majority of the failure analyses investigations do not require detail beyond the initial plan view inspections. Usually failure of the part denotes that some fairly extensive fracture, often visible, has occurred. The main responsibility of NDE inspection is to define the damage region around the primary fracture. More detailed analyses, if performed, are usually confined to other regions on the component, away from the principle fracture region, so as to identify other sites of damage or contributory defects.

A. Initial Plan View Inspections—For preliminary inspections, the major emphasis is to determine the basic outline of the damage regions such that part breakdown and sectioning can be performed without destruction of evidence or to minimize the sectioning damage if a repair scheme is considered. Plan view analyses such as ultrasonics (TTU or pulse echo) and radiography are by far the most versatile and encompassing techniques for overall determination of the basic outline of the damage region. Commonly, this coarse damage assessment is necessary for field inspection prior to part breakdown, sectioning and subsequent detailed NDE techniques performed in the laboratory. In the field, pulse echo is the preferred method, particularly desirable in conditions where only one side of the structure is accessible. When this initial inspection can be performed in the laboratory,

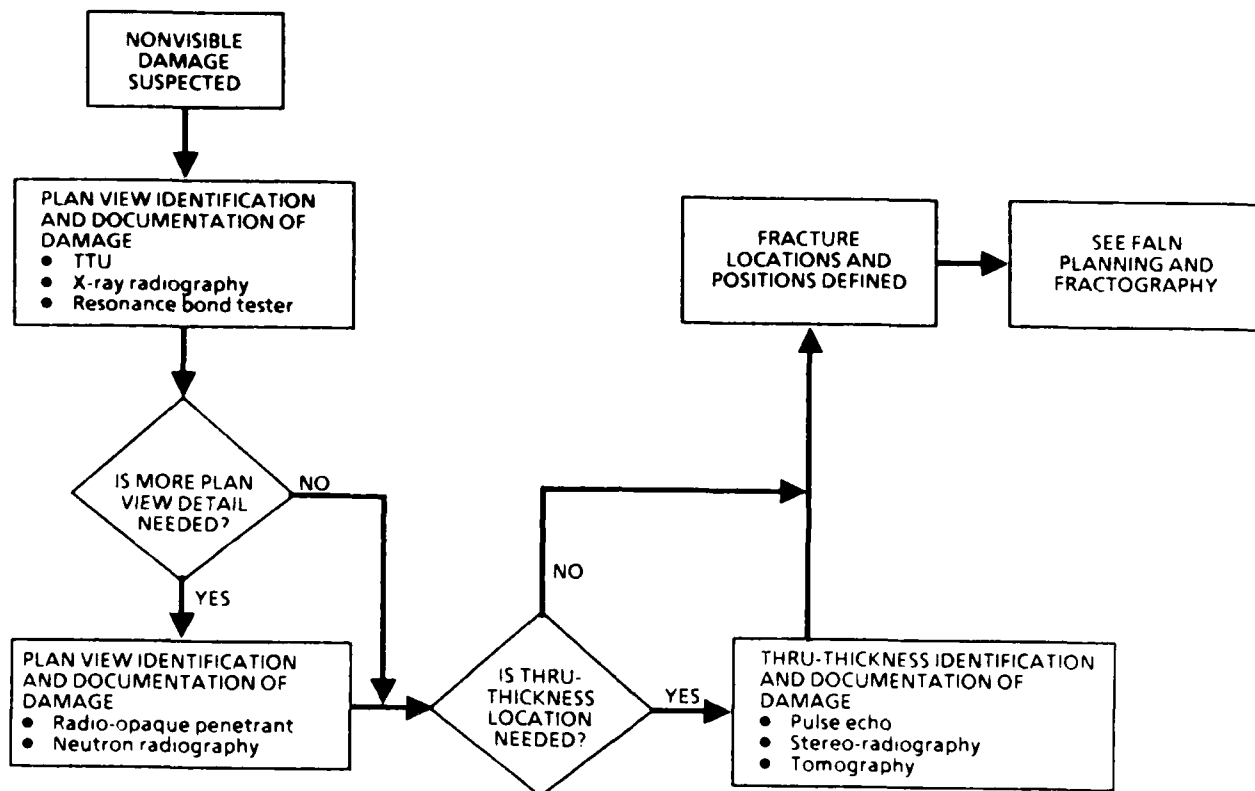


Figure 3-46. Nondestructive Evaluation Sub-FALN




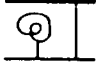
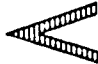


5-B70227-76

TECHNIQUE*	DESCRIPTION	USE	VALUE
Thru-transmission ultrasonic (TTU) • C-Scan	Measures ultrasonic sound attenuation • C-Scan – plan view presentation	Determines size and location of nonvisible damage, defects, fracture in plan view	<ul style="list-style-type: none"> • Plan view documentation of failure • Plan view assessment of part quality • Planning analyses
Pulse ultrasonic • B-Scan • C-Scan	Measures ultrasonic sound reflection • B-Scan – thru-transmission view presentation • C-Scan – plan view presentation	Determines size and location of damage, defects, fracture in both a plan and thru-thickness view	<ul style="list-style-type: none"> • Plan view documentation of failure • Thru-thickness view documentation of failure • Plan view assessment of part quality • Thru-thickness assessment of part quality • Planning analyses
Reasonance bond testers • Bondascope 2100 • Sondicator • Acoustic flaw detector • MIA 3000	Measures mechanical resonance changes caused by defects, meter or CRT display	Determines size and location of nonvisible damage	<ul style="list-style-type: none"> • Determining of size and location of part damage • Method can be used when only one side is accessible
X-ray radiography (tomography)	Measures X-ray attenuation plan view presentation	<ul style="list-style-type: none"> • Determines size and location of translaminar fractures and radio-opaque defects – plan view presentation • Delamination size and location determined with radio-opaque penetrant • Thru-thickness position determined by stereo-radiography or X-ray tomography 	<ul style="list-style-type: none"> • Plan-view documentation of failure • Plan view assessment of part quality and defects • Planning analyses
Neutron radiography	Measures neutron attenuation plan view presentation	<ul style="list-style-type: none"> • Determines size and location of translaminar fractures and neutron opaque defects – plan view presentation • Delamination size and locations determined with neutron-opaque penetrant • Used often where metal structure overlays composite material – neutrons are not as attenuated by metal as X-ray, and are relatively sensitive for polymers with hydrogen 	<ul style="list-style-type: none"> • Plan-view documentation of failure • Plan view assessment of part quality and defects • Planning analyses
Eddy current	Measure conditions which interrupt the flow of eddy current induced in the part	Determines differences between paint scratches and surface cracks in Gr/E fabric structures	<ul style="list-style-type: none"> • Plan view documentation of fracture with single-side access • Planning analyses

* Techniques are listed in order of preference, based on applicability, reliability, cost and sample requirements

Figure 3-47a. Failure Analysis Techniques—Nondestructive Evaluation

5-B70227-77

STRUCTURES		DEFECTS						
		DELAMINATION/ DISBOND	IMPACT DAMAGE	FASTENER HOLE DAMAGE	LIGHTNING DAMAGE	BURN DAMAGE	TRANSLAMINAR FRACTURES, SURFACE	TRANSLAMINAR FRACTURES, SUBSURFACE AND SUBSTRUCTURE
LAMINATED SKIN		C,D,E	A,C,D,E G	A,C,G,H	A,C,D,E	A,C,D,E	A,B	C,G,F, D,E
SKIN/HONEYCOMB PANEL		C,E,D	A,C,E,D	A,C,G,H	A,C,E,D	A,C,E,D	A,B	C,G,F D,E
SKIN-TO-STIFFENER JOINT		C,D,E	A,C,D,E G	A,C,G,H	A,C,D E	A,C,D E	A,B	C,G,F D,E
SKIN-TO-METAL JOINT		C,D,E	A,C,D, E	A,C,H	A,C,D E	A,C,D, E	A,B	C,I,D E
SKIN-TO-SKIN TRAILING EDGE JOINT		C,E,D	A,C,E D,G	A,C,G H	A,C,E, D	A,C,E, D	A,B	C,G, F,D,E
LAMINATED RIBS, SPARS, AND SKIN STIFFENERS		D,E	D,E, G	A,D, E,G,H	A,D,E G	A,D,E, G	A,B	C,G,F D,E
LUGS AND THICK SECTIONS		C,D,E	A,C,D,E	A,C,G H	A,C,D,E	A,C,D, E	A,B	C,G,F D,E

Key:

Inspection method

A Visual

B Penetrant

C Ultrasonic TTU

D Ultrasonic pulse echo

E Bond tester

F Low KV X-ray

G DIB-enhanced X-ray

H Eddy current

I Neutron radiography

Figure 3-47b. Method Selection (Listed in Order of Preference)

5-B70227-78

on a fairly flat panel, the TTU C-scan method is by far the most preferable method due to its ability to provide a full scale, plan view, hard copy record of the defect conditions that are aligned normal to the interrogating beam (delaminations). Defects aligned parallel to the beam direction (translaminar cracking) do not often create appreciable or detectable attenuation, and thus should be examined by X-ray methods.

B. Detailed Plan View Identification—When more plan view details are required, enhanced X-ray and neutron radiography should be used. Each technique can identify both translaminar and delamination damage, although the X-ray technique requires a free edge or surface-intersecting damage so that the penetrant can be introduced. However, when such a surface defect is present, enhanced radiography is probably the single most sensitive and accurate inspection technique for composite structures. Neutron radiography, on the other hand, can be used where metal structure overlays composite material since neutrons are not as attenuated by metal as X-rays, and are relatively sensitive to polymeric materials containing hydrogen. This method, however has not been proven to generate radiographs that exhibit much contrast or resolution. Another available technique is eddy current, in which small translaminar cracks can be identified without the requirement of a free edge.

C. Through-Thickness Identification—Where through-thickness determination of the location of planar defects such as delaminations are required, either ultrasonics (A-scan, B-scan or time-domain gated C-scan) or X-ray (stereo radiography) can be used. This provides the investigator with information similar to cross-sectional viewing of the planar defect locations.

Several techniques such as X-ray tomography, neutron radiography, and resonance/impedance bond testing are available, although their application to failure analyses is extremely limited due either to immaturity, expense, or limitation of field investigation. Holography, acoustic emission, thermography, and speckle photography are not used for post-failure analyses investigations since they require some sort of mechanical loading of the part to define damage states. For these reasons, these paragraphs describe in detail the proven and directly applicable NDE techniques such as ultrasonics, X-ray, eddy current, and edge replication. The basic operational modes and uses are presented, along with some fundamental theory with regard to evaluating fractured composite structures.

D. Evaluation Plan—Nondestructive evaluations can be extremely useful to the failure investigator by revealing visible damage as well as areas of fracture not readily discernable through the most intensive visual examination. Nondestructive evaluation is of particular importance with composite materials primarily because of their susceptibility to invisible internal delaminations within or between the laminate plies. Other identifiable defect or damage conditions include found by NDE include:

- Translaminar surface and subsurface fractures.
- Core cell damage and fluid ingestion.
- Porosity.
- Disbonds.
- Impact damage.
- Fastener hole drilling damage.
- Lightning damage.
- Heat or fire damage.

In addition to its primary benefits, NDE has several other notable advantages. Providing adequate documentation prior to destructive sectioning is of particular importance in failure analysis. With many modern and well developed nondestructive analysis techniques available for composites (ultrasonics and X-ray being the most common) a permanent record is made of both visible and invisible areas of fracture. This record, somewhat like optical photography, provides invaluable documentation for later perusal. In addition to documentation of the extent of invisible damage, the investigator often gets an added benefit of identifying the type of construction such as locations of core splicing, potting regions, and ply dropoffs or pickups. Finally, since NDE is usually performed by a support specialist, the failure analyst is freed to establish a coherent plan for more detailed evaluation prior to destructive operations (such as specimen removal by sectioning).

To provide the investigator with a better definition for the sequence of steps involved in the nondestructive evaluation of a part, the FALN presented in Figure 3-46 was developed. Several goals were considered in creating this FALN; first, the chart should provide the most basic information first, and second the techniques should progress from the most easily interpreted to the more complex. The chart begins by documenting the fracture in general terms using relatively simple techniques. Next, two operations

provide additional plan-view and through-the-thickness information using more complex techniques.

3.2.1 Ultrasonic Methods

Ultrasonic inspection techniques are useful in characterizing material flaws such as delaminations, cracks, voids, matrix rich pockets, and changes in thickness. For homogeneous materials such as metals, the techniques and the interpretation of the data is well developed and relatively simple. The anisotropic nature of composites presents an added dimension of complexity to ultrasonic inspection.

The variables affecting an ultrasonic high frequency sound source that is directionally focused on the material to be inspected, include the acoustic properties of the material and the transporting medium that the beam passes through. Any variation of the acoustic properties of these materials can produce changes in the attenuation (transmission loss), velocity, reflection amplitude, refraction angle phase and diffraction of the beam. These changes form the basis of various ultrasonic techniques.

The four primary factors that effect the ultrasound transmission in composite structures include: (1) the inherent physical properties of the material, (2) the microstructural features, (3) the condition of the surface, and (4) the thickness of the material. The first and foremost parameters that effect transmission are the physical properties of the material such as stiffness and density, which determines the directions and energy breakdown of the ultrasonic beam within the material. Second, the microstructural features such as resin content, porosity, matrix cracking, delaminations, and ply orientation all affect the ultrasonic sound propagation characteristics. It is the measurement and interpretation of the ultrasonic information that constitutes the major task involved.

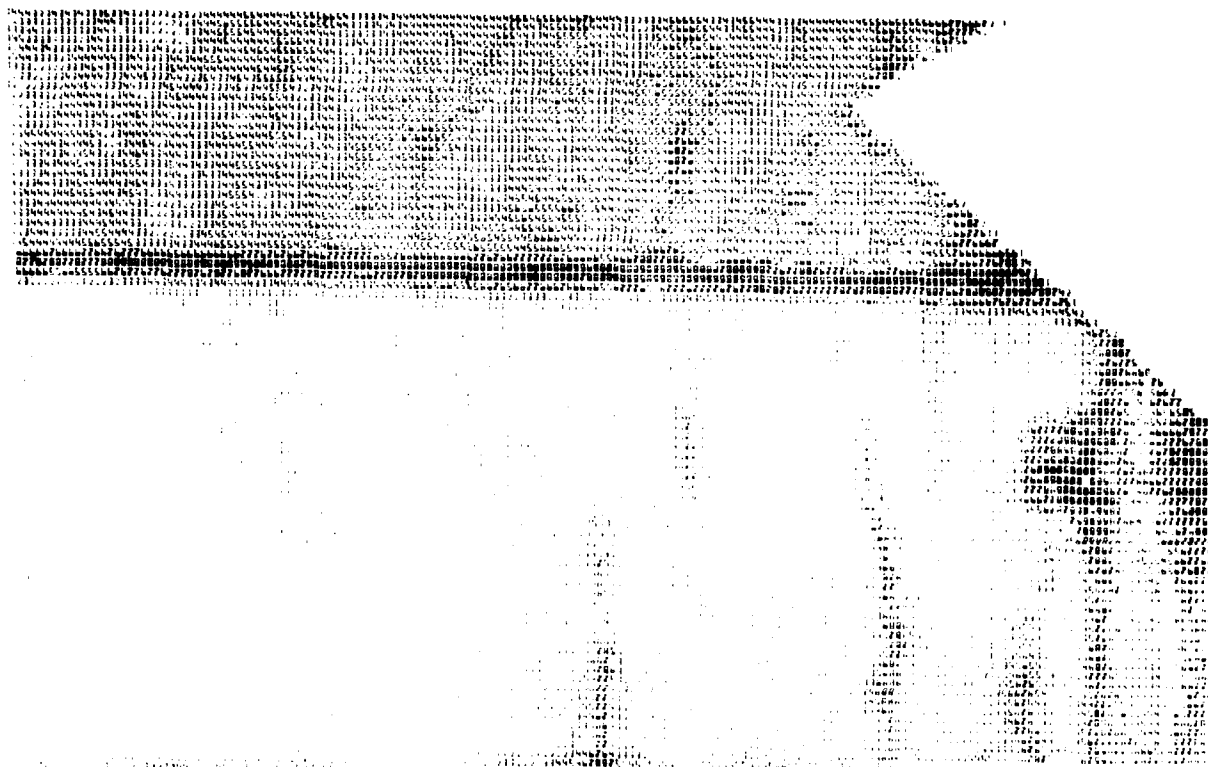
Typical ultrasonic inspection of homogeneous isotropic materials is a process that requires a trained operator using precision and care to avoid errors in the assessment of the damage conditions. The complexities that arise from analyses of extremely anisotropic materials such as composites requires knowledge of the above mentioned factors that can have pronounced effects on the information obtained. Although these factors tend to complicate the analyses, they can also contribute in a constructive manner to provide valuable information regarding the microstructure and basic construction of the component.

There are two primary methods which are recognized as the most flexible and efficient methods for obtaining ultrasonic sound propagation data from composite structures, through-transmission ultrasonic (TTU) and pulse-echo.

3.2.1.1 Through-Transmission Ultrasonic (TTU)

In the TTU method, an ultrasonic transducer is placed on one side of the material and emits an acoustic pulse. The pulse travels through the material and is received by a second transducer located on the other side of the material. These transducers are placed in axial alignment so that their common axis is perpendicular to the surface of the specimen. With this placement, the amount of energy transmitted through the material is maximized and can be easily monitored as a function of position when the material is scanned by the transducers. For a C-scan, the entire surface is inspected by moving the transducer in a series of closely spaced traverses with a mechanical system. Most mechanical systems only allow planar scanning motions of flat or circular symmetric shapes. Water jet techniques have been developed which allow inspection of parts too large to be immersed in a tank. Current technology exists for robot controlled manipulators which track complex surface geometries, but such systems are not yet commonplace. Since the speed of the test is limited primarily by the speed of the scanning, several arrayed transducers are often used for large scale inspection tasks to reduce scan times, however for most failure analyses a single transducer can inspect a large part in a few hours.

The transmitted sound can then be evaluated and broken down into several sublevels, or grey scales, with each level equivalent to a certain amount of attenuation. This energy loss can be related to either voltage or decibels (dB). Each of these sublevels can then be assigned numbers or colors and graphically presented as a plan view of the part. Regions of attenuation greater than a standard, say in the 6 to 18 dB range, indicate the presence of significant damage conditions that reflect the energy of the sound beam. Through the use of real-time computer monitoring of the attenuation, a map of the sound transmission relative to the part geometry can be produced by a plotter in which an image is formed by burning the surface layers of an ink-impregnated conductive paper. Figure 3-48 presents such a map, with a delamination identified in the areas of high attenuation. The numbers denote a range of dB sound loss, with the larger and darker numbers indicating more attenuation.



Note: Larger numbers denote higher levels of sound attenuation.

Figure 3-48. Example of an Ultrasonic Through-Transmission C-Scan

5-70227-144

In TTU, the sound attenuation results from three sources: viscoelastic effects, geometric dispersion due to material anisotropy, and dispersion due to geometric internal damage. By proper selection of the sound frequency, the attenuation due to delamination and cracks can be maximized and the attenuation due to material viscoelasticity and heterogeneity can be minimized. The use of 1 MHz has been recognized to provide the best transmittance since it has a fairly long wavelength and thus is less susceptible to scattering from smaller structural details, particularly for parts with honeycomb core. When increased sensitivity for smaller details is desired, the use of smaller wavelengths should be used, however frequencies in this range (5 to 15 MHz) do not transmit through honeycomb structure and requires a more critical alignment of the two transducers.

The transporting medium is usually water, which provides a uniform coupler to transmit the sound waves between the transducers and the specimen. This requirement for a water coupler basically limits the TTU inspections to the laboratory, however a few portable units are available. The specimen is either immersed or water jets at the transducers supply a stream of the coupler. With composite failures, surface damage in the form of edge delaminations or translaminar cracking is often present. This surface damage, if extensive, can allow water to penetrate into the cracks. Since the attenuation is commonly due to air at the crack impeding the transmittance of sound, the water penetration can displace the air and eliminate, or significantly reduce, the attenuation at these defects. Hence, special precautions are required to prevent the intrusion of water into these areas, particularly for those specimens where a contaminant is suspected and water would be very undesirable. Normally, the open surface cracks are edge sealed with adhesive tape to inhibit entry of water.

Inspection of the TTU C-scan plan view records can provide a full scale assessment of the major defect conditions. Usually this inspection method is adequate to define the general outline of the delamination, particularly surrounding the major damage region that is visible. Although the C-scan method is best used to define delaminations, much smaller defects such as porosity can also be identified in extreme cases. This technique is limited by the fact that both sides of the material must be accessible, the depth of defects within the laminate cannot be determined, extreme variations in thickness cannot be evaluated at the same time, and defects aligned parallel to the incident beam are not easily identifiable (such as translaminar cracking). Where situations exist that require a more detailed

inspection of the damage such as the determination of defect depth, access to only one side of the part, or when laboratory analysis is not possible, the pulse-echo method should be employed.

3.2.1.2 Pulse-Echo Ultrasonics

In the pulse-echo method, a single transducer transmits and receives the acoustic pulse. The transducer emits a gated pulse through the material, which is reflected by the far side of the part and then detected by the transducer again. Since the full dynamic range of the receiver is available to amplify any backscattered acoustic energy, this technique can be made quite sensitive to subtle defect conditions. The reflections from the front and back surface provide known time-related endpoints so that the depth of the defect can be determined by its time function. A potential disadvantage of this method is that flaws one ply away from the front or back surface can be hidden by the reflections from the surfaces. This problem can be alleviated by properly adjusting the instrument to distinguish between these reflections, in combination with using a delay line transducer. Additionally, it is necessary to record the returned echo trace and section it at various periods of time in order to have an accurate representation of the location of the flaws. Breaking down the echo trace allows the differentiation and separation between closely arranged flaws and prevents the investigator from mistaking several small flaws as a single large one.

For use in the C-scan format, the inspection is usually performed in either a water bath or by using columns of water sprayed upon the surface of the specimen. The water serves as the coupler and delay line for the ultrasonic signals. Information is generally recorded in which the signal levels at each (and time or depth) is printed or displayed as the transducer is moved over the specimen. The C-scan pulse echo is a plan view, two dimensional image of the internal structure of a material. With gating of the amplitude based digital signal, imaging of defects can be identified related to the position within the thickness of the material, as shown in Figure 3-49. The use of a combination of two gating zones can allow the differentiation of delaminations near the front surface (light) and the back surface (dark).

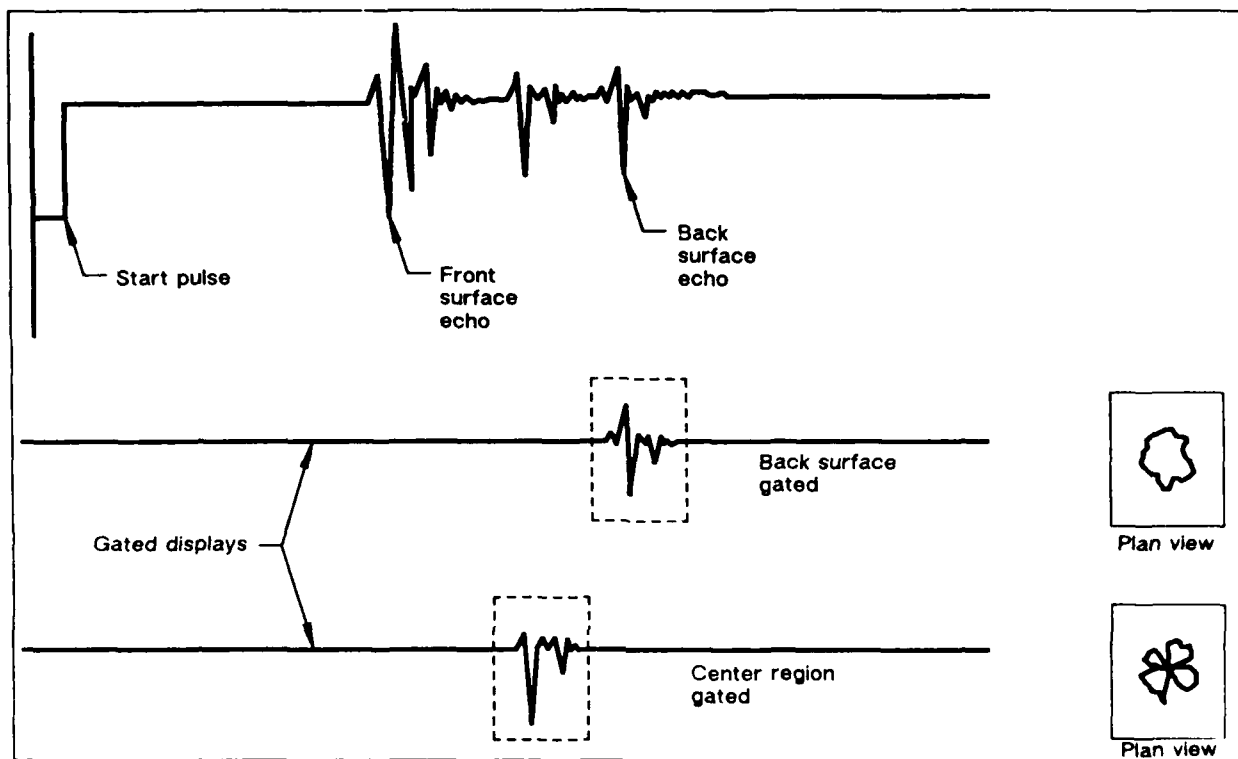


Figure 3-49. Pulse-Echo Ultrasonic C-Scan Using Time Domain Gating Zones To Identify Damage States of Impact

5-B70227-145

Short pulse (shock wave) methods can also produce a considerable amount of information, although it is limited to linear plotting of the data instead of the two dimensional C-scan. In A-scan, the reflected pulses can be real-time displayed on a cathode ray tube or permanently recorded. By comparing the reflected pulse information from a region of damage with an area containing no damage (often a calibration sample), the depth of the defect condition can be fairly accurately determined. Similar to C-scan, this method produces an image delineating the reflections between the front and back surfaces. By taking several parallel passes of the transducer over the part, a better feeling of the three-dimensional geometry of the defect can be obtained, as shown in Figure 3-50.

While the A-scan provides data regarding all reflections through the thickness, the B-scan indicates only the first echo after entering the surface. It is therefore incapable of displaying second and higher multiple reflections, as the other two methods can. The B-scan

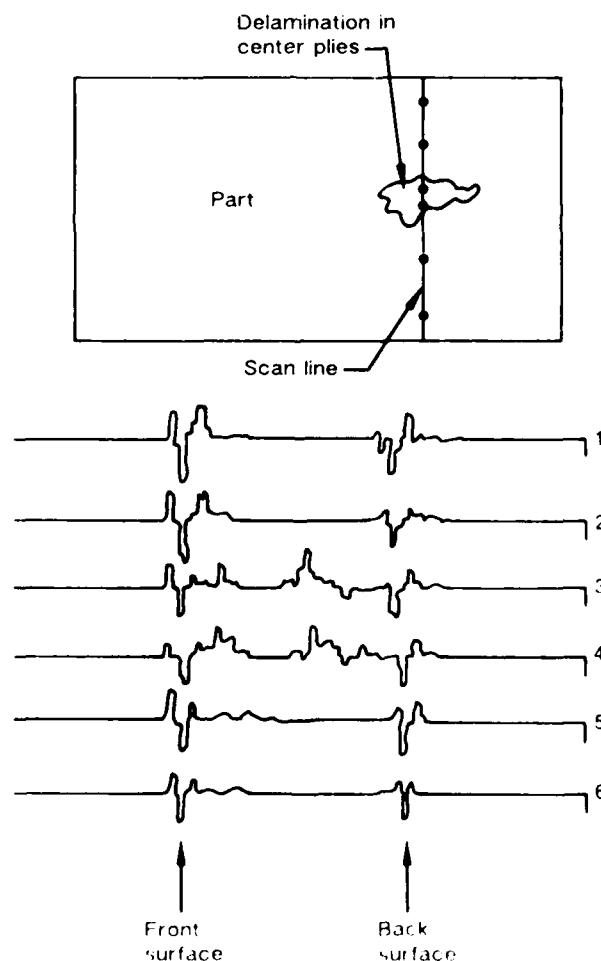


Figure 3-50. Delamination Identified by a Family of Pulse-Echo Ultrasonic A-Scans

5 B70227-146

is somewhat similar to a transverse cross-section, in that it provides a record of the depth location on a line across the specimen surface. By taking several of these scans, they also can be combined to provide a more complete view of the through-thickness damage in the material. An example of a B-scan is presented in Figure 3-51, illustrating the extent of damage in a laminate at several locations along the surface of the part. For field or initial inspections, the A-scan method using a cathode ray tube for imaging can be performed without a permanent record of the damage. For instance, early NDE investigations in large failed structures with visible damage and delamination, hand-held pulse-echo can be used to quickly define the perimeter of the delamination damage. In this case the couplant is usually a light grease, oil, or commercially available gel.

3.2.1.3 Single-Sided Ultrasonic (Backscatter)

Recent developments have provided a method of identifying transverse cracking, with resolution capable to identify cracking within a single ply. This technique is usually called single-sided ultrasonic angle beams (backscatter) and involves using an off-axis transducer that imparts the sound at an angle to the surface, as shown in Figure 3-52. This technique employs separate transmitting and receiving transducers housed in a single surface probe. A complex wavefront is created in the structure by the transmitter, and is continuously monitored by the receiving transducer. With this system, delaminations create both a phase and amplitude change, allowing their detection. Because the ultrasonic signal is

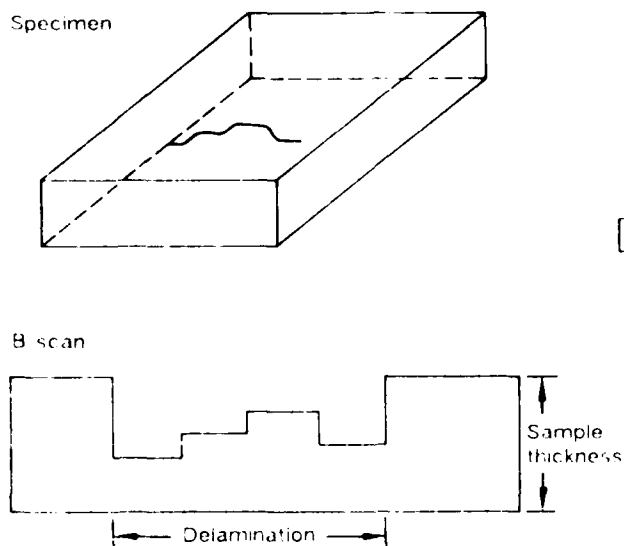


Figure 3-51. Pulse-Echo Ultrasonic B Scan of a Delamination Defect.

5-B70227-147

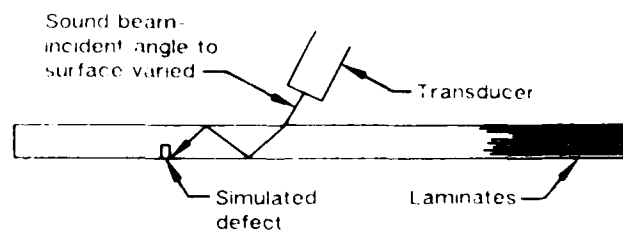


Figure 3-52. Ultrasonic Detection of Simulated Crack in Laminate Plate

5-B70227R1-148

angled with respect to the surface, this technique has enhanced sensitivity to cracks oriented in the through-the-thickness direction. A drawback is that each ply must be scanned at a specific angle of incidence to maximize the signal amplitude and properly determine the location of the microcracks. A reference standard is also required that duplicates the materials and layup of the laminate being inspected.

3.2.2 X-ray Radiography

X-ray techniques can be used to detect broken structure and large subsurface fractures when there is a displacement of members. Extensive cracks in which surface displacement has not occurred may not be detectable. Defects such as crushed core and fractures associated with impact damage lend themselves to radiographic evaluation. In addition to detecting cracks, the investigator can learn valuable information regarding the internal structure of the component, particularly if there are major differences in construction such as stiffeners and honeycomb core. Water in the core, if extensive, can also be detected. For failure analysis, the use of X-ray is most often considered as a secondary method to ultrasonics, although it possesses many advantages when faced with damage located parallel to the incident interrogating beam such as translaminar cracking.

3.2.2.1 Classical Radiography

An X-ray (radiographic) inspection is performed by transmitting a beam of penetrating radiation through an object onto a photosensitive film. This beam is partially absorbed by the composite as it passes through. Discontinuities such as translaminar cracks cause a reduction in thickness parallel to the incident beam path, and consequently results in less absorption and less reduction in the intensity of the X-ray beam. These varying beam intensities which strike the film plane form a latent image. The film is processed to form a visible image called a radiograph. The radiograph is then evaluated for information regarding the extent and nature of the defect conditions, if they exist.

Although conventional radiography readily detects through thickness fractures, it does not always present conclusive results. The information obtained from radiographic inspections are affected by the size and orientation of the defect relative to the incident beam. Defects presented normal to the beam result in insufficient changes in density so that

interlaminar defects such as delaminations and porosity are not detected by conventional radiography. Due to these limitations, the technique has been significantly improved by the use of some form of radio-opaque penetrant, which produces probably the single most sensitive inspection technique for detecting cracks in composites that are surface related. The following paragraphs focus on this valuable technique.

3.2.2.2 Penetrant-Enhanced Radiography

The procedures for making radiographs of defects and damage in composites differs from the conventional ones in that an X-ray opaque penetrant is used to enhance the damage. The penetrant provides significant improvement in contrast between the damage and the intact composite, as shown in Figure 3-53. Various penetrants have been used, with tetrabromoethane (TBE) being the first solution evaluated. This penetrant was found to be highly toxic and carcinogenic so its use was discontinued. Diiodobutane (DIB) was used for a short time, but was also found to be a toxic organic halide, expensive, and had a short shelf life. The enhancement chemical that has proven non-toxic and is relatively inexpensive is zinc iodide (ZnI_2), used with an alcohol carrier solution. The carrier solutions are as follows:

<u>Isopropal Solution</u>	<u>MEK Solution</u>
Zinc Iodide - 60 grams	Zinc Iodide - 60 grams
Water -10 milliliters (ml)	MEK - 250 milliliters
Isopropal Alcohol - 10 ml	
Kodak "Photoflo" - 1 ml	

The Isopropal solution requires about 30 minutes after application for the penetrant to reach the end of the damage. This time is reduced to about ten minutes for the MEK solution. After saturation, excess penetrant should be removed from the open surfaces with absorbant material. The use of these penetrant materials should be used with caution, since they can potentially damage or obscure the fine microstructural fracture details and prevent detection of contaminants. For fairly chemically stable matrix systems such as epoxies, the use of these penetrants have not created any undesirable effects such as damage to the fracture surface details, particularly when removed with a clean solution of the primary solvent carrier. For other material systems such as thermo-

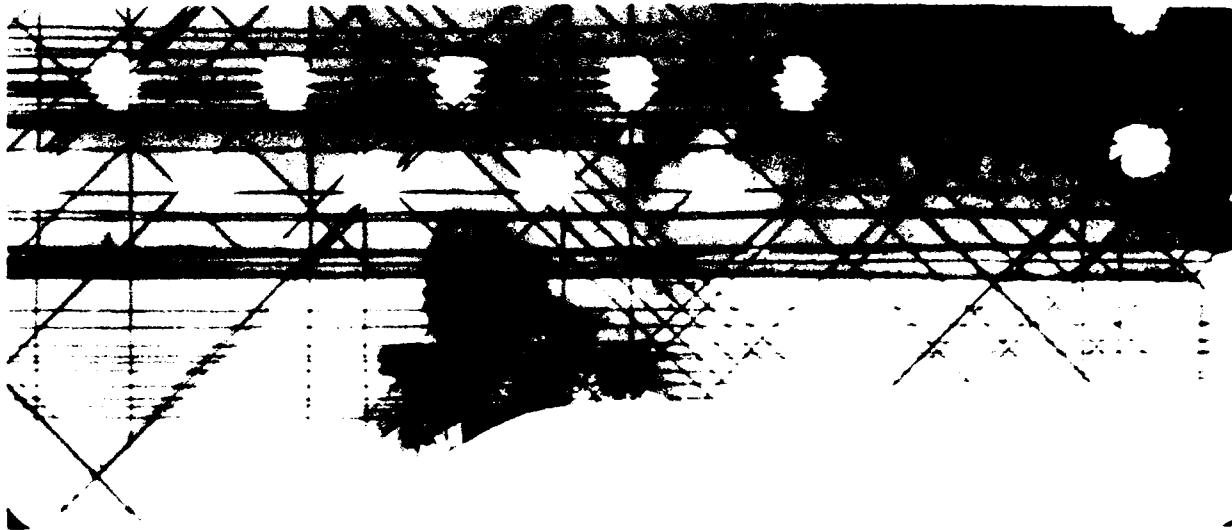


Figure 3-53. Penetrant-Enhanced X-Ray Image of Edge Delamination

5-B70227-19

plastics, the effects have not been evaluated, and thus should be spot tested prior to application to the fracture surfaces.

Various X-ray films can be used, although a high resolution, single-coat film such as Kodak Type R industrial, low speed, fine grain film gives the best contrast and resolution. Double-coat film should be avoided since it is exposed on both emulsions, leading to a double image and loss of resolution.

X-ray units emitting soft X-rays are recommended, with a small spot size in the range of 1.5 mm by 1.5 mm or less, with an inherent filtration of 1.0 mm beryllium equivalent or less. The generator tube should be capable of producing a minimum of 20 Kilovolts at 2 milliamps. The low operating voltages produces soft X-rays that provide resolution of structural details within the laminate, such as porosity and fiber spacing irregularities. For applications which require positioning the X-ray tubes at tight locations, the use of an end anode side emission is recommended. The optimum exposure times are those that produce high resolution negatives from which prints can be made. These exposure times are shorter than that used for direct viewing. It should be noted that it is difficult to obtain prints of radiographs that will reproduce adequately by normal printing methods and therefore reporting and presentation of the results are more difficult and somewhat lacking.

Inspection of the films often requires an expert to differentiate artifacts from actual damage. The interpretation requires an understanding of how the penetrant effects the X-ray beam and how it enters the damaged specimen. Regions containing penetrant appear darker than regions containing no damage or defects. Regions containing no penetrant have a uniform grayness, especially on structures that have small thickness variations, since composites have relatively low radiographic scattering or absorbence due to the elements present. Cracks such as matrix or translaminal cracking appear as long, narrow, dark lines. The interpretation of artifacts corresponding to delaminations is usually more difficult. The opening displacement of the crack is the greatest at the edge and the least at the end of the delamination, and therefore one might expect a visible lightening of the image from the free edge toward the crack tip. While this change in grey level holds true at the extreme ends of the crack, the situation at the central region is such that the capillary forces are not strong enough to hold the penetrant. This results

in a central boundary region that does not stop the X-rays and often appears light and undamaged.

Another modification to the penetrant enhanced X-ray image involves making stereo radiographs, such that a three dimensional view of the internal damage can be examined. The standard stereo radiography procedure consists of making two X-rays films of an object from slightly different orientations. The best method of creating the two views is to rotate the part through a small angle (usually about 7 to 15 degrees). The part is then allowed to remain at the center of the path of the X-rays and is also centered in the radiograph. The depth of the damage can then be identified, as well as differentiating between overlaying damage that might be masked with a single plan view. With the aid of a stereo viewer, the defects nearest the X-ray source have the largest relative displacement and the farthest defects are the least displaced.

3.2.3 Eddy Current

This technique is commonly used in metals and has provided satisfactory results for fabric laminates, particularly for locations around small, localized geometric variances such as fastener holes and edge radii. Eddy current testing involves small, hand held surface probes that produce an alternating magnetic field. This field is generated by an alternating current test instrument coil. This alternating expanding and collapsing current induces a magnetic eddy current in the specimen. The interaction of this magnetic field with the test instrument varies as the internal flaws and fractures are encountered. The use of this instrument is basically limited to solid laminates that are conductive and have appreciable magnetic permeability. This method relies on the conductivity of the carbon fiber, which is at best, limited. Figure 3-54 presents a typical inspection procedure using a probe to detect subsurface damage in fabric laminates.

3.2.4 Edge Replication

Edge replication has proven itself to be an accurate technique for documenting the state of damage in thin laminate sections. It is a direct application of the replication technique used for TEM specimen preparation. An acetate film that has been softened with acetate solution is firmly applied to the edge, then allowed to dry. The replica can then be



Figure 3-54. Subsurface Fracture Evaluation

5-B70227-20

shadowed to enhance the surface features. The result is a mirror image of the edge that can be examined at higher magnification to assess invisible damage. Cracks such as the translaminal cracks for the 90 degree plies and edge delaminations in the 0 degree plies can be readily identified and highlighted by shadowing.

3.3 FRACTOGRAPHY TECHNIQUES

Fractography, the science of studying fracture surfaces, is the key not only to the determination of the sequence of fracture events that took place during the failure process but also for the identification of the state of stress that existed at the time of fracture (tension, compression, and shear). Other factors such as environment, material defects, or other material anomalies that may have contributed to crack initiation, growth, and ultimate failure can also be evaluated using the tools presented in the following paragraphs.

Due to their laminated construction and high level of anisotropy, particularly on a localized scale, failures in composite materials tend to be extremely complex in appearance as well as in mechanism. The actual failure process and fundamental fracture mechanisms in this class of materials are not sufficiently well understood at this time. However, many of the analytical methods presently used for fractography of composite structures have been previously developed for use in failure analysis of metallic materials, and therefore have a fairly sound fundamental basis. Efforts within the past ten or so years in the area of composite fractography have been directed toward modifying these well developed metals techniques, which include:

- Visual and optical macroscopy.
- Optical microscopy.
- Scanning electron microscopy.
- Transmission electron microscopy.

Each of these analytical techniques provide the investigator with a significant amount of information regarding the fracture by examination of the morphology and other topographical features related to the fracture process. As a general rule, all failure analyses should involve each of the above techniques (with the exception of TEM) in the

order of increasing magnification. Each investigation requires a combination of the above methods, dependent on variables such as size, time available, and type of fracture.

Fractography, as an investigative post-failure analysis method, involves the use of the various techniques listed above in conjunction with the interpretation of the results as related to the fracture process. These paragraphs describe in detail the techniques used to identify the morphological fracture features. The physical principles involved in each technique are presented, including comments on how these principles can be used to control image type and the type of features observed in the fractographs. Specific examples of how to obtain suitable fractographs and gather data related to propagation type (interlaminar versus translaminar), crack propagation mode (tension versus shear), crack propagation relative to the fibers, and other divisions are illustrated.

In Section 4.0, the interpretive methods and specific examples of how the fractographic data relates to fracture mode, crack growth, and other faults are presented.

In addition to identifying the fracture morphology, the other primary responsibility of the investigator is to document the key features relevant to the determination of the cause of failure. This involves photo documentation for reports or presentations, as well as later analyses, and can often require extra effort during an investigation so that the photos convey the message to nontechnical personnel. For example, a significant portion of the analyses can be performed using optical microscopy, and although the image can be evaluated during use of the instrument, the details of resin fracture are often too fine or have too rough of a fracture topography to be documented on optical photomicrographs. In this case, the SEM is required to document these features, although it may not be required to analyze resin fracture details. In this case, the two techniques are complimentary to one another. The value and methodology of both photo documentation and the identification of the fracture morphology is presented as well as providing considerations relative to specimen preparation prior to analyses.

In fractographic analyses, primary emphasis is placed on:

- Locating the origin of the failure.
- Establishing the direction of fracture.
- Identifying the load state and modes of crack growth.

- Determining if environmental conditions or degradation were present.
- Identifying if anomalous condition contributed to reduced material strength or premature fracture.

The use of fractography for the analysis of metals dates back to the early 1900's, and well established procedures exist for its application. Recent work has reviewed and modified these guidelines to yield the detailed fractography FALN illustrated in Figure 3-55. The chart diagrams three distinct operations: classification of failure types, crack mapping, and fracture surface chemical examinations.

The first failure classification breaks down the relatively complex nature of composite fractures into two distinct types, interlaminar and translaminar. This classification is useful because different analytical methods are best suited for each type of fracture. Interlaminar fractures, or delaminations, are best analyzed for crack growth direction using optical microscopy, whereas translaminar fracture (which break the fibers) are best analyzed by scanning electron microscopy.

Determining the direction of crack propagation is one of the most significant concerns in fractography. The recommended technique for crack mapping uses the lowest magnification capable of performing the job. This recommendation is made because one of the fundamental problems in detailed microscopy of large fractures is that there is an extremely limited perspective on how the area being examined relates to the part as a whole. The situation is similar to the old adage, "one can't see the forest for the trees." With a limited perspective, it is often possible to improperly characterize the direction, mode, or load state at fracture. By emphasizing the use of lower magnifications for early investigations, the FALN imposes a sense of perspective on later, higher magnification inspections.

The chemical analysis of fracture surface features may be required to determine to sequence of fracture events. By carrying out these examinations after identifying the fracture origin, emphasis can be placed on any anomalies encountered. Figure 3-56 and Figure 3-57 summarize the techniques used in fractography.

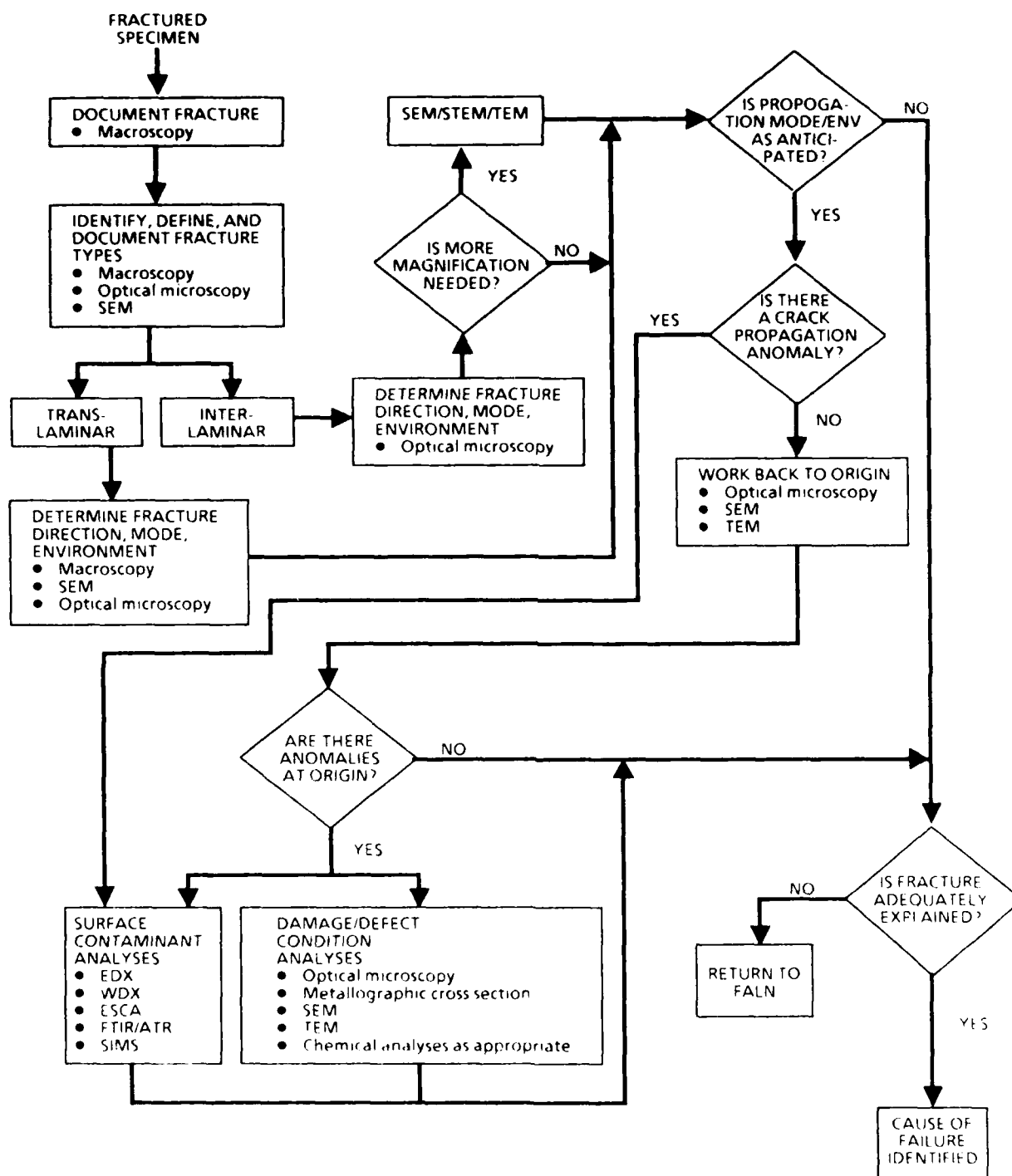


Figure 3-55. Fractography Diagnostic Technique Sub-FALN

5-B70227-100

TECHNIQUE	DESCRIPTION	USE	VALUE
Optical macroscopy	Optical examination at magnification generally at or below 10X	Plan-view examination and identification of fracture surface features, damage and defects	<ul style="list-style-type: none"> • Documentation of fracture • Identification of fracture types (translaminar vs. interlaminar) • Determination of translaminar fracture modes
Optical microscopy	Optical examination at magnifications above 10X	Plan view examination and identification of fracture surface features, damage, and defects	<ul style="list-style-type: none"> • Identification of fracture types (translaminar vs. interlaminar) • Determination of interlaminar fracture direction, mode, and environment • Determination of origin • Identification and characterization of defect and damage conditions
Optical X-section	Metallographic optical examination at magnifications above 10X	Cross-sectional examination of laminate, defect, and damage conditions	<ul style="list-style-type: none"> • Identification of fracture locations • Determination of laminate orientation and drawing compliance • Identification and characterization of defect conditions
Scanning electron microscopy (SEM)	Microscopy performed by mapping; secondary electrons from the sample generated by a primary electron beam raster	High-magnification examination of fracture surfaces and defects with excellent depth of field	<ul style="list-style-type: none"> • Documentation of fracture surface • Identification of interlaminar fracture mode, direction, and environment • Identification of translaminar fracture mode, direction, and environment • Determination of origin • Identification and characterization of defect conditions
Transmission electron microscopy (TEM)	Microscopy performed by examining the focused pattern of electrons attenuated by a thin fracture surface replica	High-magnification examination of replicated fracture surfaces with better depth of field than in optical microscopy	<ul style="list-style-type: none"> • Limited to delamination fractures • Documentation of fracture surface • Identification of interlaminar fracture mode, direction, and environment • Determination of origin • Identification and characterization of select conditions
Back-scatter electron microscopy	Microscopy performed by imaging back-reflected primary beam electrons generated by a rastered electron beam	Intermediate magnification of fracture surface and defects. Back-reflected electrons are sensitive to atomic number and can be used to distinguish surface details as a function of atomic number	<ul style="list-style-type: none"> • Documentation as a function of atomic number • Identification and characterization of defect conditions

Figure 3-56. Failure Analysis Techniques—Fractography

5-B70227-81

TECHNIQUE	DESCRIPTION	USE	VALUE
SEM/microprobe energy dispersive X-ray analysis (EDX)	Quantitative microchemical analysis, photographic mapping of X-ray energies created by primary electron beam raster	Determines microchemical elemental composition of micro-inhomogeneities and particles	<ul style="list-style-type: none"> • Identification of metallic contaminants (atomic number >1) • Particle size analyses
SEM/microprobe wavelength dispersive X-ray analysis (WDX)	Quantitative microchemical analysis, photographic mapping of X-ray wavelengths created by primary electron beam raster	Determines microchemical elemental composition of micro-inhomogeneities and particles	<ul style="list-style-type: none"> • Identification of metallic contaminants (atomic number >5) • Particle size analyses
Auger electron spectroscopy (AES)	Quantitative surface chemical analysis (top 5 nm) of Auger electrons ejected due to primary electron beam	Determines elemental chemistry of upper 5 nm of surface (requires conductive surfaces)	<ul style="list-style-type: none"> • Identification of contaminant monolayers • Identification of adhesive failure interfaces
X-ray photoelectron spectroscopy (XPS)	Quantitative surface chemical analysis (top 5 nm) of photoelectrons ejected due to primary X-ray beam	Determines elemental chemistry and chemical state of upper 5 nm of surface (does not require surface conductivity)	<ul style="list-style-type: none"> • Identification of contaminant monolayers • Identification of adhesive failure interfaces
Secondary ion mass spectroscopy (SIMS)	Qualitative surface chemical analysis of surface monolayer atoms removed by ion sputtering	Determines elemental and chemical state of surface monolayers; repeated operation allows elements to be profiled versus depth	<ul style="list-style-type: none"> • Identification of contaminant monolayers

Figure 3-57. Failure Analysis Techniques—Fracture Surface Material and Chemical Characterization

5-B70227-60

The following paragraphs describe the failure analysis methodology associated with fractography, the decision points, the use of most of the analytical tools, all combined with the background reasoning that led to the sequencing and structure of the fractography FALN.

Beginning with a failed structural component, the initial responsibility of the investigator is to document the fracture surfaces, both by extensive photodocumentation and by visual and optical macroscopy. At this important stage, while the entire part or structure is intact, significant critical information may be gained through assessment of the overall types of fracture, their locations, and obvious anomalous production or service conditions, all of which give an investigator a feeling of the primary loading events, sequence, and other contributory conditions that occurred prior to or during failure. Dependent upon the size and location of the component, further fractographic analysis may be delayed for nondestructive analysis such as hand-held pulse-echo ultrasonics and part breakdown (fastener removal) into separate components such as skin and spar. As the separated pieces become available during breakdown, the investigator should identify, define, and document the individual fracture types such as translaminar or interlaminar. Visual and optical macroscopy should be employed for these analyses.

Following definition of fracture types, and more detailed NDE examinations of the damage regions, the most labor intensive and critical portion of the fractographic examinations involve the use of detailed macroscopic and microscopic analysis. These analyses require the investigator to use specialized fractographic techniques to determine the fracture directions, modes, and environmental conditions at fracture. For translaminar fractures, the majority of the analyses involve fiber fracture details, while matrix resin fracture analyses predominates the interlaminar fractures. Emphasis should be placed upon performing as much examination as possible at the lower magnification ranges, thereby increasing confidence and reliability in the determination of crack directions, modes, and any anomalous conditions which may exist.

If determination of the fracture origin is made, through the use of detailed crack mapping or visual and macroscopic analyses, the next step is to assess whether or not an anomalous condition exists in the origin zone. If such a defect is evident or suspected, such as adhesive separation which has a general lack of fracture features, commonly associated

with contamination, then further examinations like surface chemical analysis may be required.

3.3.1 Care, Handling, and Protection of Fracture Surfaces

The preservation of the physical evidence should be viewed as one of the most important responsibilities for the investigator. Education on proper handling and protection prior to any fractographic examination is strongly recommended for anyone dealing in fractures either in the field or in the laboratory. When a fracture occurs, and there is even a slight chance that it will be submitted for laboratory examination, several important steps must be followed so that maximum information can be obtained. The important factor is prevention of damage that might preclude the use of various analytical methods. Most of the procedures described are independent of the particular fractographic techniques being employed.

The care and handling procedures that must be followed are based on general methods that have been proven for metals and modified for application to composite structures. These procedures rely on the fact that the fracture surface contains an enormous amount of valuable information and that anything done to obliterate or alter this information may obstruct important information related to the fracture. The damage that can occur can be separated into two types, either mechanical or chemical.

A. Mechanical Damage—This type may arise from several sources, including allowing the fracture to impact other objects. This can occur during the fracture process itself (for example, departure from the aircraft and subsequent ground impact), during removal of a fractured portion from the remainder of the structure, during transportation to the laboratory, or by careless accidents such as dropping the component. For composites, the consequences of damage can be detrimental to the proper determination of the cause of failure, since quite often the post failure damage cannot be differentiated from that actually created during the failure event. Notably different than metallic structures, fractures created during rapid loading such as impact from dropping, often cannot be differentiated from fractures created under slower loading which might be encountered during part service. Crack growth created during handling such as peeling delamination surfaces apart by hand are especially undesirable as they are often impossible to differentiate from delaminations created during the fracture event.

The fracture can usually be protected during shipment by properly crating the structure, if it is large and intact, so that motion of the component will not create rubbing or translation of the mating fracture surfaces. Where possible, particularly for components that have translaminar fractures, the amount of motion-induced damage can be eliminated by total separation of the fracture halves prior to shipment. Parts with only delamination damage can usually be left intact for shipment. To prevent contamination or fluid ingress such as rain, the structure should be wrapped with a clean plastic sheet. Smaller components or test coupons should be placed in zip lock bags or other airtight bagging so as to maintain the level of absorbed moisture and more completely protect the structure from contaminants. If necessary, the fracture can be protected during shipment by taping cloth or cotton to the surface, as long as loosely adhering material, commonly associated with the critical fracture regions, are not dislodged.

Touching the fracture with the fingers or rubbing it should definitely be avoided, as this can leave oils or other contaminants on the fracture surface which may alter or prevent surface chemical analysis results. One of the most common sources of fracture surface damage is when two halves of a fracture are fit together. This accomplishes nothing important and always results in some microscopic damage to the fracture surface, and thus should be avoided.

B. Chemical Damage—This type of damage to fractures can be prevented in a number of ways, each using common sense and requiring an awareness of the necessity of protecting the surface from chemical contamination or degradation. Since the identification of a foreign material (such as release agent) present on a fracture surface may be critical in the overall interpretation of the cause of fracture, all chemical protection schemes such as plastic coatings or desiccants are to be avoided. If such a condition exists where a substance must be cleaned from the part prior to shipment, such as fire retardant foams, the most desirable solvent is plenty of clean water.

C. Laboratory Cleaning—Usually some sort of cleaning of the fracture surface is required prior to examination, since small pieces of fibers and matrix are present due to either the fracture process or mechanical cutting operations. The necessity of cleaning is not always necessary, and to prevent potential loss of contamination evidence, should be avoided early in the investigations if possible. Numerous cleaning procedures have been

attempted, each suited for the extent and type of deposit, or the preference of a particular laboratory. The most commonly employed cleaning techniques, in order of least-to-most damage or destruction of evidence, are:

- A dry air blast - which will remove many loosely adhering materials. If possible, canned air for laboratory use is preferred over the piped-in compressed air which can often contain oils and moisture. A soft artist's brush will assist in the removal, but extreme care must be exercised to see that no damage is done to the fracture surface.
- Detergent wash - This method can effectively clean most specimens for high magnification investigations. A large, soft artist's brush can be used to apply a mild, water-base detergent (such as dish washing detergent), followed by a thorough rinse in lukewarm tap water and dried by air blast. Stubborn deposits of particulate dust, which can occur on cyclically loaded parts, can be removed by ultrasonic agitation while the detergent solution is present. Ultrasonic durations of only a few seconds is usually satisfactory, although up to 15 minutes have been required to remove physically imbedded dust particles.
- Chemical solvents - should be avoided and used only when other techniques do not remove the tenacious deposits or chemical coatings. Prior to using chemical solvents on critical fracture surface regions, these solvents such as acetone, methyl ethyl ketone (MEK) or alcohols should be trial tested on fracture surfaces of the same material to check for degradation or loss of morphological details. Soak durations should be kept to a minimum. These solvents may also be used with ultrasonic agitation, which may shorten the soak duration quite significantly. This should be followed by detergent wash, rinse and dry as above.

3.3.2 Photo Macrography

Photography plays an important role in fractographic reporting as well as analysis of the physical features associated with a post-failure investigation. Photographic documentation always begins with several pictures of the broken part. This is followed by successively more detailed photography of the fracture surface and associated details, including the documentation of the successive steps carried out during the analyses.

Prior to photo documenting a fractured part, a detailed and thorough visual examination of the specimen in the as-received condition should be performed. This should determine which features are most important, which aspects are extraneous (such as post-failure damage), and whether any special treatment is necessary. This inspection should begin with unaided visual examination, followed with a hand-held magnifier, and scrutinized with a low power optical stereo widefield macroscope if possible.

The next step should be to photograph the entire surface of the fractured part, with several angles and lighting conditions, to record the extent and type of damage relative to the components of the part. The documentation should begin with room overhead lighting and proceed using various angles of oblique lighting, to assess how the fracture characteristics can best be delineated and emphasized.

Accident related parts are often best photographed in the field and sometimes test parts are too large to be photographed in the laboratory. In such cases, outdoor photography using 35mm or 4-by-5-inch view cameras provide the best results. Where adequate daylight lighting exists, it should be taken advantage of, although flash or flood lighting can provide necessary illumination of shadowed or fine details.

Where most of the photography in the laboratory consists of overall pictures of fractured parts and details of fracture surfaces at low magnification, a view camera offers the highest degree of flexibility. While 8-by-10-inch cameras are available, the 4-by-5-inch cameras are most popular, lending themselves to a wider range of photographic media such as Polaroid and cut negative films. Other advantages include a wide range of magnifications with the use of the bellows and various lenses; the ground glass backing allows accurate framing and focusing, and film or lens planes can be tilted to provide focus or perspective on large components. The major disadvantages to these cameras are that they are slower to use than other smaller cameras and require a camera stand or tripod. A workable setup for photographing fracture surfaces or small specimens is a view camera mounted on an enlarger type stand. This allows vertical, or top-down view of the specimen and conveniently provides a fairly quick setup and photo documentation time.

The 35 mm single lens reflex (SLR) cameras offer ease of use with small size and, as stated above, offer a particular advantage for field work and color photography. The 35

mm SLR provides a quick, "see what you get" feature. With the closeup "macro" lenses, magnifications less than 1X can be obtained. The major disadvantages are that they offer a small viewing port which provides a limited assessment of the lighting and focus, the small negative may not always be adequate for enlargements with high speed/large grain film, and the tilt and swing functions of the lens and film planes are not available as in the view cameras.

Low magnification stereo macroscopes with attached cameras are often required to provide a light optical view and documentation of the fracture features at magnification ranges beyond those possible for the 35 mm and view cameras. These systems also permit three dimensional viewing at magnifications up to and beyond the lower limits offered by the light optical microscopes. The practical ranges of magnification for these systems range from 5X to 80X. These systems often have the additional advantage that detailed macroscopic examinations of the fracture surface details and origin regions can be performed, while allowing documentation of the features identified.

3.3.3 Optical Microscopy

Optical microscopy has proven itself as a most critical tool for failure analyses, for the examination of both fracture surfaces and cross-sections. For cross-sections, the optical microscope remains the most important technique available. The analyses of cross-sections provide insight into the microstructural features related to construction, crack propagation, and defect conditions. For fracture surfaces, particularly the delamination surfaces, the optical microscope is possibly the best technique, and at the least should be used in conjunction with the SEM and TEM, rather than as a substitute. The fractography of delaminations by optical microscopy can provide information regarding the crack growth direction, loading conditions at fracture, the origin locations, and anomalous conditions related to the origin. Undoubtedly, this information is considered paramount to the determination of the cause and sequence of failure and thus should be required for all investigations of delamination surfaces.

Microscope systems - Optical microscopes are available from a wide variety of sources and range considerably in cost and capability. Reflected light is the illumination mode used for composites. These microscopes are classified as upright or inverted, relevant to

the location of the stage with respect to the objective lenses. The upright microscope is the preferred type for examination of fracture surfaces, as the fracture surface does not contact the stage which can potentially damage the surface. The inverted stage, however, can accept an extremely large specimen, whereas the upright stage is limited to approximately 6 inches by 6 inches maximum size.

The bench type microscope is the least expensive type and often can provide all of the capabilities required to perform the investigations during fractographic analyses of composites. Various metallographs, although usually more expensive, provide more flexibility and resolution. These can range from simple to full-scale research units, with assorted illumination modes, objectives, light sources, hot stages, and other features.

Illumination - A variety of light sources for optical microscopy are available. The low-voltage tungsten filament lamp is most often used on bench microscopes and has adequate light intensity for most observation and photography requirements. Where more light intensity is required for photo documentation, xenon arc sources (intensity adjusted by neutral density filters) and tungsten halogen filament lamps (adjusted by filters or electrical current) are the most common.

Diaphragms - Two diaphragms are available within all systems to provide improve image quality. A field diaphragm is placed near the light source to minimize internal reflections and glare within the microscope. This diaphragm is stopped down to the edge of the field of view, while not impairing examination or photography. A second diaphragm, the aperture, is placed in the light path just before the vertical illuminator. Opening or closing this diaphragm alters the amount and the cone shape of light, varying the contrast, sharpness, and depth of field. As magnification is increased, the aperture should be stopped down. At a given magnification, closing the aperture increases contrast and depth of field while reducing the image sharpness. A general rule of thumb for aperture setting on rough fracture surfaces, which require maximum available depth of field, is to stop down the aperture until there is a noticeable decrease in image quality and then open it slightly to eliminate most of the aberration.

Objective lens - This forms the primary image and is therefore the most important component of the optical microscope. The apochromatic and plano type objectives provide

the highest degree of correction for aberrations, produce the best results, and reduce eye strain. There are long-distance-working objectives which are particularly valuable for examination of fracture surfaces with rough topography, and are usually only necessary for objectives in the upper ranges of magnification such as 20 to 60X. Other desirable features for fractographic examinations are parfocal lenses (maintains focus when objectives are changed) and spring loaded lenses (moves when contacted with specimen to reduce damage to lenses).

Specimen preparation - Reflected light illumination mode requires a relatively flat surface due to depth of field limitations and therefore specimen preparation is important to provide the best situation for examination and documentation. Specimen preparation for cross-sections are presented in paragraph 3.1, in which the steps for cutting, mounting and polishing are described. Specimen preparation for fracture surface examinations involve cutting the desired fracture region from the remaining structure followed by cleaning.

Fracture surface inspections - Optical fractography is by far the most efficient and cost effective method for examination of delamination surfaces. Since the specimen setup and examination times are very short, an enormous amount of fracture surface is covered with this technique. As a result, a reliable and accurate determination of the typical and representative fracture surface features is obtained in a relatively quick fashion. Translaminar fractures, on the other hand, are too rough and have too fine of features (fiber ends) to accommodate themselves for optical microscopy. Low magnification inspections can be used on delaminations to verify the plane of fracture and the location of crack growth features such as beach marks and transverse cracking. More detailed, higher magnification inspections provide resolution of the fine matrix resin fracture features. These features are used, with the interpretive methods presented in section 4.0, to identify the direction of crack growth (by evaluating river marks), the fracture mode (tension versus shear), and indications of contamination and environmental extremes. Bright field illumination, a stopped-down aperture, and long working distance objective lenses provide the best combination for examination at high magnifications required for crack mapping and identification of the fracture modes. Crack mapping methods and interpretation of the fracture features are presented in paragraphs 4.3 and 4.4. The features found with the optical microscope, even though they are visible through the eyepiece, are often too small to document with photographic film. In these situations where photomicrographs are desired, the SEM is required.

Cross-section analyses - Metallographically prepared cross-sections provide the following types of information:

- **Determination of the overall laminate quality.**
- **Quantitative evaluations of--**
 - extent of porosity
 - relative percent and morphology of phases or microconstituents
 - ply count and orientations
- **Origin examinations.**
- **Inspections of interfacial conditions.**
- **Crack propagation regions (intraply versus interply).**
- **Extent of degradation due to wear, thermal cycling, and fatigue.**

Where possible, specimens should be selected from at least two areas to most accurately characterize the features, particularly when anomalous conditions are identified. These two areas include 1) as close to the origin as possible, and 2) at an area away from damage.

Several illumination methods are available for cross-section analyses, with bright-field being the most widely used. Dark-field or oblique illumination provides an excellent image contrast for differentiating surface topographical features such as microcracks and phase interfaces. Polarized light can be used to enhance differences between ply orientations for easier ply count and orientation analyses.

3.3.4 Scanning Electron Microscopy (SEM)

Since its relatively recent origin, SEM has found a wide range of applications in failure analysis, materials research and development, and quality control. Fractography is probably the most popular application of the SEM. The three dimensional appearance of SEM fractographs, the large depth of focus, large magnification range, and simple specimen preparation with direct inspection make the SEM a versatile and indispensable tool in failure studies and fracture mechanism research. This unique instrument offers possibilities for image formation of fractured parts that are usually easy to interpret and reveal clear photomicrographs of rough surfaces as well as polished cross-sections. The develop-

ment of an assortment of related capabilities such as stereo viewing, quantitative microchemical analyses, in-situ fracture studies and image formation that is easy to interpret all contribute to the value of this investigative and research tool. Energy dispersive X-ray (EDX) analysis equipment is routinely attached to the SEM, providing semiquantitative and, in favorable situations, quantitative analysis of composition from a small volume. For composites, EDX analysis is usually only required for contamination analysis as presented in paragraph 3.1.4.

The SEM is capable of magnifications from about 5X to 250,000X, although the majority of composite fractography analyses do not go beyond 20,000X. SEM is normally a resolution of approximately 100 angstroms. The depth of field is about 300 times that of the light optical microscope, providing an excellent three dimensional view of the specimen at focal depths of over 1000 microns at 100X and 5 microns at 20,000X. Specimens can be tilted up to approximately 70 degrees to the incident beam, while maintaining focus over most of the surface. The working depth ranges from 8 mm to about 25 mm, allowing an extremely rough surface (such as with protruding fibers) to be examined. The specimen size is usually limited by the size of the chamber door. The maximum size for the latest SEM equipment is approximately 6 inches by 6 inches, with limitations in tilt and thickness at this size. Usually specimens are much smaller (0.5 to 1.0 inch square), so that thicker specimens and maximum tilting may be allowed. Since the specimen size is limited, very large specimens must be partially destroyed. This particular first presents a limiting feature to the SEM, and therefore lower magnification and less destructive inspections such as optical macroscopy and microscopy should be employed prior to SEM analyses.

3.3.4.1 SEM Specimen Preparation

Proper specimen preparation is basically simple and requires only a small amount of time. The preparation sequence is usually as follows:

- Specimen selection - commonly visual or optical inspections of the fracture surfaces to define areas of interest for analyses or documentation.

- Specimen cutting/removal - this involves mechanical methods such as abrasive cutoff machines or hand saws, as discussed in paragraph 3.1.1.
- Specimen cleaning - used to remove dust particulate (from the fracture and cutting processes) and oils, etc, as discussed earlier. Cleaning and coating should not be performed if contamination is a concern.
- Specimen mounting - this involves adhering the specimen to a mounting stub; to secure it and provide a conductive path from the specimen to the SEM chamber.
- Specimen coating - usually required for nonconducting materials such as composites when high KeV's are used.

Good imaging requires careful specimen preparation, such that electrical charging, electron beam damage, and outgasing of volatiles are minimized. Composites, due to their laminated construction and organic structure, are subject to all of these problems if the proper preparation procedures are not followed. Because of this, the latter two preparation steps (mounting and coating) are discussed in detail below.

Mounting - To prevent charging, conductive adhesives such as silver, carbon, or aluminum containing glues are used to bond the specimen to the stub. Drying times are on the order of 30 minutes, although it can be significantly reduced with the aid of a warm air blower. In order to maintain proper specimen identification, labeling the stub with a scribe is often recommended.

Conductive coating - Non-conducting materials such as composites are usually coated to prevent electron charging, caused by a buildup of a space charge region of absorbed electrons. This charging appears dark at the site of absorbed electrons and deflects the incident beam, leading to image distortion and significantly changes the emission of secondary electrons so that the surrounding region appears washed out or over-bright. Charging can be prevented by operating at low acceleration voltages (less than 5 KeV) or applying conductive coatings. The latter method is preferred by most laboratories, since the magnification ranges do not ever approach conditions where the coating would affect microstructural resolution. It should be noted that non-coated low KeV analyses offer

shorter preparation times and do not cover or obstruct surface contaminations, but do usually require an image enhancement system to properly process the limited image output.

The coating layer must be thin as feasible to minimize the possibility of obscuring fine details and thick enough to provide a conductive path for the impinging electrons. The minimum thickness is dependent upon the general roughness of the specimen surface, and may range from 10 nanometers for relatively flat specimens to 50 nanometers for extremely rough topographies. Carbon, copper aluminum, platinum, palladium, silver, gold, or gold-palladium are applied by high vacuum vapor deposition or sputtering. The gold-palladium sputtered is the preferred method, since sputtered layers provide better adhesion and more even condensation, and it provides the finest microstructure and lowest possibility of obscuring fine details. A combination that seems to work well for most fractures is to sputter coat approximately 20 nm of Au-Pd using the DC-pulse mode for 5 minutes after backfilling the vacuum chamber to 4.0 to 7.0 Pascal (30 to 50 millitorr) with argon.

It should be noted that a nondestructive method for SEM examination is available for situations where destructive cutting examination is not possible or the fracture surface may not be removable from the structure. In these situations, a two stage acetate replica may be produced with the same techniques described for TEM analyses. The only difference is that the specimen must be made conductive, and therefore requires an additional layer of vapor deposited gold or similar material.

3.3.4.2 SEM Techniques

The basic features of the SEM are presented in Figure 3-58. This instrument is a combination of electron-optical, vacuum, and electronic control devices for impinging a narrow beam of electrons from a heated cathode and focused by a system of magnets to a pinpoint spot on the surface of the specimen. An image is gained from collecting, modifying, and displaying the resulting emission from the specimen's surface. The cathode, or filament, is usually tungsten. Acceleration voltages range from 1000 to 50,000 volts, although the usual range for composites are 2 to 30 KeV. A more effective and longer life electron source is lanthanum hexaboride (LaB_6). This new cathode requires more care and

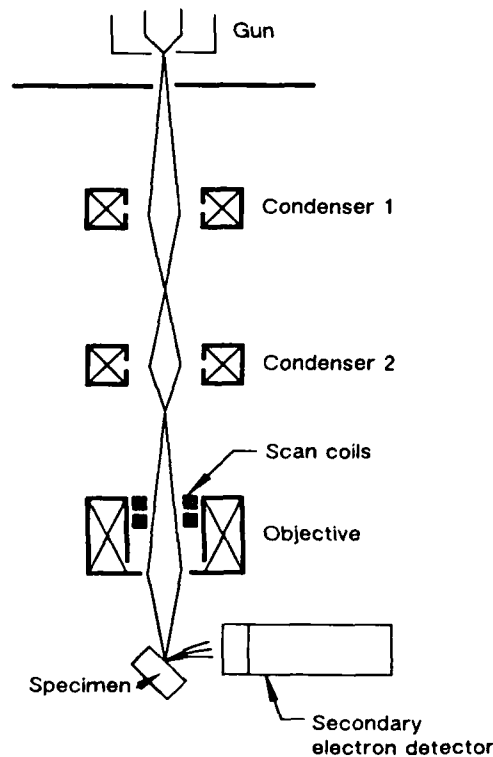


Figure 3-58. Basic Features of the SEM

5-B70227-139

warm-up time in addition to a better vacuum and higher initial cost. To generate the required vacuum, a diffusion pump or a turbomolecular pump is used.

The electron beam scans the specimen similar to the way a cathode ray tube is used to image a scanning raster on a television screen. A scanning generator controls the current to the scanning coils, which in turn, deflect the incident beam along closely spaced lines. The magnification is controlled by varying the current in the deflection coils. The electron beam impacts the specimen surface, and the electrons that return from the specimen surface are collected by a detector. Amplification of this electron signal is required for imaging the scanning cathode ray tube.

When the primary electron beam is impinged upon the specimen, electrons and other radiations are emitted from the surface that can be used to produce images and to microchemically determine the elements present. Figure 3-59 shows the types of emissions radiated from the surface and the relationship to the type of detection modes available. The most common detection modes for composite materials are: (1) the secondary electron (SE) mode, (2) the backscatter electron (BE) mode, (3) the psuedo backscatter electron (PBE) mode, and 4) X-ray spectroscopy. These are used routinely with a sound understanding of the types of information available and the limitations of each detection mode. Each of these detection techniques are described below except X-ray spectroscopy, which is presented in paragraph 3.1.

Although both secondary and backscatter electrons are used for fractography, the secondary electrons are usually the preferred source since they offer better resolution, provide an abundant signal, permit viewing areas of the specimen that are not in direct line with the detector, and provide a better three dimensional effect due to the shadowing loss of electrons at topographical features. There are situations where it is necessary to sacrifice resolution for improved image contrast and differentiation of features or phases by their atomic number. In such a case, backscatter electrons provide image contrast in specimens which are especially smooth or are viewed at low magnifications.

Secondary electrons are produced by interaction of the primary electrons with the atoms in the first 1 to 10 nm, resulting in emission of the loosely bound atomic electrons. The energy spectrum of these secondary electrons are independent of the energy of the

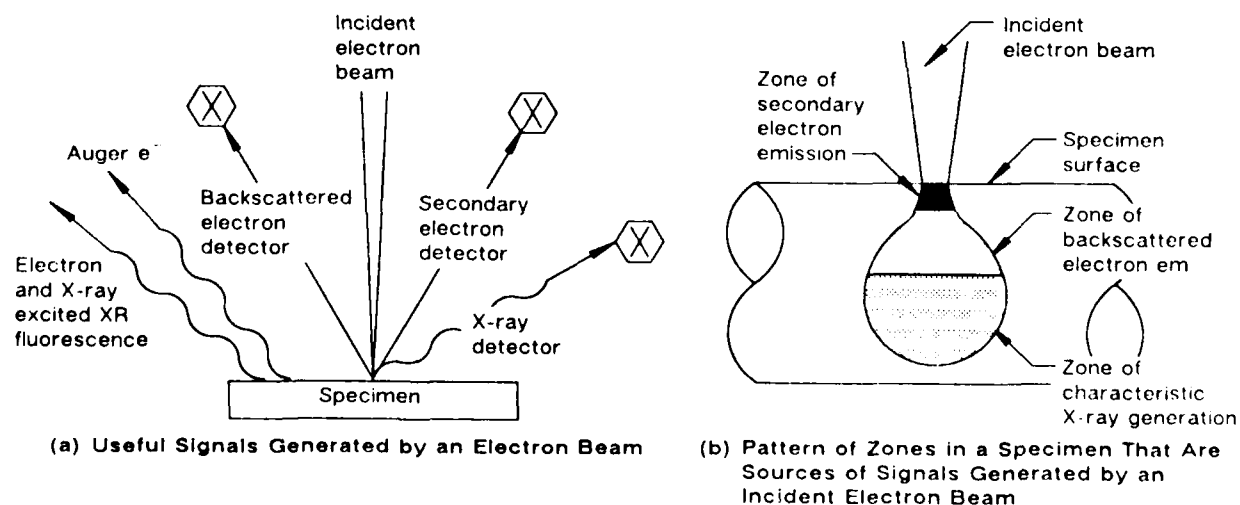


Figure 3-59. The SEM Beam-Specimen Interaction Details

incident beam and material type. The energy spectrum is fairly limited in range, with a pronounced maximum at approximately 3 eV. As a general rule, all electrons below 50 eV are considered to be secondary electrons and electrons with more energy are in the backscatter range. The primary factor for secondary yield is due to topographical features such as small variations in the surface angle. Since the secondary are emitted from the top few nanometers, the envelope of the excited and emitted electron volume moves closer to the surface when the beam contacts the surface at an angle, thus increasing secondary electron yield, and therefore brightness on the visual image.

As shown in Figure 3-59, the backscatter electrons are produced by single large-angle or multiple small-angle elastic scattering of the primary electrons as they impact the atoms from 0.1 to 1.0 μm beneath the surface of the specimen. Different than secondary electrons, the energy distribution of the backscatter electrons depend directly on the energy of the primary electrons and the atomic number of the material. In a similar manner, although with a more pronounced effect, surface inclination of the specimen provides an accentuation of the topographical features of the specimen. In specimens with high atomic numbers, which have larger atomic sizes, a larger percentage of the electrons are backscattered from atoms closer to the surface, with little change in energy. Therefore, the yield and thus the brightness is increased with materials that have higher atomic numbers. For those specimens which have a very smooth topography, the use of pseudo-backscatter electron is employed. This involves using the secondary electron detector with gating of the allowed electron energies for those electrons with more than 50 eV. This detection mode does not "see" the secondary electrons that have energies around 3 eV. Figure 3-60 illustrates the use of secondary, backscatter, and pseudo-backscatter for the imaging of a composite fracture surface.

Optimization of imaging can enhance the image for analysis and documentation. Some components of a scanning electron microscope have their own characteristics of resolution and noise, which determine the image quality, however, most instrument parameters are fixed by the designer to achieve maximum performance. The SEM provides flexibility so that the operator can adjust the instrument parameters for a specific specimen and investigation. Several commonly adjusted parameters which are available include:

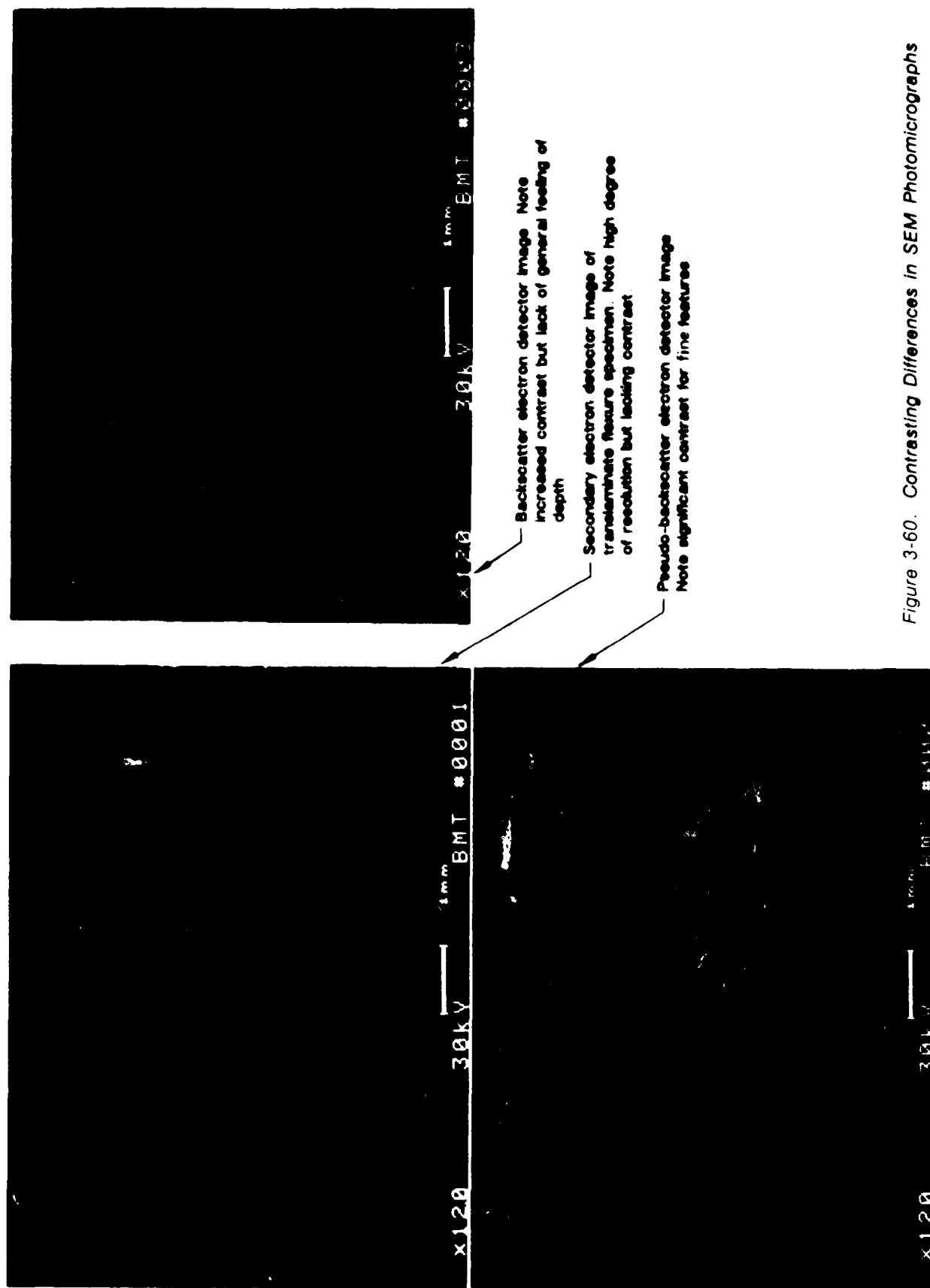


Figure 3-60. Contrasting Differences in SEM Photomicrographs

5-870227R1-014

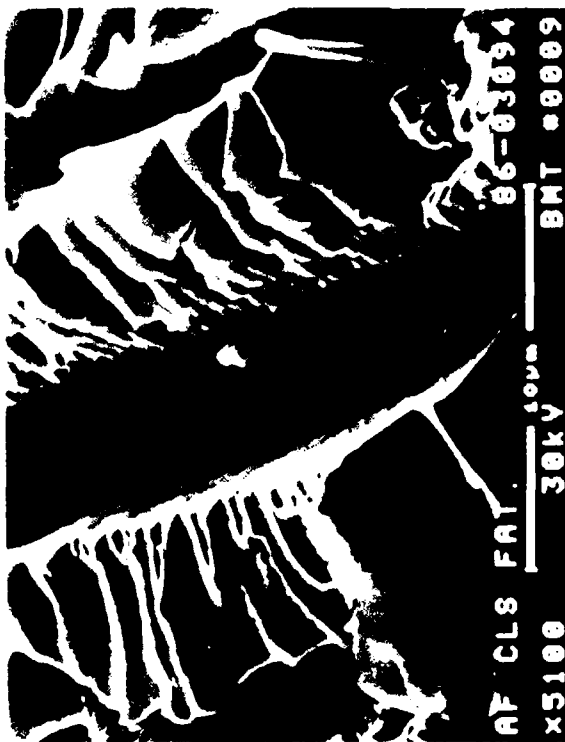
- Object tilt angle.
- The aperture size and working distance.
- The beam characteristics such as beam KeV and spot size.
- The detection method such as SE or BE.

Object tilt probably provides the greatest effect on the overall image and thus should be optimized. Specimen tilt, which causes the beam penetration depth and scattering to vary, results in contrast between topographical features, similar to side lighting in optical macroscopy or shadowing for the TEM. The effect of tilting is more pronounced for the backscatter mode than the secondary emission mode. Since tilting can be used to enhance subtle features on smooth fractures, the use of high tilts are often required for examination of fatigue features, as shown in Figure 3-61, where fatigue striations are not visible until tilts beyond 30 degrees are employed. Similarly, the use of tilt often provides a quite different perspective of the fracture morphology such as hackles, as shown in Figure 3-62.

The aperture size and working distance determine the depth of focus. For rough surfaces at low magnifications, a small aperture and large working distance are selected. For high magnifications, a short working distance, small aperture, and high lens currents must be used to minimize the spot size.

Interlaminar Fractures—The basic fracture types and the general SEM instrument optimization for each type is presented below.

- Crack mode and direction of propagation - use magnification in the range of 400X to 2000X, to inspect the direction of river marks, resin microflow, and tilt of hackles. For most observations, a tilt of approximately 30 degrees in the SE detection mode appears to be best.
- Fatigue - where this crack growth mode is suspected, high tilts beyond 60 degrees are often required, with viewing angle perpendicular to the striation. For instance, Mode II shear striations usually appear within the fiber matrix separation region, and therefore the viewing angle should be running parallel to the direction of fibers in a tape material. Pseudo backscatter and backscatter detection modes have been used successfully to identify and



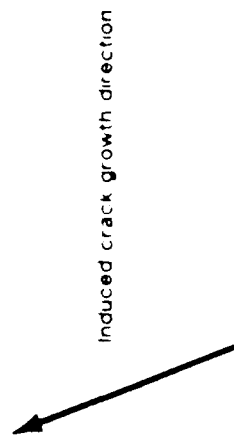
30-deg tilt



30-deg tilt



0-deg tilt



Induced crack growth direction

Figure 3-61. SEM Photomicrographs of Effect of Tilt on Striation Resolution

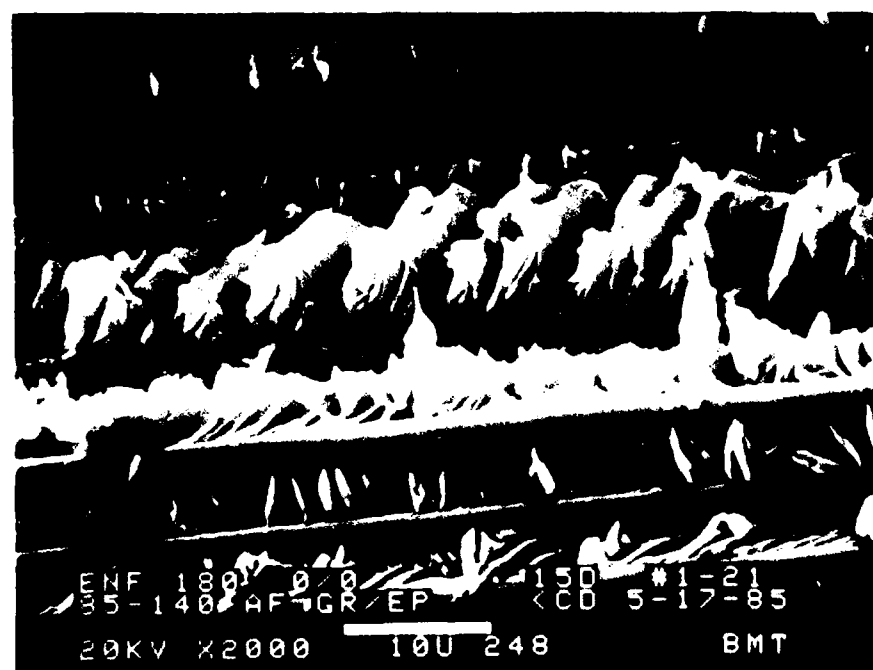


Figure 3-62. SEM Fractographs of Mode II Delamination Between Adjacent 0-deg Plies Illustrating the Effect of Tilt Angle

5-B70227-16

provide accentuated contrast to striations that are not easily detected using the secondary electron detector.

- Disbond or contamination - for areas suspected of contamination or regions suspected of having a thin coating with different atomic number, the use of backscatter is invaluable. Usually a tilt is not required for this detection method.

Translaminar Fractures—For these fractures which have a very rough topography, the use of small apertures is desirable to increase the depth of field. Increasing the working distance also provides increased depth of field, although the resolution is degraded at extremely long distances and higher magnifications. Higher accelerating voltages do not provide any additional benefit since the secondary electron emission is independent of the beam energy. For most of these investigations, the magnification range is from 5X (for macroscopic view to differentiate between compression or tension) to 2500X (to identify the individual fiber end fracture morphology). Since the translaminar fractures provide an enormous amount of contrast and topography changes, the SE detection mode is most useful since it is least sensitive to roughness extremes.

3.3.5 Transmission Electron Microscopy (TEM)

The use of transmission electron microscopy is fairly limited in investigation of composite fracture surfaces. Since the application of the SEM, which provides an excellent view of the fracture morphology, the TEM has been only applied to analyses of interlaminar fatigue. For this failure type, the striations related to cyclic crack growth are usually faint and limited to small zones in the fracture surface. The TEM has advantages over the SEM in that extremely fine resolution and a high degree of image enhancement is available through the specimen preparation methods and specimen tilt during analyses. The TEM however, requires a labor intensive specimen preparation and a trained operator to interpret the features observed. Quite different than the SEM, the transmitted electrons provide an image that is difficult to interpret and differentiate the actual fracture features from artifacts created during the replication process and microscope operation.

3.3.5.1 TEM Specimen Preparation

The basic specimen used for TEM analyses is the two-stage replica. Direct examination of the fracture surface can be made with the other techniques discussed above, but replicas offer the unique capability of transposing topographical information of composite delaminations to a high-fidelity facsimile that can be conveniently handled and transported, and readily examined in the TEM, SEM, or light optical microscope. The use of replication has significant value when the fracture surface of the failed part cannot be transported to the laboratory. Additional value is the ability to generate several replicas of the fracture surface, all of which may be destructively analyzed to determine the physical features relative to the determination of the cause of failure.

The initial cleaning of the composite fracture surface was covered in paragraph 3.3. This usually involves detergent wash with ultrasonic agitation to displace particulate that may be physically impacted into the fracture surfaces during fatigue cyclic loading. The final stage of cleaning usually consists of successively applying and stripping several acetate tape replicas. The thin acetate tape is first wetted with a small amount of acetate solution, allowed to soften, and then applied to the fracture surface which also has some acetated solution applied to the area. Hand pressure is maintained without moving for at least a full minute. Following full drying of the replica, it is carefully removed to limit the damage from lifting fibers from the fracture surface. Usually two replicas are required to properly clean the fracture surface.

For most composite laminates, the matrix material can withstand short periods of contact with solvent, even those within their own functional chemical groups. This is particularly true for chemically stable epoxy resins that are thermosetting and are highly cross-linked. For these resin systems, the use of the most common replication materials, acetate film and acetone, do not exhibit damage of even the finest fracture details. Other matrix materials, particularly those that are thermoplastic and are not cross-linked, should be spot tested in an area in the replication technique.

Following the generation of several clean replicas, they are then prepared in the same manner that is used for metals, in which the plastic replica is first shadowed with a high Z (atomic number) material such as germanium, and then coated with carbon. Figure 3-63

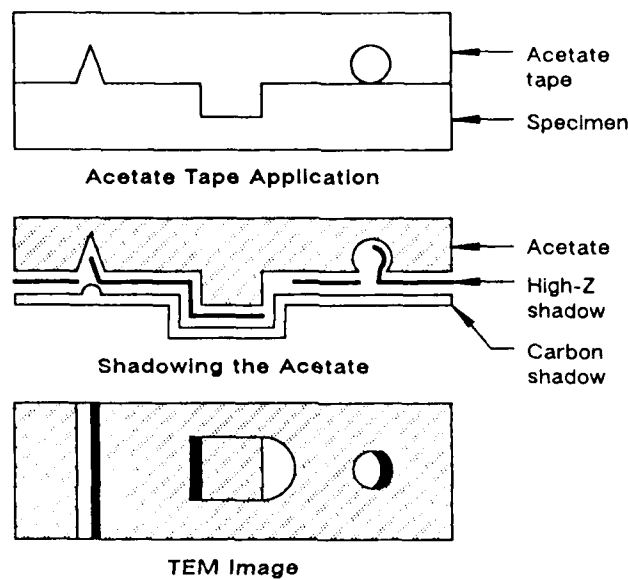


Figure 3-63. The Two-Stage TEM Replication Technique

5-B70227R1-142

illustrates the two stage replication technique. For fatigue striation evaluation and maximum enhancement of the subtle features involved, the direction of germanium shadowing should be parallel to the direction of anticipated fatigue crack growth.

These replicas are then cut to size, for fit to the copper grids, and then floated in an acetone solution to remove the plastic portion from the replica. This stage is the most difficult and often very frustrating. Due to the fiber reinforcements, the replicas have a pronounced tendency to curl along the ridges formed by the fibers. Laminate tape fractures are extremely sensitive to this problem, particularly when the fracture involves only unidirectional fiber orientation. Specialized methods can be attempted, which include:

- Dilute the acetone solution with distilled water to reduce the chemical mixing and curling, thus reducing the possibility of tearing and breakup.
- Providing more than one carbon coating, each at different angles, to provide a more complete covering of the specimen. This increases the thickness which tends to reduce the curling.
- When the above methods fail, the specimen can be scribed in the direction perpendicular to the fiber direction, creating a crosshatched effect, also reducing the chance of curling or breakup. The crosshatching has been successfully performed using a hot blade, attached to the tip of a small

soldering gun, so that the damage is lessened by the smooth cutting action on the plastic film. The cuts should be made very close together, as close as 0.01 to 0.02 inches, with very light pressure to the coated side of the replica.

- The small replica specimen can be placed between two copper grids (there are butterfly types for this purpose) and the plastic may be removed overnight by acetone vapor. (There are instruments sold for this purpose.)

3.3.5.2 TEM Techniques

The TEM shown in Figure 3-64 contains an electron source, or filament, that emits a stream of electrons into a vacuum chamber. The filament is held at high accelerating

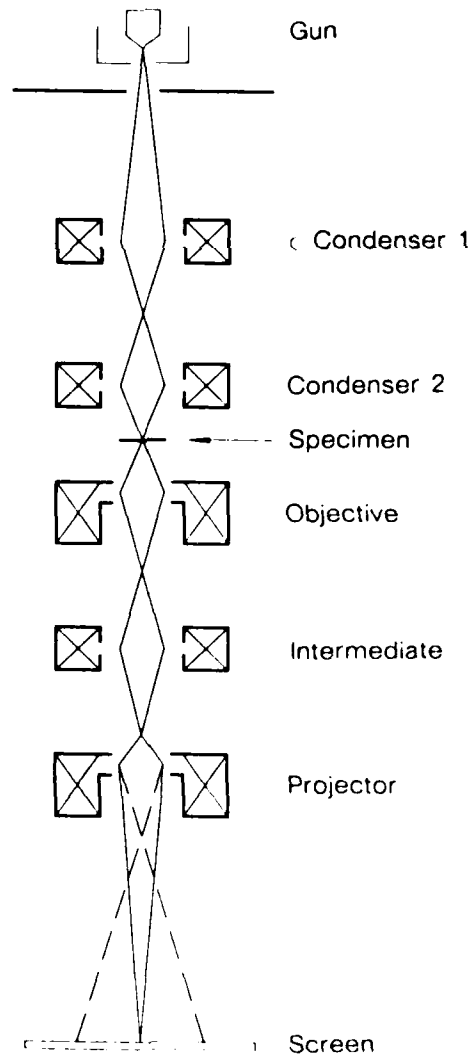


Figure 3-64. Basic Features of the Transmission Electron Microscope (TEM)

5-B70227-143

potential relative to the grounded anode beneath it. The electrons pass through the hole located in the center of the anode and then through a condenser lens which consists of a electrically variable magnet. The condenser lens focuses the beam on the specimen. The electrons are either reflected, absorbed, or transmitted. The electrons which are transmitted through the specimen are allowed to pass through three magnetic lenses, forming a succession of three images, each magnified in turn to yield the intended overall magnification. The range of magnification is from 200X to about 25,000X for two-stage replicas, however the limit of use for composite laminate resin is about 10,000X.

The quality of the TEM image is affected by magnification, image intensity, image contrast, and the resolution obtainable. For increased resolution, higher magnification and better focus is necessary. For increased contrast, the objective-lens aperture may be varied, lower KeV's can be used, or the specimen can be tilted. Specimen tilt is usually the best method for identifying the faint striations present in the resin fracture regions. Figure 3-65 presents fractographs of a specimen which had been subjected to a compression-compression fatigue cyclic loading. The faint striations are barely visible and lie perpendicular to the localized crack growth directions. River marks and resin microflow are also evident. The river marks and resin microflow features can be used to identify the localized direction so that the tilting of the specimen can be made on the correct plane to maximize the enhancement of the striations. Figure 3-66 illustrates the striations evident at the fiber/matrix interface region for crack lap shear specimens (80% interlaminar Mode II shear). Tilts between 15 and 30 degrees were required for creating enough contrast and striation enhancement for the fractograph examples presented in this paragraph.

3.4 STRESS ANALYSIS TECHNIQUES

3.4.1 Introduction to Composite Stress Analysis

The purpose of stress analysis in the context of this compendium is to provide information which may lead to defining the cause of failure damage in a composite structural component. Although other methods of analysis may identify the origin, direction, and mode of crack propagation, stress analysis most often provides a quantitative explanation for the cause of failure initiation. The following introductory paragraphs are intended to



7000X

Fiber



13,500X

Note: Striations are an indication of fatigue growth.

Figure 3-65. High-Magnification TEM Photomicrographs Showing Fatigue Striations

5-B70227-17



Note the curved striations equally spaced along the fiber surface

Figure 3-66. TEM Photomicrograph of Striation Features From a Crack Lap Shear (CLS) Specimen

5-B70227-18a

acquaint the reader with the methodologies and techniques used for stress analysis as applied to failure investigations of composite aircraft structures.

A. Stress Analysis Techniques

In the following paragraphs, literature on stress analysis is reviewed in detail. While these writings by no means encompass the entire field of stress analysis, they provide a perspective on the techniques and procedures available for composite materials. Before discussing the application of these techniques, however, it is important to recognize the role of stress analysis in a postfailure investigation.

Most components are subjected to detailed stress analyses as part of their initial design. Consequently, in the as-designed configuration, failure should not occur as long as the component is operated within its design life and envelope. However, real-world experience indicates that component fractures do occur in service. Common causes of such failures include:

- Design Deficiencies such as insufficient assessment of loads and stresses, either of design details or individual plies. Also included are the over simplification of loads, load paths, and the combined effects of load, damage, and environment.
- Manufacturing and Process Discrepancies such as mismatched radii, ply layup errors, and mislocated or misdrilled fastener holes.
- Service Damage including foreign object impact, subcritical cracking, and improper maintenance or repair.

For each case, the objective in analyzing stress is to determine if the occurrence of a failure not predicted during initial design can be explained and understood. While techniques such as *fractography* may be able to identify the origin and mode of fracture, it is stress analysis that most often determines the cause of failure.

The stress analysis required to investigate part failure can be relatively complex, but from the point of view of the failure analyst, the process involved can be divided into two discrete tasks, thus making the review of available literature most straightforward. The two tasks are:

- Assessment of the component strength in the as-fabricated condition.
- Assessment of component residual strength considering flaws, damage, and sub-critical cracks.

Figure 3-67 illustrates the relationship between the methods identified in the literature and these two tasks. The first task, assessing the part strength in the as-fabricated condition, evaluates stresses at a greater level of detail than during initial design. In most cases, this assessment focuses on the crack origin, with special attention to discrepant manufacturing and production conditions. Principal techniques at this level of assessment, likely to be of value, include individual-ply, point, and average-failure criteria, laminate strength criteria, and the Damaged Zone Model.

The individual-ply failure criterion examines stresses at the individual ply level and establishes the onset of first-ply failure. The chief benefit of this analysis method to failed structures is its ability to predict the point of initial failure on a microscale. This ability is particularly significant since most initial design analyses consider stresses on a gross-average basis. However, even though there is potential value in this methodology, some drawbacks exist. The most significant of these is that to examine edge-effect stresses of individual-ply failure criterion requires a knowledge of plan view stress distributions (surface stress flow) and detailed finite-element grids. For organizations with experts in stress analysis, neither of these factors is a limitation. More significantly, however, the individual-ply failure criterion predicts failure initiation, not catastrophic failure. It also exhibits significant inaccuracies when applied to predicting strengths of multidirectional laminates. Consequently, failure onset cannot be meaningfully determined based on the individual-ply failure criterion. As a result, prediction of the stress required for catastrophic failure is more likely to be calculated by gross area stress calculations with fine, finite-element grid structures placed in the area of failure origin.

ANAL. TASK	METHOD	DESCRIPTION	AUTHORS (ref. number)	COMMENTS
Assessment of as-fabricated strength	Laminate theory and first ply failure criteria	Laminate theory is used to identify two-dimension stresses; one of several failure criteria are applied to define occurrence of first ply failure	<ul style="list-style-type: none"> • Chamis (22) • Craddock (64) • McLaughlin (65) • Tsai (11) • Jones (15) 	<ul style="list-style-type: none"> • Valuable for simple prediction of ply failure • Laminate theory requires knowledge of local stresses • Laminate theory cannot handle edge effects/complex geometries • Predicted failure stresses vary widely with criterion used • Failure criterion not accurate • Does not predict catastrophic failure
	Finite element analysis and first ply failure criteria	Finite element analysis is used to define stresses in three dimensions for edge effects/environments/bolted joint configurations; one of several criteria are applied to define occurrence of first ply failure	<ul style="list-style-type: none"> • Crossman (20) • Herakovich (21) • Wu (66) 	<ul style="list-style-type: none"> • Valuable for simple prediction of ply failure • Finite element techniques can be used to define local stresses • Method accounts for edge effects, environment, complex geometries • Predicted failure stresses vary widely with criterion used • Failure criterion not accurate • Does not predict full failure
	Point or average failure stress criteria, DZM	A semiempirical method for describing the strength of open or filled holes; failure occurs when point or average stress at a characteristic distance from hole equals material strength	<ul style="list-style-type: none"> • Mikulas (7) • Wilson (67) • Daniel (6) • Aronsson (8) 	<ul style="list-style-type: none"> • Valuable for prediction of strength with holes • Requires knowledge of characteristic distances for material • Requires knowledge of stress distribution around hole
Assessment of residual strength	Point failure stress criterion, DZM	Adapted semiempirical method from predicting strength with holes; failure occurs when stress at a characteristic distance from damage radius equals material strength	<ul style="list-style-type: none"> • Mikulas (7) • Starnes (45) • Aronsson (8) 	<ul style="list-style-type: none"> • Valuable for predicting residual strength with impact of through-thickness cracks • Requires knowledge of characteristic distance for material • Requires knowledge of stress distribution around hole • Requires estimation of initial damage size to predict strength
	K_{IC} fracture toughness	Fracture toughness method commonly used with metals	<ul style="list-style-type: none"> • Bathias (29) • McGarry (30) • Awerbuch (31) 	<ul style="list-style-type: none"> • Valuable for predicting residual strength with through-thickness cracks under tension loads • Requires knowledge of K_{IC} for material layup • Requires estimation of initial crack size to predict strength
	G strain energy release rate	Predicts onset of delamination instability based on G_{1C} for material and G level generated by applied load	<ul style="list-style-type: none"> • O'Brien (68) • Whitcomb (9) • Rothschilds (10) 	<ul style="list-style-type: none"> • Valuable for predicting delamination instability • Requires knowledge of G for material layup • Requires calculation of buckle stability for compression case • At present, can handle only very simple geometries
	CODSTRAN	Integrated computer program that incorporates finite element model, first ply failure, and point or average failure criteria; program is iterative, allowing prediction of failure sequence and residual strength	<ul style="list-style-type: none"> • Chamis (22) 	<ul style="list-style-type: none"> • Attempts to meld various techniques discussed above • Requires expert computer programmer • Requires material data, as described above • Inaccurate prediction of strength

Figure 3-67. Stress Analysis Methods

5-B70227-116

Other considerations in estimated gross area stress are the point and the average-failure stress criteria and the Damaged Zone Model. As described in the works of Daniel (ref. 6), Mikulas (ref. 7), or Aronsson (ref. 8) on laminate failure criteria, the stress at failure can be determined for any hole, given a characteristic parameter for the particular material and layup. Based on results reported in these researchers' works, this method appears to work relatively well, its only apparent constraints being that it requires empirical measurement of the characteristic parameter and knowledge of the plan view stresses for the area of interest. In actual application, neither of these constraints should be significant; however, additional concerns that must be addressed include the effects of environment, absorbed moisture, and resin formulation on the validity of a single value used as a characteristic material property.

Figure 3-67 depicts the second major task involved in the stress analysis of a failed component—assessing its residual strength. Considerable investigation has been done that can be directly translated to the analysis of through-thickness flaws such as cracks emanating from holes. Either the Damaged Zoned Model or point-stress failure criterion appear to work well for predicting the onset of crack instability. The limit in applying either of these methodologies lies in the ability of disciplines such as fractography to identify and define the size of original damage. Given this measurement, establishing the point of stress necessary to cause failure requires only that values for the characteristic parameter be known. The literature shows that these values have been measured for a variety of layups. However, these characteristic material properties may vary with resin system and environment, making the calculation of residual strength more difficult.

Methods of evaluating the criticality of interlaminar defects has been maturing rapidly in the last five years. To accompany this, researchers have identified characteristic surface morphologies for pure Mode I or Mode II crack growth. Crack growth directions under Mode I loading can be determined quite readily from the surface micro-features. These emerging technologies in the area of delamination provide the failure analyst with useful tools for determining the cause of a structural failure.

In summary, reviewing the stress analysis literature revealed several techniques for assessing the strength of failed components either as-fabricated, or with through-thickness damage or fracture. These techniques, their value and their limitations are

summarized in Figure 3-67. Some of these techniques are somewhat inaccurate, or may require measured properties not readily available; however, at the very least, the techniques define the applicable methodologies and their attributes.

B. Stress Analysis Failure Analysis Logic Network (FALN)

Defining the cause of component failure requires the accurate understanding of the loads and stresses involved as a part functions. In metals, this understanding is commonplace. Fracture mechanic calculations are usually carried out during initial design stages as well as after component failure. Stress analyses are run after failure to review initial design stresses in more detail, to evaluate configurational and material errors, and to determine if damage (cracking) was incurred in service or during maintenance. The logical investigative sequence for metals and composites is similar. Figure 3-68 illustrates the detailed stress analysis FALN based upon existing metals procedures and inputs from experts in the area of composite materials stress analysis.

Stress analysis of a failed component is carried out at three different levels: initial design review, a structural level, and a lamina level.

At the initial design review, the analyst's objective is to verify initial design assumptions and calculations with respect to the available service history and the location of fracture. This review establishes what analyses were performed and their adequacy.

The next level of investigation encompasses the most critical stage. At the structural level, inputs from the main FALN are incorporated, and detailed strains and stability at fracture origin area are defined. Since most components are designed to gross average strain and stability criteria, the information from this analysis usually provides adequate detail to understand the cause of failure. For the analyst, investigations at this level may involve detailed finite-element modeling, depending upon the level of initial analyses.

Investigation of stress at the lamina level is unique to composite materials. Because of the highly anisotropic nature of laminated composites, internal stresses can exist on a ply-by-ply level, and individual ply stresses and failure predictions can be handled with varying degrees of detail. The simplest level of investigation employs laminate theory combined with relatively simple failure criteria. However, since individual ply failure does

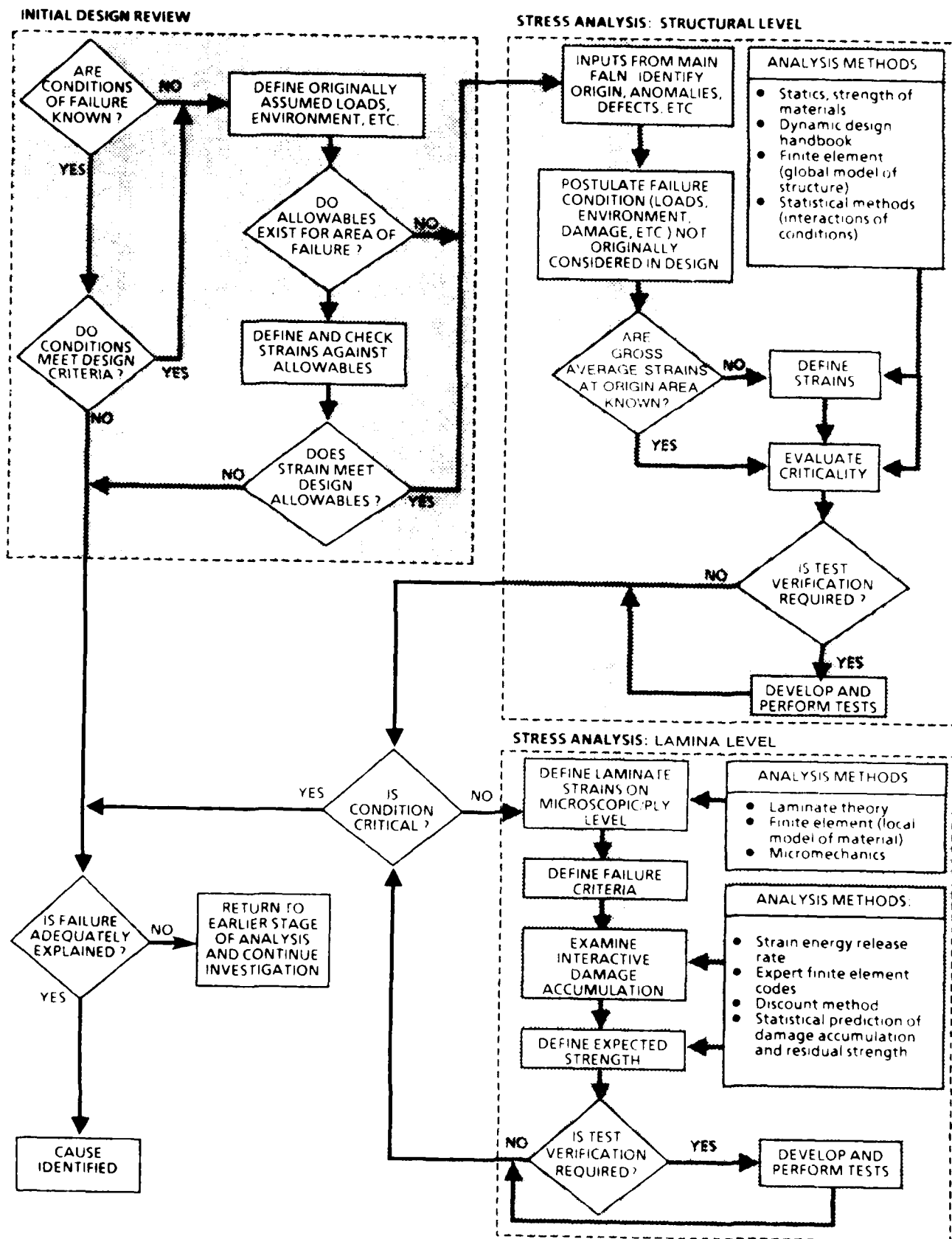


Figure 3-68. Stress Analysis Sub FALN

not usually constitute catastrophic fracture, additional iterative analyses are required. These analyses can be performed with a variety of computer programs (Figure 3-68); however, using such programs requires a detailed understanding of the methods used, their accuracy, and most importantly, their limitations.

3.4.1.1 Relevance to Stress Analysis FALN

Stress analysis as depicted by the Stress Analysis FALN (see Figure 3-69) is conducted at one or more of the following levels of complexity depending on the type of damage and economic considerations: (1) initial design review, (2) a structural level analysis, and (3) a lamina or microstructural level analysis. Throughout the investigation the failure analyst must communicate with the stress analyst to understand how the structure was loaded in the damage region (for example, tension, compression, shear, flexure).

During the initial design review, the stress analyst's objective is to verify initial design assumptions and calculations with respect to the available loading history, the location of fracture, and environmental conditions. This review establishes what analyses were performed during original design and evaluates their adequacy.

The next level of investigation encompasses the most critical analysis. At the structural level the analyst's understanding of the loads and stresses derived from the initial design review will help evaluate the significance of inputs or anomalies from the main FALN (for example, load types or errors in number of plies or ply orientation). It may be determined that these defects significantly affect the stresses or strengths in the damaged region. In this case, parts of the initial stress analysis would be repeated to assess the impact of the anomalies at the origin of failure. At the structural level, the stress analyst employs finite elements and analytical models to compare the gross average strain to strength critical strain and stability conditions. This information, incorporating the effect of anomalies, usually provides adequate detail to understand the cause of failure. Redesigns at this level of analysis would be focused towards reducing gross average design strain to account for anomalies discovered during the initial design review.

If the cause of failure has not been adequately explained in terms of gross average strains, stress analysis at the microstructural or lamina level is required. This is often the case

NAME	FEATURES	USER MANUAL	COMPUTER	APPLICATION
AC-50	Inplane laminate allowable stress	Rockwell TFD-75-1180 Nov 1975	CDC 6600	Advanced composite analysis
NASTRAN	<ul style="list-style-type: none"> • Finite element analysis • Resize for minimum weight 	NASA SP-222 (01) 1972		Analysis and resizing of complex structures
BOP (Buckling of panels)	Combined compression and shear of stiffened, variable-thickness flat rectangular orthotropic panels on discrete springs	NASA TND-7996 Oct. 1975	CDC 6600	Graphite-epoxy composite panels
SO 5	Point stress analysis of laminated composites for: <ul style="list-style-type: none"> • Inplane loads • Moments • Temperature • Transverse shear 	AFFDL tech memo FBC-74-107 July 1974	CDC 6600	Advanced composite analysis
STAGS	Stress analysis and panel stability evaluations	Lockheed document, Structural Analysis of General Shells, Volume 3, Dec 1975	CDC 6600	Plotting of buckling mode shapes
VIPASA (Vibration and instability of plate assemblies including shear and anisotropy)	Natural frequencies of loaded structures <ul style="list-style-type: none"> • Critical buckling loads • Thin, flat rectangular plates • Thermal stress 	COSMIC file ISCL Doc. ID 00 17437 Jan. 1973 NASA TMX-73914 May 1976	CDC 6600	Compression loaded stiffened graphite-epoxy panels

Figure 3-69. Computer Analysis Programs

5-B70227-82

when failure may have initiated at a design detail such as a hole, edge, or other stress concentrator. At the lamina level, highly refined finite element meshes in the region of failure initiation are employed to determine detailed three-dimensional strain distributions. Loads or displacements applied to the finite element meshes are derived from the stress analysis at the structural level. This detailed type of analysis, although not often done during the initial design, provides information needed to evaluate interlaminar normal and shear stress concentrations at free edges. Fracture mechanics, coupled with finite element analysis, have been successful at predicting the onset of interlaminar crack growth (see ref. 9 and ref.10). Redesigns, resulting from lamina level studies, may be required to eliminate or reduce the effect of design details that cause stress concentrations.

The thermoelastic properties of the anisotropic, or more specifically, orthotropic plies or lamina can be predicted from the properties of the fiber and matrix constituents with micromechanics. Lamination theory is then employed to calculate the thermoelastic properties of a group of lamina bonded together into a laminate. References (11 through 14) provide lucid descriptions of the limitations and value of lamination theory. Stress analysis of fiber reinforced polymers is quite different than that of metals for the following reasons:

- Lamina stiffness in the fiber direction is typically greater than 10 times the stiffness transverse to the fibers.
- Lamina strength in the fiber direction is generally greater than 30 times the strength transverse to the fibers.
- The differences in the stiffness coefficients between plies within a laminate causes interlaminar stresses.
- The differences in the hygrothermal expansion coefficients between fiber and matrix within a ply and between plies within a laminate may lead to significant residual stresses due to changes in temperature or moisture content.

Lamination theory can be used to determine the strains and stresses in a composite structure without considering interlaminar stresses. Finite element, finite difference and analytical methods beyond the scope of this text have been used to evaluate interlaminar stresses. However, the failure analyst must recognize that these stresses exist in composite structures and that the resistance to interlaminar crack growth is hundreds of times less than the resistance to transply crack growth. This result is expected since the fracture of fibers requires far greater energy than that needed to propagate an interlaminar crack in which matrix fracture dominates.

3.4.1.2 Overview of Topics

The following paragraphs provide the failure analyst with an overview of the techniques used to determine the stresses in laminated composites. These tools vary widely in their ease of application and accuracy of results. In addition, it is intended to familiarize the reader with design details, manufacturing and processing defects, and other considerations which must be applied to composite failure analysis.

Paragraph 3.4.1.3 deals with predicting the strength of unnotched multi-directional laminates with and without edge effects. Criteria for predicting failure of an individual ply are discussed and then applied to predicting laminate strength. Paragraph 3.4.2 addresses the influence of ply thickness and orientation on transverse cracking and delamination. Paragraph 3.4.3 describes some of the approaches for predicting reductions in strength caused by inplane stress concentrators such as cutouts and notches are described. Other strength reductions incorporated into design such as environmental effects and impact damage are also discussed. Semi-empirical fracture mechanics and stress based approaches are discussed with respect to their ease of use and generality of application. Paragraph 3.4.4 discusses, in more detail, design details causing interlaminar stress concentrations (unique to composites), such as holes and free edges. This is important because interlaminar stresses cause delamination to grow under fatigue or static loading leading to significant reductions in compressive strength. Paragraph 3.4.5 is designed to familiarize the reader with some of the extrinsic factors (for example, manufacturing defects) which may reduce the strength of laminated composites. The stress analyst would then evaluate the significance of these factors or anomalies with respect to the cause of failure.

3.4.1.3 Analytical Prediction of Strength (Of Unnotched Multidirectional Laminates)

Methods for predicting the strength of laminates composed of plies at various angles are needed to allow designers to orient the fibers in the load bearing and stiffness critical directions. The methods are semi-empirical in that they rely on measured strengths in the principal material directions for calibration. The theories are focused toward the strength of an orthotropic laminate under in-plane loading. Laminate level analysis is always based on ply level analysis. This is fundamental to the concept of lamination theory.

3.4.1.4 Individual Ply Failure Criteria

At this level of analysis the failure of an individual ply is predicted in terms of the strengths in the principal material directions and an appropriate failure criterion. The overview presented here is drawn from the excellent discussions given in references 11, 12, and 15.

Maximum Stress and Maximum Strain Theories—The maximum stress theory states that fracture occurs when the stress in any of the principal laminate orientations exceeds its respective strength. This criterion defines a failure envelope described by the following equations:

$$\sigma_1 < X^t \text{ for } \sigma_1 > 0 \text{ and } |\sigma_1| < X^c \text{ for } \sigma_1 < 0 \quad (\text{eq. 6})$$

and

$$\sigma_2 < Y^t \text{ for } \sigma_2 > 0 \text{ and } |\sigma_2| < Y^c \text{ for } \sigma_2 < 0 \quad (\text{eq. 7})$$

and

$$\sigma_{12} < S \quad (\text{eq. 8})$$

where:

- σ_1 = stress along the fiber direction
- σ_2 = stress transverse to fiber direction
- σ_{12} = in-plane shear stress
- X^t, X^c = tension and compression strength along the fiber direction

Y^t, Y^c = tension and compression strength transverse to the fiber direction

S = in-plane shear strength

For in-plane loading of an off-axis ply, the principal stresses can be calculated by the transformation equations below and then substituted into the failure criteria in the previous equations.

$$\sigma_1 = M^2 \sigma_x + n^2 \sigma_y + 2mn \sigma_{xy} \quad (\text{eq. 9})$$

$$\sigma_2 = N^2 \sigma_x + M^2 \sigma_y - 2mn \sigma_{xy} \quad (\text{eq. 10})$$

$$\tau_{12} = -MN \sigma_x + mn \sigma_y + (m^2 - n^2) \sigma_{xy} \quad (\text{eq. 11})$$

where:

$m = \cos$

$n = \sin$

An analogous failure criterion in terms of strains (see ref. 11) generates strength predictions in close agreement with the maximum stress theory. Figure 3-70 illustrates data taken by Tsai (ref. 16) that shows there are significant discrepancies between theoretical strength predictions based on the maximum stress failure criteria and experimental data for glass/epoxy. This is expected since interactions between stress components are not accounted for.

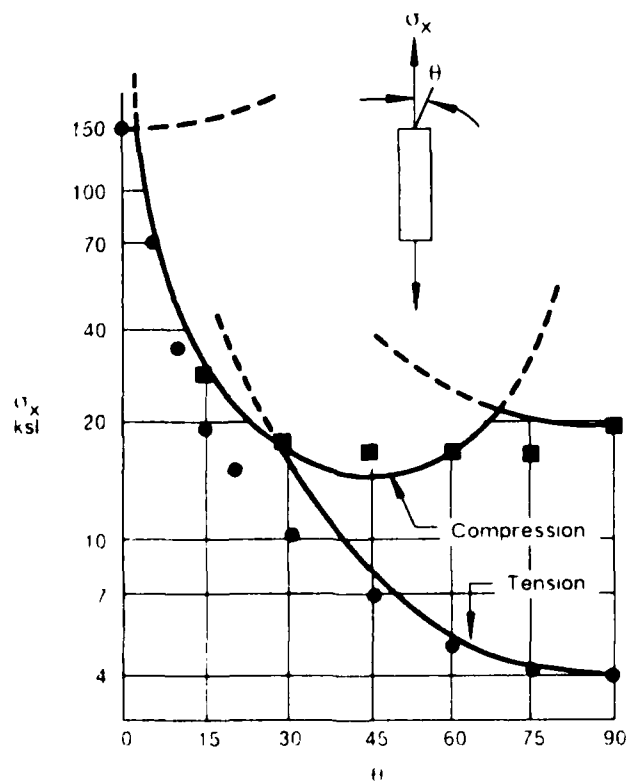


Figure 3-70 Maximum Stress Failure Theory

5 B70227-108

Tsai-Hill Theory—A strength criterion based on von Mises' isotropic yield criterion was proposed by Hill (ref. 17) for anisotropic materials. For biaxial loading and plane stress conditions, lamina failure would occur when,

$$\frac{\sigma_1^2}{X} - \frac{\sigma_1 \sigma_2}{(X)^2} + \frac{\sigma_2^2}{Y} + \frac{\sigma_{12}^2}{S} = 1 \quad (\text{eq. 12})$$

where:

$X = X^t$ when σ_1 is positive

$X = X^c$ when σ_1 is negative

$Y = Y^t$ when σ_2 is positive

$Y = Y^c$ when σ_2 is negative

X^t, X^c = tension and compression strength along the fiber direction

Y^t, Y^c = tension and compression strength transverse to the fiber direction

S = in-plane shear strength.

The Tsai-Hill strength criterion for uniaxial loading of an off-axis ply is developed by substituting equations (9), (10, and (11), into equation (12). The resulting criterion shown below provides an excellent fit to the experimental data for glass/epoxy (ref. 16) as shown in Figure 3-71.

$$\frac{m^4}{(X)^2} + \frac{m^2 n^2}{(X)^2} + \frac{n^4}{(Y)^2} + \frac{m^2 n^2}{S^2} = \frac{1}{(\sigma_x)^2} \quad (\text{eq. 13})$$

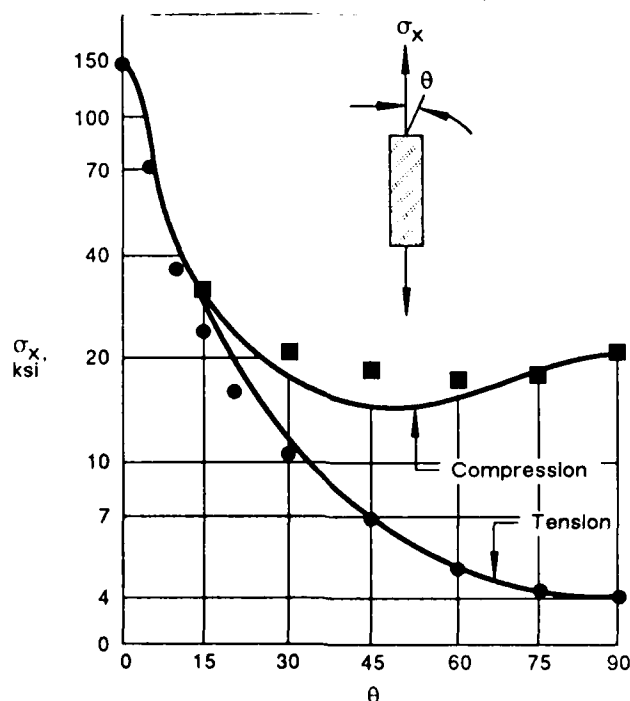


Figure 3-71. Tsai-Hill Theory

It should be noted that the Tsai-Hill criterion provides for interactions between stresses and yields a smooth curve when compared to the maximum stress or strain criteria. However, von Mises isotropic yield criterion and hence the Tsai-Hill theory is related to distortional energy as opposed to dilatational (volume change) energy. The disadvantage to Tsai-Hill's criterion is that biaxial loading of orthotropic materials always causes distortional and dilatational energy. Hence failure may not be directly related to distortional energy as it was for isotropic materials. A more general strength criterion including additional interaction terms is discussed in the next paragraph.

Tsai-Wu Quadratic Interaction Failure Criterion—The Tsai-Wu strength criterion reduces to the equation below for inplane loading of a thin (plane stress conditions) orthotropic ply.

$$F_{11}\sigma_1^2 + F_{22}\sigma_2^2 + F_{66}\sigma_6^2 + 2F_{12}\sigma_1\sigma_2 + F_1\sigma_1 + F_2\sigma_2 + F_6\sigma_6 = 1 \quad (\text{eq. 14})$$

and

$$F_1 = \frac{1}{X^t} - \frac{1}{X^c}$$

$$F_2 = \frac{1}{Y^t} - \frac{1}{Y^c}$$

$$F_6 = 0$$

$$F_{11} = \frac{1}{X^t X^c}$$

$$F_{22} = \frac{1}{Y^t Y^c}$$

$$F_{66} = \frac{1}{S^2}$$

where X^t , X^c , Y^t , Y^c , and S have the same meanings as denoted previously.

F_{12} , which represents the interaction between normal stresses, must be determined by performing a biaxial stress test. Since this test is relatively complicated, it has been recommended in references 11 and 12 to use:

$$F_{12} = F_{xy}(F_{11} F_{22})^{\frac{1}{2}}$$

where:

$$F_{xy} = -0.5$$

(eq. 15)

It should also be emphasized that for uniaxial loading of a unidirectional lamina the failure strength is insensitive to values of F_{12} within the stability limits in the following equation.

$$-(F_{11} F_2)^{\frac{1}{2}} < F_{12} < (F_{11} F_2)^{\frac{1}{2}} \quad (\text{eq. 16})$$

This insensitivity is demonstrated in Figure 3-72 where predicted strengths are in excellent agreement with experimental data for boron/epoxy (ref. 18). Figure 3-72 also demonstrates that for uniaxial loading there is little difference between the Tsai-Hill and Tsai-Wu criteria. Although the Tsai-Wu strength theory is more complicated, the well founded mathematical operations of tensor theory can be used to transform the strength parameters in these equations. This is important since it leads to straight forward computer implementation. References 11 and 12 provide invaluable discussions and examples on the Tsai-Wu strength theories in terms of stress and an analogous strain criteria.

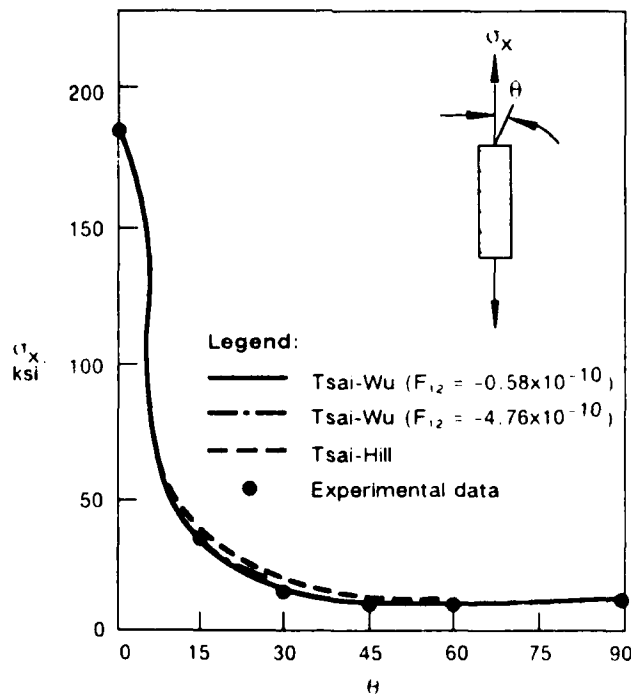


Figure 3-72. Tsai-Wu Tensor Theory

5-B70227-110

Lamina level strength theories presented in these paragraphs differ primarily in the number of empirically determined coefficients used in the curve fitting equations. The relatively simple maximum stress or strain criteria indicate the failure mode while the others do not. However, the Tsai-Hill and Tsai-Wu strength criteria are recognized as useful design tools. Predicting strength using the strain based analogies of the theories presented here is a generally accepted practice in the aircraft industry. This results from the fact that design allowables are given in terms of strain. The lamina strength theories in this paragraph will be applied to predicting laminate strength in the next paragraph.

3.4.1.5 Laminate Level Strength Criteria

First Ply Failure—At some point during loading of a multidirectional laminate, the ply or group of plies with the lowest strength will start accumulating damage. This event, often described as first ply failure, can be predicted using the lamina level theories presented in paragraph 3.4. Figure 3-73 shows a comparison between predicted strengths for plies in a uniaxially loaded multidirectional graphite/epoxy laminate based on the quadratic interaction criterion (ref. 19). It is seen that first ply failure (that is, the 90 degree plies) occurs at a lower load level than catastrophic laminate failure. This is expected, since load shedding from the damaged 90 degree plies to the rest of the plies continues until the laminate cannot carry additional load. In this case, a more accurate, but nonconservative, prediction of the strength would be based on the strength of the 0-degree plies as shown in Figure 3-73. The first ply failure envelope for a multidirectional laminate is the intersection of the failure envelopes for each ply angle in the laminate. This is shown schematically in Figure 3-74 based on the quadratic interaction criterion and ply strength data from (ref. 11).

Ply Discount Methods—First ply failure is quite conservative because the initial damage in a multidirectional laminate is cracks running parallel to the fibers. These cracks are modeled by reducing the matrix modulus of the cracked ply group. Micromechanics (refs. 11 and 12) can then be used to calculate the reduced transverse and shear modulus of the plies. In the next step, lamination theory is employed to predict the redistribution of loads within the laminate. Loads are then reapplied incrementally until compressive or tensile fiber failure occurs. Since the fibers carry most of the load, this point often corresponds to the peak load or strength of the laminate. Ply discount methods incorpo-

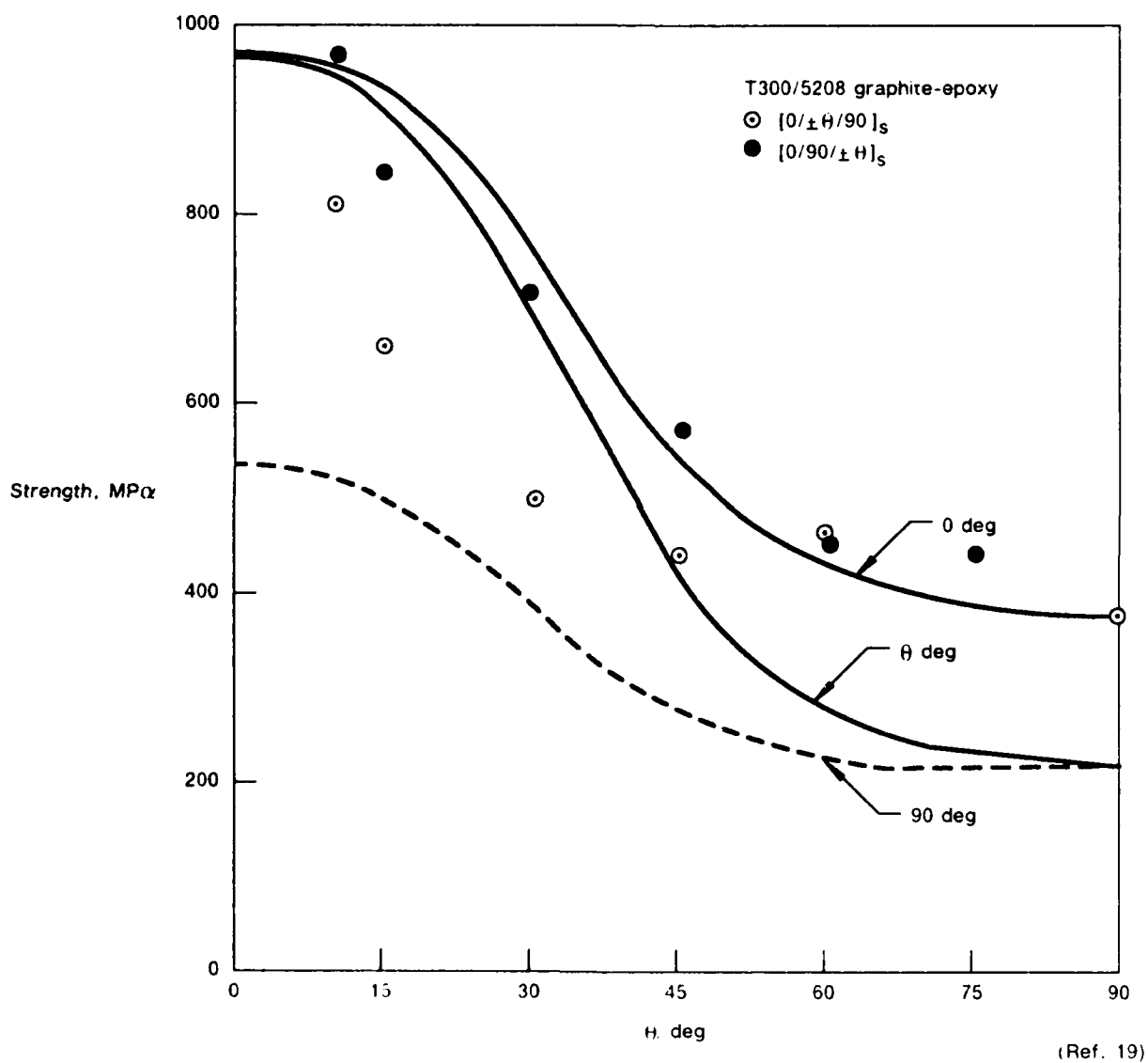


Figure 3-73. Comparison of Calculated Inplane Tensile Strength With Experiment

5-B70227R1-111

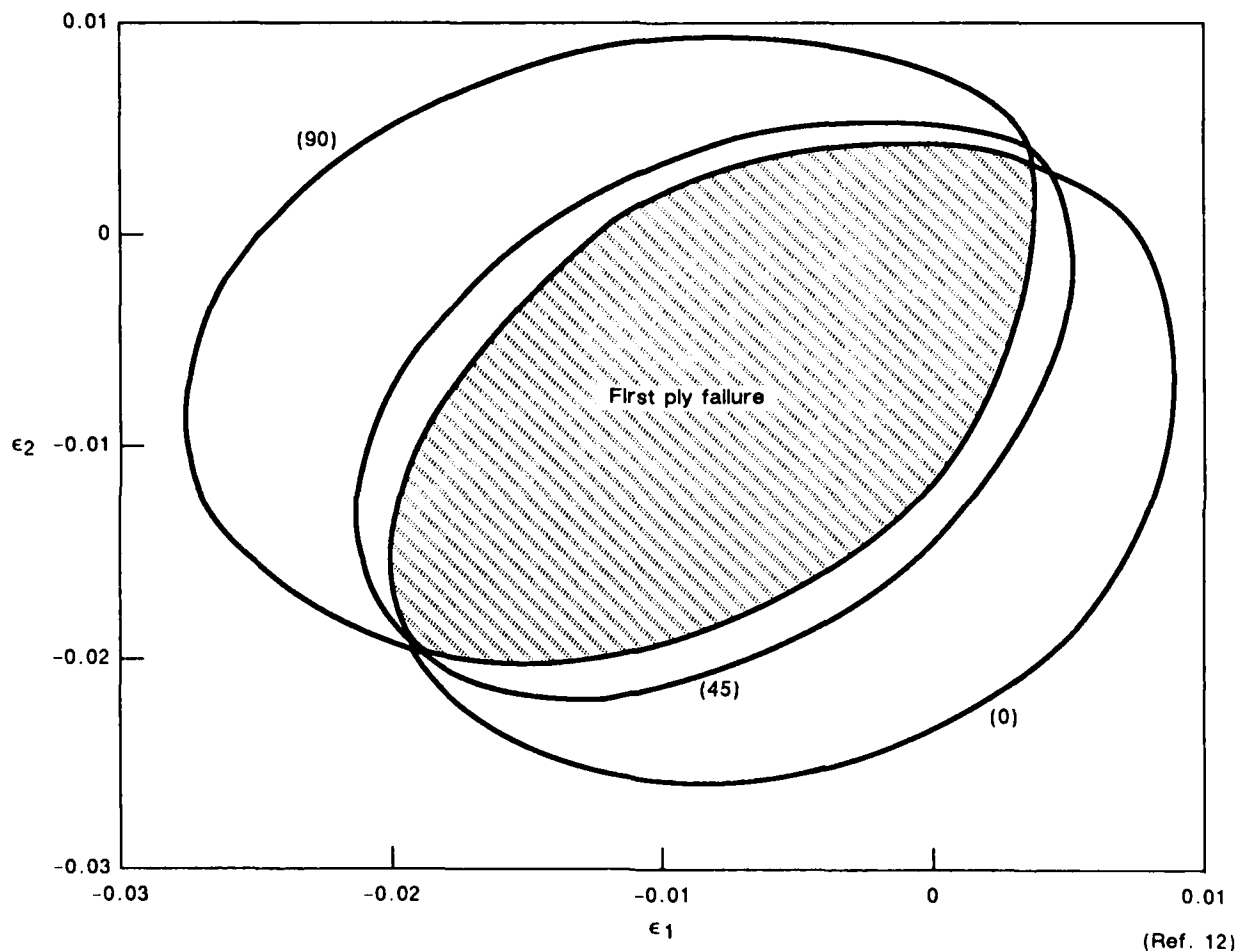


Figure 3-74. Quadratic Interaction First Ply Failure Envelope for T300/5208

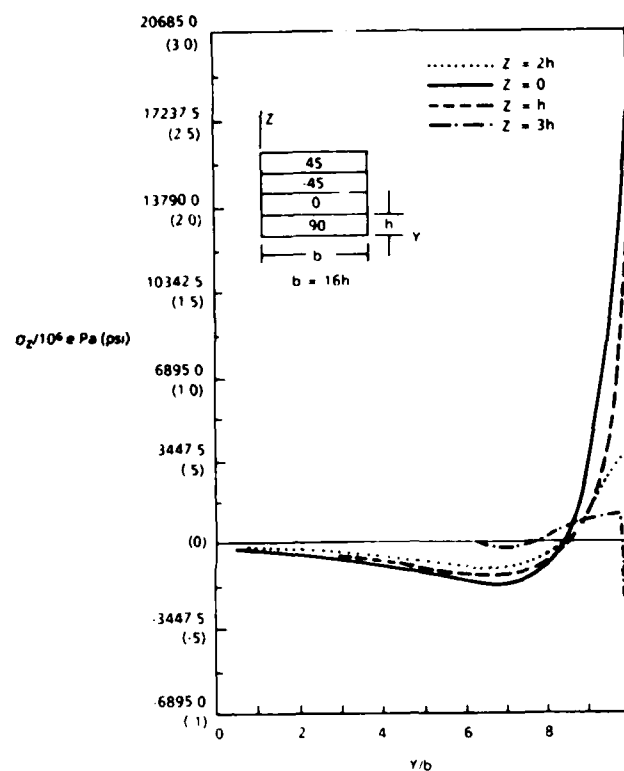
5-B70227R1-112

rating the effect of hygrothermal stresses are being used with limited success by designers.

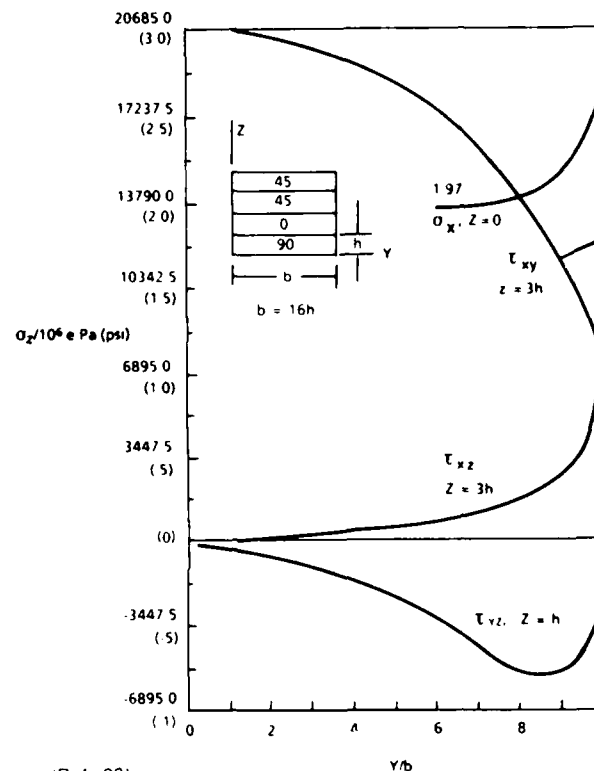
It should be noted that these methods are based on lamination theory which does not account for the interlaminar stress concentrations at the free edges. Transverse cracks also cause interlaminar stress concentrations which may lead to delamination and significant reductions in laminate strength. Two or three dimensional finite element modeling, discussed in the next paragraph, is one of the methods employed to investigate these micro-structural failure modes.

Finite Element Modeling—Incorporating the effects of free edge interlaminar stress concentrations with environmental and cure stress considerations represents the next level of complexity in predicting failure onset using individual-ply failure criteria. For the failure analyst, these works are useful in that they embody considerations likely to be necessary with real-world structures. Both Crossman and Herakovich (refs. 20 and 21, respectively) observed that significant variations in stresses and strains can occur at the free edge of specimens. Both authors show the magnitude of these stresses for relatively simple layups and specimen geometries. Generally, the most significant stresses are those developed near the specimen's free edge. In analyzing these stresses, both authors employed two-dimensional finite-element grids arranged along the specimen cross-section. Using these grids illustrates the degree of complexity involved in determining the interlaminar stresses (or strains) in microscale with such design details. As noted by Crossman, particularly large gradients can occur in both Z and Y directions near the free edge (Figure 3-75). Regarding the application of individual-ply failure criteria, the large increase in σ_z , σ_x , and τ_{xz} stresses near the edge of the specimen are particularly significant, since laminate theory methods would have ignored these increases.

Furthermore, Crossman and Herakovich predicted that stresses would be further influenced by internal cure stress, test temperature, and conditions of moisture absorption or desorption (Figure 3-76). In Herakovich's work, the relationship of these stresses to failure prediction were considered. Since his finite-element model examined stresses along three dimensions, it was necessary to develop a full three-dimensional failure criterion. Herakovich used the tensor polynomial criteria advanced by Tsai-Wu, in which strength tensors are given in terms of material principal strengths. As illustrated in



Distributions along
each ply interface for
(+45/-45/0/90 degree),

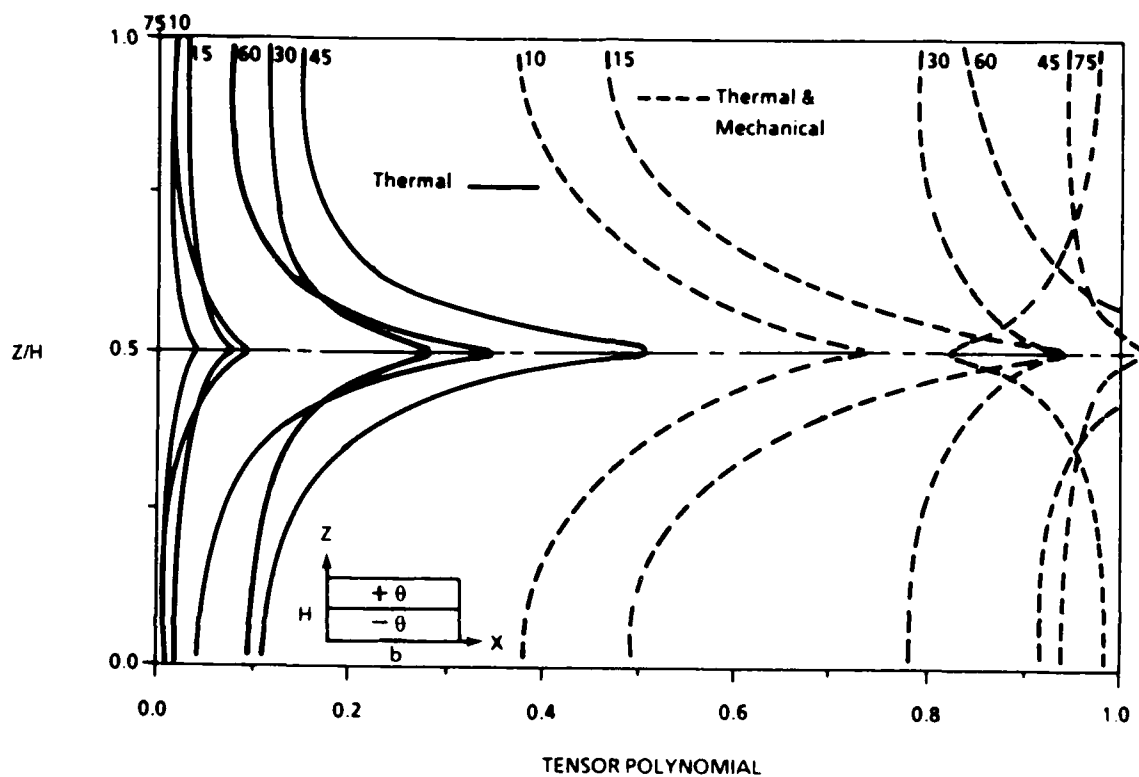


(Ref 20)

Various stress distribu-
tions along several ply
interfaces in (+45/-45/0/90 degree),

Figure 3-75. Stress Gradients Resulting From Edge Effects

5-B70227R1-117



(Ref. 21)

Figure 3-76. Through-Thickness Tensor Polynomial Distributions for Curing Stresses and Stresses at the First Failure (+/-) Laminates

5-B70227R1-118

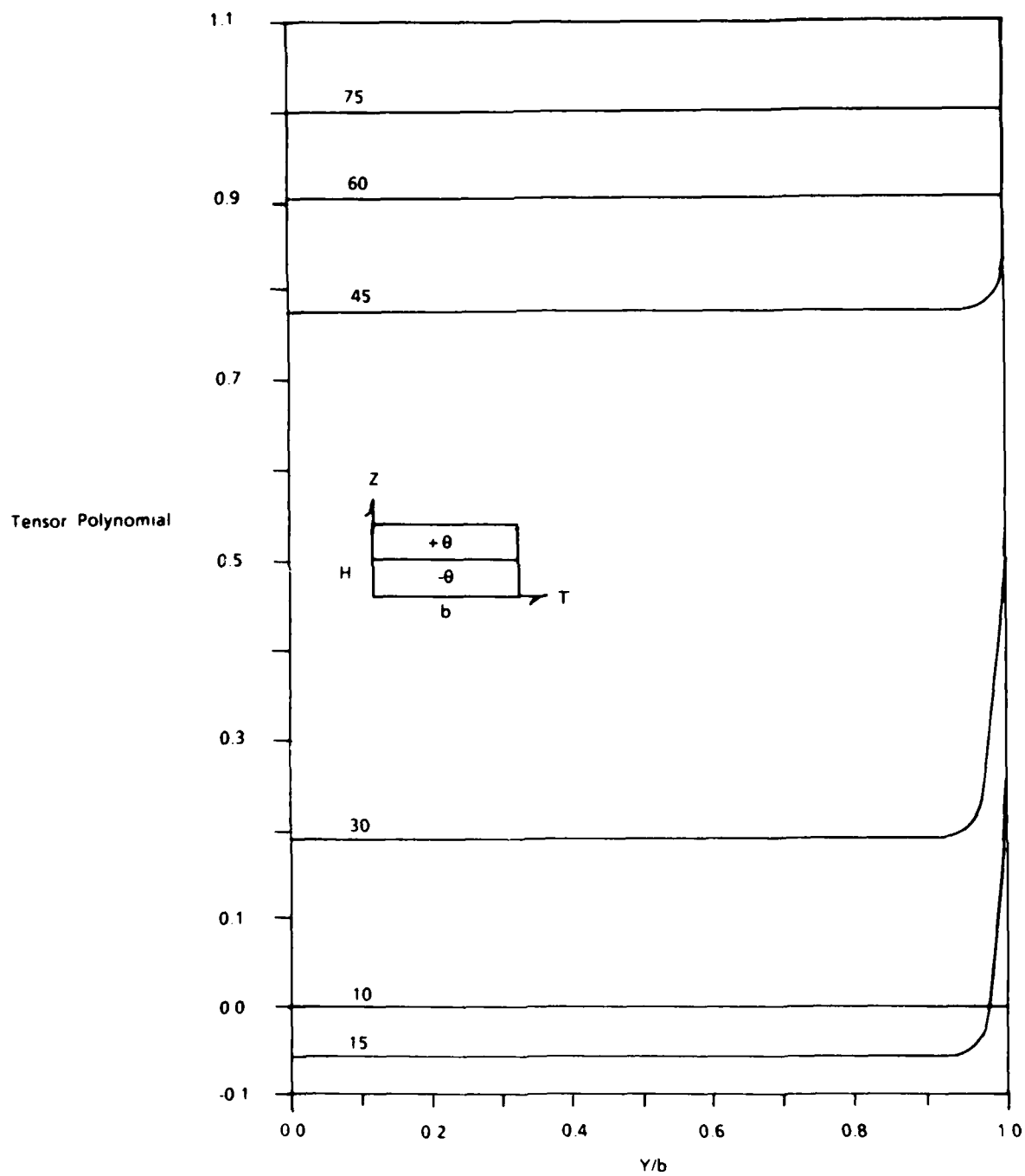
Figure 3-77, Herakovich predicted that the onset of failure depends quite strongly on edge stresses, particularly for small ($\pm\theta$) laminate angles. While not verified against actual test data, these results, when considered with Crossman's, clearly indicate that both edge and environmental stress effects must be carefully evaluated in predicting the onset of failure for whichever individual-ply criteria are employed.

Perhaps the farthest advancement of first-ply failure criteria as a method of prediction has been made by Chamis (ref. 22). In attempting to predict the defect growth and damage of composite materials subjected to load, Chamis developed an integrated computer program called CODSTRAN. Within this program, a detailed finite-element grid is constructed and evaluated for failure using both individual first-ply failure criteria and laminate-level fracture criteria. In the case of individual-ply failures, Chamis' program incorporates both general quadratic and modified distortional energy (Von Mises') criteria to predict the occurrence of failure for each element of the overall finite-element model. What is unique about Chamis' work, however, is that failed-ply elements are eliminated, and the analysis process is reiterated. As a result, CODSTRAN describes the sequence of events leading to failure, and an approximate prediction of the load at failure.

3.4.1.6 Summary - Unnotched Laminate Strength

The failure modes of composites are far more complex than those discussed in these paragraphs. At the ply-level, Tsai-Wu's quadratic interaction failure criterion seems to provide sufficiently accurate results for unidirectional laminate strength under biaxial loading. Prediction of multidirectional laminate strength is quite complex since free-edge interlaminar stress concentrations and hygrothermal stresses must be considered. Finite elements and interactive ply discount methods have been used with limited success.

It can be seen from the discussions above that computers play an important role in the stress analysis of composites. Lamination theory predictions of stiffness and the laminate strength theories discussed here have been implemented on micro-computers (that is, ref. 12 and 23).



(Ref. 21)

Figure 3-77. Tensor Polynomial Distributions Along the Interface of (+/-) Laminates

5-B70227R1-119

The methods presented in the following paragraphs can provide criteria for selecting the laminate geometry providing optimum strength in the load bearing directions. However, predictions of laminate strength, at this time, are not quantitatively accurate. Thus, the designer must rely on coupon or full scale tests to determine the actual strength for a particular laminate geometry. This requires large and expensive databases to design structural composite parts. If needed, the failure analyst should consult designers or stress analysts to find out what methods were used to establish the allowables. The overview presented in paragraph 3.4 is intended to familiarize the reader with some of the considerations, many of which are unique to composites, that must be applied to predicting laminated composite strength.

3.4.2 Influence of Ply Thickness on Transverse Cracking

In the previous paragraph, it was noted that transverse cracking and free-edge delamination reduce laminate strength. In this paragraph, the influence of ply thickness and orientation on these micro-structural failure modes is discussed. It is intended to provide the reader with an introduction to micro-structural failure features unique to laminated composites.

In the previous paragraphs, the strain required to cause cracks parallel to the fibers (transverse matrix cracking) was assumed equal to the transverse failure strain of a 90 degree ply. However, it has been shown by numerous researchers (refs. 24 to 28) that the strain to cracking of an off-axis ply group depends upon its thickness. Flaggs and Kural (ref. 24) have clearly demonstrated that the in-situ strain to cracking decreases as the thickness of an off-axis ply group (30, 60 or 90 degree) increases (see Figure 3-78). The fact that the in-situ strength of a 90-degree ply is greater than that of a laminate composed only of 90 degree plies has been attributed to the constraint provided by the stiffer surrounding ply groups. Flaggs (ref. 28) used a fracture mechanics approach combined with 2-D shear lag analysis to successfully model the in-situ strain to cracking as shown in Figure 3-78. This model has also been applied successfully to predicting in-situ cracking of 30 and 60 degree ply groups (ref. 28).

With this type of analysis, the first ply failure predictions of laminate strength could be made more accurate. To accomplish this, Flaggs' model would be used to predict the in-

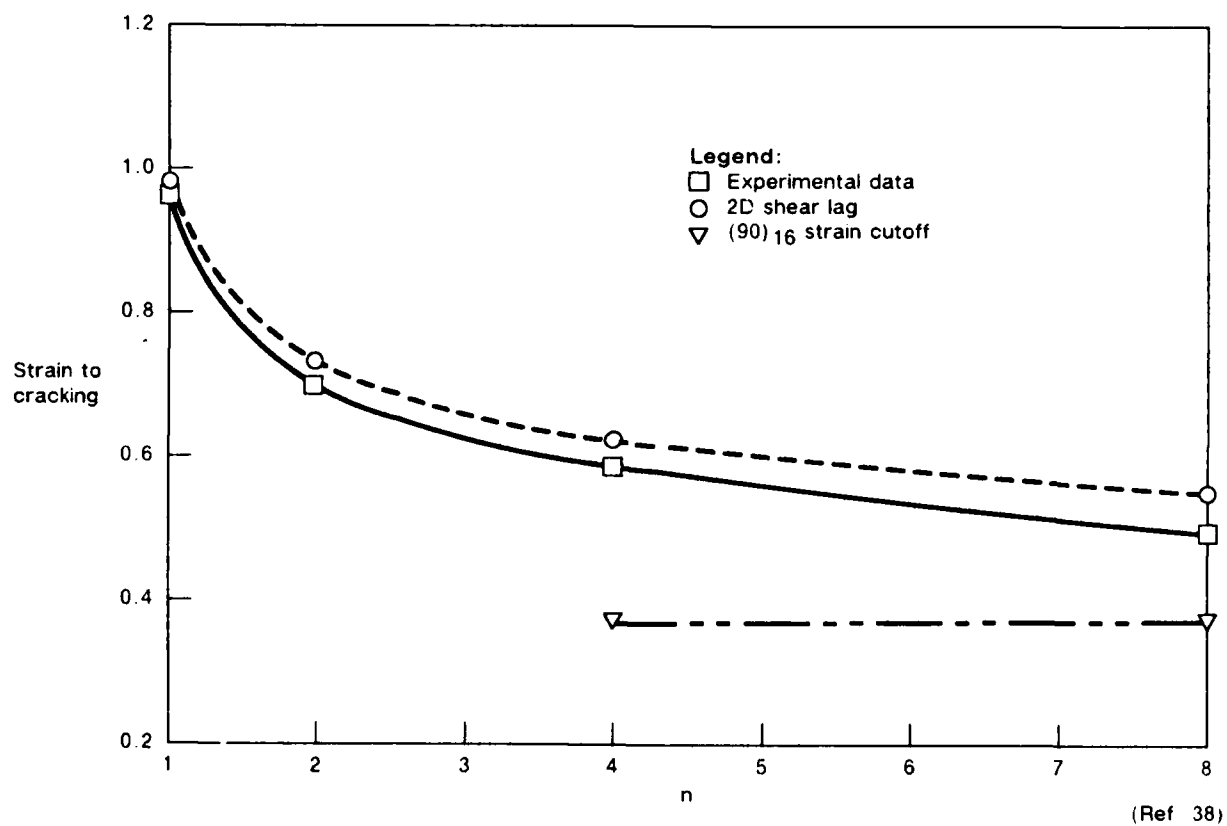


Figure 3-78. Comparison of Experimentally Derived In Situ Lamina Elastic Strains at Onset of Matrix Cracking With 2D Shear Lag Model Predictions for (0/90) T300/934 Laminate Family

5-B70227R1-113

situ strain to cracking of the off-axis ply groups in a multidirectional laminate. Then these strains would be used as the strain to failure transverse to the fibers in the lamina level failure models. This represents an effort to integrate the prediction of micro-structural failure with gross laminate failure features.

3.4.3 Strength Reductions Incorporated Into Design

The methods of paragraph 3.4 are commonly used to predict the strength of an unnotched laminate (that is, without in-plane stress concentrations). However, composite structural components may contain cutouts, fastener holes, or impact damage which reduce the in-plane strength below that of the virgin laminate. These laminates must be designed "a priori" such that the residual strength will be greater by some safety factor than the operating stresses. Some of the more popular approaches applied to predicting residual strength are reviewed in the following paragraphs.

Most of the analytic techniques for predicting residual strength employ semi-empirical approaches similar to the fracture toughness methods commonly used with metal structures. These methods typically involve the experimental determination of an intrinsic material property related to crack growth—such as material fracture toughness. This value, when considered with the size and geometry of the flaw, allows the stress at the fracture to be calculated.

The anisotropy of composites complicates the analyses considerably. Critical stress intensity factors used in metals analysis are independent of the direction of crack growth. However, the translaminar toughness of composites may be hundreds of times greater than the interlaminar toughness. This is expected since breaking fibers is a much higher energy fracture mode than matrix cracking. Often, the interaction of these two failure modes occurs as in impact damage. In this case the assessment of residual strength becomes so complicated that the designer must rely on empirical data. However, when the translaminar and interlaminar modes are acting independently, the rapidly maturing fracture mechanics approach for composites are being used successfully.

Notched Laminate Strength—The easiest-to-understand methodologies for determining laminate failure are those adapted directly from metals fracture toughness analyses.

These analyses predict the onset of component fracture through the experimental determination of a characteristic K_{IC} fracture toughness value. In these cases, K_{IC} indicates the stress intensity factor at which fracture occurs, based on the initial crack length and maximum load at failure. (For reference, this value is often referred to as $K_{apparent}$ in metals fracture toughness.) In works by Bathias (ref. 29), McGarry (ref. 30), and Awerbuch (ref. 31), K_{IC} values have been determined for a variety of layups. In measuring values, these researchers used specimens adapted directly from traditional metals toughness testing, such as compact tension coupons or large center-crack tension panels. In Bathias' work, K_{IC} values were measured for a variety of layups. As illustrated in Figure 3-79, values ranging from 16 to 43 MPa times the square root of m were measured, and demonstrated a clear dependence on the ply stacking sequence and orientations examined. (For 7075-T7351 aluminum, K_{IC} typically equals 80 to 90 MPa times the square root of m.) Each author suggests that knowledge of this material property for a layup can be used to estimate the stress at fracture instability for a given crack and component geometry.

This point of instability can be defined by using the equation:

$$K_{IC} = Y\sigma_c \text{ times the square root of } \pi a \quad (\text{eq. 17})$$

where:

- Y = geometric factor related to the crack length and location within component being examined
- σ_c = stress at instability
- a = full crack length
- K_{IC} = material fracture toughness

FRACTURE TOUGHNESS (MPa \sqrt{m})	LAYUP (DEGREES)		
	0/45/90/135/90/45/0 16 plies	0/30/60/90/120/150/0 13 plies	0/45/135/0/135/45/0 16 plies
K_{IC}	29-43	23-35	16-22

(Ref. 29)

Figure 3-79. Fracture Toughness of Various Orientations

5-B70227R1-120

A more detailed review of this technology can be found in any of several texts dealing with the fracture behavior of metals.

Numerous researchers have also attempted to predict the criticality of holes, cracks, and damage by empirically measuring other characteristic fracture properties, in much the same way as is done with fracture toughness (refs. 6 to 8 and 32 to 43). Two of the significant efforts include failure criteria which assume failure occurs when the stress at some distance away from the flaw reaches the ultimate material strength. These two are the average stress, and the point stress failure criteria models presented by Whitney and Nuismer (refs. 35, 36). As described in Daniel's paper (ref. 6), the average stress failure criterion proposes that failure occurs when the average stress over a characteristic material dimension (a_0) equals the material strength. This criterion is illustrated in Figure 3-80, where a_0 represents the length dimension of a particular layup and material. Similarly, the point-stress failure criterion presented by Mikulas (ref. 7) predicts that panel failure occurs when the axial stress at some distance (d_0) from the hole boundary equals the strength of the unnotched laminate as shown in Figure 3-81. Daniel, Mikulas, and

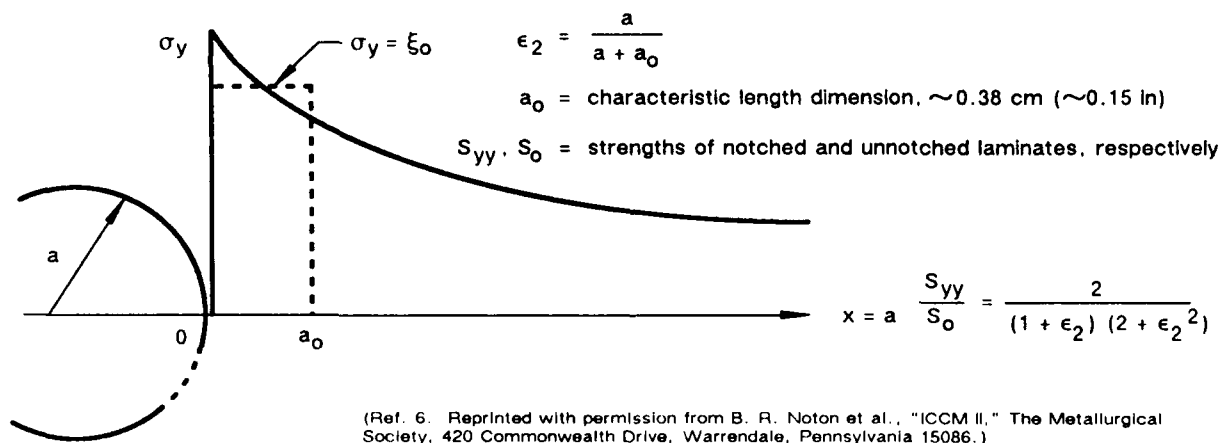


Figure 3-80. Strength Reduction of Uniaxially Loaded Plate With Circular Hole According to Average Stress Criterion

5-B70227-133

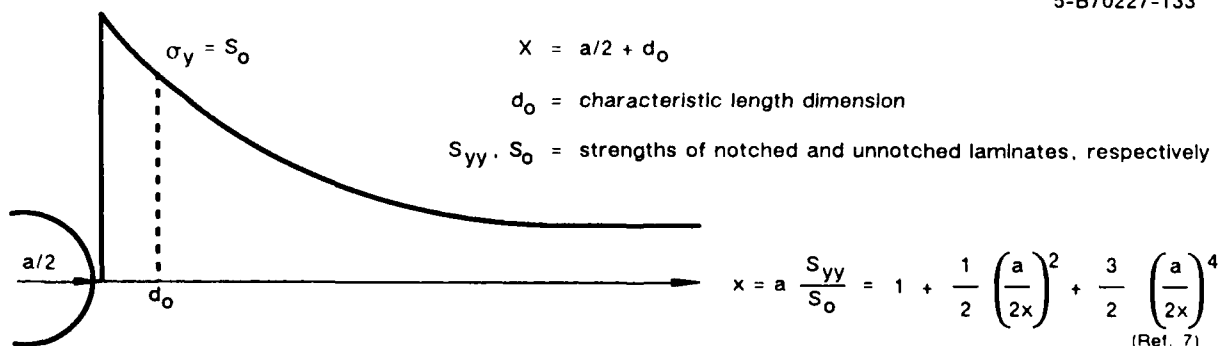


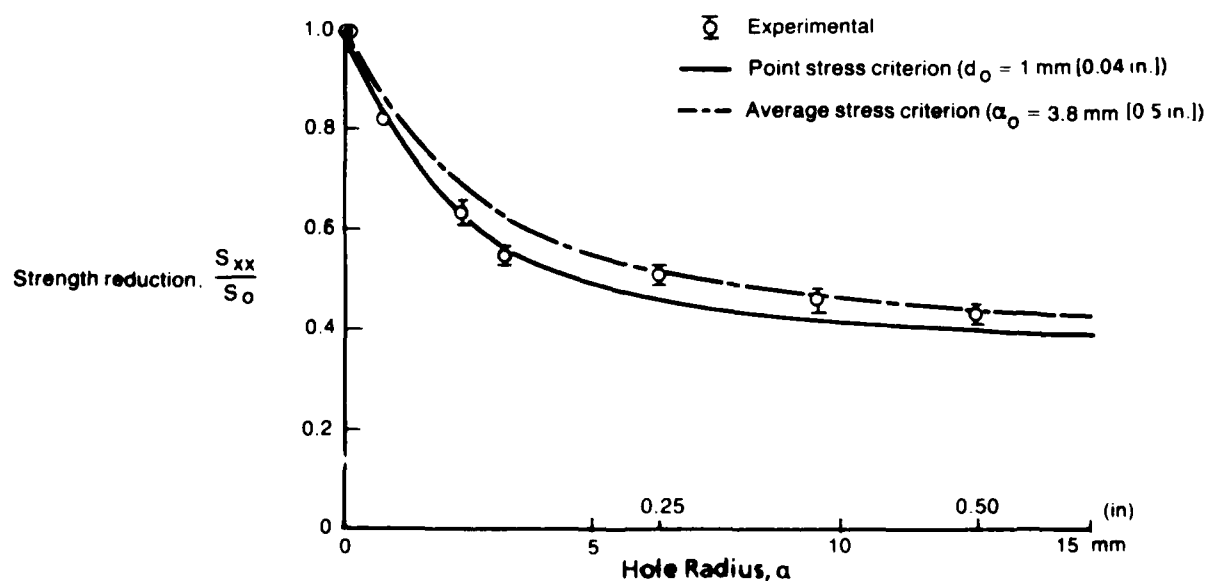
Figure 3-81. Strength Reduction of Uniaxially Loaded Hole According to Point Failure Stress Criteria

5-B70227-134

other investigators measured both a_0 and d_0 for a variety of layups and found a relatively good correspondence of predicted and measured strengths for open holes (Figure 3-82). The disadvantage of the point or average stress criteria is that they require different characteristic lengths for various notch sizes in the same type laminate (ref. 37 to 40).

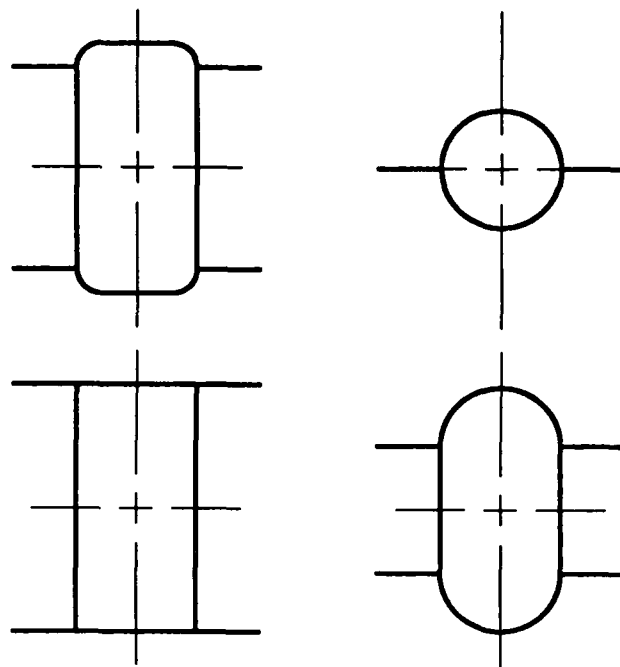
The more general Damaged Zone Model discussed by Aronsson in (ref. 8) requires only basic laminate properties (strength and stiffness) and the apparent fracture energy to predict the fracture behavior of brittle and ductile notched three point bend specimens.

In this model, the damaged (as opposed to a crack in metals) zone which develops in composites around a crack or hole is modeled by a crack with cohesive stresses acting on its surfaces. As the applied load is increased, the damage grows. This is approximated by reducing the cohesive forces on the cracked region in the model. The Damaged Zone Model (DZM) and the Point Stress Criteria (PSC) (ref. 8) accurately predicts the failure load for brittle and ductile matrix three-point bend specimens. The real utility of the DZM lies in its ability to analyze complex geometries. The PSC, which relies on exact calculations of the stress distribution around a flaw, is limited to very simple flaw geometries such as holes. Tensile failure loads have been predicted by the DZM to within 10% of the experimental values for laminates with the hole geometries in Figure 3-83 (ref. 44). The DZM should be a tool for the aerospace industry that can be used for predicting the residual strength of laminates with cutouts.



(Ref. 6. Reprinted with permission from B. R. Noton et al., "ICCM II," The Metallurgical Society, 420 Commonwealth Drive, Warrendale, Pennsylvania 15086.)

Figure 3-82. Strength Reductions as a Function of the Hole Radius for (0/+45/-45/90 deg) Graphite-Epoxy Plates With Circular Holes Under Uniaxial Tensile Loading



(Ref. 44)

Figure 3-83. Hole Geometries Analyzed With the Damage Zone Model (DZM)

5-B70227R1-114

Of particular concern to the failure analyst, however, is the ability to predict failure onset for flaw conditions such as through-cracks or impact damage. In this area, Mikulas (ref. 7) examined the applicability of the point stress failure criteria; for the case of a through-crack, stress as a function of distance from the crack was expressed as:

$$\frac{\sigma_y}{\sigma_{oo}} = \frac{X}{\text{the square root of } X^2 - \left(\frac{a}{2}\right)^2} \quad (\text{eq. 18})$$

where:

$$x = x_1 + \frac{a}{2}$$

X = distance along the x-axis, away from the crack

a = crack length

σ_{oo} = stress at infinite distance from crack

σ_y = stress
in the y direction

As a result, Mikulas indicated that the residual strength for a given crack of size a can be determined if X is set equal to d_0 .

With respect to impact damage, Mikulas reported that the characteristic length d_0 depends on the toughness of the resin system examined. As illustrated in Figure 3-84, a relatively good correlation exists for tough resin chemistries, but not for brittle, delamination-prone resin systems. These observations indicate that the accuracy of failure predictions will depend strongly on the resin system used, and the configuration of damage examined. An excellent discussion of impact damage with respect to failure modes and the effects of resin toughness has been given by Starnes, Williams, and Rhodes in references 45 to 48. Their studies have clearly shown that:

1. Tough resins reduce the size of the damage zone caused by impact.
2. Several graphite/epoxy systems with varying toughness exhibited similar residual post-impact compression strength for the same damage zone size.
3. The dominant failure mechanisms causing post-impact compression failure are delamination and shear crippling.

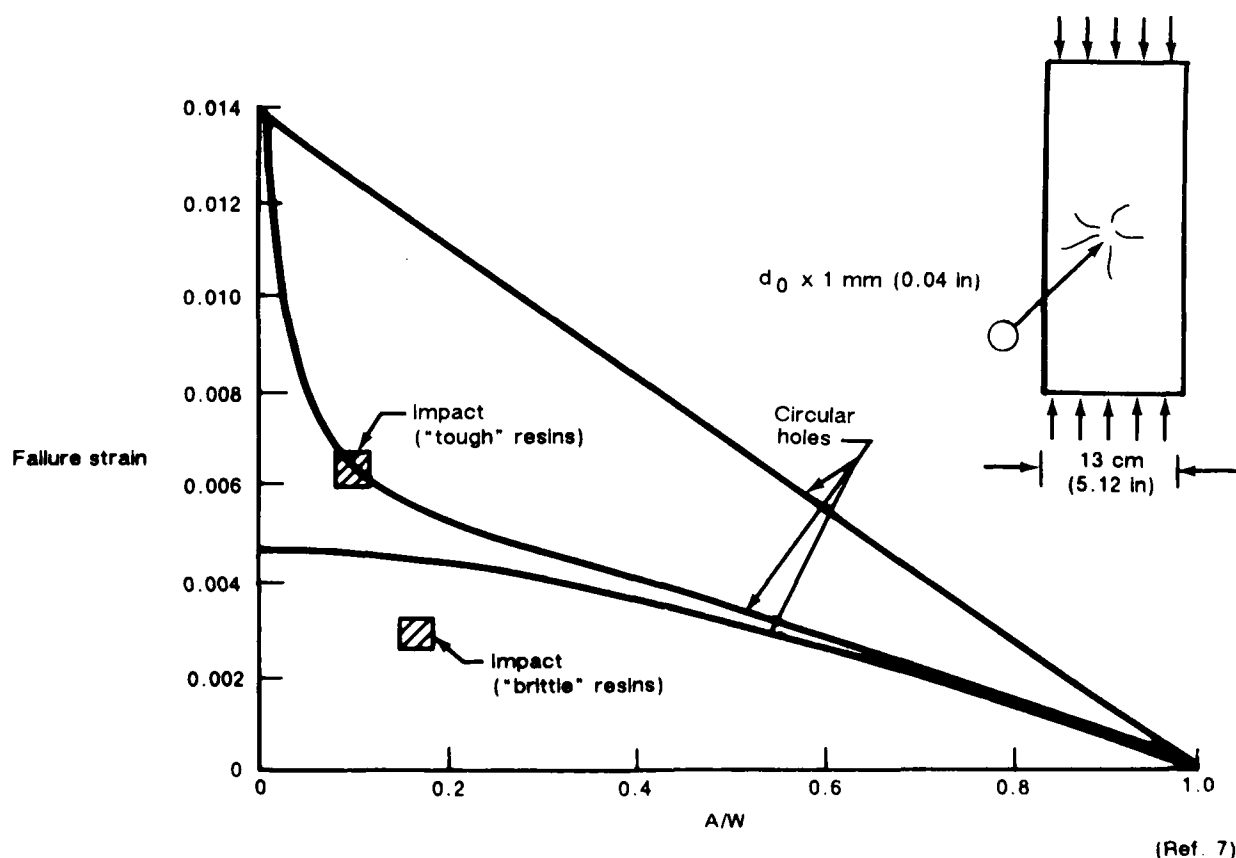


Figure 3-84. Effect of Impact Damage on the Compressive Strength of a Quasi-Isotropic Laminate

5-B70227-63

3.4.4 Introduction to Delamination

While the works discussed in paragraph 3.4 examined the residual strength of the laminates with translaminar through-thickness flaws, other investigators have considered the criticality of interlaminar defects. This paragraph has been included to acquaint the reader with some of the significant results and tests applicable to assessing the criticality of interlaminar defects in composites. Delaminations may grow and initiate component failure due to sudden loss of stiffness and strength. Fractography can be used to detect delamination and interlaminar crack growth directions, but the methods discussed here can be employed to evaluate the criticality of delaminations.

As a result of processing and service conditions, delaminations may be introduced into composite structures. Fatigue and static loading of laminated composite structure may initiate delaminations near interlaminar stress concentrations. Some of the common design features found in composite structures such as bolted joints, ply drops, and cutouts contain interlaminar stress concentrations (see Figure 3-85). In addition, multiple delaminations represent characteristic post-impact damage. Local instability of a delaminated sub-region in composite structures under compressive loading precipitates out-of-plane deformations and may lead to subsequent crack growth. Under these circumstances, it has been well documented that structural strength and stiffness reductions are significant (refs. 50 to 58).

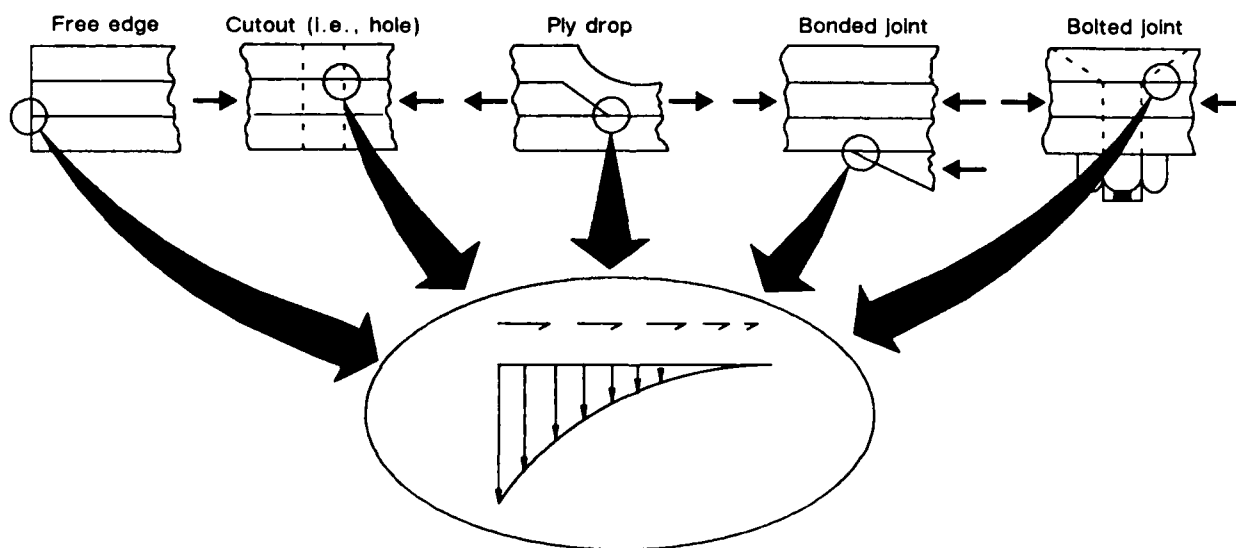


Figure 3-85. Design Details That Cause Interlaminar Stress Concentrations

(Ref. 49)

5-B70227R1-115

3.4.4.1 Fracture Analysis and Specimens (For Interlaminar Toughness)

In the presence of interlaminar stress singularities, the fracture mechanics approach is now frequently used to assess defect criticality in composites. Double cantilever beam (DCB), Mode I, and end notched flexure (ENF) Mode II specimens, as shown in Figure 3-86 (a and b), are being used to evaluate the pure mode critical strain energy release rates. Strain energy release rates are utilized in these pure mode tests because G is a physically well defined quantity experimentally measurable with compliance calibration techniques. But, in general, cracks in composite structures are subjected to all three modes of loading at the crack tip as shown in Figure 3-87.

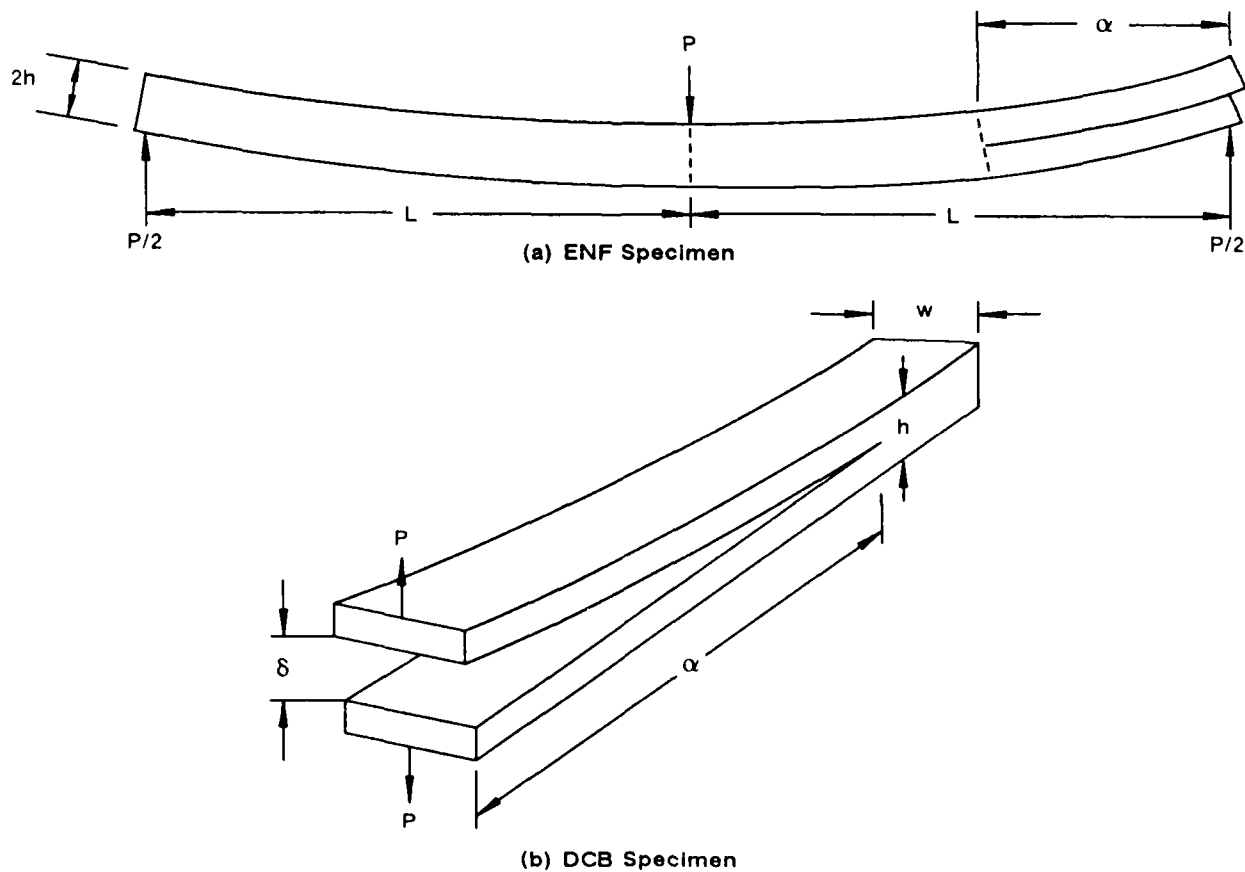


Figure 3-86. End-Notched Flexure (ENF) and Double-Cantilever Beam (DCB) Specimens

5-B70227R1-121

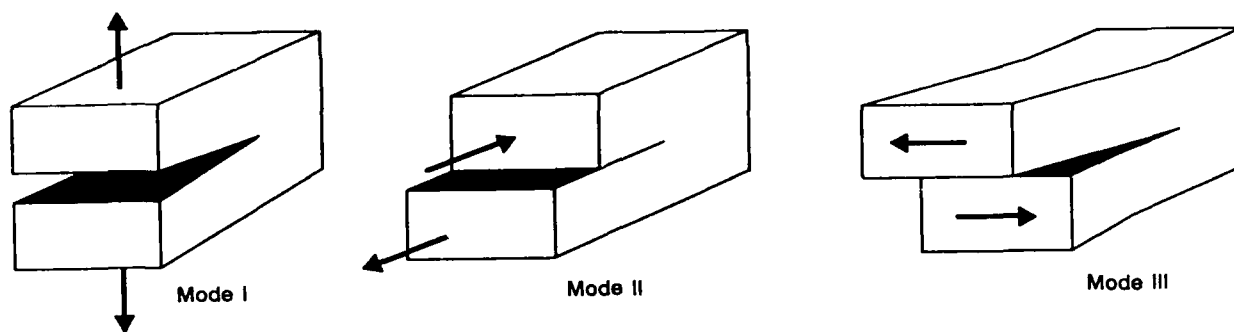
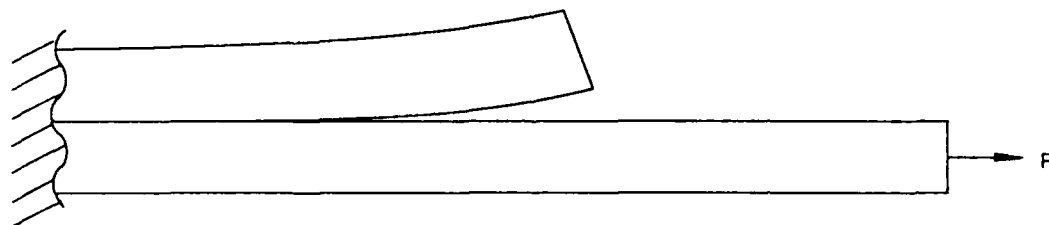


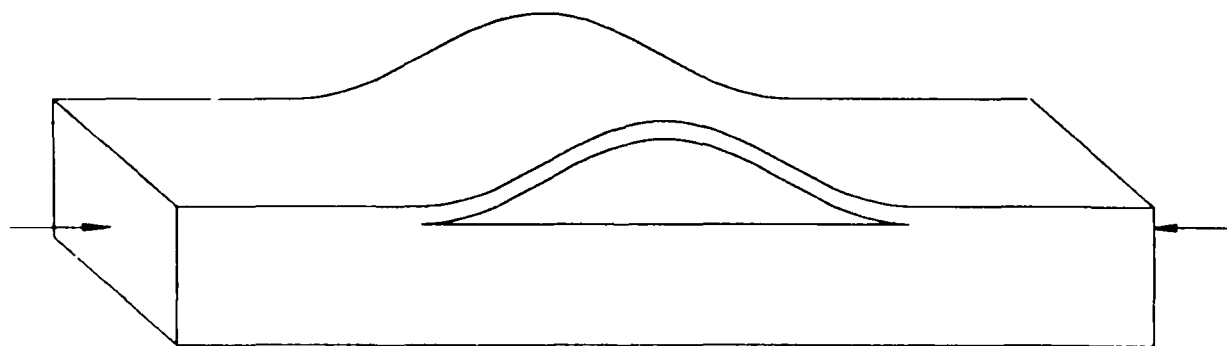
Figure 3-87. Modes of Crack Propagation

5-B70227-122

To study mixed-mode crack growth criteria, the imbedded through-width delamination (ITWD) and cracked lap shear (CLS) specimens shown in Figure 3-88 have been used by a



(a) Cracked Lap Shear (CLS) Specimen



(b) Imbedded Through-Width Delamination (ITWD) Specimen

(Ref. 10)

Figure 3-88. Mixed Modes I and II Delamination Specimens

5-B70227R1-123

number of researchers. The opening moment and the eccentricity in load path at the crack tip of the CLS and ITWD specimens are the mechanisms causing interlaminar normal (Mode I) and shear (Mode II) stress concentrations (see Figure 3-89).

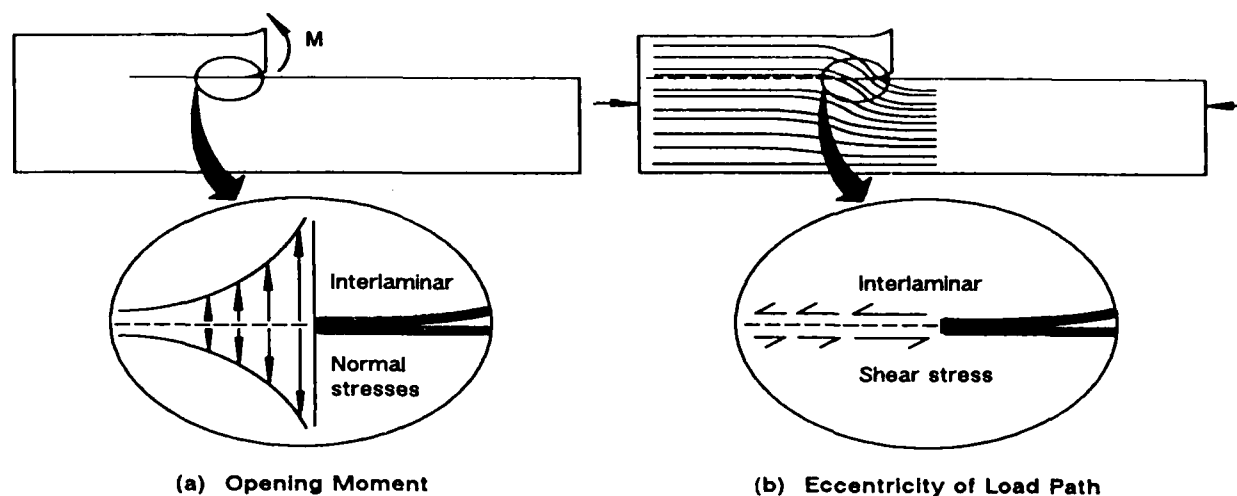
The strain energy release rate methods for evaluating the criticality of delaminations assume that G_c is a material property. This type of analysis is based on the equation below presented by Griffith (ref. 59).

$$G = \frac{P^2}{2b} \frac{dC}{da} \quad (\text{eq. 19})$$

where:

- b = width of crack
- G = strain energy release rate
- C = compliance
- a = crack length
- P = load

For a single mode of loading at the crack tip, the load on the specimen, P , is increased until G reaches its critical value G_c at the onset of crack growth. In this case, the failure criterion can be stated as crack growth occurs when G reaches G_c . Once G_c has been measured, the fracture load, P_c , can be found for any other crack length or geometry by evaluating the change in compliance with respect to crack length (dC/da). Then, dC/da can be adequately determined analytically for simple pure Mode I or Mode II geometries such as the DCB and ENF, respectively; however, finite element methods combined with the virtual crack closure analysis (ref. 60) are required to evaluate dC/da in more complicated structural applications. These types of complex geometries often have more than one mode of loading present at the crack tip (that is, mixed mode). In this case the interaction of modes must be considered, thus invalidating the simple crack growth criterion mentioned above. The mixed mode fracture criterion becomes more complicated since the critical value of the Mode II interlaminar toughness of composites can range from one



(Ref. 10)

Figure 3-89. Crack Tip Loading Mechanisms Causing Interlaminar Normal and Shear Stress Concentrations

5-B70227R1-124

to ten times that in Mode I as shown in Figure 3-90. However it has been recently shown by Rothschilds, (ref. 10) and Johnson (ref. 61) that the linear mixed-mode crack growth criterion, in the following equation, provides accurate predictions of the critical loads at the onset of mixed mode crack growth.

$$\frac{G_I}{G_{IC}} + \frac{G_{II}}{G_{IIC}} = 1 \quad (\text{eq. 20})$$

(Where the values are as defined for the previous equation.)

Material	G_{IC} kJ/m ² *	Ref. number	G_{IIC} kJ/m ² *	Ref. number
AS-4/PEEK	1.75 ± 0.13	65	1.89 ± 0.16	61
AS-4/PEEK	2.1 - 2.4	66		
AS-4/PEEK	1.54 ± 0.06	63	1.77 ± 0.24	63
T300/5208	0.103	67	0.92 ± 0.14	64
AS-1/3506-6	0.131	62		
AS-1/3501-6	0.19 ± 0.01	63	0.61 ± 0.3	63
Celion 6000/ CYCOM 982	0.25 ± 0.02	65	0.77 ± 0.07	65

*1 kJ/m² = 5.71 in lb/in².

Figure 3-90. G_{IC} and G_{IIC} Values Obtained From DCB and ENF Testing Reported in Literature

5-B70227R1-125

With this criterion, the criticality of interlaminar cracks can be evaluated in complex mixed-mode geometries. It should be noted that the criterion in the above equation reduces to the desired result in the case of pure mode loading. It is also seen that the mixed-mode criterion above requires the pure Mode I, Mode II, and or Mode III critical strain energy release rates. Fracture testing exhibits rate dependence, material nonlinearity, and subcritical crack growth. To be consistent, these effects must be considered when using the results of pure mode fracture testing in the analysis of fracture in structural components.

3.4.4.2 Interlaminar Fatigue Crack Growth

The previous paragraph discussed methods used to evaluate the criticality of interlaminar cracks under quasi-static loading. Some excellent investigations on interlaminar fatigue crack growth were performed by Wilkins (ref. 62) and Russell (ref. 63). They have shown that a power law relation exists between the change in G during a fatigue cycle and the crack growth rate. Figure 3-91 shows the crack growth rate equations in Mode I and Mode II for AS-1/3501-6 (Gr/ep). Similar equations for other materials could be used in conjunction with the methods for predicting G (discussed above) to evaluate the criticality of interlaminar fatigue in laminated composites. Figure 3-92 shows rather surprisingly that over a certain range of cyclic Mode II crack loading, the tougher thermoplastic AS4/PEEK has a higher crack growth rate than the relatively brittle epoxy. The characteristic surface micro-features have been documented in a thorough investigation of composite interlaminar crack growth by Russell (ref. 63). Failure analysts can use this information to characterize the loading (static or fatigue) and interlaminar stress state (Mode I

Mode	Governing equation	Reference number	B	n	G_{TH} , J/m ²	$\frac{\Delta G_{TH}}{G_{TC}}$
Mode I	$\left(\frac{da}{dn}\right)_I = B(\Delta G_I)^n$	62	1.47×10^{-64}	28.8	105	0.6
Mode II	$\left(\frac{da}{dn}\right)_{II} = B(\Delta G_{II})^n$	63	22.3×10^{-18}	5.8	82	0.14
Mode II	$\left(\frac{da}{dn}\right)_{mm} = B(\Delta G_T)^n$	62	1.04×10^{-20}	7.7	74	0.16

* G_{TH} is the cyclic strain energy release rate corresponding to a threshold crack growth rate of 2.54×10^{-6} mm/cycle.

Figure 3-91. Fatigue Crack Growth of AS-1/3501-6

AD-A183 783

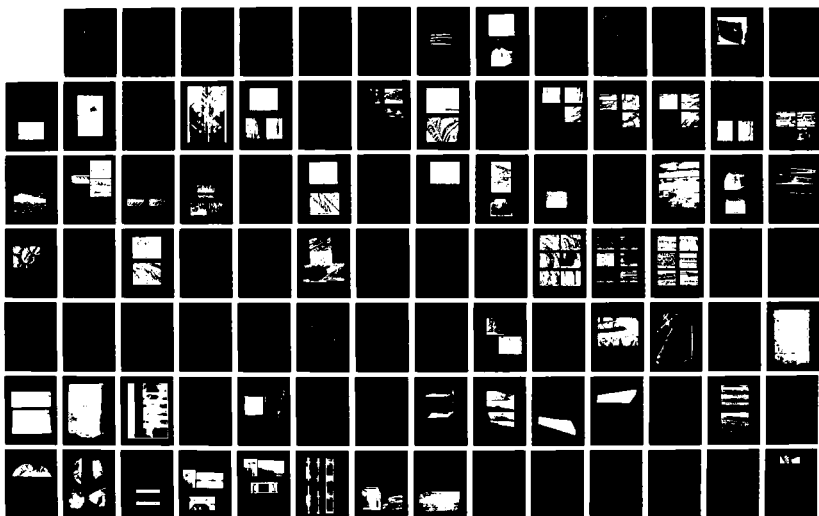
COMPENDIUM OF POST-FAILURE ANALYSIS TECHNIQUES FOR
COMPOSITE MATERIALS(U) BOEING MILITARY AIRPLANE CO
SEATTLE WA R A GROVE ET AL. JAN 87 AFMAL-TR-86-4137
F33615-84-C-5010

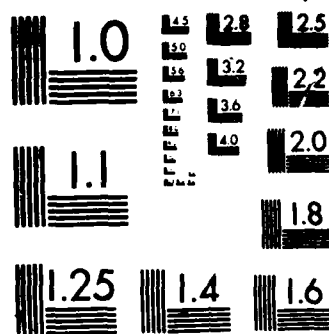
3/5

UNCLASSIFIED

F/G 11/4

NL





MICROCOPY RESOLUTION TEST CHART

NATIONAL BUREAU OF STANDARDS-1963-A

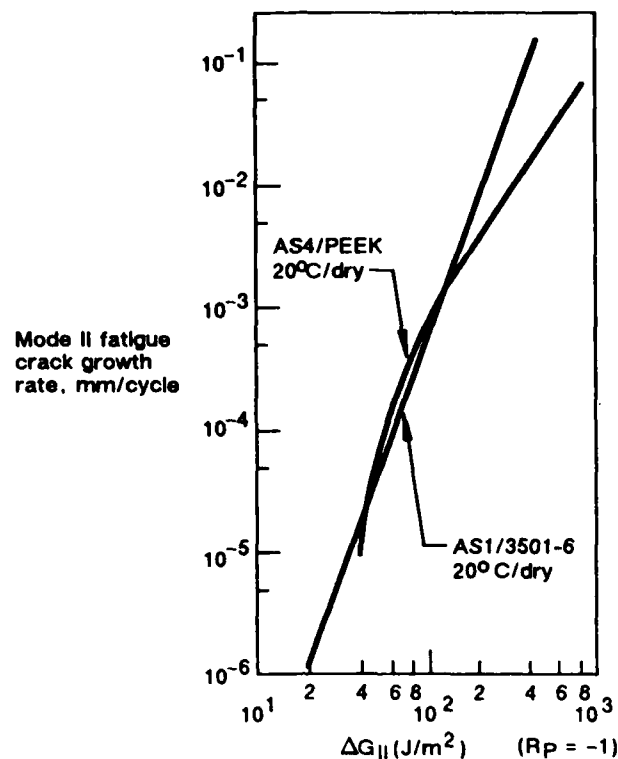


Figure 3-92. Mode II Fatigue


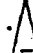







5-870227-127

or Mode II) in the region of failure initiation. Recreating the loads at the onset of failure may illuminate the cause of failure.

3.4.5 Reductions in Strength Due to Manufacturing Defects

While the strength reductions due to holes, cutouts, and impact damage are incorporated into design, manufacturing defects are not accounted for. Some of the typical manufacturing defects that may cause strength reductions are listed in Figure 3-93. This chart also lists the mechanical properties likely to be affected by the defects and some of the methods and data needed to evaluate the criticality of the flaw. Although the list in Figure 3-93 is incomplete, it provides the failure analyst with an understanding of some causes and effects related to typical manufacturing defects.

Defect	Type of defect	Cause	Mechanical properties	Stress analysis method used to evaluate critically of defects	Data needed to perform analysis
Small error in ply angle	Laminate fabrication defect	Layup technique	Strength, stiffness, and hygrothermal stability	Lamination theory, laminate fracture criterion, finite element	△
Error in number or size of plies, gross error in ply direction	Laminate fabrication defect		Strength, stiffness, resistance to edge delamination, hygrothermal stability	Lamination theory, laminate fracture criterion, finite element	△
Low-level porosity (i.e., 2%-5%)	Laminate fabrication defect	Layup technique—ply not compacted correctly, interply porosity in tapes, intraply and interply porosity in fabric	Reduction in interlaminar shear strength and interlaminar toughness	Empirical evaluation, lamination theory, finite elements, crack growth criterion	Interlaminar shear strength and/or interlaminar toughness versus percentage of porosity △
Low-level porosity (i.e., 2%-5%)	Outline-laminate held above storage temperature too long before final curing	Schedule improper or not followed, freezer malfunction	Reduction in interlaminar shear strength and interlaminar toughness	Empirical evaluation, lamination theory, finite elements, crack growth criterion	Interlaminar shear strength and/or interlaminar toughness versus percentage of porosity △
Low level porosity (i.e., 2%-5%)	Processing error	Prepreg resin content too low, too much resin flow during cure	Reduction in interlaminar shear strength and interlaminar toughness	Empirical evaluation, lamination theory, finite elements, crack growth criterion	Interlaminar shear strength and/or interlaminar toughness versus percentage of porosity △
Low-level porosity (i.e., 2%-5%)	Processing error	Cure pressure too low	Reduction in interlaminar shear strength and interlaminar toughness	Empirical evaluation, lamination theory, finite elements, crack growth criterion	Interlaminar shear strength and/or interlaminar toughness versus percentage of porosity △
Low-level porosity (i.e., 2%-5%)	Processing error	Poor impregnation of resin into fiber tow	Interlaminar toughness—susceptible to transverse cracking	Empirical evaluation, lamination theory, finite elements, crack growth criterion	Interlaminar shear strength and/or interlaminar toughness versus percentage of porosity △
High-level porosity (i.e., 5%-10%)	Same as for low-level porosity	Same as for low-level porosity	All	Empirical evaluation, lamination theory, finite elements, crack growth criterion	Interlaminar shear strength and/or interlaminar toughness versus percentage of porosity △
Low glass transition temperature (T _g)	Processing error, fabrication defects, solvent sensitivity	Incorrect processing temperature, incorrect material, exposure to solvents	Strength and stiffness at temperatures near T _g	Empirical evaluation, lamination theory, finite elements, crack growth criterion	Strength and stiffness versus temperature △
Incorrect material	Laminate fabrication defects	Layup technique	All	Lamination theory, finite elements, laminate fracture criterion, crack growth criterion	Inplane and interlaminar fracture toughness △

Low-level porosity (i.e., 2%-5%)	Processing error	Cure pressure too low	Reduction in interlaminar shear strength and interlaminar toughness	Empirical evaluation, lamination theory, finite elements, crack growth criterion	Strength and/or interlaminar toughness versus percentage of porosity 
Low-level porosity (i.e., 2%-5%)	Processing error	Poor impregnation of resin into fiber low	Interlaminar toughness—susceptible to transverse cracking	Empirical evaluation, lamination theory, finite elements, crack growth criterion	Interlaminar shear strength and/or interlaminar toughness versus percentage of porosity 
High-level porosity (i.e., 5%-10%)	Same as for low-level porosity	Same as for low-level porosity	All	Empirical evaluation, lamination theory, finite elements, crack growth criterion	Interlaminar shear strength and/or interlaminar toughness versus percentage of porosity 
Low glass transition temperature (Tg)	Processing error, fabrication defects, solvent sensitivity	Incorrect processing temperature, incorrect material, exposure to solvents	Strength and stiffness at temperatures near Tg	Empirical evaluation, lamination theory, finite elements, crack growth criterion	Strength and stiffness versus temperature 
Incorrect material	Laminate fabrication defects	Layup technique	All	Lamination theory, finite elements, laminate fracture criterion, crack growth criterion	Inplane and interlaminar fracture toughness 
Implanted defect or contamination causing delamination	Laminate fabrication defects	Layup technique	Compression and interlaminar shear strength, susceptible to static or fatigue delamination growth	Finite elements, analytical fracture mechanics, crack growth criterion	Interlaminar toughness 
Incorrect—size fastener or hole, hole or cutout, countersink depth	Assembly error	Machining error, design error, procurement error	Joint strength, laminate strength	Lamination theory, laminate strength criterion, finite elements, notched strength criterion	Notched strength data 
Incorrect fastener material	Assembly error	Machining error, design error, procurement error	Joint strength susceptible to galvanic corrosion	Lamination theory, laminate strength criterion, finite elements, notched strength criterion	Notched strength data 
Contamination, bond line thickness, improperly cured adhesive, improper surface preparation	Defective bonding	Assembly error	Bonded joint strength	Lamination theory, analytical fracture mechanics, finite elements, crack growth criterion	Fracture toughness of adhesive and interface 


 Basic laminate properties: strength, stiffness, coefficient of thermal expansion, etc.

Figure 3-93. Manufacturing Defects Chart

4.0 FRACTOGRAPHIC APPLICATIONS, EXAMPLES AND INTERPRETIVE METHODS

Some of the most extensive investigations in a failure analysis involve the examination of the fracture surface of failed components. These surfaces may provide the only true physical record of the events and conditions involved in the failure process. Through detailed macroscopic and microscopic analyses, fractography can be used to attempt reconstruction of the failure sequence. Using the tools and methods outlined in paragraph 3.3, primary emphasis is placed on interpreting the fractographic information obtained to answer the following questions:

- Where did a crack start, that is, where is a crack origin?
- What caused the crack to initiate at the origin?
- By what modes did the crack propagate?
- In what directions did the crack propagate?
- What fracture types are present?
- What loads or environmental conditions were operative at failure?
- What was the sequence of failure in a case of multiple cracks or multiple component fracture?

The development of the analytical methods and interpretive skills required to answer these questions for composite material structures have only recently been initiated. In general, fractographic studies on other materials (metals and unreinforced polymers) have made significant strides toward (1) understanding the microscopic mechanisms of cracking and (2) identifying the causes of component failure. Of these two areas, the latter is perhaps the most important. Through fractographic examinations, the origin location and the direction of crack growth and load conditions involved in premature component fractures can generally be identified. In many cases, the definition of defects, damage conditions or anomalous fracture modes by such studies may be sufficient to identify the cause of fracture. In those cases where such causes are not apparent, understanding the sequence of events leading to fracture on a microscopic scale is often crucial to accurately direct other analyses techniques such as stress analysis or materials characterization.

The information presented in this section is intended to provide the investigator with a basic fundamental understanding of how laminated composite structures fracture. Primary emphasis is placed on analyses of carbon fiber reinforced and epoxy resin matrix systems, which have been proven to provide the aerospace industry with a material which exhibits high specific strength and modulus combined with excellent environmental durability. More specifically, the vast majority of the examples are from laminates constructed from prepreg tape. Fabric or three-dimensional product forms appear to fail under basically the same mechanism, although slightly more complex in nature. Covered in this section are discussions on the following:

- Fracture type and classification.
 - Translaminar
 - Interlaminar
 - Intralaminar
- Interlaminar and intralaminar fractures.
 - Tension versus shear fracture features
 - Mixed mode fractures
 - Relationships between features and crack growth directions
 - Cross-plying interfacial effects
 - Environment and fatigue effects
- Translaminar fractures.
 - Tension
 - Compression
 - Flexure
 - Environmental effects

4.1 FRACTURE TYPES

Because of their laminated anisotropic construction, fractures in composites can occur in a number of complex ways. The types and modes of failure which can be encountered depends upon both the direction of applied load and the orientation of fibers (plies) making up the composite material. As indicated in Figures 4-1 and 4-2, variations in either of



Figure 4-1. Laminate Flexure Specimens

5-B70227R1-21



Tensile



Compression

Figure 4-2. Tensile and Compression Translaminar Fractures

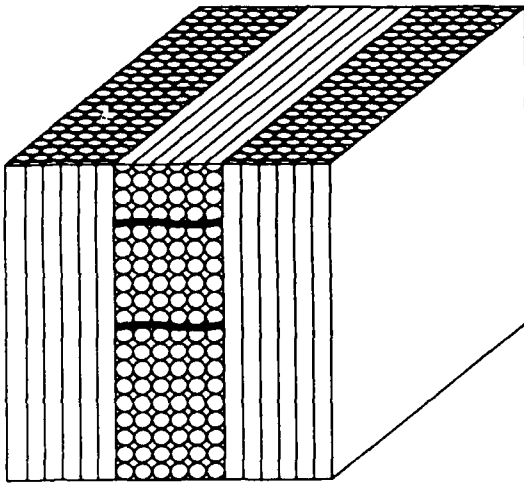
S-B70227-22

these can produce strikingly different fracture appearances on a macroscopic scale. This range of diversity precludes the ability to assign well defined macroscopic fracture types for most applications. The definition of fracture types on a microscopic scale, however, provides a relatively useful means of classifying failure modes and fracture types in much the same way as with metals.

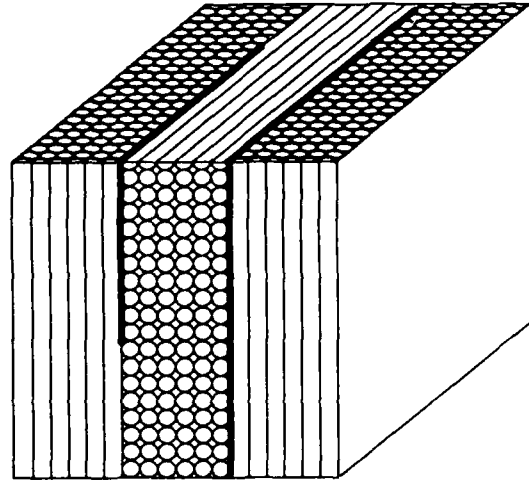
Fractures in continuous fiber reinforced composites can be divided into three basic fracture types; interlaminar, intralaminar, and translaminar. Each of these failure types are schematically illustrated in Figure 4-3. As with the intergranular and transgranular terminology commonly used with metals, each of these classifications describes the plane of fracture with respect to the microstructural constituents of the material.

Translaminar fractures are those oriented transverse to the laminated plane in which conditions of fiber fracture are generated. Interlaminar fractures, on the other hand, describe failures oriented between plies whereas intralaminar fractures are those located internally within a ply. Translaminar fractures involve significant fiber fracture, while interlaminar or intralaminar fractures occur in the laminate plane, principally fracturing matrix resin and therefore breaking few or no fibers.

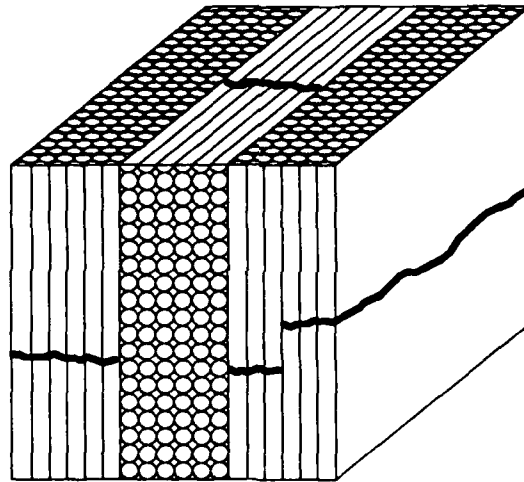
Commonly, a failed component will exhibit all three types of fracture. In this case, it is important to differentiate between the types so as to more easily prepare the analytical approach (per the fractography FALN) and to define the analytical tools to be used. For instance, the optical microscope is the most accurate and quickest method of analyzing interlaminar or intralaminar fractures, in which the fracture of the matrix resin dominates. Conversely, the optical microscope cannot be used to investigate the translaminar, fiber-fracture dominated surfaces due to the rough topography. For such fractures in which a large depth of focus is required in conjunction with high magnification capabilities, the scanning electron microscope is invaluable. Although this is rather a simple analogy, it illustrates the need to define and understand the various fracture types so that planning of detailed analysis such as crack mapping can be developed early in the investigation process.



(a) Intralaminar Fracture



(b) Interlaminar Fracture



(c) Translaminar Fracture

Figure 4-3. The Basic Fracture Modes

5-B70227-129

4.2 FRACTURE MODES, FEATURES, AND GROWTH DIRECTIONS

Failures in composites can be described in terms of the failure mechanism exhibited on translaminar, interlaminar, and intralaminar fracture types. The first evaluation method available to define and differentiate between these fracture types is visual macroscopic. The ability to define fracture types at the macroscopic level can often be the most valuable capability for many investigators, particularly for those performing field investigations. When examining a failed composite structure, the investigator must assess the nature and direction of the applied load, identify the significance and time of fracture, and select portions of the structure for laboratory analyses. Visual examination alone can often provide sufficient information to answer these questions. However, this extremely valuable capability is very much in its infancy compared to the metals field. Figure 4-4 presents a brief overview of the relationships that various investigators have observed between fracture mode/load conditions and macroscopic fracture surface features. Figure 4-5 illustrates how a consistent pattern of crack branching of the skin surface was found to indicate the direction of macroscopic crack growth, and aided in identifying the initiation site in a very large structure which experienced compression buckling.

MODE	ENVIR. CONDITION	MACROSCOPIC FRACTURE FEATURES
Interlaminar Tension Dominated	Low Temperature/Dry	<ul style="list-style-type: none"> • Smooth, glassy fracture surface • Major portion of fracture between plies
	Hot or Hot/Wet	<ul style="list-style-type: none"> • Smooth but with loose fibers strewn on surface • A majority of the fracture within plies • May be permanent deformation of laminate
Interlaminar Shear Dominated	Low Temperature/Dry	<ul style="list-style-type: none"> • Surface flat, but with "milky" appearance when held at angle to light • Major portion of fracture between plies
	Hot or Hot/Wet	<ul style="list-style-type: none"> • Also exhibits "milky" appearance • Tends to fracture within a ply • Loose fibers on surface
Translaminar Tension	_____	<ul style="list-style-type: none"> • Rough, jagged fracture surface with individual fibers protruding from surface
Translaminar Compression	_____	<ul style="list-style-type: none"> • Extreme surface damage. Large regions of fibers fractured on same plane • Very few, if any, fibers protruding from surface
Translaminar Flexure	_____	<ul style="list-style-type: none"> • Two fairly distinct regions, one exhibiting translaminar tension and the other translaminar compression, the regions being separated by a neutral axis line

Figure 4-4. Visual Microscopic Fracture Surface Features

5-B70227R1-64

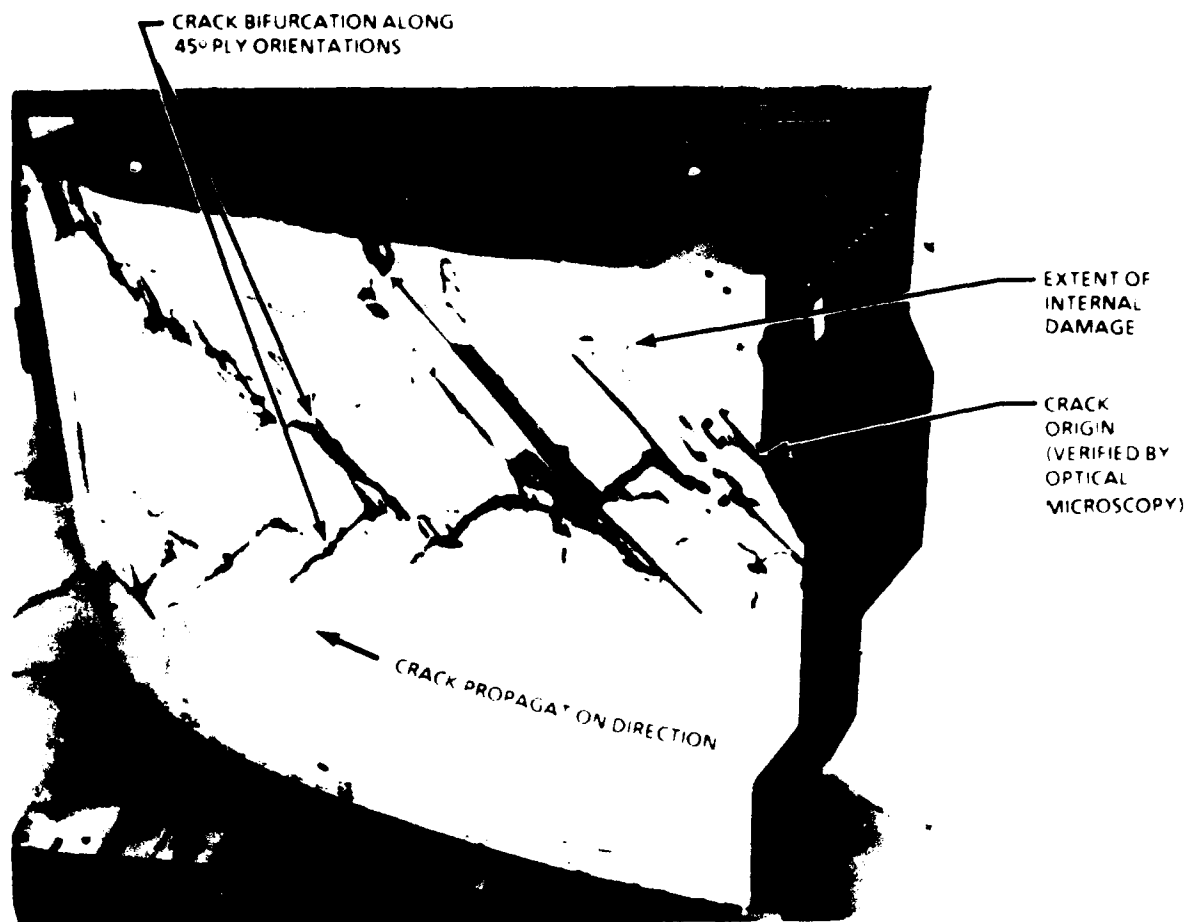


Figure 4-5. V-22 Osprey Wing Box Failure

5-B70227-86

Although macroscopic methods are currently fairly limited, an extensive capability has been developed to evaluate the microscopic fracture features in the laboratory as related to each failure mechanism. The failure mechanism reflects the load under which microscopic separation occurs, either tension, shear, or compression or fatigue. The following discussion presents each of the primary types of failure, with the interpretation of the fractographic features that identify the load type and localized crack propagation direction.

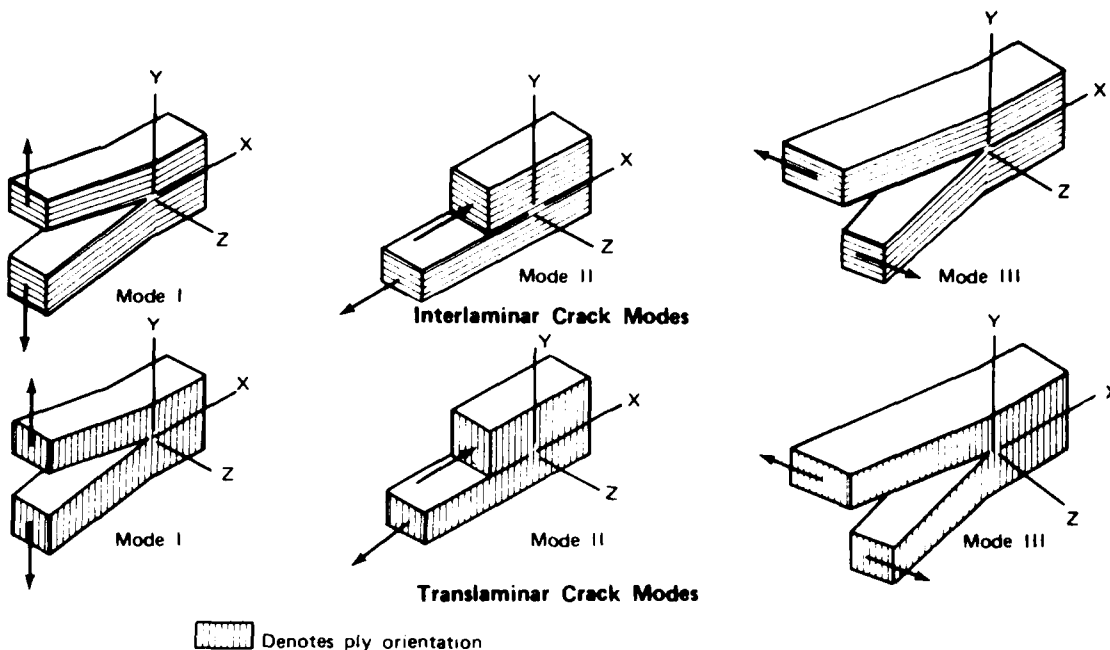
4.2.1 Interlaminar and Intralaminar

The extremely low in-plane fracture resistance ($G_{Ic} = 0.25 \text{ KJ/sg.m}$ versus translaminar G_{Ic} values of 100 KJ/sq.m) makes interlaminar and intralaminar fracture (commonly known as delaminations) a particularly significant mode of failure for nearly all composite fractures. When considered on a microscale, interlaminar and intralaminar fractures can be described similarly. In both cases fracture occurs on a plane parallel to that of the

fiber reinforcement. In a manner similar to that described for metals, fracture of either type can occur under Mode I tension, Mode II in-plane shear, Mode III anti-plane shear. These three load states are illustrated in Figure 4-6. On a microscopic scale, nearly all delaminations separate in a combination of the first two types, with a predominance of either one or the other. All modes are recognized as potentially critical in compression buckling, joint failures, and defect initiated failures such as impact. Each of these failure modes are still being actively investigated so as to further understand the actual microstructural separation mechanisms and the generated morphological features, as related to the macroscopic loading conditions. As a result, conditions such as Mode III anti-plane shear have not been thoroughly studied and will not be presented in this document. However, for Mode I tension and Mode II in-plane shear, enough data exists to accurately model their mechanisms of separation and describe their fracture characteristics.

Since interlaminar and intralaminar failures occur in the same plane as their fiber reinforcement, their fracture mechanism and appearance tend to be dominated by matrix fracture and fiber-to-matrix separation. In general, separation of the fiber from the matrix occurs at the interface for either Mode I tension or Mode II shear loading conditions. As a result, very little cohesive resin fracture occurs along the fiber, which often serves as a source of crack initiation. Fracture of the matrix resin between fibers exhibits pronounced cohesive fracture characteristics under both Mode I tension and Mode II shear loading.

For the majority of thermosetting matrices currently in use, cohesive matrix failure occurs in a brittle manner. Cohesive resin fracture characteristically exhibits relatively flat fracture planes with very little evidence of permanent material deformation. This is similar to brittle failure in metals (Figure 4-7), unreinforced polymers (Figure 4-8), and ceramics such as glass. The microscopic plane of such brittle failures is nearly always oriented normal to the direction of locally resolved tension. With reference to Figure 4-6, separation under both Mode I tension or Mode II shear occurs by the identical microscopic mechanism, (that is, brittle tension). The only difference between these two modes is the orientation of principal tensile stress under which microscopic separation occurs.



- Mode I Opening or tensile mode, where the crack surfaces move directly apart.
- Mode II Sliding or in-plane shear mode, where the crack surfaces slide over one another in a direction perpendicular to the leading edge of the crack.
- Mode III Tearing or antiplane shear mode, where the crack surfaces move relative to one another and parallel to the leading edge of the crack.

Figure 4-6. Basic Modes of Loading Involving Different Crack Types and Surface Displacements (Interlaminar and Translaminar)

5-B70227-65



Figure 4-7. Fracture Surface of 4340M Steel Illustrating Cleavage Fracture Features Indicative of Crack Growth Direction

5-B70227-23

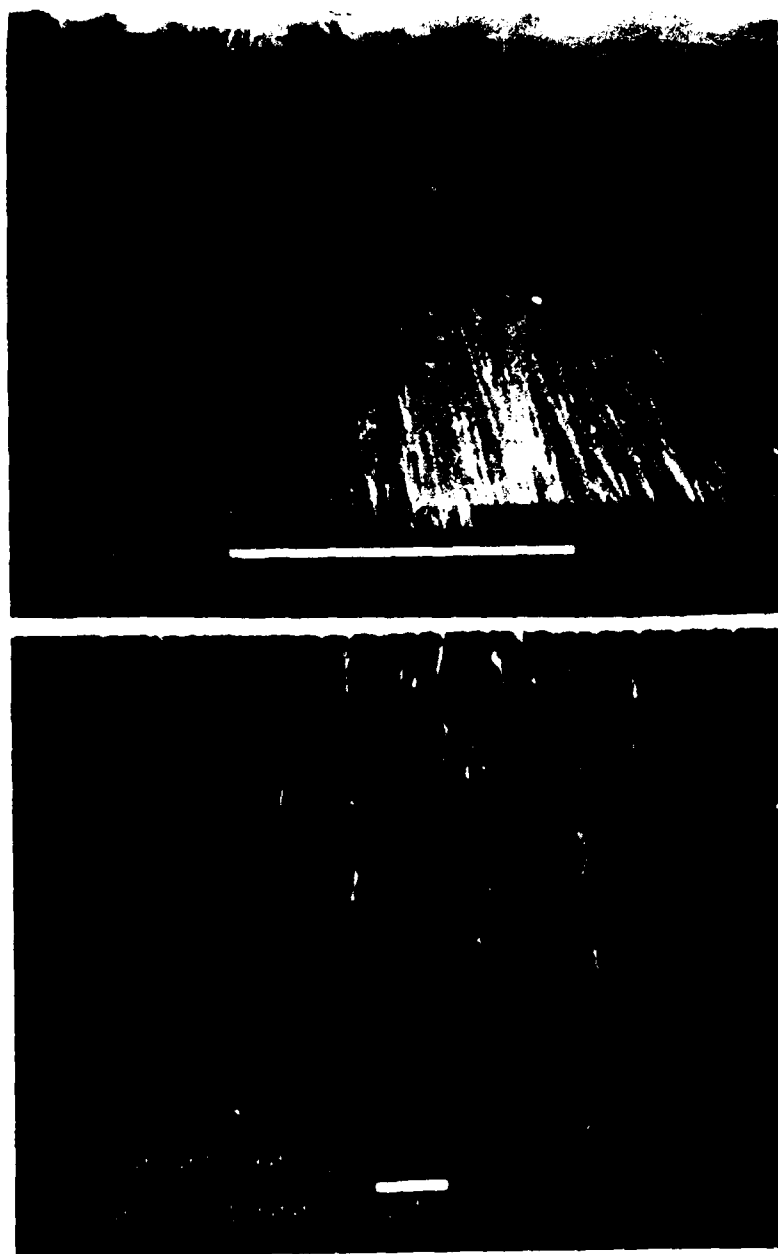


Figure 4-8. Fracture of Unreinforced Neat Epoxy Resin

5-B70227-24

4.2.1.1 Mode I Tension Delaminations

In the case of Mode I tension (which is the weakest fracture type with a G_{Ic} toughness at one-third of Mode II shear G_{IIc}), the maximum principal tensile stress lies perpendicular to the plane of failure. As a result, brittle cleavage of the matrix material occurs and fiber fracture rarely happens. These fractures are flat and are very shiny and smooth in appearance at macroscopic visual levels of magnification (Figure 4-9). Although not often identified, arced bands can be found that are similar to beach markings found in metals and unreinforced polymer fractures. Such markings, presented in Figure 4-10 from a controlled crack growth test coupon, are indicative of the crack-front geometry and are formed in response to pronounced changes in crack velocity. Numerous investigators have demonstrated that in neat polymeric materials, low crack velocities resulted in mirror-smooth fracture surfaces, and high crack velocities result in roughened, less reflective fracture topographies. This feature can be used to define the macroscopic direction of crack growth with the direction of growth moving from the concave to the convex side of the markings.

Microscopic examinations (optical and SEM) reveal distinctly flat areas of cohesive resin fracture between the areas of fiber-matrix separation. The extent to which either of these two features occur depends upon both the volume fraction of fibers and the proximity of the fracture plane to these fibers (that is, intralaminar or interlaminar). In general, cohesive resin fractures dominate the overall surface topography. Such areas typically exhibit pronounced river markings and resin microflow as discussed below. The combination of these features appear unique to Mode I tension and provide a means of identifying the relative percentage of Mode I tension at fracture and the localized direction of crack propagation.

High magnification optical photomicrographs of interlaminar tension fractures which delaminated in the direction of fiber orientation are illustrated in Figure 4-11. The surface reveals a reflective appearance with flat areas of resin fracture between the regions of fiber/matrix separation. Inspection reveals branching lines (river marks) in these flat resin fracture areas, along with an extremely fine texture or feathering (resin microflow); the direction of river mark coalescence corresponds with the direction of overall crack growth. These photomicrographs are taken from a region between plies that

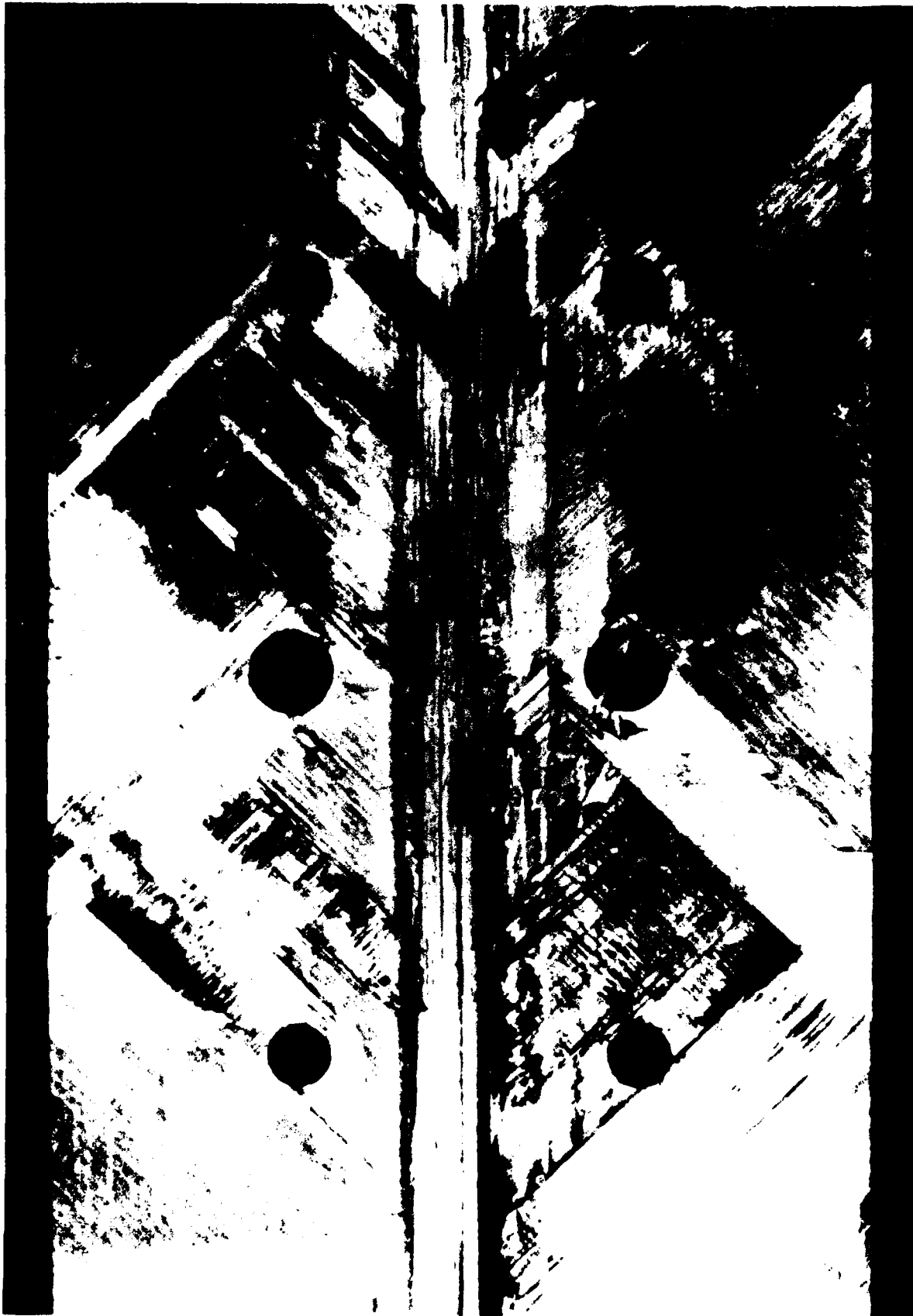
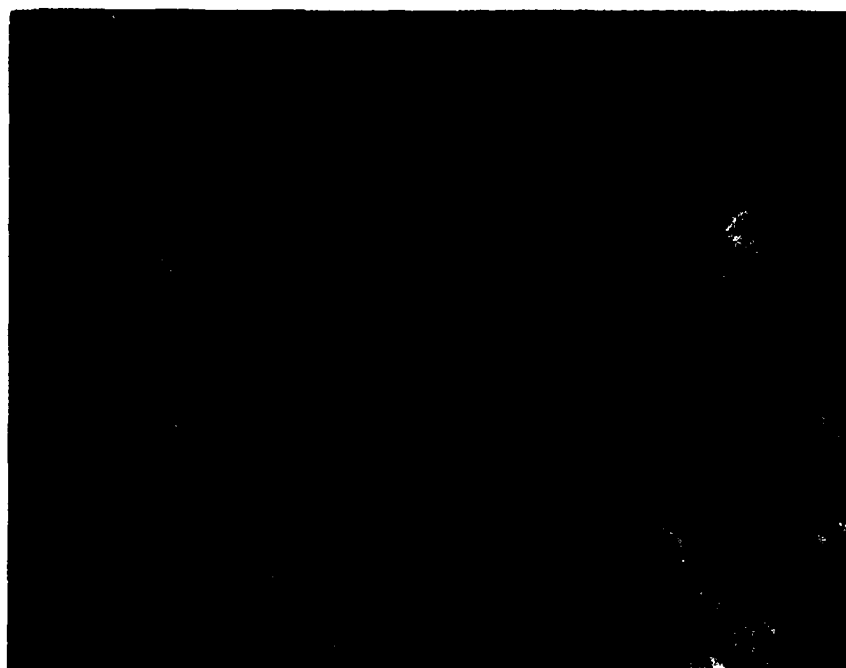


Figure 4-9. Mode I Tension Fracture

5-B70227-25



1X

Figure 4-10. Beach Marks Found in a Delamination Surface Indicative of Crack Front Shape and Growth Direction During Fracture

5-B70227-26



100X



400X

Crack propagation direction

Figure 4-11. Optical Photomicrographs of Intended Fracture Plane Between 0/0-deg Plies, DCB 21°C (70°F) Specimen

5-B70227-66

was rich in resin, primarily for illustrative purposes. Therefore more resin fracture and fewer fibers are evident than usually found. It should be noted that areas with different ratios of fiber reinforcement do not significantly effect the overall fracture features, although it can make optical inspections more difficult to resolve small resin fields between fibers.

The river markings, presented in Figure 4-12, are analogous to the cleavage fracture features commonly recognized in brittle materials such as metals, ceramics, and polymers. It has been determined through extensive studies that such features result from progressive joining of adjacent microscopic fracture planes during crack growth. More specifically, each line segment represents a local step formed when the thin ligament separating two adjacent planes is fractured during crack growth. As presented by Griffith (ref. 59), the amount of strain energy involved in fracture is proportional to the area of fracture surface created and the amount of plastic deformation at the crack tip. As a result, a large number of locally displaced fracture planes that initiate at the fiber/matrix interface represent a higher energy condition than a single continuous fracture surface. Since crack propagation tends to occur along the path requiring the least energy, there is a tendency for the planes to coalesce together. Thus the multitude of microplanes that initiate at the fiber/matrix interface link up as the crack propagates, resulting in a coalescence of the steps to form a branched pattern, or river marks.

Close inspection of the resin microplanes exhibit a distinctly textured morphology referred to as resin microflow. Microflow is discernable at high magnifications and usually requires tilting of the specimen in the SEM (Figures 4-13 and 4-14) for this subtle feature to become visible. In many ways, the textured appearance is identical to the cleavage feathers characteristic of metallic fractures as shown in Figure 4-7. These feathery patterns exhibit a distinctive chevron type appearance, with the pointed end of the chevron oriented toward the origin of propagation. This chevron pattern results from the inherent tendency of a propagating crack to take the shortest path to a free surface. On a microscopic scale, these chevrons tend to rotate from the direction of overall crack growth toward adjacent free surfaces such as microplanes, transverse cracks, or fiber/matrix interfaces. However, by examining the direction and orientation of the microflow patterns in the center of each microplane, the localized direction of crack propagation can be determined.



Vertical arrow indicates crack direction

- Legend:
 M Matrix fracture
 F Fiber fracture
 P Fiber/polymer separation
 S Surface morphology



Figure 4-12. SEM Fractographs of Mode I Delamination Between 0/0-deg Plies

5-B70227-87

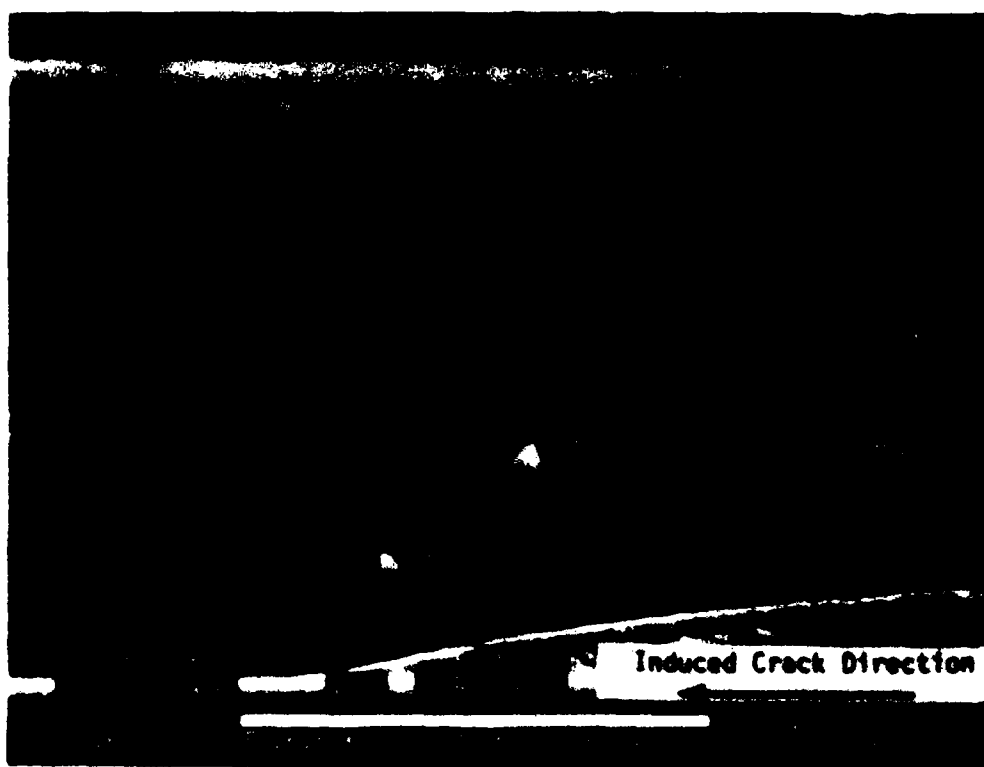


Figure 4-13. Photomicrograph Illustrating Adhesive Fracture Areas of Textured Microflow

5-B70227-89



300X

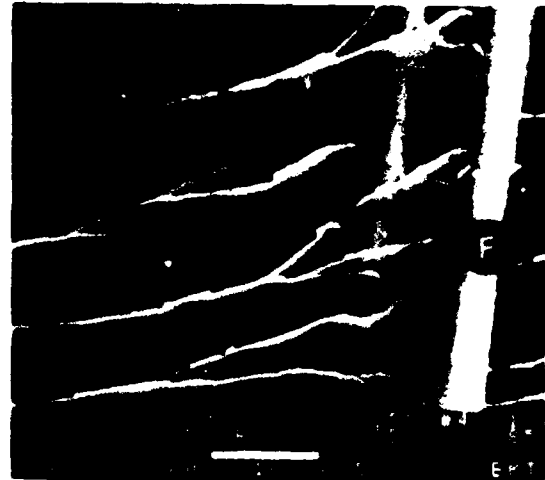
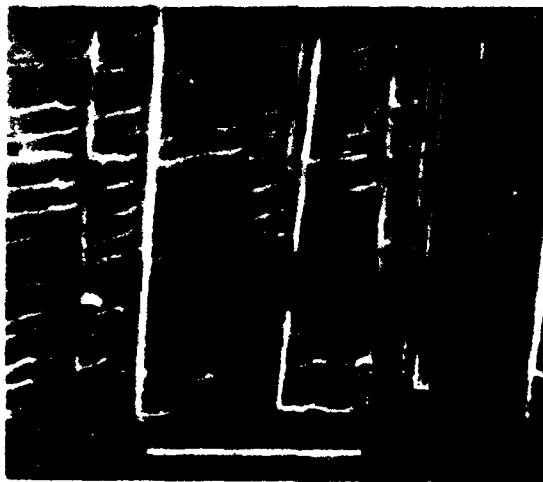
Figure 4-14. TEM Image of Resin Microplane With River Marks and Resin Microflow

5-B70227-27

Mode I tension fractures produced at angles relative to the direction of fiber reinforcement typically exhibit both the river markings and resin microflow as noted above. However, significant variations in the fracture topography can occur at the microscopic scale, depending upon the number of fibers exposed by the fracture and their orientation relative to the direction of microscopic crack growth (Figures 4-15 and 4-16). Cracking often occurs in the resin rich region between plies, particularly between plies of large angular differences (that is, 0° and 90°). Fractures which occur at the interface between plies exhibit relatively large areas of flat-resin fracture with distinct river marks in a fairly consistent microscopic direction. Alternatively, fractures which occur within a ply exhibit variable and often seemingly inconsistent localized microscopic directions of fracture. River marks and microflow are oriented in a wide variety of directions across the fracture surface. Variations in the direction of microscopic crack propagation can often be averaged together to obtain a more accurate estimate of the overall direction of crack propagation (Figure 4-17).

Variations in the direction of microscopic crack growth depend upon several factors. The two most notable factors that must be considered are the formation of localized zones due to fiber intrusion and the magnitude of stress concentration involved in fracture. In the first case, fiber/matrix areas tend to divide the crack tip into numerous microscopic zones, at which the crack must initiate a new crack front at the other side of the fiber to continue growth in this zone. In general, these zones will exhibit differing growth rates and slightly displaced planes of fracture. Consequently, the resultant crack front formed by these regions can be highly irregular, with narrow crack extensions in front of the main crack tip. This crack front profile can produce significant local variations in the crack directions as the extensions grow laterally to meet each other.

The second major condition that can lead to crack direction variations takes place when failure occurs without the formation of any appreciable stress concentration. This is similar to the condition generated with flatwise tension test coupons, in which failure tends to occur at a wide variety of locations within the laminate plane. As with ductile tensile separation rupture in metals, failure occurs when these multiple fracture planes intersect. Such fractures are characterized by the formation of an extensive number of fracture planes throughout the laminate with extreme variations in the direction of crack propagation such that no overall direction of crack propagation exists.



Mechanically induced crack direction

Legend


- M Matrix fracture
- F Fiber matrix separation
- R River markings
- T Textured microflow



Figure 4-15. SEM Photomicrographs of Mode I Delamination Between 0/90-deg Plies

5-B70227-90




 Mechanically induced crack direction

Legend

- M Matrix fracture
- F Fiber matrix separation
- R River markings
- T Textured microflow

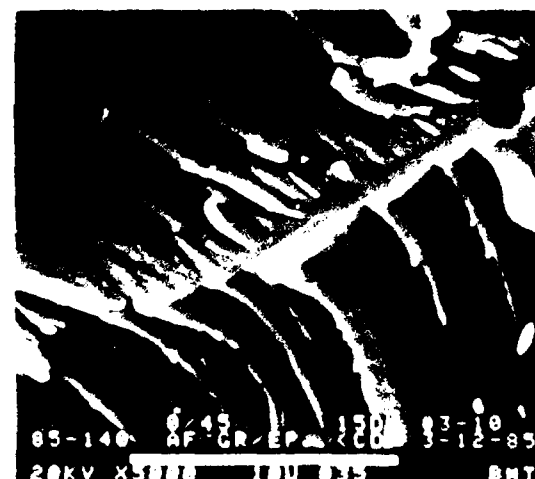
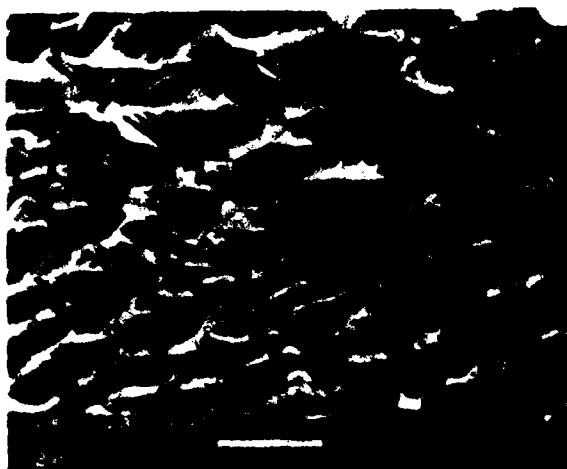


Figure 4-16. SEM Photomicrographs of Mode I Delamination Between 0/+45-deg Plies

5-B70227-92




 Mechanically induced crack direction

Legend:

- M Matrix fracture
- F Fiber matrix separation
- R River markings
- T Textured microflow



Figure 4-17. SEM Fractographs of Mode I Delamination Between +45/+45-deg Plies

5-B70227-91

4.2.1.2 Mode II Shear Delaminations

Failures by interlaminar shear can occur by macroscopic loading sources such as tension, compression, or flexure. The duty of the matrix resin is to transfer the axial loads in each fiber to the adjacent similarly oriented fibers and to adjacent plies that are not oriented in the direction of primary loading. As a result, shear fractures tend to occur within, or adjacent to, plies that are oriented in the direction of maximum loading.

Failures produced under conditions of Mode II shear, while also occurring by brittle tensile separation, exhibit a distinctly different appearance than Mode I tensile failures. Macroscopic examinations reveal a dull and often "milky" appearance when held at oblique angles to a light source, due to opaque light scattering by the rough resin fracture features. Microscopic investigations show a much rougher topography than pure Mode I tension. Optical microscopy reveals a series of translucent, vertical, and parallel resin platelets found in the narrow resin fracture zones between the fibers. As shown in Figure 4-18, the platelets are aligned normal to the direction of crack propagation. The large flat matrix regions which exhibit river mark branching typical of Mode I delaminations are not present. These distinct differences permit the use of optical analyses to rapidly differentiate between Mode I and Mode II delaminations when either load condition dominates during fracture.

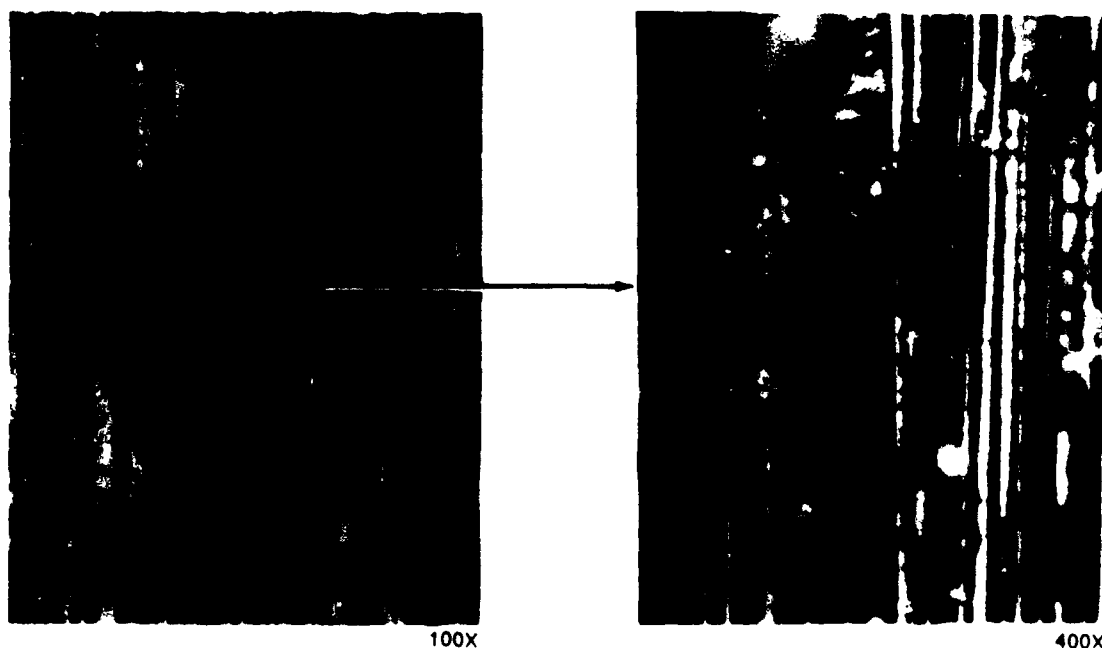


Figure 4-18. Optical Photomicrographs of Intended Fracture Plane Between 0/0-deg Plies, ENF 21°C (70°F) Specimen

Under detailed SEM examination (Figure 4-19), the rows of curved vertical platelets are found in the cohesive resin fracture regions between fibers. As described by Mohr's circle, during in-plane shear loading the principle tensile stresses are oriented at forty-five degrees to the plane of applied shear, as shown in Figure 4-20. Since matrix fracture occurs in a microscopic plane normal to resolved tensile stress, a series of distinct inclined microcracks (Figure 4-21) are formed ahead of the main crack front. Increased strain or loading causes these small parallel microcracks to grow and coalesce, resulting in the formation of a series of upright curved platelets. Based upon these observations, the directions of applied shear (clockwise or counterclockwise moment) can be determined by examining the direction of platelet tilt. Concave areas are found on the mating fracture surfaces, opposite to these platelets (Figure 4-22). High magnification inspection of the platelets and the concave regions reveals small river marks and microflow, also indicative of resolved tensile separation. Several terms have been used to describe each

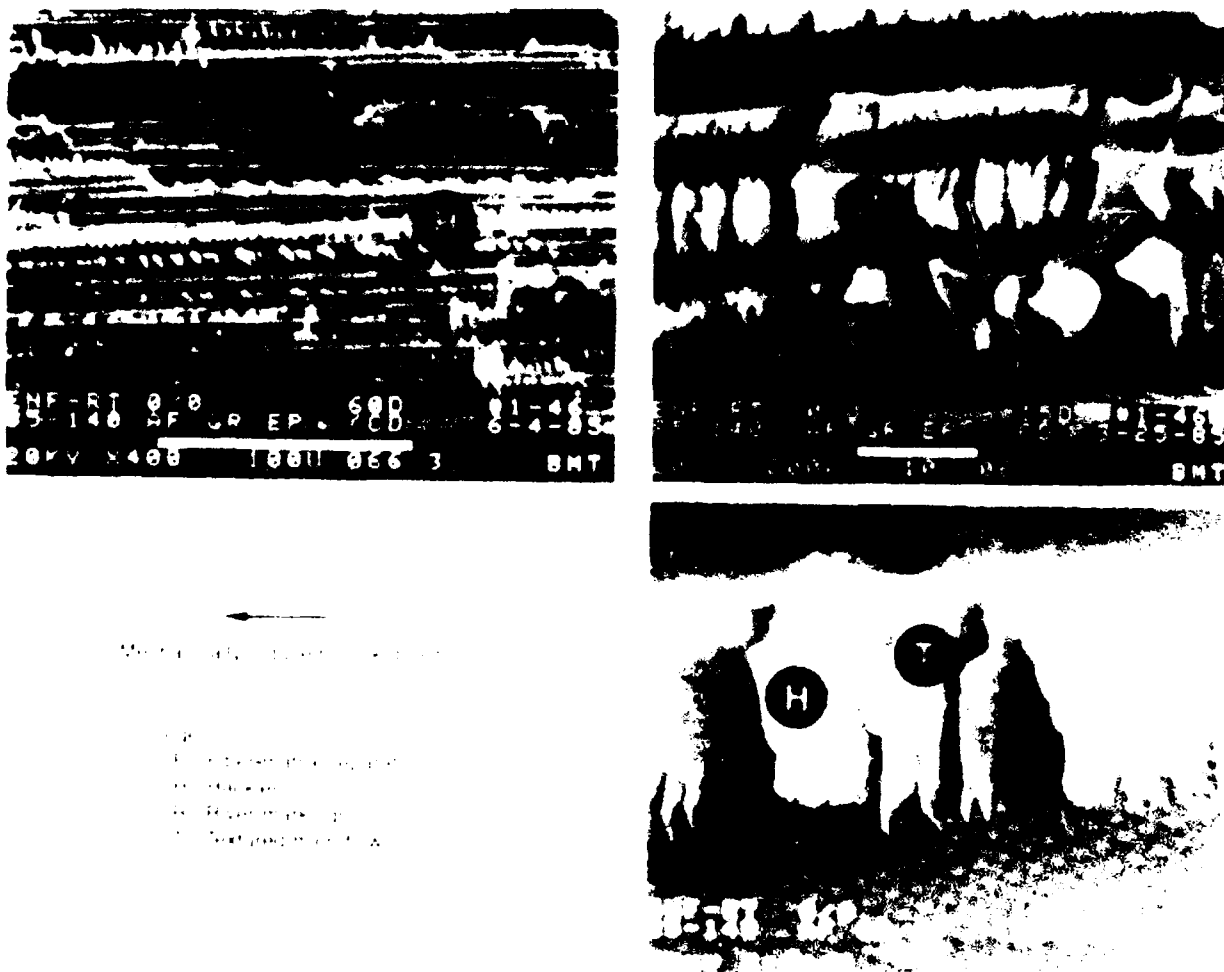


Figure 4-19. SEM Photomicrographs of Mode II Delamination Between 0/0-deg Plies

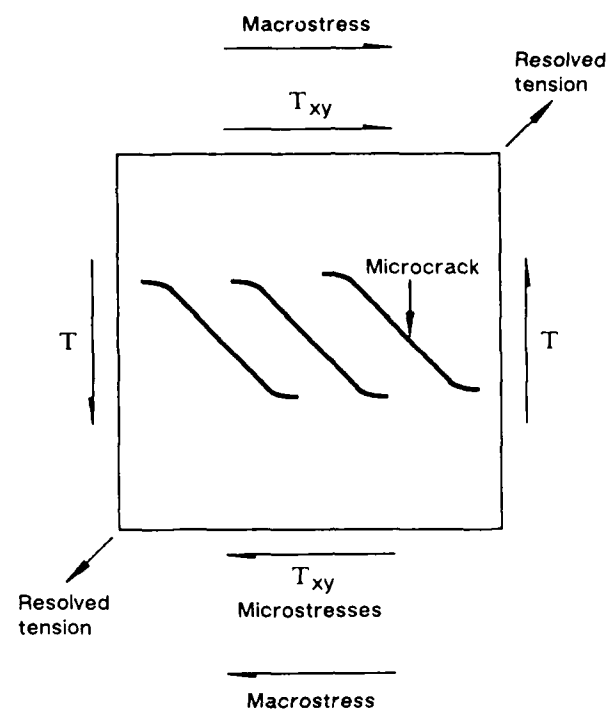
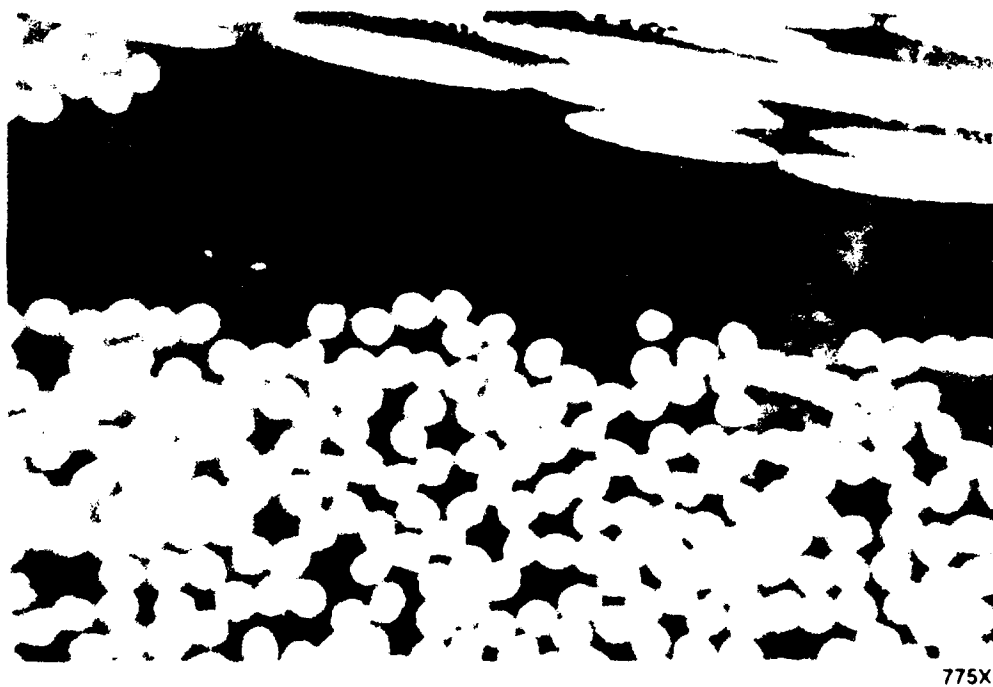


Figure 4-20. Free Body Diagram of Resolved Tensile Stresses and Inclined Microcracks

5-B70227-101



775X

(Ref. 68. Copyright © ASTM reprinted with permission.)

Figure 4-21. Microstructure of Cracks Found in Short Beam Shear Specimen Tested at 132°C (270°F)

5-B70227-94

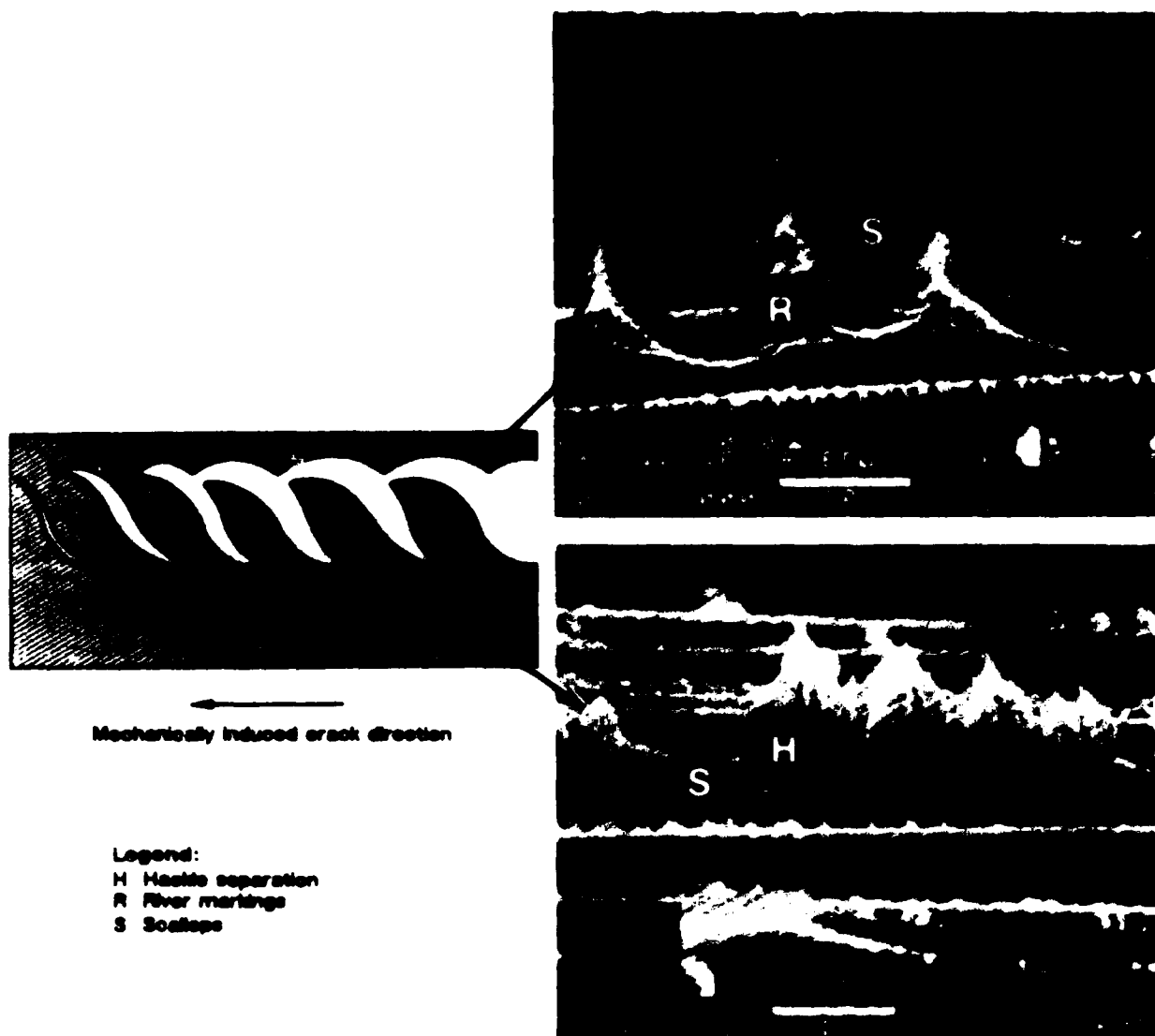


Figure 4-22. Scalloped Resin Fracture Areas and Their Development

6-B70227R1-95

of these features including lacerations or hackles for the upright platelets and scallops for the concave areas. For this document, the more common use of hackles to describe platelets and scallops to describe depressed concave areas is used.

Separation of hackles can result in two possible relationships (mechanisms A and B) between hackle tilt and the direction of crack propagation, depending on which fracture surface retains the hackle (Figure 4-23). In mechanism A, separation occurs such that the hackles are retained on the side in which the direction of crack propagation coincides with the direction of local shear component. This condition produces hackles tilted in the direction of crack propagation, and normal to the direction of resolved tension (45 degrees). Conversely, in mechanism B, separation occurs such that hackles are retained on the side in which the direction of crack propagation opposes the direction of the local shear component. In this condition, the tilt of hackles oppose the direction of crack propagation.

Comparisons of the hackle tilt, scallop features, and the mating fracture surfaces by a variety of researchers indicated that the direction of crack growth cannot be established with the same confidence possible for Mode I delaminations. Mode II and mixed mode delaminations generally occur by a combination of the two possible mechanisms such that

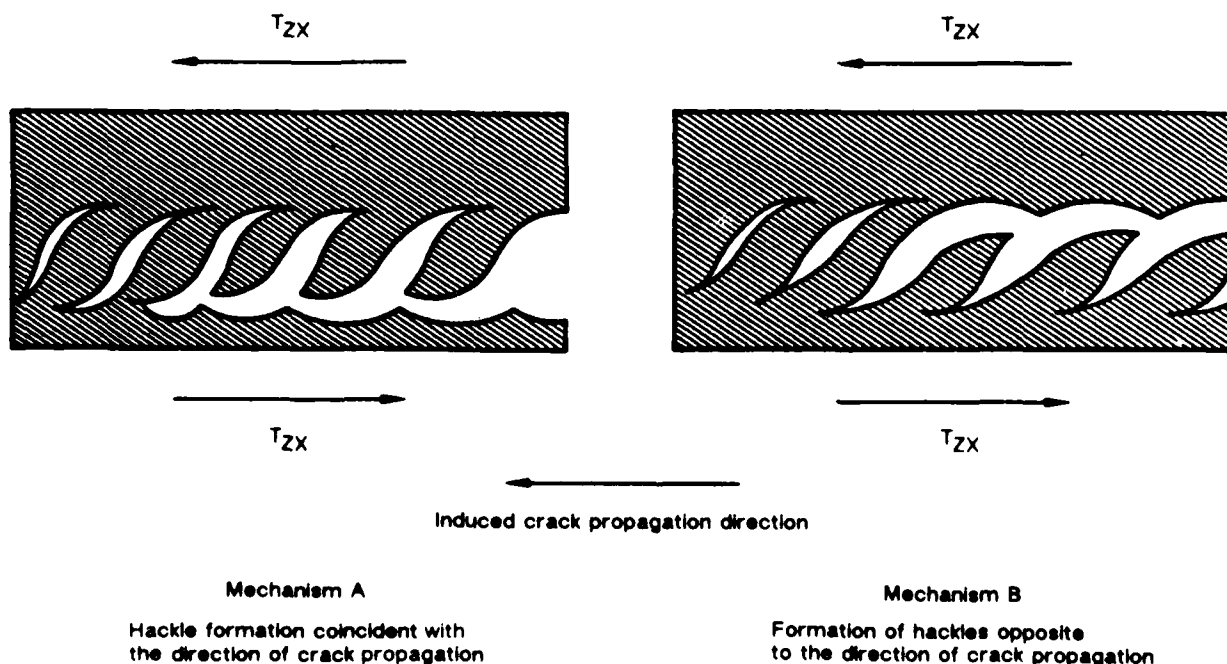


Figure 4-23. Possible Hackle Separation Mechanisms

hackles are found on each mating fracture surface, preventing a definitive conclusion of the crack growth direction. However, the direction of hackle orientation can be used to estimate the direction parallel to which crack growth occurred.

The orientation of fiber reinforcement at, or adjacent to, the delamination plane can have a significant effect on the morphology of both hackles and scallops that must be considered when determining the direction of crack propagation. Surface fibers oriented parallel to the direction of crack growth tend to form orthogonal shaped hackles and scallops (Figure 4-24), whereas fibers intersecting the fracture surface at an angle to the direction of growth tend to form roughly triangular asymmetric hackles and scallops (Figure 4-25). In the first case, a distinct branched morphology generally exists on both sides of the hackles and scallops where they intersect adjoining areas of fiber/matrix separation. Since this symmetry and the orthogonal shape of these features correspond to propagation parallel to the direction of exposed fibers, these features provide a relatively rapid and easy means of identifying the direction parallel to which crack growth occurred.



Figure 4-24. Orthogonally Shaped Symmetrical Hackles

5-B70227-68



Figure 4-25. Triangular Asymmetric Hackles, With River Marks and Fiber-Matrix Separation

5-B70227-69

In the second case, when the asymmetric features are identified, the tilt of the triangular hackles is predominantly parallel to the direction of crack propagation.

4.2.1.3 Mixed Mode Delaminations

Interlaminar mixed mode delaminations commonly fail in a mixed mode loading condition, in which neither pure tension or shear are operative. Failures due to complex loading such as flexure and compression buckling tend to exhibit delamination fracture morphologies that appear somewhat different to those found for the pure loading conditions presented in the above paragraphs. Since resin fracture separation occurs by resolved tensile forces in both pure shear and tension, so does fracture due to a mixed load state. The extent to which each of the predominant features exist, (flat regions with river marks or vertical hackles), depends upon the ratio of Mode I to Mode II macroscopic stress. Therefore, delaminations with a predominance of Mode I tension mainly exhibit river marks and flat fracture topographies, with a tendency toward a slight tilt in each of the resin fracture microplanes, indicative of the slight rotation of the resolved tensile component (Figure 4-26). For these types of fractures, river marks and resin microflow are still useful for defining the localized crack growth direction and for use in crack mapping. As the percentage of Mode II increases, the tilt of these resin microplanes also increases relative to the rotation of the resolved tensile component. At percentages of Mode II above approximately 30%, these platelets take upon an appearance of hackles, where there is pronounced separation between each hackle and scallops present on the mating surface. Figure 4-27 presents the fracture morphology at approximately 43% Mode II shear and 57% Mode I tension. This fracture surface was generated with a Mixed Mode Flexural specimen. Note the formation of the hackles, although they are not as vertical or upright as those found for pure shear fracture specimens. As indicated in the above paragraph on pure shear, the use of hackles can be used to define the direction parallel to crack propagation. As to precisely what percentage of Mode II or which fractographic features can be used to definitively define crack growth directions has not been determined. Further studies on controlled crack growth specimens across the spectrum of mixed mode must be performed to gain a firm understanding of the validity of determining crack growth directions in a mixed mode loading state.

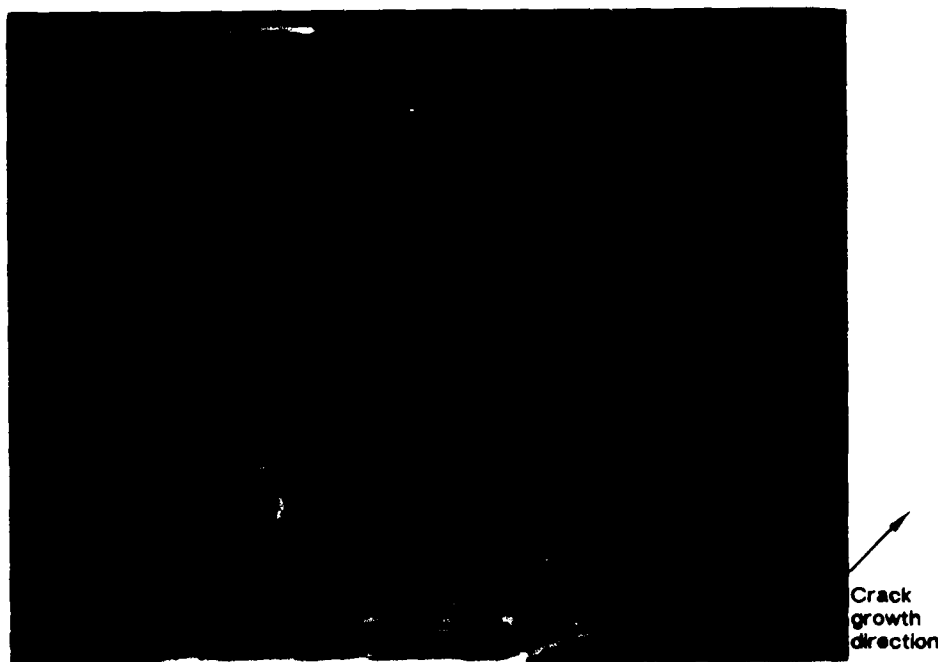


Figure 4-26. Interlaminar Mixed Mode (Tension and Shear) Fracture Morphology

5-B70227-28

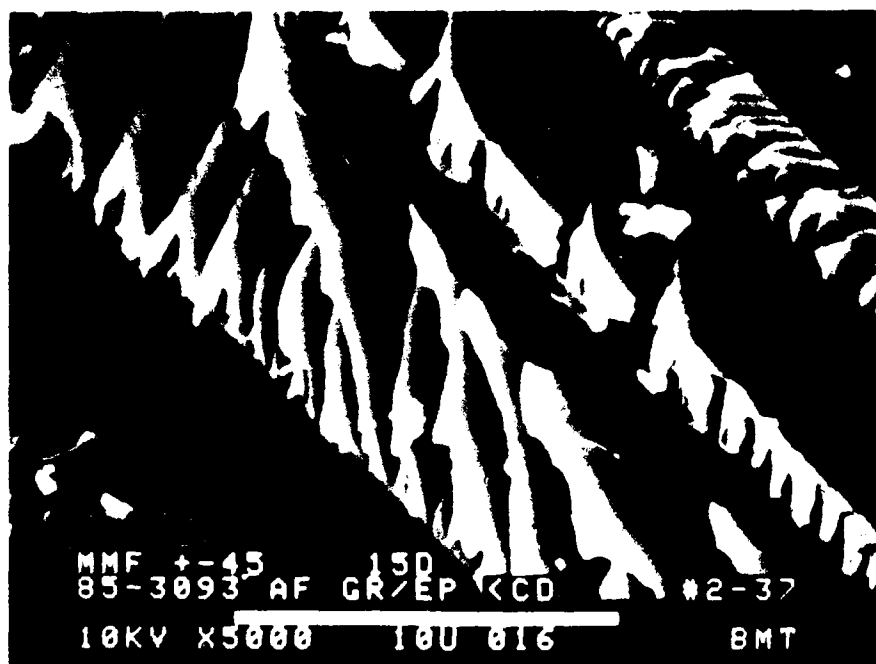


Figure 4-27. Interlaminar Mixed Mode Flexural (MMF) (Tension and Shear) Specimen Fracture Morphology

5-B70227-29

4.2.2 Translaminar

A significant portion of composite post-failure analyses involve translaminar fractures, usually in combination with delaminations located on either side of the through-thickness fracture. Due to the laminated nature of composites, combined with the excellent tensile strength of the fiber reinforcements, translaminar compression fractures tend to occur more often than the translaminar tension fractures. Tension fractures exhibit a lesser amount of delamination and tend to be relatively less damaging to the fracture surfaces and surrounding structure. Compression dominated fractures commonly fail as a result of localized buckling instability with extensive delaminations and post-failure damage to the fracture surfaces. Often the compression fracture surfaces are pushed into each other, wedging open the delaminations even further.

Fractographic analyses of translaminar fractures are generally complicated since the dominating feature is broken fibers. This generally requires the use of the SEM microscope, which is tedious and time consuming for the accurate determination of the fracture modes and crack growth directions. The optical microscope does not have the depth of focus to evaluate these extremely rough surfaces. Crack mapping can be performed by first creating a photographic montage of the fracture region at low magnifications, followed by drawing arrows delineating crack growth directions on the montage during higher magnification inspections of the fiber ends.

The following paragraphs provide insight into the use of the SEM in identifying the salient features and relating them to determination of the failure sequence. Where applicable, macroscopic methods are presented which can be used to select smaller localized areas for investigations by the SEM.

4.2.2.1 Translaminar Tension Fractures

Macroscopically, translaminar tension fractures exhibit an extremely rough topography, with large amounts of fibers protruding out of the major fracture plane, as presented in Figure 4-28. The general appearance depends largely upon the strength of the fiber matrix bond. Comparatively, strongly bonded laminates tend to be more planar and the fibers tend to fail in groups or bundles, while the lower bond strength materials are more

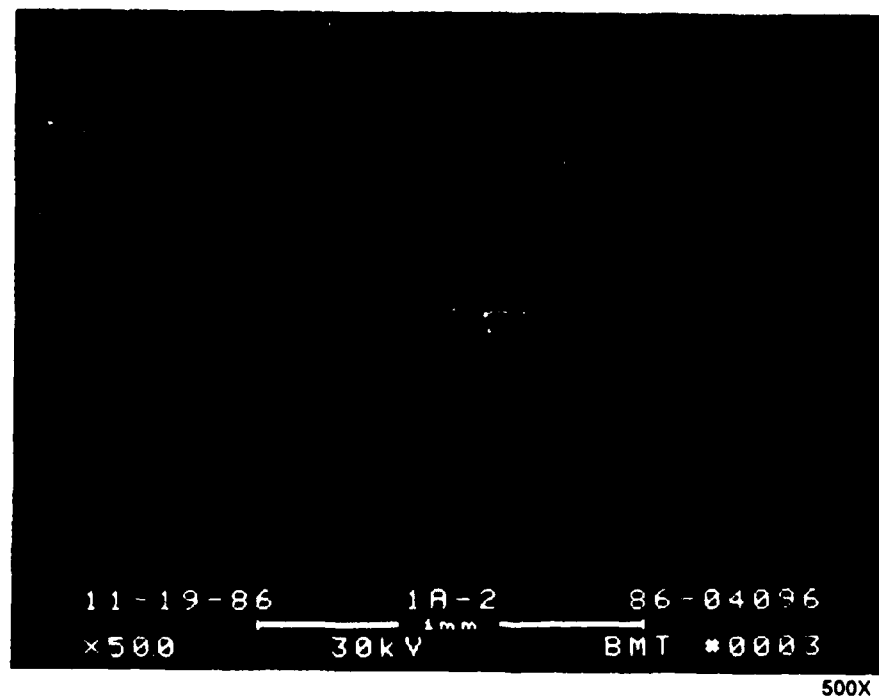
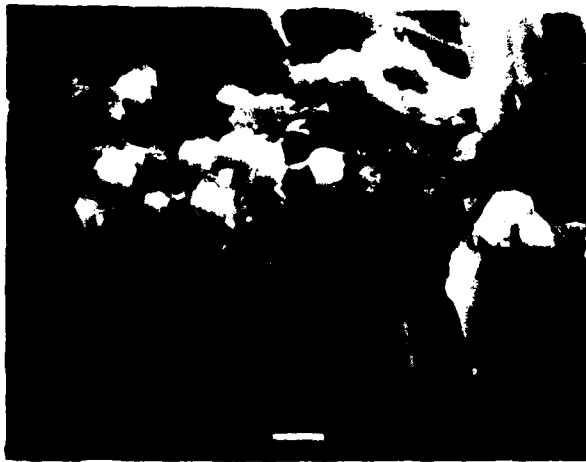


Figure 4-28. Macroscopic View of a Translaminar Tension Fracture From a Unidirectional Laminate

5-B70227-30

complex and fibrous. Macroscopic inspection of plies that are oriented parallel to the principal tensile direction often exhibit radial lines, or ridges, that radiate from an origin source and can be used to more rapidly determine the overall direction of crack propagation (Figure 4-28). Macroscopic inspection of fracture surfaces of plies that are oriented at an angle to the loading direction fail by a combination of interlaminar and translaminar shear which are extremely complicated and do not usually reveal any gross overall feature that can be used to determine fracture direction. This should be kept in mind when examining translaminar fractures of laminates that have multiple ply orientations.

Fiber end fracture, fiber pullout, and matrix fracture are the characteristic fractographic features of translaminar tension failures. Usually, little or no delamination is evident at the fracture surface, although secondary shear cracks running parallel to the fiber axis can often be found intersecting the main fracture surface. Brittle tensile failure of individual fibers is the primary operative failure mechanism, with shear fracture of the surrounding matrix considered as secondary. As stated, fibers fracture in groups (bundles) in high strength laminates, where the fibers in each bundle have a relatively flat, common fracture plane (Figure 4-29). Figure 4-30 presents the typical radial morphology found on



Note: Fracture is primarily fiber dominated with some adjacent matrix fracture.

Figure 4-29. Translaminar Fracture Morphology
5-B70227-70

Surface flaw at origin



Figure 4-30 Typical Tensile Fiber Fracture Characteristics

5-B70227-31

the broken fiber ends. This radial pattern is analogous to the chevron features of tension fractures in metals with bar or rod forms. The faint lines radiate from the point of fiber fracture initiation and thus indicate the direction of crack propagation for each individual fiber. Consistent with brittle failures, the fiber origins are primarily located at flaws or notches in the rough surfaces, although some initiate at internal flaws such as voids.

Tension failure does not usually progress by a well defined crack front. Due to flaw sensitivity, the fracture process involves a series of zones in which all the fiber breaks within each zone originate at a single fiber. Thus, the crack front actually consists of numerous isolated fracture zones (at different planes) that coalesce and propagate in the overall growth direction. This phenomena produces the distinct fracture zones commonly referred to as fiber bundles. Fiber ends tend to fracture in a variety of directions, although they are often noticeable biased in a single overall direction. Through extensive SEM mapping of the fiber ends (Figure 4-31) the macroscopic growth direction can be determined. Extreme caution must be exercised in the evaluation of isolated fibers that protrude from the main surface. To increase accuracy, many areas of crack growth

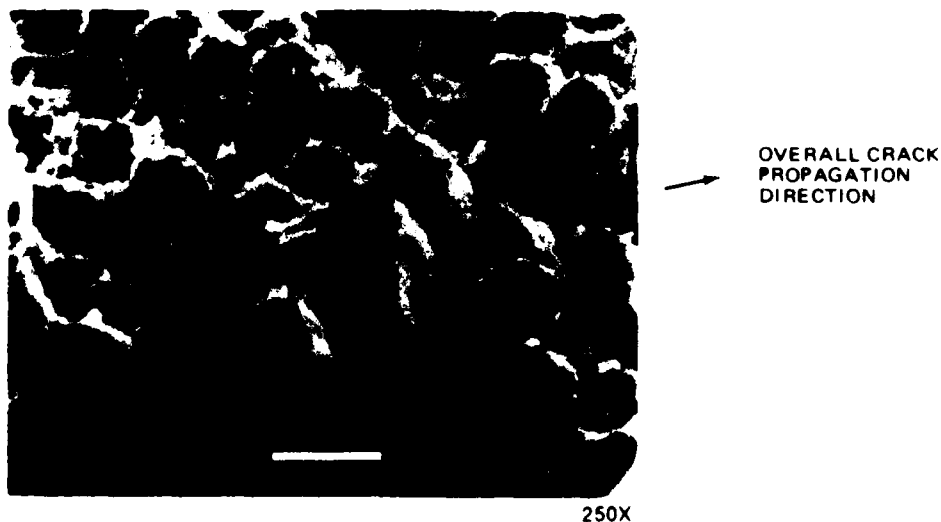


Figure 4-31. SEM Photomicrograph Showing Direction of Crack Propagation

5-B70227-71

should be evaluated during the crack mapping process; particularly bundles which fracture on a plane relatively close to the overall fracture plane.

4.2.2.2 Translaminar Compression Fractures

Macroscopically, fractures produced under uniaxial compression exhibit gross buckling, extensive delamination, and over-running of the delamination planes (Figure 4-32). An end-on view of the broken fiber ends reveals a distinct, flat fracture surface with extensive post fracture damage. This condition of flat fracture is particularly evident for plies that are oriented parallel to the axial compression loading, as shown in Figure 4-33. Often obliteration of the fracture surface details occurs due to relative post-failure motion between the fractured surfaces in contact (Figure 4-34). The surface is much flatter than the translaminar tension fractures and is virtually devoid of pulled-out fibers. Fiber buckling, fiber-end fracture, resin shear fracture, and post-fracture damage are the primary characteristic fractographic features of translaminar compression fractures.

Compression microbuckling is the primary operative failure mechanism for laminates which do not have extensive lateral through-thickness stability. This mechanism involves localized microscopic buckling of the individual fibers at a point in which a maximum lateral instability exists. Under compressive microbuckling, kinking of the fiber causes fracture at least two locations, (Figure 4-35), with each fracture separated by 5 to 10 fiber diameters. Short sections of fibers with this length can often be seen on the fracture surface. Figure 4-36 illustrates the typical flexural fracture morphology found on the fiber ends. The portion of the fiber end which exhibits a radial morphology is due to tensile separation, while the smooth, or ratcheted topography represents the compressive portion of fiber fracture. The distinct line separating these portions on the fiber end is the neutral axis line. For each individual fiber, the direction of flexure and failure occurs normal to the neutral axis line. For a given fiber, the compression and tension portions are reversed when comparing the two breaks. Therefore, a singular crack direction cannot be determined, although the individual fiber fracture propagates perpendicularly to the neutral axes lines.

The neutral axis lines are commonly found parallel to one another in a given region, indicating that microbuckling occurs on a local scale in a concerted manner and in a



Figure 4-32. Compression Buckling Failure Damage of Stringer Stiffened Laminate



Figure 4-33 End-View of Translaminar Compression Fracture

5-B70227-33

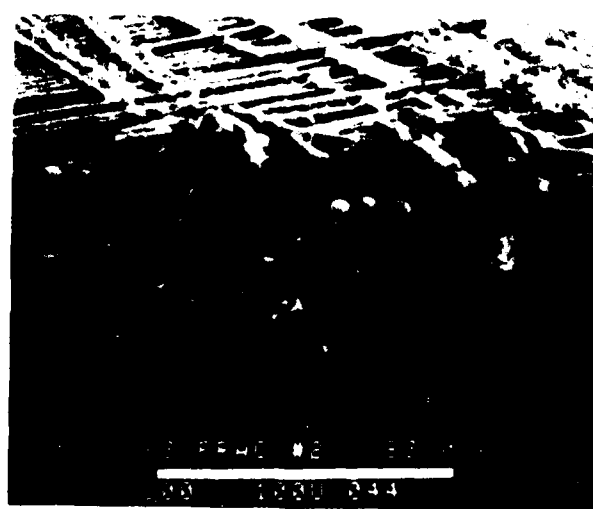


Figure 4-34. SEM Micrograph of Compression-Generated Fracture Surface Showing Severe Fracture Surface Damage

5-B70227-72

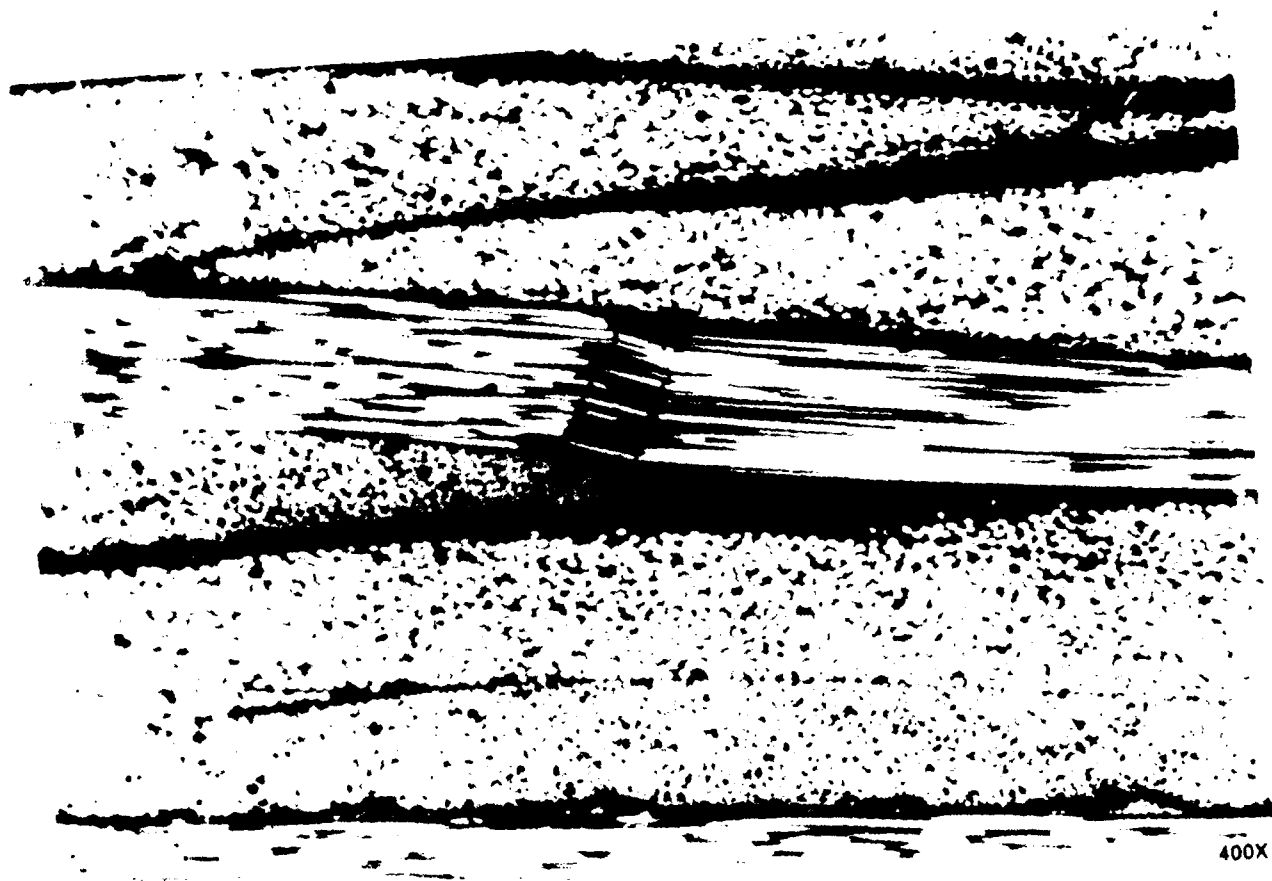


Figure 4-35. Cross Section of Compressively Loaded Laminate With Microbuckling or Kinking of the Fiber Bundles Oriented Parallel to the Axial Compressive Load

5-B70227-34



Figure 4-36. Typical Flexural Fracture Morphology Found on the Fiber Ends From a Compression Failure

5-B70227-35

unified direction, as presented in Figure 4-37. Preliminary controlled crack growth studies have shown that the neutral axis lines are often biased at an angle parallel to the direction of induced crack propagation. This indicates that flexural fiber collapse, and thus crack propagation on a microscopic scale, often occurs transverse to the gross overall crack direction; therefore, neutral axis lines cannot be used to determine the direction of crack propagation.

Laminates which have superior constraint in the through-thickness direction or excellent fiber/matrix interfacial strength are not as subject to localized delaminations or microbuckling of the plies. In this case, the fibers fracture on a microscale due to shear, with individual fiber ends exhibiting a slant type fracture, as shown in Figure 4-38.

4.3 INTERLAMINAR FRACTURE MAPPING

Crack mapping has profound significance upon the success of determining the origin locations and sequence of failure. Using microscopic techniques presented in the following paragraphs, the localized direction of crack propagation can be determined. The recommended technique of crack mapping uses the lowest magnification capable of performing the job. This recommendation is made because one of the fundamental problems in detailed microscopy of large fractures is that there is an extremely limited prospective on how the area being examined relates to the part as a whole. The situation is similar to the old adage, "one can't see the forest for the trees." With a limited perspective, it is often possible to improperly characterize the direction, mode, or load state at fracture. By emphasizing the use of lower magnifications for early investigations, the FALN imposes a sense of perspective on the value of later, high magnification inspections.

The use of optical microscopy for crack mapping interlaminar fracture surfaces has been proven to provide the most information in a given time frame and therefore the most accurate and unbiased determination of the directions of crack propagation. Optical microscopy allows direct observation of relatively large specimens in a short period, eliminating the need for specimen preparation or specimen selection required for SEM analyses. SEM analysis is basically slow and cumbersome due to the need to constantly refocus during perusal of the fracture surface. As a result, the number of crack growth

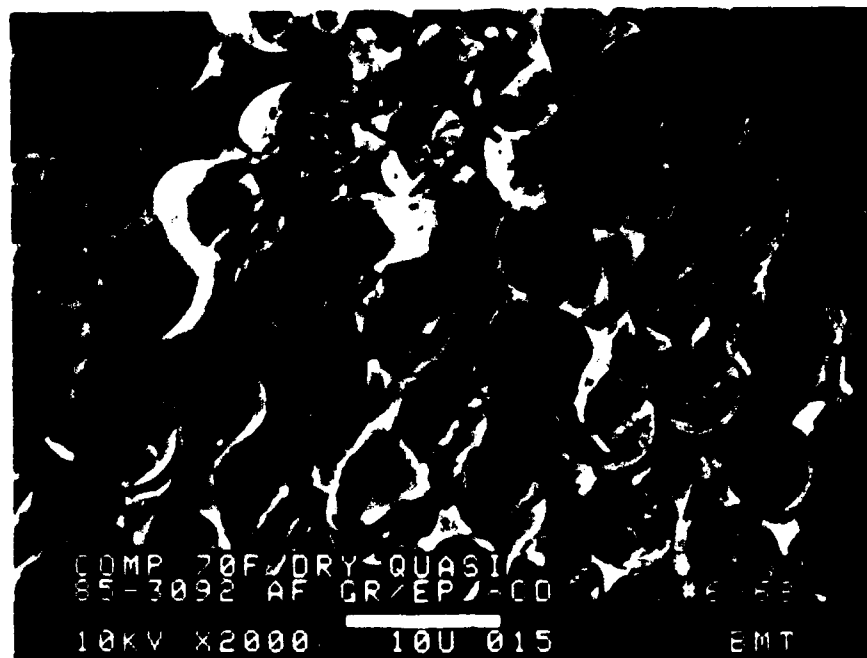
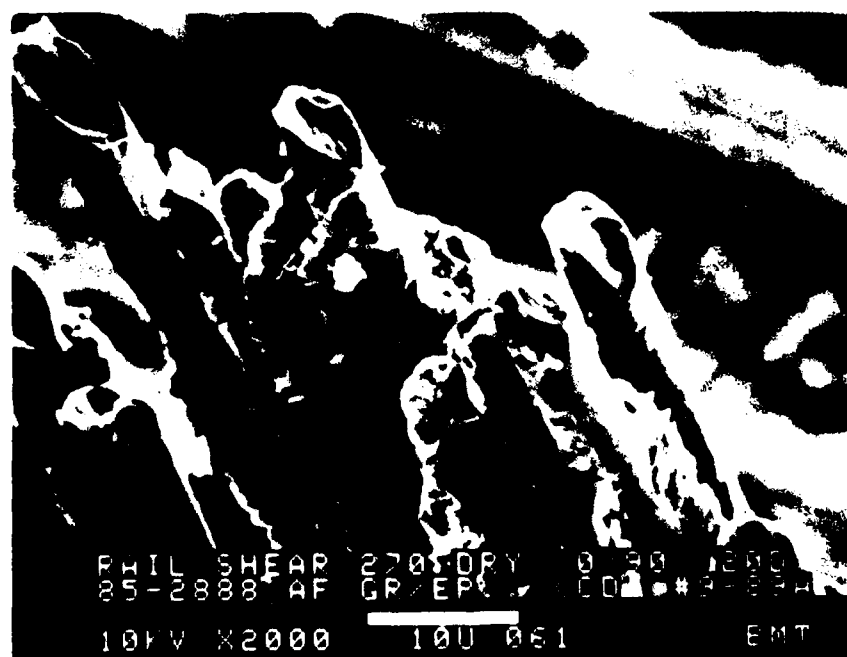


Figure 4-37. Fiber End Fracture Morphology From Compression Buckling Failure



270°F. dry

← Crack direction

Figure 4-38. Slant or Shear-Type Fracture From Compression-Induced Translaminar Failure

5-B70227-37

determinations per unit time is significantly reduced relative to optical microscopy, therefore greatly reducing the overall accuracy of the crack mapping process, particularly for ill-defined crack growth regions. Through direct scanning of the delamination surfaces with the optical microscope, features such as river marks and hackle formation can be resolved. These features, as described above, can be used to determine the localized crack propagation direction and allows the investigator to work back to the origin region. A few of the basic methods of optical crack mapping are discussed in the following paragraphs, however the photomicrographs presented were taken with the SEM, primarily due to its ability to document fracture features at higher magnifications better than the optical microscope.

The basic steps to crack mapping an interlaminar fracture surface are:

- Sectioning open the fracture surfaces to minimize artifacts.
- Reducing specimen size to fit on the optical microscope stage.
- Producing a full size copy of the fracture surface.
- Cleaning the fracture surfaces if necessary.
- Performing crack growth determinations with the optical microscope.
- Determining overall crack growth directions by averaging microscopic data.

Cutting open the delamination surfaces usually involves severing the laminate at the crack tip of the delamination as revealed by ultrasonic inspection. Successive cuts should be made until the laminate separates into two pieces. If localized fiber bridging occurs, they can be severed by cutting with a scissors. Effort should be made to prevent any delamination growth which often cannot be differentiated from cracking caused during the fracture event. Further cutting is often required to downsize the specimen to fit on the optical microscope stage (usually about 10 cm by 10 cm for an upright bench microscope).

For a worksheet by which to document the crack growth directions, a full size replica of the fracture surface can be made with a copy machine set in the lightest reproduction mode. This provides a worksheet which is superior to hand-drawn sketches (inaccurate) or photographs (expensive and time consuming).

A quick optical examination of the fracture surface can provide information regarding whether to clean the fracture surface prior to detailed crack mapping. Cleaning should not be performed if evidence of contamination is found.

Performance of the actual crack mapping process involves the interpretation of the identifiable microscopic fracture surface features as related to localized crack growth directions. Most optical microscope crack mapping requires magnifications in the range of 200X to 800X. This magnification is required to resolve the fine river marks and hackle features between the closely spaced fibers. Resin rich fracture areas such as those found between plies (or between tows for woven laminates) can be fairly easily mapped toward the lower end of this magnification range due to the larger features present. Caution should be taken when mapping these isolated resin rich regions, with direct substantiation by examination of the surrounding regions which have more fiber reinforcements. Since the fracture process actually involves a continual repetition of crack initiation at the fiber/matrix interface and subsequent crack growth in the matrix toward the next fiber, the fracture features can often be overwhelming and confusing. On a microscopic scale, the fracture details such as river marks and resin microflow are often found oriented in a variety of directions, even for delaminations with well defined crack fronts and macroscopic growth directions (Figure 4-39). As a result, accuracy during crack mapping is maximized by determining as many localized crack growth directions in a given area as economically feasible. This often requires mapping as many as 10 to 20 locations per square inch. This can be done by scanning the surface by stage translation and focussing at the same time. Once an "average" direction of the microscopic features has been obtained using the methods of determination of crack propagation described above, an arrow denoting this direction should be placed on the photocopy. For tension dominated growth regions, single-headed arrows and for shear dominated growth regions, double-headed arrows should be drawn on the map. By creating these maps for the entire fracture surface, the overall average microscopic crack growth directions, and possibly the origin location, can be determined.

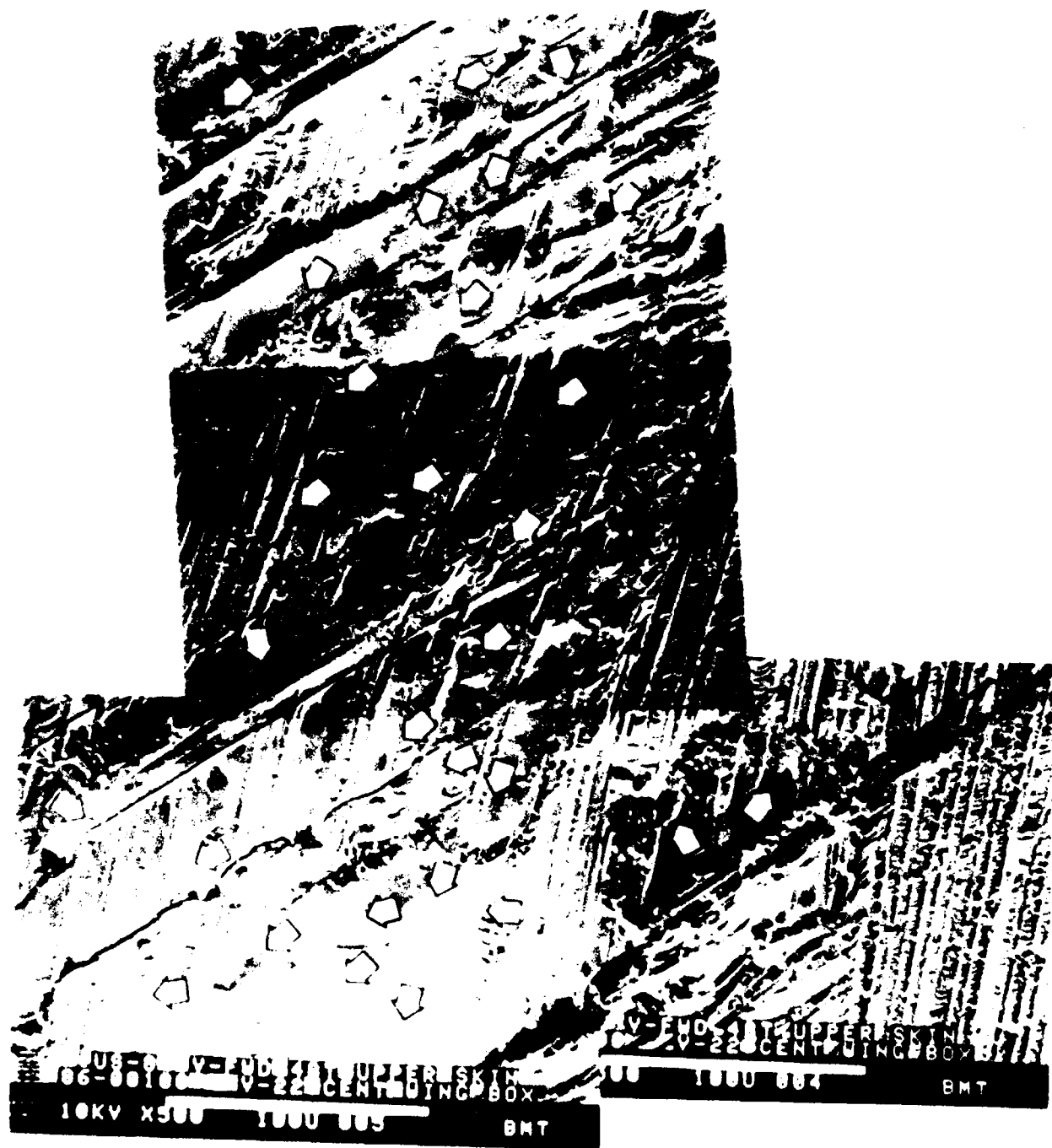


Figure 4-39. SEM Photomicrographic Montage Showing Crack Propagation Direction Mapping

5-B70227-38

4.4 CRACK ORIGIN ANALYSIS

When a crack origin has been determined, the primary emphasis is placed upon identifying the cause of crack initiation. Due to the complex nature of the fiber reinforced laminate, crack origins are often much less defined than found in metal fractures. While most metal fractures can be related to a very specific site of initiation, composites tend to exhibit origins that encompass a fairly large region. Sometimes this region can be as large as several inches in diameter, dependent upon the size of the part, the relative strain at failure, and other contributory conditions such as contamination and local part geometry. As a basic rule of thumb, fractures that have a large, relatively ill-defined origin with significant post-failure damage at the origin are exemplary of failures that occurred at a load close to the maximum strains for the entire part. This usually indicates a more desirable condition than failures exhibiting a relatively small origin which is easily defined on a microscopic scale. These origin types are often a result of localized defect conditions such that the strength at failure is low or the strains are locally magnified such as at a notch.

Analysis of the origin region should concentrate on determining if anomalous conditions existed which may have either caused or contributed to the failure event. A wide variety of defect conditions or design details should be considered when performing the analysis of the origin. Figure 4-40 presents a checklist of the possible defect conditions which can be considered. Information obtained regarding any of these defect conditions or fracture details such as local geometry, ply interfaces which delaminated, load conditions in the region (tension, shear, compression, etc) should all be evaluated for criticality. Often stress analysis is required to accurately assess the overall criticality of the specific information obtained in the origin region. Special care should be taken to not "brush off" seemingly small anomalous conditions since synergistic or accumulative situations can occur which may not be immediately obvious to the investigator.

4.5 ENVIRONMENTAL EFFECTS

Conditions of environmental extremes have been shown to significantly reduce the overall strength of composites. Therefore, the investigator should be aware of the typical fracture features that can be identified when failure occurs under conditions of

DAMAGE DEFECT CHECKLIST
<ul style="list-style-type: none"> • FASTENER HOLE DAMAGE • BACK SURFACE DELAMINATION • NOTCHED BORE • EXCESSIVE COUNTERSINK • MANUFACTURING DEFECTS <ul style="list-style-type: none"> • SAW CUT • FOREIGN OBJECT INCLUSION • CONTAMINATION • VOIDS • PART DIMENSION AND TOLERANCE • MATERIAL STRUCTURE DISCONTINUITY <ul style="list-style-type: none"> — PLY DROPOFF — LAP/GAP — PLY ORIENTATION/STACKING SEQUENCE • INSERVICE/MAINTENANCE DAMAGE <ul style="list-style-type: none"> • IMPACT • ENVIRONMENTAL EFFECTS <ul style="list-style-type: none"> — CHEMICAL ATTACK — TEMPERATURE EXTREMES • REPAIR DAMAGE • OTHER

Figure 4-40. Damage Defect Checklist

5-B70227-73

temperature and absorbed moisture. Environmental extremes at fracture tend to exhibit a more dramatic difference in the fracture features for translaminar fractures than delaminations, particularly on a macroscopic scale. Although small differences in environmental conditions cannot be readily identified in carbon/epoxy systems, large differences can be readily identified. Studies of fractures produced over a wide range of environmental conditions revealed that the general fractographic features that are used to identify the mode of fracture (tension, shear, etc) and identify the direction of crack propagation are not significantly affected.

4.5.1 Translaminar Fractures

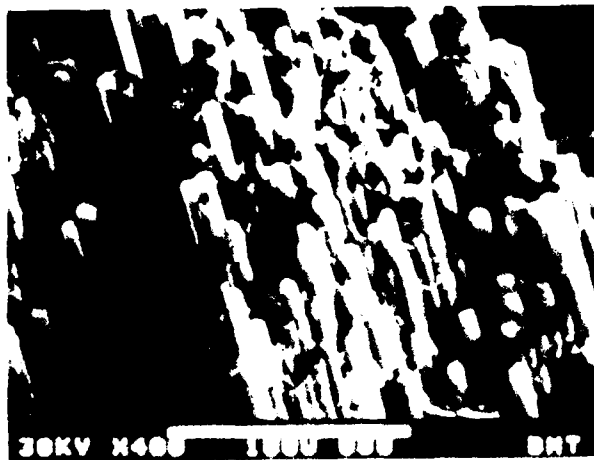
Typical translaminar fractures generated at room temperature exhibit combined features of good fiber-matrix adhesion, limited fiber pullout, and a tendency of the fibers to fail in bundles. However, translaminar fractures generated under hot/wet environmental conditions approaching the glass transition temperature exhibit greater levels of fiber pullout, combined with significantly less resin adhering to the fiber surface. Additionally, similar fractures generated under dry conditions at -65°F reveal very limited amounts of fiber pullout, with extensive amounts of residual resin on the fiber surface. In general, these observations are in agreement with published literature and illustrate the significant reduction in matrix shear strength or fiber-to-matrix interfacial strength that tends to occur under elevated-temperature and high absorbed moisture conditions. Figure 4-41 illustrates the tendency toward increased fiber/matrix separation and individual fiber pullout in wet specimens experiencing an increase in temperature.

4.5.2 Delamination Fractures

For delamination fractures, similar tendencies are evident for conditions of increasing amounts of absorbed moisture and temperature. Fractures in 177°C cure epoxy systems which occur at temperatures below approximately 90°C are very similar in appearance to the room temperature fractures. However, above this temperature range, increased fiber/matrix separation is evident and the fracture plane tends to occur within, or adjacent to, densely packed fiber regions within the lamina, resulting in a fiber-dominated fracture appearance, with small, localized regions of resin fracture (Figures 4-42 and 4-43).



-65° test condition



70° test condition



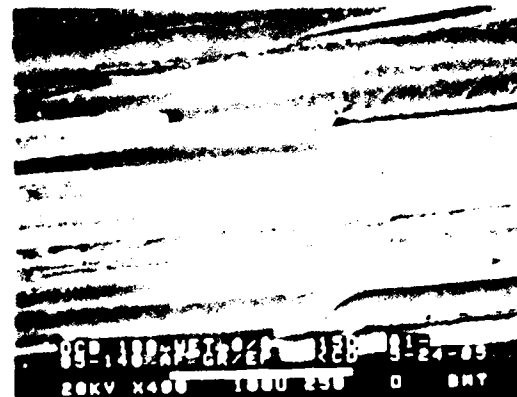
270° F wet condition

Figure 4-41. SEM Micrographs of Translamellar Fracture Conditions at Different Temperatures

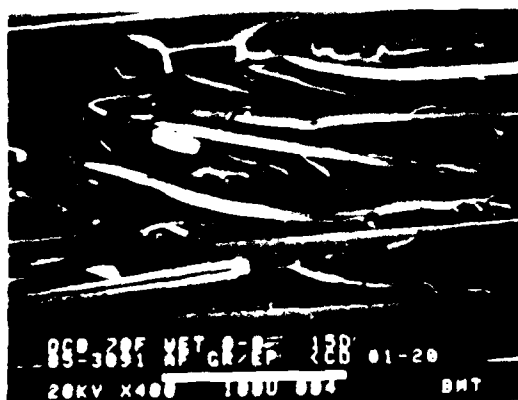
5-870227-97



-54°C (-65°F) Dry



82°C (180°F) Wet



21°C (70°F) Wet



132°C (270°F) Dry



82°C (180°F) Dry



132°C (270°F) Wet

←
Mechanically induced crack direction

Figure 4-42 Low Magnification Series of Characteristic 0°-deg Interface Mode I Fractures at Each Environmental Condition

5-B70227-98



-54°C (-65°F) Dry



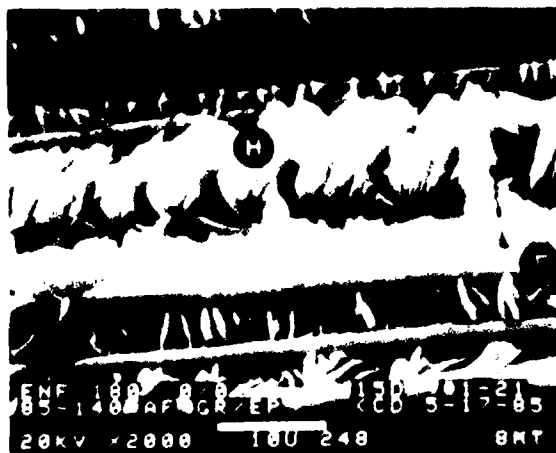
82°C (180°F) Wet



21°C (70°F) Wet



132°C (270°F) Dry



82°C (180°F) Dry



132°C (270°F) Wet

← Mechanically induced crack direction

Figure 4-43. High Magnification SEM Series of 0/0-deg Interface Mode II (Shear) Fractures Showing Features of Fiber-Matrix Separation

4.6 SUMMARY OF COMPOSITE MATERIALS FRACTOGRAPHY

The information presented in the following paragraphs provide the reader with a short summary of the current understanding of fractography of composite materials. The items included are;

- Crack propagation in brittle resin based composites.
- Crack propagation in ductile resin based composites.
- Determination of fracture modes (tension, shear, compression).
- Variables affecting fracture appearance~
 - Mixed modes
 - Temperature and absorbed moisture
 - Processing defects
 - Chemical release agents
 - Voids/porosity
 - Material forms
 - Post-failure environment
 - Water immersion after fracture
 - Fatigue loading

With an exception of the paragraph on crack growth of ductile resin based materials, the discussion is focused on the carbon fiber/epoxy resin system which currently is extensively used in the aerospace industry.

4.6.1 Brittle Resin Composite Crack Growth

The term "brittle" in regard to fractography denotes a material that fractures with very little plastic deformation during crack growth and thus absorbs a small amount of energy during failure. Obviously this is simply a relative term which can be used to compare two or more materials in terms of fracture toughness. Crosslinked thermosets and some thermoplastics (which fracture well below their T_g) are included in this category.

Microstructurally, brittle resins fracture due to locally resolved tensile stresses, resulting in a cleavage type fracture appearance with river marks and resin microflow. Mode I tension resin fractures regions appear flat, normal to the applied load. The Mode II shear

resin fracture regions exhibit the telltale 45 degree tilted resin platelets, or hackles. In these conditions of pure in-plane shear, the fracture occurs by resolved tension resulting in hackles and scallops with river marks and resin microflow present. Cracking is continually reinitiating and propagating from the fiber-matrix interface. Crack growth occurs in the direction of river mark coalescence (Mode I tension) and for Mode II shear delaminations, growth is parallel to the direction of hackle tilt. Crack mapping utilizes these features to identify macroscopic loading conditions, overall crack growth directions and origin locations.

4.6.2 Ductile Resin Composites Crack Growth

As with the term of "brittle", "ductile" is a relative term denoting material systems which exhibit high fracture toughness and ductility, or plastic deformation, at the crack tip. These materials are the thermoplastic resin based systems. Microstructurally, ductile resins fracture due to crazing, shear banding, and void coalescence. During crazing, the long chain molecules are realigned in the locally resolved tension direction and microvoids form in this region. These microvoids account for the visible stress-whitening commonly observed in many fractured or highly stressed plastics. During crack growth, extensive local deformation occurs, somewhat similar to that seen in ductile aluminum alloys during static tension fracture, in which no cleavage features are generated. To date, no conclusive methods or telltale fracture features have been identified which could be used to determine the crack growth directions. However, some resins do exhibit tilted platelets (similar to hackles) under Mode II shear conditions, such that the investigator can differentiate between Mode I tension and Mode II shear fractures.

4.6.3 Fracture Mode Determination (Tension, Shear, and Compression)

For interlaminar fractures, the mode can be determined as follows:

- Mode I tension dominated fractures exhibit flat resin fracture between each fiber, with river marks and resin microflow as the dominant features.
- Mode II shear dominated fractures exhibit rough resin fracture between each fiber, with hackles and scallops as the dominant features.

For translaminar fractures, the mode can be determined as follows:

- Tension dominated fractures exhibit a rough morphology, with fibers protruding at various heights from the surface. Close inspection of the individual fiber ends reveal radial lines indicative of tensile failure.
- Compression dominated fractures exhibit a smooth morphology, with most of the fibers broken at a common plane. Extensive damage is common due to rubbing between the mating fracture surfaces. Close inspection of the individual fiber ends reveal a neutral axis line with tensile radials on one side of the line and compression fracture on the other side.

4.6.4 Mixed Mode Loading Effects

Currently, the understanding is rather incomplete in regard to how the appearance of the interlaminar fracture surface is affected when fracture occurs under loading conditions between pure Mode I tension and pure Mode II shear (mixed mode). The accepted theory is that since cracking occurs on a microscale due to locally resolved tensile stresses, as the laminate stresses move from Mode I to Mode II the resolved principal tensile stresses rotate. As a result, the flat resin fracture regions between fibers become progressively more tilted until they reach a 45 degree angle (hackles). Until a firm understanding of how this relates to the ability to determine crack growth directions, it is advisable to concentrate analyses in delamination regions which exhibit a dominance of either tension or shear loading at fracture.

4.6.5 Temperature and Absorbed Moisture Effects

For the brittle thermoset materials systems, the effects of temperature and moisture content do not significantly alter the overall fracture mechanisms or features. As a result, examination of the characteristic fracture features remains a viable means of determining the mode and direction of crack growth. Slight differences in features are usually apparent only when temperatures exceed one half of the T_g , and temperature appears to have more of a pronounced effect than absorbed moisture. These differences are usually not great enough to verify conditions at fracture unless great care is taken to

compare features with controlled fracture specimens for the identical material system. The general theory is that increased temperatures and absorbed moisture contents decrease the strength of the fiber-matrix interface and increase the ductility of the resin. As a result, the interlaminar fractures tend to occur at locations with higher fiber volume fractions, as opposed to the resin rich region between plies. For the translaminar tension fractures, elevated temperatures and absorbed moisture contents result in increased fiber pullout and lower amounts of resin is seen adhering to the sides of the fibers.

4.6.6 Processing Defects Effects

Some of the processing defects which can have a direct effect on the fracture appearance include porosity, chemical and particulate contamination, fiber waviness, and resin rich/starved regions. These defects result in reduced strength of the laminate and often contribute to crack initiation and growth. Voids appear smooth, lack fracture features, and their perimeter is distinct and rounded. Usually the voids do not act as crack initiation sites, but rather reduce the overall delamination strength by simply a reduction in resin volume. Chemical release agents present a situation where a bondline does not cohesively bond, resulting in a smooth and featureless adhesive separation. These areas differ in appearance to voids since they affect a much larger area and are not bounded by a distinct perimeter.

4.6.7 Material Forms Effects

Generally, fractures in laminates produced from tape, fabric, or filament winding raw material forms all exhibit the basic resin and fiber fracture features that has been presented in this document. The methods used to determine the crack growth directions and the mode of fracture are identical for all forms.

For interlaminar fractures, crack mapping is easiest and often more reliable in the local regions which exhibit the highest resin volume fraction, that is between cross-ply of tape and at the intersection points of the fabric tows. This is particularly true for Mode I tension cracks where river marks are larger and more easily identified. With this in mind, it is understandable that filament winding is more difficult to analyze since very few, if any, of these resin rich regions exist.

For translaminar fractures, the filament wind and tape forms appear identical for both tension and compression features. Translaminar fabric forms exhibit each individual tow on a microscopic scale; however, at high magnifications the features present on the fiber ends are similar to the other two forms. Often less fraying and splitting of the laminate occurs with fabric since it is held together by cross-weaving each tow.

4.6.8 Post-Failure Environment Effects

Several sources of damage to the fracture surfaces exist following a component failure. These sources can be categorized as either chemical or mechanical.

The chemically induced damage sources include solvents, acids, alkaline, and complex compounds such as hydraulic fluid or flame retardant. The general result is usually a softening or loss of fine fracture surface details such as river marks, resin microflow, hackles, and scallops. Often a by-product or residue is present which can be determined by chemical analysis methods.

Mechanical damage sources include fatigue or sonic rubbing between the mating fracture surfaces during service or involves damage by poor handling practices. In nearly all cases the fracture surfaces are mechanically abraded and exhibit fine parallel lines on the fracture surfaces due to rubbing.

4.6.9 Fatigue Effects

The specific mechanisms for fatigue of brittle composite materials is not fully understood at this time. The major unanswered question is whether cracking occurs due to plastic deformation of the crack tip (such as seen in aluminum) or due to a simple crack arrest/crack initiation (similar to beach marks seen visually). Laboratory induced interlaminar fractures of small coupons have been produced which exhibit finely spaced lines similar to striations in metals. In Mode I tension the "striations" appear in the resin fracture regions, whereas the Mode II shear fractures reveal these sets of parallel line at the fiber-matrix interface. Larger structures which have been cyclically loaded to failure exhibit only very isolated and faint striations. These regions of fatigue are often extremely difficult to locate; since so far we have not visually or macroscopically

identified any differences between the slow growth and rapid fracture regions. Further studies are a must in this area since future, higher toughness materials will be pushed into higher service loads and strains which will be more susceptible to fatigue fracture.

5.0 CASE HISTORIES OF COMPOSITE FAILURE ANALYSES

The case histories presented in this section are intended to provide the investigator with a basic understanding of the overall post-failure analysis process, involving the three fundamental areas required to identify the sequence and cause of failure of the component. These fundamental areas are:

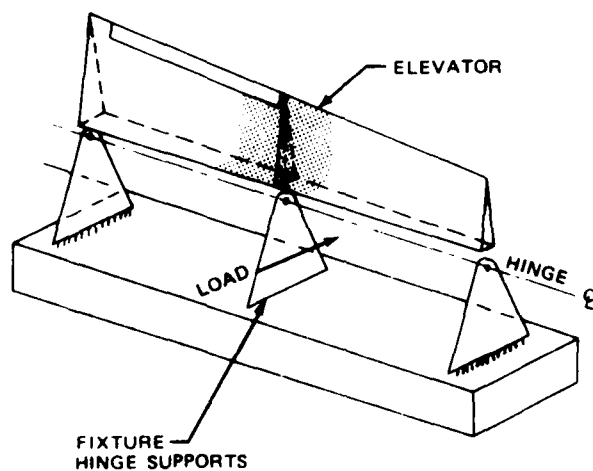
- 1) The use of the failure analysis logic networks (FALNS) which provide the guidelines delineating the logical sequence of investigative operations.
- 2) The application of the analytical tools to best determine the physical characteristics present within the failed part.
- 3) The interpretive methodology and decisions which provide the evidence and rationale to determine the causes, sequences, and contributory factors related to part failure (with the most direct, accurate, timely and cost effective methods available).

The use of these fundamental and interdependent investigative methods are applied to each of the post-failure analyses presented in this section. These case histories provide a valuable reference source of several typical fracture analyses. Each example provides a basic illustration of the sequence, analytical tools, results, and decisions involved. The collection and review of background information, nondestructive evaluations, materials characterization, fractography and stress analysis all contributed to the determination of the cause of failure.

5.1 THE 737-300 ELEVATOR TEST BOX

5.1.1 Background History

Figure 5-1 illustrates a portion of a graphite/epoxy tapered box structure which fractured during test. This graphite/epoxy box consisted of two honeycomb skin panels fastened to a spanwise spar with intermediate chordwise ribs. A review of the test history revealed that premature fracture occurred during hingeline deflection of the front spar.



NOTE Figure illustrates orientation and direction of applied loads and approximate fracture location and type.

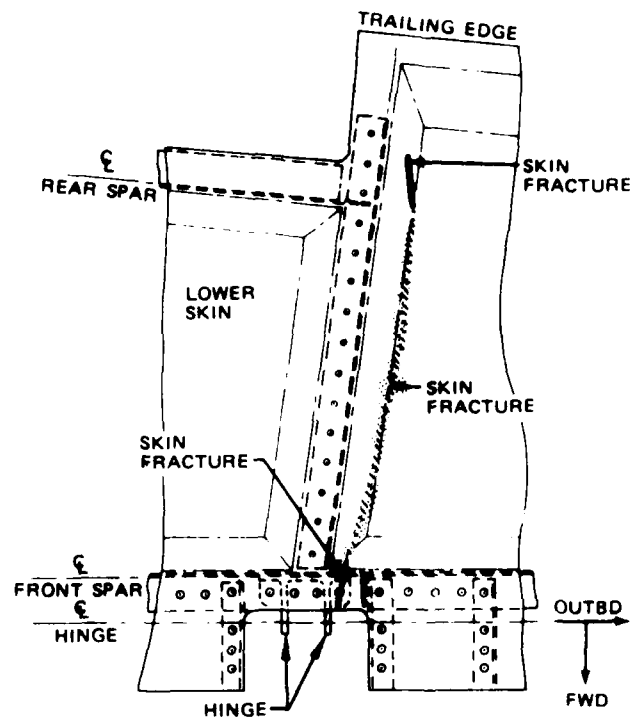


Figure 5-1. 737-300 Elevator Static Test Evaluation

5-B70227R1-74

5.1.2 Nondestructive Examination

Initial nondestructive visual inspection of the fractured box revealed several through-thickness translaminar cracks in the forward and trailing edges of the compression loaded skin panel. Upon further examination, some localized buckling of the skin panel, indicative of interlaminar fracture, was evident between each of these translaminar fractures. A nondestructive evaluation was performed using C-scan through transmission ultrasonics (TTU) to define areas of nonvisible damage so the specimen could be removed for laboratory investigations without damaging evidence. The TTU scans were performed over the entire part, and revealed a roughly four inch wide band of delamination between the areas of through-thickness skin fracture at the front and rear spar. Since a honeycomb core was involved, X-ray inspections of the core damage to determine the extent of translaminar damage was performed. Although some core crushing had occurred in the immediate vicinity of the skin fracture, the core condition was evaluated in the non-damaged area surrounding the fracture and was found to be free of defects such as poor splicing or potting.

5.1.3 Materials Characterization

Following the definition of the type and extent of fracture, tests were performed to determine if any major material discrepancies existed in either fabrication or processing. Accordingly, sections of the skin, spar and rib panels cut from nondamaged regions immediately adjacent to the fracture and were examined to verify the layup and determine the overall panel quality. In addition, thermomechanical analyses (TMA) were performed to verify the extent of cure. Since Boeing uses both 250°F (121°C) and 350°F (177°C) curing prepregs, this analysis was also performed to confirm the specified use of the 350°F prepregs. Dimensions of skin panel, spar and rib details were also measured and checked against required dimensions and tolerances. For each of these analyses, all of the individual components of the elevator were found to be in proper compliance with the drawing, materials, and process specification requirements.

5.1.4 Fractography

Since no discrepancies were identified in the above analyses, fractographic examinations were selected as the next investigative operation (see the overall FALN in section 2.0). Primary emphasis was placed on identifying the direction of crack propagation, origin, and any anomalous conditions that could be associated with fracture. To help in the examination, the delaminated interlaminar areas were removed from the skin panel and sectioned into approximately 6 inch by 6 inch squares and examined optically. The optical examinations were performed at 400 to 600X magnification, which provided a rapid and efficient means of identifying characteristic fracture features. Scanning electron microscopy (SEM) was performed on selected areas of interest requiring higher magnifications and to document specific fracture features identified during the optical analyses. The orientation of river patterns and resin microflow (Figure 5-2) observed on the fracture surface were used to generate a map of the local directions of crack propagation over the fracture surface. Although some areas of interlaminar fracture separated by shear loading (as evidenced by the presence of hackles and scallops), a majority of the fracture exhibited Mode I tension river mark features. SEM analysis of the translaminal fracture regions were not fruitful in positively identifying the direction of fracture, although the macroscopic and microscopic analyses indicated compressive buckling failure.

By reconstructing the fracture process through the interlaminar crack mapping process, it was discovered that crack initiation occurred at the periphery of a fastener hole located at the front spar. Subsequent propagation occurred in a chordwise direction across the compression loaded skin panel. See Figure 5-2 for the arrows across the skin panel illustrating the direction of the delamination process, particularly related to the fastener hole and the translaminal crack near the hole. No microscopic anomalies were identified at the origin region, and therefore no contamination analyses such as surface chemical were required.

5.1.5 Stress Analyses

Since no anomalies were identified at the origin area which might explain premature fracture, detailed stress analyses of this area were initiated. These analyses evaluated

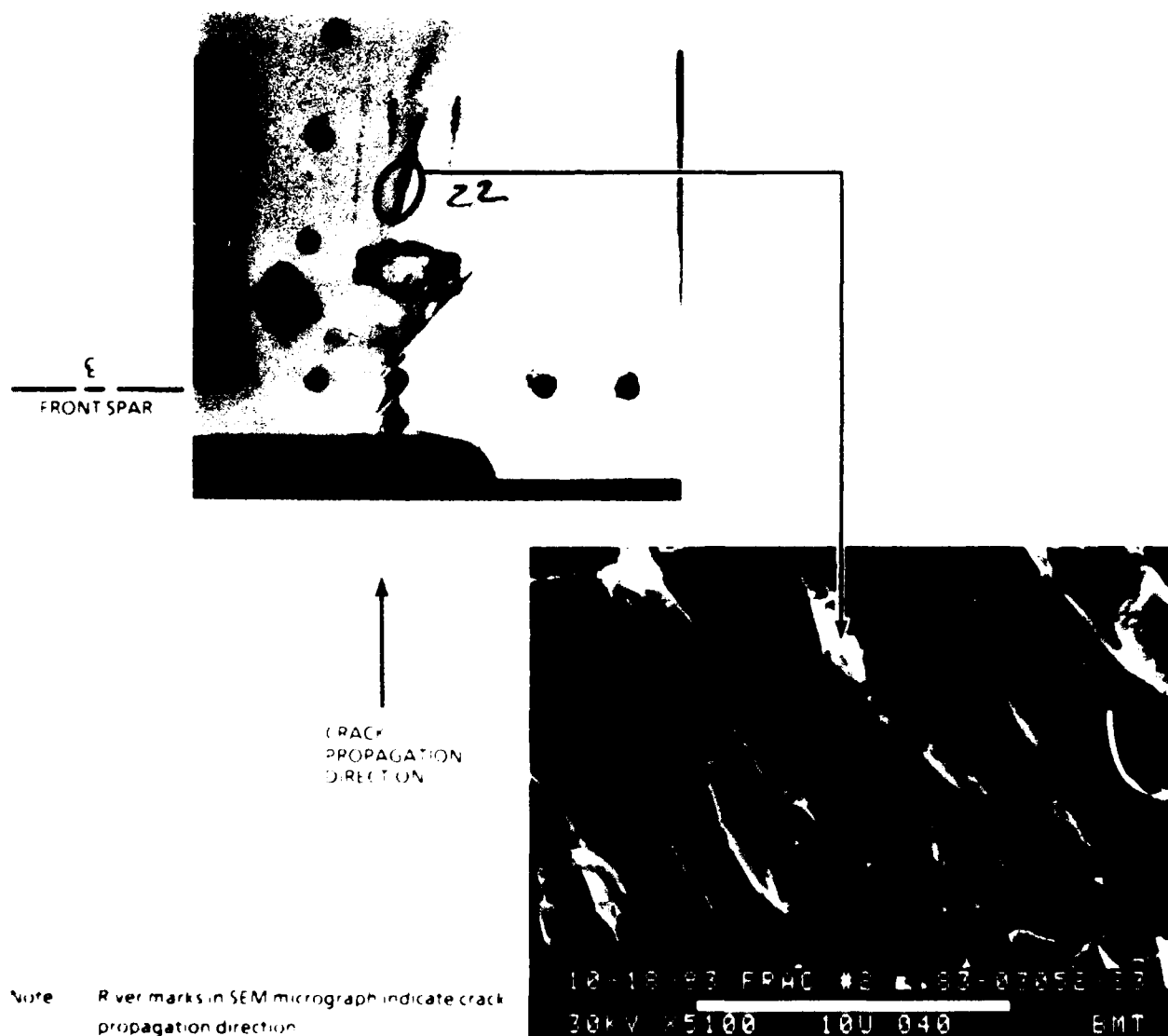


Figure 5-2. 737-300 Elevator Static Test Fracture Directions

5-B70227-75

both the basic in-plane panel strains, as well as the buckling stability of the origin area since it was in compression during fracture. These investigations revealed that premature skin buckling occurred under compression loading due to a relatively large fastener spacing in this local area. As a result of these analyses, further attention was paid to this design detail and the fastener spacing was reduced to prevent the buckling mode that precipitated premature fracture.

5.2 JVX V-22 OSPREY FULL SCALE WING TEST BOX

5.2.1 Background History

Analysis of the wing box was initiated after premature fracture had occurred during testing of the structure. Figure 5-3 illustrates the central portion of the forty five foot-long structure, immediately following fracture, with the cracking occurring in the center bay region. Discussions with the test and design engineers indicated that the loading conditions were applied to simulate upward and aft bending of the outboard ends of the box, so as to create a maximum compressive stress at the upper skin surface. The construction was found to be a stringer stiffened skin, with front and rear spars, and the ribs fabricated from graphite/epoxy tape. At this time, the manufacturing data regarding the specific materials, processes, and design (as well as the intended operational envelope) were collected.

5.2.2 Nondestructive Evaluation

Initial visual inspections of the damage region were carried out to identify the areas of visible fracture or deformation. As shown in Figure 5-4a, the upper skin surface exhibited a branching translaminar crack across the entire surface (severing all five stringers) and compression type translaminar fracture morphology for both the skin and stringers (as indicated by the flat fracture appearance). This macroscopic translaminar branching most likely indicated the gross overall fracture direction, such that the cracking progressed across the skin from the rear spar region in a chordwise direction toward the front spar. The translaminar cracking intersected the trailing edge of the skin at a radius for a runout of an overhanging tab. Extensive delamination was evident on each side of the translaminar cracking, often wedged open from mating fracture surface overrun during

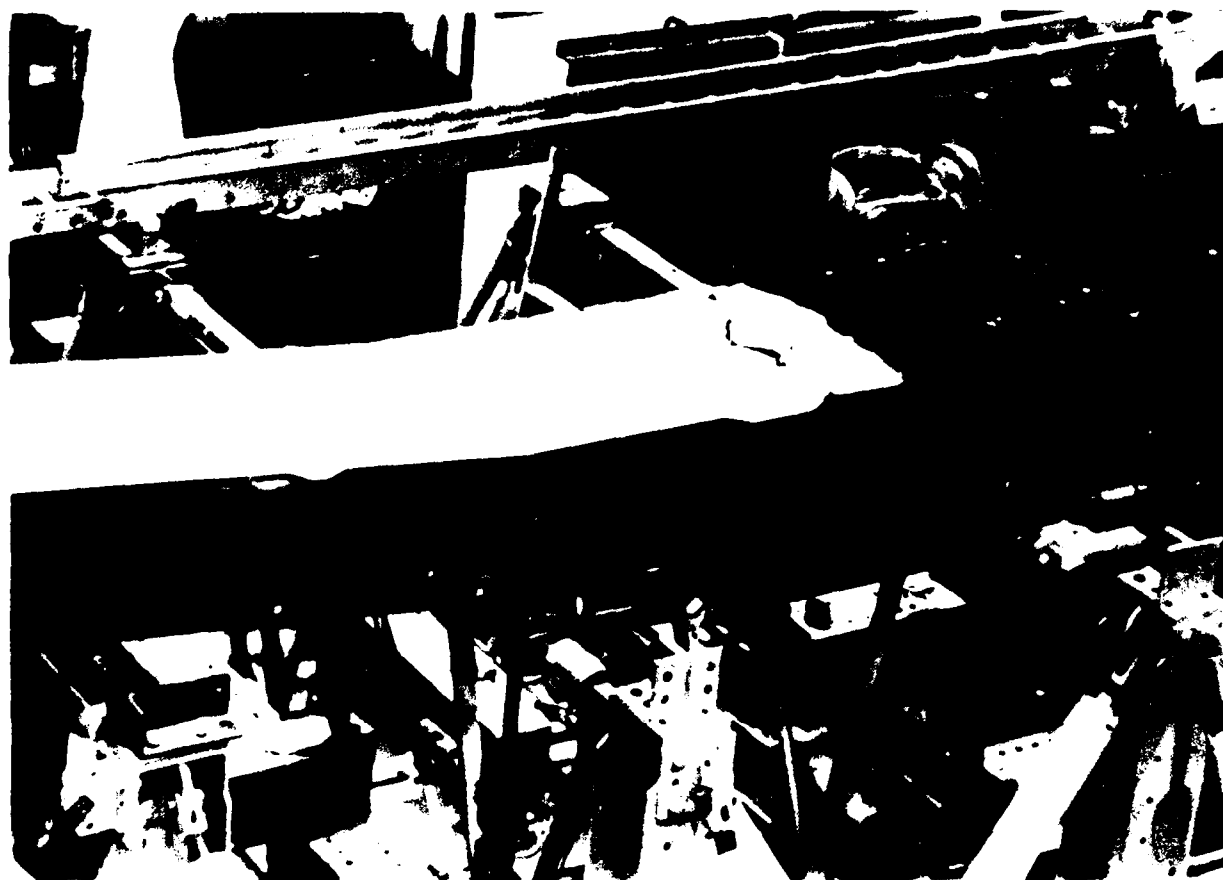


Figure 5-3. Central Portion of JVX V-22 Central Wing Test Box

5-B70227-39

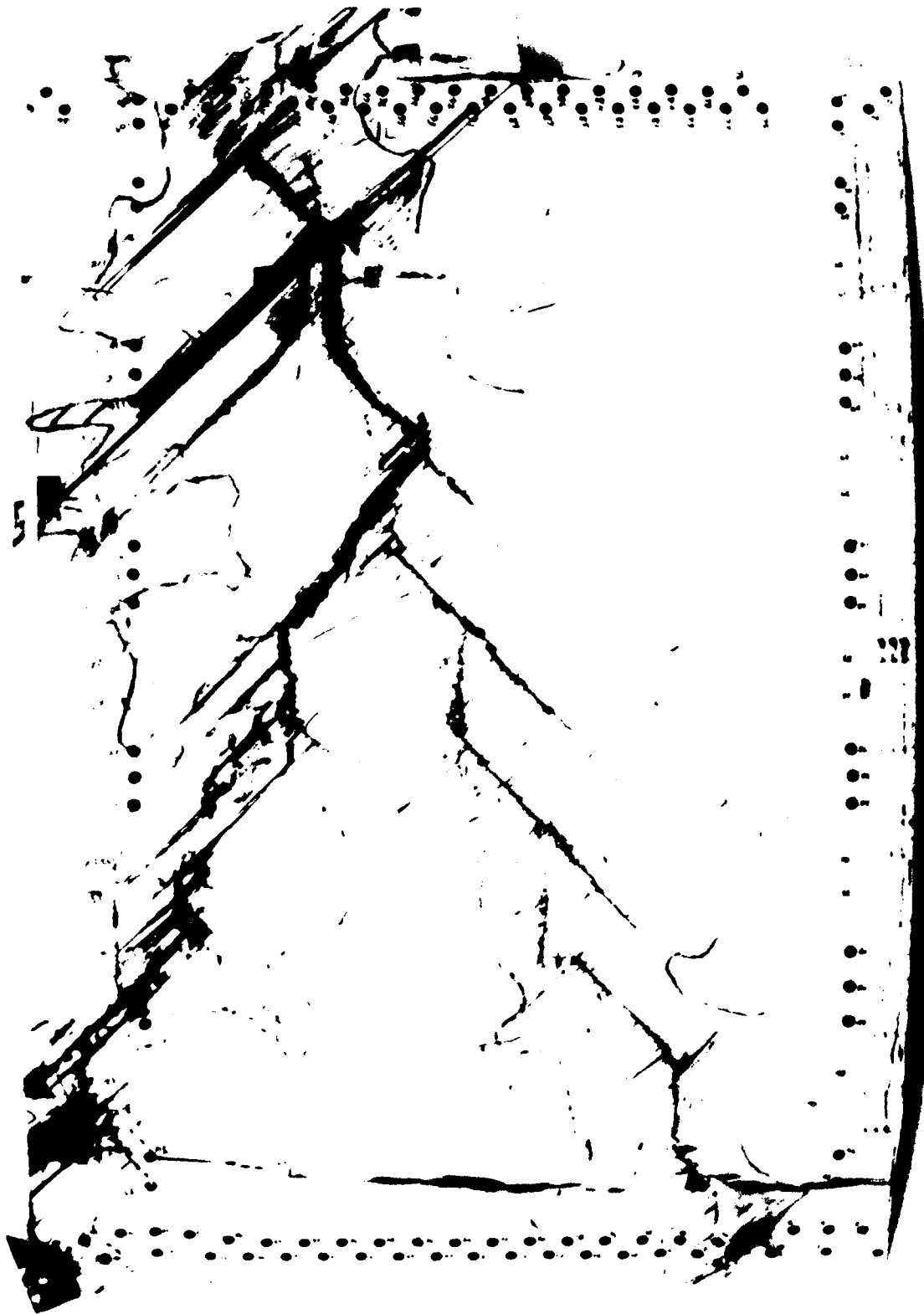


Figure 5-4a. JvX Wing Test Box Upper Skin Surface

5-B70227-40

compression loading. Figure 5-4b presents the underside of the upper skin surface, at the trailing edge tab region, illustrating the type and extent of damage.

The front and rear spars, shown in Figure 5-5, were also cracked, each exhibiting vertical translaminar fractures that appeared to intersect the upper skin fracture. The spar webs were delaminated around the translaminar cracks, with extensive buckling indicative of a compressive load at failure.

The lower skin surface, shown in Figure 5-6, was damaged in a similar manner to the upper skin, although to a lesser extent. The skin buckling also indicated a compressive loading. Since the stress prior to fracture was supposed to be tensile, the neutral axis between tension and compression must have shifted to below the lower skin surface during the failure process. As a result of these visual observations, it appeared that damage in the upper skin and spars occurred prior to cracking in the lower skin.

Nondestructive examinations were then performed to determine the extent of nonvisible damage. While still intact as a complete structure, the entire wing box was subjected to hand-held pulse echo inspection. This allowed determination of the extent of delamination surrounding the translaminar fracture as well as checking the remaining structure for any other damage that may have either contributed to, or occurred during, the failure. The outline of the delaminations surrounding the translaminar fractures as indicated by pulse echo are visible in Figures 5-3 through 5-6.

Following the visual inspections and photo documentation, the damaged central wing box portion was cut out and the major components (skins, ribs, spars, etc) were separated from one another. During component breakdown, each fastener was carefully removed and examined for proper fabrication and installation. No damage or incorrect manufacturing anomalies were identified related to fastening. Following removal of the skins, spars and ribs in the failure region, each of these components were subjected to C-scan through-transmission ultrasonic (TTU) inspections to more accurately appraise the extent of delaminations. As shown in Figure 5-7, the upper skin surface damage at the trailing edge tab radius was easily defined. Suspecting damage such as small translaminar cracking at the radius on the other side of the tab, radio-opaque penetrant X-ray inspection was performed in this region, however no damage was present.

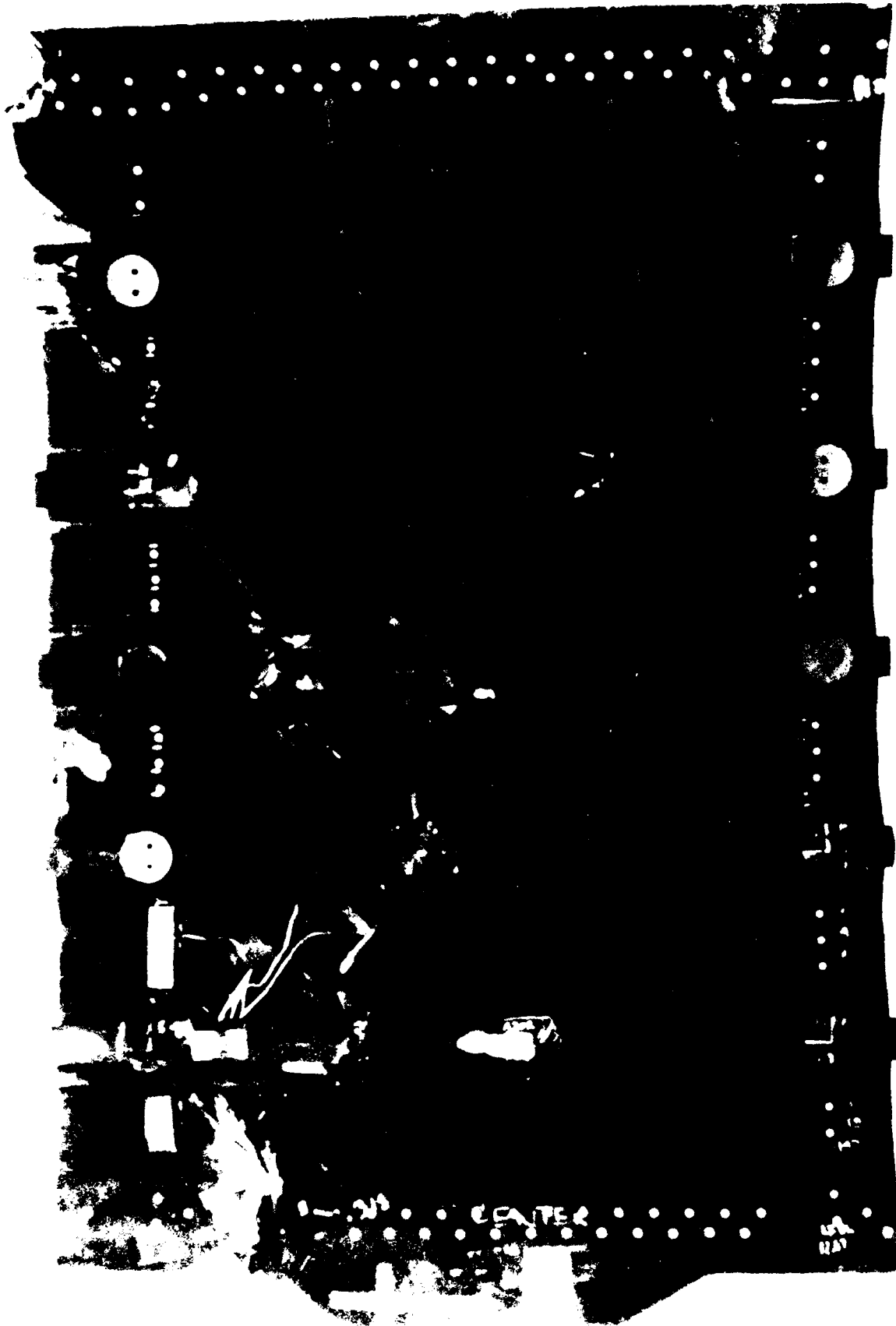
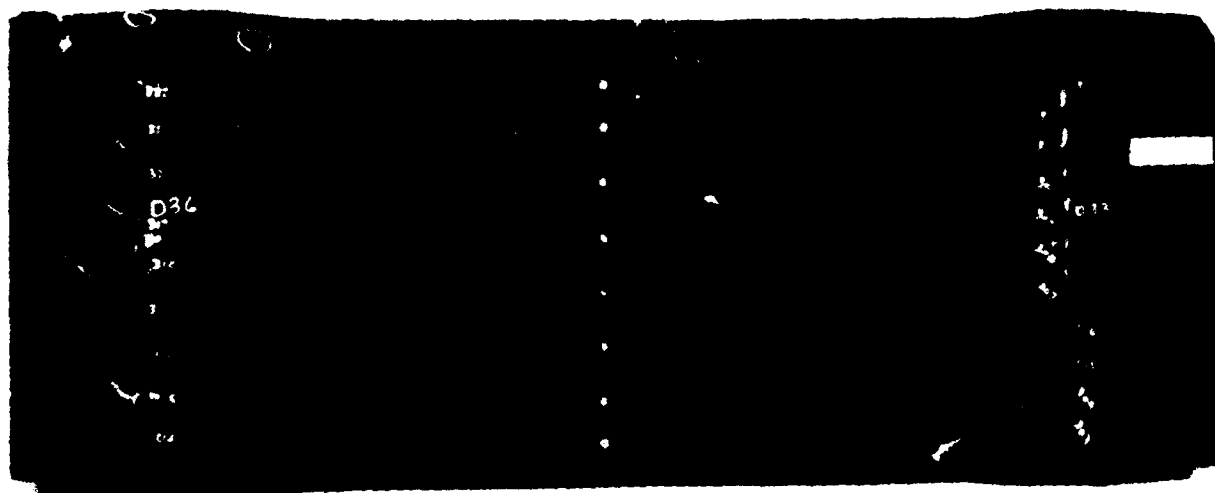
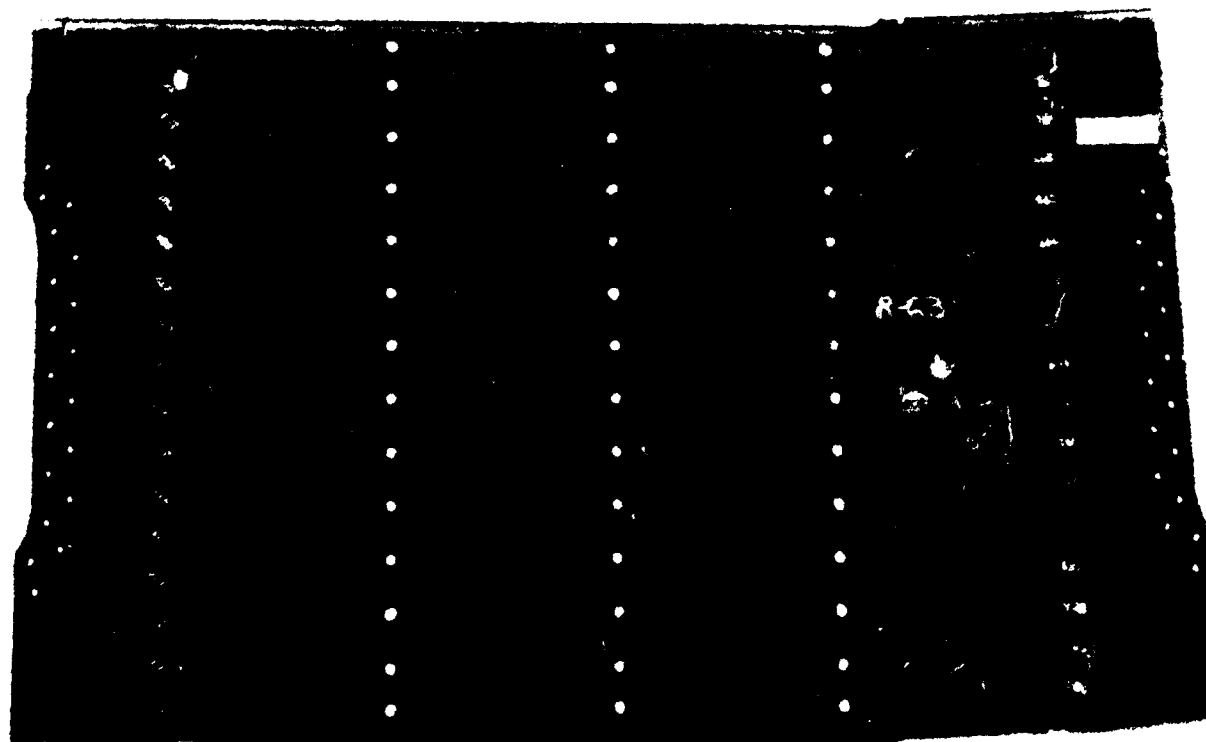


Figure 5-4b. J VX Wing Test Box Inner Side of Upper Skin

5-B70227-41



Front Spar



Rear Spar

Figure 5-5. J VX Wing Test Box Front and Rear Spars

5-B70227-42

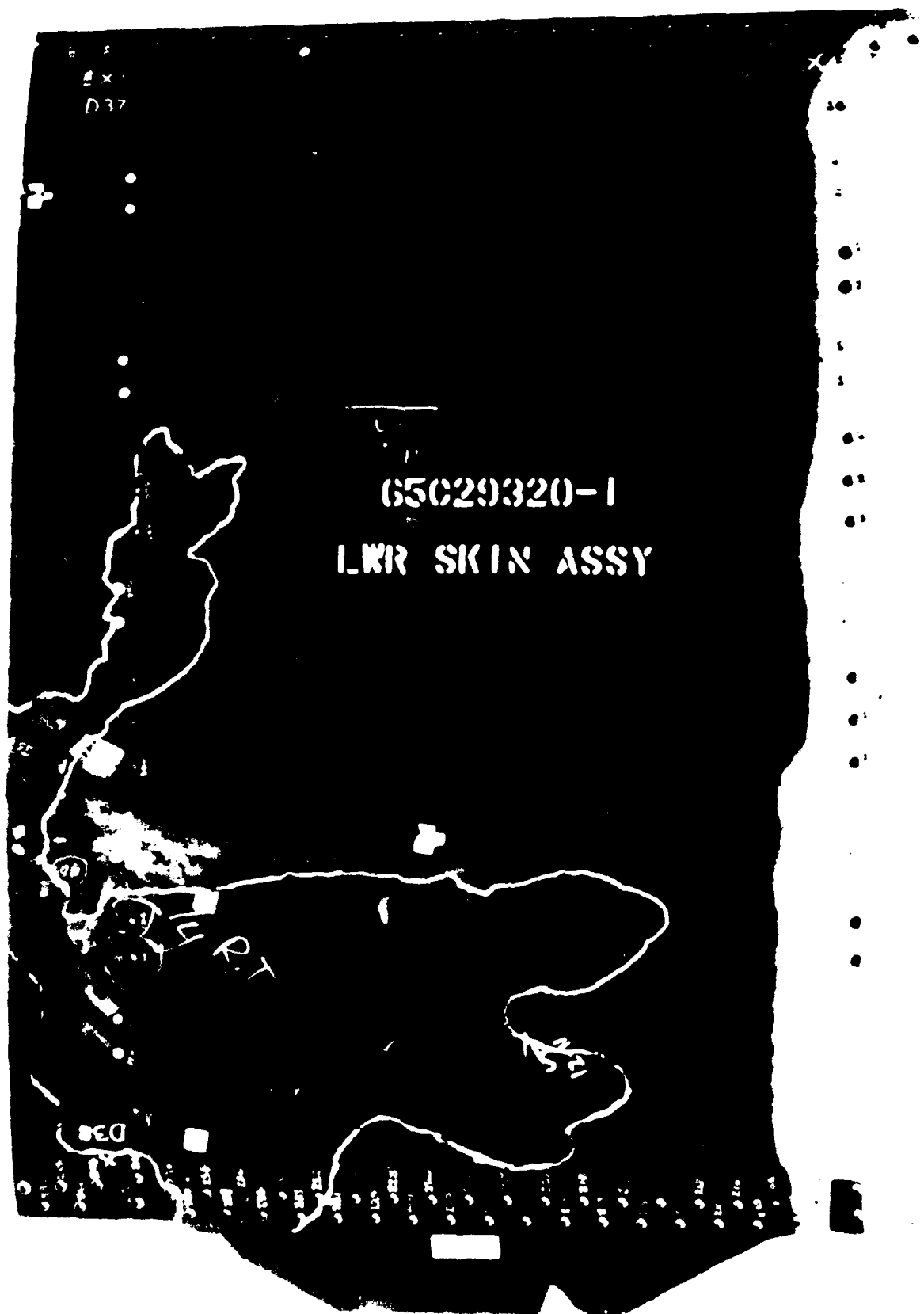


Figure 5-6 JVX Wing Test Box Lower Skin Surface

5 B70227 43



Figure 5-7 Ultrasonic C-Scan of Upper Skin Surface

5.2.3 Materials Characterization

Materials characterization involved performance of the following tests on all components, with a brief summary of the results:

- Degree of cure (T_g) using TMA flexural method;
 $T_g = 191^{\circ}\text{C}$ to 201°C - indicating a proper cure (180°C specification minimum).
- Resin content using density gradient column method;
acceptable 33.8% to 34.9% by weight (35% prepreg).
- Microstructure/porosity using optical microscopy;
no resin starvation or porosity, no fiber waviness.
- Ply count and orientation using optical microscopy;
all components in good condition except slight ply discrepancies in upper skin near trailing edge tab radius.
- Dimensional conformance to engineering drawings;
upper skin tab radius = 1.5 inch (drawing callout was 3.0 inch). This discrepancy was evaluated by analysis for stress intensity factor (K_t) effect.

5.2.4 Fractography

Using the outline of the delamination generated by NDE, the fractures were abrasively sectioned open to minimize artifacts. Detailed crack mapping of the delamination surfaces was performed by optical microscopy, with documentation of the fracture morphologies obtained by the SEM. Areas of delamination were found to be principally Mode I tension dominated, with localized Mode II shear regions. The overall crack growth directions, as well as the fracture origin regions for the upper skin surface and the rear spar are shown in Figure 5-8. These analyses revealed cracking of the upper skin initiated by compression buckling fracture mode at the trailing edge tab radius with resultant fracture propagating toward the leading edge. Similarly, the rear spar fracture originated

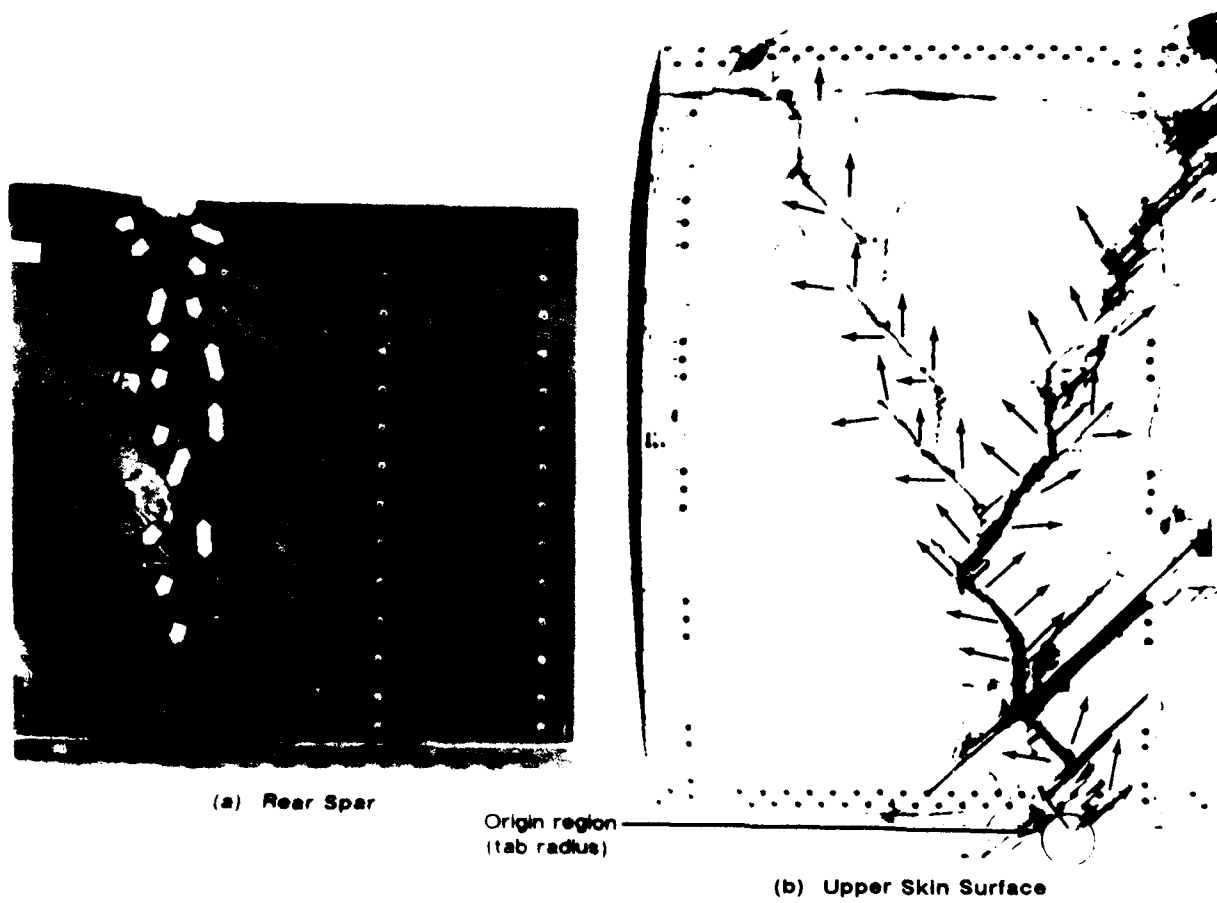


Figure 5-8. JVX Wing Test Box Crack Mapping Results

5-B70227-45

in a region adjacent to the upper skin surface. Crack mapping in this region was very inconsistent, with a nearly random variation in the microscopic river marks and hackle orientation. No anomalous conditions such as porosity, resin starvation, or chemical contamination were identified in the origin regions.

Similar fractographic analyses were performed on the lower skin and front spar, with crack mapping indicating that the fractures were a direct result of the progression of the cracking from the upper skin and the front spar.

At this point the question of the sequence of failure between the upper skin and the rear spar was asked. Experience with fracture analysis of large composite structures indicated that smaller, well defined origin regions tend to initiate at lower overall strain levels at locations such as notches or holes and therefore exhibit less damage at the origin zone. The larger, ill-defined origin zones tend to be indicative of overload, or rather, high overall strain fractures (with extensive damage); and are not usually associated with notch sensitivities or defect conditions. Using this basis for a rationale, it appeared that the upper skin surface which had the small origin region, may have initiated first, at the tab radius which served as a notch.

5.2.5 Stress Analysis

While the efforts discussed above were being performed, several levels of stress analyses were also performed. These involved the initial design review to check known test conditions against the design envelope, as well as comparing test strains from the strain gauges and coarse global analyses with the overall strain allowables. The next stage was to take inputs from the materials characterization and the fractography analyses, and evaluate the strain criticality at the structural level. Through finite-element analyses, an unanticipated strain level was identified at the upper skin tab radius, with the notch K_t effect at the radius contributing to the strain level. Subsequently, two small scale replicate panels were fabricated, tested and subjected to complete failure analysis investigations. One panel was fabricated with, and one without, the tab and radii on the skin surface. Through these verification test panels, it was shown that by elimination of the tab, and thus the radii, a premature buckling mode that precipitated fracture could be prevented.

5.3 NASA HiMAT WING

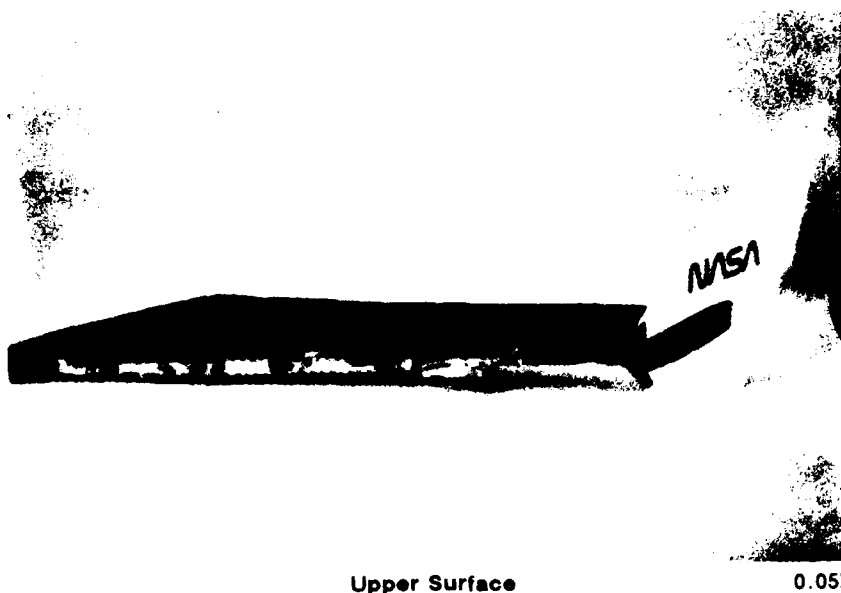
5.3.1 Background History

Figure 5-9 presents the NASA HiMAT wing section in its as-received condition. This wing was built by Rockwell International for a highly maneuverable research vehicle to study future designs for the next generation of U.S. fighters. The composite wing is a 44 percent scale model, to lower overall program cost and risk. Following numerous unmanned test flights, the outboard sweeping section of the wing was removed and subjected to simulated flight spectrum mechanical testing in the laboratory. Information supplied at this stage in the investigation regarding construction was very limited; the outboard canard was found to be fabricated from aluminum alloy and the remaining portion of the wing was fabricated from a continuous fiber reinforced laminate. Failure, denoted as a loss of structural stiffness, occurred during the mechanical testing.

5.3.2 Nondestructive Evaluation

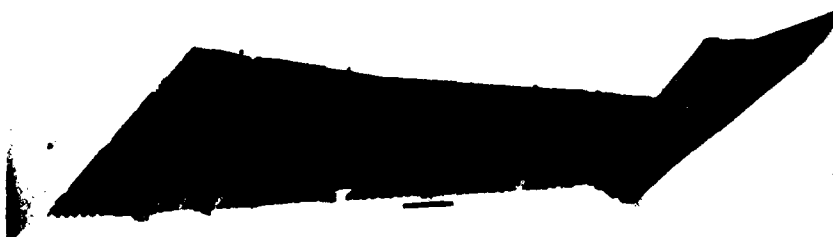
Nondestructive evaluation was performed on the entire wing to determine areas of damage or defect conditions caused from testing or manufacturing. A wide variety of NDE techniques were used, primarily to evaluate each technique and to more completely determine the construction of the wing. The following techniques were applied; visual inspection, radiography, through-transmission ultrasonics (C-scan), pulse-echo (B-scan), eddy current, and ultrasonic bond testing. Of these six, the key methods used to obtain data were visual inspection, TTU, and hand-held pulse echo.

Although no visible primary translaminar fractures were identified, visual examinations revealed several delaminations along the inboard edge (up to 13 cm in length), disbonds (up to 3 cm in length), and surface delaminations (up to 13 cm by 8 cm). Blunt gouges were found at the center of two of the delaminations along the inboard edge of upper skin, appearing to be mechanically induced after part cure. This damage may have occurred during wing removal following flight testing. These gouges are shown in Figure 5-10. On the upper skin, an area was mechanically abraded, indicative of surface repair.



Upper Surface

0.05X



Lower Surface

0.05X

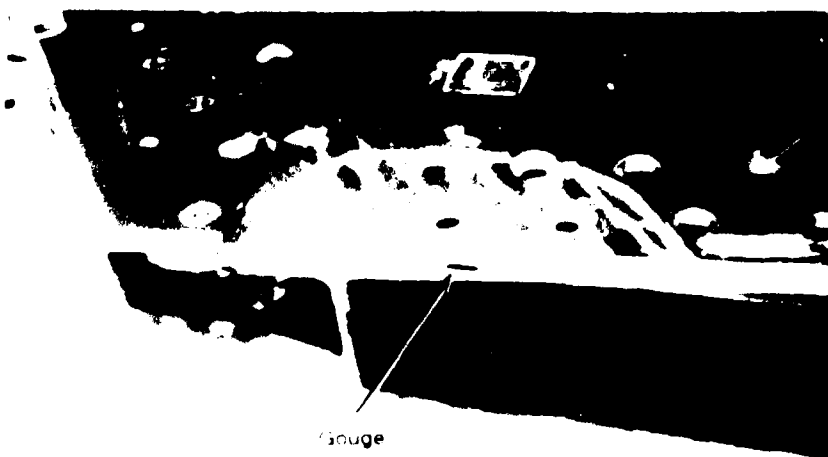
Figure 5-9. NASA HiMAT Test Wing in the As-Received Condition

5-B70227R1-46



(a) Section C

0.8X



(b) Section B

0.63X

Figure 5-10. Upper Skin Inboard Edge Damage

5-B70227-47

TTU analysis provided a thorough scan of the discontinuities along the upper and lower skins. The major delaminations and disbonds occurred along the inboard edge of the wing, with the exception of one donut-shaped delamination at the center of the wing. Figures 5-11 and 5-12 show the TTU hardcopy printout. The areas indicated by alphabetical flagnotes were delaminations or disbonds which were crack mapped during subsequent fractographic examinations. However, the areas shown with numerical flagnotes were defects indicated by X-ray such as core to skin disbonds, core crush, and water in the core cells.

The hand-held pulse-echo inspections revealed the depth of each defect. The deepest delamination occurred 0.86 cm (0.34 inches) below the skin surface. These depth measurements became very useful when the handmilling cuts were made to remove the delamination regions. This allowed precise cutting, reducing the extent of damage to the remaining portion of the wing, and allowed a more successful repair.

5.3.3 Materials Characterization

Following the nondestructive inspection, material characterization of the wing was performed to verify material composition, ply orientation, ply layup, and material processing/cure.

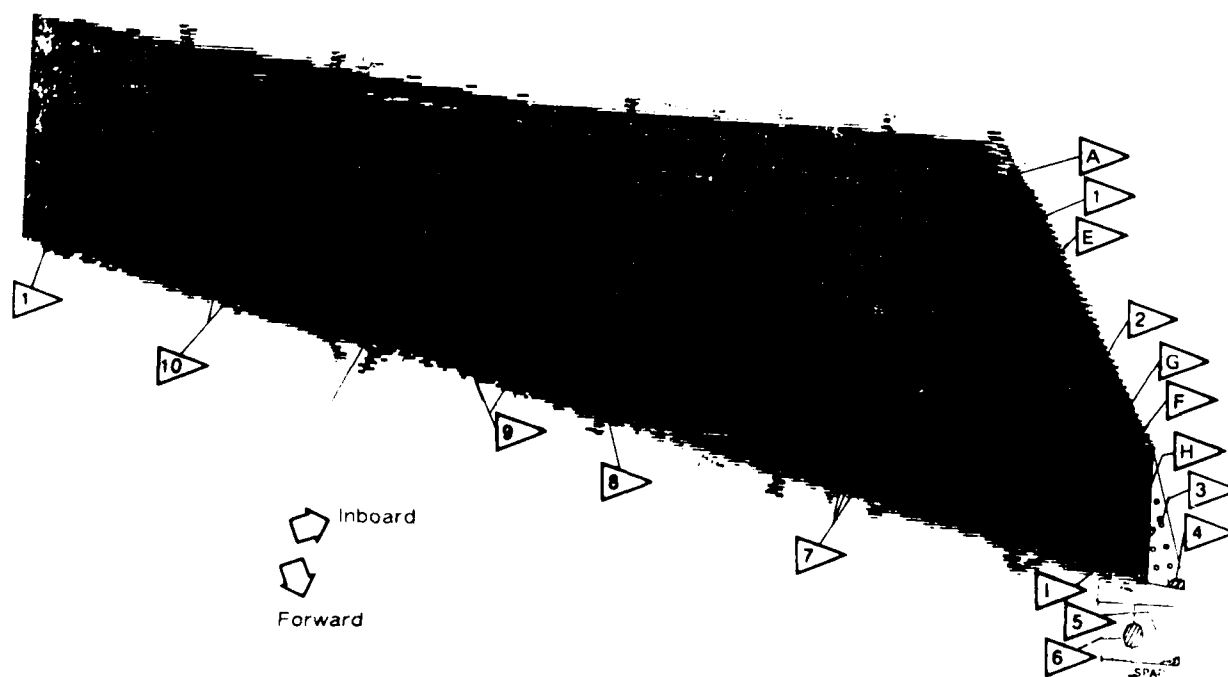


Figure 5-11. NDE Results of the Lower Surface

5-B70227-102

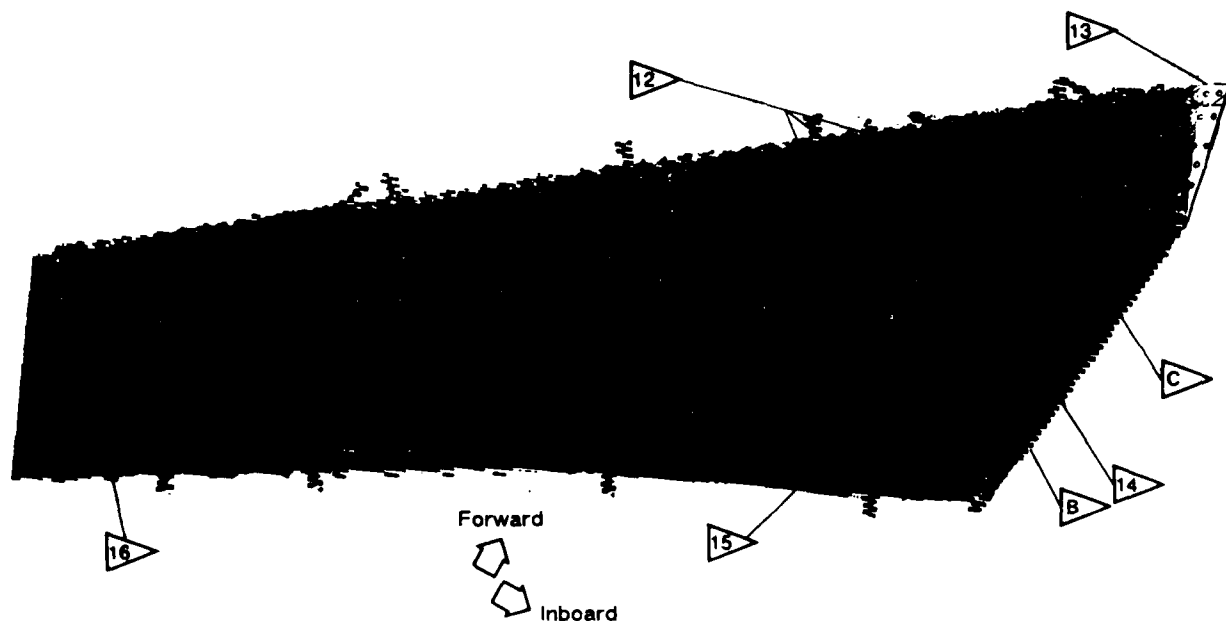
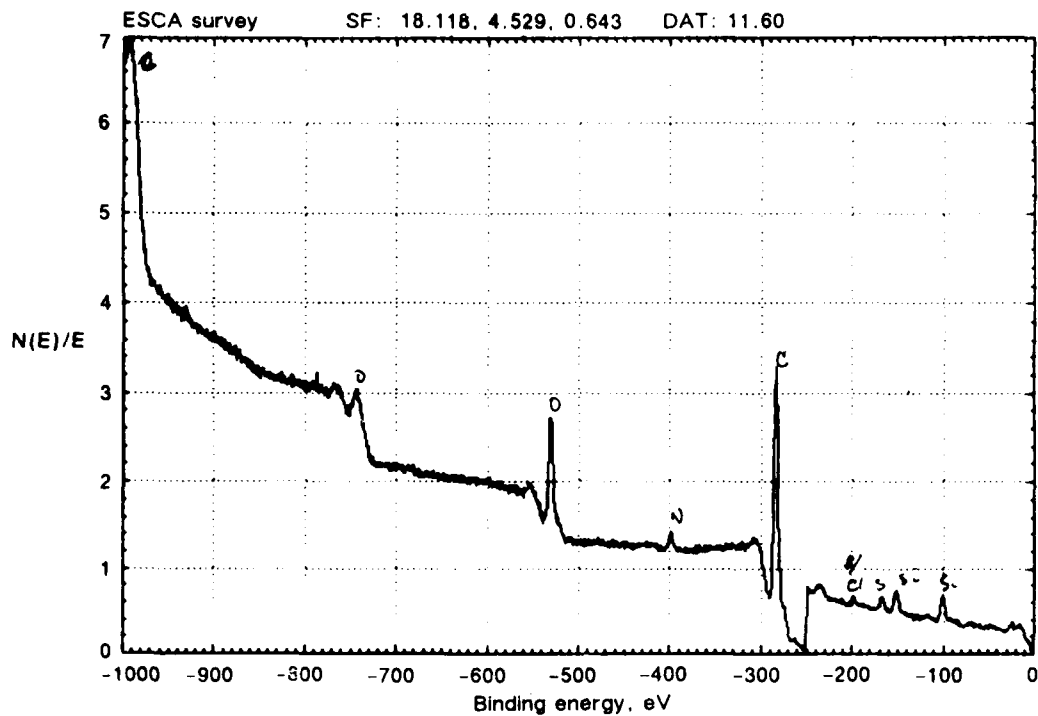


Figure 5-12. NDE Results of the Upper Surface

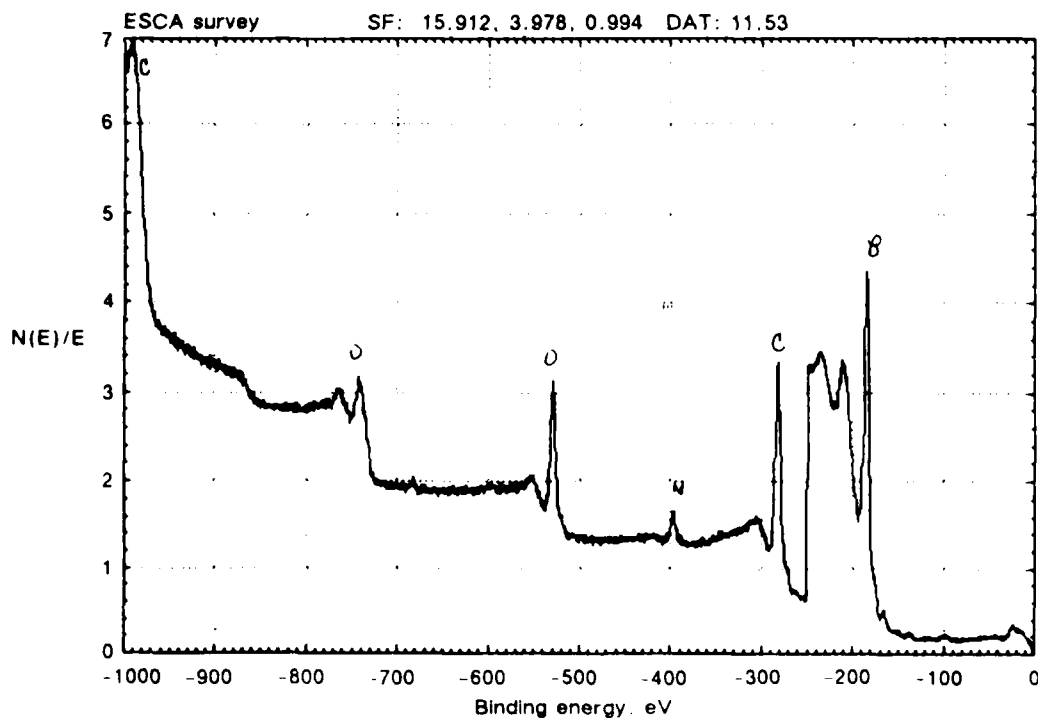
5-B70227-103

The materials used to construct the wing were found to be carbon, boron-tungsten, and fiberglass fibers in an epoxy resin. These material constituents were identified by the following techniques; scanning electron microscopy, optical microscopy, electron probe microanalysis, and electron scattering for chemical analysis (ESCA). The fibers were identified by SEM, ESCA (Figure 5-13), and optical microscopy (Figure 5-14). The novalac based epoxy resin was identified by infrared spectroscopy.

The ply orientation and number of plies were found to be consistent with engineering drawing specifications. Localized discontinuities such as resin-rich and resin-starved regions (Figure 5-15) were usually caused by misalignments of the extremely large boron fibers. A small amount of porosity was seen in the graphite/epoxy plies between the 0 and 90 degree plies. These discontinuities were not found to be associated with the delamination regions and therefore were not considered as contributory factors to the cause of part failure.



(a) Carbon Fiber Identification



(b) Boron Fiber Identification

Figure 5-13. Fiber Identification by Surface Analysis

5-B70227-104

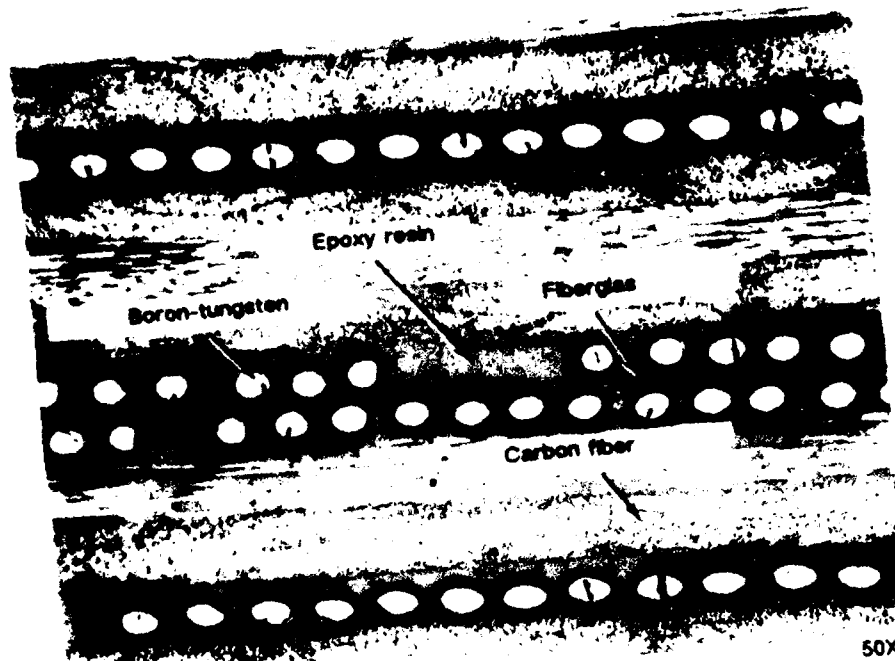


Figure 5-14. Photomicrograph of Cross-Section Damage Zone B

5-B70227-48

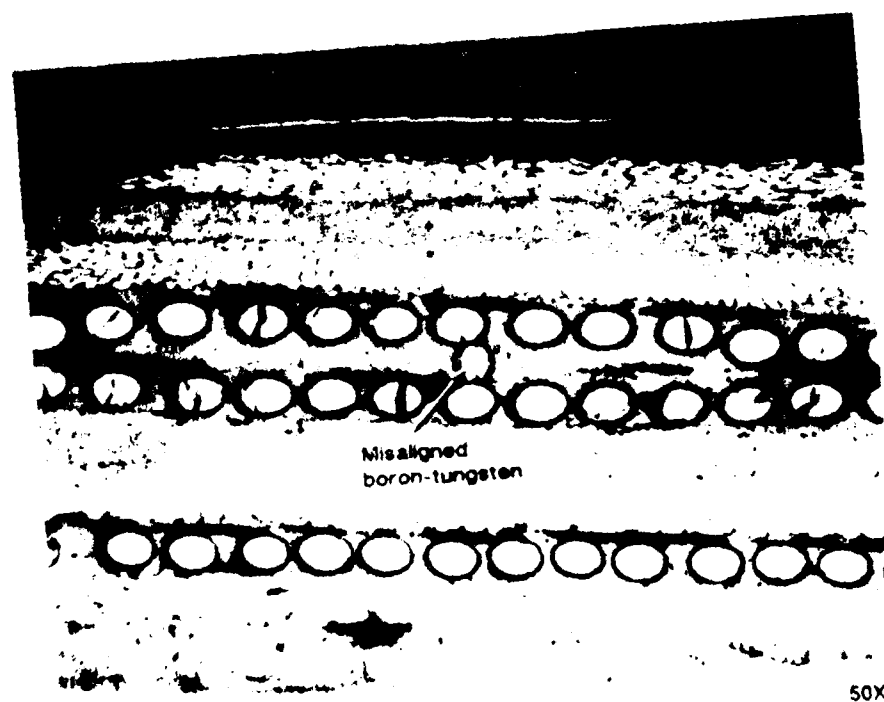


Figure 5-15. Cross Section Illustrating Boron Fiber Misalignment Resulting in Resin-Rich Adjacent Regions

5-B70227-49

Using thermomechanical analysis (TMA) in the flexure mode, the Tg was found to be 212°C, consistent with specification requirements for a 177°C cure system.

5.3.4 Fractography

Since materials characterization tests revealed that the laminate was constructed per specification and drawing requirements, efforts were directed toward the determination of the fractographic features related to each of the delaminations identified by NDE. Using optical microscopy, each of the delaminations were crack mapped to determine the mode of fracture, the origin location, and any anomalous conditions associated with the origin. The fracture mode was primarily interlaminar or intralaminar Mode I tension, with origin locations at edge defects or fastener bores. Crack initiation was found to be due to a variety of causes, including mishandling, improper bonding of the honeycomb, and improper hole drilling. The delamination interfaces were primarily between the fiberglass and boron plies or between the 0 and 90 degree graphite plies, which are often considered the weaker interfaces in a laminate. Two delaminations at the edge of the upper skin surface exhibited features indicative of crack growth by cyclic loading, evident by the presence of macroscopic beach marks (Figure 5-16) or extensive rubbing damage of the mating fracture surfaces. Both of these fractures initiated at gouges at the inboard edge, possibly due to mechanical prying with blunt instruments during separation of the outboard section of the wing (following flight tests and prior to laboratory flight spectrum loading). No indications of cyclic crack growth (due to mechanical testing) was found on the other fractures. Figure 5-17 illustrates the features identified for each of the delamination regions. Figure 5-18 presents several of the fracture surfaces with arrows defining the direction of crack growth.

5.3.5 Stress Analysis

Stress analysis was not performed. This was due to limited funding and because the majority of the delaminations were associated with defect conditions identified by the techniques described above.

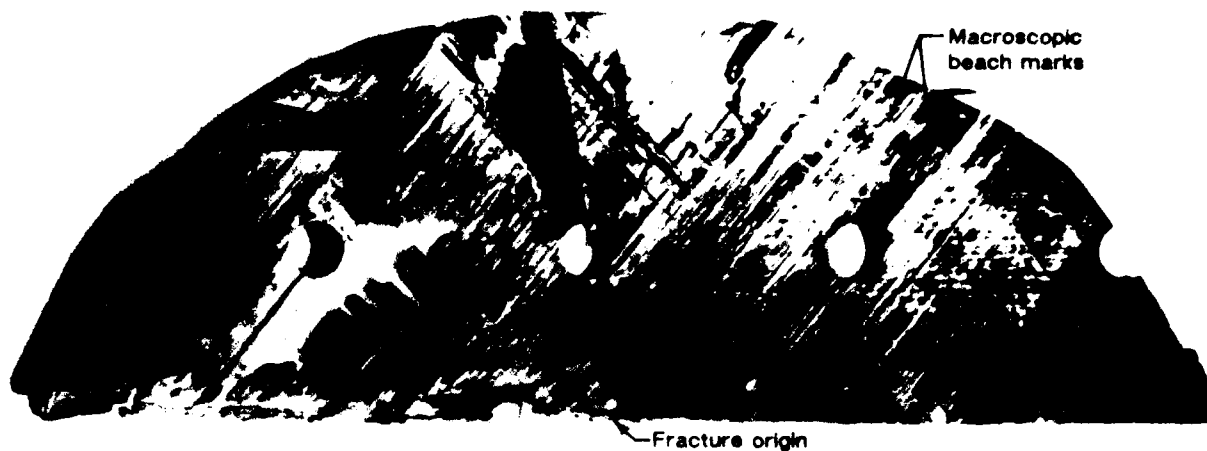


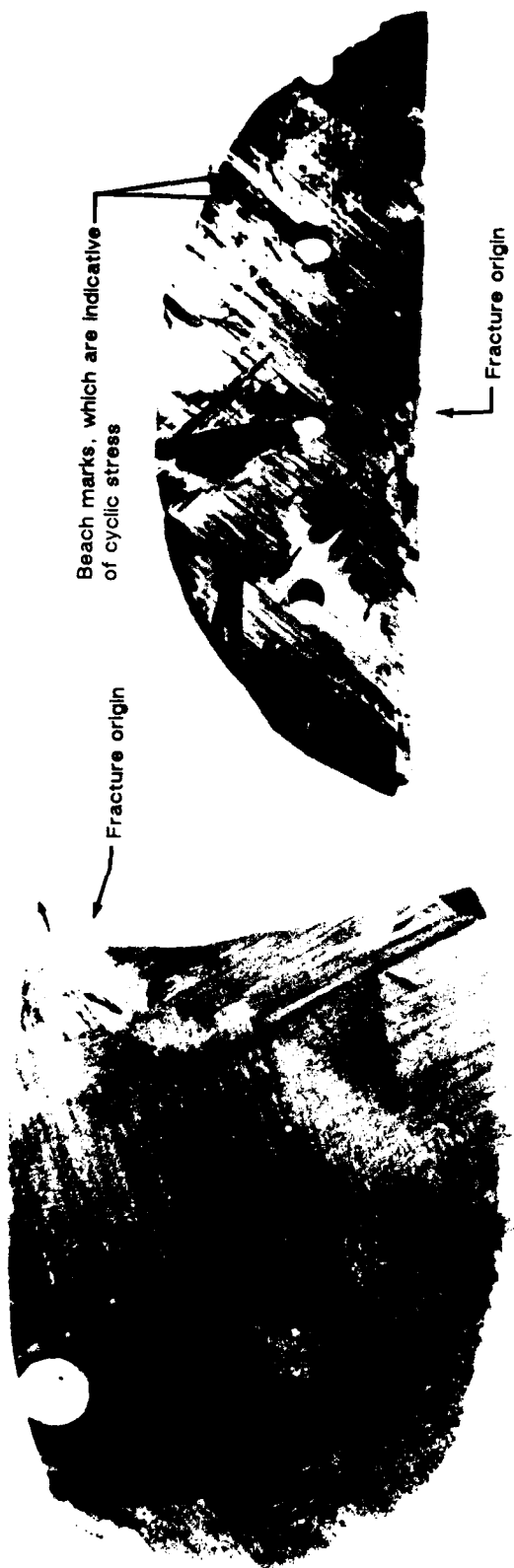
Figure 5-16. Photomicrograph of Beach Marks Indicative of Cyclic Crack Growth and Crack Propagation Direction

5-B70227-50

Delamination	Origin location	Fracture mode	Comments region
Section A	At sharp radius at edge of skin	Mode II shear at origin with mode I tension growth	Boron-fiberglass interface
Section B	Likely at an edge gouge	Not determinable	Abrasive rubbing prevented analyses
Section C	At edge gouge	Mode I tension	Radial crack growth with beach marks from cyclic loading
Section D	Not determined	Mode I tension	Donut-shaped defect
Section E	Fastener bore	Mode I tension	Boron-fiberglass interface
Section F	At edge with no defect	Mode I tension	Crack arrested at fastener bore
Section G	Fastener bore	Mode I tension	Resin particulate from drilling-induced delamination
Section H	Fastener bore	Mode I tension	Porosity aided crack initiation of fabric graphite plies

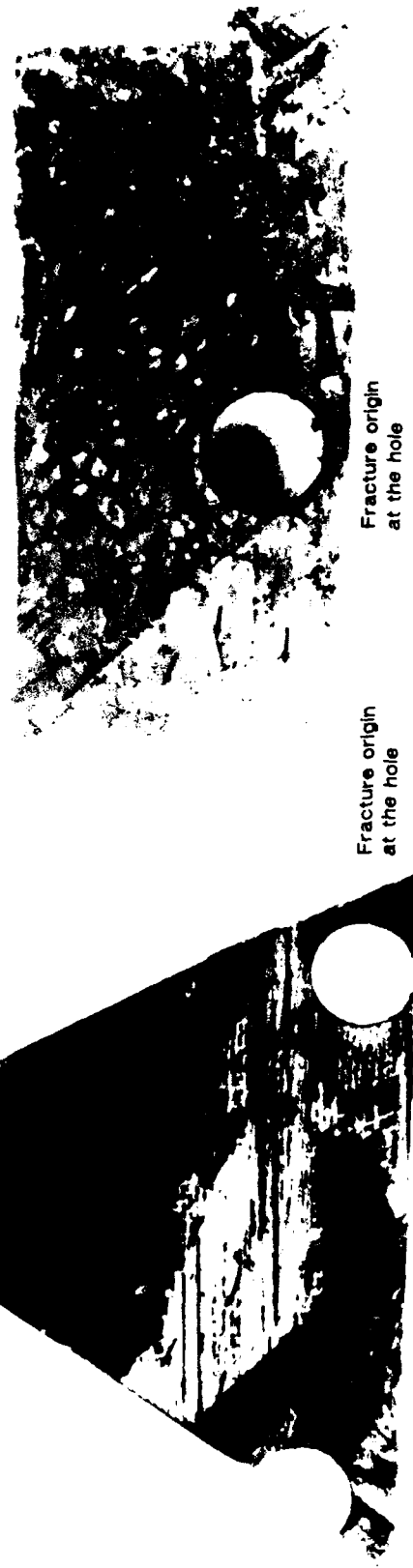
Figure 5-17. Fractography Results From NASA HiMAT Wing

5-B70227R1-105



Section A

Section C



Section E

Section I

Figure 5-18. Crack Mapping Results From Selected Delamination Regions

5.4 Carbon Fiber Reinforced Plastic I-Beam

5.4.1 Background History

Figure 5-19 shows the I-beam in its as-received condition. This component was fabricated by the personnel at the Air Force Wright Patterson Aeronautical Laboratories (AFWAL). Information regarding the component's layup, material composition, resin content, and cure temperature was provided by AFWAL. The component was tested in a four point bend test. The I-beam consisted of a tape laminate with vertical web and two horizontal caps, similar to stringers used to stiffen skins on aircraft wing construction. Small vertical stiffeners were secondarily bonded at several locations along the length to provide support of the cap flanges during loading. Efforts were aimed at determining the cause of failure with the quickest and lowest cost methods available. As a result, examinations such as fractography were performed without an SEM, relying on macroscopic and optical means of identifying the sequence and origin of fracture.

5.4.2 Nondestructive Evaluation

NDE was performed on the I-beam to determine areas of damage or defects caused from testing or manufacturing. Visual inspection of the beam revealed bearing damage on the

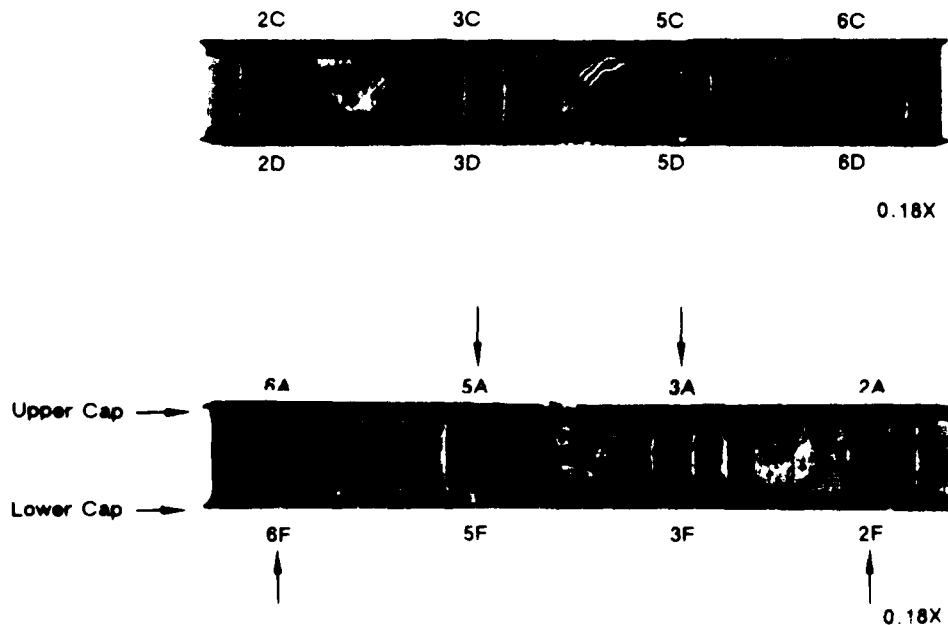


Figure 5-19. CFRP I-Beam in the As-Received Condition

5-B70227-52

caps indicative of the loading points during mechanical testing. This allowed determination of the types of stress, (that is, compression, tension or shear) imparted on the various regions of the beam. For continuity throughout this discussion, the upper cap was compressively loaded and the lower cap was in tension during flexural loading. Delaminations were found at two locations in the upper cap, with remaining damage limited to brooming (localized buckling) of the small vertical stiffeners immediately below the two center loading points, most likely due to the compressive loading. These damage conditions are presented in Figures 5-20 and 5-21. TTU inspection required three

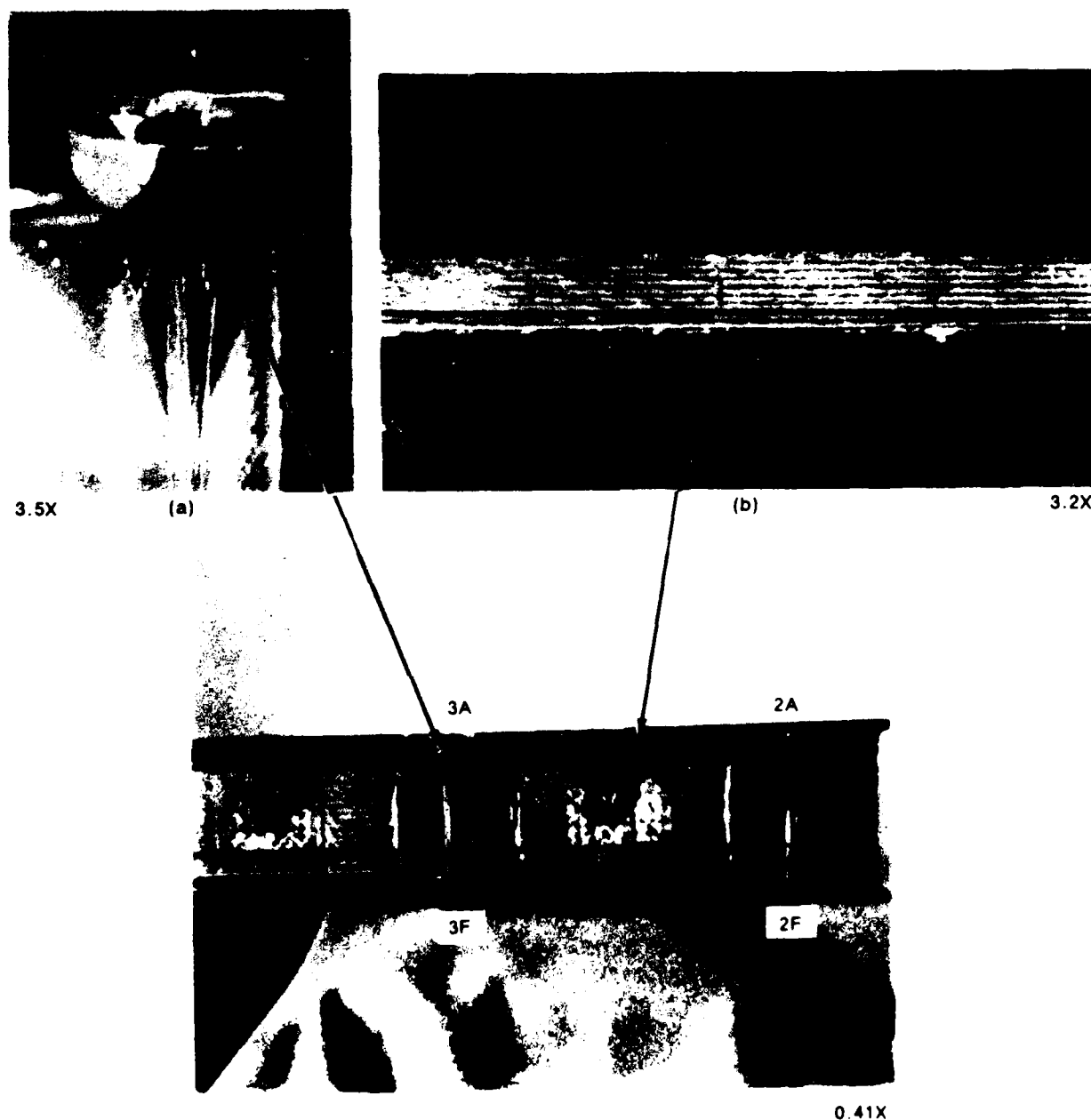


Figure 5-20. Regions of (a) Compression Buckling and (b) Delamination in the Upper Cap Section of the I-Beam

5-B70227-53

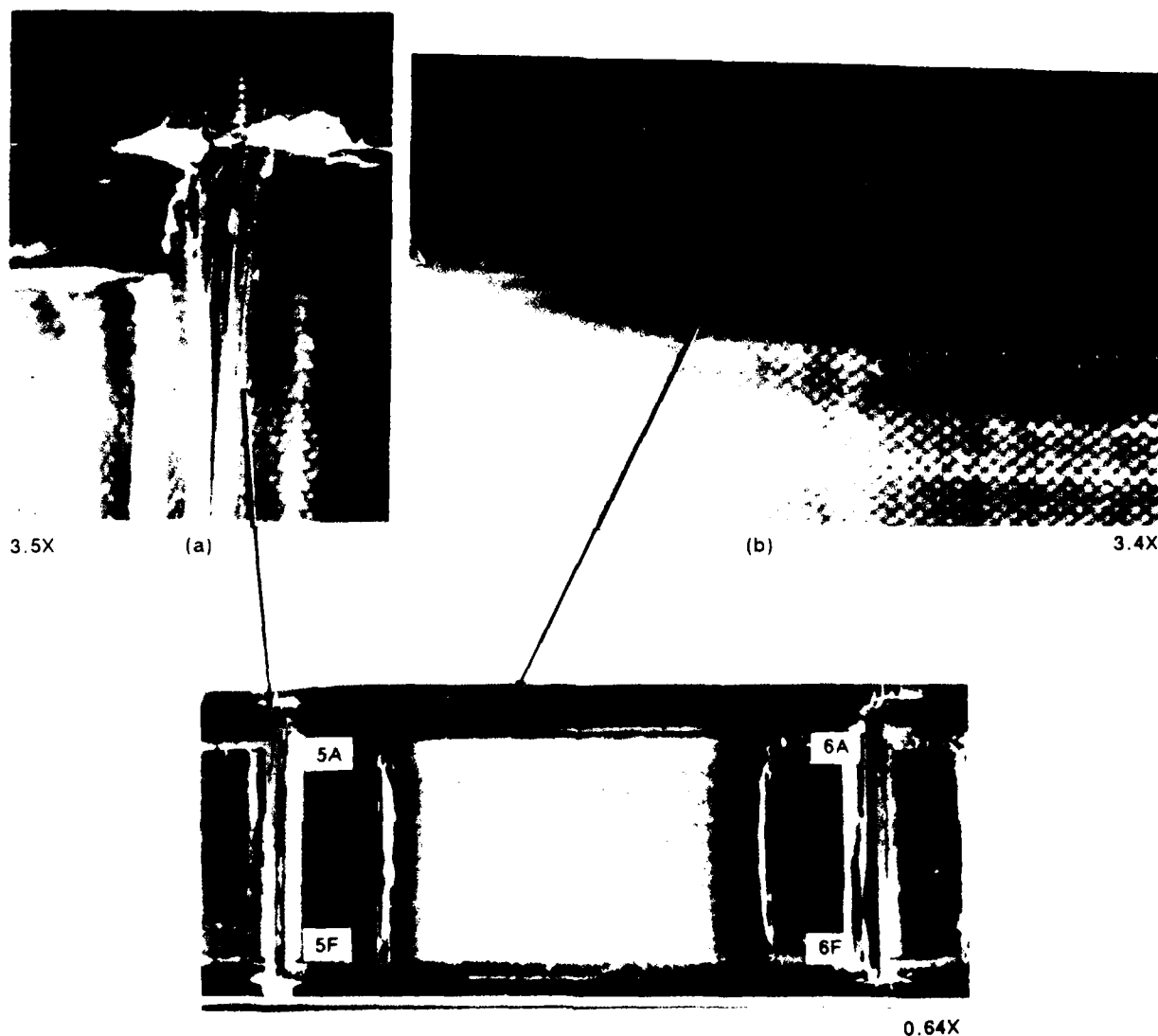


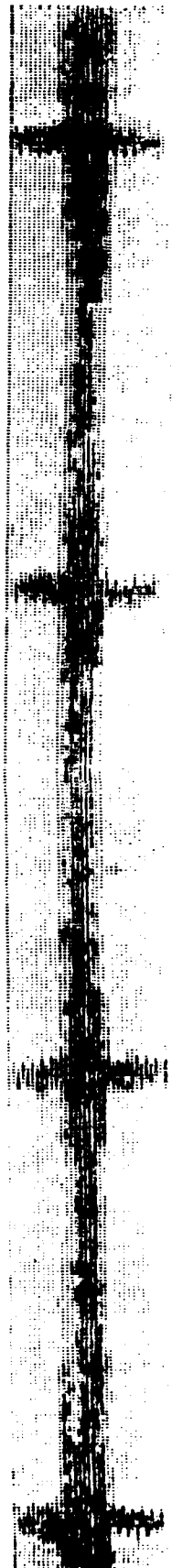
Figure 5-21. Regions of (a) Compression Buckling and (b) Delamination in the Upper Cap Section of the I-Beam

5-B70227-54

scans to evaluate the entire beam. First, the vertical web section was inspected. Since no delaminations were identified, the beam was cut longitudinally along the web to allow separate TTU inspection of the caps. The lower tensile cap was not damaged, however the upper compression cap was found to be delaminated in the identical regions which were visually identifiable (Figure 5-22). The upper cap was free of delaminations in the central region between the two loading points (an area of pure compression loading and no shear stress in the laminate plane).



Upper Cap



Lower Cap



Web Region

Figure 5-22. TTU C-Scans of the I-Beam Subcomponents

5-B70227-106

5.4.3 Materials Characterization

Cross-sections were performed on the ends of the beam to evaluate the laminate quality and construction. Ply counts indicated that the beam was fabricated with the correct number and orientation of plies. The overall part quality was found to be poor; extensive porosity was located at the web-to-cap junction and lack of adequate tooling constraint during cure allowed deformation of the entire laminate thickness (Figure 5-23).

Fiber diameters were measured to identify the fiber type (carbon AS4). Infrared spectroscopy was used to identify the novalac based epoxy resin and the presence of sulphur compounds indicative of a diaminodiphenyl sulphone (DDS) hardener used in epoxy resin systems. Thermomechanical analysis (TMA) using the flexural method was employed to determine a T_g of 379°F, verifying a complete cure of a 177°C (350°F) cure system. The resin content of the caps were determined by the density gradient column method. The resin content was 27% by weight, much less than that of the original prepreg which was approximately 34%. This was a definite concern since resin contents below 30% have been shown to significantly reduce the laminate strength, particularly for resin dominated fractures such as interlaminar shear and tension or compression buckling.



Figure 5-23. Extensive Porosity and Laminate Deformity in the Web-to-Cap Junction

5-B70227-55

5.4.4 Fractography

The delaminations in the upper caps were removed by cutting to prevent further delamination. Visual macroscopic inspection of the surfaces revealed the presence of both shiny and milky appearing regions, indicative of tension and shear dominated delaminations, respectively. The fracture occurred at the interface between the 0 and 45 degree plies, most likely due to the stress gradient between the axial 0 degree ply (which carries the primary axial flexural loads) and the off-axis 45 degree ply. Crack mapping was performed with the optical microscope, with the localized crack directions determined by examining the orientation of the hackles in the shear dominated regions and the river marks in the tension dominated regions. Cracking was found to initiate by shear at the web-to-cap junction, under the loading contact points. Cracking continued along the central region of the cap (where extensive porosity was evident) by mixed mode, although primarily tension toward the ends of the beam, as shown in Figure 5-24.

5.4.5 Stress Analysis

Although no calculations were performed, simple beam flexure theory identified the presence of an interlaminar shear stress gradient in the upper cap, being the most concentrated immediately under the central bearing points and reducing in stress toward the beam end. This gradient accounts for crack initiation by interlaminar shear at the load point, aided by the reduced strength in the cap due to extensive porosity.



Figure 5-24. Results of Fractographic Crack Mapping of an Upper Cap Delamination

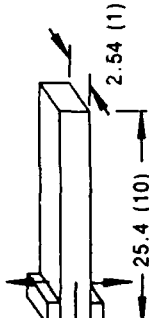
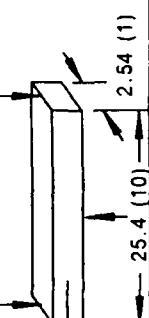
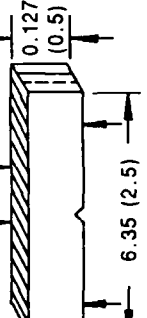
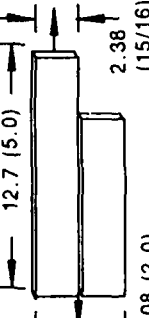
6.0 ATLAS OF FRACTOGRAPHS

An atlas of fractographs is provided in this section for use as a reference during fractographic analyses. Each of these fractographs were obtained from fracture surfaces generated from controlled fracture-toughness type coupon testing. Figure 6-1 (3 pages) presents the test matrices from which the controlled fractures were generated; also shown are paragraph numbers associated with each type of test matrix. The material system is Hercules 3501/AS4, except for a special materials group in paragraph 6.13.

In each case, fracture was produced such that the crack direction and fracture mode was controlled. Where possible, the direction of crack growth is noted, to aid the investigator in evaluation of the fracture surfaces during crack mapping. To present differences between the details identified by the various fractography tools, both optical and SEM photomicrographs are presented for each fracture condition. To further familiarize the reviewer with the typical fracture characteristics, the photomicrographs are presented in increasing order of magnification for delamination and translaminal fractures in a wide variety of ply orientations and environmental conditions.

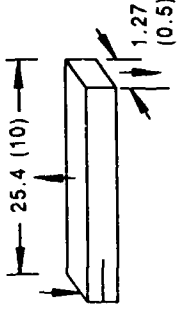
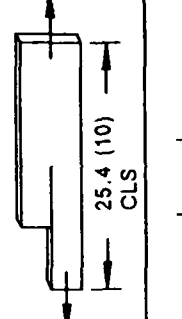
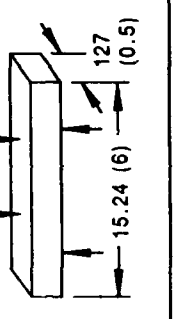
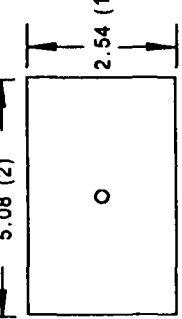
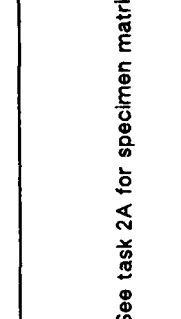
For each section, a description is provided showing the relationship between the primary fractographic features and the following:

- Load type.
- Crack growth direction.
- Mechanism.
- Environment (prior to and during fracture).

Specimen	Ply layups, number of plies, deg				Comments	Number of specimens	Specimen configuration, cm (in)	Section
Task 2A: Singular-failure-condition specimens Interlaminar • Mode I, DCB	24/0	24/+45	24/0, 45a	24/0, 90a	24/90b	a Will use 0-deg plies for buildup b Short crack stability anticipated	5 each 	6.1
• Mode II, ENF	24/0	24/+45	24/0, 45a	24/0, 90a	b	a Will use 0-deg plies for buildup b Cannot be tested in shear	5 each 	6.2
Translaminar • Mode I tension, four-point load	--	32/+45	32/quasi	32/0, 90	--	--	5 each 	6.4
• Mode I compression, four-point load	32/0	32/+45	32/quasi	32/0, 90	--	--	5 each	6.5
• Mode II, side-notched rail shear	--	--	32/quasi	32/0, 90	--	--	5 each 	6.6
Interlaminar • Mode I, DCB	24/0	24/+45	24/0, 45	24/0, 90	24/90	Water content measured 2 weeks' soak at 82°C (180°F)	5 each	6.1
• Mode II, ENF	24/0	24/+45	24/0, 45	24/0, 90	--	Environmental matrix	Same as task 2A specimens above	6.2
Translaminar • Mode I tension, four-point load	32/0	32/+45	32/quasi	32/0, 90	--	132°C (270°F) dry, wet 82°C (180°F) dry, wet 21°C (70°F) dry, wet		6.4
• Mode I compression, four-point load	32/0	32/+45	32/quasi	32/0, 90	--	-54°C (-65°F) dry		6.5
• Mode II, side-notched rail shear	32/0	32/+45	32/quasi	32/0, 90	--		5 each	6.6

Abbreviations: CLS cracked lap shear; DCB double cantilever beam; ENF end-notched flexure; MMF mixed-mode flexure

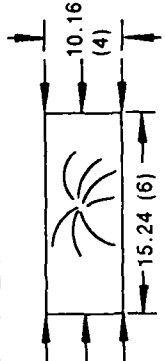
Figure 6-1. Singular- and Multiple-Failure-Condition Test Specimen Matrix (Sheet 1 of 3)

Specimen	Ply lay. ps. number of plies, deg				Comments	Number of specimens	Specimen configuration, cm (In)	Section
Task 2A: Singular-failure-condition specimens Interlaminar • Mode I, II, MMF	24/0	24/±45	24/0, 45	24/0, 90	—	5 each		6.3
	24/0	24/±45	24/0, 45	24/0, 90	—	10 each		6.8
	24/0	24/±45	24/0, 45	24/0, 90	—	10 each		6.8
	32/0	32/quasi	32/±45	32/0, 90	—	5 each		6.7
Task 2B: Multiple-failure-condition specimens Interlaminar • Drill breakout	32/0	32/quasi	32/±45	—	—	5 each		6.9
	24/0	24/±45	24/0, 45	24/0, 90	—	5 each	See task 2A for specimen matrix	6.11
	24/0	24/±45	24/0, 45	24/0, 90	—	5 each	See task 2A for specimen matrix	6.11
	24/0	24/±45	24/0, 45	24/0, 90	—	5 each	See task 2A for specimen matrix	6.11

Abbreviations: CLS cracked lap shear; DCB double cantilever beam; ENF end-notched flexure; MMF mixed-mode flexure

Figure 6-1. Singular- and Multiple-Failure-Condition Test Specimen Matrix (Sheet 2 of 3)

5-B70227-195b

Defects (continued)					Specimen configuration, cm (in)		Section	
Specimen	Ply layouts number of plies, deg				Comments	Number of specimens		
Task 2B. Multiple-failure-condition specimens • Teflon squeegee • Mode I, DCB • Mode II, ENF • Voids • Mode I, DCB • Mode II, CLS	24/0	24/±45	24/0, 45	24/0, 90	—	5 each	See task 2A for specimen matrix	
	24/0	24/±45	24/0, 45	24/0, 90	—	5 each		
	24/0	24/±45	24/0, 45	24/0, 90	—	5 each		
	24/0	24/±45	24/0, 45	24/0, 90	—	5 each		
	32/quasi	—	—	—	—	5 each		
• Impact • Compression after impact								

Abbreviations: CLS cracked lap shear; DCB double cantilever beam; ENF end-notched flexure; MMF mixed-mode flexure

Figure 6-1. Singular- and Multiple-Failure-Condition Test Specimen Matrix (Sheet 3 of 3)

5-B70227-195c

6.1 INTERLAMINAR MODE I TENSION

Figure 6-2 shows the test matrix for the Double Cantilever Beam (DCB) test type.

The primary features observed in fracture surfaces generated by Mode I tensions are as follows:

- Macroscopically and microscopically flat fracture surface.
- Flat resin fracture between fibers, exhibiting river marks and very fine resin microflow.
- Smooth appearance at the fiber-matrix separation.

Crack growth directions can be determined by examining the flat regions between fibers. The direction of river mark branching and the radiating nature of the resin microflow are oriented in the direction of crack growth (see Figure 6-3).

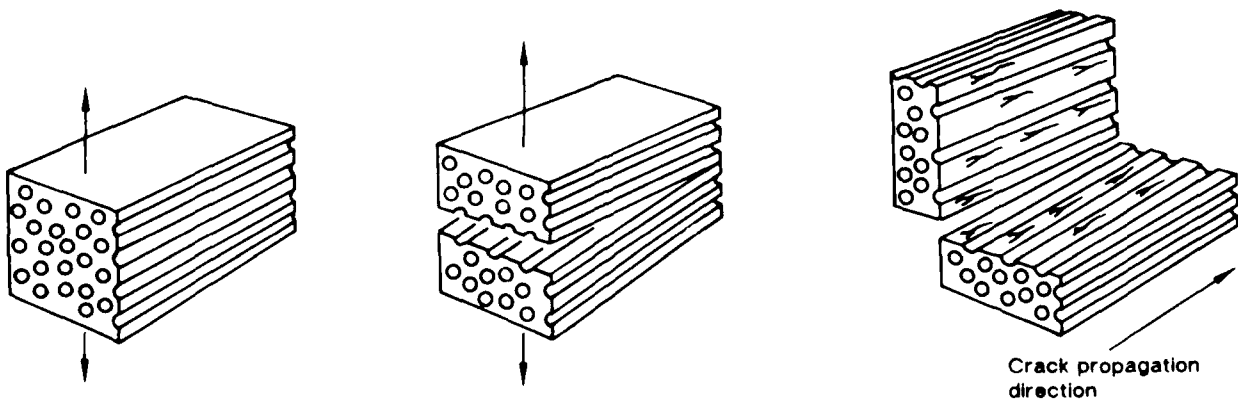


Figure 6-2. Double Cantilever Beam (DCB) Test Type

5-B70227-169

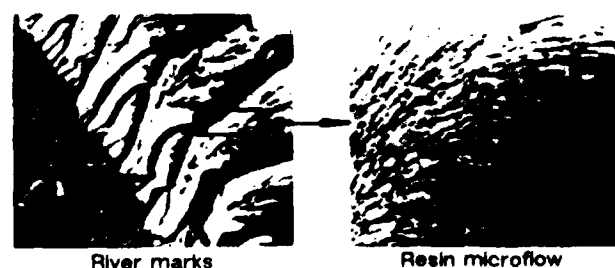


Figure 6-3. Overall Crack Growth Direction by Resin Regions Between Fibers

6-B70227-288

Care must be taken to examine many locations in the fracture surface for increased accuracy and reliability of crack growth directions.

River marks are concentrated adjacent to the fibers where cracking tends to continually reiterate on a microscale. In other cases, where overall cracking progresses in a direction other than parallel to the fibers, these river marks are concentrated on the side of the fiber away from the origin (see Figure 6-4).

Absorbed moisture or elevated temperature present during fracture does not alter the ability to determine crack growth and fracture mode. Cracking does, however, tend to occur within the undivided plies (intralaminar) as opposed to room temperature (dry features) which usually occur between plies. This is likely due to either the decreased strength of the fiber-matrix interface or the increased ductility of the resin. Fractures created at 270° F for the 350° F system often exhibited large amounts of loose fibers on the fracture surface.

See Figures 6-5 through 6-28.

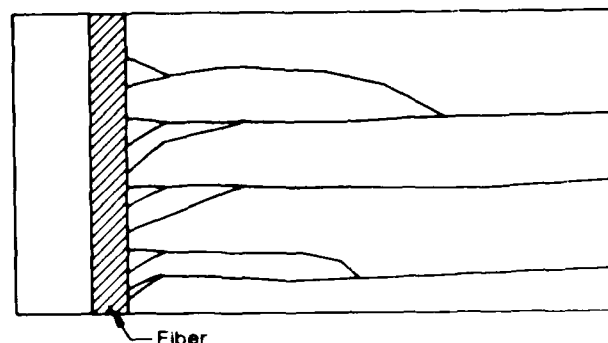


Figure 6-4. Crack Growth Direction by Resin Microflow

6-B70227-288

AD-A183 783

COMPENDIUM OF POST-FAILURE ANALYSIS TECHNIQUES FOR
COMPOSITE MATERIALS(U) BOEING MILITARY AIRPLANE CO
SEATTLE WA R A GROVE ET AL. JAN 87 AFMIL-TR-86-4137

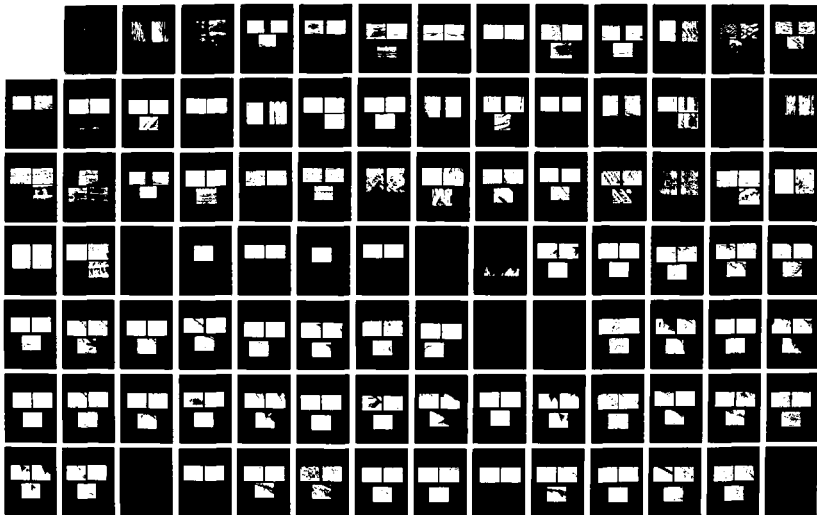
4/5

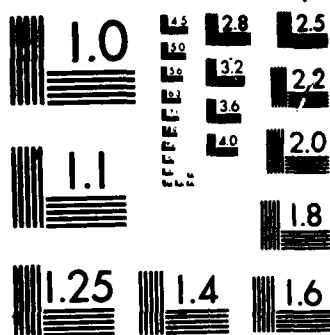
UNCLASSIFIED

F33615-84-C-5010

F/G 11/4

NL

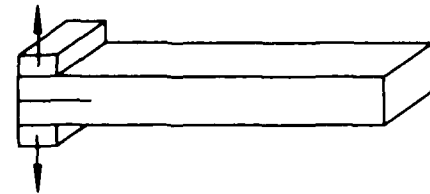




MICROCOPY RESOLUTION TEST CHART
 NATIONAL BUREAU OF STANDARDS-1963-A

Optical photomicrographs

Fracture type	Interlaminar mode I tension
Ply layup	[0]24
Test type	DCB
• Test conditions	21°C dry
• Fracture between	0/0 plies
Material	Hercules 3501-6/177° C cure AS4 fibers



100X



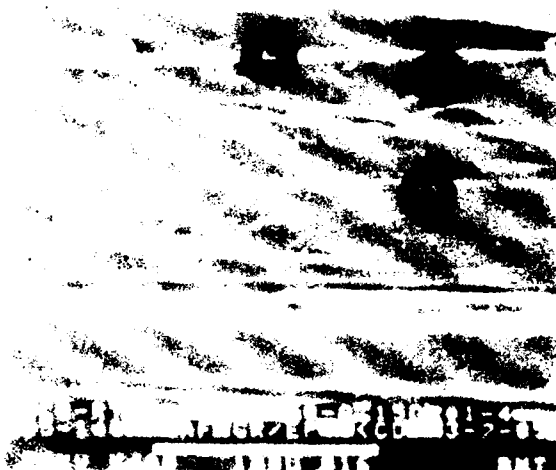
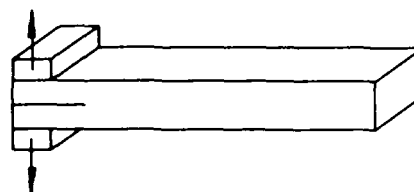
400X

Figure 6-5. 24-Ply Layup, 0 Plies

5-B70227-171

SEM photomicrographs

Fracture type	Interlaminar mode I tension
Ply layup	[0]24
Test type	DCB
• Test conditions	21°C dry
• Fracture between	0/0 plies
Material	Hercules 3501-6/177° C cure AS4 fibers



←
Mechanically induced
crack direction

Legend:

- F Fiber matrix separation
- M Matrix fracture
- R River markings

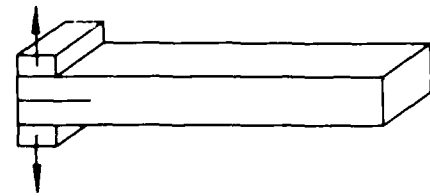


Figure 6-6. Fiber Matrix Separation, Fracture, and River Markings

5-B70227-172

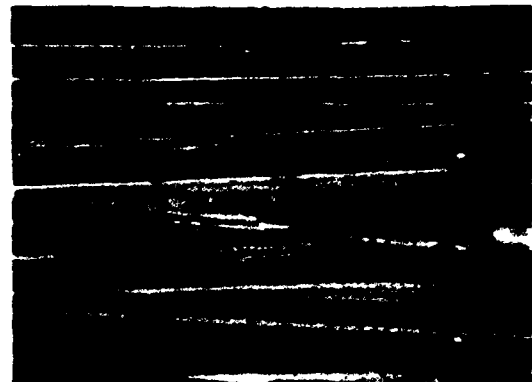
Optical photomicrographs

Fracture type	Interlaminar mode I tension
Ply layup	[0]24
Test type	DCB
• Test conditions	Dry
• Fracture between	0/0 plies
Material	Hercules 3501-6/177°C cure AS4 fibers



-65°F. dry

400X



70°F. dry

400X

→
Mechanically induced
crack direction



270°F. dry

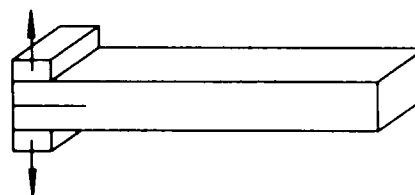
400X

Figure 6-7. -65°F, 70°F, and 270°F Conditions (Optical)

6-B70227R1-173

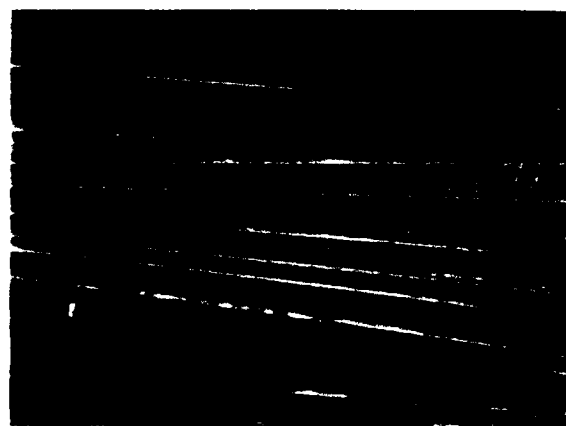
Optical photomicrographs

Fracture type	Interlaminar mode I tension
Ply layup	[0]24
Test type	DCB
• Test conditions	70°F wet
• Fracture between	0/0 plies
Material	Hercules 3501-6/177° C cure AS4 fibers



70°F wet

400X



180°F wet

400X

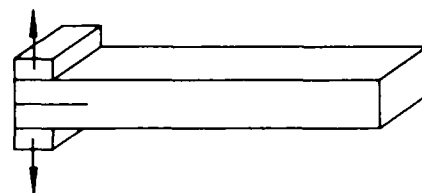
←
Mechanically induced crack direction

Figure 6-8. 70°F Wet Condition (Optical)

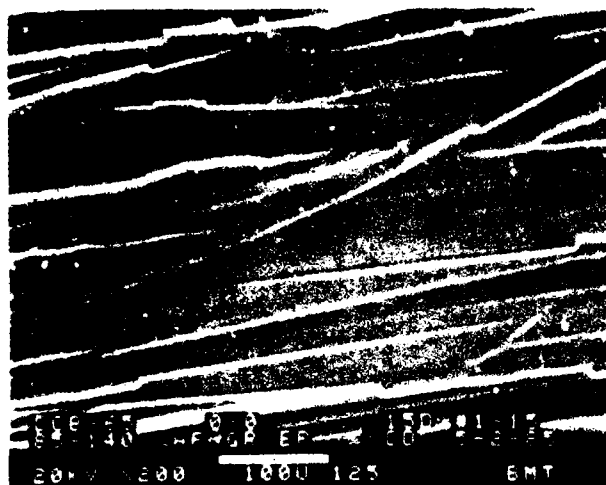
6-B70227R1-174

SEM photomicrographs

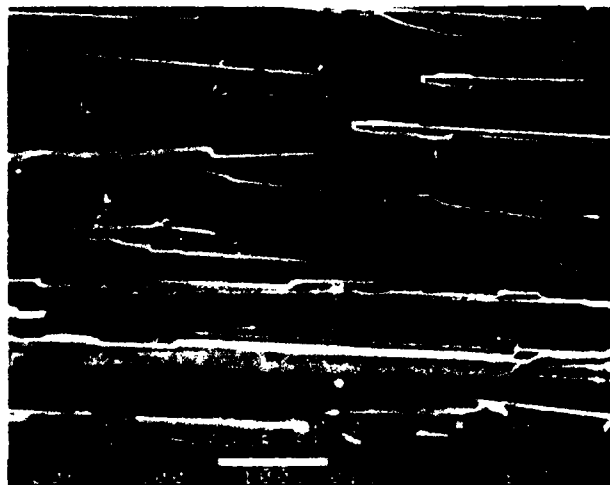
Fracture type	Interlaminar mode I tension
Ply layup	[0] 24
Test type	DCB
• Test conditions	Dry
• Fracture between	0/0 plies
Material	Hercules 3501-6/177° C cure AS4 fibers



← Mechanically induced crack direction



-65° F. dry



70° F. dry



270° F. dry

Figure 6-9. -65°F Dry, 70°F Dry, and 270°F Dry Conditions (SEM 200X)

5-B70227-175

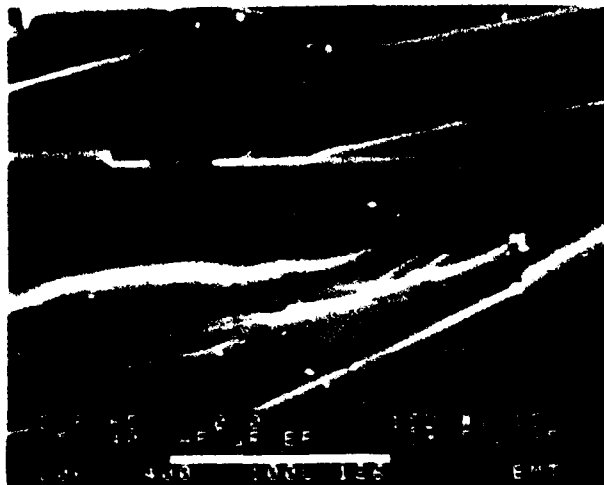
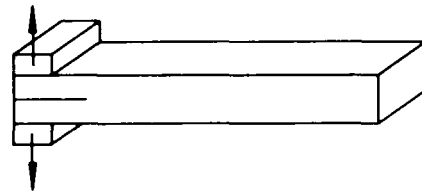
SEM photomicrographs

Fracture type	Interlaminar mode I tension
Ply layup	[0] ₂₄
Test type	DCB
• Test conditions	Dry
• Fracture between	0/0 plies
Material	Hercules 3501-6/177°C cure AS4 fibers

Legend:

F Fiber matrix separation
R River markings
M Matrix fracture

← Mechanically induced crack direction



-65°F, dry



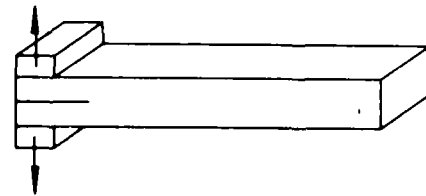
70°F, dry

Figure 6-10. -65°F and 70°F Dry Conditions (SEM)

5-B70227-176

SEM photomicrographs

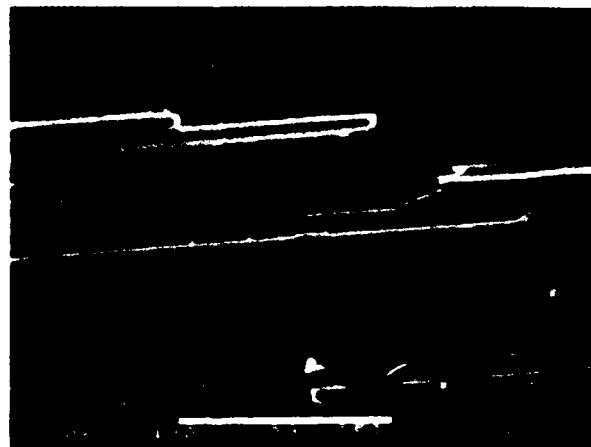
Fracture type	Interlaminar mode I tension
Ply layup	[0] 24
Test type	DCB
• Test conditions	Wet
• Fracture between	0/0 plies
Material	Hercules 3501-6/177°C cure AS4 fibers



←
Mechanically induced crack direction



70°F, wet



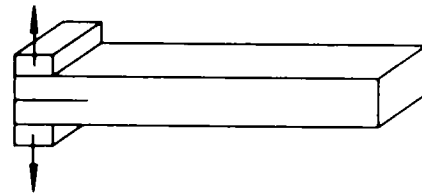
180°F, wet

Figure 6-11. 70°F Wet and 180°F Wet Conditions

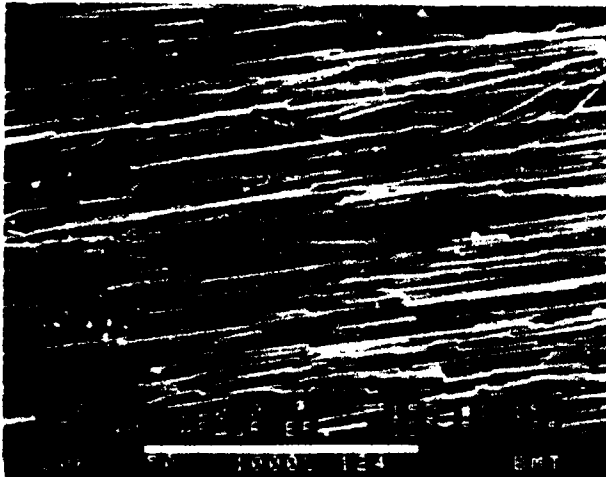
5-B70227-177

SEM photomicrographs

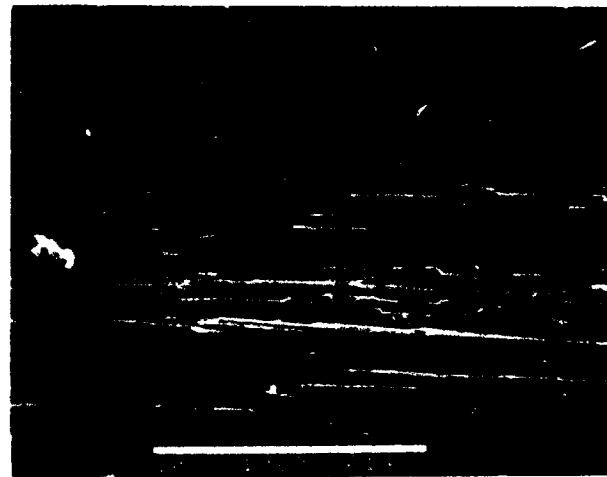
Fracture type	Interlaminar mode I tension
Ply layup	[0] 24
Test type	DCB
• Test conditions	Dry
• Fracture between	0/0 plies
Material	Hercules 3501-6/177° C cure AS4 fibers



←
Mechanically Induced crack direction



-65°F. dry



70°F. dry



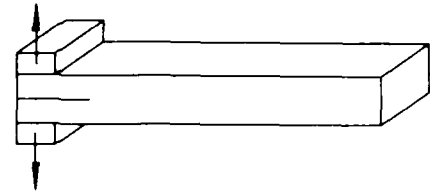
270°F. dry

Figure 6-12. -65°F Dry, 70°F Dry, and 270°F Dry Conditions (SEM 50X)

5-B70227-178

SEM photomicrographs

Fracture type	Interlaminar mode I tension
Ply layup	[0] 24
Test type	DCB
• Test conditions	Dry/wet
• Fracture between	0/0 plies
Material	Hercules 3501-6/177°C cure AS4 fibers



Mechanically induced crack direction



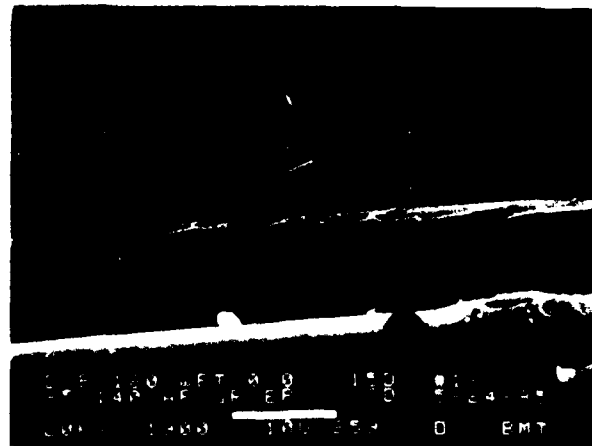
70°F wet

2000X



180°F dry

2000X



180°F, wet

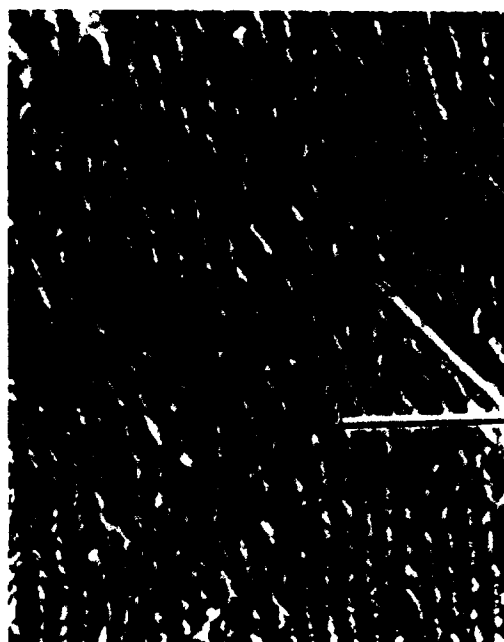
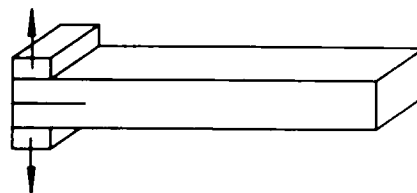
2000X

Figure 6-13. 70°F Wet, 180°F Dry, and 180°F Wet Conditions
With Fiber Separation and River Marks

6-B70227R1-179

Optical photomicrographs

Fracture type	Interlaminar mode I tension
Ply layup	[+45, -45] _{12S}
Test type	DCB
• Test conditions	21°C dry
• Fracture between	+45/-45 plies
Material	Hercules 3501-6/177°C cure AS4 fibers



100X



400X

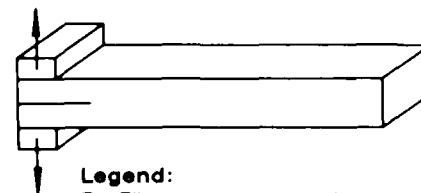
← Mechanically induced crack direction

Figure 6-14. +45/-45 Plies (Optical)

5-B70227-180

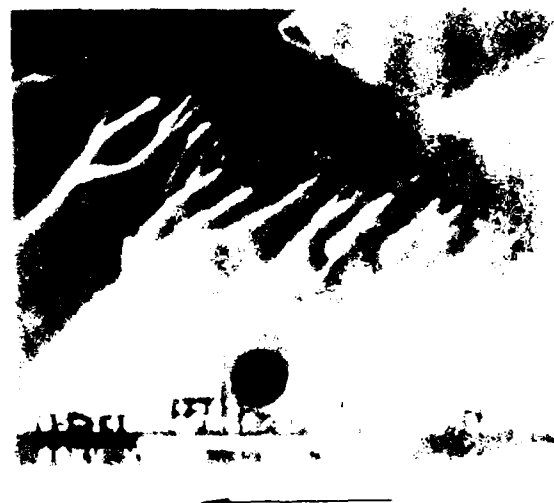
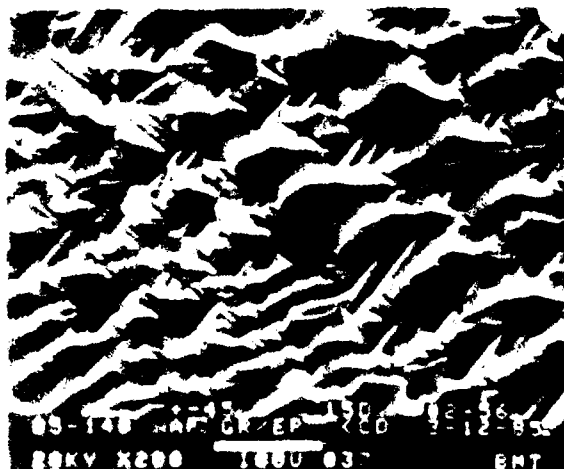
SEM photomicrographs

Fracture type	Interlaminar mode I tension
Ply layup	[+45, -45] 12S
Test type	DCB
• Test conditions	21°C dry
• Fracture between	+45/-45 plies
Material	Hercules 3501-6/177°C cure AS4 fibers



Legend:

- F Fiber matrix separation
- M Matrix fracture
- R River markings
- T Textured microflow



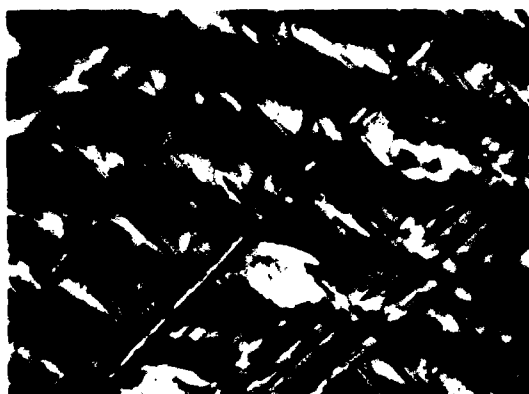
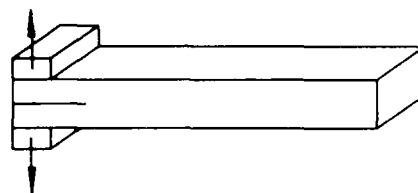
Mechanically induced crack direction

Figure 6-15. +45/-45 Plies With Matrix Fracture, Fiber Separation, River Marks, and Textured Microflow

5-B70227-181

Optical photomicrographs

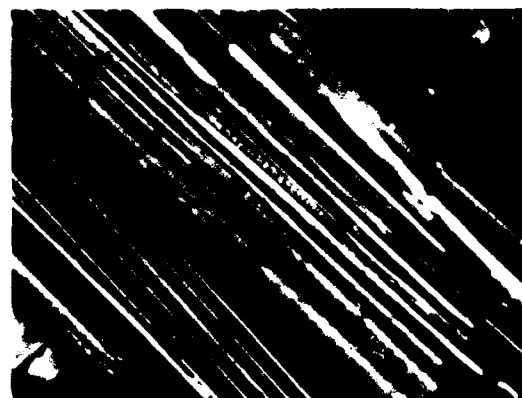
Fracture type	Interlaminar mode I tension
Ply layup	[+45, -45] ₁₂ S
Test type	DCB
• Test conditions	Dry
• Fracture between	+45/-45 plies
Material	Hercules 3501-6/177°C cure AS4 fibers



-65°F, dry 400X



70°F, dry 400X



270°F, dry 400X

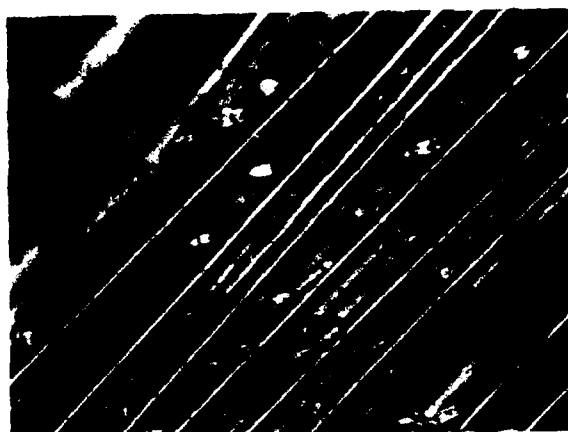
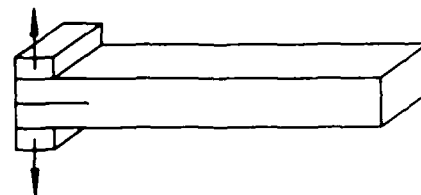
Mechanically induced crack direction

Figure 6-16. -65°F Dry, 70°F Dry, and 270°F Dry Conditions (Optical 400X)

5-B70227-182

Optical photomicrographs

Fracture type	Interlaminar mode I tension
Ply layup	[+45, -45] ₁₂ S
Test type	DCB
• Test conditions	Wet
• Fracture between	+45/-45 plies
Material	Hercules 3501-6/177°C cure AS4 fibers



70°F. wet

400X



180°F. wet

400X

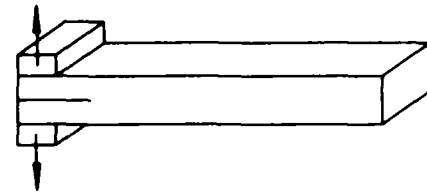
← Mechanically induced crack direction

Figure 6-17. +45/-45 Plies at 70°F Wet Conditions (Optical 400X)

5-B70227-183

SEM photomicrographs

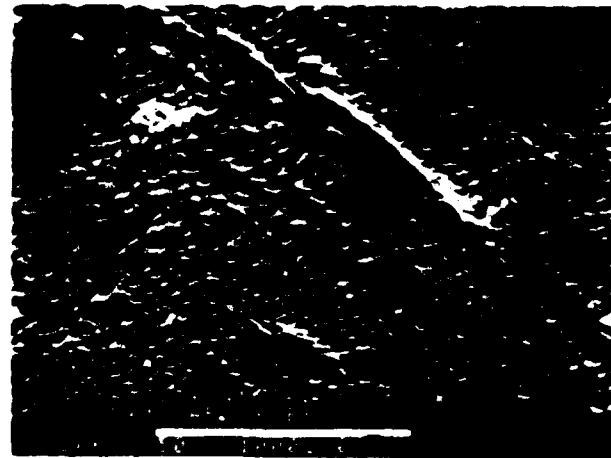
Fracture type	Interlaminar mode I tension
Ply layup	[+45,-45] 12S
Test type	DCB
• Test conditions	Dry
• Fracture between	+45/-45 plies
Material	Hercules 3501-6/177°C cure AS4 fibers



←
Mechanically induced crack direction



-65°F, Dry



70°F, Dry



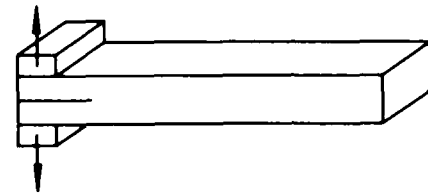
270°F, Dry

Figure 6-18. +45/-45 Plies at -65°F Dry, 70°F Dry, and 270°F Dry Conditions
(Optical 50X)

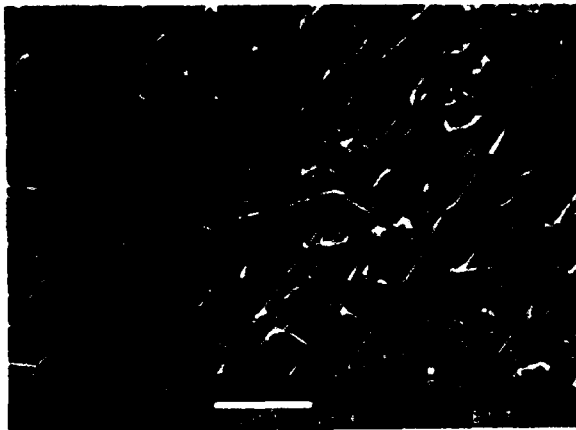
5-B70227-184

SEM photomicrographs

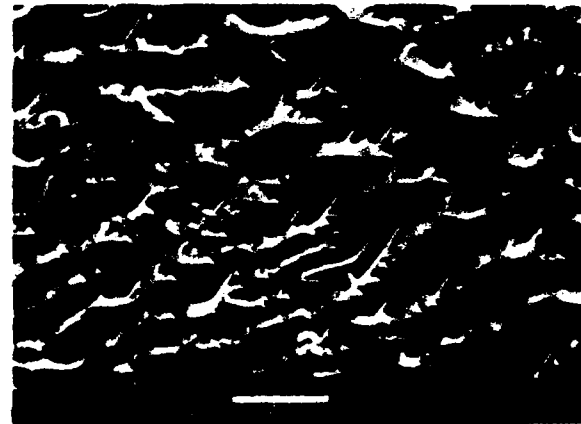
Fracture type	Interlaminar mode I tension
Ply layup	[+45,-45] 12S
Test type	DCB
• Test conditions	Dry
• Fracture between	+45/-45 plies
Material	Hercules 3501-6/177°C cure AS4 fibers



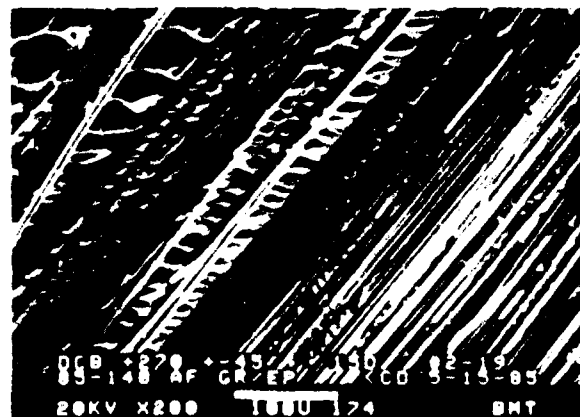
←
Mechanically induced crack direction



-65°F. Dry



70°F. Dry



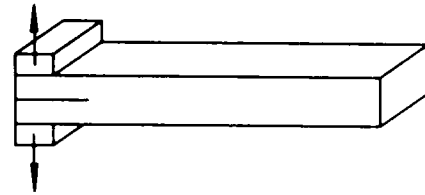
270°F. Dry

Figure 6-19. +45/-45 Plies at -65°F Dry, 70°F Dry, and 270°F Dry Conditions (SEM 200X)

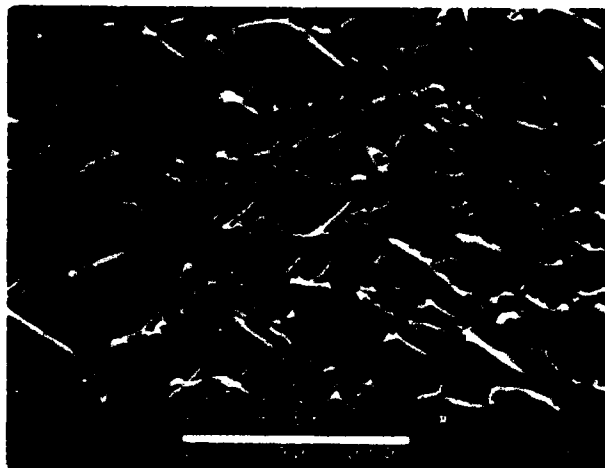
5-B70227-185

SEM photomicrographs

Fracture type	Interlaminar mode I tension
Ply layup	[+45,-45] 12S
Test type	DCB
• Test conditions	Wet
• Fracture between	+45/-45 plies
Material	Hercules 3501-6/177°C cure AS4 fibers



←
Mechanically induced crack direction



70°F. Wet



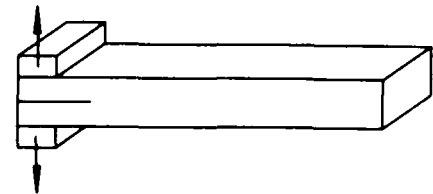
180°F. Wet

Figure 6-20. +45/-45 Plies at 70°F Wet and 180°F Wet Conditions (SEM 400X)

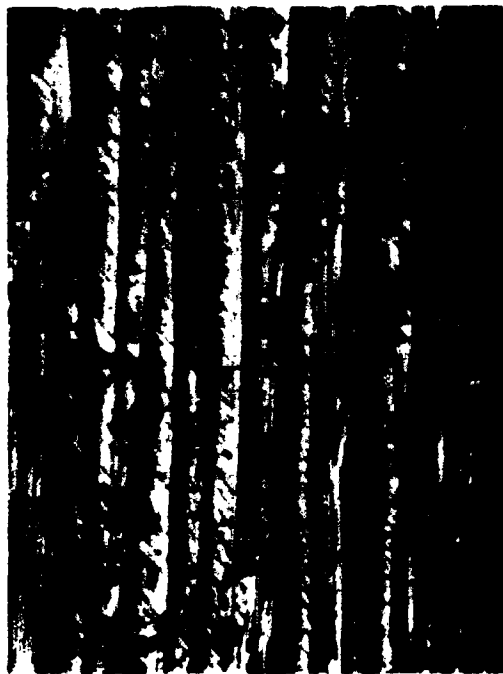
5-B70227-186

Optical photomicrographs

Fracture type	Interlaminar mode I tension
Ply layup	[0.45] _{12S}
Test type	DCB
• Test conditions	21°C dry
• Fracture between	0/45 plies
Material	Hercules 3501-6/177°C cure AS4 fibers



Mechanically
induced crack
direction



100X



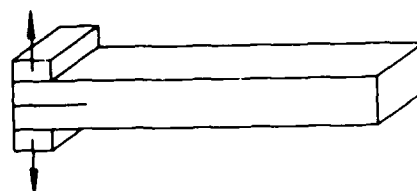
400X

Figure 6-21. 0/45 Plies at 21°C Dry (Optical 400X)

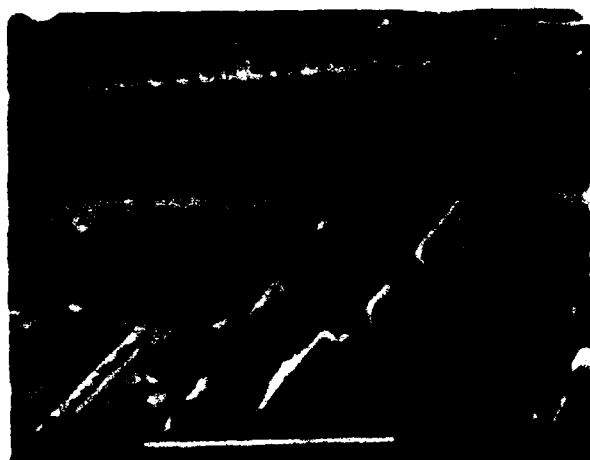
5-B70227-187

SEM photomicrographs

Fracture type	Interlaminar mode I tension
Ply layup	[0,45] _{12S}
Test type	DCB
• Test conditions	Wet
• Fracture between	0/45 plies
Material	Hercules 3501-6/177°C cure AS4 fibers



Mechanically induced crack direction



Legend:

- F Fiber matrix separation
- M Matrix fracture
- R River markings
- T Textured microflow



Figure 6-22. 0/45 Plies With Matrix Fracture, Fiber Separation, River Marks, and Textured Microflow

5-B70227-188

Optical photomicrographs

Fracture type	Interlaminar mode I tension
Ply layup	[0, 45] 12S
Test type	DCB
• Test conditions	Dry
• Fracture between	0/45 plies
Material	Hercules 3501-6/177°C cure AS4 fibers



Mechanically induced crack direction →



-65°F, dry



70°F, dry



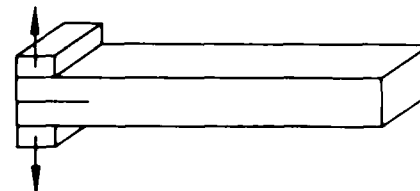
270°F, dry

Figure 6-23. 0/45 Plies at -65°F Dry, 70°F Dry, and 270°F Dry Conditions (Optical 400X)

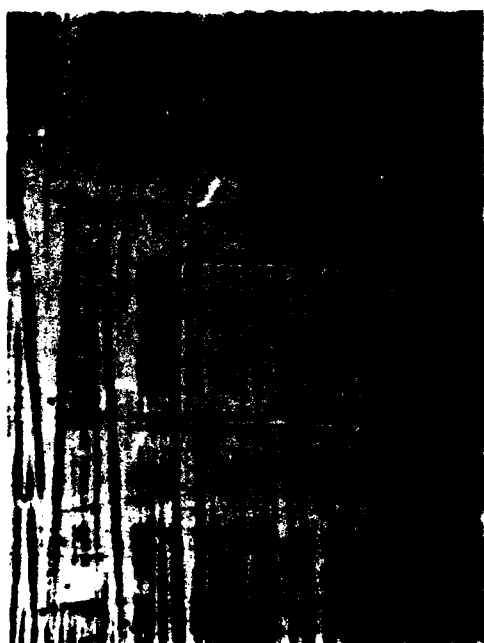
5-B70227-189

Optical photomicrographs

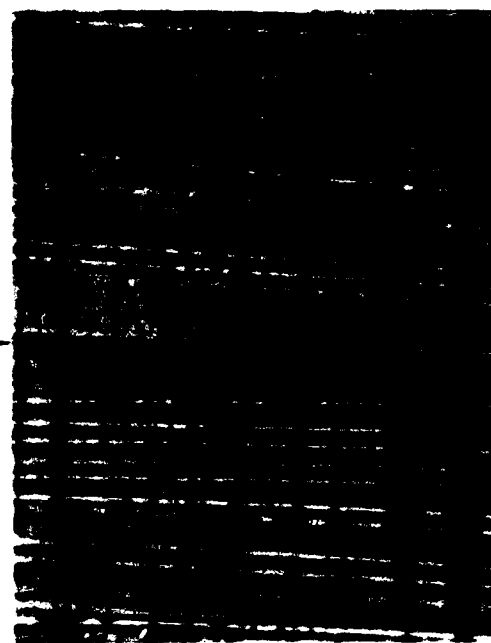
Fracture type	Interlaminar mode I tension
Ply layup	[0, 90] ₂ S
Test type	DCB
• Test conditions	21°C, dry
• Fracture between	0/90 plies
Material	Hercules 3501-6/177°C cure AS4 fibers



Mechanically induced crack direction



100X



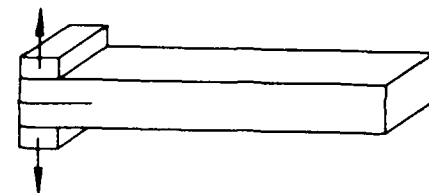
400X

Figure 6-24. 0/90 Plies at 21°C Dry Condition (Optical 100X and 400X)

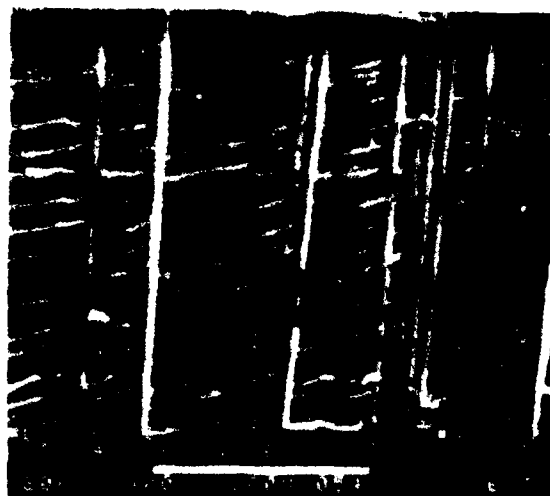
5-B70227-190

SEM photomicrographs

Fracture type	Interlaminar mode I tension
Ply layup	[0, 90] _{12S}
Test type	DCB
• Test conditions	21°C, dry
• Fiber end fracture	
Material	Hercules 3501-6/177°C cure AS4 fibers



← Mechanically induced crack direction



400X



2000X

Legend:

- F Fiber matrix separation
- M Matrix fracture
- R River markings
- T Textured microflow



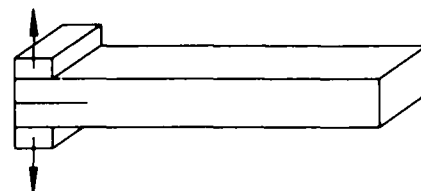
5000X

Figure 6-25. 0/90 Plies With Matrix Fracture, Fiber Separation, River Marks, and Textured Microflow

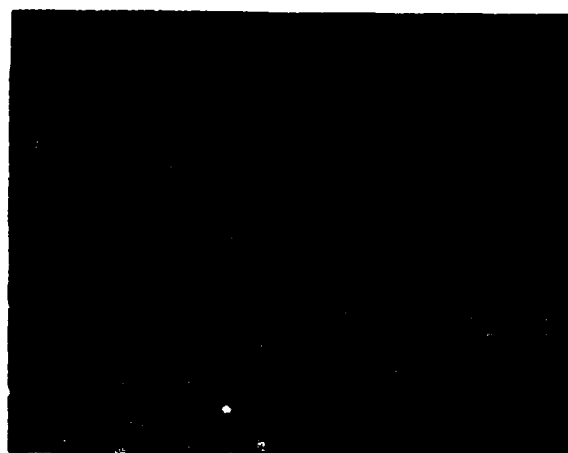
5-B70227-191

Optical photomicrographs

Fracture type	Interlaminar mode I tension
Ply layup	[0, 90] _{12S}
Test type	DCB
• Test conditions	Dry
• Fracture between	0/90 plies
Material	Hercules 3501-6/177°C cure AS4 fibers



Mechanically induced crack direction →



-65°F. dry

400X



70°F. dry

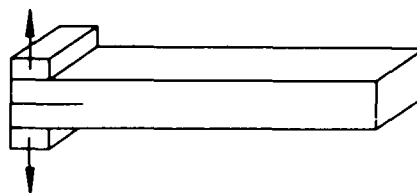
400X

Figure 6-26. 0/90 Plies at -65°F Dry and 70°F Dry Conditions (Optical 400X)

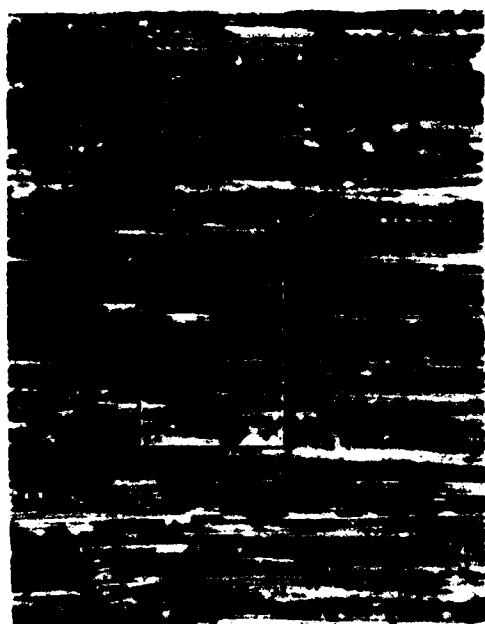
5-B70227-192

Optical photomicrographs

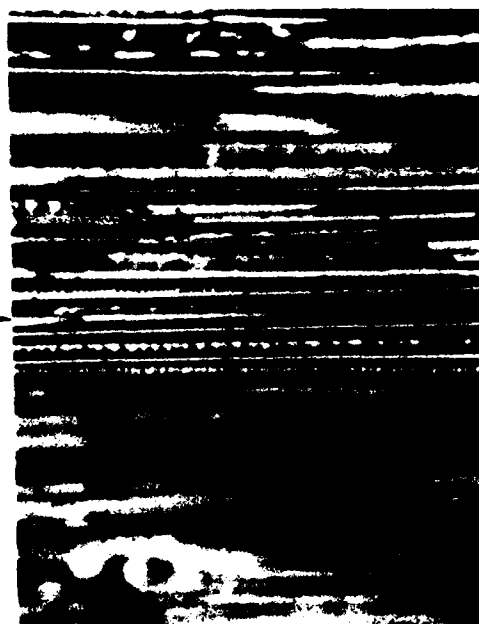
Fracture type	Interlaminar mode I tension
Ply layup	[90]24
Test type	DCB
• Test conditions	21°C, dry
• Fracture between	90/90 plies
Material	Hercules 3501-6/177°C cure AS4 fibers



Mechanically induced crack direction



100X



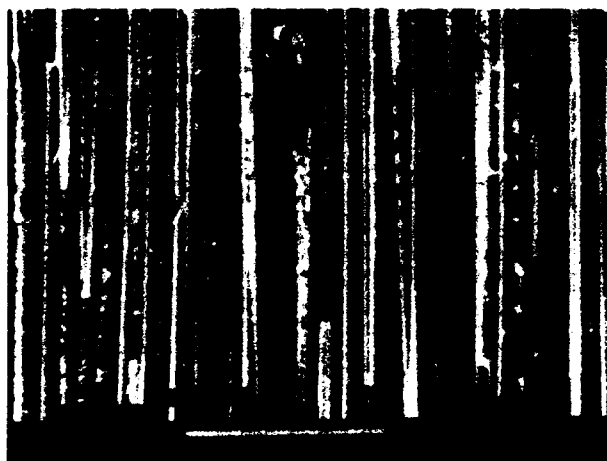
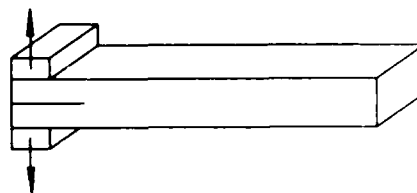
400X

Figure 6-27. 90/90 Plies at 21°C Dry Condition (Optical 100X and 400X)

5-B70227-193

SEM photomicrographs

Fracture type	Interlaminar mode I tension
Ply layup	[90] ₂₄
Test type	DCB
• Test conditions	21°C. dry
• Fracture between	0/90 plies
Material	Hercules 3501-6/177°C cure AS4 fibers



Mechanically induced crack direction



Legend:

- F Fiber matrix separation
- M Matrix fracture
- R River markings



Figure 6-28. 0/90 Plies at 21°C Dry Condition With Matrix Fracture, Fiber Separation, and River Marks

5-B70227-194

6.2 INTERLAMINAR MODE II SHEAR

Figure 6-29 shows the text matrix for the End Notch Flexural (ENF) test type.

The primary features observed in fracture surfaces generated under predominantly Mode II shear are as follows:

- Macroscopically flat surface.
- Microscopically rough resin fracture between fibers, exhibiting hackles and scallops.
- Smooth appearance at fiber-matrix separation.
- Secondary cracking (transverse to fracture plane).

The mechanisms by which hackles (vertical platelets) and scallops (concave regions) are generated in the resin are due to locally resolved tensile stresses at 45 degrees to the principle in-plane shear loads (see section 4.0). The hackles tilt in a direction parallel to the direction of crack growth. They exhibit either a symmetrical or an asymmetrical shape dependent on the crack growth direction relative to the orientation of the cross-plyed fibers, that is, symmetrical (0, 0), (0, 90) and symmetrical (0, 45), (45, 45).

Due to the locally resolved tensile stresses which occur at a microscale, river marks and resin microflow can often be seen on the hackles and scallops.

As with the interlaminar Mode I tension fractures, elevated temperatures and absorbed moisture present during fracture do not alter the ability to define fracture mode. Cracking also tends to occur interlaminarly with a more fiber dominated appearance as compared to room temperature dry fractures.

See Figures 6-30 through 6-46.

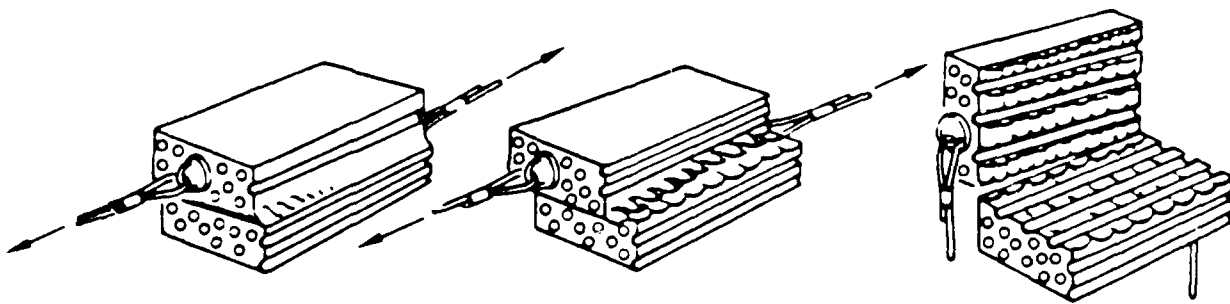


Figure 6-29. End-Notched Flexural Test Type

Optical photomicrographs

Fracture type	Interlaminar mode II shear
Ply layup	[0] ₂₄
Test type	ENF
• Test conditions	21°C dry
• Fracture between	0/0 plies
Material	Hercules 3501-6/177°C cure AS4 fibers

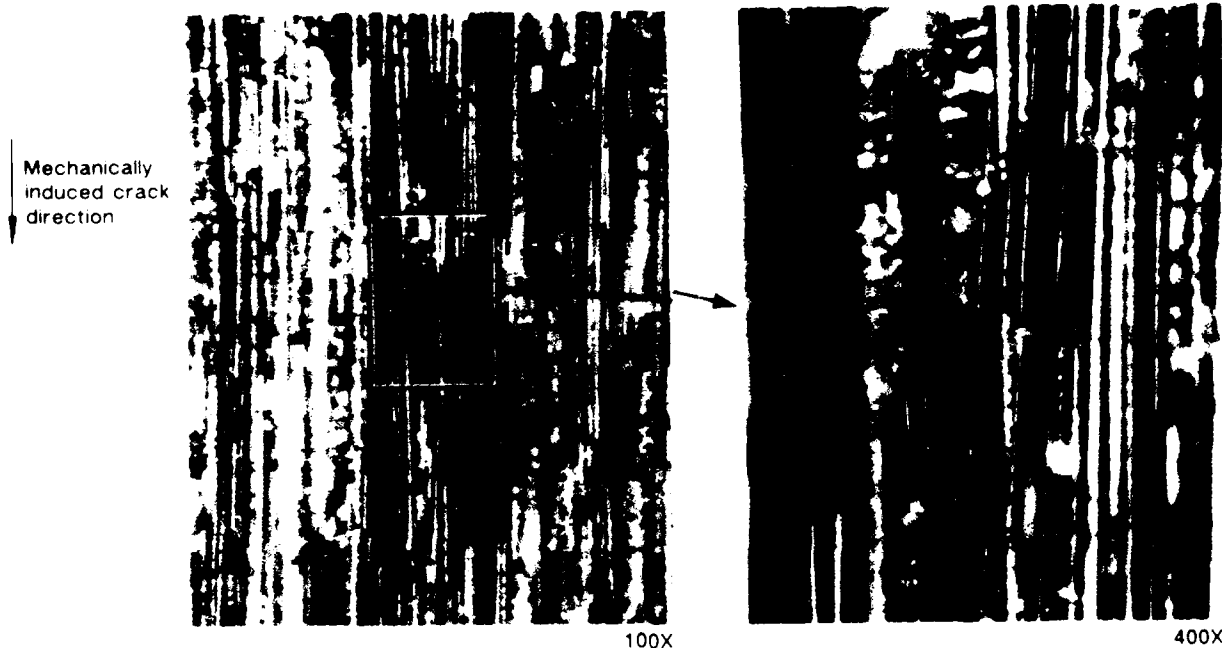
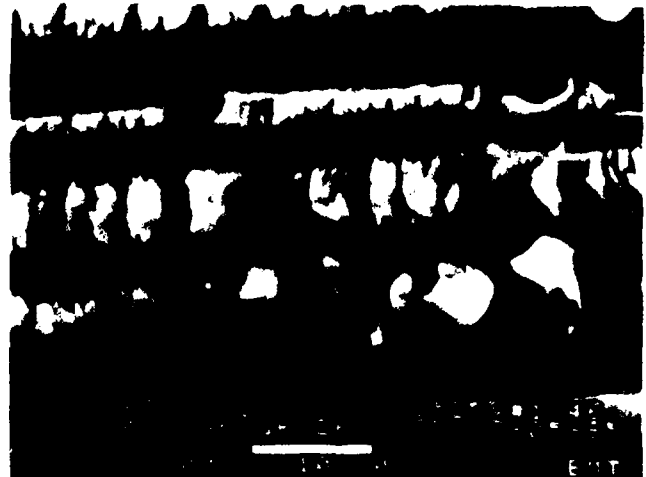
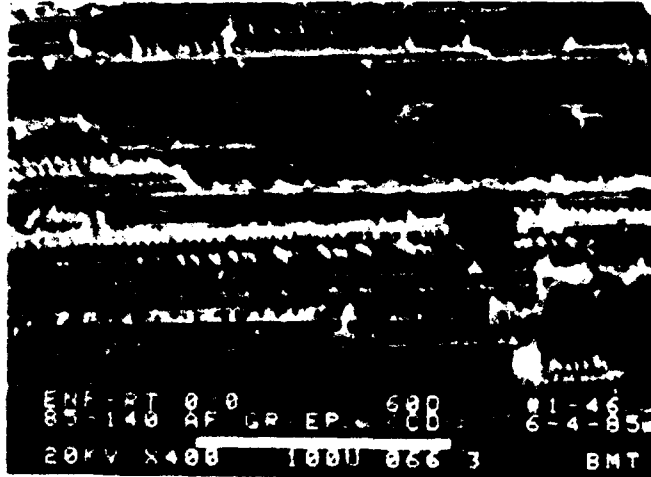


Figure 6-30. 0/0 Plies at 21°C Dry Condition (Optical 100X and 400X)

5-B70227-210

SEM photomicrographs

Fracture type	Interlaminar mode II shear
Ply layup	[0] 24
Test type	ENF
• Test conditions	21°C. dry
• Fracture between	0/0 plies
Material	Hercules 3501-6/177° C cure AS4 fibers



←
Mechanically induced crack direction

Legend:

- F Fiber matrix separation
- H Hackles
- R River markings
- T Textured microflow

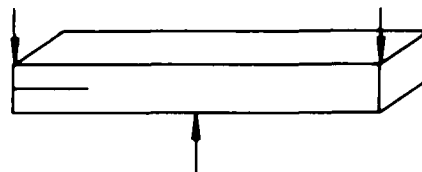


Figure 6-31. 0/0 Plies at 21°C Dry Condition With Fiber Separation, River Marks, Hackles, and Textured Microflow

5-B70227-213

Optical photomicrographs

Fracture type	Interlaminar mode II shear
Ply layup	[0, 0] ₁₂ S
Test type	ENF
• Test conditions	Dry/wet
• Fracture between	0/0 plies
Material	Hercules 3501-6/177° C cure AS4 fibers



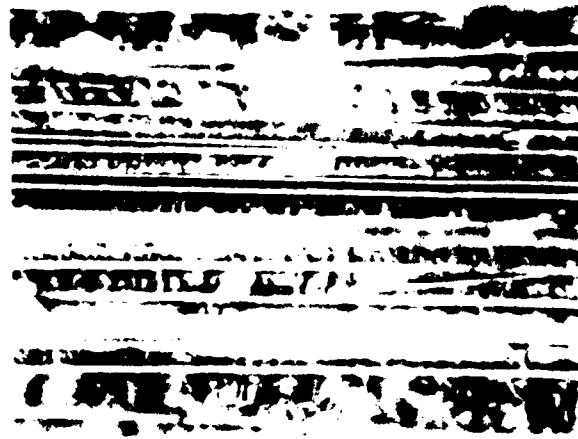
Mechanically induced crack direction



70°F, wet



180°F, dry



180°F, wet

Figure 6-32. 0/0 Plies at 70°F Wet, 180°F Dry, and 180°F Wet Conditions
(Optical 400X)

5-B70227-211

Optical photomicrographs

Fracture type	Interlaminar mode II shear
Ply layup	[0] 24
Test type	ENF
• Test conditions	Dry
• Fracture between	0/0 plies
Material	Hercules 3501-6/177° C cure AS4 fibers



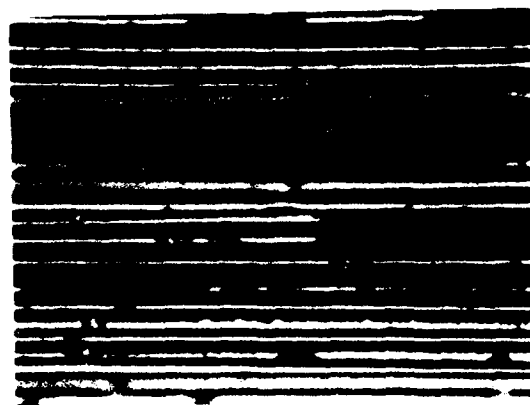
Mechanically induced crack direction



-65°F. dry



70°F. dry



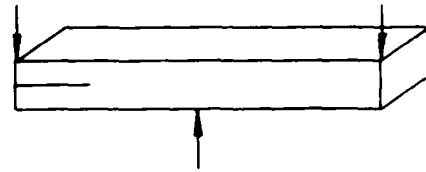
270°F. dry

Figure 6-33. 0/0 Plies at -65°F Dry, 70°F Dry, and 270°F Dry Conditions
(Optical 400X)

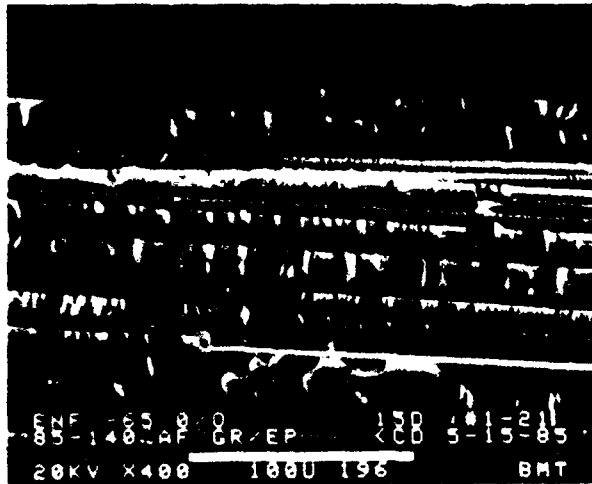
5-B70227-212

SEM photomicrographs

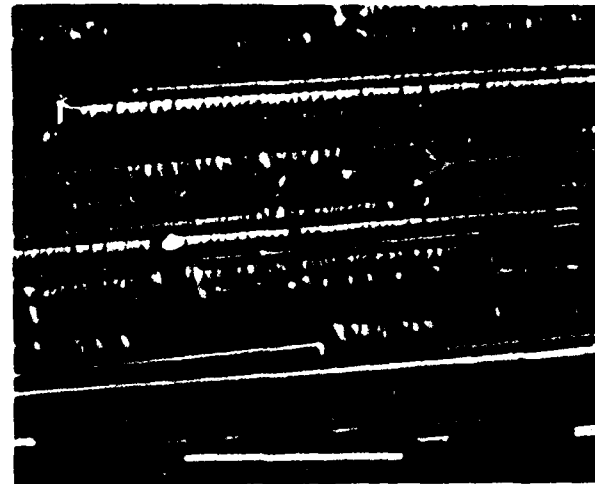
Fracture type	Interlaminar mode II shear
Ply layup	[0] ₂₄
Test type	ENF
• Test conditions	Dry
• Fracture between	0/0 plies
Material	Hercules 3501-6/177° C cure AS4 fibers



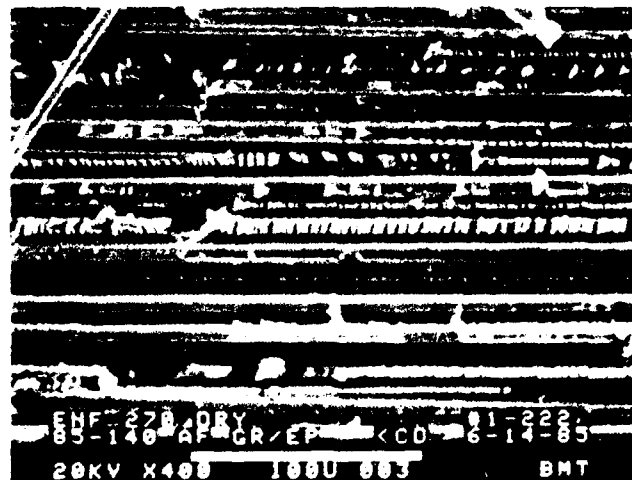
Mechanically induced crack direction



-65°F. dry



70°F. dry



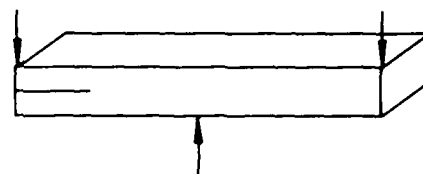
270°F. dry

Figure 6-34. 0/0 Plies at -65°F Dry, 70°F Dry, and 270°F Dry Conditions (SEM 400X)

5-B70227-214

SEM photomicrographs

Fracture type	Interlaminar mode II shear
Ply layup	[0] 24
Test type	ENF
• Test conditions	Wet
• Fracture between	0/0 plies
Material	Hercules 3501-6/177° C cure AS4 fibers



←
Mechanically induced crack direction



70°F, wet



180°F, wet

Legend:

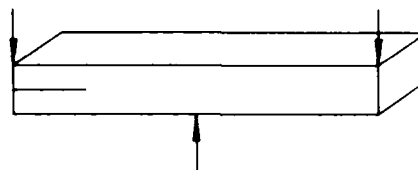
- F Fiber matrix separation
- H Hackles

Figure 6-35. 0/0 Plies at 70°F Wet and 180°F Wet Conditions With Fiber Separation and Hackles

5-B70227-215

SEM photomicrographs

Fracture type	Interlaminar mode II shear
Ply layup	[0] 24
Test type	ENF
• Test conditions	Dry
• Fracture between	0/0 plies
Material	Hercules 3501-6/177°C cure AS4 fibers



-65°F. dry



70°F. dry

←
Mechanically induced crack direction



270°F. dry

Legend:

- F Fiber matrix separation
- H Hackles

Figure 6-36. 0/0 Plies at -65°F Dry, 70°F Dry, and 270°F Dry Conditions With Fiber Separation and Hackles

5-B70227-216

Optical photomicrographs

Fracture type	Interlaminar mode II shear
Ply layup	[+45/-45] _{12S}
Test type	ENF
• Test conditions	21°C, dry
• Fracture between	+45/-45 plies
Material	Hercules 3501-6/177°C cure AS4 fibers

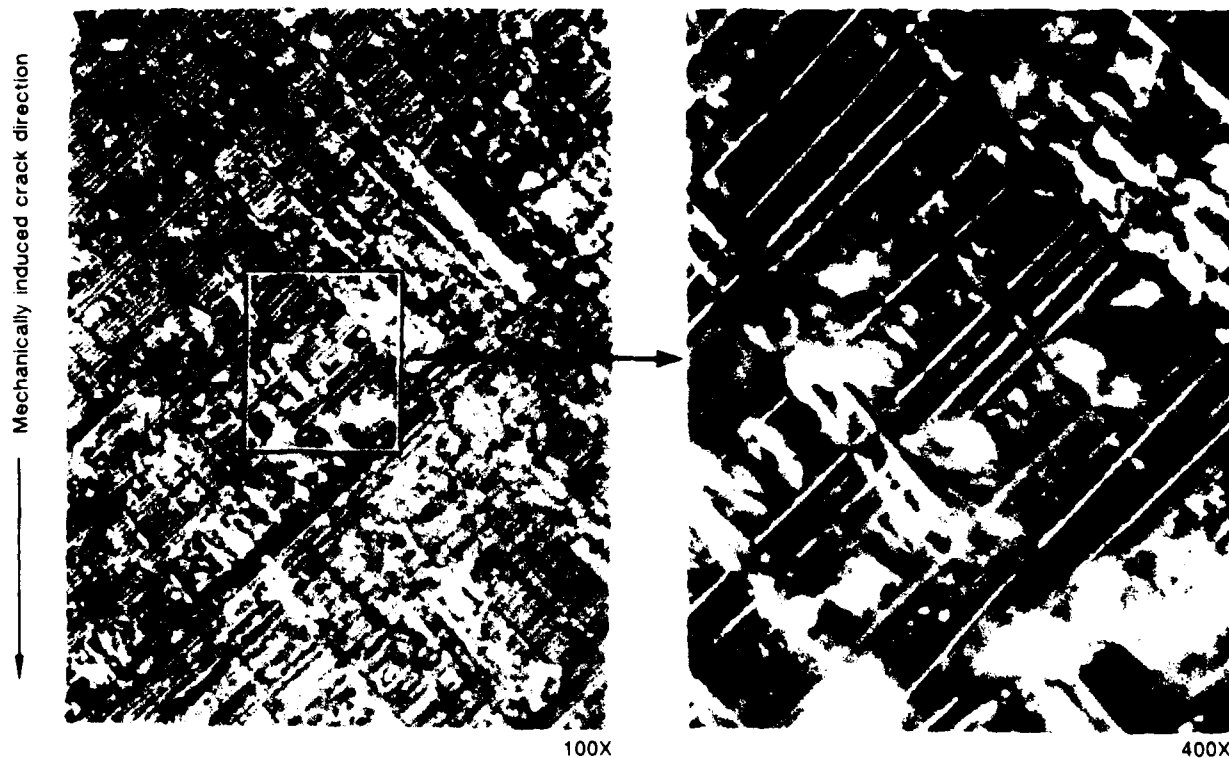
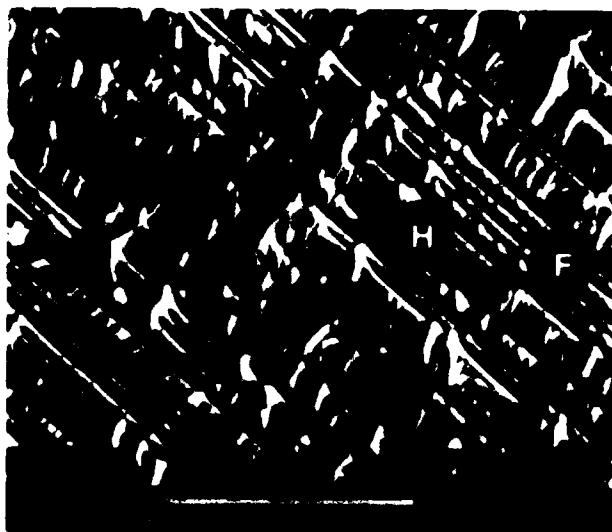


Figure 6-37. +45/-45 Plies at 21°C Dry Condition (Optical 100X and 400X)

5-B700227-217

SEM photomicrographs

Fracture type	Interlaminar mode II shear
Ply layup	[+45/-45] 12S
Test type	ENF
• Test conditions	21°C, dry
• Fracture between	+45/-45 plies
Material	Hercules 3501-6/177°C cure AS4 fibers



←
Mechanically induced crack direction



Legend:

- F Fiber matrix separation
- H Hackles
- R River markings

Figure 6-38 +45/-45 Plies at 21°C Dry Condition With Fiber Separation, River Marks, and Hackles

6-B70227R1-218

Optical photomicrographs

Fracture type	Interlaminar mode II shear
Ply layup	[+45/-45] 12S
Test type	ENF
• Test conditions	Dry
• Fracture between	+45/-45 plies
Material	Hercules 3501-6/177°C cure AS4 fibers



-65°F, dry

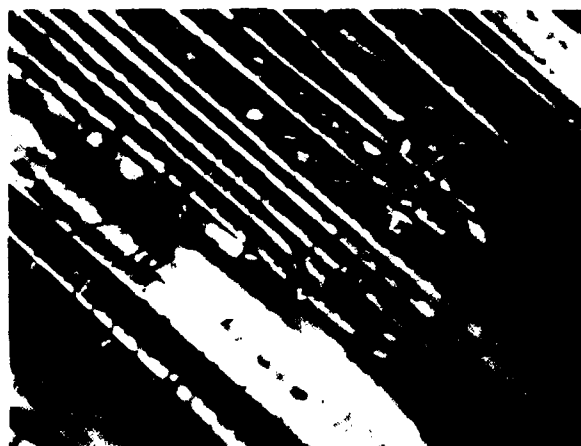
400X



70°F, dry

400X

Mechanically induced crack direction →



270°F, dry

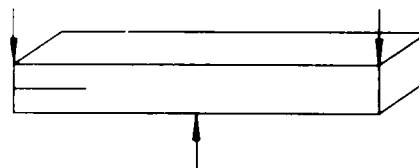
400X

Figure 6-39. +45/-45 Plies at -65°F Dry, 70°F Dry, and 270°F Dry Conditions (Optical 400X)

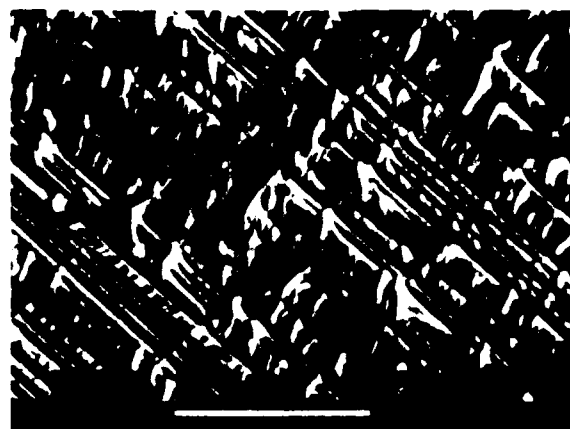
5-B70227-219

SEM photomicrographs

Fracture type	Interlaminar mode II shear
Ply layup	[+45, -45] _{12S}
Test type	ENF
• Test conditions	Dry
• Fracture between	+45/-45 plies
Material	Hercules 3501-6/177°C cure AS4 fibers

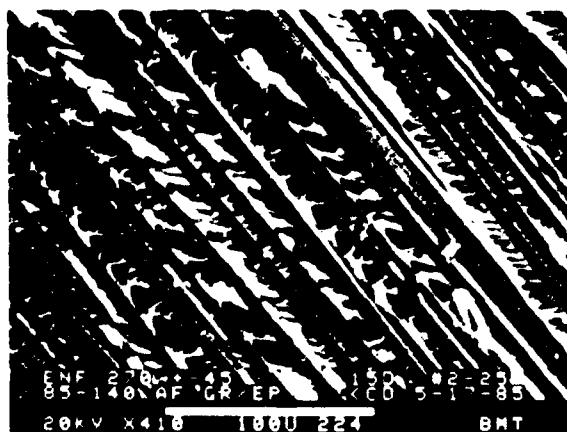


-65°F, dry



70°F, dry

Mechanically induced crack direction



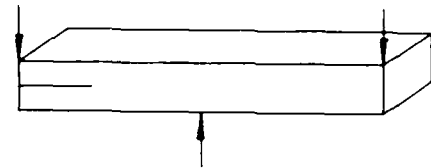
270°F, dry

Figure 6-40. +45/-45 Plies at -65°F Dry, 70°F Dry, and 270°F Dry Conditions (SEM 400X)

5-B70227-220

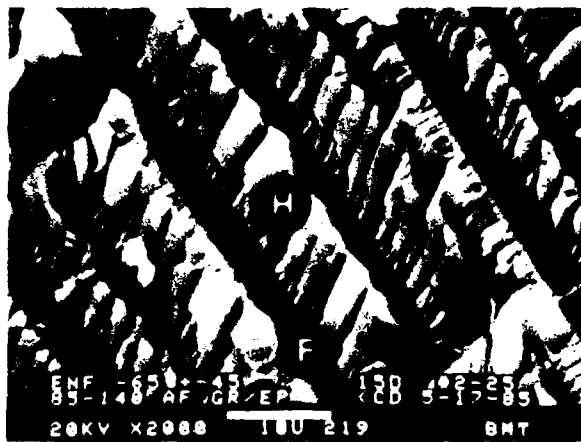
SEM photomicrographs

Fracture type	Interlaminar mode II shear
Ply layup	[+45/-45] 12S
Test type	ENF
• Test conditions	Dry
• Fracture between	+45/-45 plies
Material	Hercules 3501-6/177°C cure AS4 fibers



Legend:

F Fiber matrix separation
H Hackles



-65°F, dry



70°F, dry

← Mechanically induced crack direction



270°F, dry

Figure 6-41. +45/-45 Plies at -65°F Dry, 70°F Dry, and 270°F Dry Conditions (SEM 2000X)

5-B70227-221

Optical photomicrographs

Fracture type	Interlaminar mode II shear
Ply layup	[0, 45] ₁₂ S
Test type	ENF
• Test conditions	21°C, dry
• Fracture between	0/45 plies
Material	Hercules 3501-6/177°C cure AS4 fibers

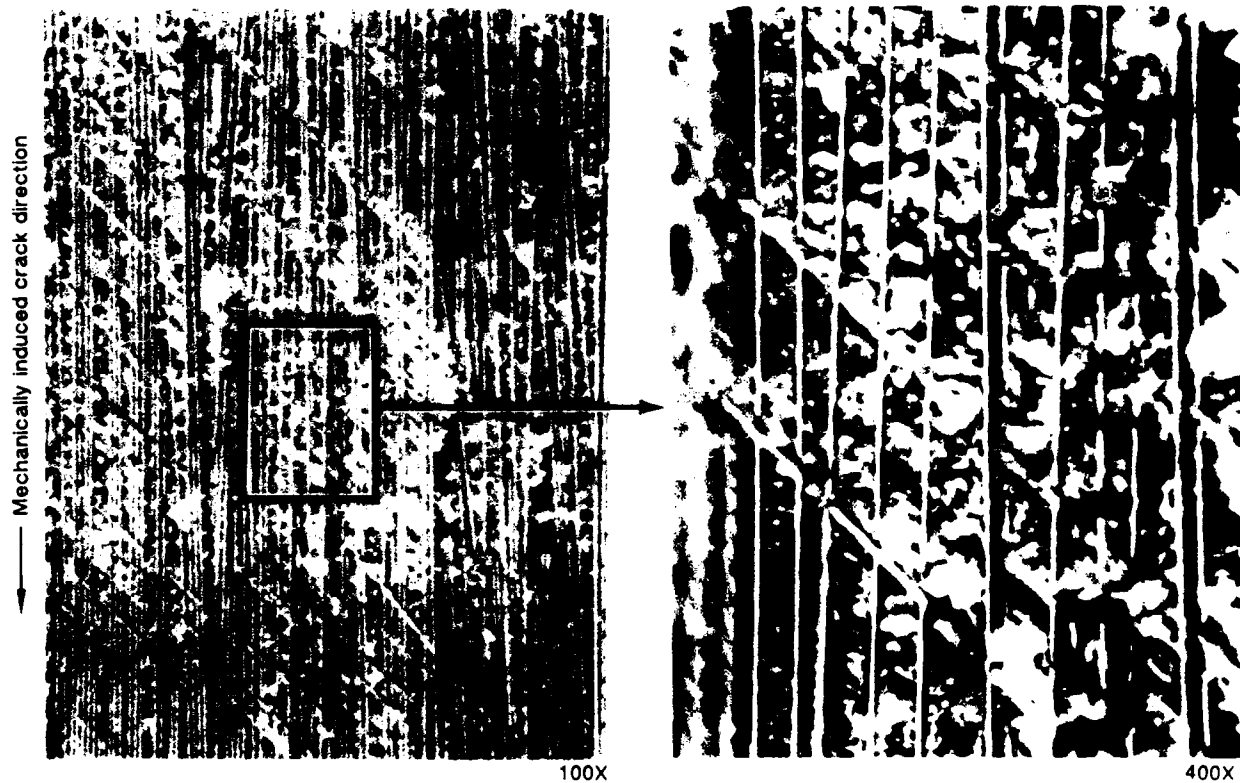
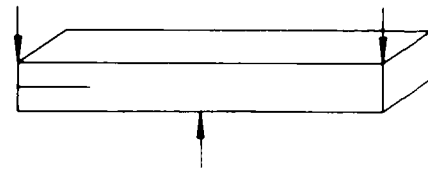
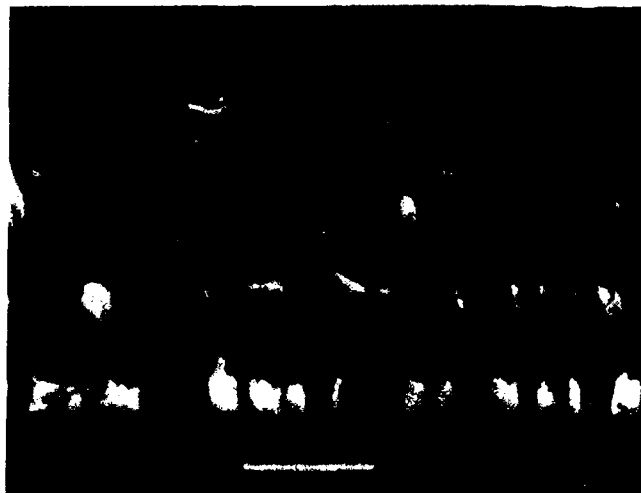
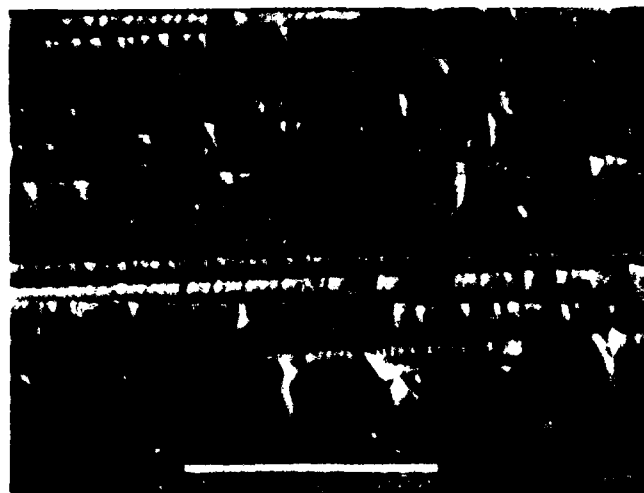
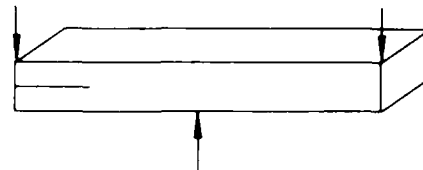


Figure 6-42. 0/45 Plies at 21°C Dry Condition (Optical 100X and 400X)

5-B70227-222

SEM photomicrographs

Fracture type	Interlaminar mode II shear
Ply layup	[0, 45] ₁₂ S
Test type	ENF
• Test conditions	RT
• Fracture between	0/45 plies
Material	Hercules 3501-6/177°C cure AS4 fibers



Mechanically induced crack direction



Legend:

- F Fiber matrix separation
- H Hackles
- R River markings
- T Textured microflow



Figure 6-43. 0/45 Plies With Fiber Separation, River Marks, Hackles, and Textured Microflow

5-B70227-223

Optical photomicrographs

Fracture type	Interlaminar mode II shear
Ply layup	[0, 90] _{12S}
Test type	ENF
• Test conditions	21°C, dry
• Fracture between	0/90 plies
Material	Hercules 3501-6/177°C cure AS4 fibers

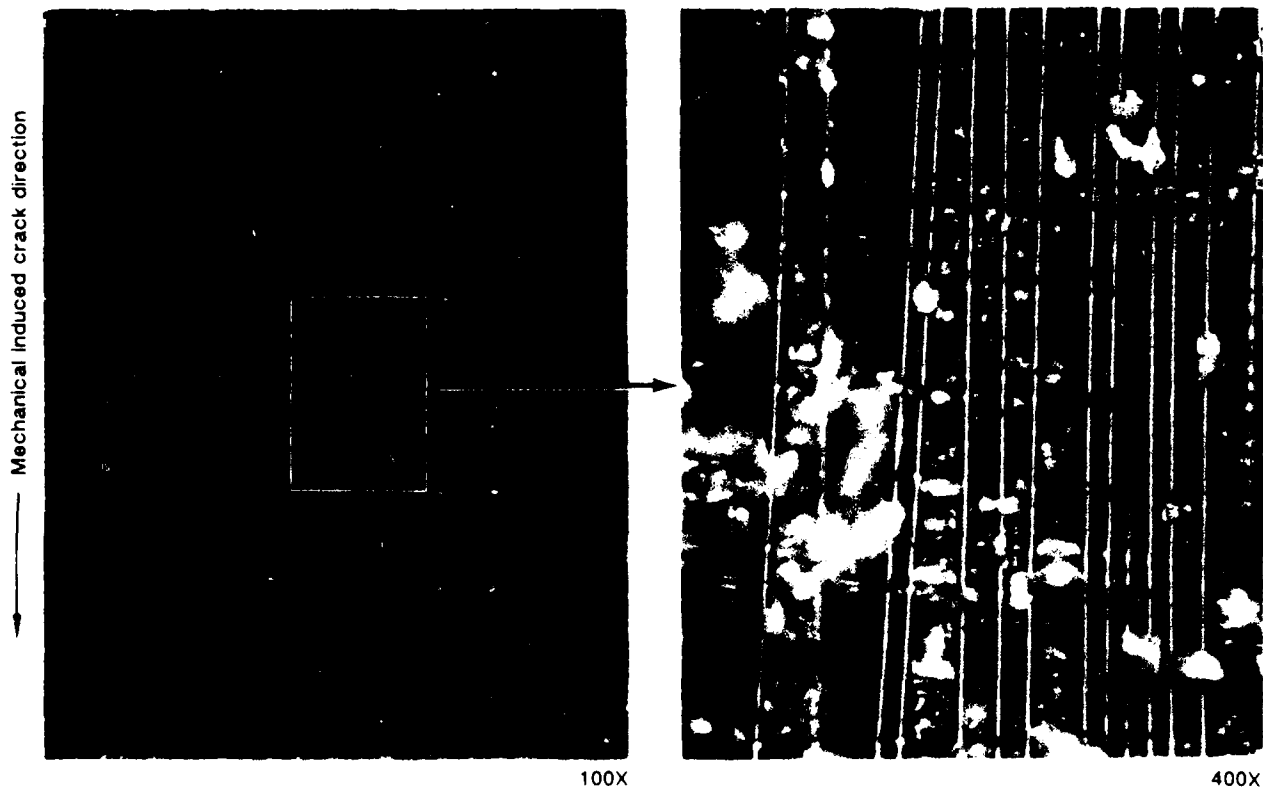


Figure 6-44. 0/90 Plies at 21°C Dry Condition (Optical 100X and 400X)

5-B70227-225

Optical photomicrographs

Fracture type	Interlaminar mode II shear
Ply layup	[90] 24
Test type	ENF
• Test conditions	21°C, dry
• Fracture between	90/90 plies
Material	Hercules 3501-6/177°C cure AS4 fibers

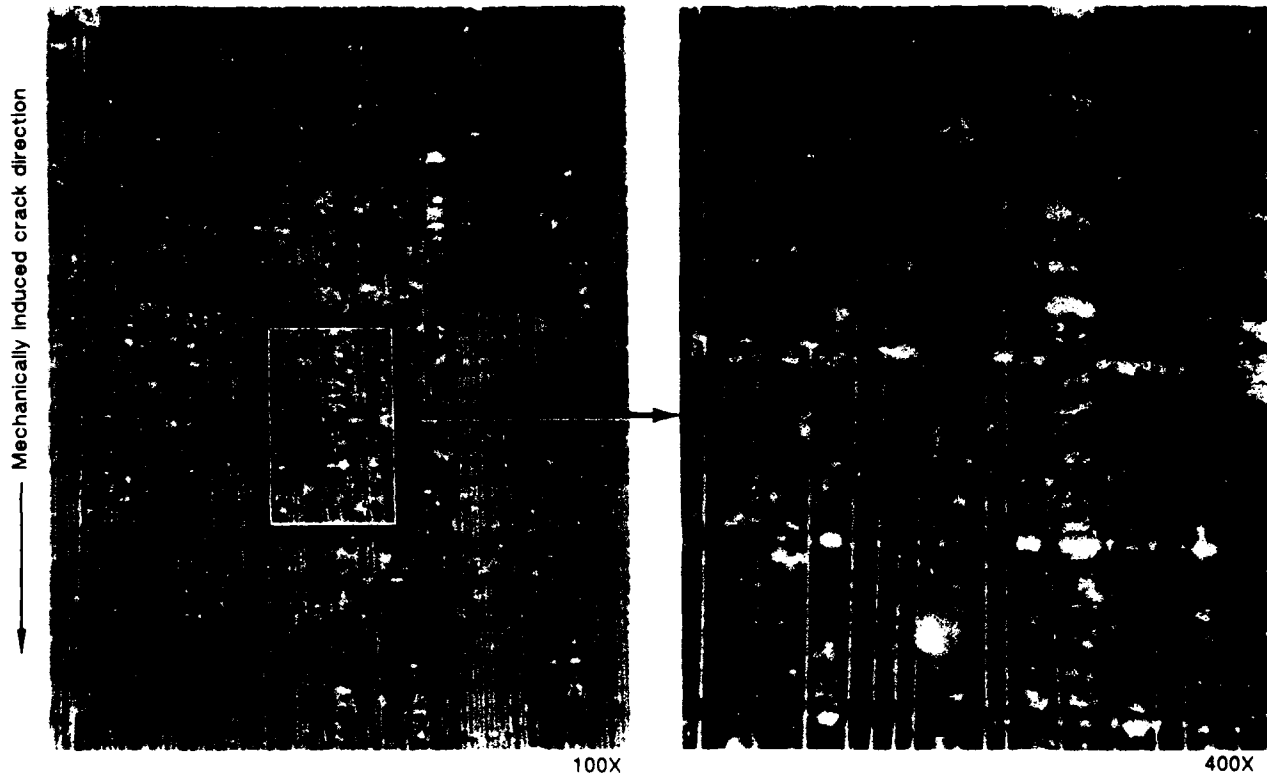
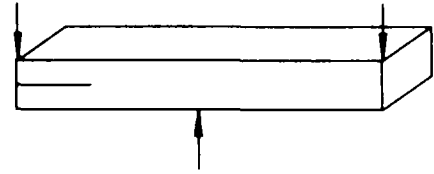
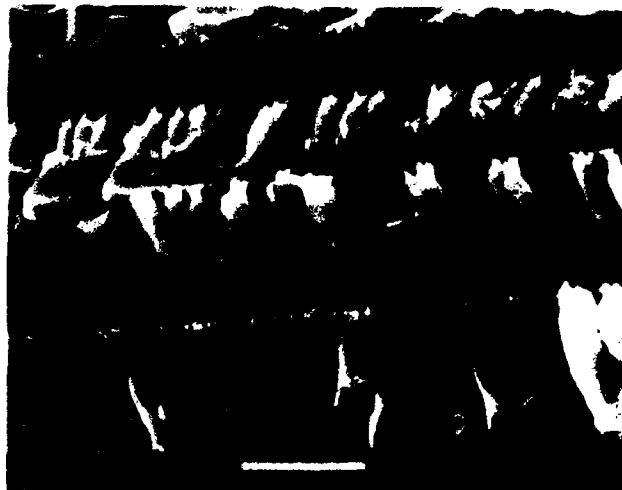
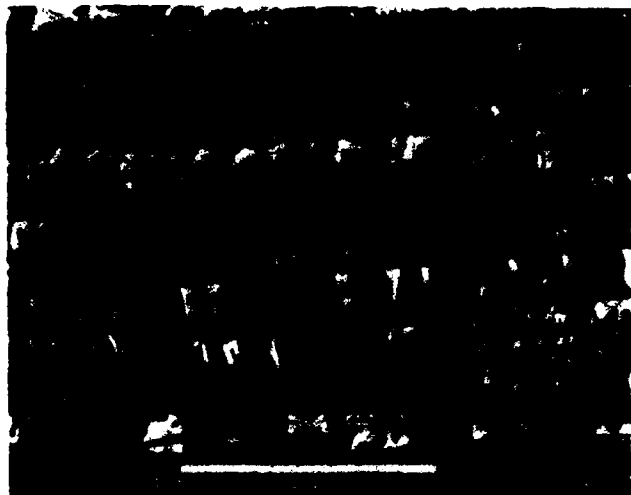
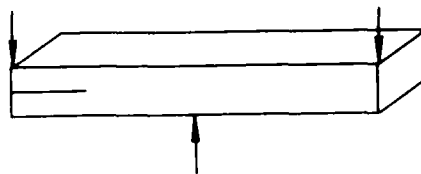


Figure 6-45. 90/90 Plies at 21°C Dry Condition (Optical 100X and 400X)

6-B70227R1-226

SEM photomicrographs

Fracture type	Interlaminar mode II shear
Ply layup	[90] 24
Test type	ENF
• Test conditions	21°C, dry
• Fracture between	90/90 plies
Material	Hercules 3501-6/177°C cure AS4 fibers



Mechanically induced crack direction



Legend:

- F Fiber matrix separation
- H Hackles
- R River markings



Figure 6-46. 90/90 Plies at 21°C Dry Condition With Fiber Separation River Marks and Hackles

5-B70227-227

6.3 INTERLAMINAR MIXED MODE FLEXURAL

Figure 6-47 shows the test matrix for the Mixed Mode Flexural (MMF) test type.

The MMF test geometry produces 57 percent Mode I tension and 43 percent Mode II shear at the crack tip. The primary features observed are quite similar to those found in 100 percent Mode II shear fracture presented in the previous paragraph; the features are listed as follows:

- Macroscopically flat surface.
- Microscopically rough resin fracture with a predominance of hackles and scallops.
- Small localized regions of flat resin fracture exhibiting only river marks and resin microflow.

A large amount of fiber bridging tends to occur in which delaminations are actually occurring, both coincident with and opposite to, the direction of crack growth. As a result, the determination of crack growth direction is limited to examining the direction of hackle tilt similar to the 100 percent Mode II shear specimens.

See Figures 6-48 through 6-51.

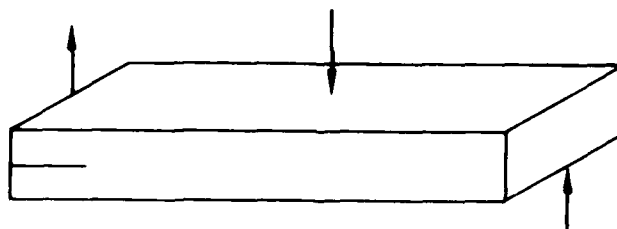
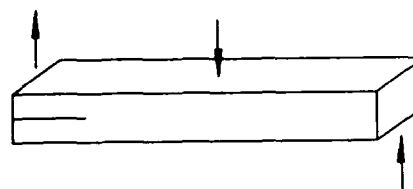


Figure 6-47. Mixed Mode Flexural Test Type

5-B70227-228

SEM photomicrographs

Fracture type	Interlaminar mixed mode (I and II)
Ply layup	[0] 24
Test type	Mixed mode flexure (MMF)
• Test conditions	21°C, dry
• Fracture between	0/0 plies
Material	Hercules 3501-6/177°C cure AS4 fibers



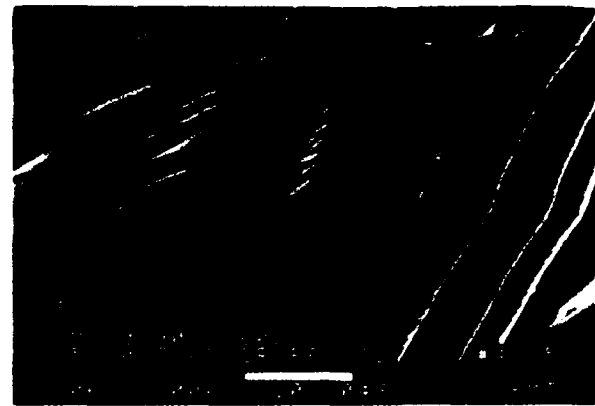
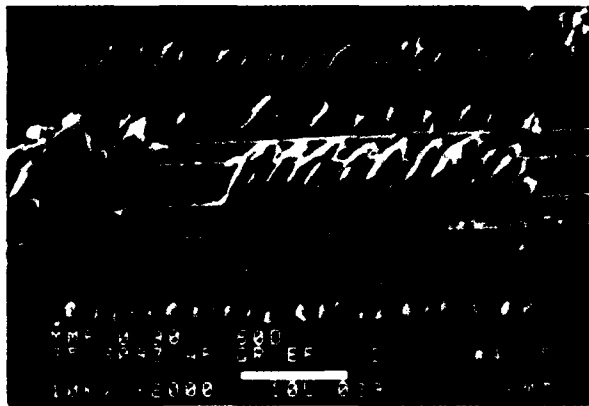
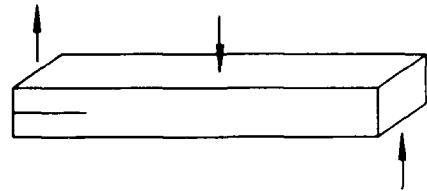
←
Mechanically induced crack direction

Figure 6-48. 0/0 Plies at 21°C Dry Condition (SEM 2000X)

5-B70227-229

SEM photomicrographs

Fracture type	Interlaminar mixed mode (I and II)
Ply layup	[0, 90] ₁₂ S
Test type	Mixed-mode flexure (MMF)
• Test conditions	21°C, dry
• Fracture between	0/90 plies
Material	Hercules 3501-6/177°C cure AS4 fibers



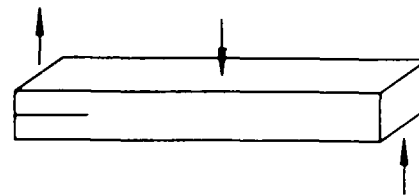
← Mechanically induced crack direction

Figure 6-49. 0/90 Plies at 21°C Dry Condition (SEM 2000X)

5-B70227-230

Optical photomicrographs

Fracture type	Interlaminar mixed mode (I and II)
Ply layup	[+45, -45] 12S
Test type	Mixed-mode flexure (MMF)
• Test conditions	21°C, dry
• Fracture between	+45/-45 plies
Material	Hercules 3501-6/177°C cure AS4 fibers



Mechanically induced crack direction

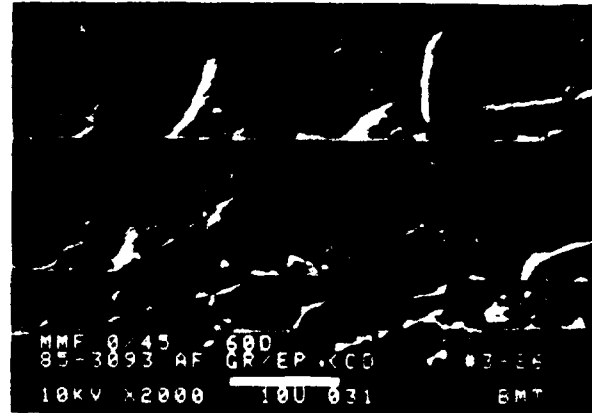
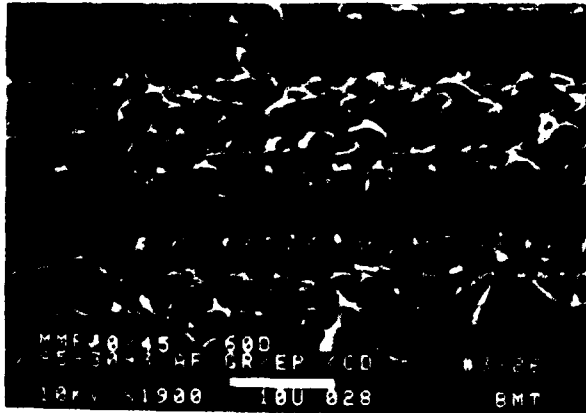
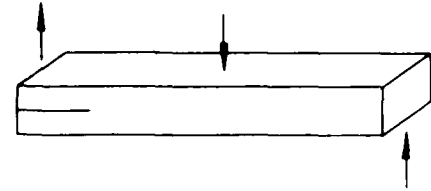


Figure 6-50. +45/-45 Plies at 21°C Dry Condition (SEM 2000X)

5-B70227-231

SEM photomicrographs

Fracture type	Interlaminar mixed mode (I and II)
Ply layup	[0, 45] _{12S}
Test type	Mixed-mode flexure (MMF)
• Test conditions	21°C, dry
• Fracture between	0/45 plies
Material	Hercules 3501-6/177°C cure AS4 fibers



←
Mechanically induced crack direction

Figure 6-51. 0/45 Plies at 21°C Dry Condition (SEM 1900X and 2000X)

5-B70227-232

6.4 TRANSLAMINAR MODE I TENSION

Figure 6-52 shows the test matrix for a tension four-point bend test type.

The primary features observed in translaminar fracture surfaces generated by Mode I tension are as follows:

- Macroscopically rough fracture surface.
- Fibers protruding from the surface (fiber pullout) at a wide variety of heights.
- Radial feature on each fiber end.
- Fractured resin on sides of fibers, ranging from shear dominated hackle morphology to a very smooth nearly adhesive fracture.

During the fracture process an individual fiber will break, leading to fracture of adjacent fibers. This process continues at various planes throughout the laminate, resulting in a rough surface and groups of fibers or bundles. Close inspection of the fiber ends (using SEM) reveals a radiating pattern indicative of the fracture direction for each individual fiber. Inspection of the fiber ends at several locations along the fracture surface is required to determine the overall crack growth directions. For laminates with a wide variety of ply orientations, the fibers which are oriented 90 degrees to the fracture plane should be examined to obtain the best resulting reliability. When plies with fibers oriented parallel to the fracture plane are present, inspection of the intralaminar river marks may also be used to determine crack growth direction.

See Figures 6-53 through 6-66.

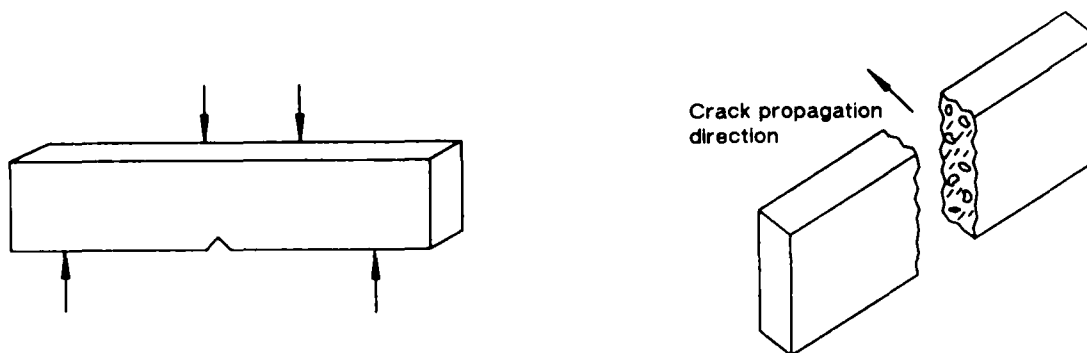
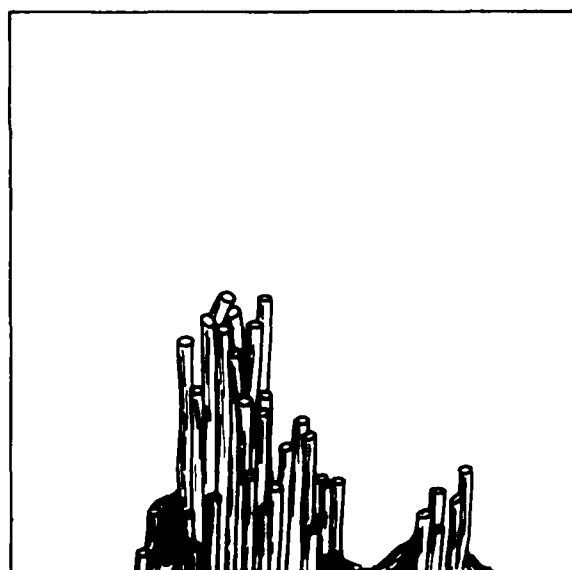
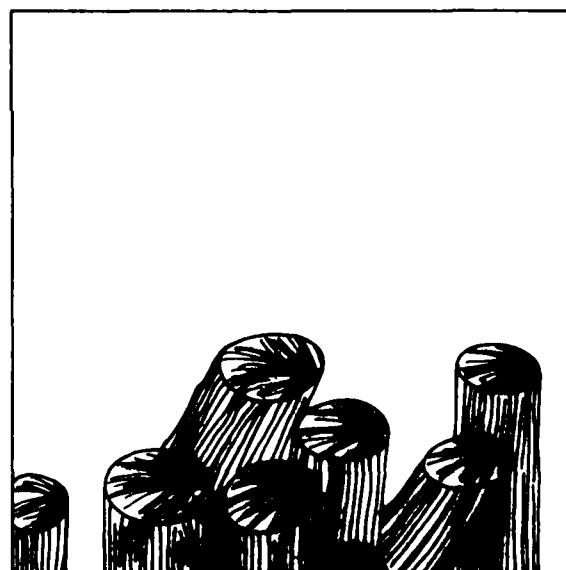


Figure 6-52. Four-Point Bend Test Type Tension

6-B70227-289



Low magnification



High magnification

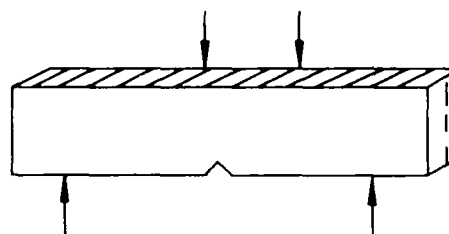
←
Overall crack growth direction

Figure 6-53. Fracture of Adjacent Files

5-B70227-224

SEM photomicrographs

Fracture type	Translaminar mode I tension
Ply layup	[0, 90] 16S
Test type	Four-point bend
• Test conditions	Dry
• Fiber end fracture	
Material	Hercules 3501-6/177°C cure AS4 fibers



-65°F, dry



180°F, dry

← Mechanically induced crack direction



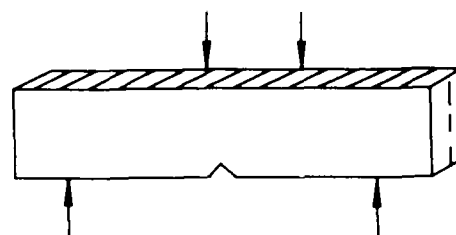
270°F, dry

Figure 6-54. 0/90 Plies at -65°F Dry, 180°F Dry, and 270°F Dry Conditions (SEM Low Magnification)

5-B70227-196

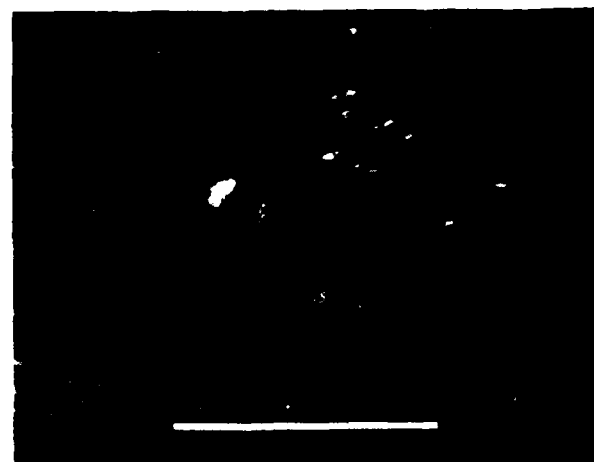
SEM photomicrographs

Fracture type	Translaminar mode I tension
Ply layup	[+45, -45] 16S
Test type	Four-point bend
• Test conditions	Wet
• Fiber end fracture	
Material	Hercules 3501-6/177°C cure AS4 fibers



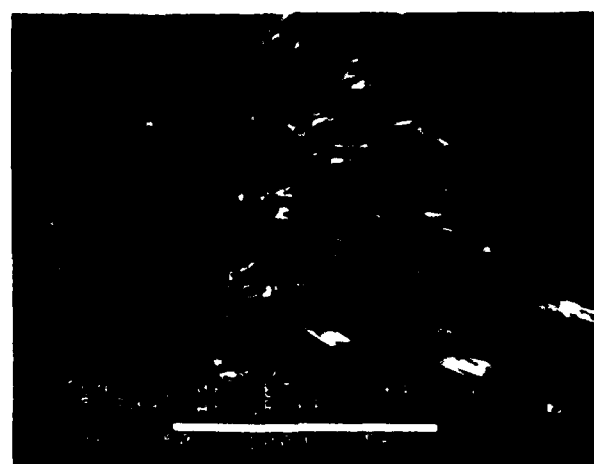
70°F. wet

← Mechanically induced crack direction



180°F. wet

← Mechanically induced crack direction



270°F. wet

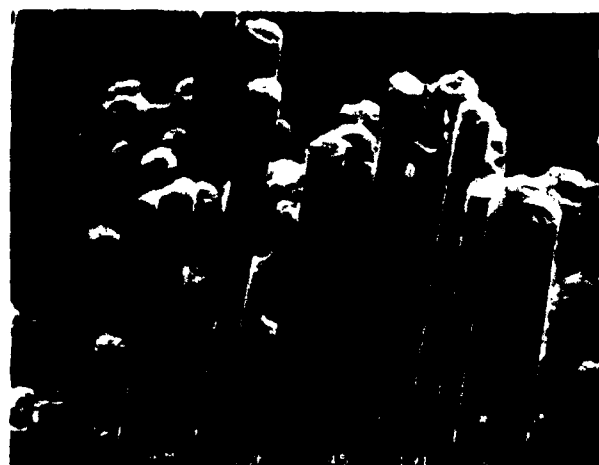
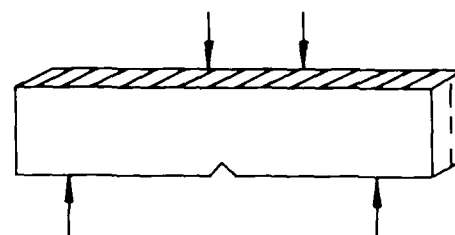
→ Mechanically induced crack direction

Figure 6-55. +45/-45 Plies at 70°F Wet, 180°F Wet, and 270°F Wet Conditions (SEM 50X)

5-B70227-197

SEM photomicrographs

Fracture type	Translaminar mode I tension
Ply layup	[0, 90] _{16S}
Test type	Four-point bend
• Test conditions	82°C, dry
• Fiber end fracture	
Material	Hercules 3501-6/177°C cure AS4 fibers



Mechanically induced crack direction

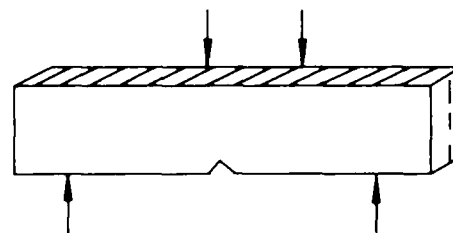


Figure 6-56. 0/90 Plies at 82°C Dry Condition (Various SEM Magnification)

5-B70227-198

SEM photomicrographs

Fracture type	Translaminar mode I tension
Ply layup	[0, 90] 16S
Test type	Four-point bend
• Test conditions	Dry
• Fiber end fracture	
Material	Hercules 3501-6/177°C cure AS4 fibers

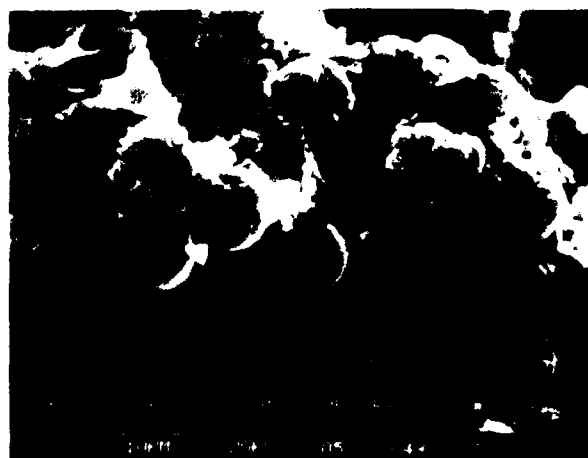


-65°F, dry



180°F, dry

Mechanically induced crack direction



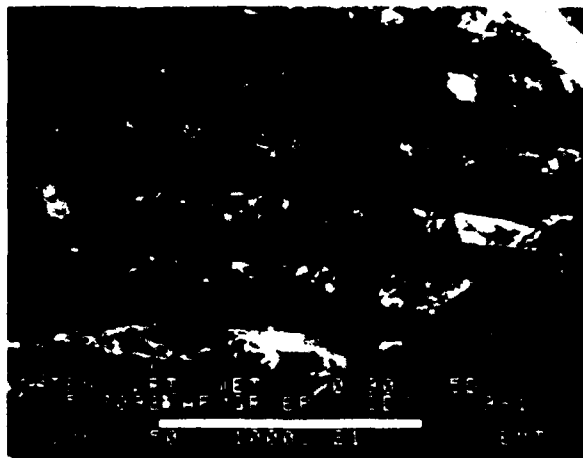
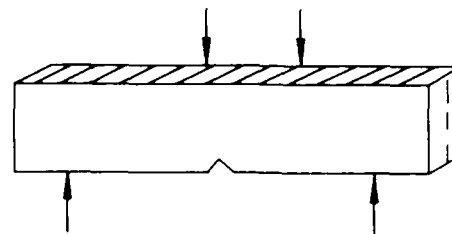
270°F, dry

Figure 6-57 0/90 Plies at -65°F Dry, 180°F Dry, and 270°F Dry Conditions (SEM)

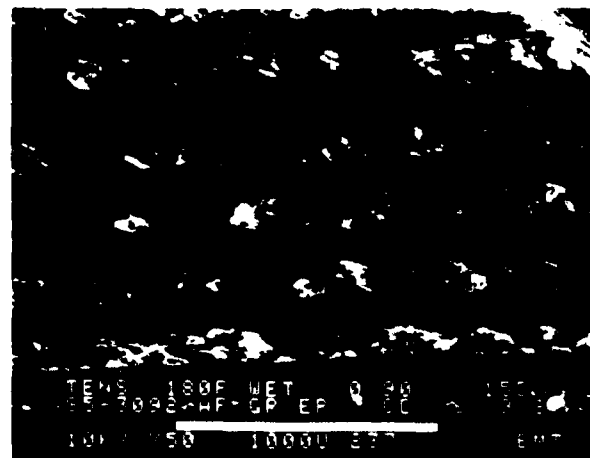
5-B70227-199

SEM photomicrographs

Fracture type	Translaminar mode I tension
Ply layup	[0, 90] _{16S}
Test type	Four-point bend
• Test conditions	Wet
• Fiber end fracture	
Material	Hercules 3501-6/177°C cure AS4 fibers

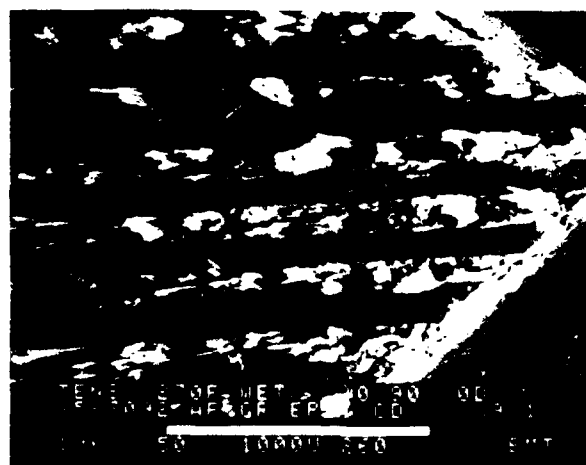


70°F, wet



180°F, wet

Mechanically induced crack direction



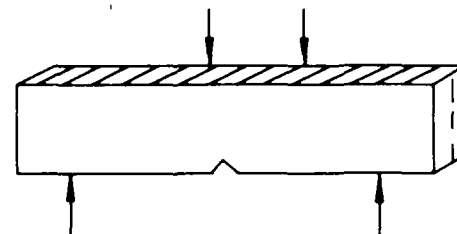
270°F, wet

Figure 6-58. 0/90 Plies at 70°F Wet, 180°F Wet, and 270°F Wet Conditions (SEM 50X)

5-B70227-200

SEM photomicrographs

Fracture type	Translaminar mode I tension
Ply layup	[0, 90] ₁₆ S
Test type	Four-point bend
• Test conditions	Wet
• Fiber end fracture	
Material	Hercules 3501-6/177°C cure AS4 fibers



70°F, wet



180°F, wet

← Mechanically induced crack direction



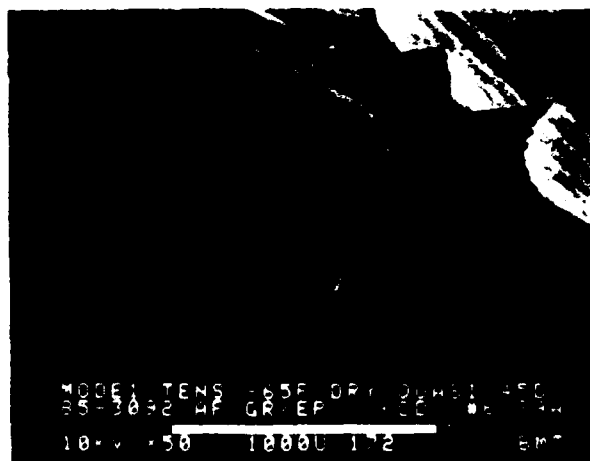
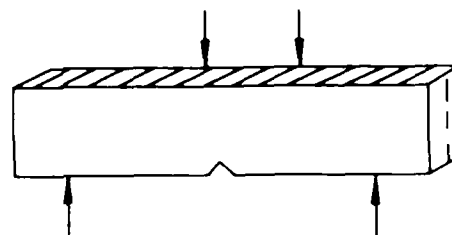
270°F, wet

Figure 6-59. 0/90 Plies at 70°F Wet, 180°F Wet, and 270°F Wet Conditions (SEM 2000X)

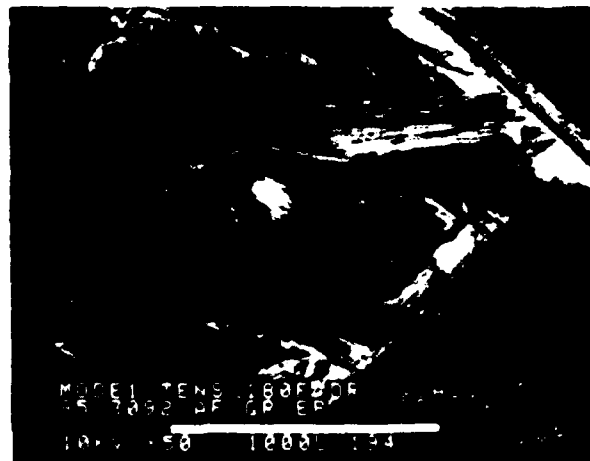
5-B70227-201

SEM photomicrographs

Fracture type	Translaminar mode I tension
Ply layup	[0, 45, 90] _{16S}
Test type	Four-point bend
• Test conditions	Dry
• Fiber end fracture	
Material	Hercules 3501-6/177°C cure AS4 fibers



-65°F, dry



180°F, dry

Mechanically induced crack direction



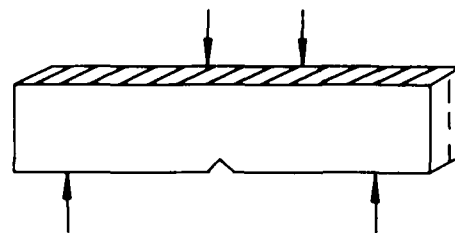
270°F, dry

5-B70227-202

Figure 6-60. 0/45/90 Plies at -65°F Dry, 180°F Dry, and 270°F Dry Conditions (SEM 50X)

SEM photomicrographs

Fracture type	Translaminar mode I tension
Ply layup	[0, 45, 90] ₁₆ S
Test type	Four-point bend
• Test conditions	Dry
• Fiber and fracture	
Material	Hercules 3501-6/177°C cure AS4 fibers

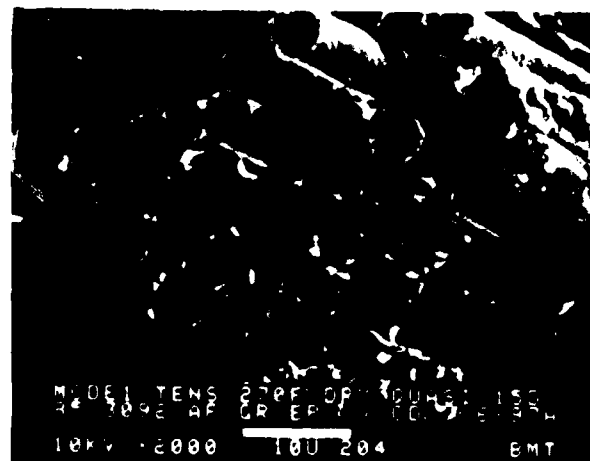


-65°F, dry



180°F, dry

Mechanically induced crack direction



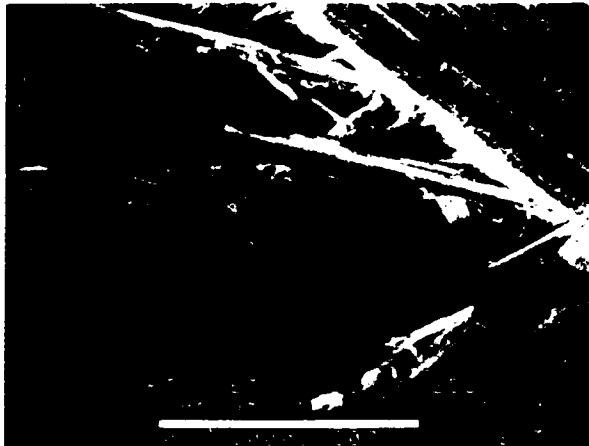
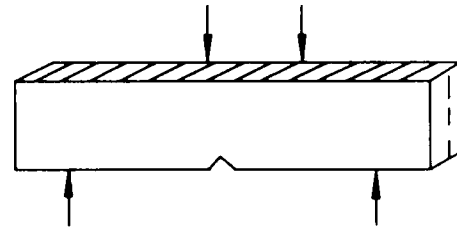
270°F, dry

Figure 6-61. 0/45/90 Plies at -65°F Dry, 180°F Dry, and 270°F Dry Conditions (SEM 2000X)

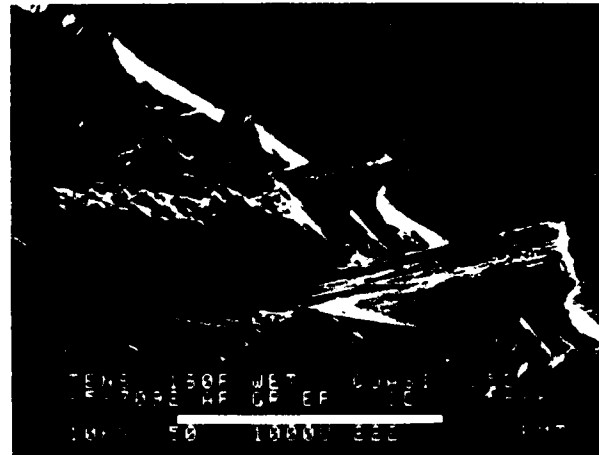
5-B70227-203

SEM photomicrographs

Fracture type	Translaminar mode I tension
Ply layup	[0, 45, 90] ₁₆ S
Test type	Four-point bend
• Test conditions	Wet
• Fiber end fracture	
Material	Hercules 3501-6/177°C cure AS4 fibers



70°F, wet



180°F, wet

← Mechanically induced crack direction



270°F, wet

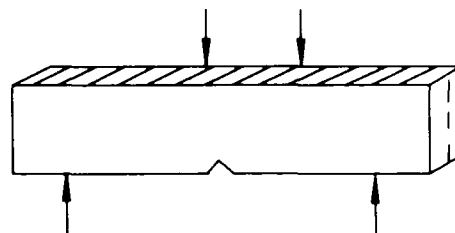
→ Mechanically induced crack direction

Figure 6-62. 0/45/90 Plies at 70°F Wet, 180°F Wet, and 270°F Wet Conditions (SEM 50X)

5-B70227-204

SEM photomicrographs

Fracture type	Translaminar mode I tension
Ply layup	[0, 45, 90] _{16S}
Test type	Four-point bend
• Test conditions	Wet
• Fiber end fracture	
Material	Hercules 3501-6/177°C cure AS4 fibers



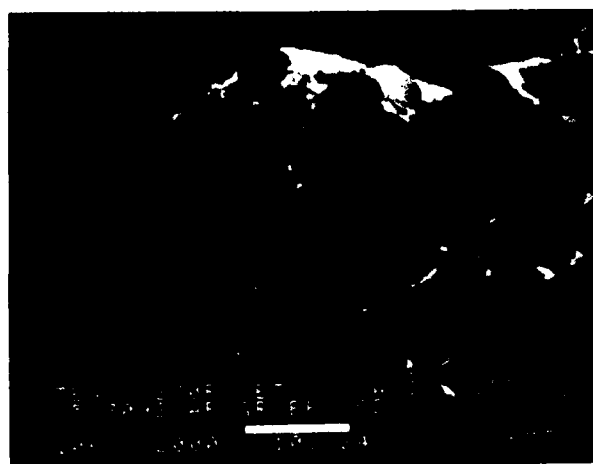
← Mechanically induced crack direction



70°F, wet



180°F, wet



270°F, wet

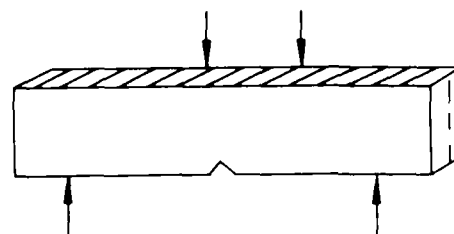
→ Mechanically induced crack direction

Figure 6-63. 0/45/90 Plies at 70°F Wet, 180°F Wet, and 270°F Wet Conditions (SEM 2000X)

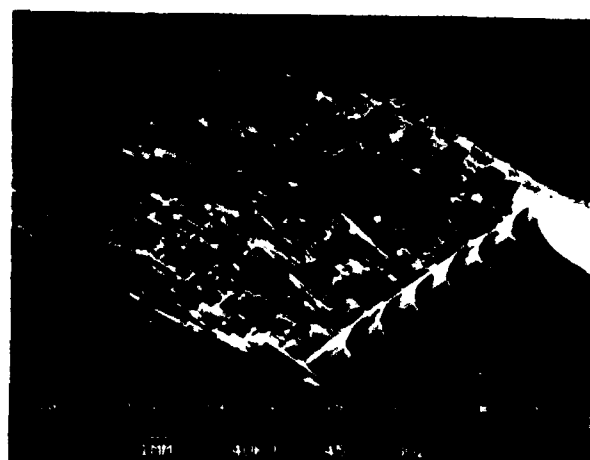
5-B70227-205

SEM photomicrographs

Fracture type	Translaminar mode I tension
Ply layup	[+45, -45] 16S
Test type	Four-point bend
• Test conditions	Dry
• Fiber end fracture	
Material	Hercules 3501-6/177°C cure AS4 fibers



-65°F, dry



180°F, dry

←
Mechanically induced crack direction



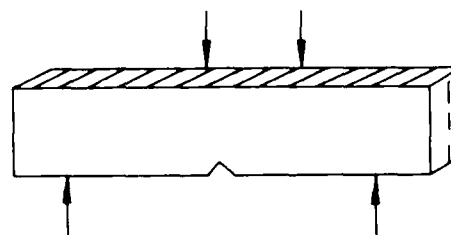
270°F, dry

Figure 6-64. +45/-45 Plies at -65°F Dry, 180°F Dry, and 270°F Dry Conditions (Fiber Pullout)

5-B70227-206

SEM photomicrographs

Fracture type	Translaminar mode I tension
Ply layup	[+45, -45] ₁₆ S
Test type	Four-point bend
• Test conditions	Dry
• Fiber end fracture	
Material	Hercules 3501-6/177°C cure AS4 fibers

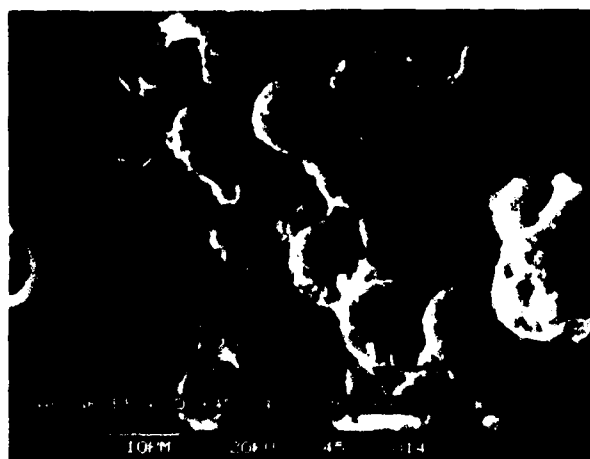


-65°F, dry



180°F, dry

←
Mechanically induced crack direction



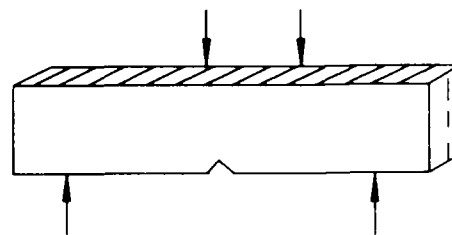
270°F, dry

Figure 6-65. +45/-45 Plies at -65°F Dry, 180°F Dry, and 270°F Dry Conditions (Fiber Breakage)

5-B70227-207

SEM photomicrographs

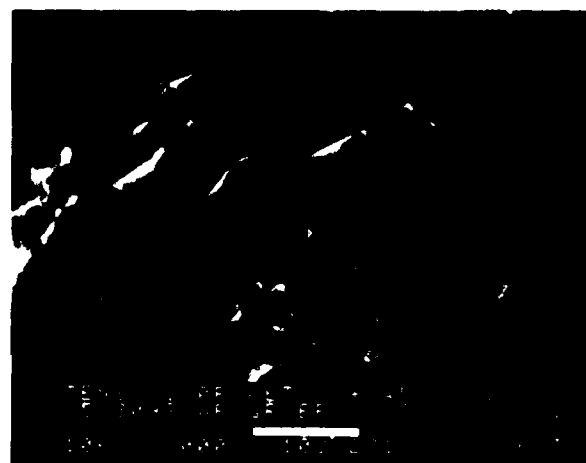
Fracture type	Translaminar mode I tension
Ply layup	[+45, -45] ₁₆ S
Test type	Four-point bend
• Test conditions	Wet
• Fiber end fracture	
Material	Hercules 3501-6/177°C cure AS4 fibers



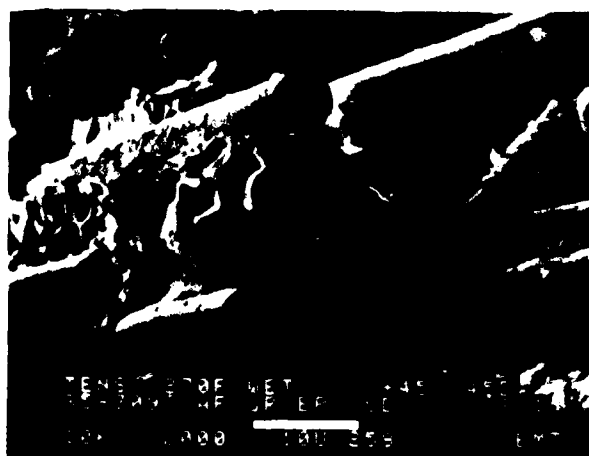
Mechanically induced crack direction



70°F, wet



180°F, wet



270°F, wet

Mechanically induced crack direction



Figure 6-66. +45/-45 Plies at 70°F Wet, 180°F Wet, and 270°F Wet Conditions (SEM 2000X)

5-B70227-208

6.5 TRANSLAMINAR MODE I COMPRESSION

Figure 6-67 shows the test matrix for compression four-point bend test type.

The primary features observed in translaminar fractures generated under Mode I compression are as follows:

- Macroscopically and microscopically flat fracture surface, particularly on plies oriented parallel to axial compression load.
- Fiber chop (short fiber segments).
- Fiber end flexural fracture exhibiting tension and compression features on each side of a neutral axis line.
- Post-failure damage due to rubbing contact between mating fracture surface.

(This last feature can often completely obscure the features normally found on individual fiber ends.)

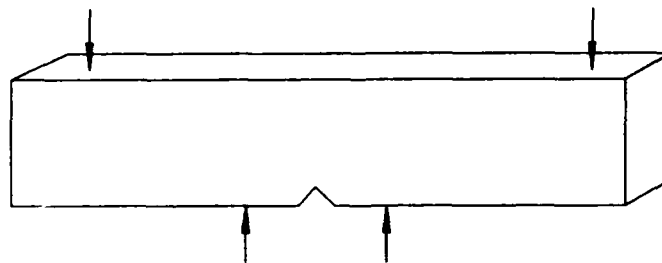


Figure 6-67. Four-Point Bend Test Type

5-B70227-233

Translaminar compression fractures occur by a combination of fiber microbuckling and delamination fractures. Examination of the fiber ends indicate a flexural fiber fracture.

Studies of these neutral axis lines have indicated that no direct correspondence to crack propagation is inferred. However, analysis of the delamination adjacent to the translaminar fracture may be used to identify crack growth direction if there is a predominance of Mode I tension during the fracture event.

Fractures produced at high temperatures and absorbed moisture content exhibit a rougher macroscopic fracture surface, with longer fiber chop and more secondary intralaminar shear cracks on the microscopic scale.

The reader should note that the low-magnification SEM photomicrographs reveal both compression fracture (flat) and tension fracture (fibers protruding). This is because the flexural nature of the test specimen, where cracking is initiated at the notch in compression. The high magnification photographs are from the compression fracture region.

See Figures 6-68 through 6-88.

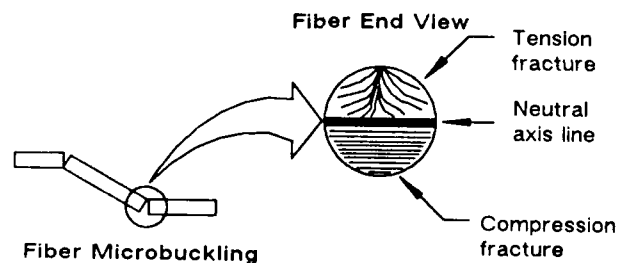
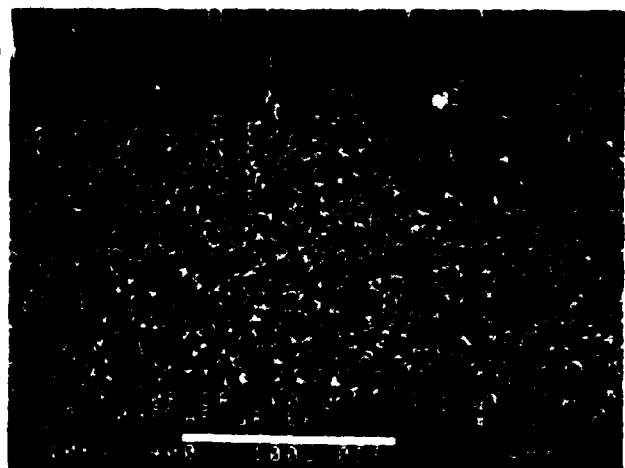
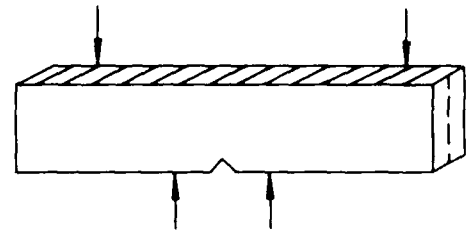


Figure 6-68. Translaminar Compression Fractures

5-B70227-234

SEM photomicrographs

Fracture type	Translaminar mode I compression
Ply layup	[0] 32
Test type	Four-point bend
• Test conditions	21°C, dry
• Fiber end fracture	
Material	Hercules 3501-6/177°C cure AS4 fibers



Mechanically induced crack direction

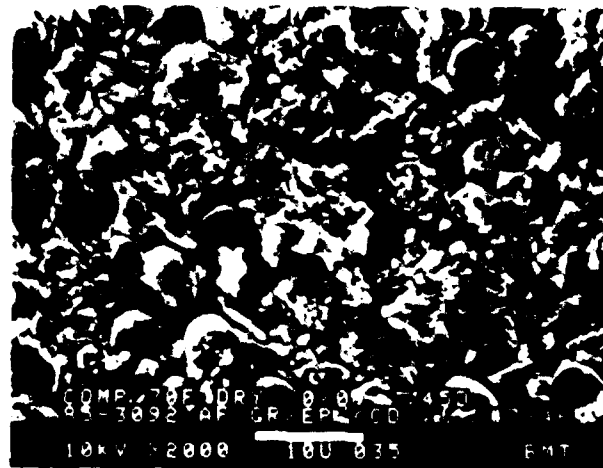
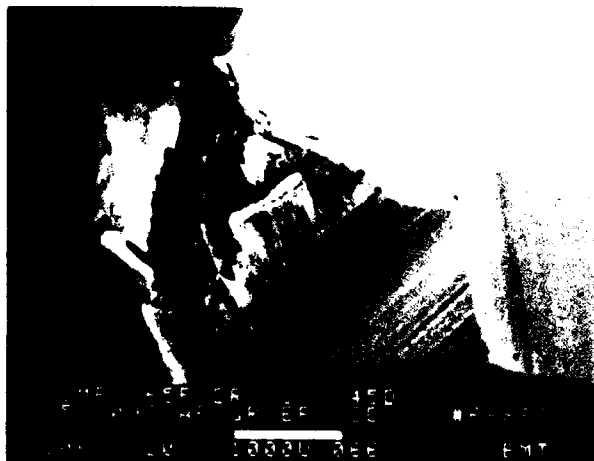
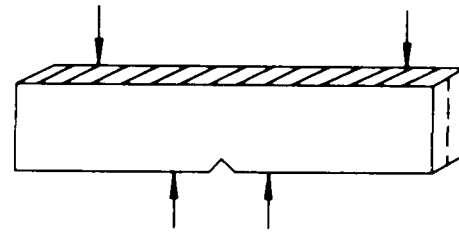


Figure 6-69. 0 (32) Ply at 21°C Dry Condition (SEM 50X, 400X, and 2000X)

SEM photomicrographs

Fracture type	Translaminar mode I compression
Ply layup	[0] 32
Test type	Four-point bend
• Test conditions	Dry
• Fiber end fracture	
Material	Hercules 3501-6/177°C cure AS4 fibers

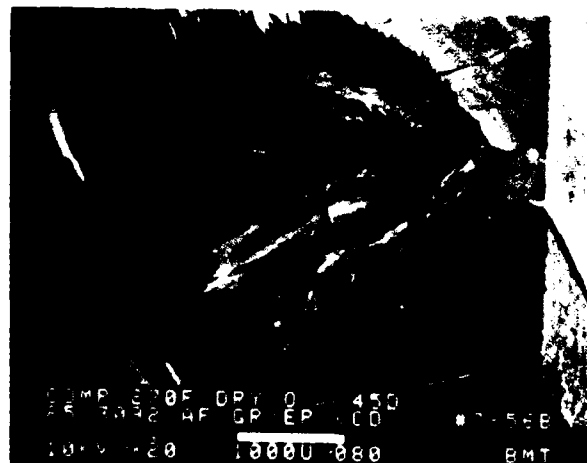


-65°F. dry



180°F. dry

← Mechanically induced crack direction



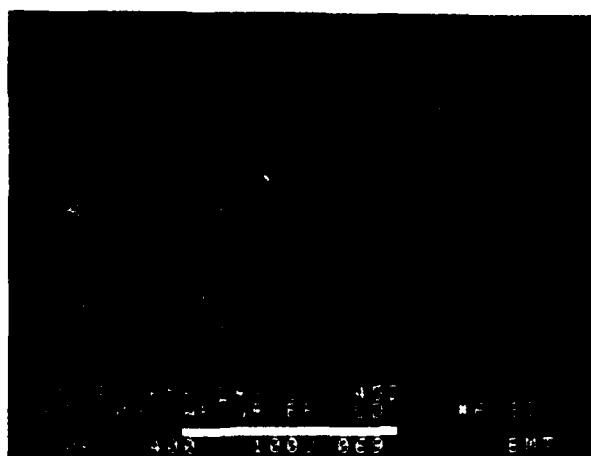
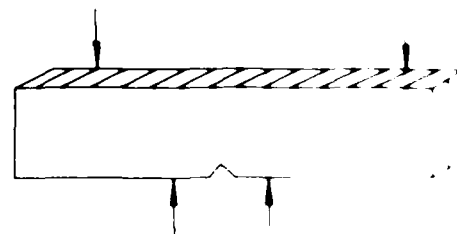
270°F. dry

Figure 6-70. 0 (32) Ply at -65°F Dry, 180°F Dry, 270°F Dry Conditions (SEM Low Magnification)

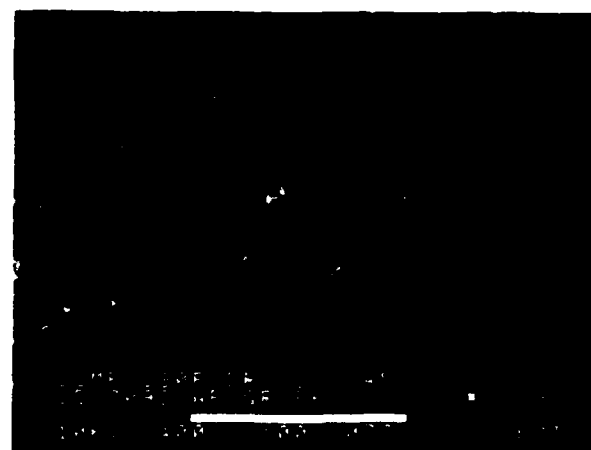
5-B70227-236

SEM photomicrographs

Fracture type	Translaminar mode I compression
Ply layup	[0] 32
Test type	Four-point bend
• Test conditions	Dry
• Fiber end fracture	
Material	Hercules 3501-6/177°C cure AS4 fibers

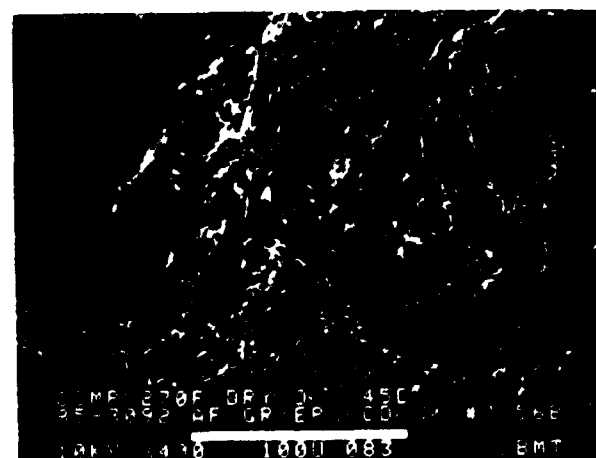


-65°F, dry



180°F, dry

← Mechanically induced crack direction



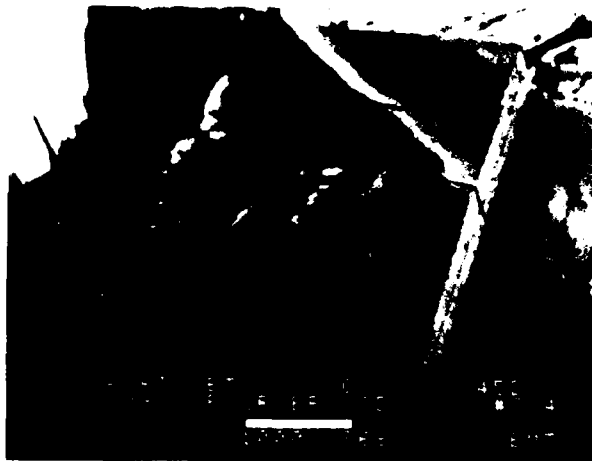
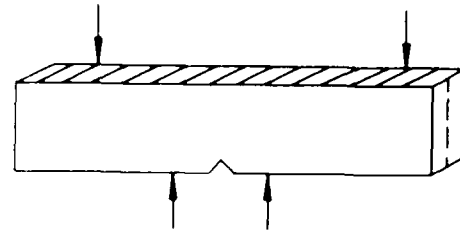
270°F, dry

Figure 6-71. 0 (32) Ply at -65°F Dry, 180°F Dry, and 270°F Dry Conditions (SEM 400X)

5-B70227-237

SEM photomicrographs

Fracture type	Translaminar mode I compression
Ply layup	[0] 32
Test type	Four-point bend
• Test conditions	Wet
• Fiber end fracture	
Material	Hercules 3501-6, 177°C cure AS4 fibers

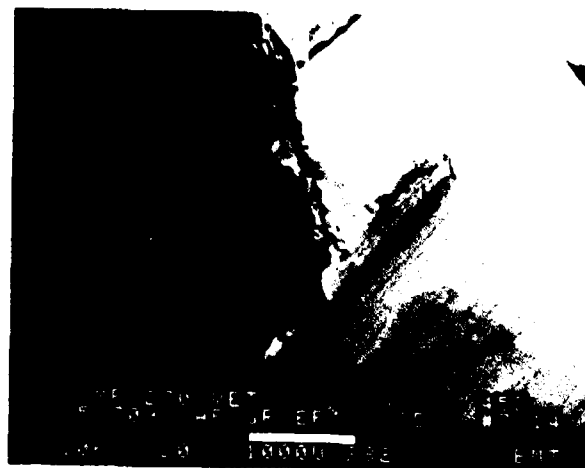


70°F. wet



180°F. wet

← Mechanically induced crack direction



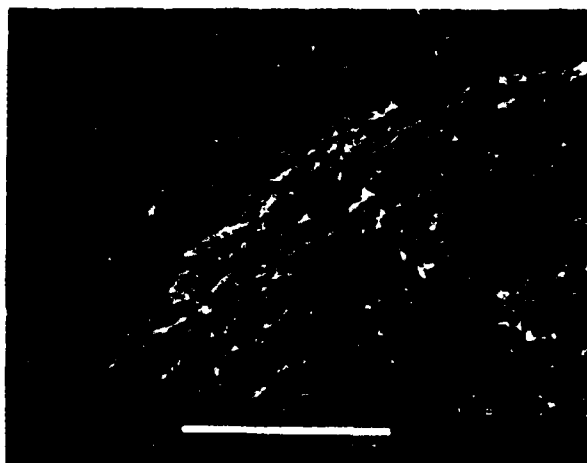
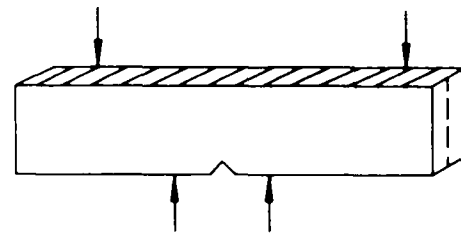
270°F. wet

Figure 6-72. 0 (32) Ply at 70°F Wet, 180°F Wet, and 270°F Wet Conditions (SEM 20X)

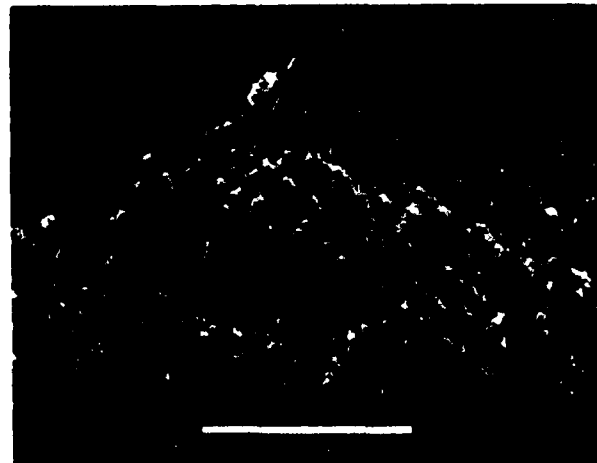
5-B70227-238

SEM photomicrographs

Fracture type	Translaminar mode I compression
Ply layup	[0]32
Test type	Four-point bend
• Test conditions	Dry
• Fiber end fracture	
Material	Hercules 3501-6/177°C cure AS4 fibers

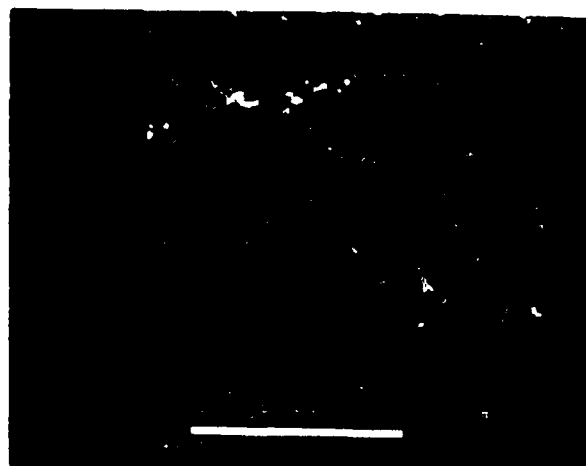


70°F. wet



180°F. wet

Mechanically induced crack direction

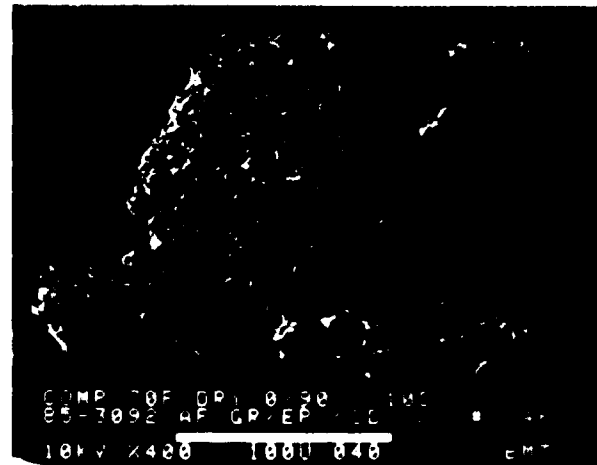
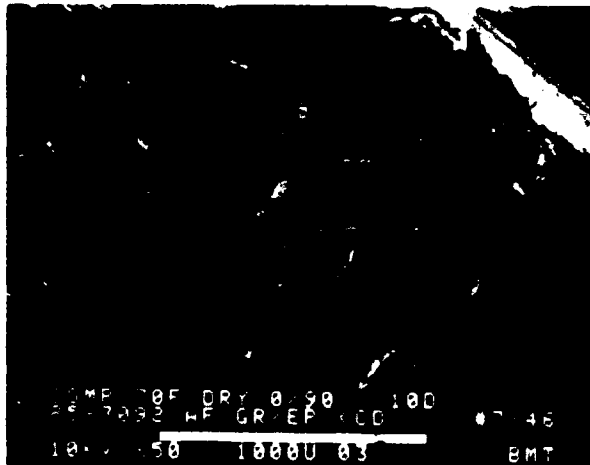
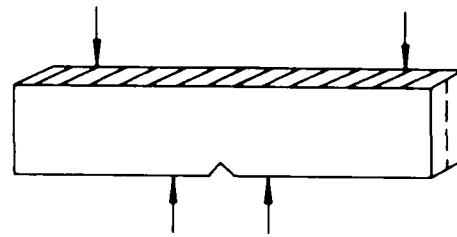


270°F. wet

Figure 6-73. [0]32 Ply at 70°F Wet, 180°F Wet, and 270°F Wet Conditions (SEM 400X)

SEM photomicrographs

Fracture type	Translaminar mode I compression
Ply layup	[0, 90] 16S
Test type	Four-point bend
• Test conditions	21°C, dry
• Fiber end fracture	
Material	Hercules 3501-6/177°C cure AS4 fibers



← Mechanically induced crack direction

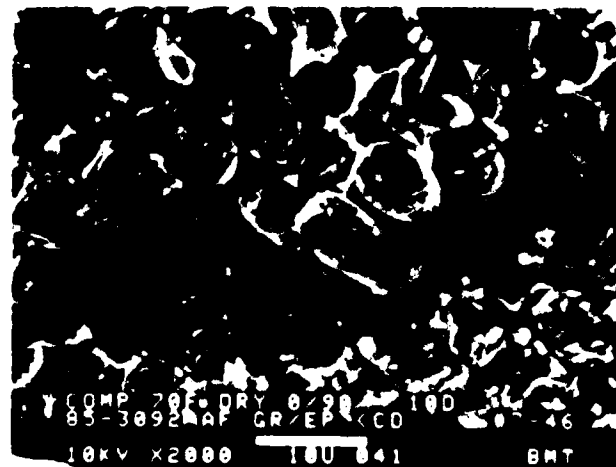
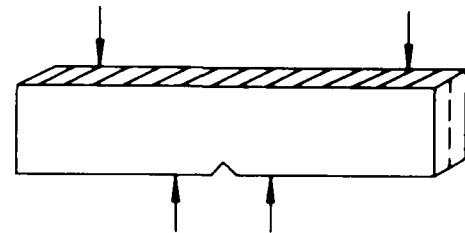


Figure 6-74. 0/90 Plies at 21°C Dry Conditions (SEM 50X, 400X, and 2000X)

5 B70227 240

SEM photomicrographs

Fracture type	Translaminar mode I compression
Ply layup	[0, 90] ₁₆ S
Test type	Four-point bend
• Test conditions	Dry
• Fiber end fracture	
Material	Hercules 3501-6/177°C cure AS4 fibers

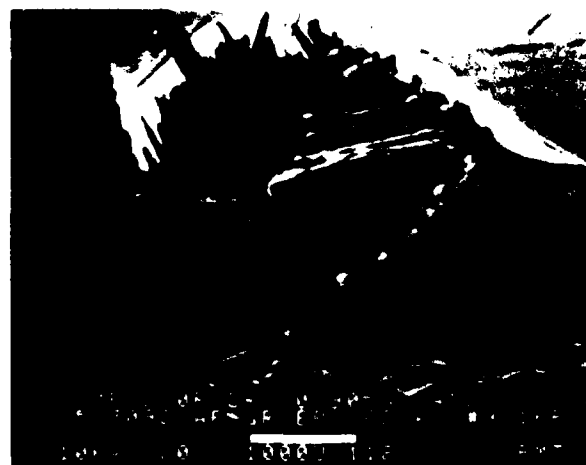


-65°F, dry



180°F, dry

Mechanically induced crack direction

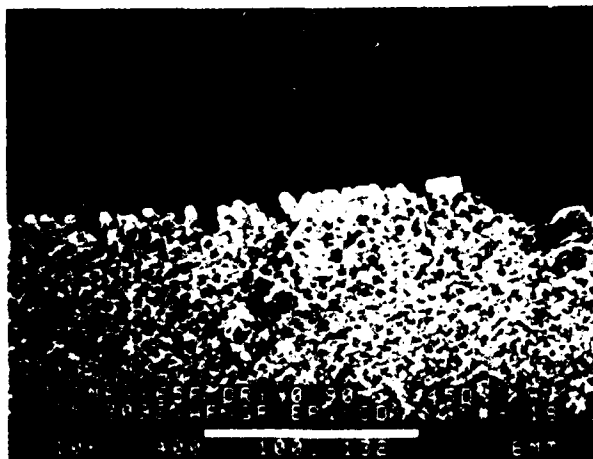
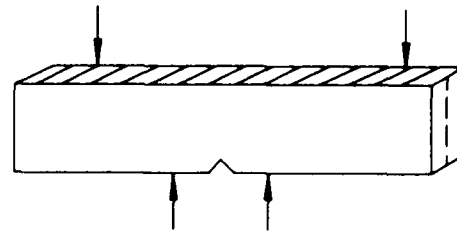


270°F, dry

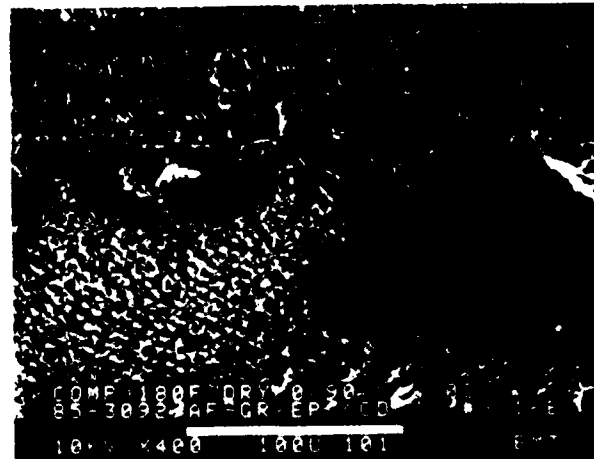
Figure 6-75. 0/90 Plies at -65°F Dry, 180°F Dry, and 270°F Dry Conditions (SEM 20X)

SEM photomicrographs

Fracture type	Translaminar mode I compression
Ply layup	[0, 90] ₁₆ S
Test type	Four-point bend
• Test conditions	Dry
• Fiber end fracture	
Material	Hercules 3501-6/177°C cure AS4 fibers

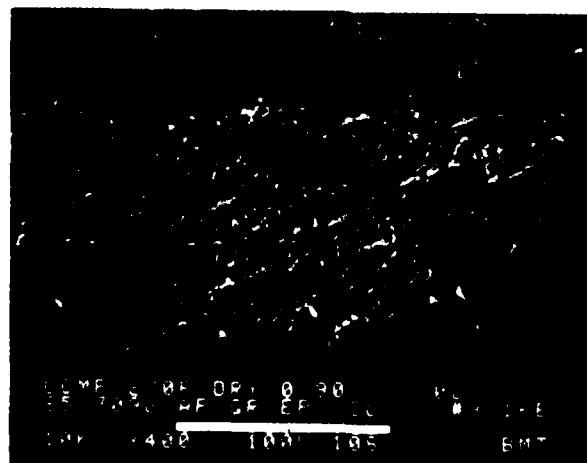


-65°F, dry



180°F, dry

Mechanically induced crack direction



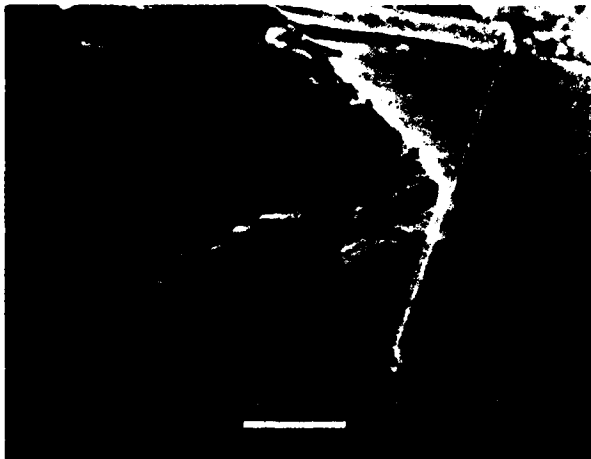
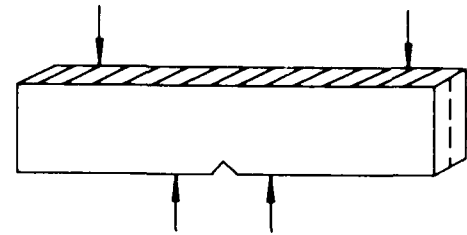
270°F, dry

Figure 6-76. 0/90 Plies at -65°F Dry, 180°F Dry, and 270°F Dry Conditions (SEM 400X)

5-B70227-242

SEM photomicrographs

Fracture type	Translaminar mode I compression
Ply layup	[0, 90] ₁₆ S
Test type	Four-point bend
• Test conditions	Wet
• Fiber end fracture	
Material	Hercules 3501-6/177°C cure AS4 fibers



70°F. wet



180°F. wet

↖ Mechanically induced crack direction

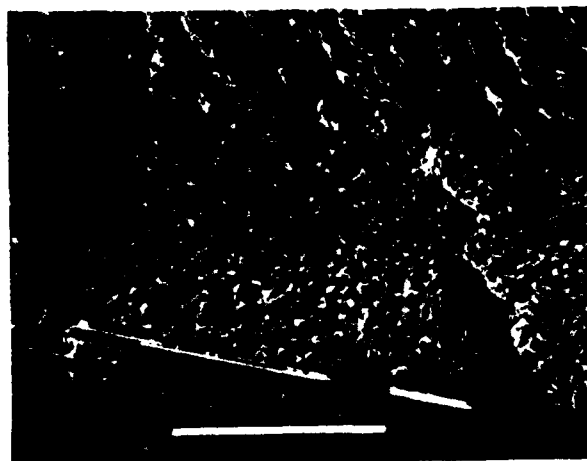
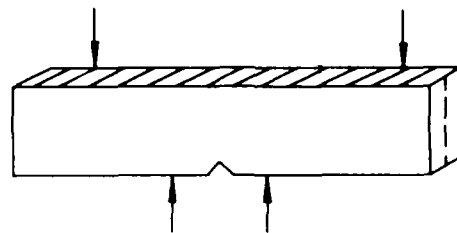


270°F. wet

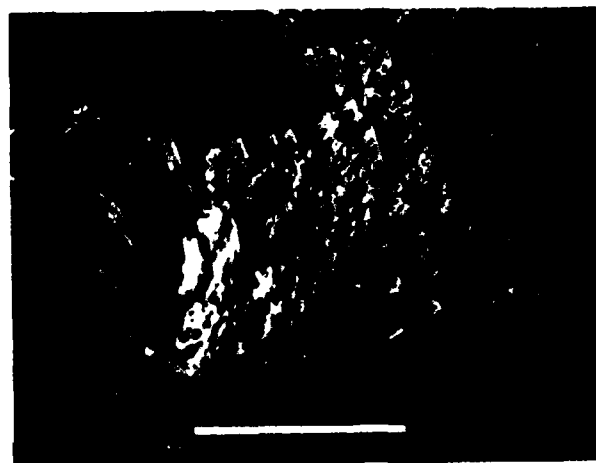
Figure 6-77. 0/90 Plies at 70°F Wet, 180°F Wet, and 270°F Wet Conditions (SEM 20x)

SEM photomicrographs

Fracture type	Translaminar mode I compression
Ply layup	[0, 90] ₁₆ S
Test type	Four-point bend
• Test conditions	Wet
• Fiber end fracture	
Material	Hercules 3501-6/177°C cure AS4 fibers

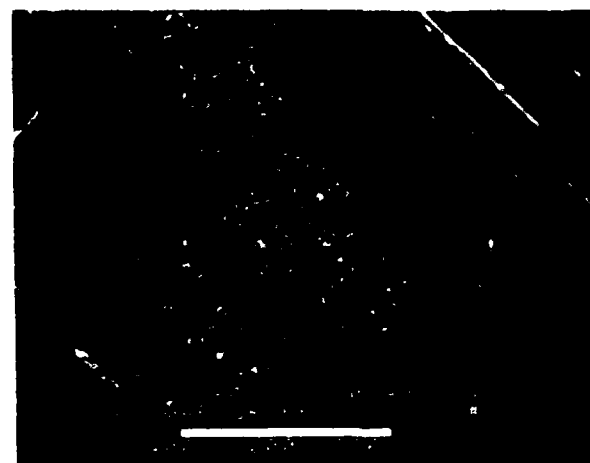


70°F. wet



180°F. wet

↖ Mechanically induced crack direction



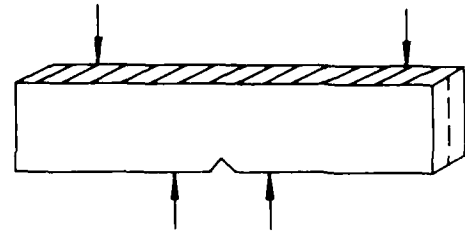
270°F. wet

Figure 6-78. 0/90 Plies at 70°F Wet, 180°F Wet, and 270°F Wet Conditions (SEM 400X)

5-B70227-244

SEM photomicrographs

Fracture type	Translaminar mode I compression
Ply layup	[0, 45, 90] 16S
Test type	Four-point bend
• Test conditions	21°C, dry
• Fiber end fracture	
Material	Hercules 3501-6/177°C cure AS4 fibers



Mechanically induced crack direction

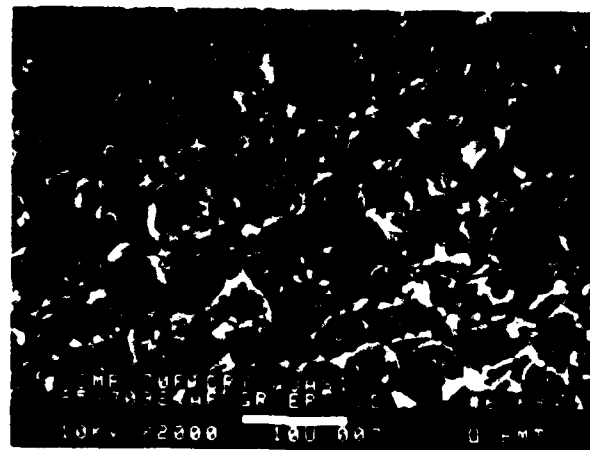
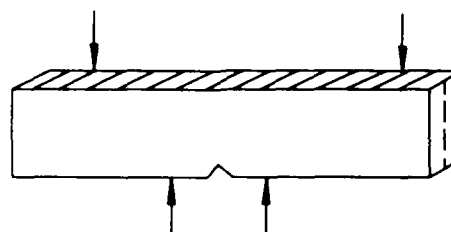


Figure 6-79. 0/45/90 Plies at 21°C Condition (SEM 50X, 400X, and 2000X)

SEM photomicrographs

Fracture type	Translaminar mode I compression
Ply layup	[0, 45, 90] _{16S}
Test type	Four-point bend
• Test conditions	Dry
• Fiber end fracture	
Material	Hercules 3501-6/177°C cure AS4 fibers



-65°F, dry



180°F, dry

← Mechanically induced crack direction



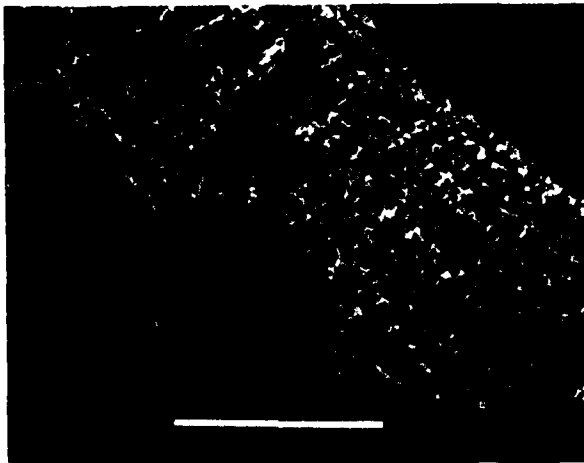
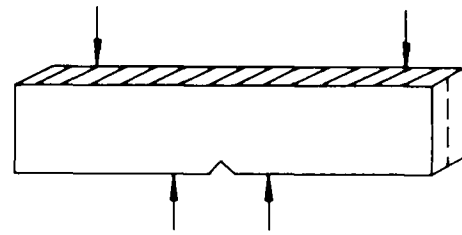
270°F, dry

Figure 6-80. 0/45/90 Plies at -65°F Dry, 180°F Dry, and 270°F Dry Conditions (SEM 20X)

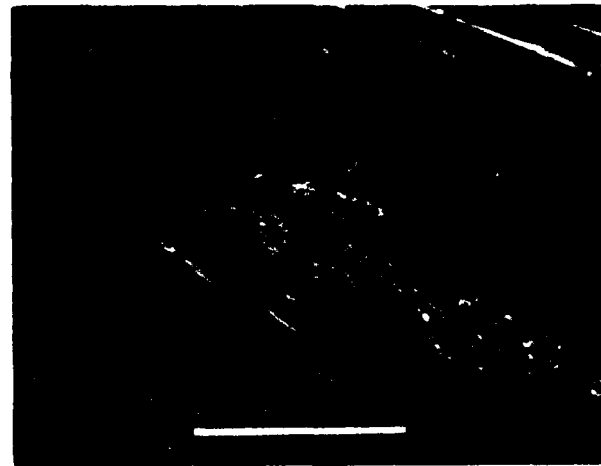
5-B70227-252

SEM photomicrographs

Fracture type	Translaminar mode I compression
Ply layup	[0, 45, 90] 16S
Test type	Four-point bend
• Test conditions	Wet
• Fiber end fracture	
Material	Hercules 3501-6/177°C cure AS4 fibers

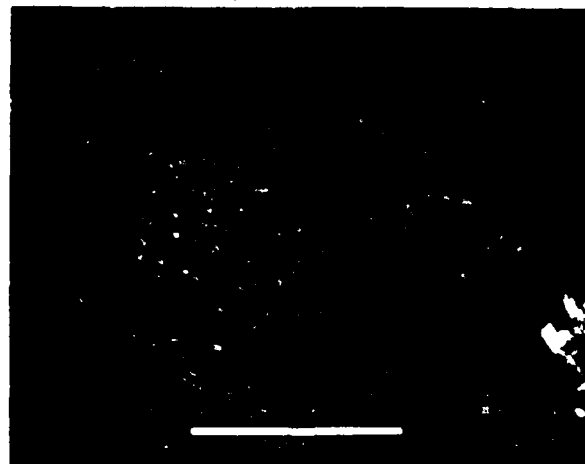


70°F, wet



180°F, wet

Mechanically induced crack direction



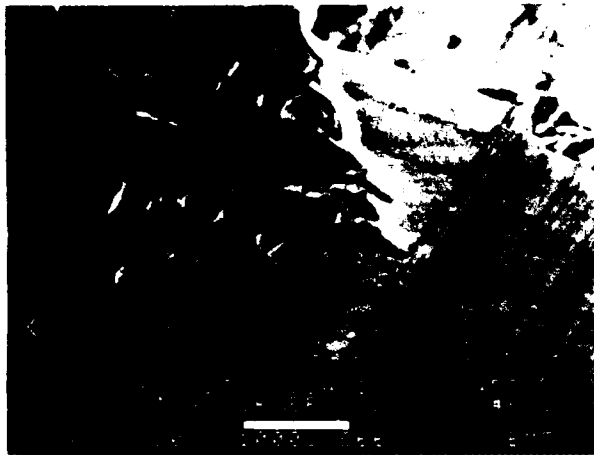
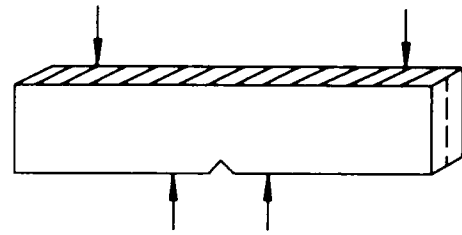
270°F, wet

Figure 6-81. 0/45/90 Plies at 70°F Wet, 180°F Wet, and 270°F Wet Conditions (SEM 400X)

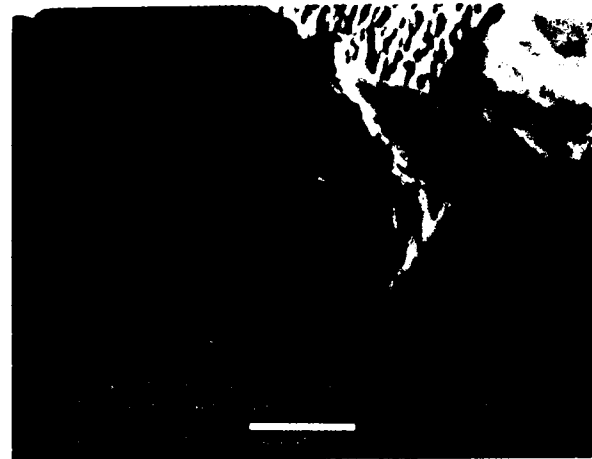
5 B70227-253

SEM photomicrographs

Fracture type	Translaminar mode I compression
Ply layup	[0, 45, 90] _{16S}
Test type	Four-point bend
• Test conditions	Wet
• Fiber end fracture	
Material	Hercules 3501-6/177°C cure AS4 fibers

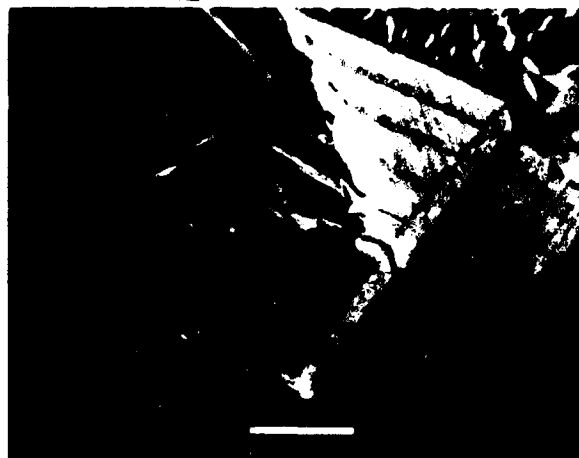


70°F, wet



180°F, wet

Mechanically induced crack direction



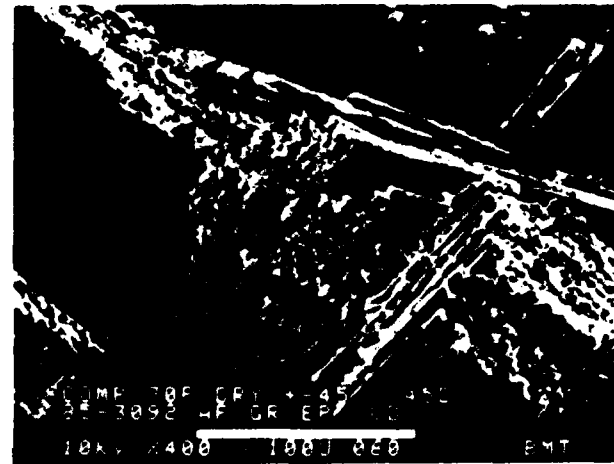
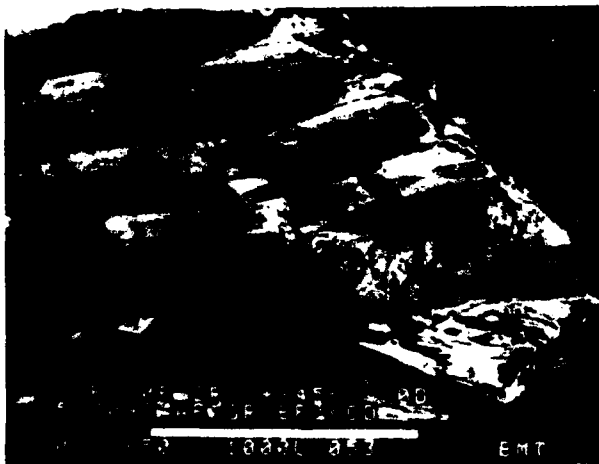
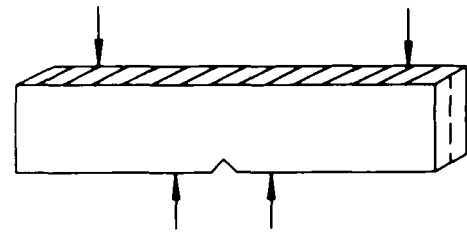
270°F, wet

Figure 6-82. 0/45/90 Plies at 70°F Wet, 180°F Wet, and 270°F Wet Conditions (SEM 20X)

5-B70227-254

SEM photomicrographs

Fracture type	Translaminar mode I compression
Ply layup	[+45, -45] 16S
Test type	Four-point bend
• Test conditions	21°C, dry
• Fiber end fracture	
Material	Hercules 3501-6/177°C cure AS4 fibers



Mechanically induced crack direction

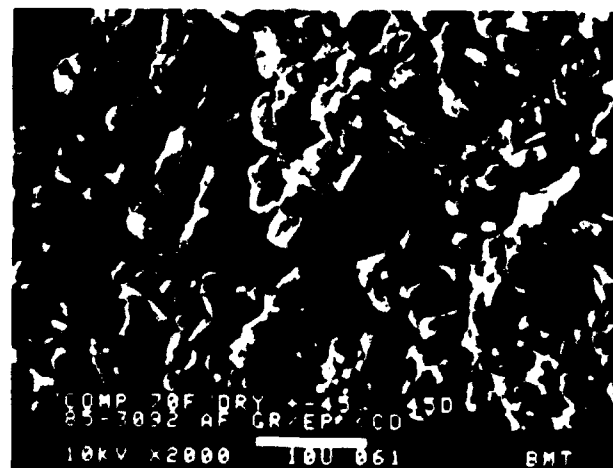
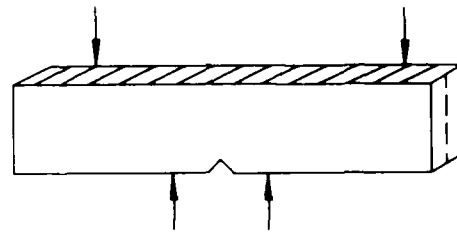


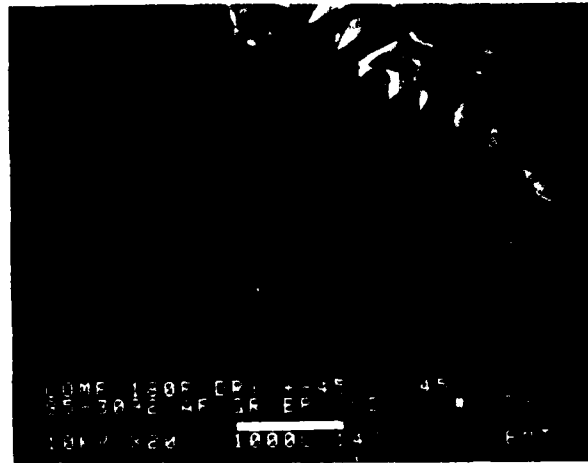
Figure 6-83 +45/-45 Plies at 21°C Dry Condition (SEM 50X, 400X, and 2000X)

SEM photomicrographs

Fracture type	Translaminar mode I compression
Ply layup	[+45, -45]16S
Test type	Four-point bend
• Test conditions	Dry
• Fiber end fracture	
Material	Hercules 3501-6/177°C cure AS4 fibers

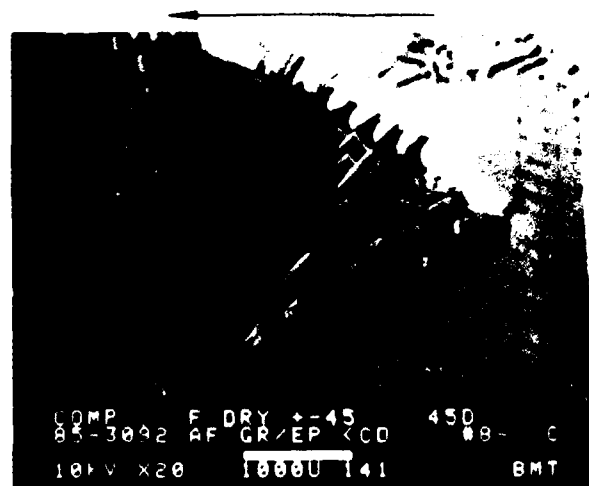


-65°F, dry



180°F, dry

Mechanically induced crack direction



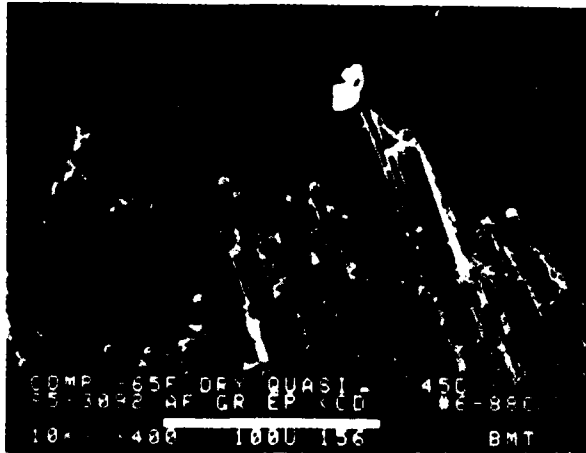
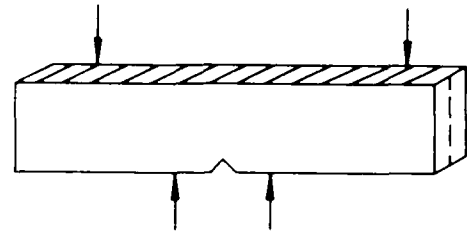
270°F, dry

Figure 6-84. +45/-45 Plies at -65°F Dry, 180°F Dry, and 270°F Dry Conditions (SEM 20x)

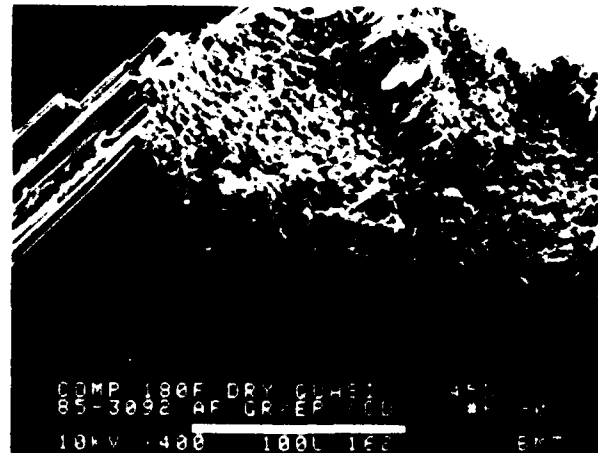
5-B70227 247

SEM photomicrographs

Fracture type	Translaminar mode I compression
Ply layup	[0, 45, 90] _{16S}
Test type	Four-point bend
• Test conditions	Dry
• Fiber end fracture	
Material	Hercules 3501-6/177°C cure AS4 fibers



-65°F, dry



180°F, dry

Mechanically induced crack direction



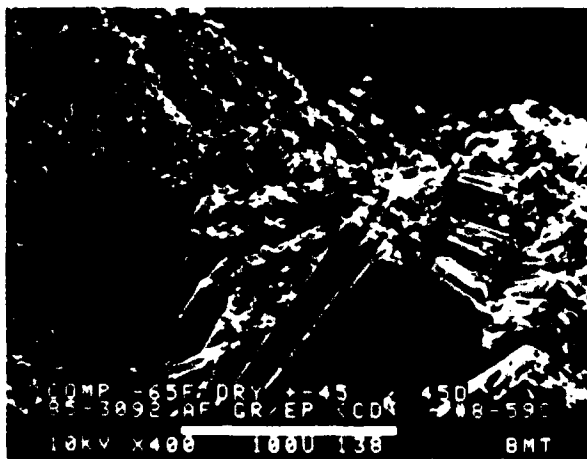
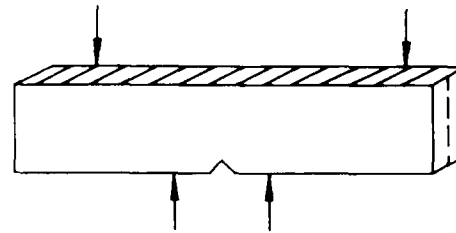
270°F, dry

Figure 6-85. 0/45/90 Plies at -65°F Dry, 180°F Dry, and 270°F Dry Conditions (SEM 400X)

5 B70227 248

SEM photomicrographs

Fracture type	Translaminar mode I compression
Ply layup	[+45, -45] 16S
Test type	Four-point bend
• Test conditions	Dry
• Fiber end fracture	
Material	Hercules 3501-6/177°C cure AS4 fibers



-65°F. dry



180°F. dry

← Mechanically induced crack direction



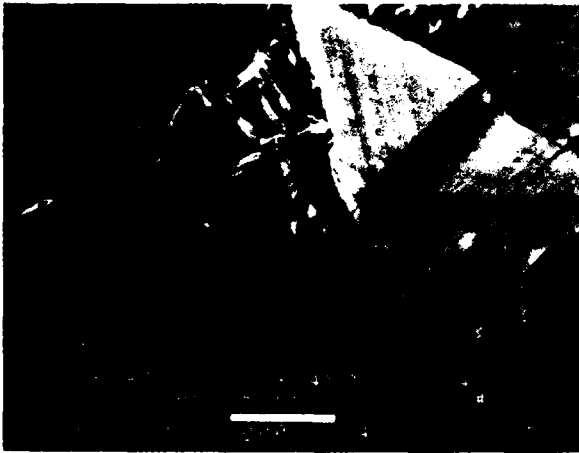
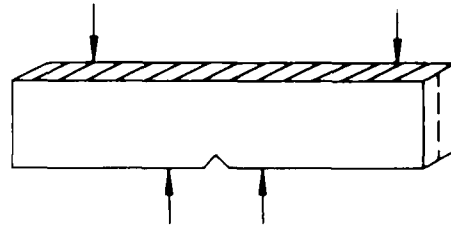
270°F. dry

Figure 6-86. +45/-45 Plies at -65°F Dry, 180°F Dry, and 270°F Dry Conditions (SEM 400X)

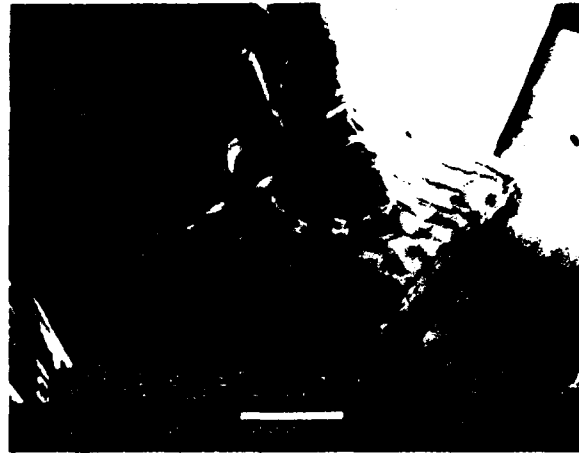
5-B70227-249

SEM photomicrographs

Fracture type	Translaminar mode I compression
Ply layup	[+45, -45] 16S
Test type	Four-point bend
• Test conditions	Wet
• Fiber end fracture	
Material	Hercules 3501-6/177°C cure AS4 fibers



-65°F. wet



180°F. wet

Mechanically induced crack direction



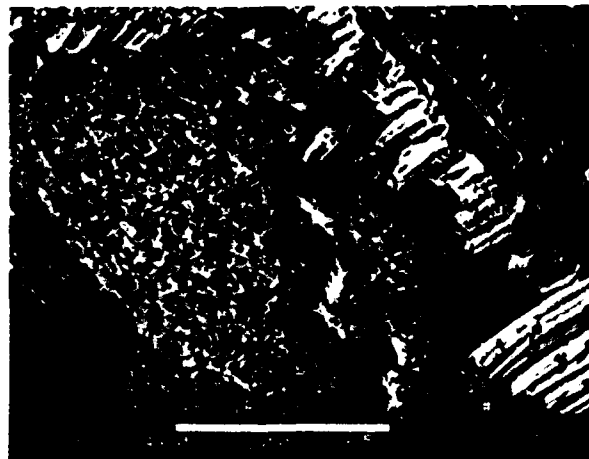
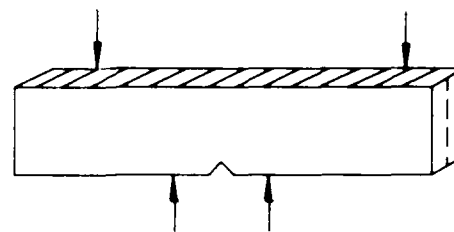
270°F. wet

+45/-45 Plies at 70°F Wet, 180°F Wet, and 270°F Wet Conditions (SEM 20X)

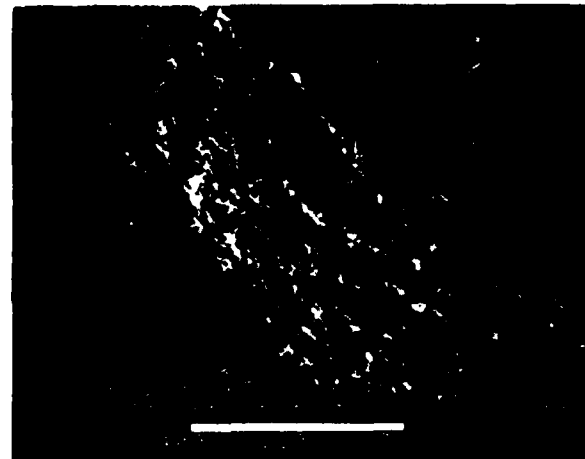
5-B70227-250

SEM photomicrographs

Fracture type	Translaminar mode I compression
Ply layup	[+45, -45] 16S
Test type	Four-point bend
• Test conditions	Dry
• Fiber end fracture	
Material	Hercules 3501-6/177°C cure AS4 fibers



70°F. wet



180°F. wet

Mechanically induced crack direction



270°F. wet

Figure 6-88. +45/-45 Plies at 70°F Wet, 180°F Wet, and 270°F Wet Conditions (SEM 400X)

5-B70227-251

6.6 TRANSLAMINAR MODE II SHEAR

Figure 6-89 shows the test matrix for a side-notched rail shear test type.

The primary features observed in these specimens were very complex and generally a combination of features identified for the laminar Mode I tension and compression fractures. The key features were as follows:

- Fiber microbuckling and fiber slant fracture.
- Post-failure compression damage to fiber ends.
- Fiber pullout and extensive lateral displacement between the protruding fibers.
- Hackle features on sides of the fibers.

As with compression dominated fractures, fractographic features by which the direction of fracture can be identified, do not exist.

See Figures 6-90 through 6-99.

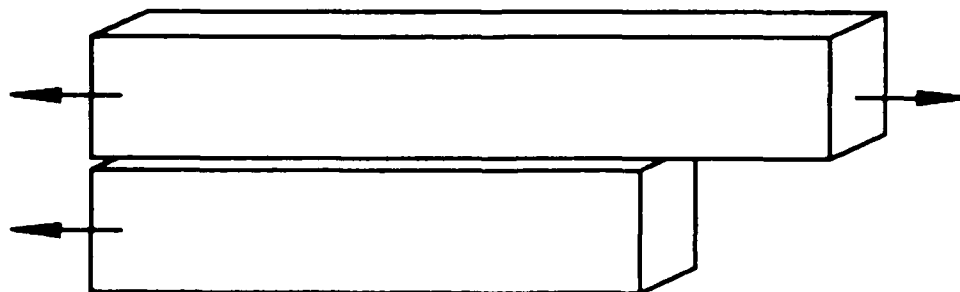
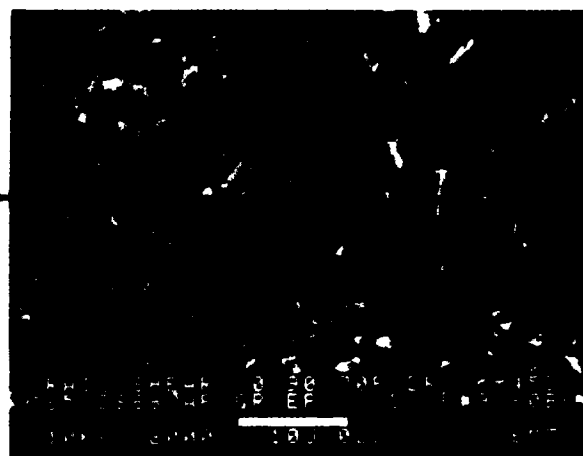
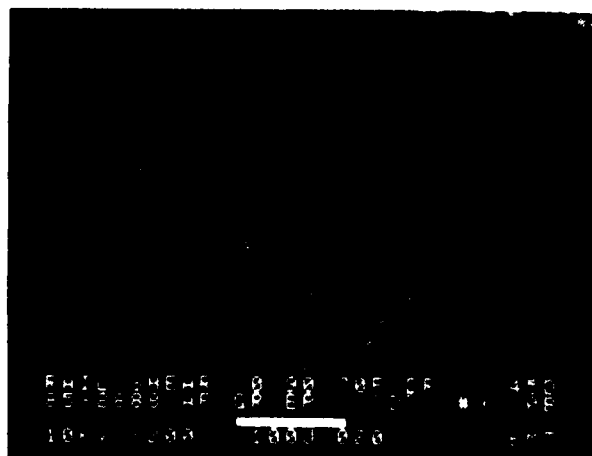
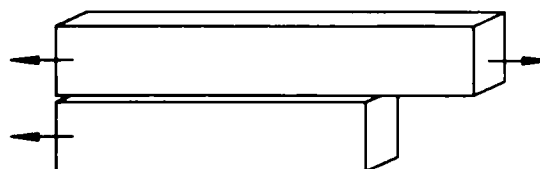


Figure 6-89. Side-Notched Rail Shear Test Type

5-B70227-255

SEM photomicrographs

Fracture type	Translaminar mode II shear
Ply layup	[0, 90] _{16S}
Test type	Side-notched rail shear
• Test conditions	21°C, dry
• Fiber end fracture	
Material	Hercules 3501-6/177°C cure AS4 fibers



Mechanically induced crack direction

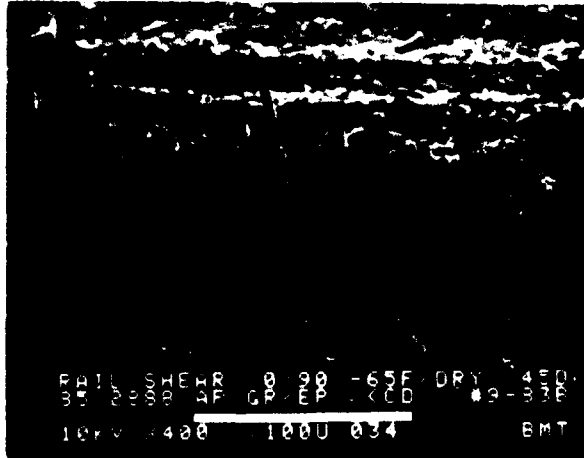
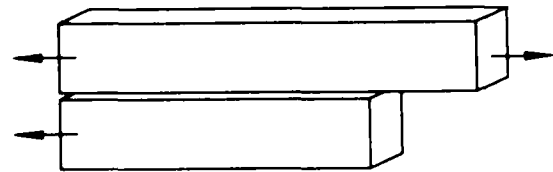


5-B70227-256

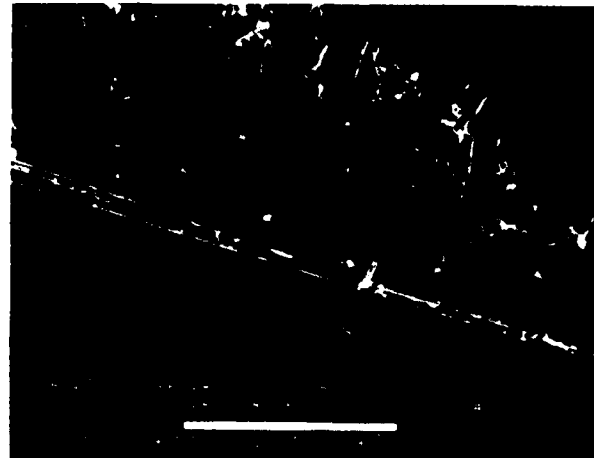
Figure 6-90. 0/90 Plies at 21°C Dry (SEM 200X and 2000X)

SEM photomicrographs

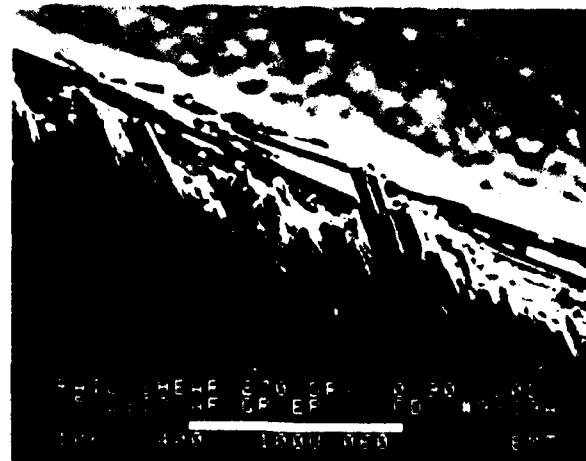
Fracture type	Translaminar mode II shear
Ply layup	[0, 90] _{16S}
Test type	Side-notched rail shear
• Test conditions	Dry
• Fiber end fracture	
Material	Hercules 3501-6/177°C cure AS4 fibers



-65°F, dry



180°F, dry



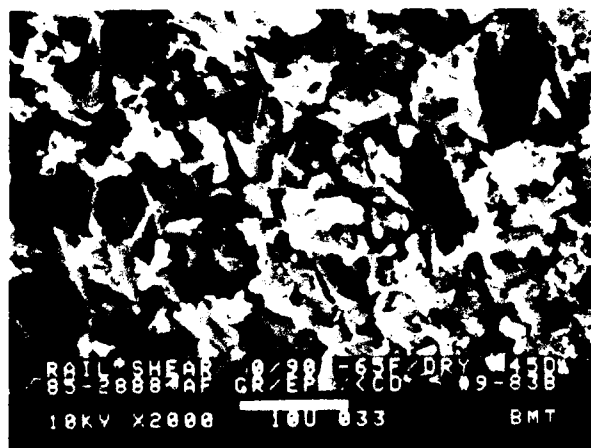
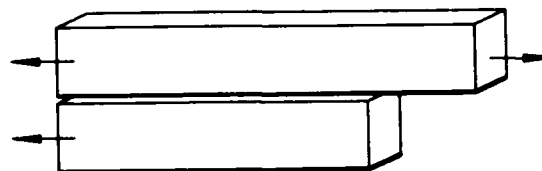
270°F, dry

Figure 6-91. 0/90 Plies at -65°F Dry, 180°F Dry, and 270°F Dry Conditions (SEM 400X)

5-B70227-257

SEM photomicrographs

Fracture type	Translaminar mode II shear
Ply layup	[0, 90] _{16S}
Test type	Side-notched rail shear
• Test conditions	Dry
• Fiber end fracture	
Material	Hercules 3501-6/177°C cure AS4 fibers



-65°F, dry



180°F, dry

Mechanically Induced crack direction



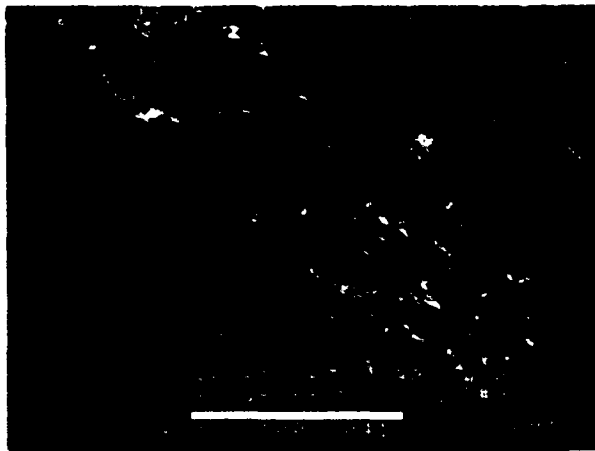
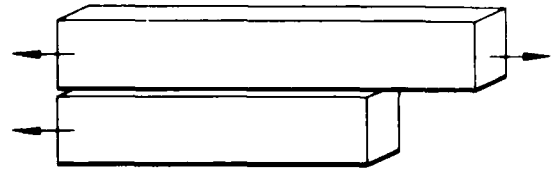
270°F, dry

Figure 6-92. 0/90 Plies at -65°F Dry, 180°F Dry, and 270°F Dry Conditions (SEM 2000X)

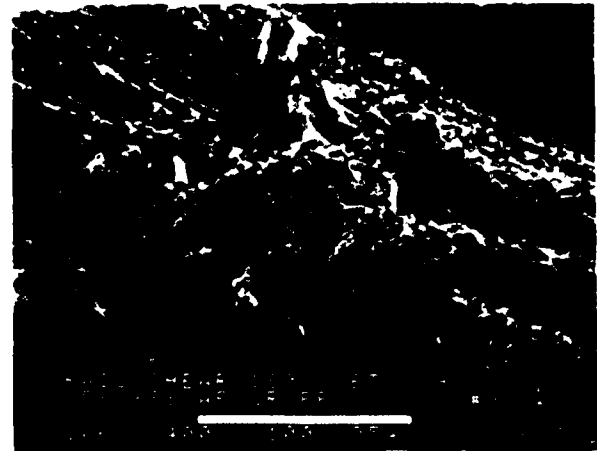
5-B70227-258

SEM photomicrographs

Fracture type	Translaminar mode II shear
Ply layup	[0. 90] ₁₆ S
Test type	Side-notched rail shear
• Test conditions	Wet
• Fiber end fracture	
Material	Hercules 3501-6/177°C cure AS4 fibers

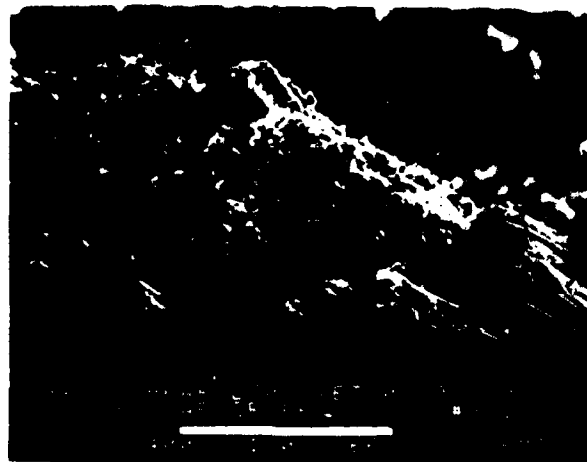
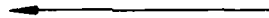


70°F, wet



180°F, wet

Mechanically induced crack direction

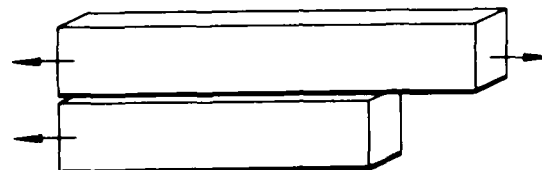


270°F, wet

Figure 6-93. 0/90 Plies at 70°F Wet, 180°F Wet, and 270°F Wet Conditions (SEM 400X)

SEM photomicrographs

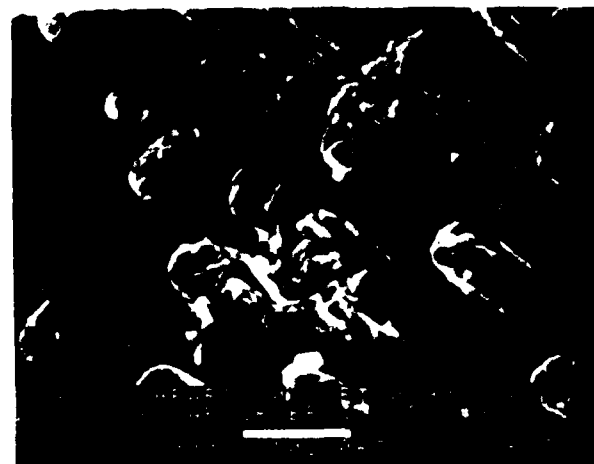
Fracture type	Translaminar mode II shear
Ply layup	[0, 90] _{16S}
Test type	Side-notched rail shear
• Test conditions	Wet
• Fiber end fracture	
Material	Hercules 3501-6/177°C cure AS4 fibers



70°F. wet



180°F. wet



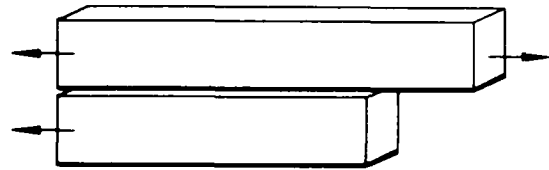
270°F. wet

Figure 6-94. 0/90 Plies at 70°F Wet, 180°F Wet, and 270°F Wet Conditions (SEM 2000X)

5-B70227-260

SEM photomicrographs

Fracture type	Translaminar mode II shear
Ply layup	[0, 45, 90] _{16S}
Test type	Side-notched rail shear
• Test conditions	21°C, dry
• Fiber end fracture	
Material	Hercules 3501-6/177°C cure AS4 fibers



Mechanically induced crack direction



Mechanically induced crack direction

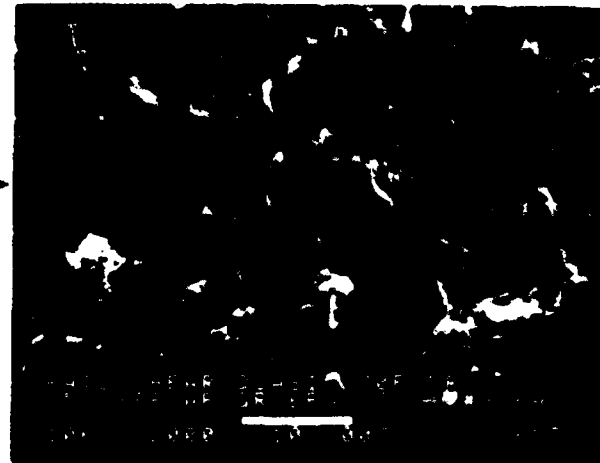
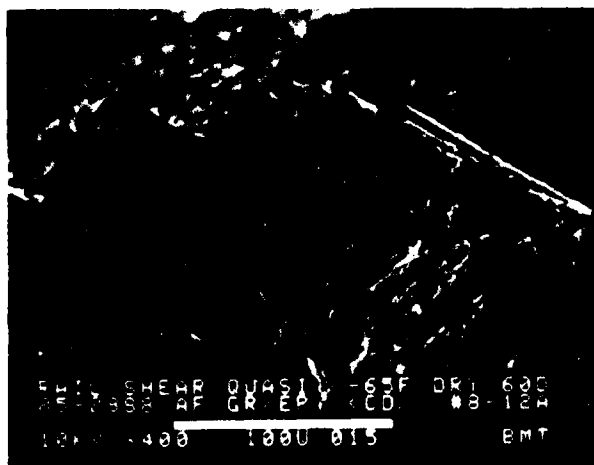
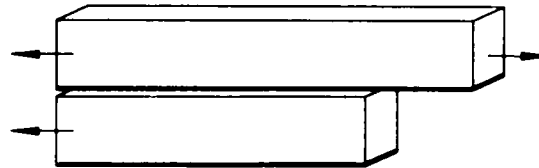


Figure 6-95. 0/45/90 Plies at 21°C Dry (SEM 200X and 2000X)

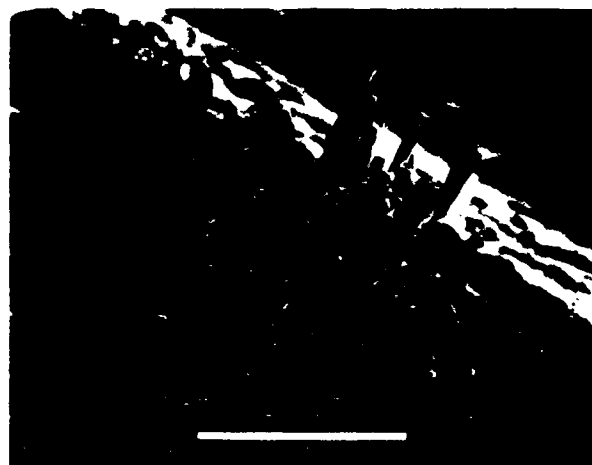
5-B70227-261

SEM photomicrographs

Fracture type	Translaminar mode II shear
Ply layup	[0.45, 90] _{16S}
Test type	Side-notched rail shear
• Test conditions	Dry
• Fiber end fracture	
Material	Hercules 3501-6/177°C cure AS4 fibers

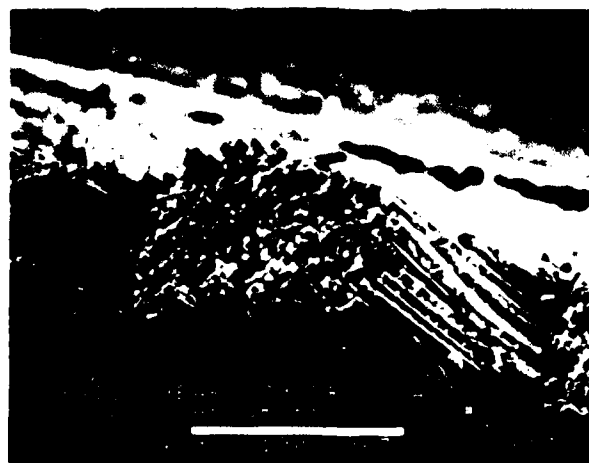


-65°F, dry



180°F, dry

Mechanically induced crack direction



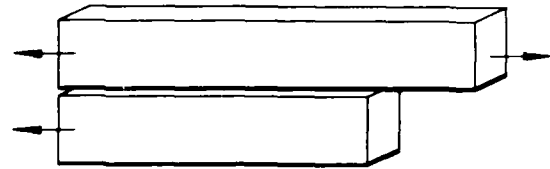
270°F, dry

Figure 6-96. 0/45/90 Plies at -65°F Dry, 180°F Dry, and 270°F Dry Conditions (SEM 400X)

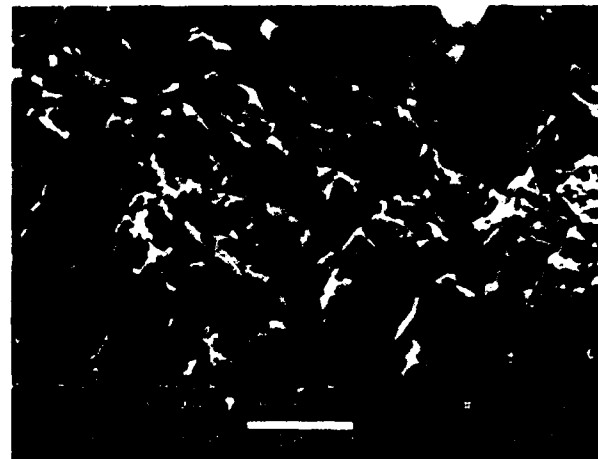
5-B70227-262

SEM photomicrographs

Fracture type	Translaminar mode II shear
Ply layup	[0, 45, 90] _{16S}
Test type	Side-notched rail shear
• Test conditions	Dry
• Fiber end fracture	
Material	Hercules 3501-6/177°C cure AS4 fibers

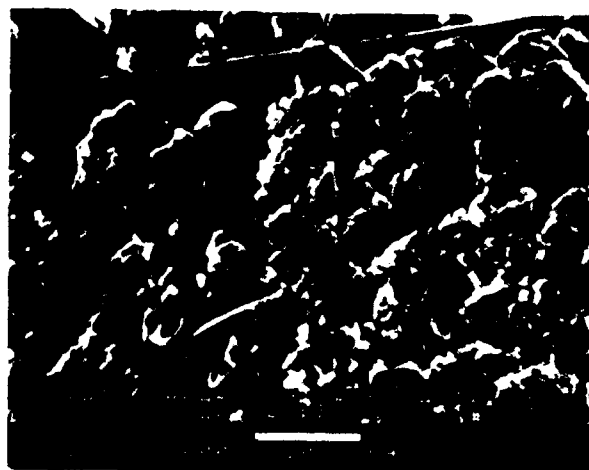


-65°F, dry



180°F, dry

Mechanically induced crack direction



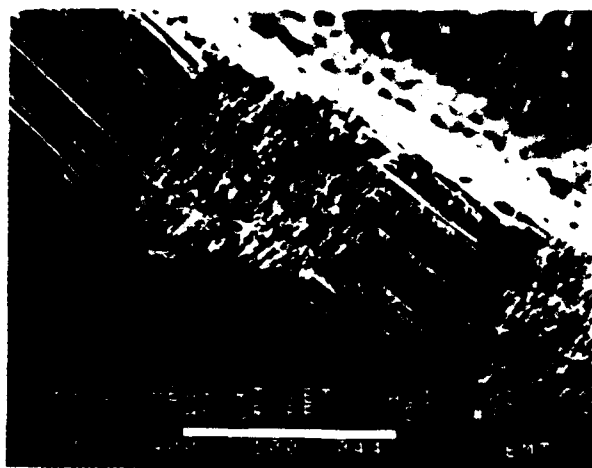
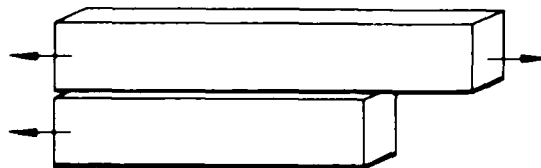
270°F, dry

Figure 6-97. 0/45/90 Piles at -65° F Dry, 180° F Dry, and 270° F Dry Conditions (SEM 2000X)

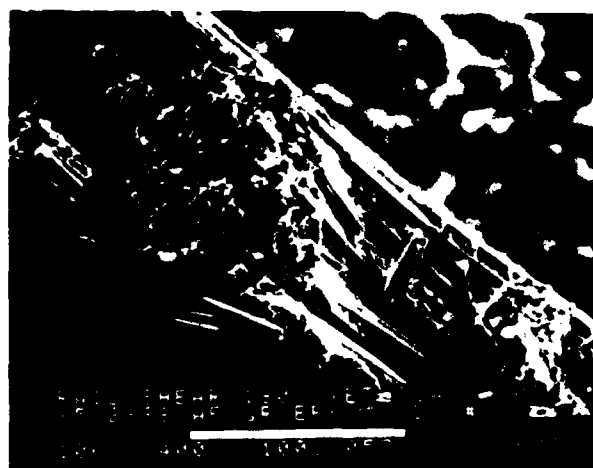
5-B70227-263

SEM photomicrographs

Fracture type	Translaminar mode II shear
Ply layup	[0, 45, 90] _{16S}
Test type	Side-notched rail shear
• Test conditions	Wet
• Fiber end fracture	
Material	Hercules 3501-6/177°C cure AS4 fibers

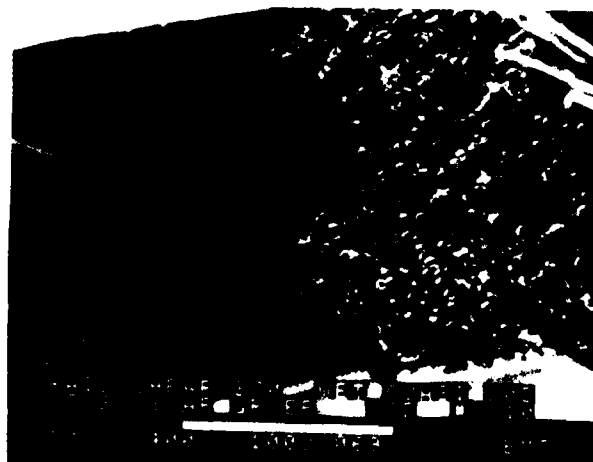


70°F. wet



180°F. wet

Mechanically induced crack direction



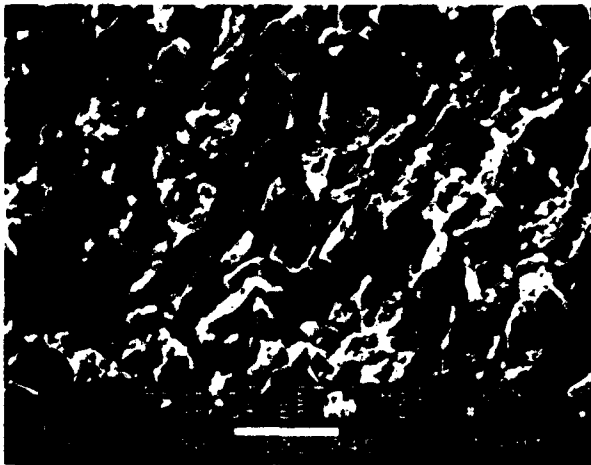
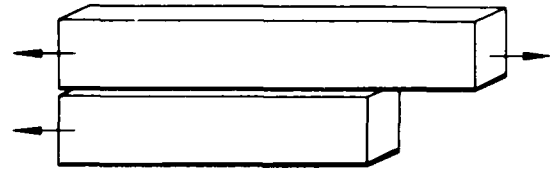
270°F. wet

Figure 6-98. 0/45/90 Plies at 70°F Wet, 180°F Wet, and 270°F Wet Conditions (SEM 400X)

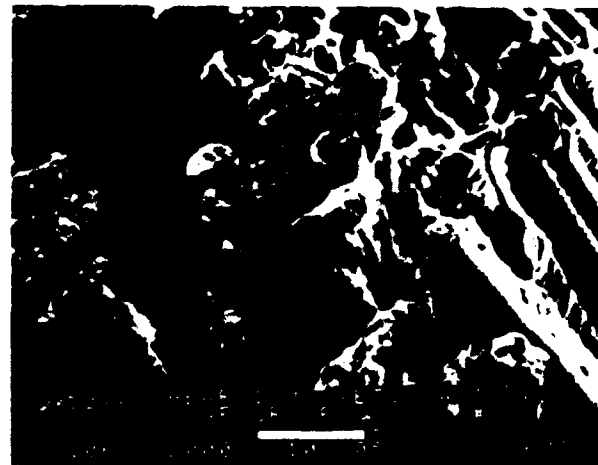
5-B70227-264

SEM photomicrographs

Fracture type	Translaminar mode II shear
Ply layup	[0, 45, 90] ₁₆ S
Test type	Side-notched rail shear
• Test conditions	Wet
• Fiber end fracture	
Material	Hercules 3501-6/177°C cure AS4 fibers

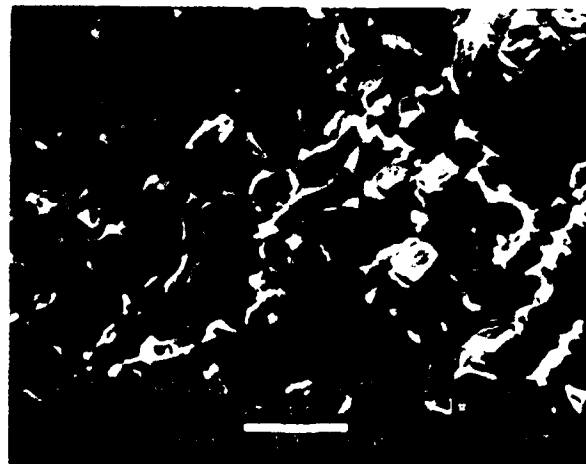


70°F, wet



180°F, wet

← Mechanically induced crack direction



270°F, wet

Figure 6-99. 0/45/90 Plies at 70°F Wet, 180°F Wet, and 270°F Wet Conditions (SEM 2000X)

5-B70227-265

6.7 TRANSLAMINAR FLEXURE

Figure 6-100 shows the test matrix for a laminate flexure test type.

The primary features observed in unnotched specimens which fail because of flexural loading are as follows:

- Macroscopic identification of rough (tensile) and smooth (compressive) fracture regions.
- Distinct separation between tension and compression regions (as indicated by a neutral axis region).
- Tensile fractures tend to initiate along the outer surface and progress toward the neutral line (as indicated by analysis of fiber end radials).

See Figure 6-101.

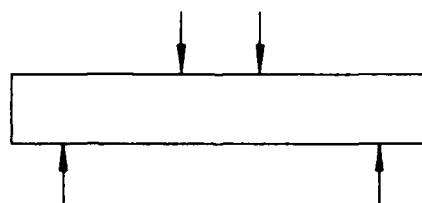


Figure 6-100. Laminate Flexure Test Type

5-B70227-266

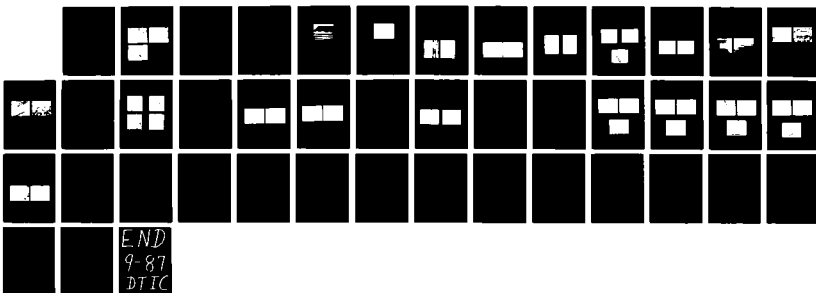
AD-A183 783

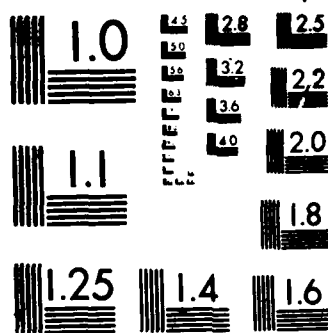
COMPENDIUM OF POST-FAILURE ANALYSIS TECHNIQUES FOR
COMPOSITE MATERIALS(U) BOEING MILITARY AIRPLANE CO
SEATTLE WA R A GROVE ET AL. JAN 87 AFMAL-TR-86-4137
F33615-84-C-5010 F/G 11/4

5/5

UNCLASSIFIED

NL





MICROCOPY RESOLUTION TEST CHART
 NATIONAL BUREAU OF STANDARDS-1963-A

SEM photomicrographs

Fracture type	Translaminar flexure
Ply layup	[0]32
Test type	Laminate flexure
• Test conditions	20°C, dry
• Fiber end fracture	
Material	Hercules 3501-6/177°C cure AS4 fibers



Compression Fracture Region



Tensile Fracture Region

Overall growth direction →

Mechanically induced crack direction →

Figure 6-101. 0 (32) Plies at 21°C Dry (SEM 20X, 800X, and 2000X)

5-B70227-267

6.8 INTERLAMINAR FATIGUE

Figure 6-102 shows the text matrix of Double Cantilever Beam (DCB) for Mode I fractures and Crack Lap Shear (CLS) for Mode II fractures.

The primary features observed in DCB Mode I tension fatigue features are:

- Striations.
- River marks and resin microflow features identical to static fractures.

(DCB striations are parallel sets of curved lines oriented to the direction of crack growth, located in the resin fracture regions between fibers.)

The primary function observed in CLS Mode II shear fatigue fractures are:

- Striations
- Hackle and scallop features identical to static features.

(CLS striations are present mainly at the fiber-matrix separation region, with isolated locations exhibiting striations in the resin fracture planes.)

Currently, it is unclear whether these striations are being formed due to a plastic deformation mechanism at the crack tip (as seen in aluminum alloys) or whether these are simply crack arrest features. (However, the striation spacing does not appear to increase as the test loads are increased. Spacing between striations often vary greatly along the length of a single fiber, as well as large variations in spacing between immediately adjacent fibers. This inconsistency prevents the investigator from accurately determining crack growth rates or loads at fracture.

Faint appearing striations can be enhanced by SEM or TEM analysis but high amounts of specimen are required.

See Figures 6-103 through 6-109.

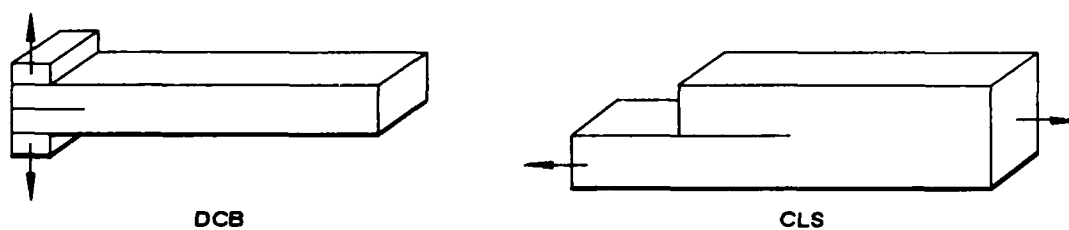
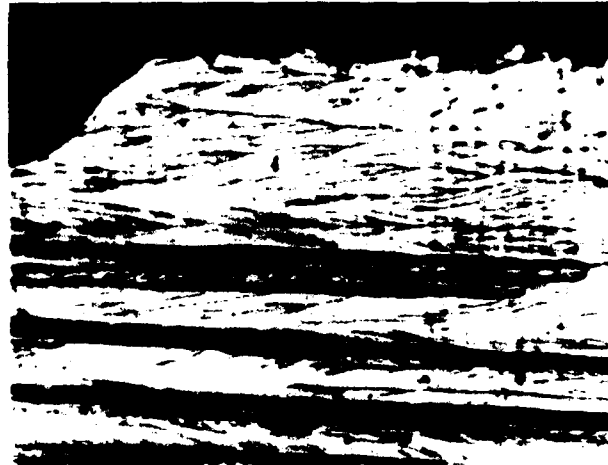
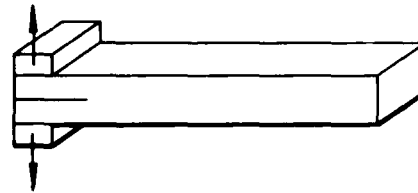


Figure 6-102. Double Cantilever Beam (DCB) for Mode I Fractures Crack Lap Shear (CLS) for Mode II Fractures

5-B70227-268

Optical photomicrographs

Fracture type	Interlaminar fatigue mode I tension
Ply layup	[0] ₂₄
Test type	Fatigue DCB
• Test conditions	21°C, dry
• Fracture between	0/0 plies
Material	Hercules 3501-6/177°C cure AS4 fibers



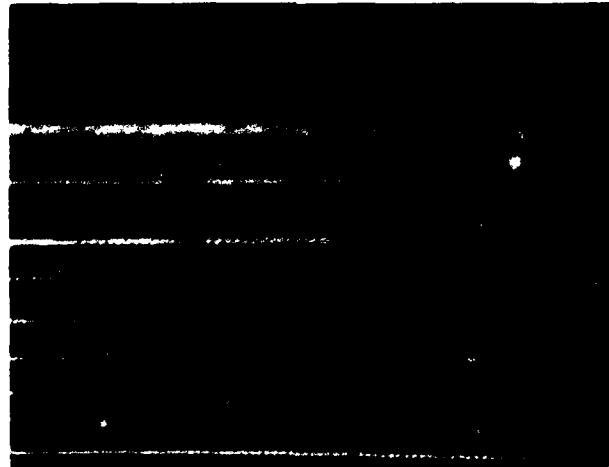
Mechanically induced crack direction →

Figure 6-103. 0/0 Plies at 70°F Dry Condition (Fatigue DCB Mode I, Optical)

5-B70227-269

Optical photomicrographs

Fracture type	Interlaminar fatigue mode II shear
Ply layup	[0] ₂₄
Test type	Fatigue CLS
• Test conditions	21°C, dry
• Fracture between	0/0 plies
Material	Hercules 3501-6/177°C cure AS4 fibers



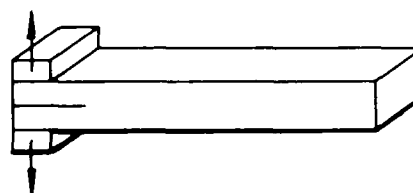
Mechanically induced crack direction →

Figure 6-104. 0/0 Plies at 70°F Dry Condition (Fatigue CLS Mode II, Optical)

5-B70227-270

Optical photomicrographs

Fracture type	Interlaminar fatigue mode I tension
Ply layup	[0]24
Test type	Fatigue DCB
• Test conditions	21°C, dry
• Fracture between	0/0 plies
Material	Hercules 3501-6/177°C cure AS4 fibers



Mechanically induced crack direction

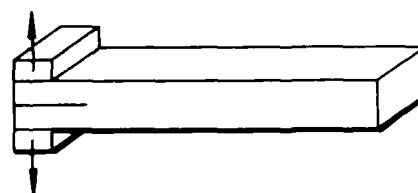


Figure 6-105. 0/0 Plies at 21°C Dry Condition (Fatigue DCB Mode I, Optical)

5-B70227-271

SEM photomicrographs

Fracture type	Interlaminar fatigue mode I tension
Ply layup	[0]24
Test type	Fatigue DCB
• Test conditions	21°C, dry
• Fracture between	0/0 plies
Material	Hercules 3501-6/177°C cure AS4 fibers



Mechanically induced crack direction

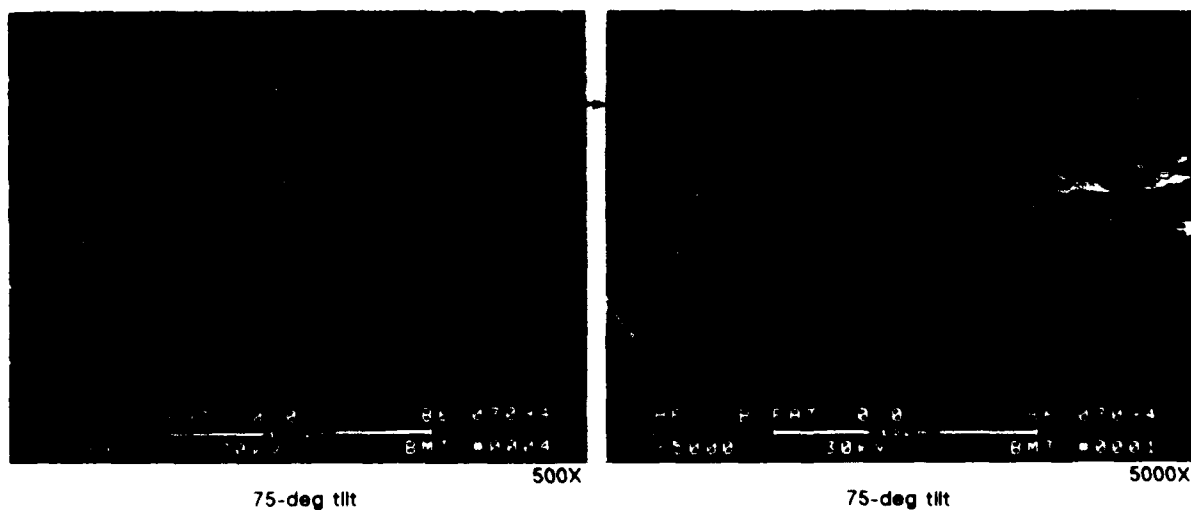


Figure 6-106. 0/0 Plies at 21°C Dry Condition (Fatigue DCB Mode I, SEM)

5-B70227-272

Optical photomicrographs

Fracture type	Interlaminar fatigue mode II shear
Ply layup	[0] 24
Test type	Fatigue CLS
• Test conditions	21°C, dry
• Fracture between	0/0 plies
Material	Hercules 3501-6/177°C cure AS4 fibers

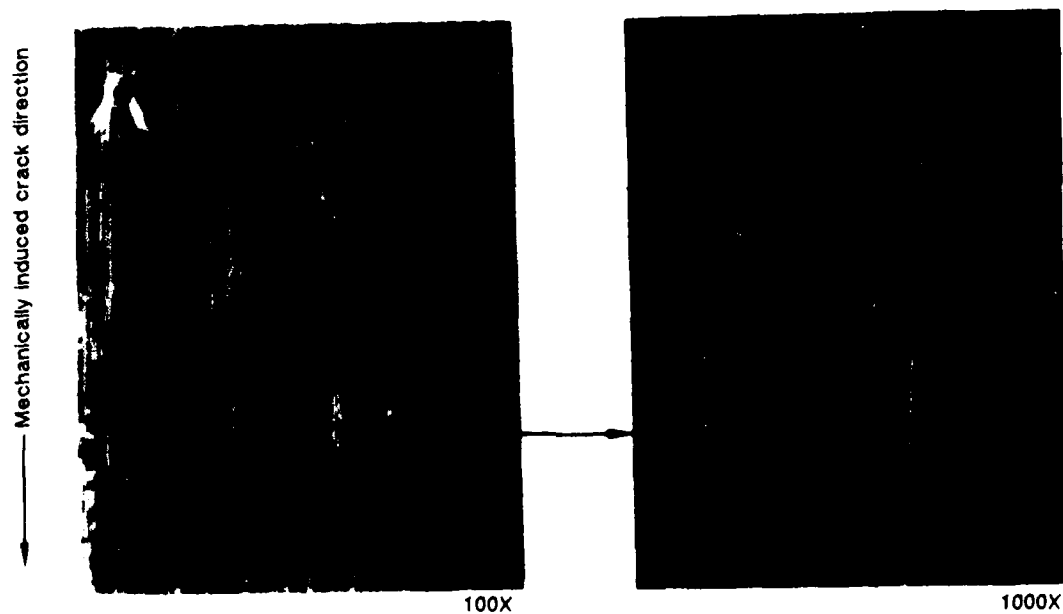
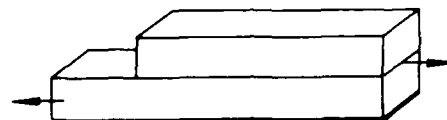
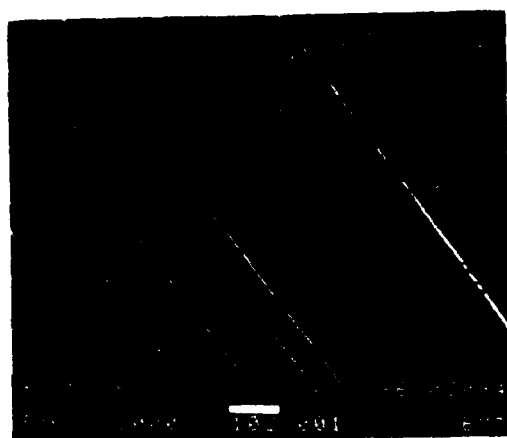
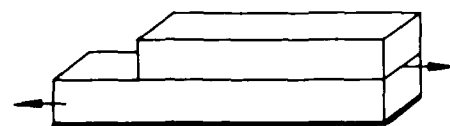


Figure 6-107. 0/0 Plies at 21°C Dry Condition (Fatigue CLS Mode II, Optical)

5-B70227-273

SEM photomicrographs

Fracture type	Interlaminar fatigue mode II shear
Ply layup	[0] 24
Test type	Fatigue CLS (80% to 40% G _{II} C)
• Test conditions	21°C, dry
• Fracture between	0/0 plies
Material	Hercules 3501-6/177°C cure AS4 fibers



1000X



5000X

Mechanically induced crack direction



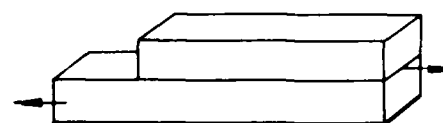
15000X

Figure 6-108. 0/0 Plies at 21°C Dry Condition (Fatigue CLS Mode II, 40% to 80% Static)

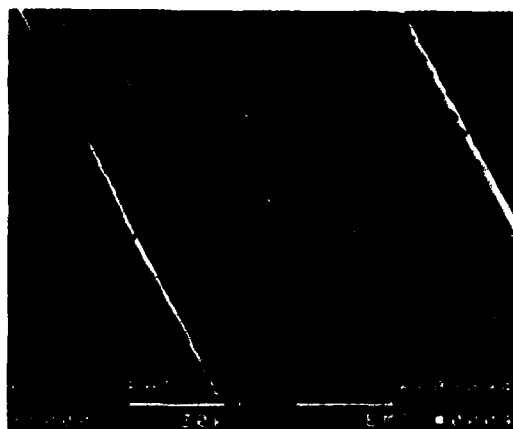
5-B70227-274

SEM photomicrographs

Fracture type	Interlaminar fatigue mode II shear
Ply layup	[0] 24
Test type	Fatigue CLS (60% to 20% GIIIC)
• Test conditions	21°C, dry
• Fracture between	0/0 plies
Material	Hercules 3501-6/177°C cure AS4 fibers



Mechanically induced crack direction



5000X



15000X

Figure 6-109. 0/0 Plies at 21°C Dry Condition (Fatigue CLS Mode II, 20% to 60% Static)

5-B70227-275

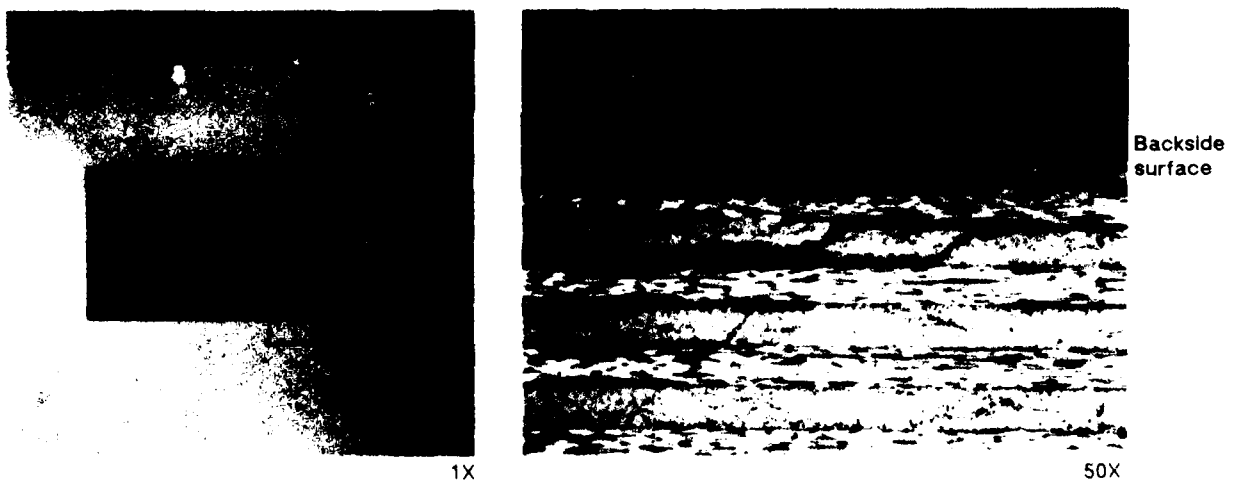
6.9 DRILL BACKSIDE BREAKOUT

Figure 6-110 shows an example of heavy drill pressure on laminate without proper backside pressure, resulting in delamination on the drill exit side.

The primary features are:

- Small localized delaminations with Mode I features (river marks and resin microflow).
- Extreme amounts of particulate present on the delamination surfaces.

See Figures 6-111 and 6-112.



Visual and optical details from a drill breakout specimen are shown above. The photo on the left illustrates the extent of backside damage around the hole and the right photo presents cross-section A-A.

Figure 6-110. Drill Breakout Specimen

6-B70227-276

SEM photomicrographs

Fracture type	Interlaminar mode I tension
Ply layup	[0] 32
Test type	Drill breakout
• Test conditions	21°C, dry
• Fracture between	0/0 plies
Material	Hercules 3501-6/177°C cure AS4 fibers

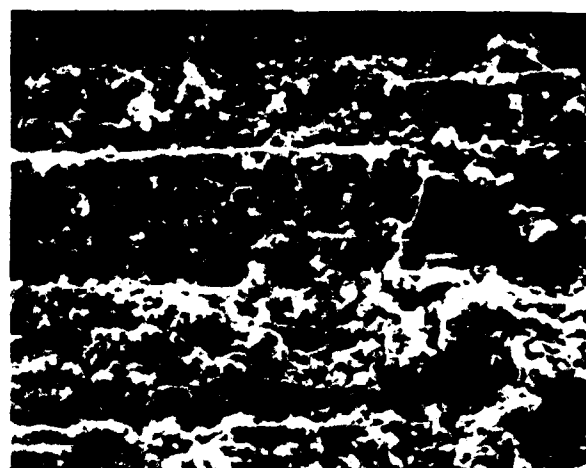
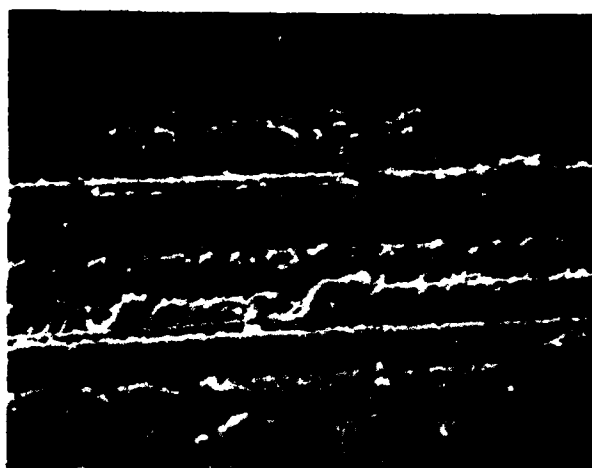
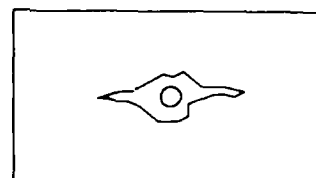
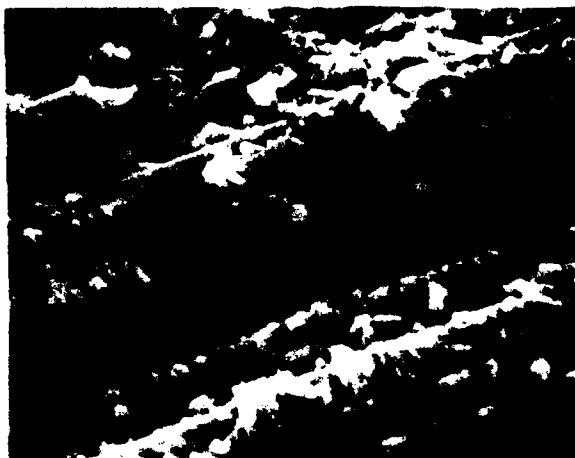
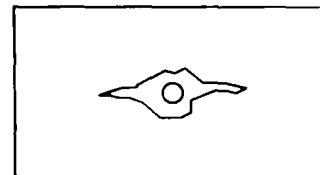


Figure 6-111. 0/0 Plies at 21°C Dry Conditions (Example A)

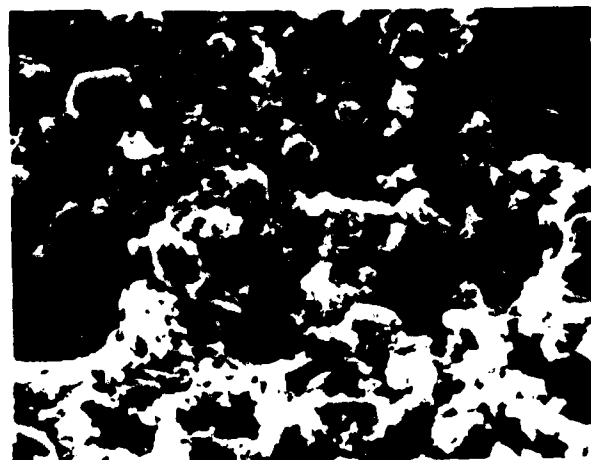
5-B70227-277

SEM photomicrographs

Fracture type	Interlaminar mode I tension
Ply layup	[0] 32
Test type	Drill breakout
• Test conditions	21°C, dry
• Fracture between	0/0 plies
Material	Hercules 3501-6/177°C cure AS4 fibers



2000X



2000X

Figure 6-112. 0/0 Plies at 21°C Dry Conditions (Example B)

5-B70227-278

6.10 COMPRESSION AFTER IMPACT (CAI)

Figure 6-113 shows an example of a Compression After Impact (CAI) test type. The test consisted of:

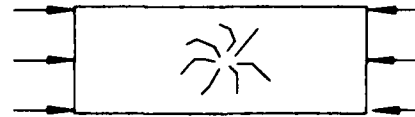
- Impact a 4-inch by 6-inch coupon until visible failure.
- In-plane compression load failure.

The primary features associated with fractures produced with a CAI specimen are as follows:

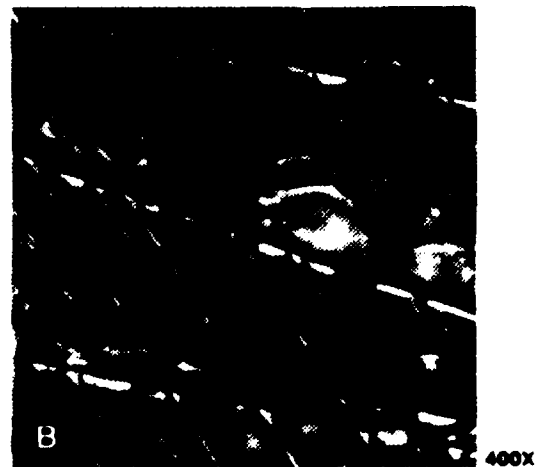
- Compression buckling of the laminate through the impact site (with extensive delamination).
- Shear dominated interlaminar fracture features at the impact region (origin).
- Tension dominated interlaminar fracture features at the specimen outer edges.
- Crack mapping of the river marks and resin microflow to identify crack growth direction (and thus the origin).

Optical photomicrographs

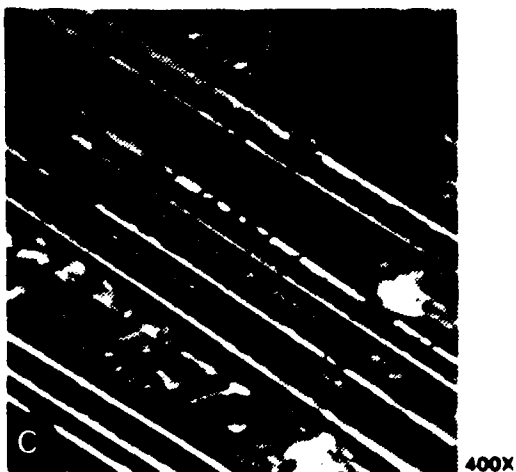
Fracture type	Interlaminar/translaminar
Ply layup	[0, 45, 90] 8S
Test type	Compression after impact
• Test conditions	Dry
• Fracture between	0/45/90 plie.
Material	Hercules 3501-6/177°C cure AS4 fibers



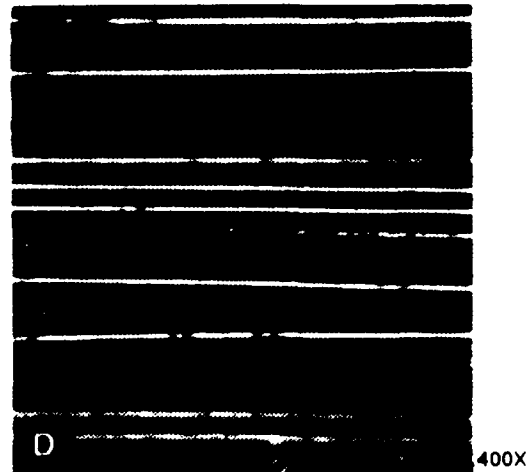
Crack propagation direction



Crack propagation direction



Crack propagation direction



Crack propagation direction

Key to crack growth
direction arrows
— Mode I tension
— Mode II shear

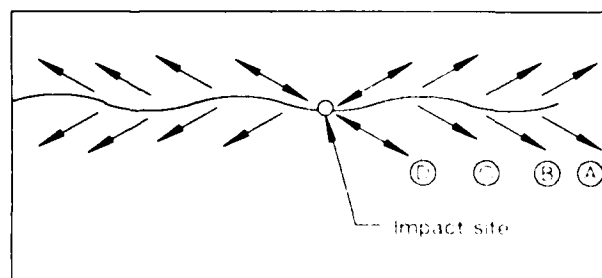


Figure 6-113. 0/45/90 Plies, Dry Conditions (Compression After Impact)

6.11 CONTAMINANTS

Figures 6-114 and 6-115 shows two test types of contaminants, Teflon and Frekote.

The primary key features observed in the contaminant containing specimens were as follows:

Teflon Contamination

- Interconnected and fibrous appearing contamination regions.
- Matrix region fracture surface surrounding Teflon regions exhibit morphologies typical of the induced loading mode.

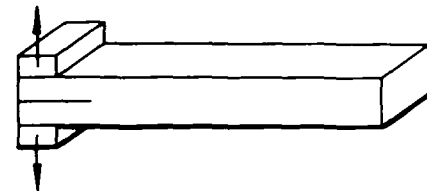
Frekote Contamination

- Interconnected and very smooth contaminated regions.
- Areas without resin fracture features (indicative of adhesive type separation).
- Matrix resin fracture surface surrounding Frekote regions exhibit morphologies typical of the induced loading mode.

Note: When photomicrographs exhibit fractured resin particulate in the regions of contamination it becomes more difficult to identify smooth adhesive separation.

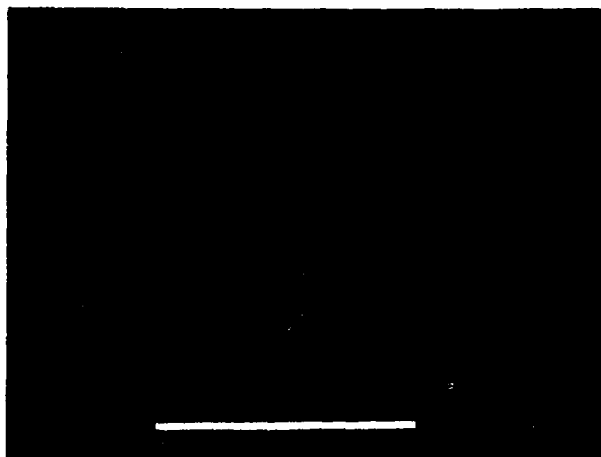
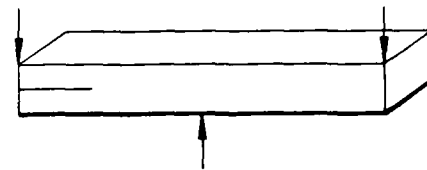
SEM photomicrographs

Fracture type	Interlaminar mode I tension
Ply layup	[0, 90] ₁₂ S
Test type	DCB with Teflon contamination
• Test conditions	21°C, dry
• Fracture between	0/90 plies
Material	Hercules 3501-6/177°C cure AS4 fibers



SEM photomicrographs

Fracture type	Interlaminar mode II shear
Ply layup	[0, 90] ₁₂ S
Test type	ENF with Teflon contamination
• Test conditions	21°C, dry
• Fracture between	0/90 plies
Material	Hercules 3501-6/177°C cure AS4 fibers



50X
Mode I tension

Mechanically induced crack direction

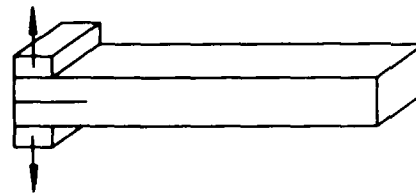
2000X
Mode II shear

Figure 6-114. Teflon Contamination

5-B70227-280

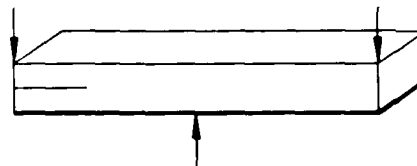
SEM photomicrographs

Fracture type	Interlaminar mode I tension
Ply layup	[0, 45] 12S
Test type	DCB with Frekote contamination
• Test conditions	21°C, dry
• Fracture between	0, 45 plies
Material	Hercules 3501-6/177°C cure AS4 fibers

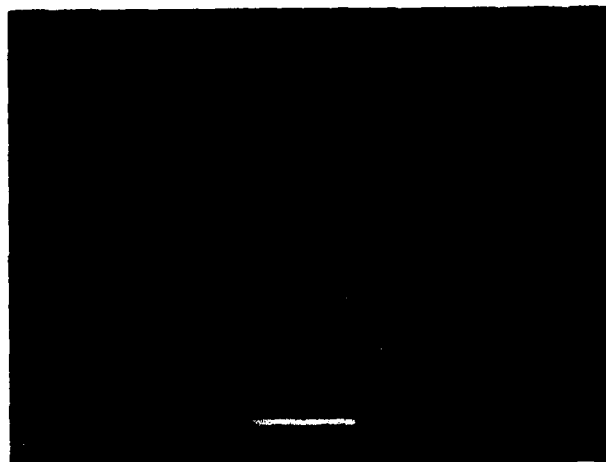


SEM photomicrographs

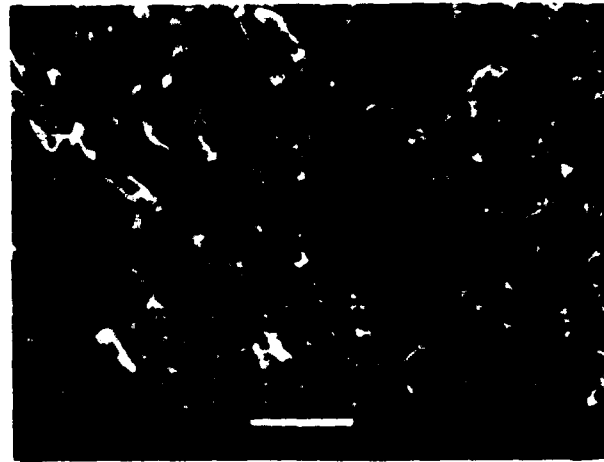
Fracture type	Interlaminar mode II shear
Ply layup	[+ 45, -45] 12S
Test type	ENF with Frekote contamination
• Test conditions	21°C, dry
• Fracture between	+45/-45 plies
Material	Hercules 3501-6/177°C cure AS4 fibers



Mechanically induced crack direction



200X
Mode I tension



2000X
Mode II shear

Figure 6-115. Frekote Contamination

6-B70227R1-281

6.12 VOIDS

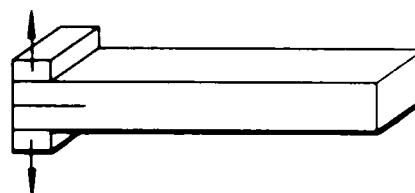
Figure 6-116 shows two test types of voids, DCB and ENF.

The primary features observed in specimens with high void areas are as follows:

- Smooth, featureless, resin surface with underlying fibers at voids (often with rounded corners)
- Fracture surface surrounding void region exhibits a matrix fracture morphology typical of the induced mode (allows determination of crack growth and mode).
- Cracking does not appear to locally initiate at the voids.

SEM photomicrographs

Fracture type	Interlaminar mode I tension
Ply layup	[0, 90] 12S
Test type	DCB—high void content
• Test conditions	21°C, dry
• Fracture between	0/90 plies
Material	Hercules 3501-6/177°C cure AS4 fibers

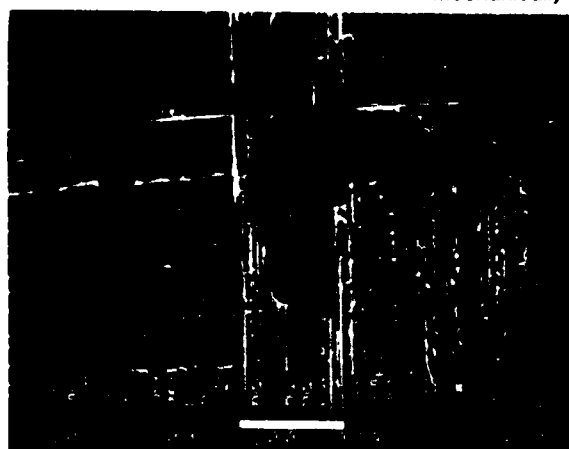


SEM photomicrographs

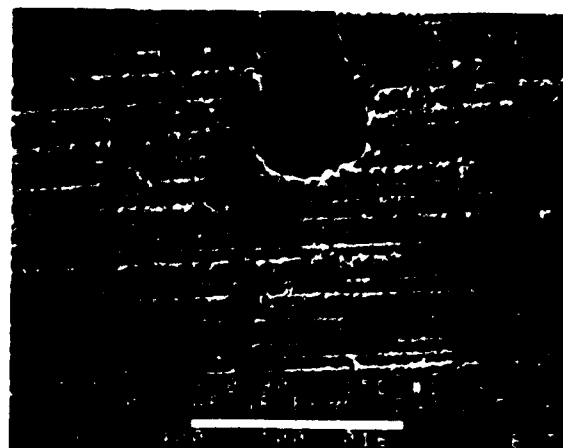
Fracture type	Interlaminar mode II shear
Ply layup	[0, 90] 12S
Test type	ENF—high void content
• Test conditions	21°C, dry
• Fracture between	0/90 plies
Material	Hercules 3501-6/177°C cure AS4 fibers



← Mechanically induced crack direction



200X



400X

Figure 6-116. Voids, DCB, and ENF

6-B70227-282

6.13 OTHER MATERIAL SYSTEMS

The systems discussed in this paragraph are:

Epoxy Based

121°C (250°F) Cure Fiberglass/Epoxy (see Figure 6-117)

177°C (350°F) Cure Fiberglass/Epoxy (see Figure 6-118)

121°C (250°F) Cure Aramid/Epoxy (see Figure 6-119)

Carbon Based

- PEEK/Carbon (see Figure 6-120)
- PMR-15/Carbon (see Figure 6-121)

6.13.1 Epoxy Resin Based Systems

Interlaminar Fractures—These types of fractures are epoxy resin dominated and exhibit features similar to those previously presented with river marks and microflow. As a result, crack mapping and determination of fracture mode is possible.

Translaminar Fractures—These types of fractures are fiber dominated and vary in appearance depending upon the fiber type. The fiberglass fibers fracture very similar to the carbon fibers, with radial features on the fiber ends. The Aramid fibers, however, tend to fibrilate (split longitudinally) and do not exhibit features useful for mapping fiber end fractures or differentiating between translaminar tension or compression.

6.1.3.2 Carbon Fiber Based Systems

For carbon based systems, the primary features presented on the fractures surface are as follows:

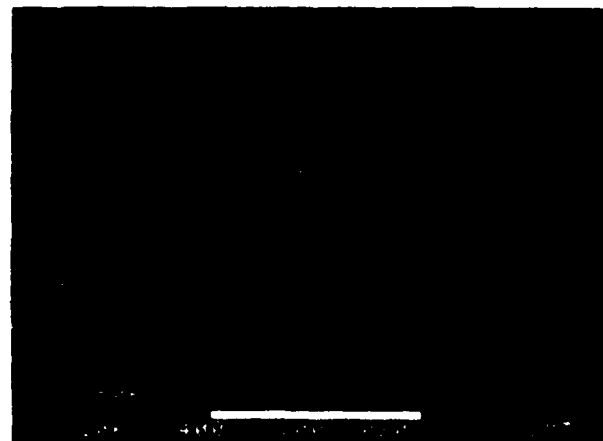
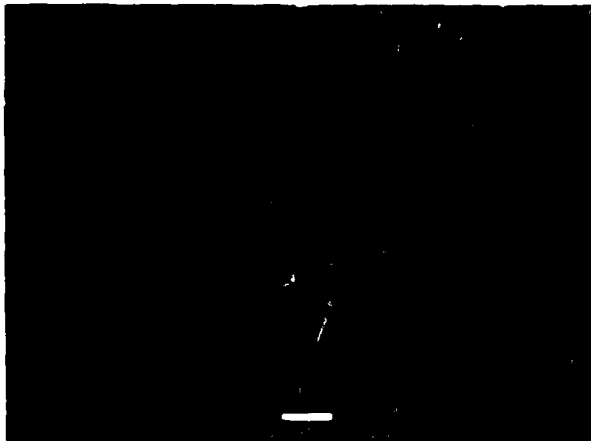
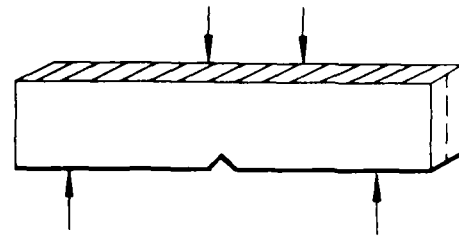
Interlaminar Fractures—These types of fractures exhibit features indicative of the resin ductibility. The PEEK resin appears to be highly deformed such that river marks and resin

microflow are either not present or identifiable. For PEEK, studies have shown the appearance of hackles for Mode II fractures, thus providing the investigator with the capability to differentiate between Mode I and Mode II fractures. The PMR-15 resin system exhibits river marks, resin microflow, and hackles due to the more brittle nature of this resin system.

Translaminar Fractures—These types of fractures exhibit fiber end features similar to those presented for the carbon/epoxy systems. Crack mapping of the fiber end radials (for tension cracks) and differentiation between tension and compression fracture is possible.

SEM photomicrographs

Fracture type	Translaminar mode I tension
Ply layup	[0, 90] _{4S} tape
Test type	Four-point bend
• Test conditions	21°C, dry
• Fracture between	0/90 plies
Material	Fiberglass-epoxy 250°F cure



Mechanically induced crack direction

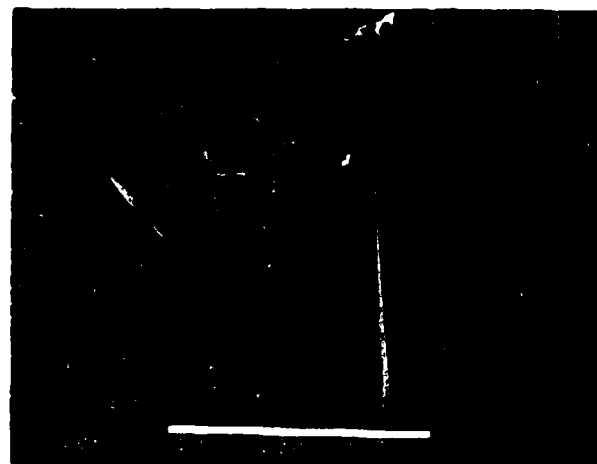
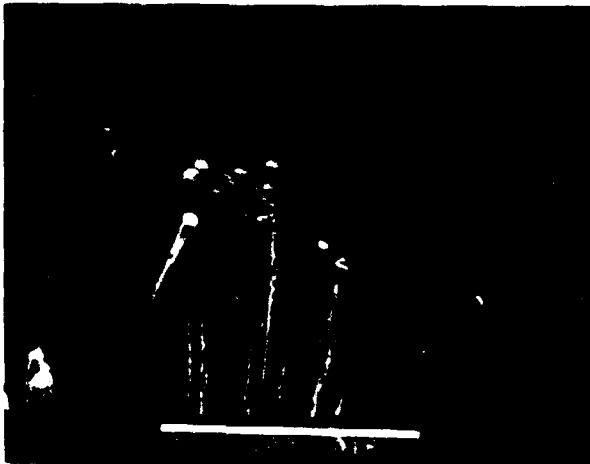
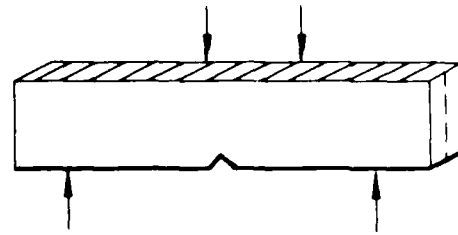


Figure 6-117. Fiberglass/Epoxy 250°F Cure

6-B70227-283

SEM photomicrographs

Fracture type	Translaminar mode I tension
Ply layup	[0, 90] _{4S} tape
Test type	Four-point bend
• Test conditions	21°C, dry
• Fracture between	0/90 plies
Material	Fiberglass-epoxy 350°F cure



Mechanically induced crack direction

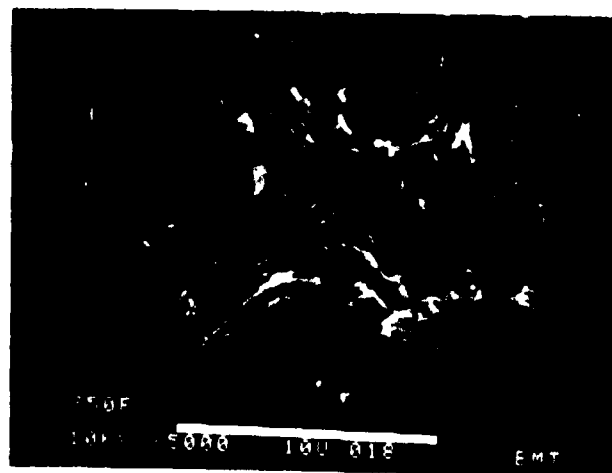
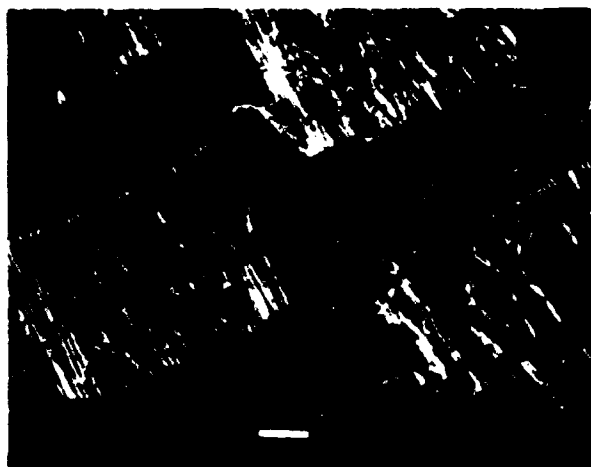
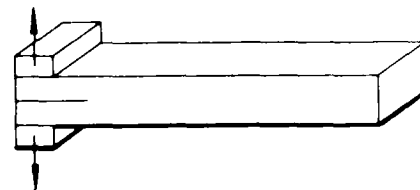


Figure 6-118 Fiberglass Epoxy, 350°F Cure

6-B70227-284

SEM photomicrographs

Fracture type	Interlaminar mode I tension
Ply layup	[0, 90] ₄ fabric
Test type	DCB
• Test conditions	21°C, dry
• Fracture between	0/90 plies
Material	Aramid fibers/epoxy



Mechanically induced crack direction

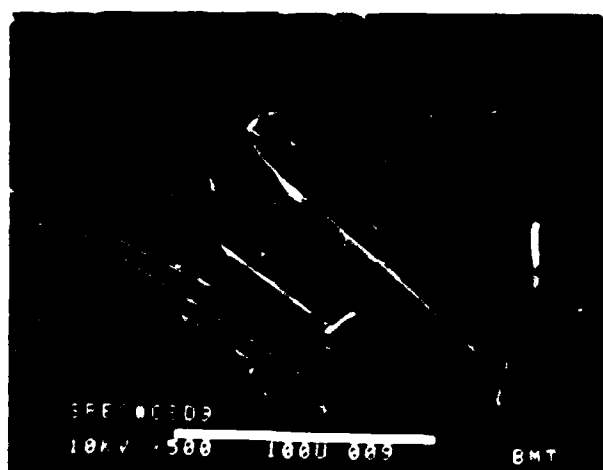
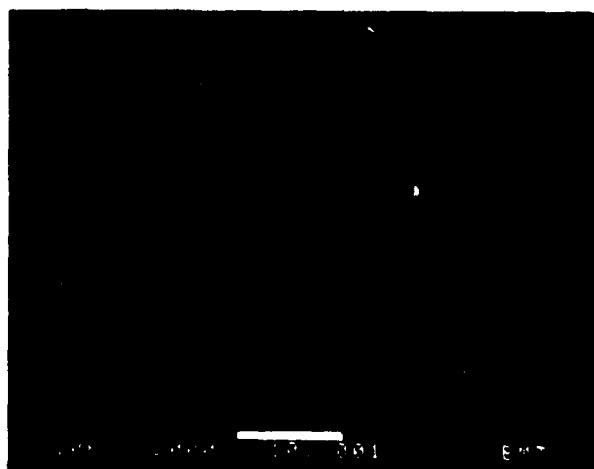
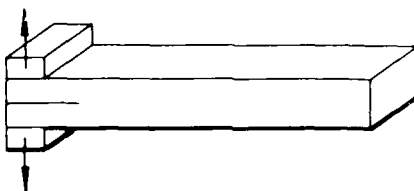


Figure 6-119. Aramid Fibers/Epoxy

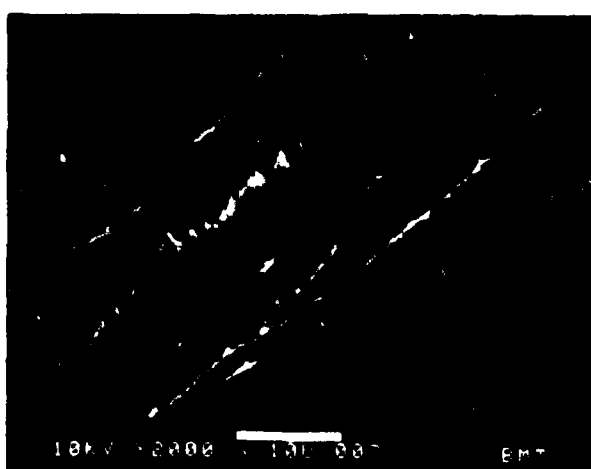
6-B70227-285

SEM photomicrographs

Fracture type	Interlaminar mode I tension
Ply layup	[0] 24
Test type	DCB
• Test conditions	21°C, dry
• Fracture between	0/0 plies
Material	PEEK/AS4 fibers



Mechanically induced crack direction



Mechanically induced crack direction



Mechanically induced crack direction

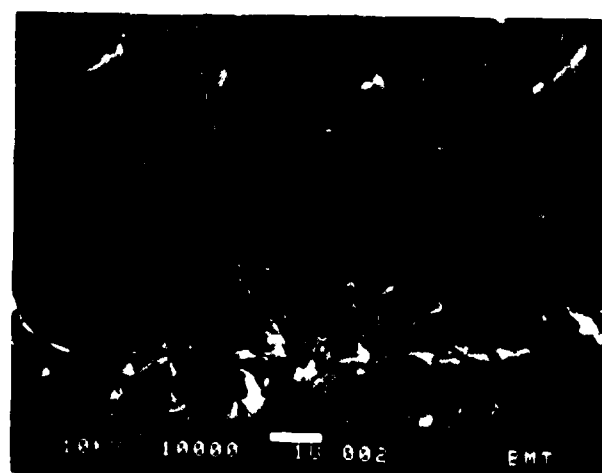
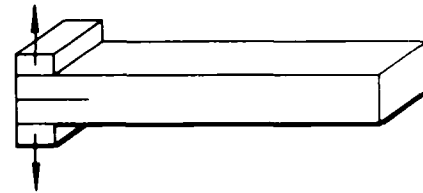


Figure 6-120 PEEK/AS4 Fibers

6-B70227-286

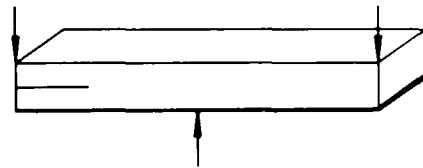
SEM photomicrographs

Fracture type	Interlaminar mode I tension
Ply layup	[0, 90] ₁₂ S
Test type	ENF
• Test conditions	21°C, dry
• Fracture between	0/90 plies
Material	PMR-15/Celion-3000

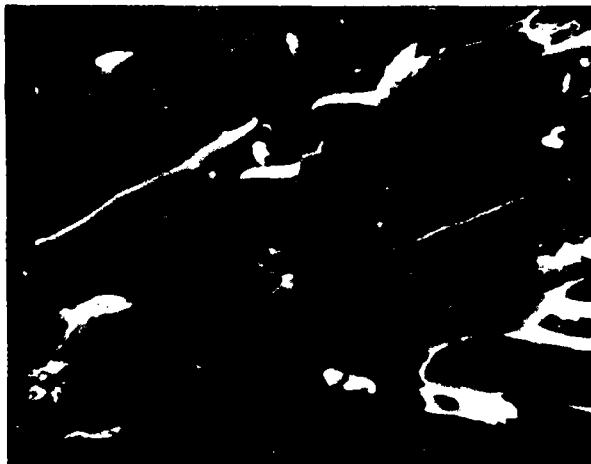


SEM photomicrographs

Fracture type	Interlaminar mode II shear
Ply layup	[0, 90] ₁₂ S
Test type	ENF
• Test conditions	21°C, dry
• Fracture between	0/90 plies
Material	PMR-15/Celion-3000



Mechanically induced crack direction



Mode I



Mode II

Figure 6-121. PMR-15/Celion-3000

6-B70227-287

7.0 TEXT REFERENCES

- (1) 1984 AF F33615-84-C-5010.
- (2) AFWAL-TR-81-4180, Chemical Composition Processing for Air Force/Navy Advanced Composite Matrix Material, T. A. Sewell, final report, 1982.
- (3) Young, P. R., Stein B. A., and Chang A. C., "Resin Characterization in Cured Graphite Fiber Reinforced Composites Using Diffuse Reflectance-FTIR", 28th National SAMPE Symposium and Exhibition, Vol. 28, 1983, pp. 824-837.
- (4) Handbook of Chemistry and Physics , 65th edition, Weast, R. C., ed., CRC Press Inc. Boca Raton, Florida, 1985, p. E-130.
- (5) Ratner, B. D., McElroy, B. J., in Spectroscopy in the Biomedical Sciences: Gendreau, R. M., ed., CRC Press Inc., Boca Raton, Florida, 1986, pp. 107-140.
- (6) Daniel, I. M., "The Behavior of Uniaxial Loaded Graphite/Epoxy Plates with Holes," Proceedings of the Second International Conference on Composite Materials, published by the Metallurgical Society of AIME, 1978, pp. 1019-1034.
- (7) Mikulas, M. M., "Failure Prediction Techniques for Compression-Loaded Composite Laminates with Holes," Selected NASA Research in Composite Materials and Structures, NASA Conference Publication 2142, August 1980.
- (8) Aronsson, C. G. and Bachklund, J., "Damage Mechanics Analysis of Matrix Effects in Notched Laminates," Composite Materials: Fatigue and Fracture, ASTM STP 907, H. T. Hahn, Ed., ASTM, Philadelphia, Pennsylvania, 1986, pp. 134-157.
- (9) Whitcomb, J. D., Analysis of Instability Related Growth of a Through-Width Delamination, NASA TM 86301, September 1984.

- (10) Rothschilds, R. J., Instability-Related Delamination Growth in Thermoset and Thermoplastic Composites, Presented at ASTM Composite Materials Testing and Design: Eighth Symposium, Charleston, South Carolina, April 1986.
- (11) Tsai, S. W. and Hahn, H. T., "Introduction to Composite Materials", Technomic Pub. Co., Inc., Westport, Connecticut, 1980.
- (12) Tsai, S. W., "Composites Design - 1986", published by Think Composites, Dayton, Ohio, 1986.
- (13) Halpin, J. C., "Primer on Composite Materials", Technomic Pub. Co., Inc., Lancaster, Pennsylvania, 1984.
- (14) Ashton, J. E. and Whitney, J. M., "Theory of Laminated Plastics", Technomic Pub. Co., Inc., Stanford, Connecticut, 1970.
- (15) Jones, R. M. Mechanics of Composite Materials, Scripta Book Co., Washington, D.C., 1975.
- (16) Tsai, S. W., "Strength Theories of Filamentary Structures", in Fundamental Aspects of Fiber Reinforced Plastic Composites, R. T. Schwartz and H. S. Schartz, Eds., Wiley Interscience, New York, 1968, pp. 3-11.
- (17) Tsai, S. W. and Wu, E. M., "A General Theory of Strength for Anisotropic Materials", J. Composite Materials, January 1971, pp. 58-80.
- (18) Pipes, R. B. and Cole, B. W., "On Off-Axis Strength Tests for Anisotropic Materials", J. Composite Materials, April 1973, pp. 246-256.
- (19) Kim, R. Y., In-Plane Tensile Strength of Multidirectional Composite Laminates, University of Dayton Research Institute, Technical Report UDR-TR-81-84, 1981.
- (20) Crossman, F. W., "Analysis of Free Edge Induced Failure of Composite Laminates," First USA-USSR Symposium on Fracture of Composite Materials, Sijthoff and Noordhoff International Publishers, 1979, pp. 291-302.

- (21) Herakovich, C. T., "On Failure Modes in Finite Width Angle Ply Laminates," Advances in Composite Materials; Proceedings of the Third International Conference on Composite Materials, Vol. 1, Pergamon Press, 1980, pp. 425-435.
- (22) Chamis, C. C. and Smith, G. T., "CODSTRAN: Composite Durability Structural Analysis," NASA-TM-79070, 1978.
- (23) Gillespie, J. W., Jr. Microcomputer Software, Center for Composites Manufacturing, Science, and Engineering, Newark, Delaware, 1984.
- (24) Flaggs, D. L. and Kural, M. H., "Experimental Determination of the In Situ Transverse Lamina Strength in Graphite/Epoxy Laminates," J. Composite Materials, Vol. 16, March 1982, pp. 103-116.
- (25) Parvizi, A., Garrett, K. W. and Bailey, J. E., "Constrained Cracking in Glass Fibre-reinforced Epoxy Cross-ply Laminates," J. Materials Science, 13, 1978, pp. 195-201.
- (26) Bader, M. G., Bailey, J. E., Curtis, P. T. and Parvizi, A., "The Mechanisms of Initiation and Development of Damage in Multi-Axial Fibre-Reinforced Plastic Laminates," ICCM3, Vol. 3, Cambridge, England, August 1979, pp. 227-239.
- (27) Bailey, J. E., Curtis, P. T. and Parvizi, A., "On the Transverse Cracking and Longitudinal Splitting Behavior of Glass and Carbon Fibre Reinforced Epoxy Cross Ply Laminates and the Effect of Poison and Thermally Generated Stain," Proc. R. Soc. Lond., 366, 1979, pp. 599-623.
- (28) Flaggs, D. L., "Prediction of Tensile Matrix Failure in Composite Laminates," J. Composite Materials, Vol. 19, January 1985, pp. 29-50.
- (29) Bathias, C., Esnault, R., and Pellas, J., "Application of Fracture Mechanics to Graphite Fibre-Reinforced Composites," Composites, Vol. 12, July 1981, pp. 195-200.

- (30) McGarry, F. J., Mandell, J. F., and Wang, S. S., "Fracture of Fiber-Reinforced Composites," Polymer Engineering and Science, Vol. 16, No. 9, September 1976, pp. 609-613.
- (31) Awerbuch, J. et al., "Determination Characteristics and Failure Modes of Notched Graphite Polyimide Composites at Room and Elevated Temperatures," NASA-CR-159375, August 1980.
- (32) Lagace, P. A., "Notch Sensitivity and Stacking Sequence of Laminated Composites," Composite Materials: Testing and Design (Seventh Conference), ASTM STP 893, J. M. Whitney, Ed., ASTM, Philadelphia, Pennsylvania, 1986, pp. 161-176.
- (33) Wu, E. M., "Fracture Mechanics of Anisotropic Plates," in Composite Materials Workshop, S. W. Tsai, J. C. Halpin and N. J. Pagano, Eds., Techomic Pub. Co., Inc., Stanford, Connecticut, 1968, pp. 20-43.
- (34) Waddoups, M. E., Eisemann, J. R. and Kaminski, B. E., "Macroscopic Fracture Mechanics of Advanced Composite Materials," J. Composite Materials, Vol. 5, 1971, pp. 446-454.
- (35) Whitney, J. M. and Nuismer, R. J., "Stress Fracture Criteria for Laminated Composites Containing Stress Concentrations," J. Composite Materials, Vol. 8, 1974, pp. 253-265.
- (36) Nuismer, R. J. and Whitney, J. M., "Uniaxial Failure of Composite Laminates Containing Stress Concentrations," in Fracture Mechanics of Composites, ASTM STP 593, American Society of Testing and Materials, 1975, pp. 117-142.
- (37) Karlak, R. F., "Hole Effects in a Related Series of Symmetrical Laminates," in Proceedings of Failure Modes in Composites, IV., The Metallurgical Society of AIME, Chicago, Illinois, 1977, pp. 105-117.

- (38) Pipes, R. B., Wetherhold, R.C. and Gillespie, J. W., Jr., "Notched Strength of Composite Materials," J. Composite Materials, Vol. 12, 1979, pp. 148-160.
- (39) Pipes, R. B., Gillespie, J. W., Jr. and Wetherhold, R. C., "Superposition of the Notched Strength of Composite Laminates," Polymer Engineering and Science, Vol. 19, No. 16, 1979, pp. 1151-1155.
- (40) Pipes, R. B., Wetherhold, R. C. and Gillespie, J. W., Jr., "Macroscopic Fracture of Fibrous Composites," Materials Science and Engineering, Vol. 45, 1980, pp. 247-253.
- (41) Kin, K. Y., "Fracture of Filamentary Composite Materials," Ph.D. Dissertation, Department of Aeronautics and Astronautics, M.I.T., Cambridge, Massachusetts, Jan. 1976.
- (42) Mar, J. W. and Lin, K. Y., "Fracture Mechanics Correlation for Tensile Failure of Filamentary Composites with Holes," J. of Aircraft, Vol. 14, No. 7, July 1977, pp. 703-704.
- (43) Poe, C. C., Jr., and Sova, J. A., "Fracture Toughness of Boron/Aluminum Laminates with Various Proportions of 0° and +45° Plies," NASA Technical Paper 1707, November 1980.
- (44) Aronsson, C. G., Tensile Fracture of Composite Laminates With Holes and Cracks, The Royal Institute of Technology, Report No. 84-5, Stockholm, Sweden, 1984.
- (45) Starnes, J. H., Jr., Rhodes, M. D., and Williams, J. G., "Effect of Impact Damage and Holes on the Compressive Strength of a Graphite-Epoxy Laminate", ASTGM STP 696, 1979, pp. 145-171.
- (46) Williams, J. G. and Rhodes, M. D., "Effect of Resin on the Impact-Damage Tolerance of Graphite-Epoxy Laminates," ASTM STP 787, 1983, pp. 450-480.

- (47) Starnes, J. H., Jr. and Williams, J. G., "Failure Characteristics of Graphite-Epoxy Structural Components Loaded in Compression," Mechanics of Composite Materials - Recent Advances, Hashin and Herakovich, Editors, Pergamon Press, 1983.
- (48) Williams, J. G., "Effect of Impact Damage and Open Holes on the Compression Strength of Tough Resin/High Strain Fiber Laminates," in Tough Composite Materials - Recent Developments, Noyes Publications, Park Ridge, New Jersey, 1985.
- (49) Wilkins, D. J., "A Preliminary Damage Tolerance Methodology for Composite Structures," in Failure Analysis and Mechanisms of Failure of Fibrous Composite Structures, NASA CP 2278, 1983, pp. 67-93.
- (50) Gillespie, J. W., Jr. and Pipes, R. B., "Compressive Strength of Composite Laminates with Interlaminar Defects," Composite Structures, Vol. 2, 1984, pp. 49-69.
- (51) Webster, J. D., "Flaw Criticality of Circular Disbond Defects in Composite Laminates," CCM-81-03, Center for Composite Materials, Univ. of Delaware, 1981.
- (52) Ashizawa, M., "Fast Interlaminar Fracture of a Compressively Loaded Composite Containing a Defect," Douglas Paper 6994, January 1981.
- (53) Ashizawa, M., "Improving Damage Tolerance of Laminated Composites Through the Use of New Tough Resins," Douglas Paper 7250, January 1983.
- (54) Ramkumar, R. L., "Performance of a Quantitative Study of Instability Related Delamination Growth," NASA Contractor Report 166046, March 1983.
- (55) Ramkumar, R. L., Kulkarni, S. V. and Pipes, R. B., "Definition and Modeling of Critical Flaws in Graphite Fiber Reinforced Epoxy Resin Matrix Composite Materials," Naval Air Development Center Report No. NADC-76228-30, January 1978.

- (56) Chatterjee, S. N., Hashin, Z. and Pipes, R. B., "Definition and Modeling of Critical Flaws in Graphite Fiber Reinforced Resin Matrix Composite Materials," Naval Air Development Center Report No. NADC 77278-30, August 1979.
- (57) Chatterjee, S. N. and Pipes, R. B., "Composite Defect Significance," Proceedings of the Mechanics of Composites Review Meeting, Dayton, Ohio, October 1982.
- (58) Yin, W. L., Sallam, S. N. and Simites, G. J., "Ultimate Axial Load Capacity of a Delaminated Beam-Plate," AIAA Journal, Vol. 24, No. 1, January 1986.
- (59) Griffith, A. A., "The Phenomena of Rupture and Flow in Solids," Phil. Trans. Royal Soc. of London, A221, 1921.
- (60) Rybicki, E. F., and Kanninen, M. F., "A Finite Element Calculation of Stress Intensity Factors by a Modified Crack Closure Integral," Engineering Fracture Mechanics, Vol. 9, No. 4, 1977, pp. 931-38.
- (61) Johnson, W. S. and Mangalgiri, P. D., "Influence of the Resin on Interlaminar Mixed-Mode Fracture," NASA TM 87571, July 1985.
- (62) Wilkins, D. J., "A Comparison of the Delamination and Environmental Resistance of a Graphite/Bismaleimide," NAV-GD-0037, General Dynamics, Fort Worth, Texas, September 1981.
- (63) Russell, A. M. and Street, K. N., "The Effect of Matrix Toughness on Delamination: Static and Fatigue Fracture Under Mode II Shear Loading of Graphite Fiber Composites," presented at NASA/ASTM Symposium on Toughened Composites, Houston, Texas, March 13-15, 1985.
- (64) Murri, G. B and O'Brien, T. K., "Interlaminar G_{IIC} Evaluation of Toughened Resin Matrix Composites Using the End-Notched Flexure Test," NASA Langley Research Center, Hampton, Virginia, 1985.

- (65) Gillespie, J. W., Jr., "Delamination Growth in Composite Materials," Center for Composite Materials, Newark, DE, NASA Grant Number NAS6-1-475, 1986.
- (66) "Aromatic Polymer Composites APC 2," Performance Resins Department, ICI Americas, Inc., Wilmington, Delaware, 1984.
- (67) Ramkumar, R. L., "Performance of a Quantitative Study of Instability-Related Delamination Growth," NASA Contract Report No. NASA-16727, March 1983.
- (68) Miller, A. G., and Wingert, A. L., "Fracture Surface Characterization of Commercial Graphite/Epoxy Systems," ASTM STP 696, Edited by R. B. Pipes, 1979, pp. 223-273.
- (69) Carpenter, J. F., "Test Program Evaluation of Hercules 3501-6 Resin," N00019-77-C-0155, May 1978.

8.0 BIBLIOGRAPHY

1. Miller, A. G., and Wingert, A. L., "Fracture Surface Characterization of Commercial Graphite/Epoxy Systems," ASTM STP 696, Edited by R. B. Pipes, 1979, pp. 223-273.
2. Clements, L. L., and Adamson, M. J. "Failure Morphology of (0 deg.) 8 Graphite/Epoxy as Influenced by Environment and Processing," NASA-TM-81318, August 1981.
3. Purslow, D., "Some Fundamental Aspects of Composites Fractography," Composites, October 1981.
4. Adams, D. F., "Analysis of the Compression Fatigue Properties of a Graphite/Epoxy Composite," 1981 Advances in Aerospace Structures and Materials, Proceeding of the Winter Annual Meeting, published by American Society of Mechanical Engineers, 1981, pp. 43-49.
5. Freeman, S. M., "Damage Progression in Graphite-Epoxy by a Deplying Technique," AFWAL-TR-81-3157, December 1981.
6. Morris, G. E. "Determining Fracture Directions and Fracture Origins on Failed Graphite/Epoxy Surfaces," ASTM STP 696, Edited by R. B. Pipes, 1979, pp. 274-297.
7. Liechti, K. M. et al., "SEM/TEM Fractography of Composite Materials," AFWAL-TR-82-4085, September 1982.
8. Kline, R. A., and Chang, F. H., "Composite Failure Surface Analysis," Journal of Composite Materials, Vol. 14, October 1980, pp. 315-324.
9. Sinclair, J. H., "Fracture Modes in High Modulus Graphite/Epoxy Angleplied Laminates Subjected to Off-Axis Tensile Loads," Rising to the Challenge of the 80's; 35th Annual Conference and Exhibit, published by Society of the Plastics Industry, Inc., 1980, pp. 12-C1 to 12-C8.

10. Johannesson, T., Sjoblom, P., and Seldon, R., "The Detailed Structure of Delamination Fracture Surfaces in Graphite/Epoxy Laminates," Journal of Materials Science **19**, 1984, pp. 1171-1177.
11. Donaldson, S. L., "Fracture Toughness Testing of Graphite/Epoxy and Graphite/PEEK Composites," Composites, April 1985.
12. Robertson, R. et al., "The Stacked Lamellar Texture on the Fracture Surface of Fibre Composites," Journal of Materials Science **20**, 1985, pp. 2801-2806.
13. Robertson, R. et al., "Fracture in Epoxy Matrix Resins," Composites Science and Technology **22**, 1985, pp. 197-207.
14. Browning, C. E. et al., "A Four-Point Shear Test for Graphite/Epoxy Composites," Composite Materials, ASTM Proceedings, Philadelphia Pennsylvania, 1983.
15. Craddock, J. N. and Champagne, P. J., "A Comparison of Failure Criteria for Laminate Composite Materials," Structures, Structural Dynamics and Materials Conference, published by American Institute of Aeronautics and Astronautics, 1982, pp. 268-278.
16. Crossman, F. W., "Analysis of Free Edge Induced Failure of Composite Laminates," First USA-USSR Symposium on Fracture of Composite Materials, Sijthoff and Noordhoff International Publishers, 1979, pp. 291-302.
17. Herakovich, C. T., "On Failure Modes in Finite Width Angle Ply Laminates," Advances in Composite Materials; Proceedings of the Third International Conference on Composite Materials, Vol. I, Pergamon Press, 1980, pp. 425-435.
18. Chamis, C. C. and Smith, G. T., "CODSTRAN: Composite Durability Structural Analysis," NASA-TM-79070, 1978.
19. Bathias, C., Esnault, R., and Pellas, J., "Application of Fracture Mechanics to Graphite Fibre-Reinforced Composites," Composites, Vol. 12, July 1981, pp. 195-200.

20. McGarry, F. J., Mandell, J. F., and Wang, S. S., "Fracture of Fiber-Reinforced Composites," Polymer Engineering and Science, Vol. 16, No. 9, September 1976, pp. 609-613.
21. Awerbuch, J. et al., "Determination Characteristics and Failure Modes of Notched Graphite Polyimide - Composites at Room and Elevated Temperatures," NASA-CR-159375, August 1980.
22. Daniel, I. M., "The Behavior of Uniaxial Loaded Graphite/Epoxy Plates with Holes," Proceedings of the Second International Conference on Composite Materials, published by the Metallurgical Society of AIME, 1978, pp. 1019-1034.
23. Mikulas, M. M., "Failure Prediction Techniques for Compression-Loaded Composite Laminates with Holes," Selected NASA Research in Composite Materials and Structures, NASA Conference Publication 2142, August 1980.
24. O'Brien, T. K., "Analysis of Local Delaminations and Their Influence on Composite Laminate Behavior," NASA-TM-85728, January 1984.
25. Webster, J. D., "Flaw Criticality of Circular Dishone Defects in Compressive Laminates," NASA-CR-164830, June 1981.
26. Wilson, D. W., Gillespie, J. W., York, J. L., and Pipes, R. B., "Failure Analysis of Composite Bolted Joints," NASA-CR-16372, July 1980.
27. Starnes, J. H. et al., "Failure Characteristics of Graphite-Epoxy Structural Components Loaded in Compression," NASA-TM-84552, September 1982.
28. Wu, E.M., "Failure Analysis of Composites with Stress Gradients," First USA-USSR Symposium on Fracture of Composite Materials, Sijthoff and Noordhoff International Publisher, 1979, pp. 63-76.
29. McLaughlin, P. V., and Dasgupta, A., "BILAM: A Composite Laminate Failure Analysis Code Using Bilinear Stress Strain Approximations," UCRL-15371, October 1980.

30. Phelps, M. L. "In-Service Inspection Methods for Graphite-Epoxy Structures on Commercial Transport Aircraft," NASA-CR-165746, November 1981.
31. Reynolds, W. N., "Nondestructive Testing (NDT) of Fiber-Reinforced Composite Materials," SAMPE Quarterly, Vol. 16, No.4, July 1985, pp. 1-16.
32. Schramm, S. W., Daniel, I. M., and Hamilton, "Evaluation of Sensitivity of Ultrasonic Detection of Disbonds in Graphite/Epoxy to Metal Joints," 36th Annual Conference, Reinforced Plastics/Composites Institute, published by The Society of the Plastics Industry, Inc., February 16-20, 1981.
33. Ulman, D. A., and Hennecke, E. G., II, "Nondestructive Evaluation of Damage in F. P./Aluminum Composites," Composite Materials: Testing and Design, ASTM STP 787, 1982, pp. 323-342.
34. Bar-Cohen, Y. et al., "Acoustic Backscattering Imaging of Subcritical Flaws in Composites," Material Evaluation, Vol. 40, August 1982.
35. Moran, T. J. et al., "High-Resolution Imaging of Microcracks in Composites," Materials Evaluation, Vol. 43, April 1982.
36. Baumann, K. J., Kennedy, W. H., and Herbert, D. L., "Composite Tomography X-ray Scanning NDE of Graphite/Epoxy Coupons," Journal of Composite Materials, Vol. 18, November 1984.
37. Sendekyj, G. P., and Maddux, G. E., "Comparison of Holographic, Radiographic, and Ultrasonic Techniques for Damage Detection in Composite Materials," ASTM-STP-696, Edited by R. P. Pipes, 1979, pp. 26-44.
38. Reifsnider, K. L. et al., "Defect Property Relationship in Composite Materials," AFML-TR-76-81, (Part III), June 1978.
39. Soni, S. R., "Failure Analysis of Composite Laminates with a Fastener Hole," Joining of Composite Materials; Proceeding of the Symposium, published by the American Society for Testing and Materials, 1981, pp. 145-164.

40. Gibbons, M. N., and Stinchcomb, W. W., "Fatigue Response of Composite Laminates with Internal Flaws," Composite Materials: Testing and Design, ASTM STP 787, 1982, pp. 305-322.
41. Teagle, P. R., "The Quality Control and Nondestructive Evaluation of Composite Aerospace Components," Composites, Vol. 14, No. 2, April 1983.
42. Bar-Cohen, Y., and Crane, R. L., "Nondestructive Evaluation of Fiber - Reinforced Composites with Acoustic Backscattering Measurements," Composite Materials, ASTM-STP-787, 1982, pp. 343-354.
43. Raatz, C. F., "Nondestructive Inspection," Airliner, October-December 1985.
44. Duke, J. C., Jr., "Nondestructive Evaluation of Composite Materials: A Philosophy, An Approach, and An Example," Composite Materials: Quality Assurance and Processing, ASTM-STP-797, 1983, pp. 75-95.
45. Wickham, A. A., Rice, D. D., and DuBois, R. J., "Chemical Analysis of Advanced Composite Prepregs and Resins," 24th National SAMPE Symposium and Exhibition, Vol. 24, 1979, pp. 506-521.
46. May, C. A., "Composite Matrix Quality Assurance - An Art Becomes a Science," 24th National SAMPE Symposium and Exhibition, Vol. 24, 1979, pp. 390-403.
47. Crozier, D., Morse, G., and Tajima, Y., "The Development of Improved Chemical Analysis Methods for Epoxy Resins," SAMPE Journal, September/October 1982, pp. 17-22.
48. Rogers, A. K., Tajima, Y. and Young, R. C., "The Development of a Material Specification for 177°C (350°F) Curing Graphite/Epoxy Composites," Composite Materials: Quality Assurance and Processing, ASTM-STP-797, Edited by C. E. Browning, 1983, pp. 15-28.

49. Tung, C. M., and Dynes, P. J., Chemorheological Characterization of B-Stage Printed Wiring Board Resins," Composite Materials: Quality Assurance and Processing, ASTM-STP-797, Edited by C. E. Browning, 1983, pp. 38-53.
50. Chen, J. S., Hunter, B. A., and Katsumoto, M. T., "Development of Quality Assurance Methods for Epoxy Graphite Prepeg," NASA CR-3531, March 1982.
51. Carpenter, J. F., "Test Program Evaluation of Hercules 3501-6 Resin," N00019-77-C-0155, May 1978.
52. Sewell, T. A., "Quality Assurance of Graphite/Epoxy by High-Performance Liquid Chromatography," Composite Materials: Quality Assurance and Processing, Edited by C. E. Browning, 1983, pp. 3-14.
53. Mones, E. T., Walkup, C. M., Happe, J. A., and Morgan, R. J., "The Characterization of Diaminodiphenyl Sulfone (DDS) Cured Tetraglycidyl 4,4' Diaminodiphenyl Methane (TGDDM) Epoxies," 14th National SAMPE Technical Conference, Vol. 14, 1982, pp. 89-100.
54. Stark, E. B., Ibrahim, A. M., and Seferis, J. C., "Experimental Analysis of the Network Structure for the High-Performance TGDDM-Novalac-DDS Epoxy Matrix System," 28th National SAMPE Symposium and Exhibition, Vol. 28, 1983, pp. 581-589.
55. Carpenter, J. F., "Physiochemical Testing of Altered Composite 3501-6 Epoxy Resin," 24th National SAMPE Symposium and Exhibition, Vol. 24, 1979, pp. 446-457.
56. Munns, T. E., and Seferis, J. C., "Coupling of DSC and Dynamic Mechanical Experiments for Probing Processing-Structure-Property Relationship of Catalyst Modified High-Performance Epoxy Matrices," Analytical Calorimetry, Vol. 5, Edited by J. F. Johnson and P. S. Gill, Plenum Press, 1984, pp. 1-12.

57. Chu, H. S. and Seferis, J. C., "Network Structure Description and Analysis of Amine-Cured Epoxy Matrices," The Role of the Polymeric Matrix in the Processing and Structural Properties of Composite Materials, Edited by J. C. Seferis and L. Nicolais, Plenum Press, 1983, pp. 53-125.
58. Young, P. R., Stein, B. A., and Chang, A. C., "Resin Characterization in Cured Graphite Fiber Reinforced Composites Using Diffuse Reflectance - FTIR," 28th National SAMPE Symposium and Exhibition, Vol. 28, 1983, pp. 824-837.
59. Burroughs, P., and Leckenby, J. N., "Analysis of Composite Materials by Dynamic Thermomechanometry (Dynamic Mechanical Analysis)," Composite Structures: Proceedings of the First International Conference, Applied Science, 1981, pp. 438-449.
60. Chu, H. S. and Seferis, J. C., "Dynamic Mechanical Experiments for Probing Process-Structure-Property Relations in Amine-Cured Epoxies," Polymer Composites, Vol. 5, No. 2, 1984, pp. 124-140.
61. Baumgartner, W. E., and Lemming, H., "Cure Monitoring and Properties Assessment of Graphite Epoxy Composites Using Dynamic Mechanical Test Methods," 22nd National SAMPE Symposium and Exhibition, Vol. 22, 1977, pp. 650-662.
62. Putter, S., Buchanan, D. L., and Rehfield, L. W., "Influence of Frequency and Environmental Conditions on Dynamic Behavior of Graphite/Epoxy Composites," Composite Materials: Testing and Design (Sixth Conference), ASTM-STP-787, Edited by I. M. Daniel, 1982, pp. 414-424.
63. Jackson, W. T., "Critical Evaluation of Several Methods for Determining Fiber Fraction of Cured Graphite/Epoxy Composites," 23rd National SAMPE Symposium and Exhibition, Vol. 23, 1978, pp. 160-174.

END

9-87

DTIC